MICROBIAL STRESS RESPONSES: ANTIOXIDANTS, THE PLASMA MEMBRANE, AND BEYOND

EDITED BY: Sukesh Chander Sharma, Joaquin Arino, Jose M. Mulet, Cristina Mazzoni and Amparo Pascual-Ahuir

PUBLISHED IN: Frontiers in Microbiology

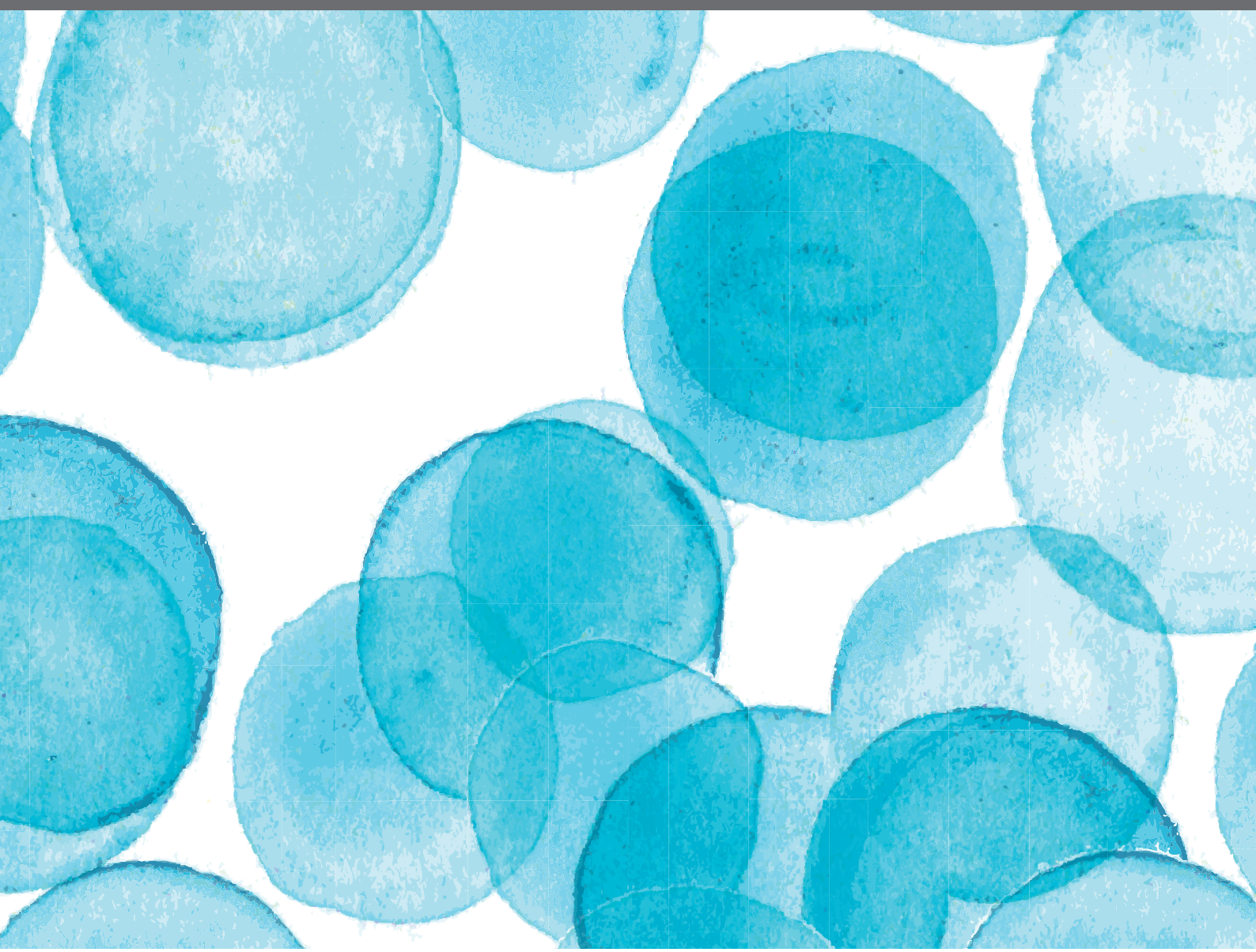

frontiers Research Topics

ISSN 1664-8714
ISBN 978-2-88974-728-3
DOI 10.3389/978-2-88974-728-3

About Frontiers

Frontiers is more than just an open-access publisher of scholarly articles: it is a pioneering approach to the world of academia, radically improving the way scholarly research is managed. The grand vision of Frontiers is a world where all people have an equal opportunity to seek, share and generate knowledge. Frontiers provides immediate and permanent online open access to all its publications, but this alone is not enough to realize our grand goals.

Frontiers Journal Series

The Frontiers Journal Series is a multi-tier and interdisciplinary set of open-access, online journals, promising a paradigm shift from the current review, selection and dissemination processes in academic publishing. All Frontiers journals are driven by researchers for researchers; therefore, they constitute a service to the scholarly community. At the same time, the Frontiers Journal Series operates on a revolutionary invention, the tiered publishing system, initially addressing specific communities of scholars, and gradually climbing up to broader public understanding, thus serving the interests of the lay society, too.

Dedication to Quality

Each Frontiers article is a landmark of the highest quality, thanks to genuinely collaborative interactions between authors and review editors, who include some of the world's best academicians. Research must be certified by peers before entering a stream of knowledge that may eventually reach the public - and shape society; therefore, Frontiers only applies the most rigorous and unbiased reviews.
Frontiers revolutionizes research publishing by freely delivering the most outstanding research, evaluated with no bias from both the academic and social point of view. By applying the most advanced information technologies, Frontiers is catapulting scholarly publishing into a new generation.

What are Frontiers Research Topics?

Frontiers Research Topics are very popular trademarks of the Frontiers Journals Series: they are collections of at least ten articles, all centered on a particular subject. With their unique mix of varied contributions from Original Research to Review Articles, Frontiers Research Topics unify the most influential researchers, the latest key findings and historical advances in a hot research area! Find out more on how to host your own Frontiers Research Topic or contribute to one as an author by contacting the Frontiers Editorial Office: frontiersin.org/about/contact

MICROBIAL STRESS RESPONSES: ANTIOXIDANTS, THE PLASMA MEMBRANE, AND BEYOND

Topic Editors:
Sukesh Chander Sharma, Panjab University, India
Joaquin Arino, Universitat Autònoma de Barcelona, Spain
Jose M. Mulet, Universitat Politècnica de València, Spain
Cristina Mazzoni, Sapienza University of Rome, Italy
Amparo Pascual-Ahuir, Universitat Politècnica de València, Spain

Citation: Sharma, S. C., Arino, J., Mulet, J. M., Mazzoni, C., Pascual-Ahuir, A., eds. (2022). Microbial Stress Responses: Antioxidants, the Plasma Membrane, and Beyond. Lausanne: Frontiers Media SA. doi: 10.3389/978-2-88974-728-3

Table of Contents

frontiers | Frontiers in Microbiology

EDITORIAL
published: 02 June 2022
doi: 10.3389/fmicb.2022.891964

Editorial: Microbial Stress Responses: Antioxidants, the Plasma Membrane, and Beyond

Sukesh Chander Sharma[1]*, *Joaquin Arino*[2], *Amparo Pascual-Ahuir*[3], *Jose M. Mulet*[3] and *Cristina Mazzoni*[4]

[1] Department of Biochemistry, Panjab University, Chandigarh, India, [2] Department de Bioquimica I Biologia Molecular, Universitat Autonoma de Barcelona, Cerdanyola del Valles, Spain, [3] Instituto de Biología Molecular y Celular de Plantas, Universitat Politècnica de València-Consejo Superior de Investigaciones Científicas, Valencia, Spain, [4] Department of Biology and Biotechnologies "C. Darwin", Sapienza University of Rome, Rome, Italy

Keywords: oxidative stress, yeasts, transporter, antioxidant, membrane

Editorial on the Research Topic

Microbial Stress Responses: Antioxidants, the Plasma Membrane, and Beyond

OPEN ACCESS

Edited by:
Nelson da Cruz Soares, University of Sharjah, United Arab Emirates

Reviewed by:
Yosuke Tashiro, Shizuoka University, Japan
Eva Torres Sangiao, "Marqués de Valdecilla" University Hospital, Spain

***Correspondence:**
Sukesh Chander Sharma
sukeshcs@pu.ac.in

Specialty section:
This article was submitted to Microbial Physiology and Metabolism, a section of the journal Frontiers in Microbiology

Received: *08 March 2022*
Accepted: *19 May 2022*
Published: *02 June 2022*

Citation:
Sharma SC, Arino J, Pascual-Ahuir A, Mulet JM and Mazzoni C (2022) Editorial: Microbial Stress Responses: Antioxidants, the Plasma Membrane, and Beyond. Front. Microbiol. 13:891964. doi: 10.3389/fmicb.2022.891964

Over the past decade, our understanding of the mechanisms involved in microbial responses to stressful environmental conditions have expanded greatly. We are now able to observe both microbial toxicity sensing and microbial adaptations to environmental perturbation. During stressful situations, such as extremes in pH, temperature, humidity and pressure, the microbial cell membrane is always the first target both in bacteria and fungi (Guan and Liu, 2020; Lanze et al., 2020). As the activities of cell membranes are crucial in the functioning of all cells, it is essential to study them during periods of stress, in particular, how the functioning of ATPases is disturbed, whether changes are observed in cation uptake or if membrane potentials are drastically altered. Emerging technologies, such as transcriptomics, proteomics, metabolomics, lipidomics and glycomics, can help us to understand the molecular mechanisms that interplay within the cell membrane during microbial exposure to stressful conditions. Investigation into aspects of the cell membrane, such as membrane raft structure characterization, ion homeostasis, and the role of ion transporters and antioxidants could shed valuable light on the holistic microbial response to stress. Frontiers in Microbiology took initiative in bringing out a special issue on this cutting-edge theme. In this Research Topic we collected 1 review and 9 original research articles which combined give an overview on the current status of this field.

In the review (Ferraz et al.), the authors consider the harsh conditions applied to microorganisms during industrial fermentations and how the plasma membrane is involved in strains productivity. They present an overview of membrane engineering strategies applied to *Saccharomyces cerevisiae* to enhance its fitness under industrially relevant conditions as well as strategies to increase microbial production of the metabolites of interest. The knowledge on this topic is not yet exhaustive and will require the collaboration of different disciplines ranging from lipidomics, molecular dynamics simulations and membrane biophysics to gain more information on the plasma membrane that could be used at systems level.

The study of Camponenschi et al. deals with the effects of light on oxidative stress and lipid biosynthesis in the *Kluyveromyces lactis* yeast. Although yeast lacks specialized light-sensing proteins, it has been reported that budding yeast *S. cerevisiae* respond to light by increasing hydrogen peroxide level and triggering nuclear translocation of the stress-response transcription factor Msn2 (Bodvard et al., 2011). In this paper, the authors show a role in light response of the regulatory factor KlMga2, involved in response to ROS, life span, and general cellular fitness

(Santomartino et al., 2019), opening new perspectives on the role of lipids and membranes in the response to light stress.

Membranes posses a unique feature called "homeoviscous adaptation" in order to maintain normal function of that system while undergoing stressful conditions. The key need for this feature is dependent upon the compositional changes of membrane matrix to control its fluidity. Paullucci et al. studied the long term response to temperature stress in Synorhizobium in Medicago sativa is due *de novo* synthesis of fatty acid composition of phospholipids and where fluidity played a key role in symbiosis.

Da Silva Rovida et al. addressed the problem of the toxicity of herbicides, used in agriculture to control weeds, toward non-target organisms. Some herbicides have electronegative and oxidizing chemical elements, such as fluorine and chlorine that can affect the stress response genes in microorganisms compromising their physical structure and causing oxidative stress through the generation of reactive oxygen species (ROS) which interact with the cell membrane and can cause lipid peroxidation. As a way of preventing or reducing these types of imbalances, bacteria have developed response systems to protect membrane integrity, such as modulating the activity of antioxidant enzymes. To test the toxicity of various commercial herbicides, the authors studied the modulation of antioxidant mechanisms of a *Pseudomonas* strain collected from biofilms in a specific herbicide packaging washing tank. This strain shows a higher tolerance to herbicides and biofilms containing this strain could protect the herbicide-sensitive isolates, opening a possibility of using biofilms containing such a kind of resistant bacterial strains for the bioremediation of contaminated areas.

For Gram-negative bacteria, the cell envelope structure, composed by the outer membrane (OM), the peptidoglycan and the inner membrane (IM), has a multitude of functions and it's fundamental to maintain the envelope homeostasis through a sophisticated regulatory network that comprises Cpx two-component regulatory system (Hews et al., 2019). Tsviklist et al. found that *E. coli* cells require the integrity of the two-component system Cpx envelope stress response especially during respiration. Moreover, the authors demonstrate that the Cpx two-component system serves as a sentry of inner membrane protein biogenesis, ensuring the function of large envelope protein complexes and maintaining the cellular energy status of the cell.

Some papers focused on stress induced by environmental factors such as temperature, salt or water stress. Goh et al. provide a molecular description of the stress response in *E. coli*. The paper describes how cold shock induces translational stress response via GTPase Bip A, a factor affecting the growth, swimming mobility and ribosome assembly. These results suggest that BipA is a *bona fide* 50s assembly factor in the bacterial ribosome biogenesis. Liu et al. investigated the effect of salt and osmotic stress on the phytofungus *Setosphaeria turcica*, a plant pathogen which causes the corn leaf blight disease. The report shows that osmotic stress increases the fungal pathogeneicity, and that this is dependent on the HOG-MAPK pathway. Moreover, the aquaglyceroporin StFPS1, a target of regulation of the HOG-MAPK pathway, is involved in the penetration ability of *S. turcica*. Following a similar approach (the interplay between environmental stress and pathogenicity). Li F. et al. investigated this phenomenon in the *Escherichia coli* BW25113 bacteria pointing to a pivotal role of trehalose in this process, This is of major interest as trehalose has also been found to have an important role in salt stress in fungi (Mulet et al., 2004). Li P.-S. et al. brought new insight into the rhizosphere bacterium *Rahnella aquatilis* JZ-GX1 and found that is moderately halophilic, and that the secretion of exopolysaccharides has a role in salt tolerance. *R. aquatilis* is a good growth promoter for plants, providing aknowledge that may be useful for agronomy. Finally Luo and Tian contributed with a report comparing two different strains of *Epichloë sinensis* aiming at gaining knowledge on the environmental adaptation of this endophyte and the role of phytohormones.

The most of the article are with the theme of the issue. The role of another important antioxidant molecular GSH has not found its place. Role of membrane rafts, alterations in the lipid- protein interactions, role of sterols, signaling lipids, their dynamics, homeostasis, lipidome, glycome, and transbilayer asymmetric distribution. Aforementioned studies can further help to gain more understanding of the role of plasma membrane, antioxidants in stress tolerance.

AUTHOR CONTRIBUTIONS

SS, JM, and CM wrote the draft of the manuscript. SS, JA, AP-A, JM, and CM contributed to manuscript revision. All authors contributed to the article and approved the submitted version.

ACKNOWLEDGMENTS

All the reviewers also deserve due appreciation for their kind help without which it is extremely difficult to move ahead.

REFERENCES

Bodvard, K., Wrangborg, D., Tapani, S., Logg, K., Sliwa, P., Blomberg, A., et al. (2011). Continuous light exposure causes cumulative stress that affects the localization oscillation dynamics of the transcription factor Msn2p. *Biochim. Biophys. Acta* 1813, 358–366. doi: 10.1016/j.bbamcr.2010.12.004

Guan, N., and Liu, L. (2020). Microbial response to acid stress: mechanisms and applications. *Appl. Microbiol. Biotechnol.* 104, 51–65. doi: 10.1007/s00253-019-10226-1

Hews, C. L., Cho, T., Rowley, G., and Raivio, T. L. (2019). Maintaining integrity under stress: envelope stress response regulation of pathogenesis in gram-negative bacteria. *Front. Cell. Infect. Microbiol.* 9, 313. doi: 10.3389/fcimb.2019.00313

Lanze, C. E., Gandra, R. M., Foderaro, J. E., Swenson, K. A., Douglas, L. M., and Konopka, J. B. (2020). Plasma membrane MCC/eisosome domains promote stress resistance in fungi. *Microbiol. Mol. Biol. Rev.* 84, e00063–e00019. doi: 10.1128/MMBR.00063-19

Mulet, J. M., Alejandro, S., Romero, C., and Serrano, R. (2004). The trehalose pathway and intracellular glucose phosphates as modulators of potassium transport and general cation homeostasis in yeast. *Yeast* 21, 569–582. doi: 10.1002/yea.1126

Santomartino, R., Camponeschi, I., Polo, G., Immesi, A., Rinaldi, T., Mazzoni, C., et al. (2019). The hypoxic transcription factor KlMga2 mediates the response to oxidative stress and influences longevity in the yeast Kluyveromyces lactis. *FEMS Yeast Res*. 19, foz020. doi: 10.1093/femsyr/foz020

Conflict of Interest: The authors declare that the research was conducted in the absence of any commercial or financial relationships that could be construed as a potential conflict of interest.

Publisher's Note: All claims expressed in this article are solely those of the authors and do not necessarily represent those of their affiliated organizations, or those of the publisher, the editors and the reviewers. Any product that may be evaluated in this article, or claim that may be made by its manufacturer, is not guaranteed or endorsed by the publisher.

frontiers in Microbiology

ORIGINAL RESEARCH
published: 08 June 2021
doi: 10.3389/fmicb.2021.657238

Salt Tolerance Mechanism of the Rhizosphere Bacterium JZ-GX1 and Its Effects on Tomato Seed Germination and Seedling Growth

Pu-Sheng Li[1,2], *Wei-Liang Kong*[1,2] *and Xiao-Qin Wu*[1,2]*

[1] *Co-Innovation Center for Sustainable Forestry in Southern China, College of Forestry, Nanjing Forestry University, Nanjing, China,* [2] *Jiangsu Key Laboratory for Prevention and Management of Invasive Species, Nanjing Forestry University, Nanjing, China*

Salinity is one of the strongest abiotic factors in nature and has harmful effects on plants and microorganisms. In recent years, the degree of soil salinization has become an increasingly serious problem, and the use of plant growth-promoting rhizobacteria has become an option to improve the stress resistance of plants. In the present study, the salt tolerance mechanism of the rhizosphere bacterium *Rahnella aquatilis* JZ-GX1 was investigated through scanning electron microscopy observations and analysis of growth characteristics, compatible solutes, ion distribution and gene expression. In addition, the effect of JZ-GX1 on plant germination and seedling growth was preliminarily assessed through germination experiments. *R. aquatilis* JZ-GX1 was tolerant to 0–9% NaCl and grew well at 3%. Strain JZ-GX1 promotes salt tolerance by stimulating the production of exopolysaccharides, and can secrete 60.6983 mg/L of exopolysaccharides under the high salt concentration of 9%. Furthermore, the accumulation of the compatible solute trehalose in cells as the NaCl concentration increased was shown to be the primary mechanism of resistance to high salt concentrations in JZ-GX1. Strain JZ-GX1 could still produce indole-3-acetic acid (IAA) and siderophores and dissolve inorganic phosphorus under salt stress, characteristics that promote the ability of plants to resist salt stress. When the salt concentration was 100 mmol/L, strain JZ-GX1 significantly improved the germination rate, germination potential, fresh weight, primary root length and stem length of tomato seeds by 10.52, 125.56, 50.00, 218.18, and 144.64%, respectively. Therefore, *R. aquatilis* JZ-GX1 is a moderately halophilic bacterium with good growth-promoting function that has potential for future development as a microbial agent and use in saline-alkali land resources.

Keywords: ***Rahnella aquatilis*, salt tolerance mechanism, compatible solute, growth-promoting function, plant growth-promoting rhizobacteria**

OPEN ACCESS

Edited by:
Jose M. Mulet, Universitat Politècnica de València, Spain

Reviewed by:
Jogendra Singh, Central Soil Salinity Research Institute (ICAR), India
Golam Jalal Ahammed, Henan University of Science and Technology, China

***Correspondence:**
Xiao-Qin Wu
xqwu@njfu.edu.cn

Specialty section:
This article was submitted to Microbial Physiology and Metabolism, a section of the journal Frontiers in Microbiology

Received: *22 January 2021*
Accepted: *03 May 2021*
Published: *08 June 2021*

Citation:
Li P-S, Kong W-L and Wu X-Q (2021) Salt Tolerance Mechanism of the Rhizosphere Bacterium JZ-GX1 and Its Effects on Tomato Seed Germination and Seedling Growth. Front. Microbiol. 12:657238. doi: 10.3389/fmicb.2021.657238

INTRODUCTION

Soil salinization is a worldwide soil degradation problem that not only causes damage to resources but also harms environmental and economic development (Zhang et al., 2010). Therefore, the remediation, development and use of saline-alkali soil are of great significance. Some microorganisms can survive in adverse conditions, among which halophilic bacteria have attracted

a great deal of attention due to their great potential applications. Therefore, elucidation of the mechanisms by which halophilic bacteria adapt to salt stress is of great significance in the future development and use of saline-alkali soil.

Microorganisms living under salt stress require specific adaptation mechanisms, and halophilic bacteria have been shown to use different strategies to deal with excessive salt in the external environment (Roy and Colin, 2002). The first strategy is the accumulation of potassium/chloride ions to maintain the internal osmotic balance of cells under high salt conditions (Hnelt and Volker, 2013), and adaptation that is common in extremely anaerobic halophilic bacteria (Oren, 2004). However, most halotolerant and moderately halophilic bacteria use a second strategy: the accumulation of compatible solutes. These complex solutes (including amino acids, carbohydrates and their derivatives, sugars and polyols) can be absorbed from the medium or synthesized by organisms themselves (Shivanand and Mugeraya, 2011). In cells, these solutes accumulate at high concentrations to maintain the balance between intracellular and extracellular osmotic pressure (Sabine et al., 2018), which is the most widely used salt tolerance strategy in bacteria, eukaryotes and some methanogenic bacteria (Lai and Gunsalus, 1992; Gupta et al., 2015). Studies have shown that betaine plays an important role in the maintenance of cell osmotic pressure. Betaine has the advantages of having no electrostatic charge and high solubility and does not affect many enzymes or other biological macromolecules, even at high concentrations (Yu et al., 2017). Betaine is the most common osmotic protective agent in prokaryotes (Farooq et al., 2015), and *Rhodococcus* sp. W2 has been reported to use intracellular betaine to resist high-salt environments (Shen et al., 2013). Trehalose is also a well-known osmotic protective agent (Jha et al., 2011). Under high-salt stress, the halophilic fungus *Aspergillus montevidensis* ZYD4 can alleviate the effects of salt stress by regulating the changes in cellular trehalose contents (Ding et al., 2019). In addition, many bacteria produce extracellular polysaccharides (EPSs) as a growth strategy that enables their survival under adverse conditions (Iwabuchi et al., 2003; Sivan et al., 2006; Urai et al., 2006; Perry et al., 2007). EPSs form a layer around cells to reduce cell damage under abiotic stress conditions, and the production of EPSs is essential for adhesion of other organisms, biofilm formation and nutrient absorption (Sutherland, 2001; Nichols et al., 2005).

In recent years, the biological engineering plants that are fully tolerant of saline-alkali environments has become a new research direction at home and abroad with the goal of improving plant yields in saline-alkali soil. At present, the use of plant growth-promoting rhizobacteria (PGPR) has been emphasized as an effective means improving soils with high-salt concentrations and promoting plant growth (Walia et al., 2005; Bashan, 2012). Studies on plant seed germination have shown that at a soil salt content of 0.2–0.3%, seedlings typically exhibit difficultly in emerging, while in soil with a salt content of 0.4–0.5%, seeds cannot unearth, and germination is difficult at soil salt contents greater than 0.65% (Liu et al., 1993). Mo et al. (2006) and other researchers have shown that *Arthrobacter* sp. Rs15-4 can improve the germination rate of cotton seeds and promote the growth of cotton seedlings under salt stress. In addition, many PGPRs have been shown to promote plant growth through a variety of other mechanisms. For example, indole-3-acetic acid (IAA) produced by PGPRs is an important plant hormone that controls many physiological processes (Spaepen et al., 2007; Leveau and Gerards, 2008). *Bacillus subtilis* pk5-26 can grow under severe salt stress and has a remarkable growth-promoting effect on *Arabidopsis thaliana*, as it is capable of dissolving phosphorus and secreting siderophores (Bokhari et al., 2019).

Preliminary studies conducted in our laboratory resulted in the isolation of the rhizosphere growth-promoting bacterium *Rahnella aquatilis* JZ-GX1 from the rhizosphere soil of 28-year-old Masson pine in Nanning, Guangxi. Strain JZ-GX1 exhibited high phytase activity, and its ability to produce IAA was shown to have significant growth-promoting effects on pine and poplar (Li and Wu, 2014). To date, research on *Rahnella* sp. has primarily focused on the biocontrol of plant diseases, the environmental remediation of selenium pollution, plant growth promotion, etc., while few studies have investigated the mechanisms associated with its salt tolerance. While PGPR aid in the ability of plants to resist stress, they must also deal with osmotic pressure changes. Thus, an in-depth understanding of the relevant mechanisms by which PGPRs cope with such stress is important for promoting PGPR-mediated strategies to improve plant abiotic stress. Thus, the goal of the present study was to elucidate the salt tolerance mechanism of *R. aquatilis* JZ-GX1 by investigating its growth characteristics under salt stress, accumulation of compatible solutes, ion distribution and expression of salt tolerance genes and to investigate the effect of this strain on tomato germination under salt stress. The results lay a foundation for expanding the application of this strain and promoting plant growth through the use of PGPRs to improve the ecological environment of salinized soil.

MATERIALS AND METHODS

Tested Strains and Culture Medium

R. aquatilis JZ-GX1 is a plant growth-promoting bacterium isolated from the rhizosphere soil of 28-year-old *P. massoniana* in Nanning, Guangxi, and is stored in the Culture Preservation Center of China (CCTCC, No: M2012439). After activation, strain JZ-GX1 was cultured overnight in LB liquid medium at 28°C (Kong et al., 2020). LB solid medium was prepared with 10 g of peptone, 5 g of yeast powder, 10 g of NaCl, and 15–20 g of agar (pH 7.2), and the NaCl concentration of the medium was set to 0, 3, 6, and 9% (0, 0.51, 1.02, and 1.53 mol/L, respectively). The activated strains were inoculated into the prepared media and cultured to the logarithmic phase at 28°C with shaking 200 r/min.

Determination of the Growth of *R. aquatilis* JZ-GX1 Under Salt Stress

Strain JZ-GX1 was inoculated on plates with different salt concentrations, and its growth on was observed after 24–48 h. Then, 50 μL of an activated bacterial solution was inoculated into test tubes containing 4,950 μL of LB medium with different salt concentrations and shaken. Subsequently, the culture broth was pipetted into each well of a 96-well plate and cultured

in a microplate reader (Bioscreen C, FP-110-C, Finland) at 28°C to determine the growth curves, with measurements automatically collected every 2 h for 48 h. The activated strain was inoculated (1%) in LB medium with different salt concentrations, and after cultivating for 24, 48, and 72 h, the cells were collected by centrifugation and dried to a constant weight to determine the dry weight.

Morphological Observation of Strain JZ-GX1 in the Presence of Different Salt Concentrations

Scanning electron microscopy observations of the tested strain JZ-GX1 were obtained as described by Castelijn et al. (2012). For sample preparation, the cells were first fixed with glutaraldehyde, washed with 0.2 M phosphate buffer (pH 7.4) and dehydrated with gradient ethanol. The dehydrated sample was dried with a CO_2 critical point desiccator (liquid CO_2, EMITECH K850), after which the dried sample was divided into fragments of suitable length, glued to the table and sprayed with gold (HITACHE-1010). Subsequently, the morphology of strain JZ-GX1 cells in the presence of different salt concentrations was observed with a scanning electron microscope (QUANTA200, FEI, United States).

Determination of Extracellular Polysaccharides Produced by Strain JZ-GX1 in the Presence of Different Salt Concentrations

The EPS content in the culture medium was determined using the phenol-sulfuric acid method (Wang, 2015).

Determination of Compatible Solutes Accumulated by Strain JZ-GX1 in the Presence of Different Salt Concentrations

LB media with different salinities (0, 3, 6, and 9%) was prepared. The bacteria were inoculated (1%) and cultured on a shaking table (28°C, 180 rpm) for 1, 2, 3, and 4 days. Subsequently, 500 μL of bacterial suspension was collected and centrifuged at 10,000 rpm for 3 min, and the supernatant was discarded.

Samples were prepared to assess the proline content of cells using a ratio of bacteria (10^4 cfu/mL) to extract volume (mL) of 500:1 (ultrasonic power 200 w, 3 s, interval 10 s, repeated 30 times). Thee samples were extracted in a 95°C water bath for 10 min. Then, after cooling, the samples were centrifuged at 25°C for 10 min at 10,000 rpm, and the supernatant was reserved. Samples were prepared to assess the trehalose content of cells by lysing bacteria with an ultrasonicator at a ratio of bacteria (10^4 cfu/ml) to extract volume (mL) of 500:1 (ultrasonic power 200 w, 3 s, interval 10 s, repeated 30 times). Then, after incubating at room temperature for 45 min, the samples were shaken 3–5 times, cooled, centrifuged at 8,000 rpm at 25°C for 10 min, and the supernatant was reserved. Samples were prepared to assess the betaine contents of cells by continuously shaking the samples with 1.2 mL of water for 60 min prior to extraction for 30 s. Subsequently, 400 μL of extract was added, mixed thoroughly, and centrifuged at 10,000 rpm at 25°C for 10 min to obtain the supernatant.

Three replicates of each treatment were evaluated, and the proline, betaine and trehalose contents accumulated by strain JZ-GX1 in the presence of different salt concentrations were determined using a commercial kit (Suzhou Keming Biotechnology Co., Ltd.).

Determination of the Na^+ and K^+ Concentrations of Strain JZ-GX1 in the Presence of Different Salt Concentrations

Na^+ and K^+ were extracted according to Nagata's method, and the concentrations of Na^+ and K^+ were determined by flame photometry (Nagata et al., 2005).

Differential Expression of Salt Tolerance-Related Genes in Strain JZ-GX1 in the Presence of Different Salt Concentrations

For quantitative RT-PCR, strain JZ-GX1 was cultured in LB medium for 72 h with shaking, after which RNA was extracted from cells using the TRIzol method. cDNA samples were prepared using HiScript II Q Select RT SuperMix for qPCR (China). The expression of salt tolerance-related genes was determined by qRT-PCR with an ABI 7500 instrument (Applied Biosystems, United States), and atpD was used as an internal control (Li et al., 2019). Three genes related to salt tolerance were selected from the genome of *R. aquatilis* JZ-GX1 (unpublished) for analysis (**Table 1**). The relative gene expression changes were calculated with the $2^{-\Delta\Delta CT}$ method. The RT-PCR assay consisted of three independent experiments, with three replicates performed for each experiment.

Determination of Growth-Promoting Characteristics of Strain JZ-GX1 in the Presence of Different Salt Concentrations

The siderophile production capacity of strain JZ-GX1 was determined as described in the literature (Schywn and Nielands, 1987); the indole acetic acid production capacity was assessed in accordance with the literature (Glickmann and Dessaux, 1995); and the phosphorus dissolving ability was determined according to the method reported by Li et al. (2012).

TABLE 1 | Primers used in the RT-qPCR analysis.

Gene name	Gene functions	Primers
nhaB	Na^+/H^+ antiporter NhaB	CGCTATTACTTCTCCAATCC ATCCACAATCTGCTCGTA
betB	Betaine-aldehyde dehydrogenase	ATGCATCACCCGCAGTTGTA TGAACGCTTTACCGCTCAGT
lgbT	L-Proline/glycine/betaine transporter	ATGAGCACTTCAACCATAA ATCCACCGAAGGATCTAA
atpD	Proton motive force generation	TAAAGTCGGTCTGTTCGGTG CGTGATAGAAGTCGTTACCCTC

Assessment of Seed Germination

Tomato seeds with similar breakage, size and fullness were selected, surface-sterilized with 10% hydrogen peroxide for 10 min, and washed thoroughly with aseptic distilled water to remove the residual hydrogen peroxide, after which the seeds were air-dried. Two groups were established: the control group (H_2O and LB) and the experimental group (JZ-GX1). The surface-sterilized seeds were soaked in sterile water and then cultured in LB liquid medium with 1×10^7 cfu/mL JZ-GX1 for 24 h. Subsequently, seeds of the same size were evenly distributed in a Petri dish (20 seeds in each dish) containing 10 mL of 100 mmol/L NaCl solution. Four replicates of each treatment were included. Starting on the 2nd day of observation of the artificial climate box, the number of germinated seeds based on a radicle length of 0.2 cm as the germination standard was counted every day. On the 7th day, 10 plants from each treatment were randomly selected to measure their germination length, root length, and fresh weight and to calculate their germination rate and germination energy (Fu et al., 2017).

$$\text{Germination rate (\%)} = \left(\text{number of germinated seeds by day 7} / \text{total number of test seeds}\right) \times 100.$$

$$\text{Germination energy (\%)} = \left(\text{number of germinated seeds by day 3} / \text{total number of test seeds}\right) \times 100.$$

Statistical Analysis

The data were analyzed by analysis of variance and Duncan's multiple comparison using SPSS 17.0, and the standard errors of the mean values were calculated ($P < 0.05$).

RESULTS

Salt-Tolerant Growth Characteristics of *R. aquatilis* JZ-GX1

The growth of bacteria in media with high salt concentrations is an important indicator of their salt tolerance. *R. aquatilis* JZ-GX1 was able to grow on plates containing 0–9% NaCl, indicating that strain JZ-GX1 is a moderately halophilic bacterium. In the presence of 9% NaCl concentration of, the growth rate was slow, and the colonies were small. Thus, the decrease in the growth rate of strain JZ-GX1 was related to the increase in salt concentration (**Figure 1A**).

A microplate reader was used to generate growth curves of strain JZ-GX1 cultured in LB medium with different salt concentrations. Strain JZ-GX1 had the shortest lag phase when cultured in the presence of 1%, while the lag phase reached 18 h in the presence of 9% NaCl. After entering the logarithmic phase of growth, the fastest growth rate of strain JZ-GX1 was obtained with a salt concentration of 3%, and the lowest growth rate of strain JZ-GX1 was observed with a salt concentration of 9%. After entering the stationary phase, the maximum OD600 value exceeded 1.0 for strain JZ-GX1 when cultured in the presence of 3% NaCl, with this phase

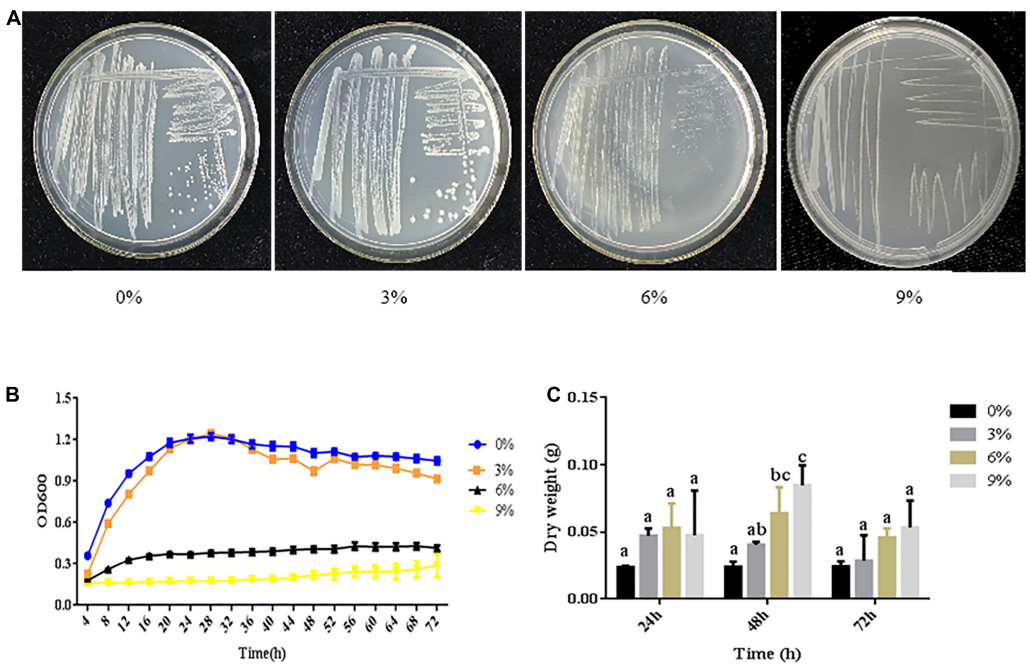

FIGURE 1 | Growth of *R. aquatilis* JZ-GX1 in media with different salt concentrations. **(A)** Images of culture plates. **(B)** Growth curves. **(C)** Cell dry weights. The vertical bars represent the standard deviations of the averages. One-way ANOVA was performed, and Duncan's *post hoc* test was applied. Different letters indicate significant differences ($P < 0.05$) among the treatments.

lasting longer when cultured in medium containing 0 and 3% NaCl than 6% NaCl. Increasing the NaCl concentration to 9% significantly prolonged the lag phase, decreased the growth rate at each growth period, and significantly inhibited the growth of *R. aquatilis* JZ-GX1. In addition, the lowest OD value observed after entering the stationary phase was detected at this salt concentration, with a maximal OD value of 0.241. Furthermore, almost no growth in the logarithmic phase was detected at this salt concentration, and the growth was seriously inhibited (**Figure 1B**). A further increase in the salt concentration reduced the tolerance and survival rate of the bacteria.

In terms of biomass, salt stress (3, 6, and 9%) increased the biomass of strain JZ-GX1 compared to that obtained in the absence of salt stress. At a salt concentration of 0%, no significant difference in the cell dry weight was observed over time. At a salt concentration of 3% NaCl, the dry weight of JZ-GX1 decreased slowly over time. At salt concentrations of 6 and 9%, the dry weight of strain JZ-GX1 first increased and then decreased over time (**Figure 1C**).

Electron Microscopy Observations of *R. aquatilis* JZ-GX1 in the Presence of Different Salt Concentrations and Secretion of Extracellular Polysaccharides

As shown in **Figure 2**, the cell morphology of *R. aquatilis* JZ-GX1 was altered under different levels of salt stress. In the presence of 0% NaCl, the cells were relatively short and regular in shape and presented many visible folds on the surface. In the presence of 3% NaCl, the bacteria became slightly longer and showed a sparse arrangement, and the visible folds on the cell surface were decreased and relatively smooth. In medium containing 6% NaCl, the bacteria adsorbed and adhered together, presumably due to the secretion of EPSs by the cells. In the presence of 9% NaCl, the bacteria were notably longer and arranged in a disorderly manner, cell fragments were detected, the cell morphology was damaged, and breakage was observed during the cell division. In general, increases in the degree of salt stress were associated with increases in cell length. The length and width of the cells treated with 9% salt were 5.12- and 1.41-fold higher than those observed with 0% salt, respectively. The results showed that strain JZ-GX1 can resist a high salt environment by altering its cell morphology.

The production of EPSs by many halotolerant bacteria is a growth strategy that can promote the formation of a protective layer around cells under adverse conditions to protect cells from the external environment. Therefore, the potential role of EPSs in the salt tolerance of JZ-GX1 was evaluated. As shown in **Figure 3**, strain JZ-GX1 could secrete EPSs in the presence of

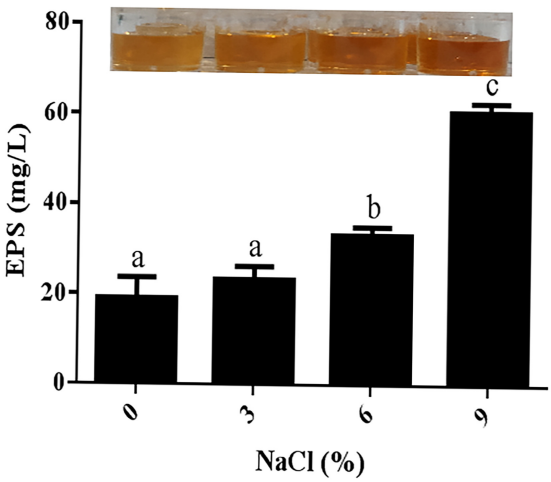

FIGURE 3 | Determination of extracellular polysaccharide levels produced by *R. aquatilis* JZ-GX1 at different salt concentrations. The vertical bars represent the standard deviations of the averages. One-way ANOVA was performed, and Duncan's *post hoc* test was applied. Different letters indicate significant differences ($P < 0.05$) among the treatments.

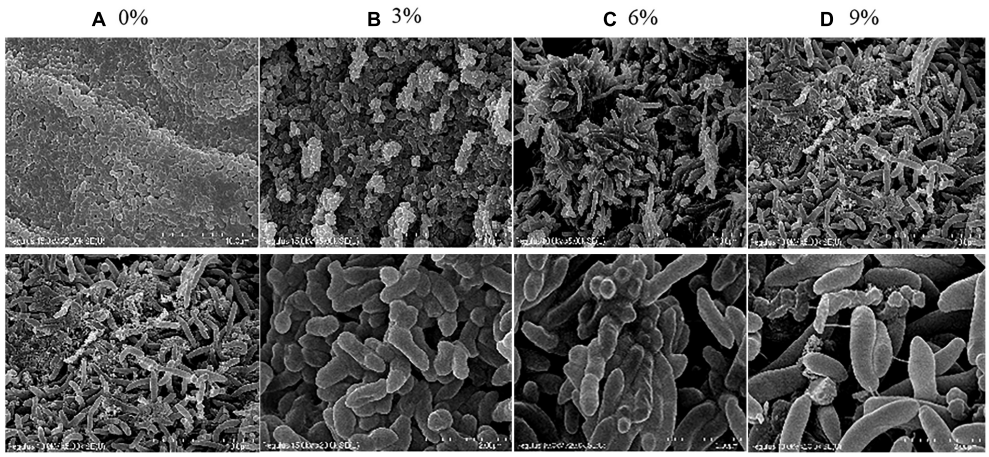

FIGURE 2 | Morphological changes in *R. aquatilis* JZ-GX1 at different salinities. **(A–D)** show scanning electron microscopy images of cells in the presence of 0, 3, 6, and 9% NaCl, respectively, with the scale bars indicating 10 or 2 μm.

different salinities, and the EPS yield increased with increasing salt concentration (0, 3, 6, and 9% NaCl), reaching maximum levels at 9% NaCl (60.6983 mg/L).

Accumulation of Compatible Solutes by *R. aquatilis* JZ-GX1 in the Presence of Different Salt Concentrations

To determine the type and content of compatible solutes in the JZ-GX1 strain, the accumulation of proline, betaine and trehalose in the presence of different concentrations of NaCl (0, 3, 6, and 9%) was assessed. As shown in **Figure 4**, the accumulation of proline and trehalose gradually increased with increases in the NaCl concentration on the 1st day, but no obvious change in the betaine content was detected. The highest accumulation of proline, betaine and trehalose was detected with 9% NaCl on the 1st, 2nd, and 3rd days, respectively, and on the 4th day of fermentation with 6% NaCl. Compared to the results obtained under salt-free conditions, the contents of proline, betaine and trehalose increased by 28.15, 46.55, and 66.63%, respectively. In addition, on the 1st day, strain JZ-GX1 primarily relied on proline to resist salt stress, while trehalose was relied upon at later stage, indicating that were selective in the accumulation of soluble solutes. These results suggest that strain JZ-GX1 may alleviate salt stress by regulating the content of compatible solutes *in vivo*, and the accumulation of trehalose is the primary protective mechanism used by this bacterium against high salt stress.

Analysis of Na^+ and K^+ Concentrations in *R. aquatilis* JZ-GX1 in the Presence of Different Salt Concentrations

R. aquatilis JZ-GX1 cells were analyzed by flame photometry, and a large amount of Na^+ was detected in the intracellular/extracellular spaces (**Figure 5**). The concentration of Na^+ in strain JZ-GX1 was lower than that in LB liquid medium (CK), a finding that was observed both intracellularly and extracellularly. Analysis of the accumulation of K^+ showed that the intracellular K^+ concentration was lower than that of CK, whereas the extracellular K^+ concentration was higher than that of CK. Further analysis of the extracellular Na^+/K^+ concentrations showed that the intracellular and extracellular Na^+/K^+ concentrations of strain JZ-GX1 were lower than those of CK under the four salt concentration gradients. These findings show that *R. aquatilis* JZ-GX1 can accumulate K^+ and increase the Na^+/K^+ ratio to cope with high salt environments,

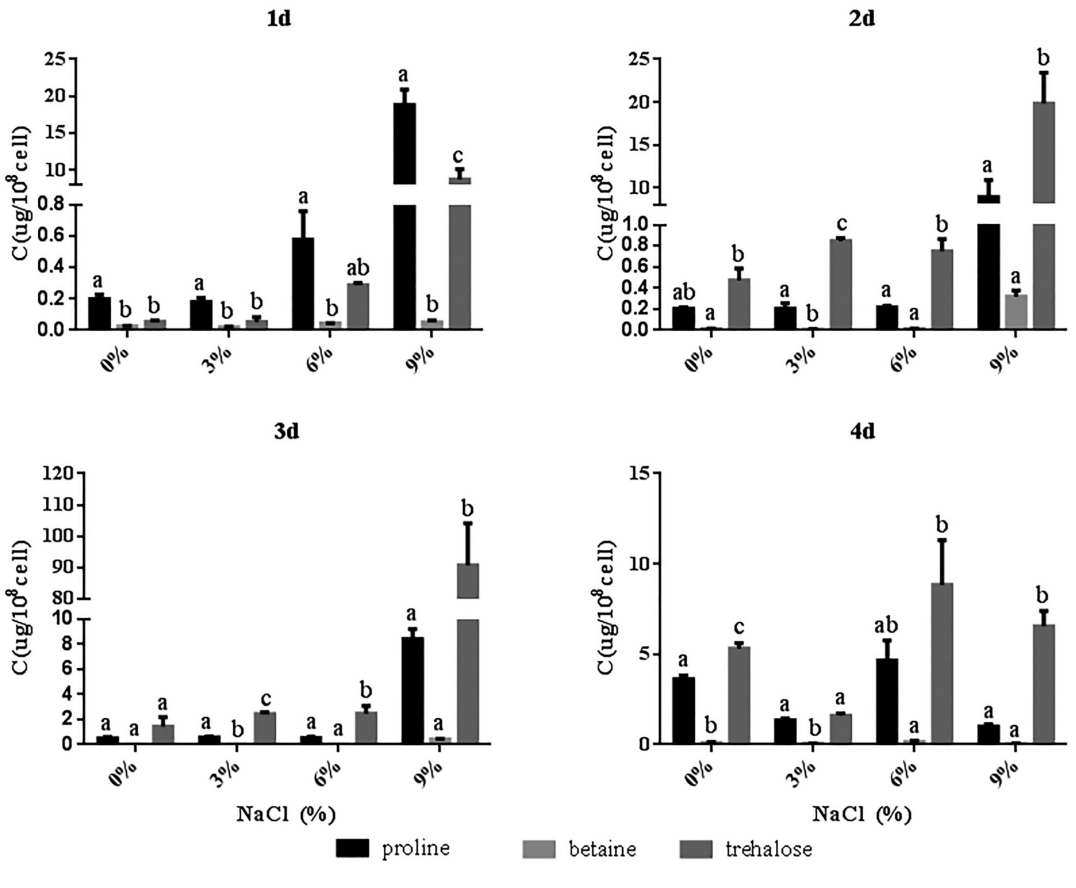

FIGURE 4 | Compatible solutes accumulated by *R. aquatilis* JZ-GX1 in the presence of different salt concentrations. The vertical bars represent the standard deviations of the averages. One-way ANOVA was performed, and Duncan's *post hoc* test was applied. Different letters indicate significant differences ($P < 0.05$) among the treatments.

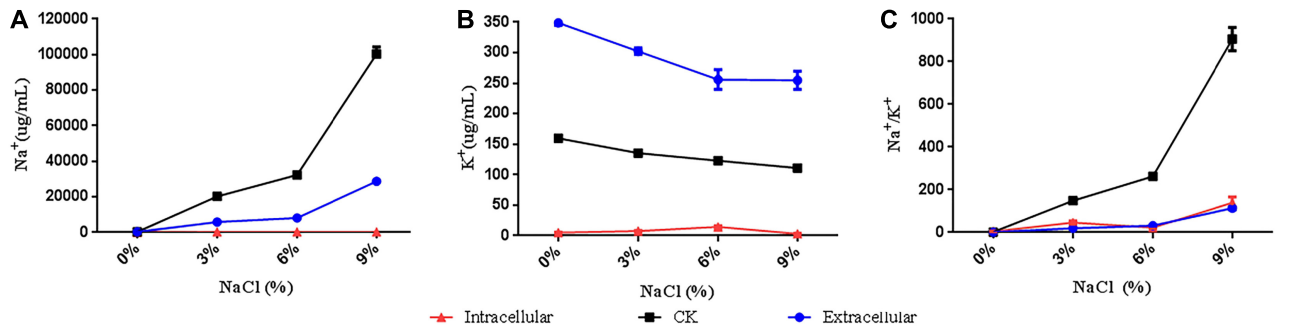

FIGURE 5 | Na^+ and K^+ concentrations of *R. aquatilis* JZ-GX1 in the presence of different salt concentrations. **(A)** Na^+ content. **(B)** K^+ content. **(C)** Na^+/K^+.

demonstrating another osmotic adaptation mechanism of *R. aquatilis* JZ-GX1.

Differential Expression of Salt Tolerance-Related Genes in *R. aquatilis* JZ-GX1 in the Presence of Different Salt Concentrations

To further elucidate the molecular mechanism underlying the salt tolerance of JZ-GX1, the target genes NhaB (encoding Na^+/H^+ antiporter NhaB), lgbT (encoding L-proline/glycine) and betB (encoding betaine) were selected to analyze the effect of NaCl on the expression of salt tolerance-related genes in strain JZ-GX1 at the transcriptional level. As shown in **Figure 6**, the level of NhaB transcription decreased with increasing salinity (0, 3, and 6% NaCl). In contrast, whereas the transcriptional levels of lgbT and betB first increased and then decreased with increasing salinity, the maximal values of these genes were obtained with 3% NaCl and reached 2.23- and 2.94-fold higher values than those observed in the absence of NaCl, respectively.

Effects of Different Salt Concentrations on the Growth-Promoting Characteristics of *R. aquatilis* JZ-GX1

Some PGPRs can promote plant growth under stress by secreting IAA. Therefore, the ability of strain JZ-GX1 to secrete IAA was also assessed in the present study, and the results are shown in **Figure 7A**. Quantitative analysis showed that strain JZ-GX1 could secrete a high concentration of IAA, even in TSB medium with a salt concentration of 3%. Siderophores are bioactive substances secreted by PGPRs that can increase the absorption of iron in plants and inhibit the growth of pathogens. In the present study, the ability of strain JZ-GX1 to synthesize siderophores was determined. As shown in **Figure 7B**, the siderophore production of strain JZ-GX1 first increased and then decreased as the salt concentration increased, and the

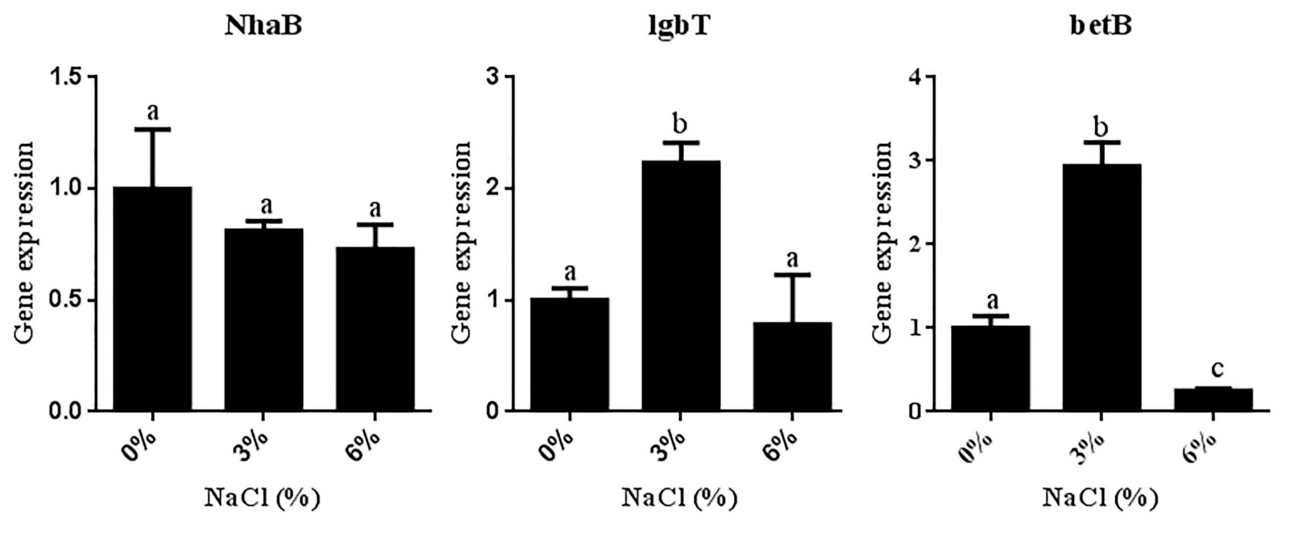

FIGURE 6 | Differential expression of salt tolerance-related genes in *R. aquatilis* JZ-GX1 in the presence of different salt concentrations. The vertical bars represent the standard deviations of the averages. One-way ANOVA was performed, and Duncan's *post hoc* test was applied. Different letters indicate significant differences ($P < 0.05$) among the treatments.

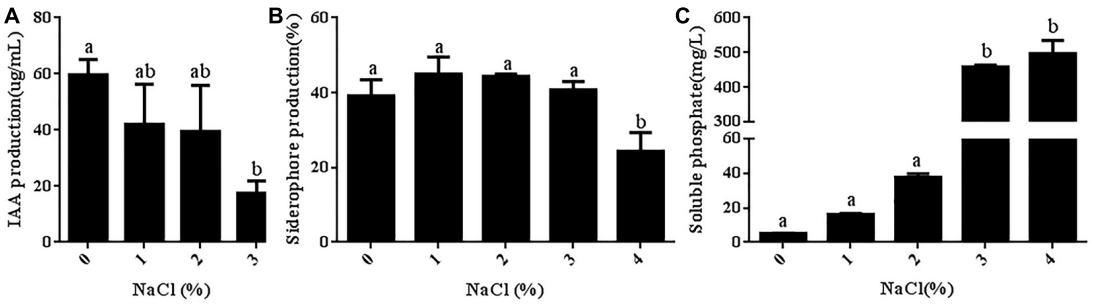

FIGURE 7 | Determination of JZ-GX1-related growth-promoting characteristics in the presence of different salt concentrations. **(A)** IAA content. **(B)** Siderophore content. **(C)** Phosphorus concentration. The vertical bars represent the standard deviations of the averages. One-way ANOVA was performed, and Duncan's *post hoc* test was applied. Different letters indicate significant differences ($P < 0.05$) among the treatments.

highest content of siderophores (44.93%) was obtained with a salt concentration of 1%. Appropriate salt concentrations could promote the secretion of siderophores by strain JZ-GX1, but the level of secreted siderophores began to decrease when the salt concentration reached 4%. By producing iron carriers, strain JZ-GX1 can help plants obtain iron from soil while controlling plant pathogens. An analysis of the ability of strain JZ-GX1 to dissolve inorganic phosphorus under different salt concentrations showed that increases in the salt concentration significantly improved the phosphorus-solubilizing ability of strain JZ-GX1 (**Figure 7C**).

Effect of *R. aquatilis* JZ-GX1 on Tomato Seed Germination Under Salt Stress

To determine whether strain JZ-GX1 can promote plant growth under salt stress, we used tomato as the target plant (**Figure 8A**). After being subjected to salt stress for 7 days, the fresh weight of the seedlings treated with strain JZ-GX1 was 23.97 and 50.005% higher than those obtained with the H_2O and LB treatments, respectively (**Figure 8B**). In addition, the primary root length of the JZ-GX1 strain-treated seedlings was approximately 1.9- and 3.2-fold longer than those of the seedlings subjected to the H_2O and LB treatments, respectively (**Figure 8C**). Furthermore, the stem length of the seedlings treated with strain JZ-GX1 was 41.88 and 144.64% higher than those obtained with the H_2O and LB treatments, respectively (**Figure 8D**). As shown in **Figures 8E,F**, treatment with strain JZ-GX1 significantly increased the germination rate and germination energy of tomato seedlings under salt stress. The results showed that the germination percentage and germination potential of tomato seeds treated with strain JZ-GX1 were significantly higher than those of the seeds treated with H_2O and LB, and the fresh weight, primary root length and stem length of the tomato seedlings were significantly increased by treatment with strain JZ-GX1.

DISCUSSION

Salinity is an abiotic stress in nature that exerts harmful effects on organisms. When cells are exposed to high-salt conditions, osmotic pressure pulls unbound water molecules out of the cells to yield a highly concentrated cytoplasm, which impairs cell function and can lead to cell death. Therefore, organisms living in high-salt environments need to have specific adaptation mechanisms (Weinisch et al., 2018). As cells adapt to a new osmotic environment, their biomass will change. In the present study, salt stress (3, 6, and 9%) increased the biomass of strain JZ-GX1 compared to that observed under non-salt stress conditions. The highest biomass of strain JZ-GX1 was obtained after 48 and 72 h of exposure to 9% NaCl, and the dry weight of strain JZ-GX1 at high salt concentrations was higher than that observed at low salt concentrations. Some studies have shown that EPSs can protect PGPRs from external stress during inoculation (Arora et al., 2020). According to relevant studies, the EPS yield shows a positive correlation with salt concentrations of 0–6% NaCl, reaching a maximum value (222.67 mg/g) at 6% NaCl. In the presence of higher NaCl concentrations (8–10%), the EPSs yield was shown to gradually decrease (Qiu et al., 2020). Khanna (2015) also observed similar results. In the present study, the EPS content produced by strain JZ-GX1 increased as the salt concentration increased, an effect was observed up to a salt concentration of 9%, which promoted the formation of a biofilm barrier. These findings indicated that one of the strategies used by strain JZ-GX1 to limit salt absorption involves reducing the intake of sodium by capturing sodium ions in its EPS matrix.

Previous studies have shown that halophilic bacteria under high salinity need to change their morphology to adapt to salt stress (Kogej et al., 2006). The phenomenon of early bacterial cell lengthening has been observed in *Pseudomonas* sp., but in *Rhodopseudomonas palustris*, this process is limited to the metabolism of selenium (Manter, 2009; Li et al., 2014). Mccready et al. (1966) suggested that the changes in growth of bacterial cells treated with selenium is due to the inhibition of cell division. The results of the present study are consistent with previously results describing significant lengthening of PGPR cells under abiotic stress (Yanyun et al., 2018). To date, it remains unclear why bacteria have evolved to produce larger cells under stressful conditions, but it might be because when bacteria encounter harmful substances in the environment (such as heavy metals, active oxygen species, drugs, etc.), mother cells can store more nutrients needed for the life activities of future generations by increasing the cell surface area (Philippe et al., 2009). Interestingly, although strain JZ-GX1 cells were damaged

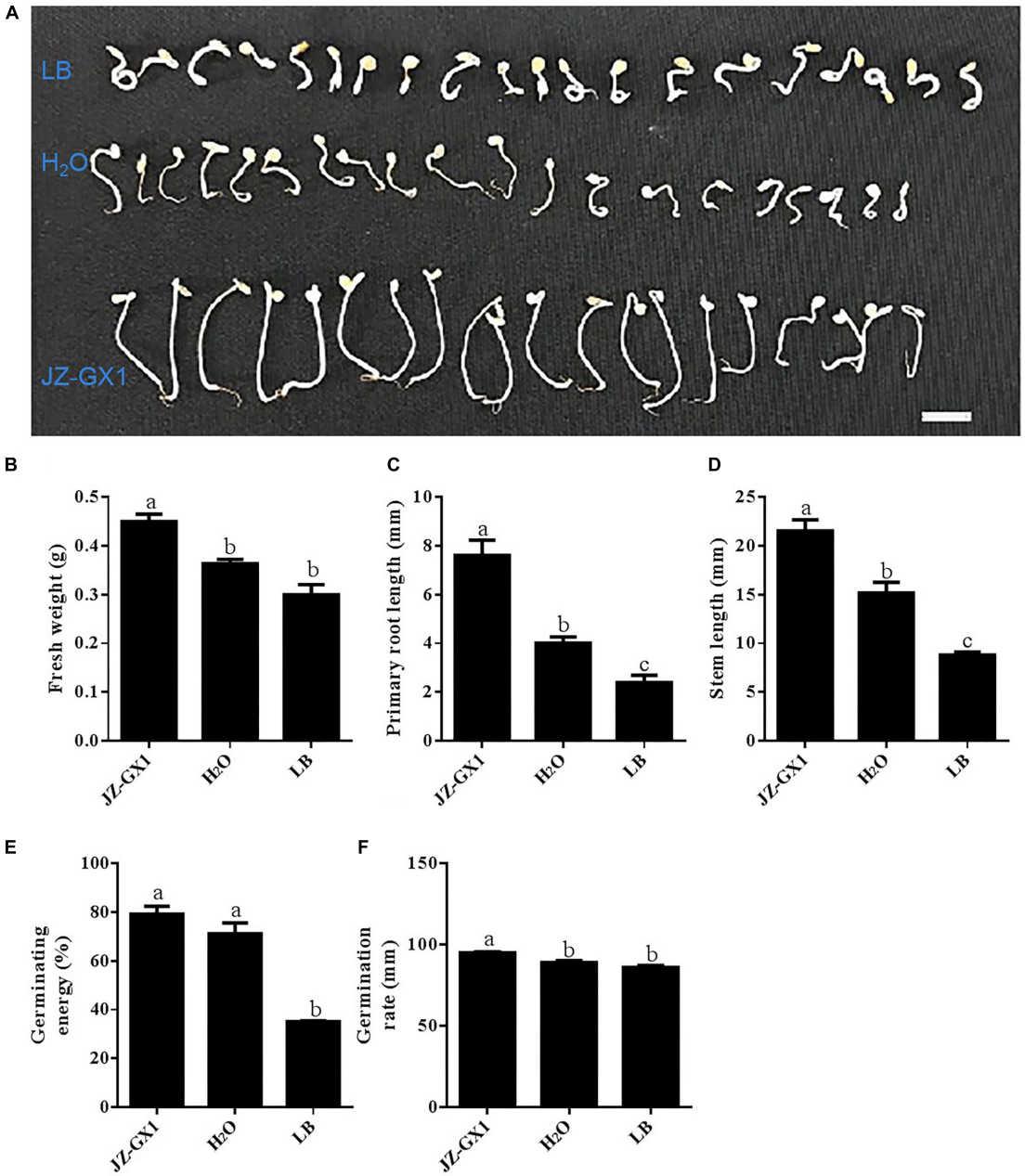

FIGURE 8 | Effects of *R. aquatilis* JZ-GX1 on tomato seed germination and seedling growth under salt stress (100 mM). **(A)** Phenotype. **(B)** Fresh weight. **(C)** Primary root length. **(D)** Stem length. **(E)** Germination energy. **(F)** Germination rate. The vertical bars represent the standard deviations of the averages. One-way ANOVA was performed, and Duncan's *post hoc* test was applied. Different letters indicate significant differences ($P < 0.05$) among the treatments.

to different degrees under different salt concentrations, they could still grow normally.

In a high salt environment, the establishment of intracellular ion homeostasis is important for the survival and growth of microorganisms (Plemenitas et al., 2016). Another strategy for avoiding high salt concentrations in the cytoplasm is to pump ions out of the cell. Na^+/H^+ antiporters, such as NhaA, an antiporter of *Escherichia coli* and many bacteria (Hunte et al., 2005), aid in pumping out excess sodium ions (Ruppel et al., 2013). In prokaryotes, Na^+/H^+ antiporters play an important role in salt tolerance. The results of the present study revealed that the expression of NhaB in *R. aquatilis* JZ-GX1 decreased with as the salt concentration increased, which could effectively reduce the continuous intake of sodium ions. In addition to NhaB, *R. aquatilis* JZ-GX1 can also resist high osmotic pressure by altering the expression of other salt tolerance-related genes. It is worth noting that Na^+ not only participates in the regulation of osmotic pressure in the form of ions but also plays an

important role in the regulation of the osmotic equilibrium of organically compatible solutes as some important substances for the transport of amino acids. Some microorganisms also produce organic osmotic substances that accumulate in the cytoplasm and resist osmotic pressure under high salt stress. To adapt to the balance of intracellular osmotic pressure, some osmotic regulators and protective substances, such as betaine (Wu et al., 2018) and proline (Nadeem et al., 2007), need to be synthesized and accumulate. Some moderately halophilic bacteria often exhibit selectivity for the accumulation of compatible solutes, reflecting the selective accumulation of several specific compatible solutes at different growth periods and in the presence of different salt concentrations. For example, when *Halomonas israelensis* was cultured at salinities lower than 3.5%, the major compatible solute that accumulated was trehalose, whereas the primary compatible solute that accumulated during cultivation at high salinities was tetrahydropyrimidine (He et al., 2005). *Bacillus* sp. I121 primarily accumulates proline under high salt concentrations and tetrahydropyrimidine at higher environmental salt concentrations, primarily maintaining its cellular osmotic pressure by accumulating tetrahydropyrimidine as a compatible solute (Jiang et al., 2010). In the present study, an analysis of the accumulation of three common compatible solutes (proline, betaine and trehalose) by *R. aquatilis* JZ-GX1 in the presence of different salt concentrations revealed that this strain primarily accumulated trehalose in the presence of high environmental salt concentrations, but no obvious trend was detected at low salt concentrations. In addition, the storage of osmotic substances represents a successful stress response mechanism that promotes the ability of bacteria to limit their water loss and increase the concentration of potassium ions in their cytoplasm. These results indicate that *R. aquatilis* JZ-GX1 adopts the "salting-out" strategy (the process of removing sodium ions and accumulating compatible solutes) to address high osmotic damage.

Microorganisms inhabiting plant roots form a complex ecological community with plants, affecting plant growth and productivity through their metabolic activities (Baek et al., 2010). The interactions between plants and beneficial microorganisms such as PGPRs can alleviate abiotic stress and increase the tolerance of plants to adverse growth conditions (Rodriguez et al., 2008; Aghili et al., 2014). In addition, PGPRs can also improve plant growth through indirect and direct mechanisms, including atmospheric nitrogen fixation, inorganic phosphorus hydrolysis, iron chelation, antibiotics, volatile compound production, hydrolase synthesis or plant hormone production (Babalola, 2010). A quantitative analysis confirmed that *R. aquatilis* JZ-GX1 can produce IAA and siderophores and has the ability to dissolve phosphorus under salt stress. Our results are consistent with those reported by Fatima et al. (2020). *Alcaligenes* AF7 has the ability to dissolve phosphorus under salt stress, and this ability promotes the ability of plants to grow under salt stress. Seed germination and early seedling growth are typically the most sensitive stages affected by salinity (Foolad, 2004), and mitigating the effects of salt at these early stages will increase the probability of successful crop growth under salt stress (Ashraf et al., 2003). In the present study, JZ-GX1 promoted the germination rate of tomato seeds under salt stress and enhanced the tolerance of tomato to salt stress by promoting shoot and root development and photosynthesis. This finding was consistent with those reported by Nadeem et al. (2013). Compared to the untreated control, seedings in natural saline land inoculated with *Pseudomonas putida*, *Enterobacter cloacae*, *Serratia ficaria,* and *Pseudomonas fluorescens* significantly increased the germination rate and germination index of wheat seeds and significantly increased wheat yields in saline-alkali land (Nadeem et al., 2013). The results of the present study demonstrated that strain JZ-GX1 has good application prospects for promoting plant growth under salt stress.

PGPR have value in a wide range of applications by inducing plants to resist adverse environmental conditions. We will perform pot experiments in the future to assess how the PGPR JZ-GX1 can improve early tomato seedling growth, including by studying its metabolic regulatory processes and associated molecular mechanisms in depth.

DATA AVAILABILITY STATEMENT

The raw data supporting the conclusions of this article will be made available by the authors, without undue reservation.

AUTHOR CONTRIBUTIONS

P-SL completed the data analysis and the first draft of the manuscript. P-SL and W-LK completed the experiments. X-QW directed the experimental design, data analysis, and manuscript writing and revision. All the authors read and agreed on the final text.

FUNDING

This work was supported by the National Key Research and Development Program of China (2017YFD0600104) and the Priority Academic Program Development of the Jiangsu Higher Education Institutions (PAPD).

REFERENCES

Aghili, F., Jansa, J., Khoshgoftarmanesh, A. H., Afyuni, M., and Gamper, H. A. (2014). Wheat plants invest more in mycorrhizae and receive more benefits from them under adverse than favorable soil conditions. *Appl. Soil Ecol.* 84, 93–111. doi: 10.1016/j.apsoil.2014.06.013

Arora, N., Sunita, K., Mishra, I., Mishra, J., and Prakash, J. (2020). Secondary metabolites from halotolerant plant growth promoting rhizobacteria for ameliorating salinity stress in plants. *Front. Microbiol.* 11:567768. doi: 10.3389/fmicb.2020.567768

Ashraf, M., Zafar, R., and Ashraf, M. Y. (2003). Time-course changes in the inorganic and organic components of germinating sunflower achenes under

salt (NaCl) stress. *Flora Morphol. Distribut. Funct. Ecol. Plants* 198, 26–36. doi: 10.1078/0367-2530-00073

Babalola, O. (2010). Beneficial bacteria of agricultural importance. *Biotechnol. Lett.* 32, 56–77.

Baek, D., Jiang, J., Jung-Sung, C., Wang, B., Chen, J., and Xin, Z. (2010). Regulated AtHKT1 gene expression by a distal enhancer element and DNA methylation in the promoter plays an important role in salt tolerance. *Plant Cell Physiol.* 52:149. doi: 10.1093/pcp/pcq182

Bashan, Y. (2012). *Enhancement of Plant Drought Tolerance by Microbes*. Berlin: Springer.

Bokhari, A., Essack, M., Lafi, F. F., Andres-Barrao, C., and Saad, M. M. (2019). Bioprospecting desert plant *Bacillus* endophytic strains for their potential to enhance plant stress tolerance. *Sci. Rep.* 9:18154.

Castelijn, G. A., Veen, S. V. D., Zwietering, M. H., Moezelaar, R., and Abee, T. (2012). Diversity in biofilm formation and production of curli fimbriae and cellulose of *Salmonella Typhimurium* strains of different origin in high and low nutrient medium. *Biofouling* 28, 51–63. doi: 10.1080/08927014.2011.648927

Ding, X., Liu, K., Lu, Y., and Gong, G. (2019). Morphological, transcriptional, and metabolic analyses of osmotic-adapted mechanisms of the halophilic *Aspergillus montevidensis* ZYD4 under hypersaline conditions. *Appl. Microbiol. Biotechnol.* 103, 3829–3846. doi: 10.1007/s00253-019-09705-2

Farooq, M., Hussain, M., Wakeel, A., and Siddique, K. (2015). Salt stress in maize: effects, resistance mechanisms, and management. a review. *Agron. Sustain. Dev.* 35, 461–481. doi: 10.1007/s13593-015-0287-0

Fatima, T., Mishra, I., Verma, R., and Arora, N. K. (2020). Mechanisms of halotolerant plant growth promoting *Alcaligenes* sp. involved in salt tolerance and enhancement of the growth of rice under salinity stress. *3 Biotech.* 10, 88–90. doi: 10.3390/microorganisms8010088

Foolad, M. R. (2004). Recent Advances in genetics of Salt Tolerance in Tomato. *Plant Cell Tissue Organ Cult.* 76, 101–119. doi: 10.1023/b:ticu.0000007308.47608.88

Fu, L., Li, X., Gao, L., Jiang, J. X., and Sun, J. Z. (2017). Effects of *Panthenia endophytic* bacteria on germination and physiology of hybrid pennisetum under salt stress. *Pratacult. Sci.* 34, 2099–2108.

Glickmann, E., and Dessaux, Y. (1995). A critical examination of the specificity of the salkowski reagent for indolic compounds produced by phytopathogenic bacteria. *Appl. Environ. Microbiol.* 61, 793–796. doi: 10.1128/aem.61.2.793-796.1995

Gupta, S., Sharma, P., Dev, K., Srivastava, M., and Sourirajan, A. (2015). A diverse group of halophilic bacteria exist in Lunsu, a natural salt water body of Himachal Pradesh, India. *Springerplus* 4:274.

He, J., Wang, T., Sun, J. Q., Gu, L. F., and Li, S. P. (2005). Isolation and characterization of moderately halophilic bacteria I15 with tetrahydropyrimidine as the main compatible solute. *J. Microbiol.* 45, 84–88.

Hnelt, I., and Volker, M. (2013). Molecular mechanisms of adaptation of the moderately *Halophilic* bacterium *Halobacillis halophilus* to its environment. *Life* 3, 90–99.

Hunte, C., Screpanti, E., Venturi, M., Rimon, A., Padan, E., and Michel, H. (2005). Structure of a Na^+/H^+ antiporter and insights into mechanism of action and regulation by pH. *Nature* 435:1197. doi: 10.1038/nature03692

Iwabuchi, N., Sunairi, M., and Anzai, H. (2003). Relationships among colony morphotypes, cell-surface properties and bacterial adhesion to substrata in *Rhodococcus*. *Coll. Surf. B Biointerf.* 30, 51–60. doi: 10.1016/s0927-7765(03)00036-5

Jha, Y., Subramanian, R. B., and Patel, S. (2011). Combination of Endophytic and Rhizospheric plant growth promoting rhizobacteria in *Oryza Sativa* shows higher accumulation of Osmoprotectant against saline stress. *Acta Physiol. Plant.* 33, 797–802. doi: 10.1007/s11738-010-0604-9

Jiang, W., Li, L., and Zhang, W. (2010). Proteomic analysis of plasma membrane of moderately halophagous bacteria *Bacillus* sp. I121. *J. Biol.* 27, 1–4.

Khanna, V. (2015). ACC-deaminase and EPS production by salt tolerant rhizobacteria augment growth in chickpea under salinity stress. *Intern. J. Bioresour. Stress Manag.* 9, 34–45.

Kogej, T., Gorbushina, A. A., and Gunde-Cimerman, N. (2006). Hypersaline conditions induce changes in cell-wall melanization and colony structure in a halophilic and a xerophilic black yeast species of the genus *Trimmatostroma*. *Mycol. Res.* 110, 713–724. doi: 10.1016/j.mycres.2006.01.014

Kong, W. L., Rui, L., Ni, H., and Wu, X. Q. (2020). Antifungal effects of volatile organic compounds produced by *Rahnella aquatilis* JZ-GX1 against *Colletotrichum gloeosporioides* in *Liriodendron chinense*× *tulipifera*. *Front. Microbiol.* 11:1114. doi: 10.3389/fmicb.2020.01114

Lai, M. C., and Gunsalus, R. P. (1992). Glycine betaine and potassium ion are the major compatible solutes in the extremely Halophilic methanogen methanohalophilus strain Z7302. *J. Bacteriol.* 174, 74–77.

Leveau, J. H. J., and Gerards, S. (2008). Discovery of a bacterial gene cluster for catabolism of the plant hormone indole 3-acetic acid. *FEMS Microbiol. Ecol.* 9, 34–45.

Li, B., Liu, N., Li, Y., Jing, W., Fan, J., and Li, D. (2014). Reduction of selenite to red elemental selenium by *Rhodopseudomonas palustris* strain N. *PLoS One* 9:e95955. doi: 10.1371/journal.pone.0095955

Li, G. E., and Wu, X. Q. (2014). Study on phytase characteristics of highly efficient phytate-degrading bacteria JZ-GX1. *J. Central S. Univ. For. Sci. Technol.* 8, 90–93.

Li, L., Li, J., Peng, J., Wu, W., and Guo, Y. (2019). Identification of atpD as an optimal reference gene to explore antibiotic resistance and stress tolerance in *Rahnella aquatilis*. *J. Appl. Microbiol.* 126, 1096–1107. doi: 10.1111/jam.14215

Li, Y., Yu, L., Li, H. X., Xu, L., Jiao, J. G., and Xu, F. (2012). Screening, identification and characterization of a growth-promoting strain in thrhizosphere of peanut. *J. Ecol. Rural Environ.* 28, 416–421.

Liu, G. Q., Lu, L. M., and Liu, J. D. (1993). Study on identification of salt tolerance of cotton variety resources. *China Seed Indust.* 6, 45–77.

Manter, H. D. K. (2009). Reduction of selenite to elemental red selenium by *Pseudomonas* sp. strain CA5. *Curr. Microbiol.* 11, 35–45.

Mccready, R. G. L., Campbell, J. N., and Payne, J. I. (1966). Selenite reduction by *Salmonella heidelberg*. *Can. J. Microbiol.* 12:703. doi: 10.1139/m66-097

Mo, W. P., Zheng, Y. Y., Yue, H. T., Li, C., and Li, H. (2006). Screening of desalination-promoting bacteria from cotton and preliminary study on its mechanism. *J. Shihezi Univ.* 24, 79–82.

Nadeem, S. M., Zahir, Z. A., Naveed, M., and Arshad, M. (2007). Preliminary investigations on inducing salt tolerance in maize through inoculation with rhizobacteria containing ACC deaminase activity. *Can. J. Microbiol.* 53, 1141–1149. doi: 10.1139/w07-081

Nadeem, S. M., Zahir, Z. A., Naveed, M., and Nawaz, S. (2013). Mitigation of salinity-induced negative impact on the growth and yield of wheat by plant growth-promoting rhizobacteria in naturally saline conditions. *Ann. Microbiol.* 63, 225–232. doi: 10.1007/s13213-012-0465-0

Nagata, S., Sasaki, H., Oshima, A., Takeda, S., Hashimoto, Y., and Ishida, A. (2005). Effect of proline and K^+ on the stimulation of cellular activities in *Escherichia coli* K-12 under high salinity. *J. Agric. Chem. Soc. Jpn.* 69, 740–746. doi: 10.1271/bbb.69.740

Nichols, C. A. M., Guezennec, J., and Bowman, J. P. (2005). Bacterial Exopolysaccharides from extreme marine environments with special consideration of the Southern Ocean, Sea Ice, and deep-sea hydrothermal vents: a review. *Mar. Biotechnol.* 7, 23–55.

Oren, A. (2004). Adaptation of *Halophilic archaea* to life at high salt concentrations. *Salin. Environ. Plants Mol.* 306, 81–96. doi: 10.1007/0-306-48155-3_4

Perry, M. B., Maclean, L. L., Patrauchan, M. A., and Evgeny, V. (2007). The structure of the exocellular polysaccharide produced by *Rhodococcus* sp. RHA1. *Carbohyd. Res.* 342, 2223–2229. doi: 10.1016/j.carres.2007.07.002

Philippe, N., Pelosi, L., Lenski, R. E., and Schneider, D. (2009). Evolution of penicillin-binding protein 2 concentration and cell shape during a long-term experiment with *Escherichia coli*. *J. Bacteriol.* 191, 909–921. doi: 10.1128/jb.01419-08

Plemenitas, A., Konte, T., Gostincar, C., and Cimerman, N. G. (2016). Transport systems in halophilic fungi. *Adv. Exper. Med. Biol.* 892, 307–325. doi: 10.1007/978-3-319-25304-6_13

Qiu, K. X., Wu, S., Fu, Y. Y., Cao, J. C., Guan, Z. G., Guo, P., et al. (2020). Studies on the mechanism of salt tolerance and betaine transporter gene of petroleum-degrading bacteria HX-2. *Microbiol. Bull.* 47, 40–53.

Rodriguez, R. J., Henson, J., Volkenburgh, E. V., Hoy, M., Wright, L., and Beckwith, F. (2008). Stress tolerance in plants via habitat-adapted symbiosis. *ISME J.* 2:404. doi: 10.1038/ismej.2007.106

Roy, D. S., and Colin, H. (2002). Bacterial osmoadaptation: the role of osmolytes in bacterial stress and virulence. *FEMS Microbiol. Rev.* 26, 89–99.

Ruppel, S., Franken, P., and Witzel, K. (2013). Properties of the halophyte microbiome and their implications for plant salt tolerance. *Funct. Plant Biol.* 40, 940–951. doi: 10.1071/fp12355

Sabine, J., Zeidler, S., Nig, P., Ngu, N. D., Scholz, A., Averhoff, B., et al. (2018). Salt induction and activation of MtlD, the key enzyme in the synthesis of the compatible solute mannitol in *Acinetobacter baumannii*. *Microbiol. Open* 9, 55–78.

Schywn, B., and Nielands, J. B. (1987). Universal chemical assay for the detection and determination of siderophores. *Analyt. Biochem.* 16, 47–56. doi: 10.1016/0003-2697(87)90612-9

Shen, E., Wang, P., Zhou, H., Kong, C. L., Ma, Q., Qu, Y. Y., et al. (2013). Isolation, identification and salt-tolerant mechanism of a salt-tolerant phenol-degrading bacteria. *J. Environ. Sci.* 33, 377–382.

Shivanand, P., and Mugeraya, G. (2011). Halophilic bacteria and their compatible solutes Osmoregulation and potential applications. *Curr. Ence* 100:25.

Sivan, A., Szanto, M., and Pavlov, V. (2006). Biofilm development of the polyethylene-degrading bacterium *Rhodococcus ruber*. *Appl. Microbiol. Biotechnol.* 72, 346–352. doi: 10.1007/s00253-005-0259-4

Spaepen, S., Vanderleyden, J., and Remans, R. (2007). Indole-3-acetic acid in microbial and microorganism-plant signaling. *FEMS Microbiol. Rev.* 31, 425–448. doi: 10.1111/j.1574-6976.2007.00072.x

Sutherland, I. W. (2001). Microbial polysaccharides from Gram-negative bacteria. *Intern. Dairy J.* 9, 34–45.

Urai, M., Anzai, H., Ogihara, J., Iwabuchi, N., Harayama, S., Sunairi, M., et al. (2006). Structural analysis of an extracellular polysaccharide produced by *Rhodococcus rhodochrous* strain S-2. *Carbohyd. Res.* 341, 766–775. doi: 10.1016/j.carres.2005.12.013

Walia, H., Wilson, C., Condamine, P., Liu, X., Ismail, A. M., Zeng, L., et al. (2005). Comparative transcriptional profiling of two contrasting rice genotypes under salinity stress during the vegetative growth stage. *Plant Physiol.* 139, 822–835. doi: 10.1104/pp.105.065961

Wang, G. (2015). Effects of salt stress on chemical structure and antioxidant activity of extracellular polysaccharides from nostoc flagelliforme[D]. *Shaanxi Univ. Sci. Technol.* 9, 34–45.

Weinisch, L., Steffen, K., Roth, R., Grimm, M., Roth, T., Netz, D., et al. (2018). Identification of osmoadaptive strategies in the halophile, heterotrophic ciliate *Schmidingerothrix salinarum*. *PLoS Biol.* 16:e2003892. doi: 10.1371/journal.pbio.2003892

Wu, H., Yu, P., Zhang, L., Zhao, S., Zhang, L., and Han, X. (2018). Glycine betaine transport conditions of Lactobacillus delbrueckii subsp. bulgaricus in salt induce hyperosmotic stress. *Intern. Dairy J.* 20, 359–487.

Yanyun, Z., Baoyu, R., Huafen, L., Zhiqing, L., and Gary, B. (2018). Biosynthesis of selenium nanoparticles and effects of selenite, selenate, and selenomethionine on cell growth and morphology in *Rahnella aquatilis* HX2. *Appl. Microbiol. Biotechnol.* 9, 34–47.

Yu, D. S., Wu, G. D., Li, J., Zhou, T., and Wang, X. J. (2017). Enhanced nitrogen removal of ANAMMOX treating saline wastewater with betaine addition. *Huan Jing Ke Xue* 39, 1688–1696.

Zhang, J., Chen, L. X., Qiao, L., Huang, L. Y., Meng, L., Liang, J., et al. (2010). Salinization characteristics and evaluation of different soil types in Daqing. *J. Northeast For. Univ.* 38, 119–122.

Conflict of Interest: The authors declare that the research was conducted in the absence of any commercial or financial relationships that could be construed as a potential conflict of interest.

frontiers in Microbiology

ORIGINAL RESEARCH
published: 22 June 2021
doi: 10.3389/fmicb.2021.673211

Herbicides Tolerance in a *Pseudomonas* Strain Is Associated With Metabolic Plasticity of Antioxidative Enzymes Regardless of Selection

*Amanda Flávia da Silva Rovida[1], Gessica Costa[2], Mariana Inglês Santos[2], Caroline Rosa Silva[2], Paloma Nathane Nunes Freitas[2], Elizangela Paz Oliveira[1], Sônia Alvim Veiga Pileggi[2], Ricardo Luiz Olchanheski[2] and Marcos Pileggi[2]**

[1] Department of Biotechnology, Genetics and Cell Biology, State University of Maringá, Maringá, Brazil, [2] Laboratory of Environmental Microbiology, Biological and Health Sciences Sector, Department of Structural and Molecular Biology and Genetics, State University of Ponta Grossa, Ponta Grossa, Brazil

OPEN ACCESS

Edited by:
Cristina Mazzoni, Sapienza University of Rome, Italy

Reviewed by:
Jay Prakash Verma, Banaras Hindu University, India
Rafael Vazquez-Duhalt, Universidad Nacional Autónoma de México, Mexico

***Correspondence:**
Marcos Pileggi
mpileggi@uepg.br

Specialty section:
This article was submitted to Microbial Physiology and Metabolism, a section of the journal Frontiers in Microbiology

Received: *27 February 2021*
Accepted: *10 May 2021*
Published: *22 June 2021*

Citation:
Rovida AFdS, Costa G, Santos MI, Silva CR, Freitas PNN, Oliveira EP, Pileggi SAV, Olchanheski RL and Pileggi M (2021) Herbicides Tolerance in a Pseudomonas Strain Is Associated With Metabolic Plasticity of Antioxidative Enzymes Regardless of Selection. Front. Microbiol. 12:673211. doi: 10.3389/fmicb.2021.673211

Agriculture uses many food production chains, and herbicides participate in this process by eliminating weeds through different biochemical strategies. However, herbicides can affect non-target organisms such as bacteria, which can suffer damage if there is no efficient control of reactive oxygen species. It is not clear, according to the literature, whether the efficiency of this control needs to be selected by the presence of xenobiotics. Thus, the *Pseudomonas* sp. CMA 6.9 strain, collected from biofilms in an herbicide packaging washing tank, was selected for its tolerance to pesticides and analyzed for activities of different antioxidative enzymes against the herbicides Boral®, absent at the isolation site, and Heat®, present at the site; both herbicides have the same mode of action, the inhibition of the enzyme protoporphyrinogen oxidase. The strain showed tolerance to both herbicides in doses up to 45 times than those applied in agriculture. The toxicity of these herbicides, which is greater for Boral®, was assessed by means of oxidative stress indicators, growth kinetics, viability, and amounts of peroxide and malondialdehyde. However, the studied strain showed two characteristic antioxidant response systems for each herbicide: glutathione-s-transferase acting to control malondialdehyde in treatments with Boral®; and catalase, ascorbate peroxidase, and guaiacol peroxidase in the control of peroxide induced by Heat®. It is possible that this modulation of the activity of different enzymes independent of previous selection characterizes a system of metabolic plasticity that may be more general in the adaptation of microorganisms in soil and water environments subjected to chemical contaminants. This is relevant to the impact of pesticides on the diversity and abundance of microbial species as well as a promising line of metabolic studies in microbial consortia for use in bioremediation.

Keywords: antioxidant enzymes, oxidative stress, selective pressure, bacterial adaptation, herbicide bioremediation, herbicide degradation, metabolic plasticity

INTRODUCTION

The herbicides used to combat weeds have become indispensable in agriculture, increasing productivity but also causing several environmental problems, such as impacts on non-target organisms (Thiour-Mauprivez et al., 2019).

Bacterial communities can undergo intense changes in their diversity when in contact with herbicides, which can affect soil and water quality, as in cases of exposure to 2,4-D (Moretto et al., 2017; Meena et al., 2020), atrazine, diuron (Moretto et al., 2017) and mesotrione (Du et al., 2018), by triazines in groundwater (Mauffret et al., 2017), and atrazine, glyphosate, malathion, carbaryl, and permethrin in container aquatic habitats (Muturi et al., 2017). The herbicide alachlor caused a reduction in biomass and inhibited bacterial growth in river waters collected from the Saskatchewan River, Saskatoon, SK, Canada, when they were inoculated in bioreactors (Paule et al., 2016).

When subjected to stressful environmental conditions, bacterial strains can naturally produce reactive oxygen species (ROS) in large quantities. Contaminants, such as herbicides, cause oxidative stress through the generation of ROS, which interact with the cell membrane and can cause lipid peroxidation (Dourado et al., 2015). As a way of preventing or reducing these types of imbalances, bacteria have developed response systems to protect membrane integrity, such as modulating the activity of antioxidant enzymes (Martins et al., 2011; Lemire et al., 2017). Bacteria can become tolerant to oxidative stress by secreting extracellular polymeric substances (EPS) and forming biofilms (Tolker-Nielsen, 2015). The efficiency of these responses can lead to different levels of susceptibility and sensitivity of bacterial communities to stressors, leading to changes in their diversity and ecological functions (Polst et al., 2018).

Microorganisms have stress response mechanisms, including increased expression of enzymes that transform ROS, such as superoxide dismutase (SOD), which catalyzes the dismutation of superoxide ($O_2^{\cdot -}$) into oxygen (O_2) and hydrogen peroxide (H_2O_2), and catalase (CAT), which decomposes H_2O_2 into water (H_2O) and oxygen (O_2) (Prione et al., 2016), in addition to peroxidases such as glutathione S-transferase (GST) (Wongsaroj et al., 2018). However, there are no in-depth studies analyzing the efficiency of this mechanism in the presence of xenobiotics. Even for some enzymes, there are no recent reports of the effects on bacteria, but only indirect on enzymes from bacteria-colonized plants, such as guaiacol peroxidase (GPX) (Eke et al., 2019), and ascorbate peroxidase (APX) (Fan et al., 2020).

The genus *Pseudomonas* stands out for its tolerance to chemical stressors because of its metabolic and physiological versatility, and it can be isolated from soil, fresh water, biofilms, and other places, with potential for application in bioremediation (Venturi, 2006; Karami et al., 2016; Melo et al., 2016). Lima et al. (2020) obtained collections of bacteria capable of tolerating different herbicides, including *Pseudomonas* sp. CMA 6.9, assessed in this study. This strain was isolated from a tank containing water for washing pesticide packaging in which the Heat® herbicide was present.

Boral® and Heat® are herbicides whose mode of action inhibits the enzyme protoporphyrinogen oxidase (protox) (Beffa et al., 2019). These herbicides have electronegative and oxidizing chemical elements, such as fluorine (F) and chlorine (Cl), that can affect the stress response genes in microorganisms (Li et al., 2020), compromise the physical structure, and affect metabolic processes, efflux pumps, and regulation of gene expression (Ye et al., 2020).

The use of cycles of chemical substances, such as fungicides, insecticides, antibiotics, and herbicides, is considered key for the selection of resistance in organisms through specific strategies, based on the mode of action of these substances. These are the target-site resistance (TSR) models. New proposals have been designed, called non-target-site resistance (NTSR), and are based on related genes in different systems of detoxification, transport, efflux, and sequestration. These systems can give resistance to chemical substances with different modes of action, being, therefore, more general mechanisms (Comont et al., 2020). Metabolic mechanisms, described in plants are also included in NTSR, such as those reactions involving the esterase enzymes, GSTs, uridine 5′ diphospho-glucosyl transferases, and cytochrome P450s (Jugulam and Shyam, 2019; Gaines et al., 2020).

This study aimed, therefore, to compare the mode of modulation of antioxidant mechanisms of *Pseudomonas* sp. CMA 6.9 in the presence of the herbicide Boral®, which was absent at the isolation site of this strain, and of the Heat®, which exerts selective pressure at the isolation site of this strain.

MATERIALS AND METHODS

In accordance with the objectives of this work, the following experimental design (**Figure 1**) was carried out.

Bacterial Strain

Pseudomonas sp. CMA 6.9 was from the Collection of Environmental Microorganisms of the Laboratory of Environmental Microbiology of the State University of Ponta Grossa (UEPG). This collection consists of 67 bacterial biofilm isolates from water storage tanks used to wash agrochemical packaging (Lima et al., 2020) at the BASF experimental station, Fazenda Escola Capão da Onça of UEPG.

Herbicides

The commercially sold herbicides Boral® and Heat® were used in this work.

The Boral® 500 SC herbicide (FMC, Philadelphia, PA, United States) contains 500 g/L (50% w/v) of the active ingredient sulfentrazone (2′,4′-dichloro-5′ - (4-difluoromethyl-4,5-dihydro-3-methyl-5-oxo-1H-1,2,4-triazole-1-yl) methanesulfonanilide). The doses used in the experiments were 15x (B15) and 45x (B45) the concentration used in the field, with concentrations of 7.3 mMol and 22.0 mMol, respectively.

The herbicide Heat® (BASF, Ludwigshafen, Rhein, Germany) contains 700 g/L (70% w/v) of the active ingredient saflufenacil (N′- {2-chloro-4-fluoro-5- [1,2,3, 6-tetrahydro-3-methyl-2,6-dioxo-4- (trifluoromethyl) pyrimidin-1-yl] benzoyl} -N-isopropyl-N-methylsulfamide). The doses used in

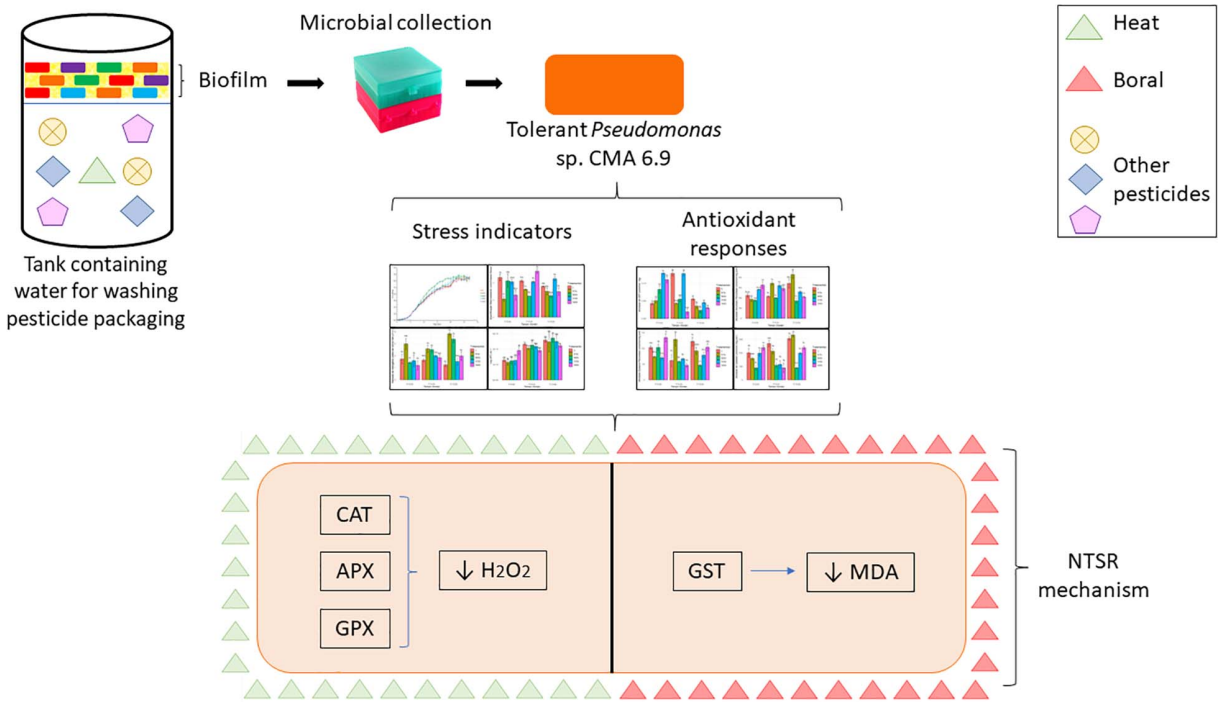

FIGURE 1 | Experimental design showing the tests performed for the preliminary characterization of the lineage and evaluations of oxidative stress indicators and stress response systems.

the experiments were 15x (H15) and 45x (H45) at concentrations of 0.7 mMol and 2.2 mMol, respectively.

Herbicide Tolerance Test

The herbicides were added to Luria Bertani Agar (LA) at 45°C. The treatments H15, H45, B15, and B45 were compared to the control (C) in triplicate without herbicides. The plates were incubated at 30°C for 24 h. Isolates that grew in culture medium were considered tolerant.

Molecular Identification by Sequencing the 16S Ribosomal Gene

The strain was grown in a plate containing LA. After incubation for 48 h at 30°C, isolated colonies were collected for molecular identification. The identity of the isolate was determined by sequencing the 16S ribosomal gene. The total DNA was extracted using the DNA isolation kit from Promega (Madison, WI, United States). Primers fD1 (5′-CCGAATTCGT CGACAACAGAGTTTGATCCTGGCTCAG-3′) and rD1 (5′-CCCGGGATCCAAGCTTAAGGAGGTGATCCAGCC-3′) were used for amplification (Benson et al., 1996). This reaction consisted of an initial denaturation cycle at 95°C for 5 min, 94°C for 45 s, annealing at 55°C for 45 s, extension at 72°C for 2 min, and a final extension cycle for 10 min at 72°C. The PCR products were purified using the QIAquick PCR kit (no. 28104). After purifying the PCR products and analyzing the integrity of the bands using electrophoresis, the material obtained was sent for sequencing at Ludwig Biotec (Alvorada, Brazil). The sequences were analyzed using the resources of the "Ribosomal Database Project" site. The strain was identified as belonging to the genus *Pseudomonas*, accession number MT072022 – NCBI, named as *Pseudomonas* sp. CMA 6.9. It is deposited at the Center for Biological Resources Johanna Döbereiner (CRB-JD) – Embrapa Agrobiologia, under the code BR 14567 and is part of the UEPG's Collection of Environmental Microorganisms.

Oxidative Stress Analysis

Bacterial Growth Curve

The bacterial strain was incubated at 30°C at 120 rpm overnight in Luria Bertani Broth (LB) to produce the pre-inoculum. Thereafter, the inoculum was placed in 250-ml flasks containing 100 ml of the treatments in LB at an initial optical density (OD) of 0.05–600 nm. Bacterial growth was monitored every 1 h for 27 h in a spectrophotometer at 600 nm. The growth values were obtained multiplying the OD obtained in a diluted suspension of bacteria by the dilution factor. The experiments were conducted in triplicate.

Cell Viability

After preparing the pre-inoculum (Section "Bacterial Growth Curve"), the inoculum was transferred to the control and treatments B15, B45, H15, and H45. Aliquots of 100 μL were removed in three growth phases established from the growth curves (6 h, 9 h, and 12 h). The samples were diluted sequentially in the proportion of 1–10, inoculated on LA, and incubated at 30°C. After 24 h, colony forming units (CFU) were counted, containing 25–300 colonies.

Sample Preparation for Cell Damage

After preparing the pre-inoculum (Section "Bacterial Growth Curve"), the cells were cultured in the established phases (Section "Cell Viability"). The cultures were centrifuged at 8000 × *g* for 10 min at 4°C, the supernatant was discarded, and the precipitate was macerated in liquid nitrogen. Then 100-mg aliquots of samples were frozen at −80°C until analyzed (Alexieva et al., 2001).

Quantification of H_2O_2

The extracted samples were homogenized with 1 ml of trichloroacetic acid (TCA) to 0.1% and centrifuged at 10,000 × *g* for 15 min at 4°C. Subsequently, 0.2 mL of the supernatant was collected and transferred to a tube containing 0.2 mL of a 100 mM solution of potassium phosphate buffer (14.52 g/L K_2HPO_4, 2.26 g/L KH_2PO_4, pH 7.5) and 0.8 mL of 1 M potassium iodide (KI) solution. The sample was stored in the dark and on ice for 1 h. The reading was performed on a spectrophotometer at 390 nm. The results were expressed in μmol H_2O_2/g of fresh weight (Dourado et al., 2013).

Quantification of lipid peroxidation

Quantification of lipid peroxidation was carried out by measuring the release of malondialdehyde (MDA), a reactive metabolite of 2-thiobarbituric acid (TBA) (Heath and Packer, 1968, with modifications). For this test, 0.1 g of each sample (Section "Quantification of H_2O_2") was homogenized with 1 ml of TCA to 0.1% and centrifuged at 11,600 × *g* for 5 min. The samples were collected in a 0.25 mL aliquot of supernatant and transferred to a test tube containing 1 ml of 20% TCA and 0.5% TBA. The reaction mixture was placed in a dry bath for 30 min at 95°C, cooled on ice for 10 min, and centrifuged at 11,600 × *g* for 10 min. The MDA concentration was monitored at 535 nm (all lipids) and 600 nm (all lipids except for MDA) and calculated using an extinction coefficient of 155 mM/cm. The amount of MDA was expressed in μmol MDA/g fresh weight.

Protein Extraction for Oxidative Stress Analysis

After pre-inoculation preparation (Section "Bacterial Growth Curve"), cultures were centrifuged at 8,000 × *g* for 10 min. The precipitate was macerated in liquid nitrogen, homogenized (10:1 w/v) in 100 mM potassium phosphate buffer (pH 7.5) containing 1 mM ethylene diamine tetra-acetic acid (EDTA), 3 mM dithiothreitol (DTT), and 5% (w/v) polyvinylpolypyrrolidone and kept at 4°C. The homogenate was centrifuged at 10,000 × *g* for 30 min, and the supernatant was collected and frozen for further enzymatic analysis. The protein concentration was determined using bovine serum albumin (BSA) as a standard (Bradford, 1976). The results were expressed as μmol of protein/g of fresh weight.

Total proteins – SDS

As a quality control of the control protein extracts and treatments (Section "Protein Extraction for Oxidative Stress Analysis"), SDS-polyacrylamide gel electrophoresis (PAGE) gel (**Supplementary Material 1**) was performed. The electrophoresis experiments in discontinuous and denaturing buffer systems were performed using an 8.3 × 10.2 cm mini-gel system at 10% acrylamide concentration (Laemmli, 1970). Protein denaturation was performed by heating at 95°C for 5 min, and 10% SDS was used in the running buffer and in the packaging buffer. For resolution, the gels were washed in distilled water and incubated overnight in 0.05% Coomassie blue R-250 in water/methanol/acetic acid 45/45/10 (v/v/v) and color removed by successive washing in the water/methanol/acetic acid 45/45/10 (v/v/v) solution.

Determination of SOD isoforms

We performed 12% non-denaturing polyacrylamide gel electrophoresis (PAGE) with protein extract (Section "Protein Extraction for Oxidative Stress Analysis"), and the gel was divided vertically into three parts. The first part was maintained at 4°C in 100 mM potassium phosphate buffer, pH 7.8. The second was immersed in 100 ml of the same buffer containing 2 mM KCN and 0.0292 g of EDTA. The third was immersed in 100 ml of said buffer containing 5 mM H_2O_2 and 0.0292 g of EDTA. The experiments were carried out in the dark. After 20 min in these solutions, the gels were stained with nitroblue tetrazolium (NBT) and riboflavin, as previously mentioned, and bands appeared. Isoforms were classified as Mn-SOD if resistant to both inhibitors (KCN and H_2O_2), Fe-SOD if resistant to KCN and inhibited by H_2O_2, and Cu/Zn-SOD if inhibited by both substances (Azevedo et al., 1998).

PAGE SOD activity

Electrophoresis was performed on non-denaturing polyacrylamide separating gels at 12% and a stacking gel of polyacrylamide at 4% at a current of 15 mA for 3 h. A 20-ng aliquot of protein (Section "Protein Extraction for Oxidative Stress Analysis") was applied to each well. SOD activity was determined as described by Peters et al. (2014). The gels were washed in distilled water and incubated in the dark for 30 min in 50 mM potassium phosphate buffer (pH 7.8) containing 1 mM EDTA, 0.005 mM riboflavin, 0.1 mM nitroblue tetrazolium and N, N, N′, 0.03 mM N′-tetramethylethylenediamine (TEMED). The gels were exposed to white light and immersed in water until the bands corresponding to the SOD bands became visible. Since there are differences between measurements of enzymatic activities (Faria et al., 2015), in the case of SOD we prefer to use the electrophoretic method to the enzymatic one.

CAT activity

Catalase activity was determined in a solution containing 1 ml of 100 mM potassium phosphate buffer (pH 7.5) and 2.5 μL de H_2O_2 (30% solution) and quantified in a spectrophotometer at 25°C. The reaction was started with the addition of 50 μL of protein extract (Section "Protein Extraction for Oxidative Stress Analysis"), and the activity was determined following the decomposition of H_2O_2 at 240 nm for 1 min using the molar extinction coefficient of 43.6 M^{-1} cm^{-1}. The results were expressed in μmol/min/mg protein (Kraus et al., 1995).

APX activity

Ascorbate peroxidase activity was determined in a reaction mixture with 650 μL of potassium phosphate buffer (80 mM, pH 7.0), 100 μL EDTA (1 mM), 100 μL ascorbic acid

(5 mM), 100 μL H_2O_2 (1 mM) and quantified in a spectrophotometer at 25°C. The reaction was started with the addition of 50 μL of protein extract (Section "Protein Extraction for Oxidative Stress Analysis") and the activity was determined following the decomposition of H_2O_2 by APX at 290 nm for 1 min assuming a molar extinction coefficient of 2.8 mM^{-1} cm^{-1}. The activity was expressed in μmol/min/mg protein (Nakano and Asada, 1981).

GPX activity

Guaiacol peroxidase activity was determined by adding 25 μL of protein extract (section "Protein Extraction for Oxidative Stress Analysis") to a solution of 390 μL of citrate buffer (0.2 M of dibasic disodium phosphate and 0.1 M of citric acid, pH 5.0), 25 μL of guaiacol, and 25 μL of H_2O_2 (3%), which were homogenized and immersed in a water bath at 30°C for 15 min. Then 25 μL of sodium metabisulfite (2%) was added and GPX activity was measured in a spectrophotometer at 450 nm. The activity was expressed in μmol/min/mg protein (Matsuno and Uritani, 1972).

GST activity

Glutathione S-transferase activity was measured in a solution containing 900 μL of 100 mM potassium phosphate buffer (pH 6.8), adding 25 μL of 40 mM 1-chloro-2,4-dinitrobenzene (CDNB) and 50 μL of reduced glutathione (GSH) 0.1 M and incubating at 30°C (Zablotowicz et al., 1995). The reaction was started with the addition of 25 μL of protein extract (Section "Protein Extraction for Oxidative Stress Analysis") and was monitored for 2 min at 340 nm. The activity was expressed in μmol/min/mg protein.

Statistical Analysis

Data on quantification of the growth curve, H_2O_2, MDA, CAT, APX, and GPX were obtained in triplicate for each treatment and statistically analyzed using a randomized complete block design. Significance analyses were obtained with the R 1.3.1056 program using the Duncan test ($p < 0.05$) (**Supplementary Material 2**). All these data were processed by principal component analysis (PCA) (Gotelli et al., 2011).

RESULTS

Herbicide Tolerance Test

The evaluation of tolerance to the Boral® and Heat® herbicides showed that of the 67 isolates tested, 45 (67.2%) did not show growth and therefore were considered sensitive to these herbicides. The 22 (32.8%) that were herbicide tolerant were grown on LB + herbicides and based on OD data, the most tolerant strain was identified as *Pseudomonas* sp. CMA 6.9.

Indicators of Oxidative Stress in Bacteria

Data on Growth Kinetics of *Pseudomonas* sp. CMA 6.9 in Media Containing Herbicides

The growth rates of *Pseudomonas* sp. CMA 6.9 in the treatments were significantly greater or equal in comparison to the control (**Figure 2** and **Supplementary Material 2**). Based on the growth curves, three phases were established in the logarithmic period in which the samples were obtained, and analyses were made of stress indicators and enzyme response systems as follows: early-log (at 6 h of incubation), early mid-log (at 9 h), and mid-log (in 12 h).

Viability Data for *Pseudomonas* sp. CMA 6.9 Against Boral® and Heat® Herbicides

Viability data were measured in *Pseudomonas* sp. CMA 6.9 under the described growth conditions (Section "Bacterial Growth Curve"). The feasibility data (**Figure 3**) showed significant increases over the three evaluated periods (**Supplementary Material 2**).

Quantification of H_2O_2

The concentrations of H_2O_2 found to s in *Pseudomonas* sp. 6.9 CMA were significantly lower in control than in treatments with Boral® and Heat® most prevalently in the early stage. The concentrations of H_2O_2 in the treatments with Boral®, especially in the mid-log stage of growth, were significantly greater (**Supplementary Material 2**) than in the other treatments (**Figure 4**).

Quantification of MDA

The concentration of MDA in the controls and treatments with Boral® and Heat® was evaluated as an indicator of lipid peroxidation and cytotoxicity caused by these herbicides (**Figure 5**).

The concentrations of MDA in the control showed significant decreases over the analyzed growth periods. In general, the concentrations in treatments with Heat® were significantly higher, mainly in the early mid-log phase in the H45 treatment, while concentrations in the treatments with Boral® were significantly lower in relation to the control.

Activities of Antioxidative Enzymes in *Pseudomonas* sp. CMA 6.9

The *Pseudomonas* sp. CMA 6.9 in response to the toxicity of Boral® and Heat® herbicides was evaluated by quantifying the activities of the enzymes SOD, CAT, APX, GPX, and GST.

SOD Enzymatic Activity

Iron superoxide dismutase (Fe-SOD) was the only isoform characterized for *Pseudomonas* sp. CMA 6.9 (data not shown). There were no significant variations in activity between control and treatments, except for B45, which showed a greater variation in the relative band intensity in the three growth phases evaluated (**Figure 6**).

CAT, APX and GPX Enzymatic Activities

The activities of CAT, APX, and GPX were analyzed in this section because they are enzymes with the H_2O_2 metabolizing function; the data are shown in **Figure 7**.

The enzymes CAT, APX, and GPX showed a significant increase in activities throughout the growth phases, analyzing the behavior in control. The treatments with the Boral® herbicide

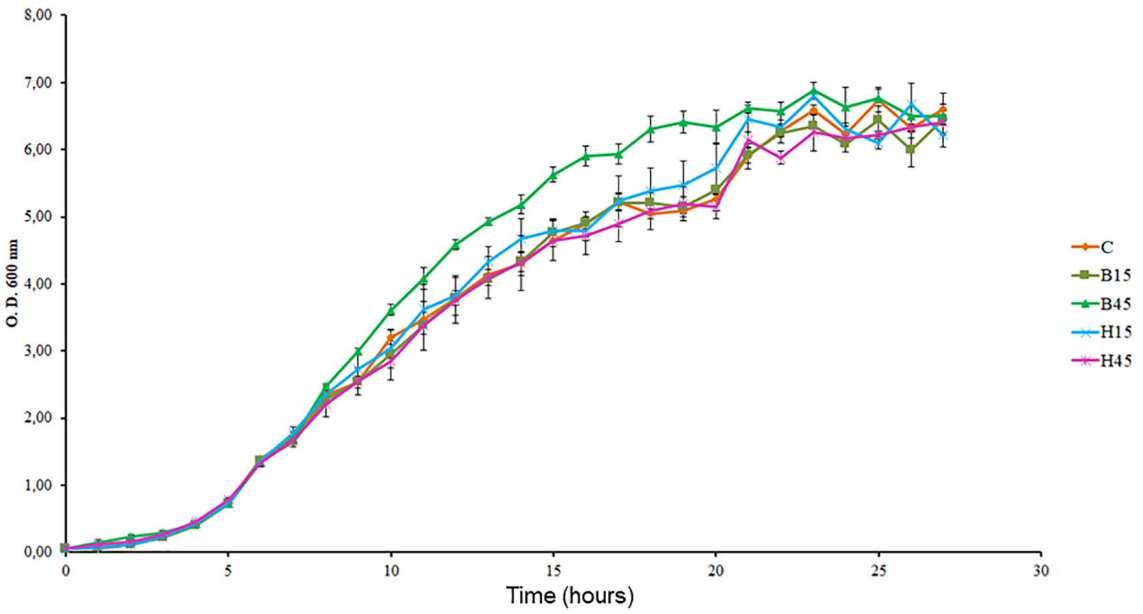

FIGURE 2 | Growth curves of *Pseudomonas* sp. CMA 6.9 in control treatments (C) and with the herbicides Boral® (B15 and B45) and Heat® (H15 and H45), determined by OD at 600 nm. Data were obtained in triplicate for each treatment and statistically analyzed using a randomized complete block design using the Duncan test ($p < 0.05$). Error bars represent standard errors of the means.

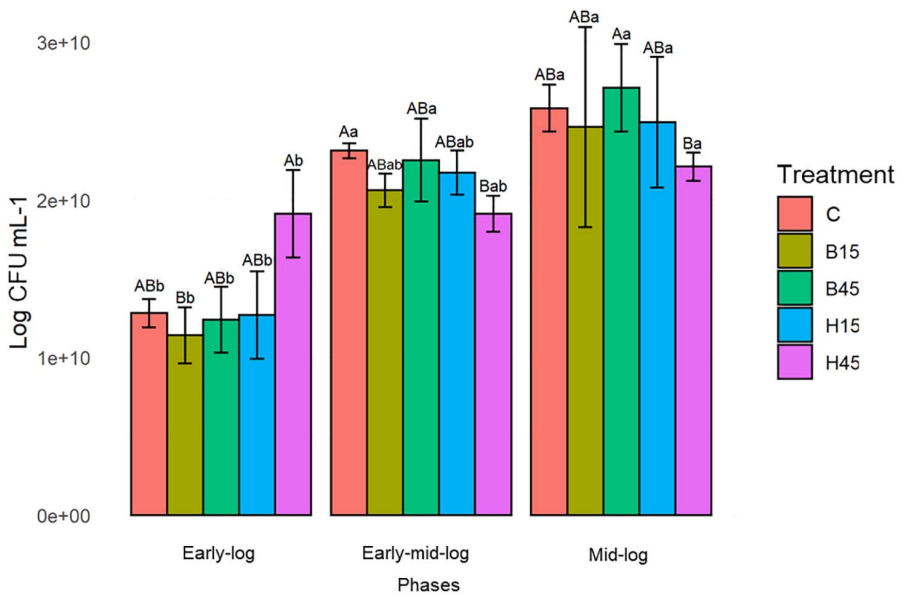

FIGURE 3 | Cell viability of *Pseudomonas* sp. CMA 6.9 in control treatments (C) and with the herbicides Boral® (B15 and B45) and Heat® (H15 and H45) in the three growth phases indicated. Data were obtained in triplicate for each treatment and statistically analyzed using a randomized complete block design using the Duncan test ($p < 0.05$). Error bars represent standard errors of the means. Different uppercase letters represent statistically significant differences between treatments at the same time; lower-case letters represent statistically significant differences between treatments at different times.

were also characterized by higher activities of the three enzymes, mainly in B15, and in general increasing throughout the growth phases. In the B45 treatment, the enzyme activities were generally lower than in the control and B15. Variations in the activities of the three enzymes in the studied growth phases were similar. In treatments with the herbicide Heat®, however, the general behavior of enzymatic activities was to decrease significantly.

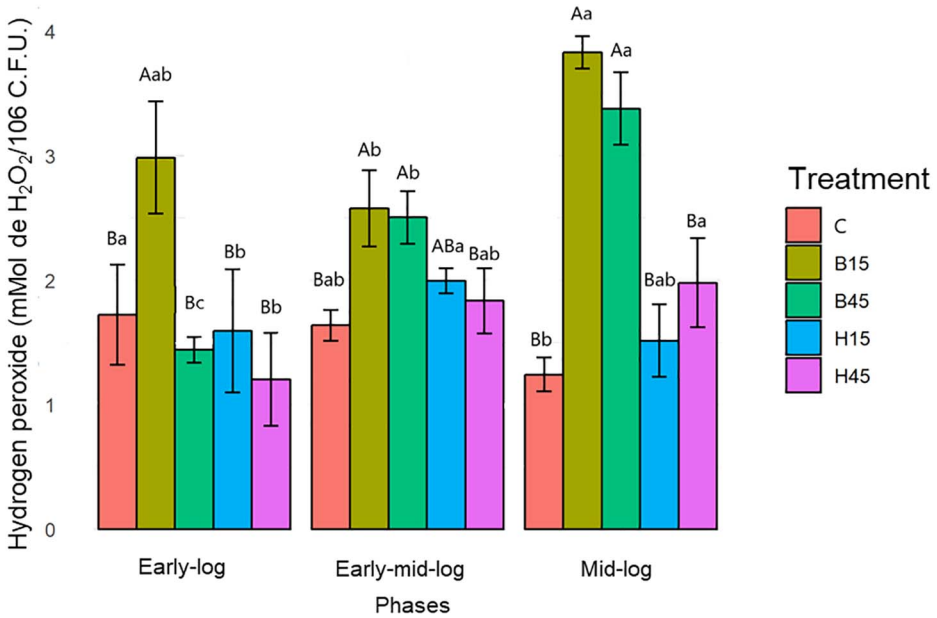

FIGURE 4 | Quantification of H_2O_2 from *Pseudomonas* sp. CMA 6.9 in control treatments (C) and with the herbicides Boral® (B15 and B45) and Heat® (H15 and H45) in the three growth phases indicated. Data were obtained in triplicate for each treatment and statistically analyzed using a randomized complete block design using the Duncan test ($p < 0.05$). Error bars represent standard errors of the means. Different uppercase letters represent statistically significant differences between treatments at the same time; lower-case letters represent statistically significant differences between treatments at different times.

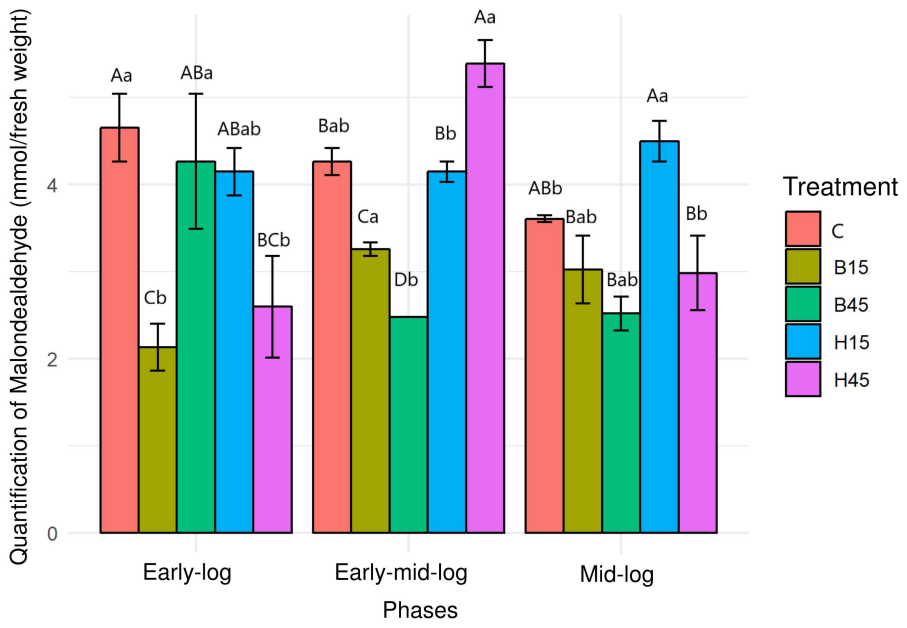

FIGURE 5 | Quantification of MDA from *Pseudomonas* sp. CMA 6.9 in control treatments (C) and with the herbicides Boral® (B15 and B45) and Heat® (H15 and H45) in the three growth phases indicated. Data were obtained in triplicate for each treatment and statistically analyzed using a randomized complete block design using the Duncan test ($p < 0.05$). Error bars represent standard errors of the means. Different uppercase letters represent statistically significant differences between treatments at the same time; lower-case letters represent statistically significant differences between treatments at different times.

Enzymatic Activity of GST

Quantitative analysis of GST for *Pseudomonas* sp. CMA 6.9 is shown in **Figure 8**.

Glutathione S-transferase activity for *Pseudomonas* sp. CMA 6.9, under control conditions, showed significantly higher activity in the early mid-log phase compared to other growth phases.

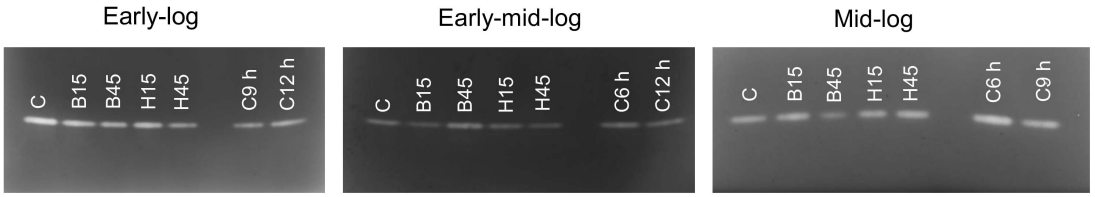

FIGURE 6 | SOD activity of *Pseudomonas* sp. CMA 6.9 in control treatments (C) and with the herbicides Boral® (B15 and B45) and Heat® (H15 and H45) in the three growth phases indicated. In each of the growth phases, replicates of the other controls were made, with C6 h, 6 h control; C9 h, 9 h control; C12 h, 12 h control.

In treatments with the Boral® herbicide, there was a drop-in activity throughout the growth phases, with a more pronounced drop for B45. With the Heat® treatment, the variation in enzyme activity was more complex, depending on the concentration of the herbicide. For H15, the high activities, which were higher among the different experiments, followed a significant drop in the mid-log phase. In H45, the high rate in the early phase was followed by a significant drop in the early mid-log and mid-log phase.

Interrelationships Between Stress Indicators and Enzymatic Activities in *Pseudomonas* sp. CMA 6.9 in Treatments With Boral® and Heat®

Principal component analysis was used to assess data interrelationships in the quantification of stress indicators, H_2O_2 and MDA, and activities of the antioxidant enzymes CAT, APX, GPX, and GST (**Figure 9**). The most significant interrelationships were important for the elaboration of the enzymatic response systems of *Pseudomonas* sp. CMA 6.9 against the toxicity of herbicides Boral® (not present in the isolation tanks) and Heat® (present in the isolation tanks).

DISCUSSION

Tolerance to Herbicides by *Pseudomonas* sp. CMA 6.9

The tolerance evaluation of bacteria obtained in tanks containing washing water from pesticide containers (Lima et al., 2020) showed that 67.2% of the isolates were sensitive to herbicides Boral® and Heat® at 15x and 45x concentrations. It is known that herbicides can be toxic for non-target organisms because of the electronegative characteristics of their active molecules (Pileggi et al., 2020) and can reduce microbial diversity, such as that of *Actinobacter* in the presence of Granstar, a sulfonylurea herbicide, and that prior exposure to the herbicide acts as a selective agent (Rachedi et al., 2018). However, the 32.8% of tolerant isolates to these herbicides, from which the *Pseudomonas* sp. 6.9 CMA was selected, suggests that there are adaptation mechanisms that do not need specific selective agents as inducers. No articles were found on bacterial strains carrying tolerance systems without prior selection events. Sensitive bacteria can be protected in communities structured in biofilms, where a part of the community can contain tolerance systems, but selected by stressors, such as the case of marine periphytic biofilms under ecotoxicological effect of copper (Corcoll et al., 2019).

Indicators of Oxidative Stress in Bacteria

Oxidative stress occurs when there is an imbalance between the production of ROS and their removal by enzymatic and non-enzymatic action, by which more toxic molecules are transformed into less harmful ones (Imlay, 2019). Population growth kinetics, cell viability, and quantification of H_2O_2 and MDA were evaluated as indicators of oxidative stress induced by herbicides, since it is important to let it be characterized that these substances, even when targeting weeds, are toxic to bacteria.

Growth Kinetics

The times corresponding to the first phases of logarithmic growth were determined to evaluate the differences in the induction of the response systems of the strain to the two herbicides, because the growth phases indicate the adaptability of the strain to the medium (Molina et al., 2019; Ram et al., 2019). The early-log (6 h), early mid-log (9 h), and mid-log (12 h) phases were standardized to obtain data on stress indicators and enzyme responses. According to the data obtained, such as growth rates of *Pseudomonas* sp. CMA 6.9 in control was not significantly higher than in the treatments with herbicides, this strain was considered tolerant to Boral® and Heat®, and the isolates that did not show any growth, even in the presence of 1x the herbicides, were considered sensitive.

Viability of *Pseudomonas* sp. CMA 6.9

Cell viability is one of the most important indicators for determining whether cells are under oxidative stress and undergoing damage (Ye et al., 2019). Stressors such as herbicides can decrease cell viability. The cyanobacterium *Microcystis aeruginosa*, for example, when exposed to glyphosate showed an increase in oxidative stress levels, indicated by MDA and cell apoptosis, and consequently, a decrease in cell viability levels, even with an increase in the activity of antioxidant enzymes such as SOD, CAT, and peroxidases (Wu et al., 2016). The collection that was screened in this work showed 67.2% of its isolates were herbicide-sensitives. Even so, no data were found in the literature on the effects on Boral® and Heat® on the viability of bacteria. In contrast, *Pseudomonas* sp. CMA 6.9 showed significant increases in growth rates (**Figure 2**) and viability (**Figure 3**) during the three time periods evaluated, indicating

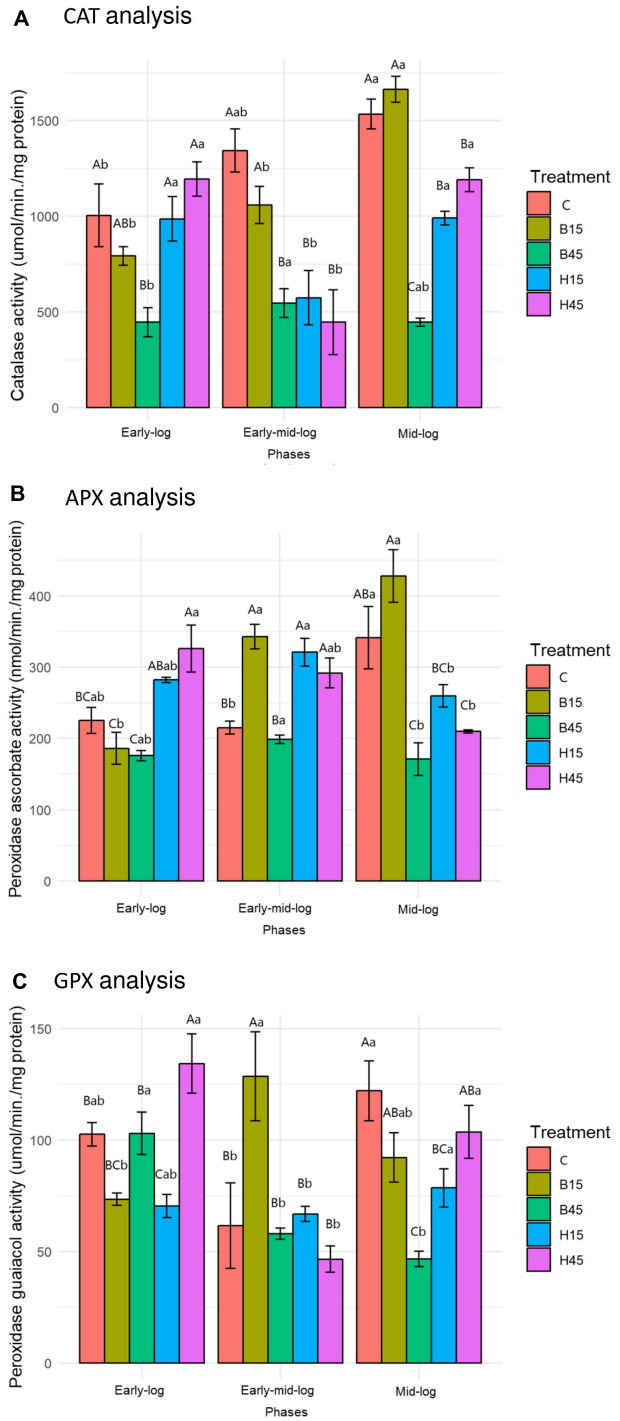

FIGURE 7 | CAT **(A)**, APX **(B)**, and GPX **(C)** activity of *Pseudomonas* sp. CMA 6.9 in control treatments (C) and with the herbicides Boral® (B15 and B45) and Heat® (H15 and H45) in the three growth phases indicated. Data were obtained in triplicate for each treatment and statistically analyzed using a randomized complete block design using the Duncan test ($p < 0.05$). Error bars represent standard errors of the means. Different uppercase letters represent statistically significant differences between treatments at the same time; lower-case letters represent statistically significant differences between treatments at different times. CAT, catalase; APX, ascorbate peroxidase; GPX, guaiacol peroxidase.

that it has efficient response systems for adaptation to herbicide absent at the isolation site (Boral®), as well as herbicide present (Heat®), not seen in other isolates from the same environment.

Quantification of H_2O_2

Reactive oxygen species, such as H_2O_2 and O_2^-, are generated via normal aerobic metabolic processes in the electron transport chain; however, these molecules are toxic to cells, especially when their levels are high because of the presence of stressors (Prione et al., 2016).

Boral® was considered to have a greater potential to cause oxidative stress in *Pseudomonas* sp. CMA 6.9 than Heat®, considering the comparisons between the concentrations of H_2O_2 in the treatments of these herbicides and in the control. Other herbicides have this characteristic of increasing the amount of H_2O_2 in two strains of *Bacillus megaterium*, leading to the combined toxic effects of adjuvants and the active molecule mesotrione (Dobrzanski et al., 2018). In the same way, the herbicide gramoxone was seen to cause this effect in strains of *Escherichia coli* (Gravina et al., 2017).

Quantification of MDA

Malondialdehyde is an indicator of damage to unsaturated fatty acids in the membrane caused by H_2O_2 (Heath and Packer, 1968) and so is used as a representative biomarker of oxidative damage in ecotoxicology (Liu et al., 2019). Therefore, the concentration of MDA in the controls and treatments with Boral® and Heat® was evaluated as an indicator of lipid peroxidation and cytotoxicity caused by these herbicides (**Figure 5**). Using only these data and definitions, it would be possible to infer that Heat® produces more oxidative damage to *Pseudomonas* sp. CMA 6.9 compared to Boral®, and this would produce less damage than in the control. Another hypothesis that could be proposed is a response related to the dose of Heat® in the early mid-log phase (**Figure 5**), as described for *Pseudomonas stutzeri* after exposure to increasing doses of silver nanoparticles (Wu et al., 2020). However, considering the whole period of analysis and data for Boral®, this hypothesis cannot be confirmed.

The data on growth kinetics (**Figure 2**) and viability (**Figure 3**) show that the correlation between cytotoxicity and the amounts of MDA are also unclear. In addition, the data on the amount of H_2O_2 (**Figure 4**) and MDA (**Figure 5**) do not indicate a relationship between peroxide and peroxidation in the studied strain. Studies by our research group have indicated that different bacterial species can modify their lipid composition in response to the toxicity of different herbicides, changing, therefore, the proportion of unsaturated fatty acids in membranes and the amount of MDA. This has been observed for different mutated strains for SOD isoforms in *E. coli* in treatment with gramoxone (Gravina et al., 2017), for *Pantoea ananatis* (Prione et al., 2016), for *E. coli* (Olchanheski et al., 2014), and for different strains of *B. megaterium* (Dobrzanski et al., 2018), all with treatment with the herbicide mesotrione. Generally, alterations in fatty acids in the cytoplasmic membrane of Gram-negative bacteria are considered important mechanisms in adaptation to toxic compounds, such as herbicides (Murínová and Dercová, 2014).

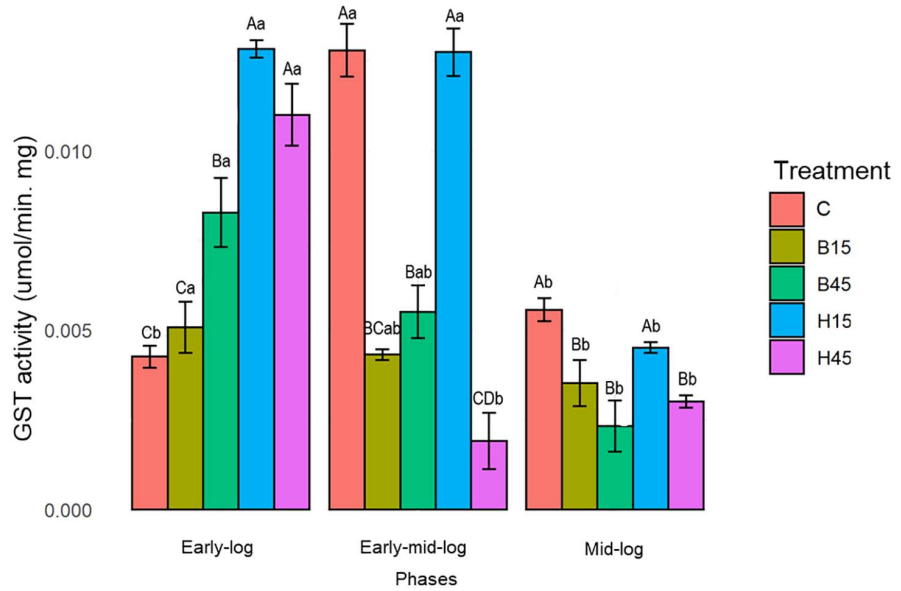

FIGURE 8 | GST activity of *Pseudomonas* sp. CMA 6.9 in control treatments (C) and with the herbicides Boral® (B15 and B45) and Heat® (H15 and H45) in the three growth phases indicated. Data were obtained in triplicate for each treatment and statistically analyzed using a randomized complete block design using the Duncan test ($p < 0.05$). Error bars represent standard errors of the means. Different uppercase letters represent statistically significant differences between treatments at the same time; lower-case letters represent statistically significant differences between treatments at different times.

Enzymatic Control of Oxidative Stress Caused by the Herbicides Boral® and Heat® in *Pseudomonas* sp. CMA 6.9

Pseudomonas sp. CMA 6.9 did not degrade the active molecules of the herbicides Boral® (sulfentrazone) and Heat® (saflufenacil) (**Supplementary Material 3**); therefore, only the antioxidant enzymes were considered as a possible mechanism of response to the toxicity of these substances. Thus, enzymatic control of oxidative stress is necessary for tolerant bacteria to survive in environments in which herbicides can cause an increase in ROS and, consequently, structural and genomic damage and impaired bacteria viability. Oxidative stress is a considerable impact caused by herbicides in bacteria, such as the case of glyphosate on the intestinal microbiota of rats, according to methods of shotgun metagenomics and metabolomics, techniques with good precision to assess the presence of genes and production of related metabolites with responses to the herbicide (Mesnage et al., 2021). Therefore, to evaluate the antioxidative system of the *Pseudomonas* sp. CMA 6.9 is relevant in this context and can be considered a basis for understanding their survival as well as the sensitive isolates that cohabited biofilms in the presence of pesticides.

SOD Enzymatic Activity

Superoxide dismutase acts to reduce oxidative stress, catalyzing the dismutation of superoxide in O_2 and H_2O_2. SOD is a metalloenzyme classified according to its metallic cofactor, such as manganese (Mn), iron (Fe), or copper-zinc (Cu-Zn). Fe-SOD was the only isoform characterized for *Pseudomonas* sp. CMA 6.9 (data not shown) for which a cytoplasmic location and constitutive synthesis is attributed (Barnes et al., 1996; Touati, 2000). The culture medium can induce differential expression of SOD isoenzymes, such as Luria Bertani, which induces the expression of Fe-SOD in *Pseudomonas aeruginosa* (Pedersen et al., 2009). There were no significant variations in activity between the control and the treatments, except for B45, which showed high activity in the early mid-log phase (**Figure 9**), with the probable consequence of higher production of H_2O_2 in the mid-log phase (**Figure 4**). Therefore, SOD was induced in *Pseudomonas* sp. CMA 6.9 only for Boral, but not for Heat. Regardless of the isoenzyme type, increased SOD activity in bacteria is considered an adaptive response to stress induced by some herbicides. For example, *Rhodobacter sphaeroides* and *Acinetobacter lwoffii* strains increased SOD activity in response to treatments with the herbicide atrazine (Zhang et al., 2012). This induction also occurred for a *Stenotrophomonas maltophilia* strain treated with quinclorac or bensulfuron-methyl herbicides, but not for *E. coli* (Lü et al., 2009).

CAT, APX and GPX Enzymatic Activities

Hydrogen peroxide has the potential to cause cell damage, thus requiring control of its concentration. The action of CAT in response to cell defense is important for bacterial adaptation and surviving herbicide-induced H_2O_2 (Bučková et al., 2010). CAT operates more than that produced in ROS metabolism, while APX enzymes, which use ascorbate with an electron donor, and GPX, which uses guaiacol, act to split the remaining H_2O_2. APX and GPX are mainly described in plants and occur in the presence of stressors (Mittler, 2002; Lesser, 2006; Fijalkowski and Kwarciak-Kozlowska, 2020).

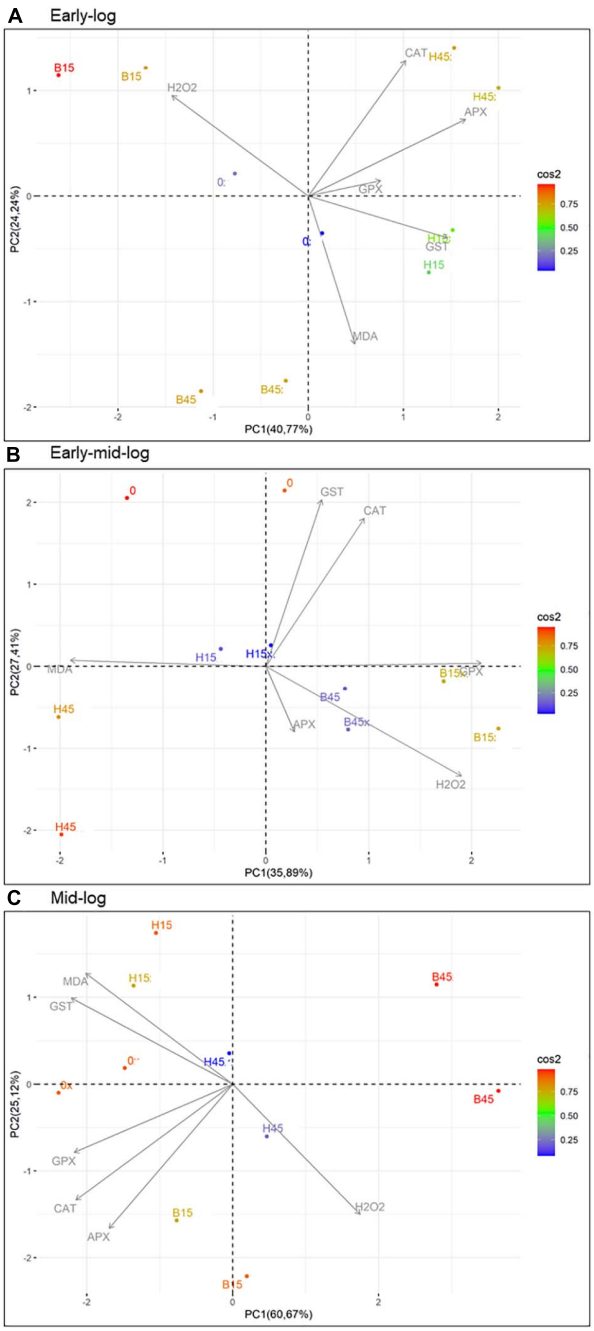

FIGURE 9 | PCA of the relationships between quantifications of stress indicators H_2O_2 and MDA and profiles of enzymatic activities of CAT, APX, GPX, and GST of *Pseudomonas* sp. CMA 6.9 in the three growth phases indicated. **(A)** Early-log phase; **(B)** Early mid-log phase; **(C)** Mid-log. Color scale indicates the degree of contribution of the data distribution. CAT, catalase; APX, ascorbate peroxidase; GPX, guaiacol peroxidase; GST, glutathione S-transferase.

The increase in CAT activity in the controls of the strain *Pseudomonas* sp. CMA 6.9 throughout the evaluated growth phases (**Figure 7A**) was accompanied by the reduction of H_2O_2 (**Figure 4**), showing the efficiency of this enzyme in conditions without herbicides. The APX and GPX enzymes (**Figures 7B,C**) also showed a significant increase only in the mid-log stage, characterizing the cooperative action with CAT for the control of H_2O_2. The same efficiency in the control of H_2O_2 was not observed in treatments with the Boral® herbicide (**Figure 4**). In B15 there were variations in the activities of three enzymes, which were not observed for B45, for which the activities were relatively the lowest of all (**Figure 7**). CAT is an important antioxidant enzyme in bacteria exposed to xenobiotics. The activity of this enzyme has been observed in freshwater bacterial biofilms exposed to the herbicide oxyfluorfen (Bonnineau et al., 2013), and *P. aeruginosa* PAO1 WT exposed to nicotine (Tang et al., 2018). Despite the importance of CAT, other enzymes participate in the metabolism of H_2O_2, such as glutathione peroxidases (Gebicka and Krych-Madej, 2019). Different *Chlamydomonas* strains showed variation at APX activities when exposed to methyl viologen, indicating that this enzyme contributes to tolerance to this herbicide (Tanaka et al., 2011). APX was also important in ERO control induced by heavy metals, such as zinc, in *Pseudomonas putida* (Hussein and Ho, 2013).

The joint action of CAT, APX, and GPX enzymes in controlling H_2O_2 in bacteria is described in only a few reports in the literature. These effects are limited to bacteria in modulating the activity of these enzymes in plants (Shahid and Khan, 2018). A strain of rhizosphere *Variovorax* sp. was considered tolerant to water stress because of its activity profile of antioxidative enzymes and used to stimulate these characteristics for a symbiotic plant. This strain showed high CAT activity and low APX during stress experiments (Kim et al., 2020). Even for CAT, one of the most studied enzymes in the control of oxidative stress, few reports have followed its activity in relation to the use of herbicides, such as an endophytic strain of *Klebsiella pneumoniae* isolated in evening primrose, used as a bio-herbicide (Kang et al., 2020). However, no similar reports were found on the modulation of the activity of these enzymes in the control of oxidative stress in *Pseudomonas* sp. CMA 6.9.

Enzymatic Activity of GST

Bacterial GST specializes in the detoxification of many molecules via conjugation by GSH (Allocati et al., 2009). Glutathione is an ROS reducing agent produced from cysteine and participates in the glutaredoxin system (Hufnagel et al., 2017). An important feature, however, has been studied in relation to GST, the regulation of cell signaling pathway lipid peroxidation products (Awasthi et al., 2017).

Glutathione S-transferase activity in *Pseudomonas* sp. CMA 6.9 (**Figure 8**) showed a relationship with MDA (**Figure 5**), which is little explored in the literature. Especially in H15 treatment, GST activity was proportional in the early-log and mid-log phases and inversely proportional in the early mid-log phase. GST may be related to the control of lipid peroxidation in this strain, in response to the stress induced mainly by the herbicide Heat®. Temperature stress can change the fluidity of membranes, which may be compensated by the action of desaturases, responsible for substitutions of saturated and unsaturated fatty acids, and GST may be related to the removal of lipids damaged by

peroxide and restoration of the fluidity of the membranes (Kammerscheit et al., 2019).

Changes in the composition of membrane lipids were correlated with lower rates of MDA and changes in permeability in response to the toxicity of the herbicide mesotrione in *E. coli* (Olchanheski et al., 2014) and *B. megaterium* (Dobrzanski et al., 2018). The response system for this same herbicide in *P. ananatis* probably involved the formation of GST-mesotrione conjugates, altering lipid saturation and providing a protective effect for the bacterium by decreasing the permeability of membranes to the herbicide (Prione et al., 2016).

Metabolic Plasticity as a Response System for *Pseudomonas* sp. CMA 6.9 to Boral® and Heat® Herbicides

Antioxidative Enzymes and H_2O_2

In the early-log phase of growth, the enzymes CAT, APX, and GPX had a direct proportional correlation (most obviously with APX) in the H45 treatment but was inversely proportional with B45. A positive correlation of enzymes activities with H_2O_2 was observed for B15 treatment, but inversely proportional for H15. These enzymes seem to work cooperatively by the control of peroxide, mainly in the treatment with Heat®.

The mid-log phase is characterized by a modulation like that of the initial growth phase in *Pseudomonas* sp. CMA 6.9, featuring more efficient control of these three enzymes over the stress generated by Heat® than by Boral®, as already discussed in Section "Quantification of H_2O_2," in terms of the toxicity of Boral®.

There are few reports on the activities of APX and GPX enzymes in microorganisms. In floating aquatic plants, *Hydrocharis dubia*, when exposed to different concentrations of glyphosate, the increase in H_2O_2 production was accompanied by an increase in CAT, APX, and GPX activities (Zhong et al., 2018).

Antioxidative Enzymes and Lipid Peroxidation

In this work we studied a little-explored relationship in the literature, the control of lipid peroxidation by the enzyme GST in bacteria (Awasthi et al., 2017). In the initial growth phase of *Pseudomonas* sp. CMA 6.9, there is a positive correlation between GST and MDA in treatment H15 but inversely proportional to treatment B15. In the early mid-log phase, GST activity is low for H45, while MDA is inversely proportional in treatments with Boral®. In the mid-log phase, as well as for the enzymes discussed in the previous phase, the pattern of interrelations resembles the early-log phase again. Therefore, it appears that lipid peroxidation in treatments with Boral® is affected more by the activity of GST, although the amounts of H_2O_2 are higher, explaining the tolerance to this herbicide, as shown by the data on enzymatic kinetics (**Figure 2**) and viability (**Figure 3**). As noted, GST has the function of controlling oxidative stress induced by cytotoxic substances through conjugation with lipid aldehydes (Singhal et al., 2015).

Metabolic Plasticity

The biofilm strain *Pseudomonas* sp. CMA 6.9 is tolerant to the herbicide Heat®, based on the joint action of the enzymes CAT, APX, and GPX in the control of H_2O_2. The literature points out that previous exposure to herbicides can alter the sensitivity, diversity, and functioning of microorganism species in aquatic biofilms, such as in exposure to the herbicides promethrin (Polst et al., 2018) or alachlor (Paule et al., 2015). However, the strain studied in this work tolerated the toxicity and oxidative stress induced by Boral® by means of another enzymatic system, GST, to control the amounts of MDA, even when this herbicide did not exert selective pressure at the isolation site. The genus *Pseudomonas* is metabolically versatile and plastic, with the ability to metabolize different toxic substances (Orellana-Saez et al., 2019). Thus, the two enzymatic systems of *Pseudomonas* sp. CMA 6.9 to deal with oxidative stress, induced by two different herbicides – one without prior selection – are related to two groups of genes linked to different antioxidative systems, possibly allowing tolerance to both herbicides as more general NTSR mechanisms (Comont et al., 2020). GSTs have already been proposed as NTSR mechanisms (Jugulam and Shyam, 2019; Gaines et al., 2020). In this work, in addition to GST, we are proposing the CAT, APX, and GST systems as NTSR mechanisms in *Pseudomonas* sp. CMA 6.9.

Approaches to Unresolved Issues

Pseudomonas sp. CMA 6.9, selected from the collection of bacteria isolated from biofilms in tanks used to wash pesticide packaging, was evaluated for enzyme systems that possibly induce tolerance to Boral® and Heat® herbicides, as shown by growth and viability kinetics data. The H_2O_2 and MDA data indicated the toxicity of these herbicides, especially Boral®. Although these herbicides act to inhibit the enzyme protoporphyrinogen oxidase, two systems of antioxidative responses were characteristic for each of them: CAT, APX, and GPX in the control of H_2O_2 induced by Heat®, present at the isolation site; and GST acting to control MDA in treatments with Boral®, not present at the isolation site. This modulation of the activity by different enzymes dependent on previous selection characterizes a system of metabolic plasticity. However, 67.2% of the isolates studied in this work were sensitive to these herbicides, suggesting that changes in diversity in soil and water microbiota may occur in the presence of pesticides. Meanwhile, diversity molecular studies revealed that trace metal contamination in water environment have higher impacts on the functional profiles than on the structure of biofilm communities (Coclet et al., 2021). The authors consider that biofilms are less impacted than planktonic communities to metal contamination due to a protection offered by the resistant species to all members in the community, and a wide range of specific mechanism of protection. Taking this in consideration, studies involving metabolome and identification of quorum-sensing signaling molecules should be carried out to test hypotheses regarding the modulations of the enzymatic response systems for the herbicides Boral® and Heat® in *Pseudomonas* sp. CMA 6.9. Biofilms containing this strain could protect the herbicide-sensitive isolates, opening a possibility of using biofilms containing biodegrade communities of biofilms in recovery from contaminated areas.

DATA AVAILABILITY STATEMENT

The datasets presented in this study can be found in online repositories. The names of the repository/repositories and accession number(s) can be found in the article/ **Supplementary Material**.

AUTHOR CONTRIBUTIONS

AR, CS, and PF: data curation, formal analysis, investigation, methodology, software, visualization, and writing original draft, review, and editing. GC and MS: methodology. EO: investigation, methodology, and visualization. SP: writing, review, and editing. RO: conceptualization, data curation, formal analysis, resources, supervision, validation, and writing original draft, review, and editing. MP: conceptualization, data curation, formal analysis, funding acquisition, project administration, resources, supervision, validation, and writing original draft, review, and editing. All authors contributed to the article and approved the submitted version.

FUNDING

This work was supported by the Coordination for the Improvement of Higher Level Personnel (CAPES), the National Council for Scientific and Technological Development (CNPq), and the Foundation for Research Support of the State of Paraná (Fundação Araucária).

ACKNOWLEDGMENTS

The authors would like to thank Maria Janina Pinheiro Diniz for assisting in the preparation and execution of the experiments.

SUPPLEMENTARY MATERIAL

The Supplementary Material for this article can be found online at: https://www.frontiersin.org/articles/10.3389/fmicb.2021.673211/full#supplementary-material

REFERENCES

Alexieva, V., Sergiev, I., Mapelli, S., and Karanov, E. (2001). The effect of drought and ultraviolet radiation on growth and stress markers in pea and wheat. *Plant Cell Environ.* 24, 1337–1344. doi: 10.1046/j.1365-3040.2001.00778.x

Allocati, N., Federici, L., Masulli, M., and Di Ilio, C. (2009). Glutathione transferases in bacteria. *FEBS J.* 276, 58–75. doi: 10.1111/j.1742-4658.2008.06743.x

Awasthi, Y. C., Ramana, K. V., Chaudhary, P., Srivastava, S. K., and Awasthi, S. (2017). Regulatory roles of glutathione-S-transferases and 4-hydroxynonenal in stress-mediated signaling and toxicity. *Free Radic. Biol. Med.* 111, 235–243. doi: 10.1016/j.freeradbiomed.2016.10.493

Azevedo, R. A., Alas, R. M., Smith, R. J., and Lea, P. J. (1998). Response of antioxidant enzymes to transfer from elevated carbon dioxide to air and ozone fumigation, in the leaves and roots of wild-type and a catalase-deficient mutant of barley. *Physiol. Plant.* 104, 280–292. doi: 10.1034/j.1399-3054.1998.1040217.x

Barnes, A. C., Horne, M. T., and Ellis, A. E. (1996). Effect of iron on expression of superoxide dismutase by *Aeromonas salmonicida* and associated resistance to superoxide anion. *FEMS Microbiol. Lett.* 142, 19–26. doi: 10.1111/j.1574-6968.1996.tb08401.x

Beffa, R., Menne, H., and Köcher, H. (2019). *Herbicide Resistance Action Committee (HRAC): Herbicide Classification, Resistance Evolution, Survey, and Resistance Mitigation Activities*. Available online at: http://weedscience.org/ (accessed February 21, 2020)

Benson, D. R., Stephens, D. W., Clawson, M. L., and Silvester, W. B. (1996). Amplification of 16S rRNA genes from *Frankia* strains in root nodules of *Ceanothus griseus*, *Coriaria arborea*, *Coriaria plumosa*, *Discaria toumatou*, and *Purshia tridentata*. *Appl. Environ. Microbiol.* 62, 2904–2909. doi: 10.1128/AEM.62.8.2904-2909.1996

Bonnineau, C., Tlili, A., Faggiano, L., Montuelle, B., and Guasch, H. (2013). The use of antioxidant enzymes in freshwater biofilms: temporal variability vs. toxicological responses. *Aquat. Toxicol.* 136–137, 60–71. doi: 10.1016/j.aquatox.2013.03.009

Bradford, M. M. (1976). A rapid and sensitive method for the quantitation of microgram quantities of protein utilizing the principle of protein-dye binding. *Anal. Biochem.* 72, 248–254. doi: 10.1016/0003-2697(76)90527-3

Bučková, M., Godočíková, J., Zámocký, M., and Polek, B. (2010). Screening of bacterial isolates from polluted soils exhibiting catalase and peroxidase activity and diversity of their responses to oxidative stress. *Curr. Microbiol.* 61, 241–247. doi: 10.1007/s00284-010-9601-x

Coclet, C., Garnier, C., D'Onofrio, S., Durrieu, G., Pasero, E., Le Poupon, C., et al. (2021). Trace metal contamination impacts predicted functions more than structure of marine prokaryotic biofilm communities in an anthropized coastal area. *Front. Microbiol.* 19:589948. doi: 10.3389/fmicb.2021.589948

Comont, D., Lowe, C., Hull, R., Crook, L., Hicks, H. L., Onkokesung, N., et al. (2020). Evolution of generalist resistance to herbicide mixtures reveals a trade-off in resistance management. *Nat. Commun.* 11:3086. doi: 10.1038/s41467-020-16896-0

Corcoll, N., Yang, J., Backhaus, T., Zhang, X., and Eriksson, K. M. (2019). Copper affects composition and functioning of microbial communities in marine biofilms at environmentally relevant concentrations. *Front. Microbiol.* 8:3248. doi: 10.3389/fmicb.2018.03248

Dobrzanski, T., Gravina, F., Steckling, B., Olchanheski, L. R., Sprenger, R. F., Espírito Santo, B. C., et al. (2018). *Bacillus megaterium* strains derived from water and soil exhibit differential responses to the herbicide mesotrione. *PLoS One* 13:e0196166. doi: 10.1371/journal.pone.0196166

Dourado, M. N., Franco, M. R., Peters, L. P., Martins, P. F., and Souza, L. A. (2015). Antioxidant enzymes activities of *Burkholderia* spp. strains - oxidative responses to Ni toxicity. *Environ. Sci. Pollut. Res. Int.* 22, 19922–19932. doi: 10.1007/s11356-015-5204-1

Dourado, M. N., Martins, P. F., Quecine, M. C., Piotto, F. A., Souza, L. A., Franco, M. R., et al. (2013). *Burkholderia* sp. SCMS54 reduces cadmium toxicity and promotes growth in tomato. *Ann. Appl. Biol.* 163, 494–507. doi: 10.1111/aab.12066

Du, Z., Zhu, Y., Zhu, L., Zhang, J., Li, B., Wang, J., et al. (2018). Effects of the herbicide mesotrione on soil enzyme activity and microbial communities. *Ecotoxicol. Environ. Saf.* 30, 571–578. doi: 10.1016/j.ecoenv.2018.08.075

Eke, P., Kumar, A., Sahu, K. P., Wakam, L. N., Sheoran, N., Ashajyothi, M., et al. (2019). Endophytic bacteria of desert cactus (*Euphorbia trigonas* Mill) confer drought tolerance and induce growth promotion in tomato (*Solanum lycopersicum* L.). *Microbiol. Res.* 228:126302. doi: 10.1016/j.micres.2019.126302

Fan, D., Subramanian, S., and Smith, D. L. (2020). Plant endophytes promote growth and alleviate salt stress in *Arabidopsis thaliana*. *Sci. Rep.* 10:12740. doi: 10.1038/s41598-020-69713-5

Faria, G., Guimaraes, R. M., Carvalho, E. R., and Sousa, D. P. (2015). Methods for the assessment of isoenzymes activity in sunflower seeds. *J. Seed Sci.* 37, 211–217. doi: 10.1590/2317-1545v37n3149041

Fijalkowski, K. L., and Kwarciak-Kozlowska, A. (2020). Phytotoxicity assay to assess sewage sludge phytoremediation rate using guaiacol peroxidase activity

(GPX): a comparison of four growth substrates. *J. Environ. Manage.* 263:110413. doi: 10.1016/j.jenvman.2020.110413

Gaines, T. A., Duke, S. O., Morran, S., Rigon, C. A. G., Tranel, P. J., Küpper, A., et al. (2020). Mechanisms of evolved herbicide resistance. *J. Biol. Chem.* 295, 10307–10330. doi: 10.1074/jbc.REV120.013572

Gebicka, L., and Krych-Madej, J. (2019). The role of catalases in the prevention/promotion of oxidative stress. *J. Inorg. Biochem.* 197:110699. doi: 10.1016/j.jinorgbio.2019.110699

Gotelli, N. J., Ellison, A. M., Dunn, R. R., and Sanders, N. J. (2011). Counting ants (Hymenoptera: Formicidae): biodiversity sampling and statistical analysis for myrmecologists. *Myrmecol. News* 15, 13–19.

Gravina, F., Dobrzanski, T., Olchanheski, L. R., Galvão, C. W., Reche, P. M., Pileggi, S. A. V., et al. (2017). Metabolic interference of sod gene mutations on catalase activity in *Escherichia coli* exposed to Gramoxone® (paraquat) herbicide. *Ecotoxicol. Environ. Saf.* 139, 89–96. doi: 10.1016/j.ecoenv.2017.01.027

Heath, R. L., and Packer, L. (1968). Photoperoxidation in isolated chloroplasts: I. Kinetics and stoichiometry of fatty acid peroxidation. *Arch. Biochem. Biophys.* 125, 189–198. doi: 10.1016/0003-9861(68)90654-1

Hufnagel, D. A., Price, J. E., Stephenson, R. E., Kelley, J., Benoit, M. F., and Chapman, M. R. (2017). Thiol starvation induces redox-mediated dysregulation of *Escherichia coli* biofilm components. *J. Bacteriol.* 200:e00389-17. doi: 10.1128/JB.00389-17

Hussein, K. A., and Ho, J. J. (2013). Heavy metal resistance of bacteria and its impact on the production of antioxidant enzymes. *Afr. J. Microbiol. Res.* 7, 2288–2296. doi: 10.5897/AJMR12.1764

Imlay, J. A. (2019). Where in the world do bacteria experience oxidative stress? *Environ. Microbiol.* 21, 521–530. doi: 10.1111/1462-2920.14445

Jugulam, M., and Shyam, C. (2019). Non-target-site resistance to herbicides: recent developments. *Plants* 8:417. doi: 10.3390/plants8100417

Kammerscheit, X., Chauvat, F., and Cassier-Chauvat, C. (2019). From cyanobacteria to human, MAPEG-type Glutathione-S-transferases operate in cell tolerance to heat, cold, and lipid peroxidation. *Front. Microbiol.* 10:2248. doi: 10.3389/fmicb.2019.02248

Kang, S. M., Bilal, S., Shahzad, R., Kim, Y. N., Park, C. W., Lee, K. E., et al. (2020). Effect of ammonia and indole-3-acetic acid producing endophytic *Klebsiella pneumoniae* YNA12 as a bio-herbicide for weed inhibition: special reference with evening primroses. *Plants (Basel).* 9:761. doi: 10.3390/plants9060761

Karami, S., Maleki, A., Karimi, E., Poormazaheri, H., Zandi, S., Davari, B., et al. (2016). Biodegradation of 2,4-dichlorophenoxyacetic acid by bacteria with highly antibiotic-resistant pattern isolated from wheat field soils in Kurdistan, Iran. *Environ. Monit. Assess.* 188:659. doi: 10.1007/s10661-016-5673-9

Kim, Y., Khan, M. A., Kang, S., Hamayun, M., and Lee, I. (2020). Enhancement of drought-stress tolerance of *Brassica oleracea* var. *italica* L. by newly isolated *Variovorax* sp. YNA59. *J. Microbiol. Biotechnol.* 30, 1500–1509. doi: 10.4014/jmb.2006.06010

Kraus, T. E., McKersie, B. D., and Fletcher, R. A. (1995). Paclobutrazol-induced tolerance of wheat leaves to paraquat may involve increased antioxidant enzyme activity. *J. Plant Physiol.* 145, 570–576. doi: 10.1016/S0176-1617(11)81790-6

Laemmli, U. K. (1970). Cleavage of structural proteins during the assembly of the head of bacteriophage T4. *Nature* 227, 680–685. doi: 10.1038/227680a0

Lemire, J., Alhasawi, A., Appanna, V. P., Tharmalingam, S., and Appanna, V. D. (2017). Metabolic defence against oxidative stress: the road less travelled so far. *J. Appl. Microbiol.* 123, 798–809. doi: 10.1111/jam.13509

Lesser, M. P. (2006). Oxidative stress in marine environments: biochemistry and physiological ecology. *Annu. Rev. Physiol.* 68, 253–278. doi: 10.1146/annurev.physiol.68.040104.110001

Li, M., Song, J., Ma, Q., Kong, D., Zhou, Y., Jiang, X., et al. (2020). Insight into the characteristics and new mechanism of nicosulfuron biodegradation by a *Pseudomonas* sp. LAM1902. *J. Agric. Food Chem.* 68, 826–837. doi: 10.1021/acs.jafc.9b06897

Lima, J. Y., Moreira, C., Nunes Freitas, P. N., Olchanheski, L. R., Pileggi, S. A. V., Etto, R. M., et al. (2020). Structuring biofilm communities living in pesticide contaminated water. *Heliyon.* 6:e03996. doi: 10.1016/j.heliyon

Liu, X., Chen, Q., Ali, N., Zhang, J., Wang, M., and Wang, Z. (2019). Single and joint oxidative stress–related toxicity of sediment-associated cadmium and lead on *Bellamya aeruginosa*. *Environ. Sci. Pollut. Res.* 26, 24695–24706. doi: 10.1007/s11356-019-05769-9

Lü, Z., Sang, L., Li, Z., and Min, H. (2009). Catalase and superoxide dismutase activities in a *Stenotrophomonas maltophilia* WZ2 resistant to herbicide pollution. *Ecotoxicol. Environ. Saf.* 72, 136–143. doi: 10.1016/j.ecoenv.2008.01.009

Martins, P. F., Carvalho, G., Gratão, P. L., Dourado, M. N., Pileggi, M., Araújo, W. L., et al. (2011). Effects of the herbicides acetochlor and metolachlor on antioxidant enzymes in soil bacteria. *Process Biochem.* 46, 1186–1195. doi: 10.1016/j.procbio.2011.02.014

Matsuno, H., and Uritani, I. (1972). Physiological behavior of peroxidase isozymes in sweet potato root tissue injured by cutting or with black rot. *Plant Cell Physiol.* 13, 1091–1101. doi: 10.1093/oxfordjournals.pcp.a074815

Mauffret, A., Baran, N., and Joulian, C. (2017). Effect of pesticides and metabolites on groundwater bacterial community. *Sci. Total Environ.* 576, 879–887. doi: 10.1016/j.scitotenv.2016.10.108

Meena, R. S., Kumar, S., Datta, R., Lal, R., Vijayakumar, V., Brtnicky, M., et al. (2020). Impact of agrochemicals on soil microbiota and management: a review. *Land* 9:34. doi: 10.3390/land9020034

Melo, C. A. D., Massenssini, A. M., Passos, A. B. R. J., Carvalho, F. P., Ferreira, L. R., Silva, A. A., et al. (2016). Isolation and characteristics of sulfentrazone-degrading bacteria. *J. Environ. Sci. Heal. Part B Pestic. Food Contam. Agric. Wastes* 52, 115–121. doi: 10.1080/03601234.2016.1248136

Mesnage, R., Teixeira, M., Mandrioli, D., Falcioni, L., Ducarmon, Q. R., Zwittink, R. D., et al. (2021). Use of shotgun metagenomics and metabolomics to evaluate the impact of glyphosate or roundup MON 52276 on the gut microbiota and serum metabolome of Sprague-Dawley rats. *Environ. Health Perspect.* 129:17005. doi: 10.1289/EHP6990

Mittler, R. (2002). Oxidative stress, antioxidants and stress tolerance. *Trends Plant Sci.* 7, 405–410. doi: 10.1016/S1360-1385(02)02312-9

Molina, L., La Rosa, R., Nogales, J., and Rojo, F. (2019). *Pseudomonas putida* KT2440 metabolism undergoes sequential modifications during exponential growth in a complete medium as compounds are gradually consumed. *Environ. Microbiol.* 21, 2375–2390. doi: 10.1111/1462-2920.14622

Moretto, J. A. S., Altarugio, L. M., Andrade, P. A., Fachin, A. L., Andreote, F. D., and Stehling, E. G. (2017). Changes in bacterial community after application of three different herbicides. *FEMS Microbiol. Lett.* 364:fnx113. doi: 10.1093/femsle/fnx113

Murínová, S., and Dercová, K. (2014). Response mechanisms of bacterial degraders to environmental contaminants on the level of cell walls and cytoplasmic membrane. *Int. J. Microbiol.* 2014:873081. doi: 10.1155/2014/873081

Muturi, E. J., Donthu, R. K., Fields, C. J., Moise, I. K., and Kim, C. H. (2017). Effect of pesticides on microbial communities in container aquatic habitats. *Sci. Rep.* 7:44565. doi: 10.1038/srep44565

Nakano, Y., and Asada, K. (1981). Hydrogen peroxide is scavenged by ascorbate-specific peroxidase in spinach chloroplasts. *Plant Cell. Physiol.* 22, 867–880. doi: 10.1093/oxfordjournals.pcp.a076232

Olchanheski, L. R., Dourado, M. N., Beltrame, F. L., Zielinski, A. A. F., Demiate, I. M., Pileggi, S. A. V., et al. (2014). Mechanisms of tolerance and high degradation capacity of the herbicide mesotrione by *Escherichia coli* strain DH5-a. *PLoS One* 9:e99960. doi: 10.1371/journal.pone.0099960

Orellana-Saez, M., Pacheco, N., Costa, J. I., Mendez, K. N., Miossec, M. J., Meneses, C., et al. (2019). In-depth genomic and phenotypic characterization of the antarctic psychrotolerant strain *Pseudomonas* sp. MPC6 reveals unique metabolic features, plasticity, and biotechnological potential. *Front. Microbiol.* 10:1154. doi: 10.3389/fmicb.2019.01154

Paule, A., Lamy, A., Roubeix, V., Delmas, F., and Rols, J. L. (2015). Influence of the natural growth environment on the sensitivity of phototrophic biofilm to herbicide. *Environ. Sci. Pollut. Res.* 22, 8031–8043. doi: 10.1007/s11356-014-3429-z

Paule, A., Roubeix, V., Swerhone, G. D. W., Roy, J., Lauga, B., Duran, R., et al. (2016). Comparative responses of river biofilms at the community level to common organic solvent and herbicide exposure. *Environ. Sci. Pollut. Res.* 23, 4282–4293. doi: 10.1007/s11356-015-5141-z

Pedersen, H. L., Willassen, N. P., and Leiros, I. (2009). The first structure of a cold-adapted superoxide dismutase (SOD): biochemical and structural characterization of iron SOD from *Aliivibrio salmonicida*. *Acta Crystallog.*

Sect. F Struct. Biol. Cryst. Commun. 65, 84–92. doi: 10.1107/S1744309109001110

Peters, L. P., Carvalho, G., Martins, P. F., Dourado, M. N., Vilhena, M. B., Pileggi, M., et al. (2014). Differential responses of the antioxidant system of ametryn and clomazone tolerant bacteria. *PLoS One* 9:e112271. doi: 10.1371/journal.pone.0112271

Pileggi, M., Pileggi, S. A. V., and Sadowsky, M. J. (2020). Herbicide bioremediation: from strains to bacterial communities. *Heliyon* 6, e05767. doi: 10.1016/j.heliyon.2020.e05767

Polst, B. H., Anlanger, C., Risse-Buhl, U., Larras, F., Hein, T., Weitere, M., et al. (2018). Hydrodynamics alter the tolerance of autotrophic biofilm communities toward herbicides. *Front. Microbiol.* 9:2884. doi: 10.3389/fmicb.2018.02884

Prione, L. P., Olchanheski, L. R., Tullio, L. D., Santo, B. C. E., Reche, P. M., Martins, P. F., et al. (2016). GST activity and membrane lipid saturation prevents mesotrione-induced cellular damage in *Pantoea ananatis*. *AMB Express* 6:70. doi: 10.1186/s13568-016-0240-x

Rachedi, K., Zermane, F., Tir, R., Ayache, F., Duran, R., Lauga, B., et al. (2018). Effect of sulfonylurea tribenuron methyl herbicide on soil Actinobacteria growth and characterization of resistant strains. *Braz. J. Microbiol.* 49, 79–86. doi: 10.1016/j.bjm.2017.05.004

Ram, Y., Dellus-Gur, E., Bibi, M., Karkare, K., Obolski, U., Feldman, M. W., et al. (2019). Predicting microbial growth in a mixed culture from growth curve data. *Proc. Natl. Acad. Sci. U.S.A.* 116, 14698–14707. doi: 10.1073/pnas.1902217116

Shahid, M., and Khan, M. S. (2018). Glyphosate induced toxicity to chickpea plants and stress alleviation by herbicide tolerant phosphate solubilizing *Burkholderia cepacia* PSBB1 carrying multifarious plant growth promoting activities. *3 Biotech* 8:131. doi: 10.1007/s13205-018-1145-y

Singhal, S. S., Singh, S. P., Singhal, P., Horne, D., Singhal, J., and Awasthi, S. (2015). Antioxidant role of glutathione S-transferases: 4-hydroxynonenal, a key molecule in stress-mediated signaling. *Toxicol. Appl. Pharmacol.* 289, 361–370. doi: 10.1016/j.taap.2015.10.006

Tanaka, S., Ikeda, K., Miyasaka, H., Shioi, Y., Suzuki, Y., Tamoi, M., et al. (2011). Comparison of three *Chlamydomonas* strains which show distinctive oxidative stress tolerance. *J. Biosci. Bioeng.* 112, 462–468. doi: 10.1016/j.jbiosc.2011.07.019

Tang, H., Zhang, Y., Ma, Y., Tang, M., Shen, D., and Wang, M. (2018). Regulation of nicotine tolerance by quorum sensing and high efficiency of quorum quenching under nicotine stress in *Pseudomonas aeruginosa* PAO1. *Front. Cell. Infect. Microbiol.* 8:88. doi: 10.3389/fcimb.2018.00088

Thiour-Mauprivez, C., Martin-Laurent, F., Calvayrac, C., and Barthelmebs, L. (2019). Effects of herbicide on non-target microorganisms: towards a new class of biomarkers? *Sci. Total Environ.* 684, 314–325. doi: 10.1016/j.scitotenv.2019.05.230

Tolker-Nielsen, T. (2015). Biofilm development. *Microbiol. Spectr.* 3:MB-0001-2014. doi: 10.1128/microbiolspec.mb-0001-2014

Touati, D. (2000). Iron and oxidative stress in bacteria. *Arch. Biochem. Biophys.* 373, 1–6. doi: 10.1006/abbi.1999.1518

Venturi, V. (2006). Regulation of quorum sensing in *Pseudomonas*. *FEMS Microbiol. Rev.* 30, 274–291. doi: 10.1111/j.1574-6976.2005.00012.x

Wongsaroj, L., Saninjuk, K., Romsang, A., Duang-nkern, J., Trinachartvanit, W., Vattanaviboon, P., et al. (2018). *Pseudomonas aeruginosa* glutathione biosynthesis genes play multiple roles in stress protection, bacterial virulence and biofilm formation. *PLoS One* 13:e0205815. doi: 10.1371/journal.pone.0205815

Wu, L., Qiu, Z., Zhou, Y., Du, Y., Liu, C., Ye, J., et al. (2016). Physiological effects of the herbicide glyphosate on the cyanobacterium *Microcystis aeruginosa*. *Aquat. Toxicol.* 178, 72–79. doi: 10.1016/j.aquatox.2016.07.010

Wu, L., Zhu, G., Zhang, X., and Si, Y. (2020). Silver nanoparticles inhibit denitrification by altering the viability and metabolic activity of *Pseudomonas stutzeri*. *Sci. Total Environ.* 706:135711. doi: 10.1016/j.scitotenv.2019.135711

Ye, C., Lin, H., Zhang, M., Chen, S., and Yu, X. (2020). Characterization and potential mechanisms of highly antibiotic tolerant VBNC *Escherichia coli* induced by low level chlorination. *Sci. Rep.* 10:1957. doi: 10.1038/s41598-020-58106-3

Ye, J., Huang, C., Qiu, Z., Wu, L., and Xu, C. (2019). The growth, apoptosis and oxidative stress in *Microcystis viridis* exposed to glyphosate. *Bull. Environ. Contam. Toxicol.* 103, 585–589. doi: 10.1007/s00128-019-02691-1

Zablotowicz, R. M., Hoagland, R. E., Locke, M. A., and Hickey, W. J. (1995). Glutathione-s-transferase activity and metabolism of glutathione conjugates by rhizosphere bacteria. *Appl. Environ. Microbiol.* 61, 1054–1060.

Zhang, Y., Meng, D., Wang, Z., Guo, H., Wang, Y., Wang, X., et al. (2012). Oxidative stress response in atrazine-degrading bacteria exposed to atrazine. *J. Hazard Mater.* 229–230, 434–438. doi: 10.1016/j.jhazmat.2012.05.054

Zhong, G., Wu, Z., Liu, N., and Yin, J. (2018). Phosphate alleviation of glyphosate-induced toxicity in *Hydrocharis dubia* (Bl.) Backer. *Aquat. Toxicol.* 201, 91–98. doi: 10.1016/j.aquatox.2018.05.025

Conflict of Interest: The authors declare that the research was conducted in the absence of any commercial or financial relationships that could be construed as a potential conflict of interest.

frontiers in Microbiology

ORIGINAL RESEARCH
published: 13 July 2021
doi: 10.3389/fmicb.2021.686049

Translational GTPase BipA Is Involved in the Maturation of a Large Subunit of Bacterial Ribosome at Suboptimal Temperature

*Kwok Jian Goh[1], Rya Ero[1], Xin-Fu Yan[1], Jung-Eun Park[1], Binu Kundukad[2], Jun Zheng[3], Siu Kwan Sze[1] and Yong-Gui Gao[1]**

[1] School of Biological Sciences, Nanyang Technological University, Singapore, Singapore, [2] Singapore Centre for Environmental Life Sciences Engineering, Nanyang Technological University, Singapore, Singapore, [3] Faculty of Health Sciences, University of Macau, Macau, China

OPEN ACCESS

Edited by:
Amparo Pascual-Ahuir, Universitat Politècnica de València, Spain

Reviewed by:
Kaoru Nakasone, Kindai University, Japan
Cinthia Nuñez, Instituto de Biotecnología, Mexico

***Correspondence:**
Yong-Gui Gao
ygao@ntu.edu.sg

Specialty section:
This article was submitted to Microbial Physiology and Metabolism, a section of the journal Frontiers in Microbiology

Received: *26 March 2021*
Accepted: *09 June 2021*
Published: *13 July 2021*

Citation:
Goh KJ, Ero R, Yan X-F, Park J-E, Kundukad B, Zheng J, Sze SK and Gao Y-G (2021) Translational GTPase BipA Is Involved in the Maturation of a Large Subunit of Bacterial Ribosome at Suboptimal Temperature. Front. Microbiol. 12:686049. doi: 10.3389/fmicb.2021.686049

BPI-inducible protein A (BipA), a highly conserved paralog of the well-known translational GTPases LepA and EF-G, has been implicated in bacterial motility, cold shock, stress response, biofilm formation, and virulence. BipA binds to the aminoacyl-(A) site of the bacterial ribosome and establishes contacts with the functionally important regions of both subunits, implying a specific role relevant to the ribosome, such as functioning in ribosome biogenesis and/or conditional protein translation. When cultured at suboptimal temperatures, the *Escherichia coli bipA* genomic deletion strain (Δ*bipA*) exhibits defects in growth, swimming motility, and ribosome assembly, which can be complemented by a plasmid-borne *bipA* supplementation or suppressed by the genomic *rluC* deletion. Based on the growth curve, soft agar swimming assay, and sucrose gradient sedimentation analysis, mutation of the catalytic residue His78 rendered plasmid-borne *bipA* unable to complement its deletion phenotypes. Interestingly, truncation of the C-terminal loop of BipA exacerbates the aforementioned phenotypes, demonstrating the involvement of BipA in ribosome assembly or its function. Furthermore, tandem mass tag-mass spectrometry analysis of the Δ*bipA* strain proteome revealed upregulations of a number of proteins (e.g., DeaD, RNase R, CspA, RpoS, and ObgE) implicated in ribosome biogenesis and RNA metabolism, and these proteins were restored to wild-type levels by plasmid-borne *bipA* supplementation or the genomic *rluC* deletion, implying BipA involvement in RNA metabolism and ribosome biogenesis. We have also determined that BipA interacts with ribosome 50S precursor (pre-50S), suggesting its role in 50S maturation and ribosome biogenesis. Taken together, BipA demonstrates the characteristics of a *bona fide* 50S assembly factor in ribosome biogenesis.

Keywords: BipA, ribosome biogenesis, large subunit maturation, conditional protein expression, stress response, suboptimal temperature growth

INTRODUCTION

The ability of bacteria to respond, adapt, and grow at suboptimal temperature is known as cold shock response, which is activated in *Escherichia coli* under a condition of a sudden drop in culturing temperature (usually from 37 to 15°C) (Barria et al., 2013). Suboptimal temperature can cause both physiological and morphological changes in the bacteria and even cell death if the temperature shift is beyond bacterial tolerance. The majority of cold-inducible proteins involves RNA metabolism, indicating that regulation of RNA metabolism is crucial for suboptimal temperature adaptation (Barria et al., 2013). The most notable examples include the following: (i) cold shock protein (Csp) family proteins, which are RNA chaperones and able to prevent formation of RNA secondary structures (Phadtare et al., 2003; Barria et al., 2013; Uppal and Jawali, 2015); (ii) DEAD-box RNA helicase (DeaD) that can unwind RNA secondary structure to promote degradation (Charollais et al., 2004; Prud'homme-Généreux et al., 2004; Resch et al., 2010); and (iii) RNase R, the only 3′–5′ exonuclease in *E. coli* that degrades double-stranded RNA without the help of a helicase (Cairrão et al., 2003; Awano et al., 2010; Barria et al., 2013).

The translational stress response involves a key component of protein-synthesizing machinery, the ribosome. Bacteria utilize a series of protein factors that bind ribosome to modulate translation in order to cope with stress. For example, the RelA/SpoT homolog (RSH) proteins bind ribosome when there is a surge of uncharged tRNAs caused by the shortage of amino acids. Consequently, binding of RSH to ribosome triggers the alarmone synthesis and is followed by the stringent response (Hauryliuk et al., 2015). Notably, there are two proteins that bind to the ribosome to exert their stress response function: ObgE and BPI-inducible protein A (BipA). ObgE is an essential GTPase, and its homologs have been ubiquitously found across all kingdoms of life (Sato et al., 2005; Jiang et al., 2006). An analysis of those immature 50S particles, accumulated in cells with the ObgE depleted, showed that late assembling r-proteins (L33, L34, and L16) were under-represented, indicating that ObgE is an important factor during the late step of 50S biogenesis (Jiang et al., 2006).

BipA has been implicated in various functions of pathogenic bacteria, such as *Salmonella typhimurium* (*S. typhimurium*), *Pseudomonas aeruginosa* (*P. aeruginosa*), and enteropathogenic *E. coli* (EPEC). BipA is upregulated by ∼7-fold when *S. typhimurium* is "attacked" by bactericidal/permeability increasing (BPI) antimicrobial peptide (Qi et al., 1995). BipA is also known as TypA, referring to tyrosine phosphorylated protein A, and this is the case in *P. aeruginosa* where TypA was found to be involved in virulence, antimicrobial resistance, and biofilm formation (Neidig et al., 2013). In EPEC, BipA has been reported to upregulate the virulence and reduce flagella-mediated motility (Grant et al., 2003). The *bipA* deletion would result in growth delay of *E. coli* K12 strain while cultured at low temperature (e.g., 20°C) (Pfennig and Flower, 2001). Furthermore, Choudhury and Flower (2015) reported that the ribosomal particle distribution of the *bipA* deletion strain changes dramatically, with the accumulation of the 30S and the presence of 50S precursor (pre-50S), indicating a possible role of BipA in ribosome biogenesis (Choudhury and Flower, 2015). Interestingly, a transposon-mediated random insertion mutation into *E. coli* K12 strain genome revealed that the disruption of the *rluC* gene can suppress the phenotype of the *bipA* deletion (Krishnan and Flower, 2008). RluC is a pseudouridine synthase, which converts three uridines (U955, U2504, and U2580) in 23S rRNA to pseudouridines (Ψ955, Ψ2504, and Ψ2580). Pseudouridine is a uridine isomer where the uracil base is linked to the pentose sugar by a carbon-to-carbon bond, resulting in the ability to form an additional hydrogen bond and thereby increasing the stability compared to uridine (Kierzek et al., 2013). In addition, Choudhury and Flower (2015) discovered that the deletion of DeaD exacerbates both the growth and ribosomal particle distribution defects (Choudhury and Flower, 2015). Since DeaD is involved in 50S biogenesis, it is not surprising that *bipA* and *deaD* double mutations could cause an evident defect in ribosome biogenesis. Crystal structures of the apo-, as well as the nucleotides [GDP, (p)ppGpp, and GDPCP] bound BipA, showed no significant difference in their overall conformations (Fan et al., 2015; Kumar et al., 2015). However, a drastic conformational change was observed in domains III, V, and the C-terminal domain (CTD), upon GTP form BipA binding to 70S ribosome (Kumar et al., 2015). The conformational change of the CTD was particularly interesting because the CTD loop extends into the ribosomal A site to establish extensive contacts with the tRNA acceptor stem; however, the precise role of such interactions is largely unknown (Kumar et al., 2015). Nevertheless, the structure of BipA with ribosome demonstrated an activated form of BipA in the ribosome, with the catalytic residue, histidine 78 (H78), situated close to the 23S rRNA sarcin–ricin loop (SRL) in a ratcheting ribosome as well as interacting with the bound nucleotide (GDPCP). Collectively, BipA is an authentic ribosome-dependent trGTPase. However, how BipA in association with 70S ribosome is correlated with bacterial stress response as well as how BipA functions in conditional translation for bacterial cells at suboptimal temperature require further studies.

Notably, recent quantitative mass spectrometry data nicely showed the accumulated pre-50S intermediates in *bipA* mutant cells at suboptimal temperature, with several r-proteins absent, further demonstrating the role of BipA in 50S subunit assembly (Gibbs et al., 2020). Furthermore, a paper published during our manuscript preparation revealed that bacteria can remodel their protein expression relevant to biofilm formation in a temperature-dependent manner by modulating BipA abundance (Del Peso Santos et al., 2021). With the desire to support the ongoing effort in BipA-related studies and to expand our efforts on structural study of ribosome-associated proteins and biofilm formation as well as its relevant pathogenesis and resistance (Tanaka et al., 2008; Selmer et al., 2012; Kumar et al., 2015; Yu et al., 2015; Ero et al., 2016; Kumar et al., 2016; Yang et al., 2017), here we report additional evidence to demonstrate the role of BipA in ribosome biogenesis, specifically in large subunit 50S maturation, and conditional protein translation at suboptimal temperature through combinative approaches. In particular, our findings by tandem mass tag (TMT)-based

quantitative proteomic analysis identified proteins relevant to RNA metabolism (e.g., DeaD) with increased expression levels upon BipA deletion, such an effect can be suppressed by a further mutation of RluC or complementation by BipA. The upregulation of these protein possibly indicates that bacterial cells can compensate for the loss of BipA during 50S biogenesis.

MATERIALS AND METHODS

Bacterial Strains and Culturing

The *E. coli* strains used in this project are listed in **Table 1**. Strains were grown in Lysogeny broth (LB) at 37°C for optimal growth and at 25°C for suboptimal growth. The antibiotics chloramphenicol (34 μg/ml), gentamicin (15 μg/ml) and kanamycin (30 μg/ml) were added when required for selection.

Deletion of *rluC* gene was carried out using the pRed/ET system (Heermann et al., 2008), replacing *rluC* with gentamicin resistance cassette through sequence-specific homologous recombination. Linear DNA fragments consisting of the homologous arms (50-bp sequences upstream and downstream of *rluC*), sandwiching the gentamicin antibiotic cassette, were transformed into pRed/ET-harboring *E. coli* K12 strain (K12WT) using electroporation.

Deletion of genomic *bipA* and *spoT* genes was carried out using the pDS132 (Philippe et al., 2004) suicide plasmid. Approximately 500 bp upstream and downstream of *bipA* and *spoT* were amplified as the homologous arms. The upstream and downstream arms were combined through restriction site ligation and cloned into pDS132 to obtain pDS132-*bipA* and pDS132-*spoT* plasmids. The plasmids were transformed into target cells using electroporation and two rounds of selections. Kanamycin-resistant cells were selected from the first round of selection, and sucrose-sensitive cells were selected from the second round of selection.

Knock-in of *lacZ* downstream of *deaD* and *obgE* was done using pVIK111 (Zheng et al., 2007) suicide vector. In-frame insertion was created by amplifying approximately 500 bp of 3′-end of the target gene, while excluding the stop codon, and cloned into pVIK111 yielding pVIK111-*deaD* and pVIK111-*obgE*. The plasmids were then transformed into *E. coli* K12 strain (K12WT), Δ*bipA*, Δ*bipA* (pCA24N-BipA), and Δ*rluC*/Δ*bipA* using electroporation. Kanamycin-resistant clones were selected.

Site-Directed Mutagenesis

Modifications of pCA24N-BipA were done using the QuikChange method to produce pCA24N-BipA$_{H78A}$, pCA24N-BipA$_{H78Q}$, and pCA24N-BipA$_{T544_D552del}$. Primers were designed to have equal lengths of nucleotides extending toward 5′- and 3′-ends from the point of modification. Briefly, the first step was PCR amplification of pCA24N-BipA to produce two single-stranded circular DNAs by carrying out the forward and reverse amplification in separate reactions. Secondly, the samples were mixed in the presence of 1 μl *Dpn*I enzyme (NEB®), which digested the template DNA. Next was activation at 37°C for 2.5 h, followed by deactivation at 80°C for 20 min, and then denaturation at 98°C for 15 min. Lastly, samples were incubated at room temperature to allow the denatured products to re-anneal. Chloramphenicol-resistant clones were selected for sequence verification.

Growth Assay

Growth curves were determined using a 96-well microplate. The overnight cultures were diluted in LB to $OD_{600} \approx 0.02$ in a final volume of 100 μl/well. Plates were shaken in a shaker incubator at 200 RPM and temperature of 37°C for optimal growth and 25°C for suboptimal growth. The cell density was measured by a TECAN Spark^{TM} 10M multimode microplate reader without microplate lid every half an hour (37°C) or every hour (25°C) under the settings of 600-nm light absorbance, 25 flashes, and 120-ms wait time between wells. Growth curves were performed in biological triplicates.

Swimming Motility Assay

Overnight cultures were diluted to $OD_{600} \approx 1.0$ in 0.9% (*w*/*v*) NaCl. Soft LB agar (0.3% *w*/*v*) was inoculated with overnight cultures by using a drawing needle to dip into the diluted overnight cultures and then pierced through the soft agar to the middle. The plates were incubated at room temperature for 24 and 48 h. Results were recorded in the form of images and measurements of swimming diameter.

Sucrose Gradient Sedimentation Analysis

Cell pellets [K12WT, Δ*bipA*, Δ*bipA* (pCA24N-BipA), Δ*bipA* (pCA24N-BipA$_{H78A}$), Δ*bipA* (pCA24N-BipA$_{H78Q}$), Δ*bipA* (pCA24N-BipA$_{T544_D552del}$), Δ*rluC*, and Δ*rluC*/Δ*bipA*] were resuspended in RNA lysis buffer [20 mM HEPES pH 7.5, 10.5 mM MgOAc, 100 mM NH_4Cl, 0.5 mM EDTA pH 8.0, and 6 mM β-mercaptoethanol (β-ME)] in the presence of 20 U/ml DNase I and 1 mg/ml lysozyme. Cells were lysed by three rounds of freeze and thaw (30 min freezing in −80°C and complete thawing in ice water). Ten A_{260} units was layered onto 5–45% (*w*/*v*) sucrose gradient for polysome profiling. The 5% and 45% (*v*/*v*) sucrose solutions were prepared by dissolving sucrose in overlay buffer (10 mM HEPES pH 7.5, 50 mM KCl, 10 mM NH_4Cl, 10.25 mM MgOAc, and 0.25 mM EDTA pH 8.0), and 6 mM β-ME was added before use. The gradients were formed using Gradient Master (BioComp, Munich, Germany). The sucrose gradients were centrifuged at 36,000 RPM for 1.5 h ($\omega^2 t = 7.6746 \times 10^{10}$) at 4°C using SW 41 Ti rotor (Beckman Coulter, Brea, CA, United States). A density gradient fractionator system (Brandel, Gaithersburg, MD, United States) was used to analyze the ribosomal particles by continuous monitoring of A_{260} and to fractionate the samples.

Tandem Mass Tag-Mass Spectrometry-Based Quantitative Proteomics

Tandem mass tag-mass spectrometry (TMT-MS) was carried out as described in a previous work (Park et al., 2019), with slight modifications. K12WT, Δ*bipA*, Δ*bipA* (pCA24N-BipA), Δ*rluC*, and Δ*rluC*/Δ*bipA* were cultured in 200 ml LB at 25°C in a

TABLE 1 | Strains of *E. coli* and plasmids used in this project.

***E. coli* strains**	**Description of the genotype**	**Reference or sources**
K12WT	K12 BW25113 wild-type; Δ*(araD-araB)567* Δ*lacZ4787(:rrnB-3)*λ- *rph-1* Δ*(rhaD-rhaB)568 hsdR514*	Baba et al., 2006
Δ*bipA*	F-, Δ*(araD-araB)567*, Δ*lacZ4787(:rrnB-3)*, λ-, *rph-1*, Δ*bipA733:kan*, Δ*(rhaD-rhaB)568*, and *hsdR514*	Baba et al., 2006
Δ*rluC*	*rluC:: Gen*^{R}; gentamicin resistance cassette replaced entire K12WT *rluC* gene using pRed/ET	This study
Δ*rluC*/ Δ*bipA*	*rluC:: Gen*^{R}; gentamicin resistance cassette replaced entire Δ*bipA rluC* gene using pRed/ET	This study
Δ*relA*	F-, Δ*(araD-araB)567*, Δ*lacZ4787(:rrnB-3)*, λ$^-$, Δ*relA782:kan*, *rph-1*, Δ*(rhaD-rhaB)568*, *hsdR514*	Baba et al., 2006
Δ*relA*/Δ*spoT*	Homologous recombination gene replacement using upstream and downstream sequences of *spoT* on Δ*relA*	This study
Δ*relA*/Δ*spoT*/Δ*bipA*	Homologous recombination gene replacement using upstream and downstream sequences of *bipA* on Δ*relA* Δ*spoT*	This study
obgE:: pVIK111	K12WT; in frame *obgE-lacZ* translational fusion	This study
Δ*bipA obgE*:: pVIK111	Δ*bipA*; in frame *obgE-lacZ* translational fusion	This study
Δ*bipA obgE*:: pVIK111 + *bipA*	Δ*bipA obgE*:: pVIK111 harboring pCA24N-BipA	This study
Δ*rluC*/ Δ*bipA obgE*:: pVIK111	Δ*rluC*/ Δ*bipA*; in frame *obgE-lacZ* translational fusion	This study
deaD:: pVIK111	K12WT; in frame *deaD-lacZ* translational fusion	This study
Δ*bipA deaD*:: pVIK111	Δ*bipA*; in frame *deaD-lacZ* translational fusion	This study
Δ*bipA deaD*:: pVIK111 + *bipA*	Δ*bipA deaD*:: pVIK111 harboring pCA24N-BipA	This study
Δ*rluC*/ Δ*bipA deaD*:: pVIK111	Δ*rluC*/ Δ*bipA*; in frame *deaD-lacZ* translational fusion	This study
MC1061 (λpir)	*thi thr-1 leu-6 proA2 his-4 argE2 lacY1 galK2 ara-14 xyl-5 supE44 pir*	Zheng et al., 2007
Plasmids		
pCA24N-BipA	ASKA clones harboring *bipA*, Cam^R	KEIO collection
pCA24N	Modified from pCA24N-BipA, harboring no insert to act as an empty plasmid, Cam^R	This study
pCA24N-BipA$_{H78A}$	Point mutation to substitute H78 with alanine, Cam^R	This study
pCA24N-BipA$_{H78Q}$	Point mutation to substitute H78 with glutamine, Cam^R	This study
pCA24N-BipA$_{T544_552del}$	CTD loop in frame truncation of 9 amino acids (amino acids T544 to D522), Cam^R	This study
pDS132	pCVD442 modified suicide plasmid, *pir* dependent, *sacB*, Cam^R	Philippe et al., 2004
pDS132-*bipA*	pDS132 carrying homologous arms (−552 to 7; 1,803 to +730) of *bipA*, *sacB*, and Cam^R	This study
pDS132-*spoT*	pDS132 carrying homologous arms (−529 to 2; 2,073 to +713) of *spoT*, *sacB*, and Cam^R	This study
pVIK111	Contains *lacZ* for translational fusion, Kan^R	Kalogeraki and Winans, 1997
pVIK111-*obgE*	pVIK111 carrying 3′ region (623–1,172) of *obgE*, in frame with *lacZ*, Kan^R	This study
pVIK111-*deaD*	pVIK111 carrying 3′ region (1,295–1,889) of *deaD*, in frame with *lacZ*, Kan^R	This study

shaking incubator at 200 RPM to $OD_{600} \approx 1.0$. The cultures were immediately cooled on ice before centrifugation at 4,500 RPM for 8 min at 4°C. The resulting cell pellets were resuspended in 1 ml TMT lysis buffer [100 mM tetraethylammonium bromide (TEAB) pH 8.5, 1 mM PMSF, 1% Triton X-100, and EDTA-free protease inhibitor cocktail]. Lysis was done using sonication for 5 min at 40% amplitude with pulses set at 5 s on followed by 5 s off. Lysates were incubated at 4°C on a rotator for 1 h and then clarified by centrifugation at 15,000 RPM for 45 min at 4°C. The clarified lysates were filtered through a 0.22-μm spin filter (Corning® Costar® Spin-X®) and sent to the Proteomic Core Facility of the Biological Research Center of Nanyang Technological University (Singapore) for TMT-MS services. The TMT-MS was done with technical triplicates.

β-Galactosidase Assay

The β-galactosidase assay was performed using 96-well microplates by referring to a reported work (Schaefer et al., 2016). The *obgE*:: pVIK111 and *deaD*:: pVIK111 strains were cultured in 10 ml LB at 25°C with shaking at 200 RPM. When the OD_{600} reached the value of 0.2, 0.5, and 1.0, 20 μl of the culture was collected and mixed with 80 μl permeabilization solution (100 mM Na_2HPO_4, 20 mM KCl, 2 mM $MgSO_4$, 0.04% sodium deoxycholate, 5 mM β-mercaptoethanol, and 1 mg/ml lysozyme) in a 96-well microplate (Nunc^{TM} MicroWell^{TM}, Thermo Scientific, Waltham, MA, United States). Permeabilizing samples were stored at 4°C until all the samples were prepared, and then, 25 μl of permeabilized samples were mixed with 150 μl of substrate solution (60 mM Na_2HPO_4, 40 mM NaH_2PO_4, 1 mg/ml ONPG, and 5 mM β-mercaptoethanol) in a 96-well microplate (Nunc^{TM} MicroWell^{TM}, Thermo Scientific, Waltham, MA, United States) and mixed well before loading the plate without its lid into the TECAN Spark^{TM} 10M multimode microplate reader. The OD_{420} absorbance was measured every 5 min for a total of 80 min incubation at 37°C. The settings for the OD_{420} absorbance measurement were 25 flashes and 120-ms wait time between wells. Biological triplicates were analyzed for all strains.

Purification of Pre-50S Particles

E. coli Δ*bipA* strain was cultured in large scale (six flasks of 800 ml LB) at 25°C with shaking at 200 RPM, until the $OD_{600} \approx 0.4–0.5$. The cultures were immediately cooled down on ice before centrifugation at 4,000 RPM for 15 min using

JLA-8.1000 rotor (Beckman Coulter, Brea, CA, United States). The resulting pellets were pooled and resuspended in 30 ml lysis buffer (20 mM HEPES pH 7.5, 10.5 mM MgOAc, 100 mM NH_4Cl, 0.5 mM EDTA pH 8.0, 6 mM β-ME, 20 U/ml DNase I, and 1 mg/ml lysozyme) and aliquoted into Eppendorf tubes to go through three rounds of freeze and thaw for cell lysis. The lysates were centrifuged at 14,500 RPM for 30 min at 4°C, and the supernatants were pooled. The supernatant was diluted using lysis buffer to a concentration of 80 A_{260} units in a final volume of 800 μl. Then, 10–25% (*w*/*w*) sucrose gradients were formed by mixing sucrose solution with overlay buffer (10 mM HEPES pH 7.5, 50 mM KCl, 10 mM NH_4Cl, 10.2 mM MgOAc, and 0.25 mM EDTA pH 8.0). Onto the sucrose gradients, 800 μl of samples were layered in 38.5-ml polyallomer open-top tubes (Beckman Coulter, Brea, CA, United States). The gradients were centrifuged at 19,000 RPM for 17.5 h ($\omega^2 t = 2.5 \times 10^{11}$ at 4°C) in SW 28 Ti rotor (Beckman Coulter, Brea, CA, United States). Ribosomal particles were analyzed by a density gradient fractionator system (Brandel, Gaithersburg, MD, United States) by continuous monitoring of A_{260} and to fractionate the samples. Fractions that corresponded to the peak between the 30S and 50S subunit peaks were collected and pooled. Pooled samples were split into 26-ml polycarbonate bottles with cap assembly (Beckman Coulter, Brea, CA, United States) and centrifuged at 43,000 RPM for a minimum of 19 h at 4°C in Ti70 rotors. The supernatant was discarded, and the resulting pellets were washed with 70S buffer (5 mM HEPES pH 7.5, 50 mM KCl, 10 mM NH_4Cl, and 10 mM MgOAc) twice to remove the sucrose. The pellets were resuspended in 1 ml of 70S buffer and stored at −80°C.

Purification of BipA

BipA was overexpressed from the plasmid pNIC28-Bsa-*bipA* in *E. coli* BL21 (DE3) and purified through three consecutive chromatography steps. Cells transformed with the plasmid were cultured large scale at 37°C until the $OD_{600} \approx 0.8$ and then overexpression was induced by adding isopropyl β-D-thiogalactoside (IPTG) to a final concentration of 125 μM. Culture temperature was reduced to 16°C upon IPTG induction for overnight incubation. Cells were harvested by centrifugation at 4,000 RPM for 15 min at 4°C. The resulting cell pellet was resuspended in 100 ml of lysis buffer [50 mM NaH_2PO_4 pH 8.0, 300 mM NaCl, 10% (*v*/*v*) glycerol, and 5 mM β-ME] and lysed using LM20 Microfluidizer® (Microfluidics™, Newton, MA, United States) with 20,000 PSI pressure. The lysate was clarified by centrifugation at 20,000 RPM for 1 h at 4°C using a JA-25.50 rotor, filtered through a 0.45-μm filter, and kept on ice before loading onto HisTrap® HP 5 ml Ni^{2+} column for affinity chromatography using ÄKTA Purifier (GE Healthcare Life Sciences, Marlborough, MA, United States). The column was then washed with two column volumes (CV) of lysis buffer. The elution was performed by gradually increasing the concentration of His elution buffer [50 mM NaH_2PO_4 pH 8.0, 300 mM NaCl, 10% (*v*/*v*) glycerol, 5 mM β-ME, and 500 mM imidazole). The fractions containing BipA as determined by sodium dodecyl sulfate–polyacrylamide gel electrophoresis (SDS-PAGE) were pooled and diluted with 25 mM Tris pH 8.0 buffer to a final concentration of 50 mM NaCl before loading onto HiTrap® Q Fastflow 5-ml column for anion exchange chromatography using ÄKTA Purifier. The column was then washed with two CVs of Q buffer A (25 mM Tris pH 8.0, 50 mM NaCl, and 5 mM β-ME). The elution was carried out by gradually increasing the concentration of Q buffer B (25 mM Tris pH 8.0, 1 M NaCl, and 5 mM β-ME). The fractions containing BipA as determined by SDS-PAGE were pooled and concentrated to a volume of 5 ml using Amicon® Ultra-15 Centrifugal Filter Units with 30-kDa cut-off membrane (MERCK, Darmstadt, Germany). A concentrated sample was loaded onto HiLoad® 16/60 Superdex® 200-pg column equilibrated with GF buffer (25 mM Tris pH 8.0, 100 mM NaCl, and 5 mM β-ME) for size exclusion chromatography using ÄKTA Explorer. The fractions containing BipA were pooled and concentrated to 13 mg/ml using Amicon® Ultra-15 Centrifugal Filter Units with 10-kDa cut-off membrane (MERCK, Darmstadt, Germany). The concentrated proteins were snap frozen using liquid nitrogen and stored at −80°C.

Ribosome Binding Assay

For at least 30 min on ice, 50 μl of BipA (13 mg/ml) in GF buffer was incubated with 100 μM GDPCP. For western blotting of polysome profiling fractions, 10 A_{260} units of Δ*bipA* cell lysate was prepared, and BipA pre-incubated with GDPCP was added five times in excess (10 A_{260} = 23.9 nM; BipA concentration = 1.195 μM) and incubated on ice for 1.5 h. The sample was layered onto 5%–45% sucrose gradient in overlay buffer (10 mM HEPES pH 7.5, 50 mM KCl, 10 mM NH_4Cl, 10.25 mM MgOAc, and 0.25 mM EDTA pH 8) in 13.2-ml thin-wall polypropylene tubes (Beckman Coulter, Brea, CA, United States) and centrifuged at 36,000 RPM for 1.5 h ($\omega^2 t = 7.6746 \times 10^{10}$) at 4°C using an SW 41 Ti rotor (Beckman Coulter, Brea, CA, United States). The gradients were fractionated by 10 drops per 1.5-ml Eppendorf tubes. Fractions were precipitated by adding 2.5 times sample volume of ice-cold 100% ethanol and one-tenth sample volume of 3 M NaOAc and incubation at −20°C overnight. The precipitated ribosomal samples were recovered by centrifuging the samples at 14,500 RPM for 30 min at 4°C, then air-dried before resuspending in 10 μl of RNase-free water. Recovered ribosomal samples were then loaded onto 10% polyacrylamide gel followed by semi-dry transfer onto nitrocellulose membrane. Recombinant BipA was detected by western blotting using 1:2,000 of HRP-conjugated anti-His_6 antibody (Santa Cruz Biotechnology, Dallas, TX, United States), and then, Clarity ECL western blotting substrates (Bio-Rad, Hercules, CA, United States) was applied before visualization using ChemiDoc™ (Bio-Rad, Hercules, CA, United States).

BipA binding was also analyzed by co-pelleting through sucrose cushion. Two separate samples were prepared on ice. Then, 50 μl of BipA (13 mg/ml) in GF buffer was incubated with 100 μM GDPCP for at least 30 min on ice. The sample with BipA pre-incubated with GDPCP only was prepared by mixing 1X Buffer G (5 mM HEPES pH 7.5, 50 mM KCl, 10 mM NH_4Cl, 10 mM MgOAc, and 6 mM β-ME) and 144 μM of

BipA pre-incubated with GDPCP and topped up to 50 μl with RNase-free water. The BipA pre-incubated with GDPCP complex with pre-50S particles was prepared by mixing 1X Buffer G with 144 μM of BipA pre-incubated with GDPCP and 24 OD_{260} units (0.576 μM) of pre-50S particles and then topped up to 50 μl with RNase-free water. Then, samples were layered onto 1.1 M sucrose in 1X Buffer G and centrifuged at 45,000 RPM in a TLA-100 rotor for 16 h at 4°C. Post-centrifugation, 1 μl of supernatant was aliquoted from each sample. The remaining supernatant was discarded, and the pellet was washed with 1X Buffer G three times to remove the sucrose. The pellets were then resuspended in 20 μl of 1X Buffer G. The RNA concentration of sample with BipA pre-incubated with GDPCP complex with pre-50S particles was measured using a NanoDrop 2000c spectrophotometer (Thermo Fisher Scientific, Waltham, MA, United States) and adjusted to 24 OD_{260} units using 1X Buffer G if dilution was required. Samples for PAGE were prepared by mixing 1 μl of the sample, 2.5 μl of 4X loading buffer, 1 μl of β-mercaptoethanol, and 5.5 μl of RNase-free water and incubated at 70°C for 10 min. Then, samples were loaded onto 4–12% NuPAGE Bis-Tris Gel (Invitrogen, Waltham, MA, United States) and run in 1X MES buffer at 200 V.

RESULTS

Deletion of Genomic *bipA* Gene Affects *E. coli* Growth at Suboptimal Temperature

While the growth defects of *E. coli* Δ*bipA* knock-out strains at suboptimal culturing temperature (mostly at 20°C) have been reported by several groups (Pfennig and Flower, 2001; Krishnan and Flower, 2008; Choudhury and Flower, 2015; Choi and Hwang, 2018), the phenotype is not well consistent and understood. For a better understanding of the importance of BipA in cold stress conditions, we first determined the growth curves of *E. coli* K12 strain (K12WT) and its corresponding *bipA* knock-out strain (Δ*bipA*), both harboring the empty pCA24N vector, under optimal (37°C, **Figure 1A**) and suboptimal (25°C, **Figure 1B**) temperatures. While the two strains demonstrated a similar growth rate at 37°C (**Figure 1A**), the Δ*bipA* strain revealed a notable growth retardation at 25°C, resulting from a significantly longer lag phase (**Figure 1B**). Further corroborating the role of BipA in cold stress is the finding that BipA expression from plasmid pCA24N-BipA could restore the growth of Δ*bipA* strain, albeit not entirely (**Figure 1B**). In line with a previous report (Choudhury and Flower, 2015), RluC deficiency (Δ*rluC*) can complement the growth defect of Δ*bipA* at 25°C (**Figure 1B**).

Next, we sought to investigate the effect of the loss of genes linked to bacterial stress response. Namely, we examined whether the growth defect is exacerbated if alarmone synthetase genes *relA* and *spoT* were deleted in the Δ*bipA* background. Our results showed that the double mutant strains (Δ*relA*/Δ*spoT*) demonstrated a slight growth defect compared to the wild type, whereas the growth curve was similar to *relA*/*spoT* knock-out in the Δ*bipA* background (triple mutations) (**Figure 1C**), implying that alarmone level perhaps has little influence on the growth of *E. coli* at suboptimal temperature.

GTP hydrolysis activity is important for trGTPase turnover on ribosome and in turn its physiological function through conformational change (Kumar et al., 2015; Ero et al., 2016). To study the significance of GTP hydrolysis for BipA functioning under sub-optimal growth temperature, mutations were introduced into the plasmid-borne *bipA* gene and subsequently transferred to the Δ*bipA* strain. We mutated the proposed catalytic residue histidine 78 to alanine (H78A) or glutamine (H78Q) to abolish the GTP hydrolysis, respectively, based on structure and sequence comparison of BipA with other trGTPases such as EF-G and EF-Tu (Scarano I, Krab et al., 1995; Gao et al., 2009; Schmeing et al., 2009; Koripella et al., 2015). In addition, the C-terminal loop (CTL) of BipA was truncated (T544_D552del) given that the CTL is believed to be essential for BipA binding with 70S ribosome (deLivron et al., 2009; Kumar et al., 2015). Growth complementation results showed that under an optimal growth condition (37°C), leaky expression of BipA mutants $BipA_{H78A}$, $BipA_{H78Q}$, and $BipA_{T544\_D552del}$ would have a negative effect on the growth of Δ*bipA* strain whereas the native BipA expression had no effect on cell growth (**Figure 1A**). In line with the role of GTP hydrolysis essential for BipA turnover, these findings likely suggest that the aforementioned mutations cause BipA turnover defects, resulting in the "trapped" ribosomes leading to decrease in translation and, ultimately, affecting cell growth. By being "trapped," the ribosomes would be prevented from carrying out its task due to the bound translational factors being unable to dissociate itself from the ribosome, similar to that in which EF-G was trapped by fusidic acid (Gao et al., 2009).

Interestingly, the growth defects that vary in magnitude were observed when the Δ*bipA* strains transformed with diverse *bipA* mutations were grown at suboptimal temperature of 25°C (**Figure 1D**). Namely, the growth complementation of Δ*bipA* strain by plasmid-borne BipA was not achieved for $BipA_{H78A}$, $BipA_{H78Q}$, and $BipA_{T544\_D552del}$ mutants, whereas BipA could completely restore the growth of Δ*bipA* strain (**Figure 1D**). In particular, the expression of $BipA_{H78A}$ and $BipA_{T544\_D552del}$ mutants resulted in further notable defects in Δ*bipA* strain at suboptimal conditions, suggesting that ribosome binding and GTP hydrolysis are crucial for the role of BipA in bacterial growth under cold shock stress.

Taken together, our results demonstrated that the elimination of alarmone synthesis by removing RSH proteins has a minute effect on cell growth of at low temperature, whereas the loss of *bipA* would cause a significant growth defect, which could be complemented or suppressed by pCA24N-BipA supplementation and genomic *rluC* deletion, respectively.

Loss of *bipA* Gene Causes Swimming Motility Defect in *E. coli* at Suboptimal Temperature

It was recently reported that *E. coli* with *bipA* deletion demonstrated motility defects while incubated at 20°C (Choi and Hwang, 2018). Hence, we would like to examine

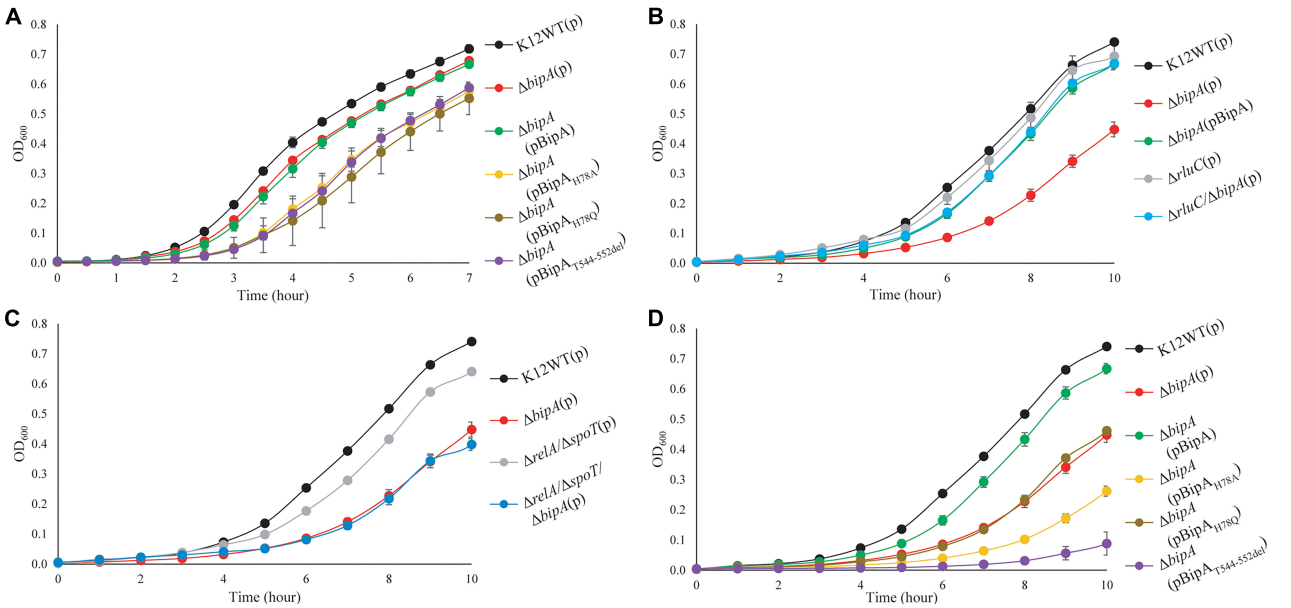

FIGURE 1 | Growth curves of *E. coli* wild-type, *bipA*-deficient, and complementation strains under optimal (37°C) and suboptimal (25°C) growth temperatures. **(A)** Growth curves at 37°C of *E. coli* with various BipA mutations. Under optimal condition, the strain Δ*bipA* did not present a significant growth defect, but the strains Δ*bipA* transformed with pCA24N-BipA variants presented a significant delay in growth. **(B)** Growth curves at 25°C of *E. coli* with deletions for *bipA* and/or *rluC*. Loss of *bipA* (Δ*bipA*) led to growth defect at 25°C, which can be complemented by the presence of BipA expression (pCA24N-BipA) or suppressed by genomic deletion of *rluC*. The complementation was judged by the growth curve progression of the diverse strains (Δ*bipA*, Δ*bipA* + pCA24N-BipA, Δ*rluC*, and Δ*bipA* + Δ*rluC*) in comparison to the wild-type strain (K12WT). **(C)** Growth curves at 25°C of *E. coli* with deletions for *bipA*, relA, and/or spoT. Deletion of both *relA* and *spoT* caused a slight growth delay but did not exacerbate the growth delay of Δ*bipA* in the triple knock-out strains. **(D)** Growth curves at 25°C of *E. coli* with various BipA mutations. The Δ*bipA* strain expressing pCA24N-BipA variants presented different growth curves at 25°C. The cells with $BipA_{H78Q}$ demonstrated the same growth rate as the strain Δ*bipA* (pCA24N), while preceding with $BipA_{H78A}$ that preceded with $BipA_{T544\_D552del}$. Note that biological triplicates were analyzed, and pCA24N without gene of interest was transformed into cells not harboring any plasmid so that all strains have the similar cellular burden of holding a plasmid. The "p" in the bracket alone or preceding "BipA" represents plasmid pCA24N.

the swimming motility of our *E. coli* strains using agar plate assay and incubation at room temperature, with the agar plate images after 24- and 48-h incubation shown (**Figures 2A,B**). The results of 24-h incubation demonstrated that the swimming motility was severely diminished for Δ*bipA* strain, and it could be complemented by plasmid harboring native *bipA* gene, but not the $bipA_{H78A}$, $bipA_{H78Q}$, and $bipA_{T544\_D552del}$ mutants (**Figure 2A**). Interestingly, all Δ*bipA* strains produced chemotactic rings after 48-h incubation (**Figure 2B**). Despite that the rings for the BipA mutants are notably smaller than those for the strains expressing BipA, the results clearly showed that swimming motility was not diminished, but rather reduced, for Δ*bipA* and the *bipA* mutants. Furthermore, Δ*bipA* strain expressing $BipA_{H78Q}$ produced significantly larger rings than Δ*bipA* strain expressing $BipA_{H78A}$ or $BipA_{T544\_D552del}$ after 48-h incubations (**Figure 2B**), which suggests that H78Q substitution retains BipA function to a certain extent, likely the ribosome binding and transition state stabilizing. In line with this hypothesis, Δ*bipA* (pCA24N-$BipA_{H78A}$) produced a significantly larger ring than Δ*bipA* (pCA24N-$BipA_{T544\_D552del}$) after 48-h incubation, indicating that the truncation of BipA CTL causes more severe motility defects for *E. coli* (**Figure 2B**), and note that BipA CTL is required for BipA binding to ribosome (deLivron et al., 2009; Kumar et al., 2015). On the other hand, while RluC-deficient (Δ*rluC*) strain behaved similarly to *E. coli* wild-type strain (K12WT), the Δ*rluC*/Δ*bipA* strain demonstrated significant suppression on the swimming defect of Δ*bipA* (**Figures 2A,B**); this revealed a functional link between BipA and RluC as previously reported (deLivron et al., 2009).

Agar plate assay alone does not provide sufficient evidence to conclude whether the chemotactic ring represents the swimming motility of the bacteria, given that the possible influence of cell growth on the ring formation cannot be completely ruled out. The rings observed on semi-solid agar might represent bacterial growth instead of swimming motility because all the strains except K12WT and Δ*bipA* (pCA24N-BipA) did not present the typical chemotactic rings where highly motile populations form an outer layer of the ring (Koster et al., 2012; Cremer et al., 2019; Liu et al., 2019). Furthermore, the cells might be defective in swimming and were tumbling, or the observations were restricted to semi-solid environment (Kinosita et al., 2020). Thus, inverted microscopy was employed to detect the diluted overnight cultures of K12WT, Δ*bipA*, Δ*bipA* (pCA24N-BipA), and Δ*rluC*/Δ*bipA* cells (**Supplementary Movies 1–4**), and these animated movies show that all four strains demonstrated swimming motility in liquid media. Taken together, strains with *bipA* yielded larger

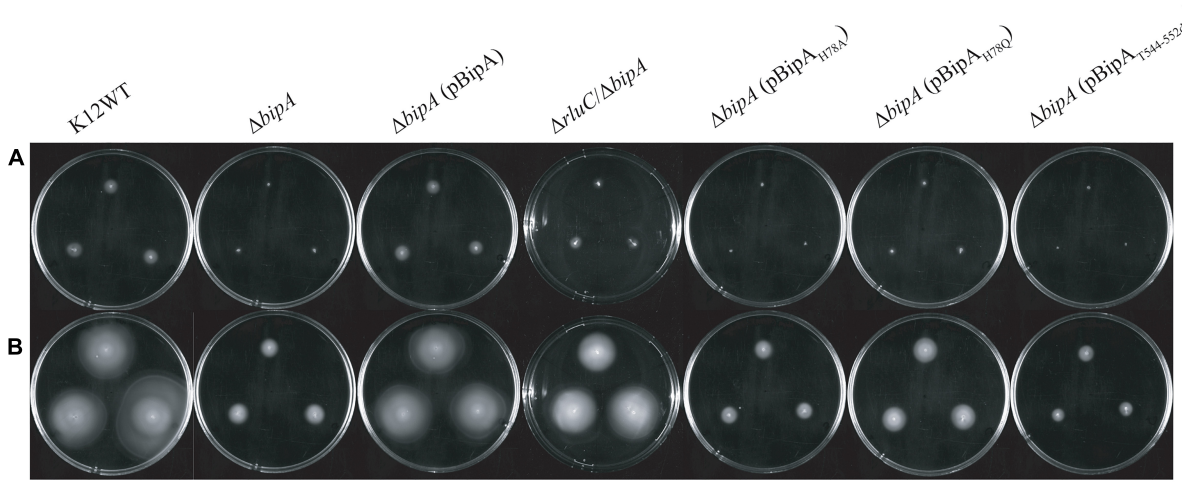

FIGURE 2 | The effect of BipA on swimming motilities of various strains of *E. coli* K12 BW25113 after **(A)** 24-h incubation and **(B)** 48-h incubation. The agar plate-based assay was employed, and it was assessed by the development of chemotactic ring. **(A)** After 24-h incubation at room temperature (suboptimal temperature), cells with *bipA* deletion showed no notable chemotactic rings except for cells with double mutations (Δ*rluC*/Δ*bipA*). Cells with the plasmid-borne BipA were compensated for the loss of genomic *bipA* and yielded chemotactic ring with similar size to the strain K12WT. The Δ*bipA* strains expressing BipA mutants also demonstrated the lack of chemotactic ring except for the strain Δ*bipA* (pCA24N-BipA$_{H78Q}$), which showed slight development of chemotactic ring as compared to the Δ*bipA* strain. **(B)** After 48-h incubation, all the strains developed chemotactic rings despite variations in size. The Δ*bipA* strain expressing BipA mutants presented significant increase in chemotactic ring size, where the strain Δ*bipA* (pCA24N-BipA$_{H78Q}$) yielded chemotactic ring larger than the strains Δ*bipA* (pCA24N-BipA$_{H78A}$ and pCA24N-BipA$_{T544_D552del}$). The "p" in the bracket alone or preceding "BipA" represents plasmid pCA24N.

chemotactic rings at room temperature, and deletion of *bipA* caused a significant delay in the appearance of chemotactic rings, which could be complemented by introducing functional BipA or suppressed by genomic deletion of *rluC*.

The Effect of BipA Mutations on the Defect of Ribosome Assembly

The loss of *bipA* had been found to cause ribosome assembly defect with the accumulation of pre-50S, which can be alleviated by expressing BipA from a plasmid or genomic deletion of *rluC* (Krishnan and Flower, 2008). Very recently, BipA has been implicated in ribosome (specifically large subunit) assembly at low temperature growth (Choi and Hwang, 2018; Gibbs et al., 2020). Here, we examine whether the *bipA*$_{H78A}$, *bipA*$_{H78Q}$, and *bipA*$_{T544\_D552del}$ mutants affect the complementation of ribosome assembly defect in the Δ*bipA* cells through sucrose gradient sedimentation analysis. As shown in **Figure 3A**, compared to the wild-type strain K12WT, *bipA* deficiency resulted in significantly reduced 70S ribosome and 50S subunit populations (**Figure 3A**), and simultaneously, a minor peak between the 30S and 50S peaks was observed, which is likely representing a population of pre-50S particles and is consistent with the previous results (Choi and Hwang, 2018; Gibbs et al., 2020). Similar to that presented by Gibbs et al. (2020), the pre-50S peak was not observed in the ribosomal particle distribution of Δ*bipA* expressing exogenous BipA (pCA24N-BipA), suggesting that BipA is involved in ribosome assembly, particularly in the maturation of the 50S subunit (**Figure 3A**). On the other hand, Δ*bipA* strain with *rluC* genomic deletion (Δ*rluC*/Δ*bipA*) yielded ribosomal particle distribution without a notable pre-50S peak, which differs from the previous study (Choudhury and Flower, 2015), and concurrent *rluC* deletion failed to fully compensate the ribosome assembly defect of *bipA* deficiency (**Figure 3A**). Note that all the strains demonstrated a similar profile of polysome level.

Comparisons among the Δ*bipA* strains expressing pCA24N-BipA mutants revealed very interesting results on the ribosomal particle distribution (**Figure 3B**). The expression of BipA$_{H78A}$ in the Δ*bipA* strain resulted in a very similar profile to that of the control (Δ*bipA* strain), suggesting that the H78A mutation might have rendered BipA non-functional (**Figure 3B**). In contrast, the ribosomal particle distribution of Δ*bipA* strain with the expression of BipA$_{T544_D552del}$ showed the lowest 70S and 50S peaks of all strains as well as an abnormal 30S peak, demonstrating the importance of intact CTL (**Figure 3B**). The relatively skewed 30S peak might be an accumulation of heterogeneous population of ribosomal subunits and likely includes the pre-50S particles; therefore, the lower 50S peak perhaps resulted from fewer 50S subunits matured in the strain Δ*bipA* (pCA24N-BipA$_{T544_D552del}$). The expression of BipA$_{H78Q}$ in the Δ*bipA* strain generated a medium level of compensation for BipA, demonstrated by the absence of pre-50S peak. In addition, the ribosomal particle distribution was significantly different from that of the Δ*bipA* (pCA24N-BipA$_{H78A}$) strain, but similar to that of the Δ*rluC*/Δ*bipA* strain, implying that H78Q substitution of BipA might have retained the function of BipA to a certain degree (**Figures 3B,C**). As *rluC* deletion is known to compensate the loss of BipA, the similarity in complementation would therefore support the notion that glutamine is able to partially substitute histidine as the catalytic residue of BipA GTPase activity (Koripella et al., 2015).

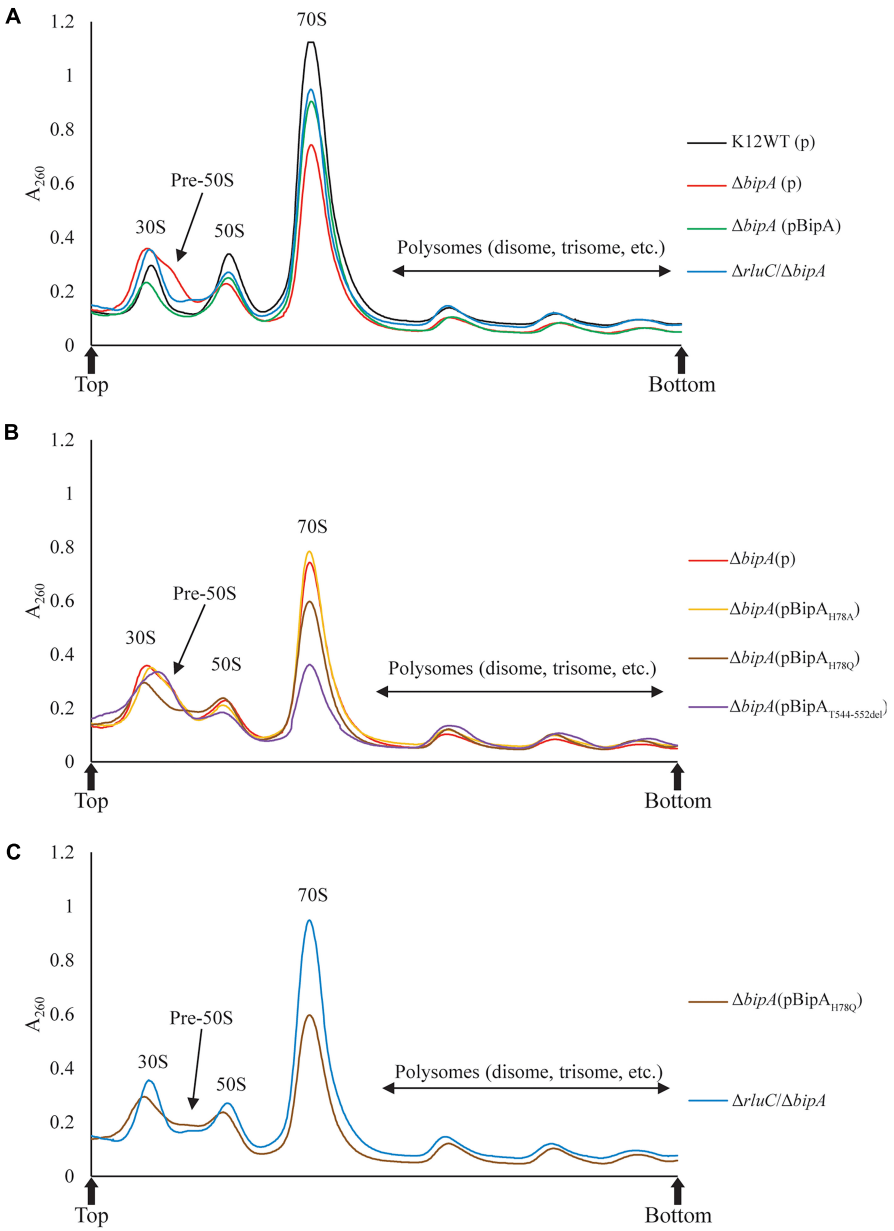

FIGURE 3 | Ribosomal particle distribution showing ribosome assembly defects caused by *bipA* deletion and BipA mutants. Peaks corresponding to polysomes, 70S ribosome, and free subunits are indicated. **(A)** Using K12WT (black) as a reference, Δ*bipA* (red) presented accumulation of ribosomal subunits and reduction of 50S and 70S ribosomal particles, deduced from the higher 30S peak and lower 50S and 70S peaks, respectively. The pre-50S peak appeared as a minor peak between 30S and 50S peaks in Δ*bipA* ribosomal particle distribution. Although with a lower 70S peak, the profile of Δ*bipA* (pCA24N-BipA) (green) was similar to K12WT. The Δ*rluC*/Δ*bipA* (blue) yielded similar 50S and 70S peaks as K12WT, but similar 30S peak as Δ*bipA*. Notably, the region between the peak of 30S and 50S subunits was slightly elevated indicating maturing pre-50S. **(B)** The Δ*bipA* (pCA24N-BipA$_{H78A}$) (yellow) yielded almost identical ribosomal particle distribution as Δ*bipA*. While Δ*bipA* (pCA24N-BipA$_{H78Q}$) (brown) had lesser 70S ribosome, the pre-50S peak was not visible. The Δ*bipA* (pCA24N-BipA$_{T544_D552del}$) (purple) produced the least 70S and 50S particles with a skewed 30S peak, which may include a large population of pre-50S particles. **(C)** A comparison between sucrose gradient profiles of the strains Δ*rluC*/Δ*bipA* and Δ*bipA* (pCA24N-BipA$_{H78Q}$). The data showed similarity in terms of reduced pre-50S with elevated area under the peak between 30S and 50S peaks, likely representing a population of pre-50S that had mature further than what was seen in Δ*bipA*. The "p" in the bracket alone or preceding "BipA" represents plasmid pCA24N. Peaks corresponding to subunits (30S, pre-50S, and 50S), monosomes (70S), and polysomes are indicated. Top and bottom of each gradient are marked with arrows.

Taken together, ribosome assembly defect caused by the loss of endogenous BipA could be partially complemented by introducing BipA and the mutant BipA$_{H78Q}$ or suppressed by genomic *rluC* deletion, but not the BipA$_{H78A}$ and BipA$_{T544_D552del}$, demonstrating varied and complicated effects of GTP hydrolysis and ribosome

binding (e.g., CTL) of BipA in ribosome assembly at low temperature.

Loss of *bipA* Resulted in Upregulation of Proteins Involved in RNA Metabolism

TMT is an isobaric mass tag-based multiplexed quantitative proteomics method by mass spectrometry (Thompson et al., 2003). Tryptic peptides from different samples are labeled with different isobaric tags for accurate relative quantitation of protein expression across the samples. Using tandem mass spectrometry, proteins can be identified by the fragment ions of peptides, and their expression levels quantitated with reported ion intensities. Next, we sought to further investigate the effect of BipA on protein expression and the rationale behind the suppression of Δ*bipA* phenotypes by genomic deletion of *rluC* for cells under suboptimal temperature with TMT approach. Volcano plots of the TMT proteomic datasets were used to determine significant changes in protein expression between different conditions. The cut-off for fold change (FC) with statistical significance ($p < 0.05$) was determined to be 1.5 ($\log_2$ abundance ratio = 0.585). Differentially expressed proteins were shortlisted for further data analysis and interpretation (**Supplementary Tables 2–7**). The data was reliable as validated by the protein expression level of the deleted genes.

As compared to wild-type strain K12WT, several proteins demonstrated higher expression level in the Δ*bipA* strain in response to cold stress (**Figure 4A**). Particular attention was drawn to two proteins DeaD and ObgE given that both have been implicated in 50S subunit biogenesis (Charollais et al., 2004; Sato et al., 2005). Other proteins, with significantly higher expression level in Δ*bipA* but not implicated in ribosome assembly, include CspA, RNase R, and RpoS. In contrast, by introducing BipA (pCA24N-BipA) to the Δ*bipA* strain, the expression levels of DeaD, ObgE, CspA, RNase R, and RpoS become similar to those in the strain K12WT (**Figure 4B**). Furthermore, a comparison of expression levels of these five proteins in the Δ*bipA* (pCA24N-BipA) and Δ*bipA* strains showed lower levels for the former (**Figure 4C**). In addition, the proteins relevant to cell motility were found significantly upregulated while the Δ*bipA* strains express exogenous BipA (pCA24N-BipA) (**Figures 4B,C** and **Supplementary Tables 3, 4**), suggesting that BipA has a direct or indirect influence on bacterial motility. Notably, upregulation of these proteins also rationalized our motility assay for the role of BipA, as observed in **Figure 2**.

Furthermore, the expression levels of these proteins (except for RpoS) in the Δ*rluC*/Δ*bipA* double mutant strain were similar to those in the strain K12WT, within cut-off value for different expression level (**Figure 4D**). In the case of RpoS, it was significantly upregulated in the Δ*rluC* strain as compared to the strain K12WT (**Figure 4E**), implying that *rluC* genomic deletion would affect RpoS expression and thereby leading to an additional effect in the Δ*rluC*/Δ*bipA* strain. A comparison of protein expression level of the Δ*rluC*/Δ*bipA* strain with that of the Δ*bipA* strain also revealed significantly lower levels of DeaD, ObgE, and CspA (**Figure 4F**). Notably, the expression level of RNase R in the Δ*rluC*/Δ*bipA* strain was about 0.7 times lower than that in the Δ*bipA* strain with high statistical significance ($\log_2$ abundance ratio = 0.432), indicating that RNase R was indeed downregulated in Δ*rluC*/Δ*bipA*, but did not meet the FC cut-off. These observations together demonstrated that the upregulation of the aforementioned proteins likely was ascribed to compensation of the *bipA* loss in *E. coli* when cultured at suboptimal temperature.

Interestingly, the upregulation of GrcA, a stress-induced alternate pyruvate formate-lyase subunit, was observed in Δ*rluC* strains. The mRNA of GrcA can be cleaved by MazF, leading to leaderless mRNA with anti-Shine–Dalgarno sequence removed; therefore, the resultant mRNA is favorably translated by a ribosome (Vesper et al., 2011). The significance of GrcA in bacterial stress and cold shock response remains poorly understood, but it is of interest for further study.

Ribosome Maturation Factor DeaD Is Upregulated in Δ*bipA* Strain at Suboptimal Growth Temperature

To further validate the upregulation of 50S biogenesis factors detected by TMT-MS, β-galactosidase reporter assay was employed. The *lacZ* gene was inserted downstream of the target gene in the genome, and its activity (β-galactosidase activity) could be easily measured. Therefore, a fusion design (target gene–*lacZ*) with the stop codon of the target gene excluded can be used to assess the expression level of this target protein based on the output of the β-galactosidase (LacZ) activity. In our case, the β-galactosidase activity was used to reflect the expression level of the fused DeaD (DeaD–LacZ) protein, which would be consequently used to validate our observation by TMT-MS.

Upon the *bipA* deletion (Δ*bipA*), the β-galactosidase activity was dramatically increased for all tests at OD_{600} ∼0.2, ∼0.5, and ∼1.0, demonstrating DeaD was highly expressed (**Figures 5A–C**). However, with further deletion of the gene *rluC* (Δ*rluC*/Δ*bipA*), the elevated β-galactosidase activity was reduced, almost to the level of the wild-type strain K12WT. Similarly, exogenous expression of BipA in its deletion strain (Δ*bipA* + pCA24N-BipA) was also able to complement the effect of *bipA* deletion on DeaD expression. Collectively, DeaD–LacZ activities for the three strains (K12WT, Δ*bipA* + pCA24N-BipA, and Δ*rluC*/Δ*bipA*) show similar time course, but lower than that for the *bipA* deletion strain (Δ*bipA*), suggesting that upregulation of DeaD was triggered by *bipA* deletion, which can be complemented or suppressed by overexpressing BipA or *rluC* genomic deletion, respectively. These data are in line with the expression changes in DeaD detected by TMT-MS and are in support of upregulated RNA helicase DeaD, which likely plays an important role in ribosome assembly at low temperature upon the loss of *bipA*. However, the precise and detailed mechanism remains unknown.

BipA Binds Pre-50S Ribosomal Subunit and 70S Ribosome *in vitro*

We next tested whether BipA can bind pre-50S particle for its proposed function as 50S maturation factor through *in vitro* reconstitution. First, we mixed the purified BipA, which was pre-incubated with GDPCP with clarified lysate of the Δ*bipA*

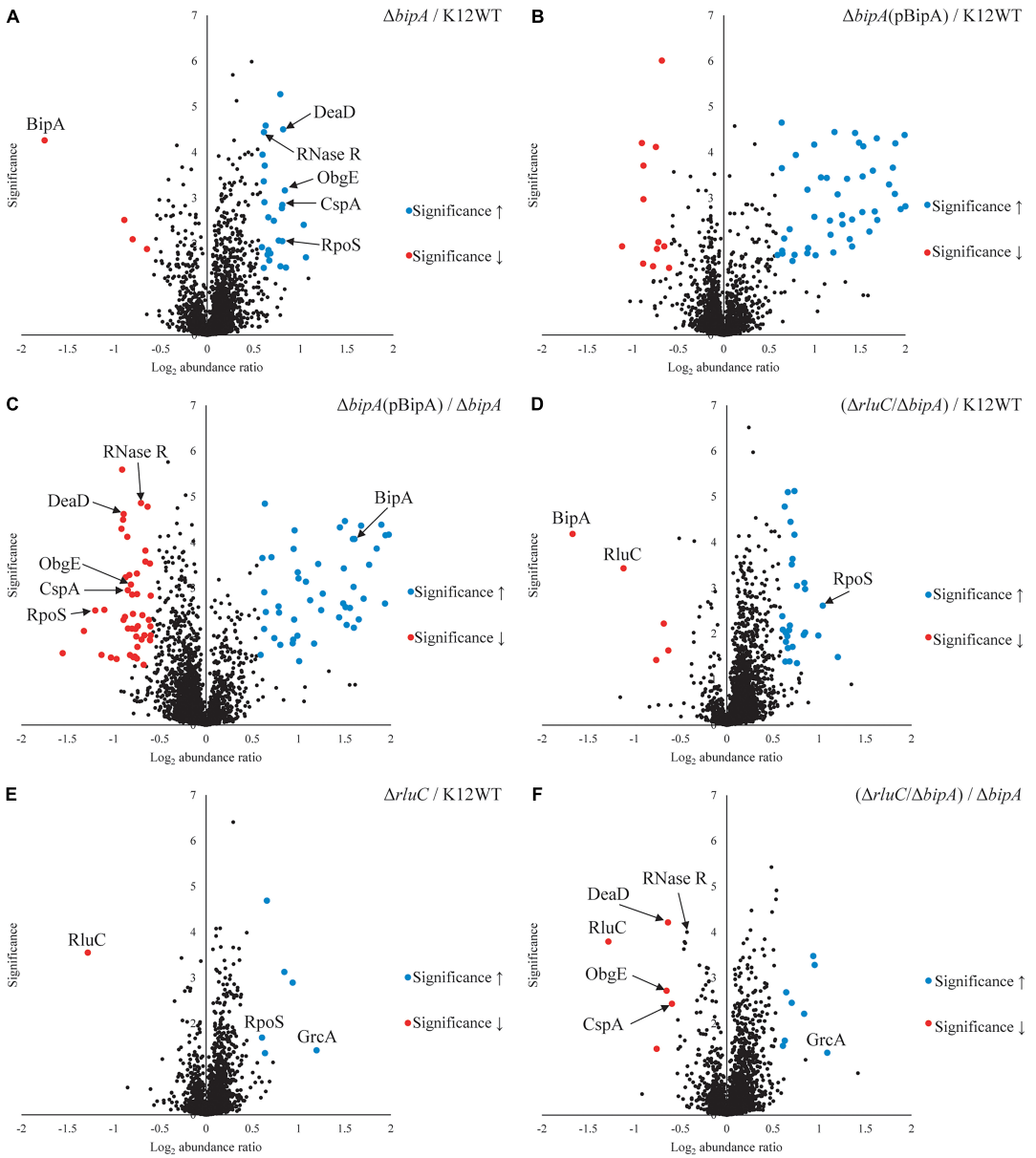

FIGURE 4 | Tandem mass tag-mass spectrometry (TMT-MS) analysis of various strains of *E. coli* K12 BW25113. A TMT-based quantitative proteomic method was used to determine differential protein expression under suboptimal cell culture condition between wild-type, Δ*bipA* (pCA24N-BipA), and ΔrluC/Δ*bipA* strains. **(A)** A volcano plot showing protein expression level of the strain Δ*bipA* against the strain K12WT. The *bipA* was indeed deleted based on significantly low $\log_2$ FC. The five proteins DeaD, ObgE, RpoS, CspA, and RNase R yielded significantly higher reads in the strain Δ*bipA* than the strain K12WT. **(B)** The expression levels of DeaD, ObgE, RpoS, CspA, and RNase R proteins were not changed between K12WT and Δ*bipA* (pCA24N-BipA) strain. **(C)** Comparison of Δ*bipA* (pCA24N-BipA) against Δ*bipA*. We put DeaD, ObgE, RpoS, CspA, and RNase R in the negative $\log_2$ abundance ratio side of the plot, meaning peptide reads of the proteins were lesser in the presence of pCA24N-BipA. The blue dot labeled as BipA was an indication that BipA was indeed expressed. **(D)** The *rluC* deletion in Δ*bipA* background produced a volcano plot similar to **(A)**, but the DeaD, ObgE, CspA, and RNase R were close to K12WT as differential expressions against K12WT were not detected. As in **(A,D)**, higher readout of RpoS was detected in Δ*rluC*/Δ*bipA*. Red dots labeled with BipA and RluC showed that these *bipA* and *rluC* were indeed deleted. **(E)** Genomic deletion of *rluC* only yielded six differentially expressed proteins relative to K12WT, and out of which, two interesting changes were RpoS and GrcA upregulations. The significant negative $\log_2$ abundance ratio of RluC indicates that the gene was indeed removed. **(F)** Comparisons between Δ*rluC*/Δ*bipA* and Δ*bipA* showed a reduced expression level of the DeaD, ObgE, and CspA to wild-type level. The RNase R readout was found to be reduced by the loss of *rluC*, close to the cut-off for FC. The pBipA refers to pCA24N-BipA.

cells followed by sucrose gradient centrifugation and ribosome fractionation, and subsequently, western blot was employed to detect BipA. Our data clearly showed that BipA is able to co-sediment with both large and small ribosomal units, as well as the pre-50S ribosomal unit (**Figure 6A**). BipA could bind to even small ribosomal unit 30S, perhaps through its β-barrel domain

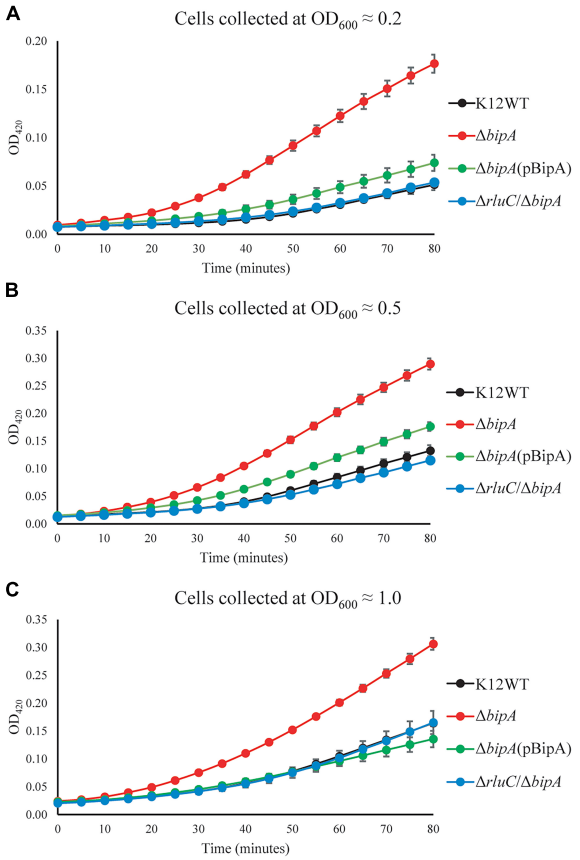

FIGURE 5 | β-galactosidase activity assays demonstrated the upregulation of DeaD in the strain Δ*bipA*. The cells were harvested at $OD_{600} \approx 0.2$ **(A)**, 0.5 **(B)**, and 1.0 **(C)**, respectively, and the activity was assessed by measuring the breakdown of ONPG through recording OD_{420}. Δ*bipA* cells (red) harvested at all three OD_{600} presented the highest β-galactosidase activity, indicated by the significantly stronger OD_{420} absorbance over time as compared to K12WT (black), Δ*bipA* (pCA24N-BipA) (green), and Δ*rluC*/Δ*bipA* (blue). The pBipA refers to pCA24N-BipA.

II, implying a yet unknown function in bacterial translational machinery ribosome (**Figure 6A**). Second, we combined BipA pre-incubated with GDPCP and purified pre-50S population of Δ*bipA* strain, layered on top of 1.1 M sucrose cushion and performed high-speed centrifuge to find out if BipA would co-sediment with pre-50S. As shown in **Figure 6B**, the results clearly demonstrated that BipA was indeed co-sedimented with pre-50S, corroborating that BipA is capable of binding to the pre-50S ribosomal particle.

DISCUSSION

GTP Hydrolysis and CTL of BipA Are Crucial for 50S Biogenesis at Low Temperature

The highly conserved *bipA* gene has been shown to be significant for bacterial growth and ribosome assembly at suboptimal temperature (Choudhury and Flower, 2015; Ero et al., 2016; Choi and Hwang, 2018; Gibbs et al., 2020). Here, we report that *bipA* deletion and mutagenesis significantly affect *E. coli* swimming motility (**Figure 2**). The experiment was carried out at room temperature (suboptimal for *E. coli* growth) and revealed that the swimming defect of the Δ*bipA* strain can be complemented or suppressed by the expression of plasmid-borne BipA (pCA24N-BipA) or the concurrent deletion of *rluC* gene (Δ*rluC*/Δ*bipA*), respectively (**Figure 2**). The possible reason for this phenotype might be the decelerated global translation due to retardation of ribosome biogenesis, which subsequently shuts down energy-costly pathways, one of which involves the cell motility (Ottemann and Miller, 1997; Martínez-García et al., 2014). The observations of agar plate assay for these mutations correlate with the change of growth trend that can be seen in growth curves (**Figure 1**) as well as with ribosomal particle distribution observed in **Figure 3**, suggesting that the loss of *bipA* leads to a condition affecting growth, motility, ribosome assembly, and protein translation. Indeed, the ribosome assembly defect likely slows down protein translation as the concentrations of 70S ribosomes and polysomes are decreased (Peil et al., 2008; Gibbs et al., 2020). This retardation in protein translation then negatively affects the downstream processes including bacterial growth and motility (Rudra and Warner, 2004).

In this work, we showed that the phenotypes presented by the *bipA* deletion (Δ*bipA*) could be complemented by pCA24N-BipA or suppressed by *rluC* genomic deletion, suggesting that BipA is important for *E. coli* to thrive at suboptimal temperature, and pseudouridylation on the correct nucleotides (such as RluC involving U955, U2504, and U2580 of 23S rRNA) can be helpful for ribosome biogenesis in *E. coli* and therefore growth as well as motility. While there is no reported relation to bacterial motility, Choudhury and Flower (2015) proposed that suboptimal temperature caused the ribosome to be dependent on BipA for efficient assembly, and loss of 23S rRNA modification by RluC actually led to an alternative folding pathway that is BipA independent. This further suggests that the improvement of Δ*bipA* swimming is perhaps not motility regulation related. The unexpected appearance of the chemotactic rings for the strains Δ*bipA* and Δ*bipA* with plasmid-expressing BipA mutants after 48-h incubation suggests that the loss of *bipA* did not diminish swimming motility. Instead, the swimming was delayed probably due to the decreased rate of protein translation and cell growth caused by ribosome assembly defect. This is supported by the microscopy visualization of the bacteria cells grown overnight in liquid culture demonstrating their swimming motility (**Supplementary Movies 1–4**).

In this study, the plasmid-borne BipA, with H78A or H78Q mutation (catalytic residue H78) or CTL truncation (T544_D552del), was transformed into the Δ*bipA* strain to examine its effect on complementation for BipA, respectively. The rationale behind the mutations was based on previous mutagenesis studies on catalytic histidine of EF-Tu and EF-G (H84 and H91, respectively) and structural study where the CTL interacts directly with the A-loop of 50S subunit (**Supplementary Figure 11**). The H84Q substitution in EF-Tu showed a reduction

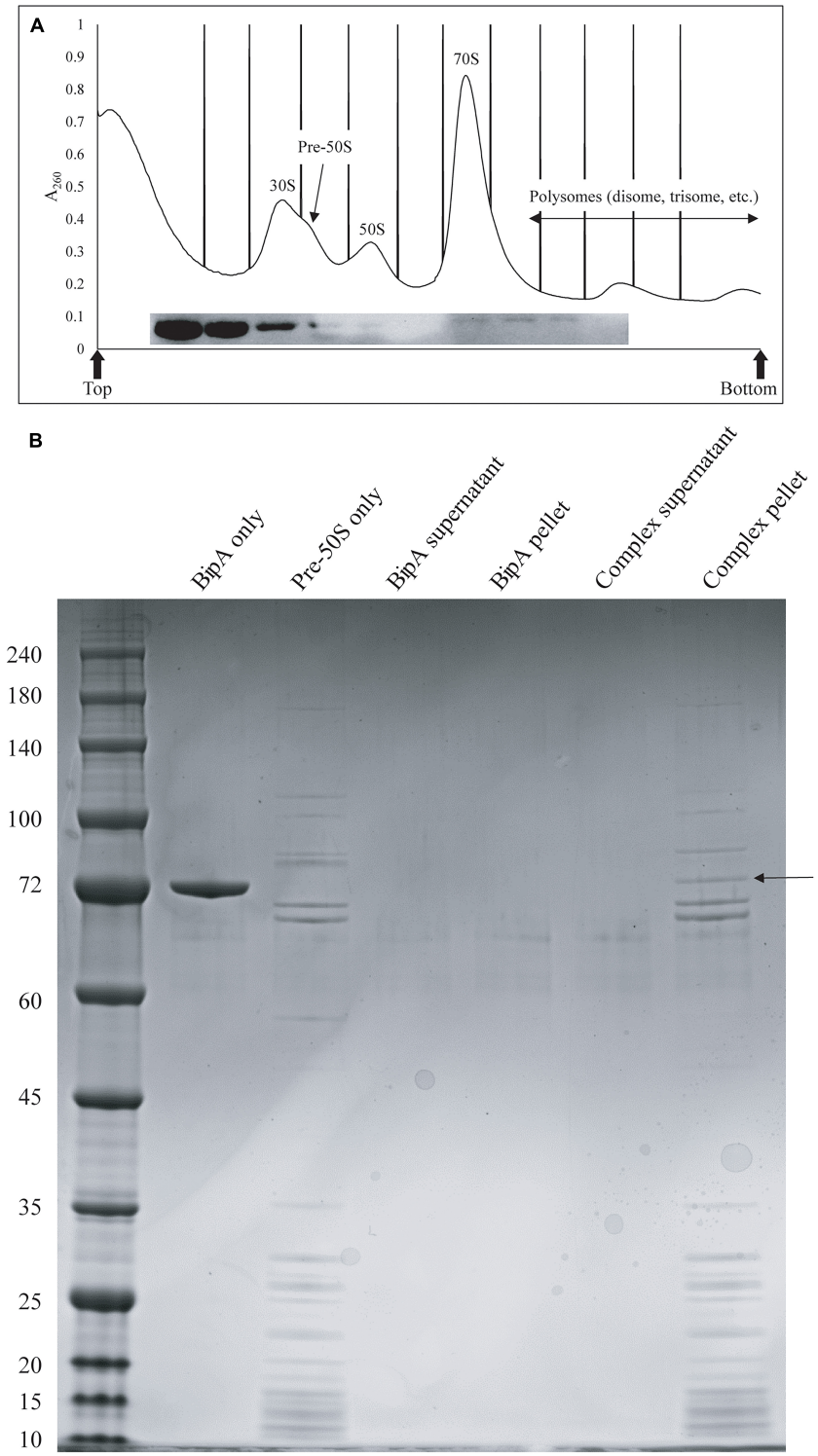

FIGURE 6 | *In vitro* binding assays showed that BipA pre-incubated with 5X excess GDPCP bound to various ribosomal particles including pre-50S particles. **(A)** Ribosomal particle distribution of *in vitro* reconstitution of BipA-GDPCP with ribosomal particles. By analyzing the fractions from ribosomal particle distribution using western blot, most of the BipA pre-incubated with GDPCP were detected in the junk fractions before 30S peak, and the band intensity decreased from 30S toward polysomes. Peaks corresponding to subunits (30S, pre-50S, and 50S), monosomes (70S), and polysomes are indicated. Top and bottom of each gradient are marked with arrows. **(B)** SDS-PAGE check of ribosome fractions from **(A)**. BipA interaction with pre-50S was observed based on the presence of co-pelleting through sucrose cushion using ultracentrifugation. The band representing co-pelleted BipA is indicated by the black arrow in the "Complex pellet" lane, which consists of pelleted BipA pre-incubated with GDPCP-bound ribosome complex, suggesting that binding occurs.

of GTP hydrolysis by 35%, and H84A abolished the GTPase activity (Scarano I, Krab et al., 1995), while the activity of ribosome-associated GTP hydrolysis of EF-G with H91Q substitution was comparable to native protein, and it was found to be defective in organic phosphate release (Koripella et al., 2015). The finding that the expression of $BipA_{H78A}$ did not restore the ribosomal particle distribution as did the wild-type BipA was also observed in a recently published study where the expression of $BipA_{H78A}$ led to slow growth for both WT and Δ*bipA* strains (Gibbs et al., 2020). On the other hand, Gibbs et al. (2020) expressed suspicion that $BipA_{H78A}$ is able to bind 70S ribosome but is unable to facilitate GTP hydrolysis as well as the subsequent factor release, which ultimately led to halt in translation. The $BipA_{H78Q}$ presented interesting outcomes that could be summarized in three points: (1) similar growth curve as Δ*bipA* at suboptimal temperature despite longer lag phase at optimum condition (**Figures 1C,D**); (2) shorter lag phase than Δ*bipA* (pCA24N-$BipA_{H78A}$) and Δ*bipA* (pCA24N-$BipA_{T544\_D552del}$) at suboptimal temperature (**Figure 1D**); (3) similar ribosomal particle distribution as Δ*rluC*/Δ*bipA*, albeit with significantly fewer 70S ribosomal particles (**Figure 3C**). Based on the aforementioned examples of H84Q and H91Q, glutamine substitution might have rendered BipA less efficient in GTP hydrolysis and/or organic phosphate release (Scarano I, Krab et al., 1995; Koripella et al., 2015), leading to the retention on 70S ribosome for longer period of time and negatively impacting the assembly efficiency. Interestingly, $BipA_{T544\_D552del}$ seemed to have an inhibitory effect on *E. coli* growth and ribosome assembly at suboptimal temperature as deduced from the exacerbated growth defect as compared with the strain Δ*bipA* (**Figure 1D**) and lesser 50S and 70S observed in ribosomal particle distribution (**Figure 3B**). Kumar et al. (2015) reported that the region L543-E553 of CTL projects deep into the peptidyl transferase center (PTC), while the region N536-K542 is critical for ribosome binding. Therefore, the truncation of T544-D552 could potentially play a role in BipA association and function by establishing direct contact with the A-loop of 23S rRNA (**Supplementary Figure 11**). This corroborates with the study by deLivron et al. (2009) revealing that alanine substitutions of amino acids within the CTL hinder the binding of BipA to the 70S ribosome.

Collectively, growth curves, ribosomal particle distribution, and swimming motility assays demonstrated a correlation whereby the defect in ribosome assembly at suboptimal temperature leads to a delay in growth and swimming motility (Pfennig and Flower, 2001; Choudhury and Flower, 2015; Choi and Hwang, 2018). Perhaps, BipA is a ribosome biogenesis factor that is crucial for ribosome biogenesis at suboptimal temperature, as a previously reported role for BipA is incorporating the ribosomal protein L6 into the 50S ribosome (Choi and Hwang, 2018). In the recent study by Gibbs et al. (2020), structural block 3 of 50S ribosomal subunit demonstrated a growth condition-dependent assembly, including suboptimal temperature. While it was not evident that BipA has a direct role in delaying block 3 folding, the loss of *bipA* led to the accumulation of pre-50S without ribosomal protein L17, an r-protein associated with block 3 (Gibbs et al., 2020).

Loss of *bipA* Leads to Upregulation of RNA Metabolism

TMT-MS revealed a significant upregulation of a number of proteins involved in RNA metabolism and chaperoning in the Δ*bipA* strain, but with expression comparable to the wild-type level in the strains Δ*bipA* (pCA24N-BipA) and Δ*rluC*/Δ*bipA*. Contrary to pCA24N-BipA complementation, the Δ*rluC*/Δ*bipA* strain presented an expression of majority of the proteins at above wild-type level while it suppressed Δ*bipA* phenotypes. Furthermore, the findings from TMT-MS seem to correlate with growth curve, ribosomal particle distribution, and swimming motility assays in a sense that significant changes observed in Δ*bipA* were found to be reversed in complementation strains. Furthermore, the proteins with significant changes in expression in the Δ*bipA* strains were involved in ribosome assembly, stress response, and growth. In particular, the expression of DeaD, ObgE, CspA, and RNase R was increased in the Δ*bipA* strain, but decreased in the complementation strains, indicating their involvement in the phenotypes of the Δ*bipA* strain. On the other hand, the expression of RpoS was higher in the absence of BipA expression as compared to K12WT, including the Δ*rluC*/Δ*bipA* strain. This observation can be explained as the influence of *rluC* deletion given that the RpoS in the Δ*rluC* strain was presented

TABLE 2 | Tabulated data adapted from Gibbs and Fredrick (2018), referring to proteins involved in ribosome assembly in *E. coli*; ObgE is included.

Assembly factor	Type	Ribosomal subunit involved
RbfA	**RNP**	**30S**
RimJ	RNP	30S
RimM	RNP	30S
RimP	RNP	30S
YhbY	**RNP**	**50S**
KsgA	**Modification enzyme**	**30S**
RsmC	Modification enzyme	30S
RlmA	Modification enzyme	50S
RlmE	Modification enzyme	50S
RluB	Modification enzyme	50S
RluC	Modification enzyme	50S
RluD	Modification enzyme	50S
DeaD	**Helicase**	**50S**
DbpA	**Helicase**	**50S**
SrmB	**Helicase**	**50S**
RhlE	Helicase	50S
DnaK/DnaJ/GrpE	Chaperone	30S, 50S
GroES/GroEL	Chaperone	50S
Era	**GTPase**	**30S**
RsgA	GTPase	30S
LepA	GTPase	30S
Der	**GTPase**	**50S**
YihA	GTPase	50S
ObgE	**GTPase**	**50S**
BipA	**GTPase**	**50S**

Ten out of 24 proteins have previously been reported to play a role in cold sensitivity when deleted or mutated (bold).

higher than the wild-type level, and thus, an additive effect of RpoS reads would be observed in the strain Δ*rluC*/Δ*bipA*. To date, no relationship between RluC and RpoS has been reported according to our knowledge, and it is an intriguing topic for further studies. Note that an increased sensitivity to several antibiotics caused by the inactivation of *rluC* has been reported (Murakami et al., 2005; Toh and Mankin, 2008). This is not surprising as the pseudouridines synthesized by RluC are situated in PTC (U955, U2504, and U2580) where a number of antibiotics bind; hence, the rluC deletion increased the antibiotic susceptibility, and *rpoS* could be upregulated as a stress response in the Δ*rluC* strain (Conrad et al., 1998).

Out of the five aforementioned proteins, DeaD and ObgE have been implicated in the biogenesis of ribosome large subunit, suggesting their upregulations may have a functional relationship with BipA *in vivo*. Similar to BipA, DeaD has been found to be associated with pre-50S particles (Charollais et al., 2004). DeaD has a role in rRNA structural rearrangement using its helicase activity, which aids in 50S biogenesis at low temperature (Charollais et al., 2004). Charollais et al. (2004) also demonstrated that the overexpression of DeaD was able to complement the growth defect of Δ*srmB* at low temperature. The finding that the DEAD-box RNA helicase SrmB facilitates 50S biogenesis during early maturation phase (Charollais et al., 2003) suggests an overlap of functions between DeaD and SrmB (Charollais et al., 2004). Such overlapping functions could be possible with BipA and DeaD as well, since both strains Δ*deaD* and Δ*bipA* showed accumulation of pre-50S, and Δ*deaD*/Δ*bipA* double knock-out produced an additive effect (Choudhury and Flower, 2015). From the study by Kitahara and Suzuki (2009), DeaD was shown to be likely to contribute to efficient assembly of circularly permuted rRNAs, implying that the cell would lose the ability to assemble rRNAs with scrambled domains in the absence of DeaD. This finding could be linked to a recent hypothesis on "limited parallel processing" of rRNA and serve as an explanation for the upregulation of DeaD upon the *bipA* deletion (Δ*bipA*), which is likely to be a strategy for *E. coli* to cope with the loss of *bipA* at suboptimal temperature (Davis et al., 2016). Davis et al. (2016) found that ribosome assembly is dynamic after observing pre-50S from L17-deficient cells mature into the 50S albeit at a slower rate, which the author considered a "limited parallel processing" (Davis et al., 2016). Such behavior confers the bacteria the flexibility in ribosome assembly should there be any factors that are undesirable for ribosome assembly. In addition, Davis et al. (2016) also found that 23S rRNA matures in the form of cooperative folding blocks, whereby different regions of 23S rRNA mature independently in parallel and come into contact with each other to form the tertiary structure. Collectively, their results indicate that ribosome maturation and assembly can occur in multiple pathways, demonstrating the flexibility of bacterial ribosome assembly when there is a bottleneck caused by the shortage of assembly factors or r-proteins.

The importance of RNA secondary structure destabilization at low temperature was demonstrated by Awano et al. (2007), where they presented the growth defect of Δ*deaD* at 15°C being complemented by the overexpression of CspA. The CspA is an RNA chaperone that is able to destabilize RNA secondary structure at low temperature with low substrate specificity (Phadtare, 2011). In addition, RNase R, the only 3′–5′ exonuclease in *E. coli*, is also able to complement the cold sensitivity of Δ*deaD*, indicating their tight relationship during cold shock (Awano et al., 2010). The RNase R consists of a helicase and an RNase domain that function independently, and its mutant with only helicase activity was able to complement the cold sensitivity of Δ*deaD*, revealing that the helicase activity was the key during cold shock (Awano et al., 2007). Notably, upregulation of RNase R by at least sevenfold is observed during cold shock in *E. coli* (Cairrão et al., 2003; Guan et al., 2005). Hence, the upregulation of DeaD, CspA, and RNase R in Δ*bipA* is probably an attempt by the cell to compensate the loss of BipA during 50S biogenesis in which BipA plays a yet unknown role.

In addition to the evidence presented in our work for BipA, the loss of various ribosome assembly factors results in the development of the common phenotype of cold sensitivity coupled with ribosome assembly defect. As summarized in **Table 2**, 10 out of 24 proteins have previously been reported to play a role in cold sensitivity when deleted or mutated (bold), and several others demonstrated involvement in cold shock. As shown in this study, the deletion of RluC suppresses the cold sensitivity of Δ*bipA*; the overexpression and deletion of RhlE complement the cold sensitivity of Δ*deaD* and Δ*srmB*, respectively (Jain, 2008); and LepA is released from the membrane during stress, including cold shock (Pech et al., 2011). Other than these, a recent report revealed that r-protein L6, RplF, an essential protein involved in ribosome biogenesis at low temperature, was missing from the pre-50S fraction of *E. coli* in the absence of *bipA* (Bosl and Böck, 1981; Shigeno et al., 2016; Choi and Hwang, 2018). These observations strengthen the connections among cold sensitivity, RNA metabolic process, ribosome biogenesis, and ribosome assembly factors and together support BipA as a *bona fide* ribosome assembly factor. In addition to the structure of BipA bound to 70S ribosome, it would be of interest to characterize the structure of BipA in complex with the intermediate state of ribosome (like pre-50S in **Figure 3**) during its biogenesis, which could offer atomic insights into how BipA facilitates ribosome assembly.

DATA AVAILABILITY STATEMENT

The raw data supporting the conclusions of this article will be made available by the authors, without undue reservation.

AUTHOR CONTRIBUTIONS

Y-GG directed the project. KJG performed most of the experiments. RE, J-EP, and BK participated in some of the experiments. KJG, X-FY, JZ, SKS, and Y-GG analyzed the data. KJG, RE, X-FY, and Y-GG wrote the manuscript with some input from all other co-authors.

FUNDING

This work was supported by a Tier I grant RG108/20 (to Y-GG) from the Ministry of Education (MOE) of Singapore.

SUPPLEMENTARY MATERIAL

The Supplementary Material for this article can be found online at: https://www.frontiersin.org/articles/10.3389/fmicb.2021.686049/full#supplementary-material

REFERENCES

Awano, N., Rajagopal, V., Arbing, M., Patel, S., Hunt, J., Inouye, M., et al. (2010). *Escherichia coli* RNase R has dual activities, helicase and RNase. *J. Bacteriol.* 192, 1344–1352. doi: 10.1128/jb.01368-09

Awano, N., Xu, C., Ke, H., Inoue, K., Inouye, M., and Phadtare, S. (2007). Complementation analysis of the cold-sensitive phenotype of the *Escherichia coli csdA* deletion strain. *J. Bacteriol.* 189, 5808–5815. doi: 10.1128/jb.00655-07

Baba, T., Ara, T., Hasegawa, M., Takai, Y., Okumura, Y., Baba, M., et al. (2006). Construction of *Escherichia coli* K-12 in-frame, single-gene knockout mutants: the Keio collection. *Mol. Syst. Biol.* 2:2006.0008.

Barria, C., Malecki, M., and Arraiano, C. (2013). Bacterial adaptation to cold. *Microbiology* 159, 2437–2443. doi: 10.1099/mic.0.052209-0

Bosl, A., and Böck, A. (1981). Ribosomal mutation in *Escherichia coli* affecting membrane stability. *Mol. Gen. Genet.* 182, 358–360. doi: 10.1007/bf00269684

Cairrão, F., Cruz, A., Mori, H., and Arraiano, C. M. (2003). Cold shock induction of RNase R and its role in the maturation of the quality control mediator SsrA/tmRNA. *Mol. Microbiol.* 50, 1349–1360. doi: 10.1046/j.1365-2958.2003.03766.x

Charollais, J., Dreyfus, M., and Iost, I. (2004). CsdA, a cold-shock RNA helicase from *Escherichia coli*, is involved in the biogenesis of 50S ribosomal subunit. *Nucleic Acids Res.* 32, 2751–2759. doi: 10.1093/nar/gkh603

Charollais, J., Pflieger, D., Vinh, J., Dreyfus, M., and Iost, I. (2003). The DEAD-box RNA helicase SrmB is involved in the assembly of 50S ribosomal subunits in *Escherichia coli*. *Mol. Microbiol.* 48, 1253–1265. doi: 10.1046/j.1365-2958.2003.03513.x

Choi, E., and Hwang, J. (2018). The GTPase BipA expressed at low temperature in *Escherichia coli* assists ribosome assembly and has chaperone-like activity. *J. Biol. Chem.* 293, 18404–18419. doi: 10.1074/jbc.ra118.002295

Choudhury, P., and Flower, A. M. (2015). Efficient assembly of ribosomes is inhibited by deletion of *bipA* in *Escherichia coli*. *J. Bacteriol.* 197, 1819–1827. doi: 10.1128/jb.00023-15

Conrad, J., Sun, D., Englund, N., and Ofengand, J. (1998). The *rluC* gene of *Escherichia coli* codes for a pseudouridine synthase that is solely responsible for synthesis of pseudouridine at positions 955, 2504, and 2580 in 23 S ribosomal RNA. *J. Biol. Chem.* 273, 18562–18566. doi: 10.1074/jbc.273.29.18562

Cremer, J., Honda, T., Tang, Y., Wong-Ng, J., Vergassola, M., and Hwa, T. (2019). Chemotaxis as a navigation strategy to boost range expansion. *Nature* 575, 658–663. doi: 10.1038/s41586-019-1733-y

Davis, J. H., Tan, Y. Z., Carragher, B., Potter, C. S., Lyumkis, D., and Williamson, J. R. (2016). Modular assembly of the bacterial large ribosomal subunit. *Cell* 167, 1610–1622.e5.

Del Peso Santos, T., Alvarez, L., Sit, B., Irazoki, O., Blake, J., Warner, B. R., et al. (2021). BipA exerts temperature-dependent translational control of biofilm-associated colony morphology in *Vibrio cholerae*. *Elife* 10:e60607.

deLivron, M. A., Makanji, H. S., Lane, M. C., and Robinson, V. L. (2009). A novel domain in translational GTPase BipA mediates interaction with the 70S ribosome and influences GTP hydrolysis. *Biochemistry* 48, 10533–10541. doi: 10.1021/bi901026z

Ero, R., Kumar, V., Chen, Y., and Gao, Y. G. (2016). Similarity and diversity of translational GTPase factors EF-G, EF4, and BipA: From structure to function. *RNA Biol.* 13, 1258–1273. doi: 10.1080/15476286.2016.1201627

Fan, H., Hahm, J., Diggs, S., Perry, J. J. P., and Blaha, G. (2015). Structural and functional analysis of BipA, a regulator of virulence in enteropathogenic *Escherichia coli*. *J. Biol. Chem.* 290, 20856–20864. doi: 10.1074/jbc.m115.659136

Gao, Y.-G., Selmer, M., Dunham, C. M., Weixlbaumer, A., Kelley, A. C., and Ramakrishnan, V. (2009). The structure of the ribosome with elongation factor G trapped in the posttranslocational state. *Science* 326, 694–699. doi: 10.1126/science.1179709

Gibbs, M. R., and Fredrick, K. (2018). Roles of elusive translational GTPases come to light and inform on the process of ribosome biogenesis in bacteria. *Mol. Microbiol.* 107, 445–454. doi: 10.1111/mmi.13895

Gibbs, M. R., Moon, K. M., Warner, B. R., Chen, M., Bundschuh, R., Foster, L. J., et al. (2020). Functional analysis of BipA in *E. coli* reveals the natural plasticity of 50s subunit assembly. *J. Mol. Biol.* 432, 5259–5272. doi: 10.1016/j.jmb.2020.07.013

Grant, A. J., Farris, M., Alefounder, P., Williams, P. H., Woodward, M. J., and O'Connor, C. D. (2003). Co-ordination of pathogenicity island expression by the BipA GTPase in enteropathogenic *Escherichia coli* (EPEC). *Mol. Microbiol.* 48, 507–521. doi: 10.1046/j.1365-2958.2003.t01-1-03447.x

Guan, Y.-X., Pan, H.-X., Gao, Y.-G., Yao, S.-J., and Cho, M.-G. (2005). Refolding and purification of recombinant human interferon-γ expressed as inclusion bodies in *Escherichia coli* using size exclusion chromatography. *Biotechnol. Bioprocess Eng.* 10, 122–127. doi: 10.1007/bf02932581

Hauryliuk, V., Atkinson, G. C., Murakami, K. S., Tenson, T., and Gerdes, K. (2015). Recent functional insights into the role of (p) ppGpp in bacterial physiology. *Nat. Rev. Microbiol.* 13, 298–309. doi: 10.1038/nrmicro3448

Heermann, R., Zeppenfeld, T., and Jung, K. (2008). Simple generation of site-directed point mutations in the *Escherichia coli* chromosome using Red®/ET® Recombination. *Microb. Cell Factor.* 7:14. doi: 10.1186/1475-2859-7-14

Jain, C. (2008). The *E. coli* RhlE RNA helicase regulates the function of related RNA helicases during ribosome assembly. *RNA* 14, 381–389. doi: 10.1261/rna.800308

Jiang, M., Datta, K., Walker, A., Strahler, J., Bagamasbad, P., Andrews, P. C., et al. (2006). The *Escherichia coli* GTPase CgtAE is involved in late steps of large ribosome assembly. *J. Bacteriol.* 188, 6757–6770. doi: 10.1128/jb.00444-06

Kalogeraki, V. S., and Winans, S. C. (1997). Suicide plasmids containing promoterless reporter genes can simultaneously disrupt and create fusions to target genes of diverse bacteria. *Gene* 188, 69–75. doi: 10.1016/s0378-1119(96)00778-0

Kierzek, E., Malgowska, M., Lisowiec, J., Turner, D. H., Gdaniec, Z., and Kierzek, R. (2013). The contribution of pseudouridine to stabilities and structure of RNAs. *Nucleic acids Res.* 42, 3492–3501. doi: 10.1093/nar/gkt1330

Kinosita, Y., Ishida, T., Yoshida, M., Ito, R., Morimoto, Y. V., Goto, K., et al. (2020). Distinct chemotactic behavior in the original *Escherichia coli* K-12 depending on forward-and-backward swimming, not on run-tumble movements. *Sci. Rep.* 10:15887.

Kitahara, K., and Suzuki, T. (2009). The ordered transcription of RNA domains is not essential for ribosome biogenesis in *Escherichia coli*. *Mol. Cell* 34, 760–766. doi: 10.1016/j.molcel.2009.05.014

Koripella, R. K., Holm, M., Dourado, D., Mandava, C. S., Flores, S., and Sanyal, S. (2015). A conserved histidine in switch-II of EF-G moderates release of inorganic phosphate. *Sci. Rep.* 5:12970.

Koster, D. A., Mayo, A., Bren, A., and Alon, U. (2012). Surface growth of a motile bacterial population resembles growth in a chemostat. *J. Mol. Biol.* 424, 180–191. doi: 10.1016/j.jmb.2012.09.005

Krishnan, K., and Flower, A. M. (2008). Suppression of Δ*bipA* phenotypes in *Escherichia coli* by abolishment of pseudouridylation at specific sites on the 23S rRNA. *J. Bacteriol.* 190, 7675–7683. doi: 10.1128/jb.00835-08

Kumar, V., Chen, Y., Ero, R., Ahmed, T., Tan, J., Li, Z., et al. (2015). Structure of BipA in GTP form bound to the ratcheted ribosome. *Proc. Natl. Acad. Sci. U.S.A.* 112, 10944–10949. doi: 10.1073/pnas.1513216112

Kumar, V., Ero, R., Ahmed, T., Goh, K. J., Zhan, Y., Bhushan, S., et al. (2016). Structure of the GTP Form of Elongation Factor 4 (EF4) Bound to the Ribosome. *J. Biol. Chem.* 291, 12943–12950. doi: 10.1074/jbc.m116.725945

Liu, W., Cremer, J., Li, D., Hwa, T., and Liu, C. (2019). An evolutionarily stable strategy to colonize spatially extended habitats. *Nature* 575, 664–668. doi: 10.1038/s41586-019-1734-x

Martínez-García, E., Nikel, P. I., Chavarría, M., and de Lorenzo, V. (2014). The metabolic cost of flagellar motion in *Pseudomonas putida* KT 2440. *Environ. Microbiol.* 16, 291–303. doi: 10.1111/1462-2920.12309

Murakami, K., Ono, T., Viducic, D., Kayama, S., Mori, M., Hirota, K., et al. (2005). Role for *rpoS* gene of *Pseudomonas aeruginosa* in antibiotic tolerance. *FEMS Microbiol. Lett.* 242, 161–167.

Neidig, A., Yeung, A. T., Rosay, T., Tettmann, B., Strempel, N., Rueger, M., et al. (2013). TypA is involved in virulence, antimicrobial resistance and biofilm formation in *Pseudomonas aeruginosa*. *BMC Microbiol.* 13:77. doi: 10.1186/1471-2180-13-77

Ottemann, K. M., and Miller, J. F. (1997). Roles for motility in bacterial–host interactions. *Mol. Microbiol.* 24, 1109–1117. doi: 10.1046/j.1365-2958.1997.4281787.x

Park, J. E., Dutta, B., Tse, S. W., Gupta, N., Tan, C. F., Low, J. K., et al. (2019). Hypoxia-induced tumor exosomes promote M2-like macrophage polarization of infiltrating myeloid cells and microRNA-mediated metabolic shift. *Oncogene* 38, 5158–5173. doi: 10.1038/s41388-019-0782-x

Pech, M., Karim, Z., Yamamoto, H., Kitakawa, M., Qin, Y., and Nierhaus, K. H. (2011). Elongation factor 4 (EF4/LepA) accelerates protein synthesis at increased Mg2+ concentrations. *Proc. Natl. Acad. Sci. U.S.A.* 108, 3199–3203. doi: 10.1073/pnas.1012994108

Peil, L., Virumäe, K., and Remme, J. (2008). Ribosome assembly in *Escherichia coli* strains lacking the RNA helicase DeaD/CsdA or DbpA. *FEBS J.* 275, 3772–3782. doi: 10.1111/j.1742-4658.2008.06523.x

Pfennig, P., and Flower, A. (2001). BipA is required for growth of *Escherichia coli* K12 at low temperature. *Mol. Genet. Genom.* 266, 313–317. doi: 10.1007/s004380100559

Phadtare, S. (2011). Unwinding activity of cold shock proteins and RNA metabolism. *RNA Biol.* 8, 394–397. doi: 10.4161/rna.8.3.14823

Phadtare, S., Hwang, J., Severinov, K., and Inouye, M. (2003). CspB and CspL, thermostable cold-shock proteins from *Thermotoga maritima*. *Genes Cells* 8:801. doi: 10.1046/j.1365-2443.2003.00675.x

Philippe, N., Alcaraz, J.-P., Coursange, E., Geiselmann, J., and Schneider, D. (2004). Improvement of pCVD442, a suicide plasmid for gene allele exchange in bacteria. *Plasmid* 51, 246–255. doi: 10.1016/j.plasmid.2004.02.003

Prud'homme-Généreux, A., Beran, R. K., Iost, I., Ramey, C. S., Mackie, G. A., and Simons, R. W. (2004). Physical and functional interactions among RNase E, polynucleotide phosphorylase and the cold-shock protein, CsdA: evidence for a 'cold shock degradosome'. *Mol. Microbiol.* 54, 1409–1421. doi: 10.1111/j.1365-2958.2004.04360.x

Qi, S. Y., Li, Y., Szyroki, A., Giles, I. G., Moir, A., and David O'Connor, C. (1995). *Salmonella typhimurium* responses to a bactericidal protein from human neutrophils. *Mol. Microbiol.* 17, 523–531. doi: 10.1111/j.1365-2958.1995.mmi_17030523.x

Resch, A., Večerek, B., Palavra, K., and Bläsi, U. (2010). Requirement of the CsdA DEAD-box helicase for low temperature riboregulation of *rpoS* mRNA. *RNA Biol.* 7, 796–802. doi: 10.4161/rna.7.6.13768

Rudra, D., and Warner, J. R. (2004). What better measure than ribosome synthesis? *Genes Dev.* 18, 2431–2436. doi: 10.1101/gad.1256704

Sato, A., Kobayashi, G., Hayashi, H., Yoshida, H., Wada, A., Maeda, M., et al. (2005). The GTP binding protein Obg homolog ObgE is involved in ribosome maturation. *Genes Cells* 10, 393–408. doi: 10.1111/j.1365-2443.2005.00851.x

Scarano, G. I, Krab, M., Bocchini, V., and Parmeggiani, A. (1995). Relevance of histidine-84 in the elongation factor Tu GTPase activity and in poly (Phe) synthesis: its substitution by glutamine and alanine. *FEBS Lett.* 365, 214–218. doi: 10.1016/0014-5793(95)00469-p

Schaefer, J., Jovanovic, G., Kotta-Loizou, I., and Buck, M. (2016). Single-step method for β-galactosidase assays in *Escherichia coli* using a 96-well microplate reader. *Anal. Biochem.* 503, 56–57. doi: 10.1016/j.ab.2016.03.017

Schmeing, T. M., Voorhees, R. M., Kelley, A. C., Gao, Y. G., Murphy, F. V. IV, Weir, J. R., et al. (2009). The crystal structure of the ribosome bound to EF-Tu and aminoacyl-tRNA. *Science* 326, 688–694.

Selmer, M., Gao, Y. G., Weixlbaumer, A., and Ramakrishnan, V. (2012). Ribosome engineering to promote new crystal forms. *Acta Crystallogr. D Biol. Crystallogr.* 68(Pt 5), 578–583. doi: 10.1107/s0907444912006348

Shigeno, Y., Uchiumi, T., and Nomura, T. (2016). Involvement of ribosomal protein L6 in assembly of functional 50S ribosomal subunit in *Escherichia coli* cells. *Biochem. Biophys. Res. Commun.* 473, 237–242. doi: 10.1016/j.bbrc.2016.03.085

Tanaka, Y., Sakamoto, S., Kuroda, M., Goda, S., Gao, Y. G., Tsumoto, K., et al. (2008). A helical string of alternately connected three-helix bundles for the cell wall-associated adhesion protein Ebh from *Staphylococcus aureus*. *Structure* 16, 488–496. doi: 10.1016/j.str.2007.12.018

Thompson, A., Schäfer, J., Kuhn, K., Kienle, S., Schwarz, J., Schmidt, G., et al. (2003). Tandem mass tags: a novel quantification strategy for comparative analysis of complex protein mixtures by MS/MS. *Anal. Chem.* 75, 1895–1904. doi: 10.1021/ac0262560

Toh, S.-M., and Mankin, A. S. (2008). An indigenous posttranscriptional modification in the ribosomal peptidyl transferase center confers resistance to an array of protein synthesis inhibitors. *J. Mol. Biol.* 380, 593–597. doi: 10.1016/j.jmb.2008.05.027

Uppal, S., and Jawali, N. (2015). Cyclic AMP receptor protein (CRP) regulates the expression of *cspA*, *cspB*, *cspG* and *cspI*, members of *cspA* family, in *Escherichia coli*. *Arch. Microbiol.* 197, 497–501. doi: 10.1007/s00203-015-1085-4

Vesper, O., Amitai, S., Belitsky, M., Byrgazov, K., Kaberdina, A. C., Engelberg-Kulka, H., et al. (2011). Selective translation of leaderless mRNAs by specialized ribosomes generated by MazF in *Escherichia coli*. *Cell* 147, 147–157. doi: 10.1016/j.cell.2011.07.047

Yang, C., Cui, C., Ye, Q., Kan, J., Fu, S., Song, S., et al. (2017). *Burkholderia cenocepacia* integrates cis-2-dodecenoic acid and cyclic dimeric guanosine monophosphate signals to control virulence. *Proc. Natl. Acad. Sci. U.S.A.* 114, 13006–13011. doi: 10.1073/pnas.1709048114

Yu, Y., Wu, Y., Cao, B., Gao, Y.-G., and Yan, X. (2015). Adjustable bidirectional extracellular electron transfer between *Comamonas testosteroni* biofilms and electrode via distinct electron mediators. *Electrochem. Commun.* 59, 43–47. doi: 10.1016/j.elecom.2015.07.007

Zheng, J., Li, N., Tan, Y. P., Sivaraman, J., Mok, Y.-K., Mo, Z. L., et al. (2007). EscC is a chaperone for the *Edwardsiella tarda* type III secretion system putative translocon components EseB and EseD. *Microbiology* 153, 1953–1962. doi: 10.1099/mic.0.2006/004952-0

Conflict of Interest: The authors declare that the research was conducted in the absence of any commercial or financial relationships that could be construed as a potential conflict of interest.

frontiers in Microbiology

ORIGINAL RESEARCH
published: 14 July 2021
doi: 10.3389/fmicb.2021.705012

Light-Stress Response Mediated by the Transcription Factor *Kl*Mga2 in the Yeast *Kluyveromyces lactis*

*Ilaria Camponeschi[1], Arianna Montanari[1], Marzia Beccaccioli[2], Massimo Reverberi[2], Cristina Mazzoni[1] and Michele M. Bianchi[1]**

[1] Department of Biology and Biotechnology 'C. Darwin', Sapienza University of Rome, Rome, Italy, [2] Department of Environmental Biology, Sapienza University of Rome, Rome, Italy

In unicellular organisms like yeasts, which do not have specialized tissues for protection against environmental challenges, the presence of cellular mechanisms to respond and adapt to stress conditions is fundamental. In this work, we aimed to investigate the response to environmental light in *Kluyveromyces lactis*. Yeast lacks specialized light-sensing proteins; however, *Saccharomyces cerevisiae* has been reported to respond to light by increasing hydrogen peroxide level and triggering nuclear translocation of Msn2. This is a stress-sensitive transcription factor also present in *K. lactis*. To investigate light response in this yeast, we analyzed the different phenotypes generated by the deletion of the hypoxia responsive and lipid biosynthesis transcription factor *Kl*Mga2. Alterations in growth rate, mitochondrial functioning, ROS metabolism, and fatty acid biosynthesis provide evidence that light was a source of stress in *K. lactis* and that *Kl*Mga2 had a role in the light-stress response. The involvement of *Kl*Msn2 and *Kl*Crz1 in light stress was also explored, but the latter showed no function in this response.

Keywords: lipid, membrane, desaturase, ROS, fungi

OPEN ACCESS

Edited by:
Nelson da Cruz Soares, University of Sharjah, United Arab Emirates

Reviewed by:
Rosaura Rodicio, University of Oviedo, Spain
Luis L. Fonseca, University of Florida, United States

***Correspondence:**
Michele M. Bianchi
michele.bianchi@uniroma1.it

Specialty section:
This article was submitted to Microbial Physiology and Metabolism, a section of the journal Frontiers in Microbiology

Received: *04 May 2021*
Accepted: *16 June 2021*
Published: *14 July 2021*

Citation:
Camponeschi I, Montanari A, Beccaccioli M, Reverberi M, Mazzoni C and Bianchi MM (2021) Light-Stress Response Mediated by the Transcription Factor KlMga2 in the Yeast Kluyveromyces lactis. Front. Microbiol. 12:705012. doi: 10.3389/fmicb.2021.705012

INTRODUCTION

Studies on yeast lipid metabolism have been mainly conducted on *S. cerevisiae* (Natter and Kohlwein, 2013): in this yeast, fatty acid (FA) biosynthesis is restricted to saturated and monounsaturated FAs (MUFAs) and essentially accomplished by acetyl-CoA carboxylase (Acc1) and FA synthase (Fas1 and Fas2) enzymes and by the unique Δ9 desaturase enzyme (Ole1) that produces the monounsaturated (MUFA) palmitoleic and oleic acids. In the lactose-utilizing yeast *Kluyveromyces lactis*, the composition of FAs is enriched with the polyunsaturated (PUFA) linoleic and α-linolenic acids generated by the Δ12 (Fad2) and ω3 (Fad3) desaturases (Kainou et al., 2006; Santomartino et al., 2017). Environmental conditions regulate the expression of desaturases and have therefore effects on the synthesis and abundance of different (mono- and poly-) unsaturated FA molecules (Rossi et al., 2009) and on properties of membranes.

Mga2 is the *S. cerevisiae* transcription factor that regulates the expression of desaturase gene *OLE1* (Zhang et al., 1999; Chellappa et al., 2001; Jiang et al., 2001) in low-oxygen conditions. Mga2 is constitutively expressed as inactive form bound into endoplasmic reticulum (ER). It is activated

in hypoxic conditions by proteasome cleavage (Hoppe et al., 2000): the 90 kDa N-terminal soluble fragment moves then into the nucleus where it induces the expression of low-oxygen responsive genes. In *K. lactis*, studies on *KlMGA2* gene, which is the ortholog gene of *S. cerevisiae MGA2* and/or *SPT23*, revealed multiple cellular roles of this regulator, including response to hypoxia, respiration, glucose metabolism, response to ROS, life span, and general cellular fitness (Micolonghi et al., 2012; Ottaviano et al., 2015; Santomartino et al., 2019a). In detail, the genetic targets of *Kl*Mga2 in FA biosynthesis are *KlACC1* and *FAD2* genes and phenotypes generated by *KlMGA2* deletion are restored by the addition of unsaturated FAs (UFA).

Light is a common environmental source of heat and energy, essential for biosynthetic organisms. Yeasts, on the other hand, lack specialized light sensing proteins such as phytochromes, opsins, and cryptochromes (Idnurm et al., 2010), but studies of light-induced stress conducted in *S. cerevisiae* have shown a response to blue light *via* activation of the stress-regulated transcription factors Msn2 and Crz1. Both factors control gene expression through nucleo-cytoplasmic translocations (Cai et al., 2008; Bodvard et al., 2011), and the homologs of these two stress-sensitive transcription factors were identified also in *K. lactis* (Bussereau et al., 2006; Barsoum et al., 2011). In *S. cerevisiae*, Ca2+ signaling, mediated by the Ca2+/calmodulin dependent phosphatase calcineurin, is required for cell survival during environmental stresses. These conditions cause an increase in cytosolic Ca2+ that induces calcineurin activation (Cyert, 2003). The phosphatase, in turn, dephosphorylates Crz1, which rapidly translocates from the cytosol to the nucleus, where it activates the transcription of genes involved in adaptation to stress (Bodvard et al., 2013; Thewes, 2014).

The second stress-response transcription factor, Msn2, exhibits similar behaviors; it moves to the nucleus where it affects the expression of target genes with STREs (stress response elements) in their promoters (Estruch, 2000). Several stresses are known to induce nucleocytoplasmic oscillations of Msn2, including high concentrations of extracellular Ca2+ (Cai et al., 2008), caloric restriction (low glucose levels 0.1%) (Medvedik et al., 2007), oxidative stress (Hao and O'Shea, 2011), as well as light (Bodvard et al., 2011, 2013, 2017), but the overall activation pathway is less clear than Crz1. Nuclear localization of Msn2 is contrasted by cyclic AMP-controlled protein kinase A (PKA) (Görner et al., 1998) and promoted by the phosphatases PP1 and PP2A (Görner et al., 1998; Santhanam et al., 2004). Another important feature is that light stimulates hydrogen peroxide production in cultured mouse, monkey, and humans cells *via* photoreduction of flavin-containing oxidases (Hockberger et al., 1999). The intermediates and the mechanism by which PKA senses light remain unclear, but it has been shown that in *S. cerevisiae* a conserved peroxisomal oxidase (Pox1) converts light into a H_2O_2 signal, which is sensed by the peroxiredoxin Tsa1 and then transduced to thioredoxin (Trx1) to inhibit PKA activity (Bodvard et al., 2017).

To our knowledge, studies on response to light have never been reported in *K. lactis* except the resonance response to light–dark 12 + 12 hour cycles generating an increase of phenotypic suppression in *KlMGA2* deletion mutant (Camponeschi et al., 2020). Interestingly, the desaturase gene *FAD2* is a light-dependent gene in plants (Kargiotidou et al., 2008; Dar et al., 2017) and its transcription is increased also at low temperatures (Byfield and Upchurch, 2007). Desaturase level and lipid unsaturation index were both light-dependent in cold stress (Yuan et al., 2012). As reported above, in *K. lactis FAD2* gene is a hypoxic target of *Kl*Mga2, suggesting that it could be possible for an overlap between light response and other conditions affecting the regulation of FA biosynthetic metabolism, such as hypoxia, also in non-photosynthetic organism.

In this work we aimed to investigate the role of the yeast multi-functional mediator *Kl*Mga2 in light response and connection with the other putative stress factors *Kl*Msn2 and *Kl*Crz1 in this yeast. Effects of light on oxidative stress and lipid biosynthesis were also studied.

MATERIALS AND METHODS

Media and Growth Condition

The yeast strains used are listed in **Table 1**. The YPD medium was composed of 1% Yeast Extract (Becton Dickinson and Company), 1% Peptone (Becton Dickinson), and 2% glucose. Solid media contained 2% Bacto-Agar (Becton Dickinson). For

TABLE 1 | Plasmids and strains.

Name	Description	References
Plasmids		
pFA6-KanMX4	Plasmid containing the *KanMX4* marker	Wach et al., 1994
pYM27	Template for C-terminal EGFP and $G418^R$	Janke et al., 2004
pYM14	Template for C-terminal 3HA and $G418^R$	Janke et al., 2004
Kp426[KlMga2^{FLAG}]	Plasmid containing Flag-tagged *KlMGA2*	Micolonghi et al., 2012
pRS416	Plasmid containing the *URA3* marker	Sikorski and Hieter, 1989
Strains		
MWL9S1	*MAT*a, *ura3*, *leu2*, *lysA1*, *trp1*, *metA1-1*, *Klnej1::loxP*	Hnatova et al., 2008
*Klcrz1*Δ	*MAT*a, *ura3*, *leu2*, *lysA1*, *trp1*, *metA1-1*, *Klcrz1::kanMX4*	This work
*Klmsn2*Δ	*MAT*a, *ura3*, *leu2*, *lysA1*, *trp1*, *metA1-1*, *Klmsn2::kanMX4*	This work
LDA2	*MAT*a, *ura3*, *leu2*, *lysA1*, *trp1*, *metA1-1*, *fad2::kanMX4*	De Angelis et al., 2016
LD2G	*MAT*a, *ura3*, *leu2*, *lysA1*, *trp1*, *metA1-1*, *FAD2-GFP*	De Angelis et al., 2016
*Klmga2*Δ	*MAT*a, *lysA1*, *trp1*, *leu2*, *metA1-1*, *ura3, Klnej1::loxP*, *Klmga2::URA3*	This work
*mga2*ΔTM	*MATa*, *lysA1*, *trp1*, *leu2*, *metA1-1*, *ura3, Klnej1::loxP*, *Klmga2*(ΔTM)*-3HA*	This work
KlMga2^{FLAG}	*MATa*, *lysA1*, *trp1*, *leu2*, *metA1-1*, *ura3*, *Klnej1::loxP*, *Klmga2::URA3*, transformed with Kp426[KlMga2^{FLAG}]	This work
*Klmga2*Δ/Fad2-GFP	*MATa*, *lysA1*, *trp1*, *leu2*, *metA1-1*, *ura3*, *Klnej1::loxP*, *Klmga2::URA3*, *FAD2-GFP*	This work

selection of transformed cells, we used YPD solid medium supplemented with Geneticin 100 μ/ml (G418; Sigma-Aldrich) or SD solid medium, composed of 0.67% Yeast Nitrogen Base (Becton Dickinson), 2% glucose, and auxotrophic requirements as needed, without uracil. GAA medium, used to select rag + phenotype cells, was composed of YP medium with 5% glucose and 5 μM Antimycin A (Sigma-Aldrich). Except when otherwise specified, culture growth was performed at 28 ± 1°C in complete darkness or in light (134 $\mu M/s/m^2$) under white LED lamps (4500K, 400–700 nm range). Cell density was determined by optical density at 600 nm or by cell counting in Burker chamber.

Construction of Strains

Strains MWL9S1/*crz1*Δ, MWL9S1/*msn2*Δ, and MWL9S1/*Klmga2*Δ were obtained by disruption of *KlCRZ1* (ORF *KLLA0E08713g*), *KlMSN2* (ORF *KLLA0F26961g*), or *KlMGA2* (ORF *KLLA0E17953g*) with the *KanMX4* cassette or *URA3* deletion cassettes, which have been generated by the short flanking sequences-PCR method (Janke et al., 2004) (Vent DNA Polymerase; New England Biolabs). DNAs were amplified using the primers 1–6 (**Supplementary Table 1**) and plasmid pFA6-KanMX4 (Addgene, **Table 1**) as DNA template containing *KanMX4* or the plasmid pRS416 (Stratagene, **Table 1**) as DNA template containing *URA3* marker. The purified PCR products were then used to transform MWL9S1 strain by electroporation. Transformed colonies were selected on YPD solid medium supplemented with Geneticin (G418) on SD solid medium without uracil and then analyzed by PCR (Taq Pol, Jena Bioscience). Strain MWL9S1/*mga2*ΔTM was obtained in the same way by disruption of C-terminal membrane-anchoring domain coding sequence in *KlMGA2* (from codon 833 of protein KLLA0E17953p) using plasmid pYM14 (Euroscarf, **Table 1**) as template bearing the *3HA-KanMX4* cassette (primers 7 and 8, **Supplementary Table 1**). *FAD2* gene was fused in frame with *GFP* sequence in *Klmga2*Δ strain, by a PCR-based strategy (Janke et al., 2004) using plasmid pYM27 (Euroscarf, **Table 1**) as template bearing the *EGFP-KanMX4* cassette to obtained *Klmga2*Δ/Fad2-GFP strain. Yeast strains were obtained by transformation with the electroporation procedure as previously described (Salani and Bianchi, 2006).

RNA Extraction and Analysis

Total RNAs were prepared by the hot phenol procedure as described by Köhrer and Domdey (1991) from cultures grown to OD_{600} = 1 ± 0.2 in light or dark conditions, and then collected or subjected to the opportune light/dark shift. Integrity of total RNAs extracts was controlled by electrophoresis on agarose-formaldehyde gel. RNA concentration was determined by measuring the absorption at 260 nm. Transcript analysis was performed by qRT-PCR. Total RNA (1 μg) was retro-transcribed to cDNA using QuantiTect Reverse Transcription Kit (Qiagen), following instructions. One sample not retro-transcribed was used as negative control. cDNA amplification was performed using KAPA Sybr Fast 2X (Sigma-Aldrich) with the appropriate couple of 10 μM primers (**Supplementary Table 1**) and 2 μl of the cDNA (100 ng). All the samples, except for the negative controls, were loaded in double for a technical replicate. The experiments were then conducted using the Rotor Gene Q (Qiagen), and data were analyzed using the provided software. The cycling was set with 3 min at 95°C for enzyme activation, then 40 cycles at 95°C for 3 s and 30 s at 60°C, followed by a final step for generation of melting curve, ranging from 60° to 95°C. Quantification was performed by the construction of a standard curve with genomic DNA from MWL9S1 with five points of serial dilutions (the R2 obtained for the curve was always higher than 0.99) and by the relative quantification of the samples of interest, using amplification of 18S rDNA as reference (Santomartino et al., 2019b).

Protein Extraction and Western Blotting

Cultures were grown to OD_{600} = 1 ± 0.2 and then collected or shifted to light or dark conditions for different time points, depending on the experiment. Cells were harvested and suspended in 200 μl of sterile water. An equal volume of 0.2 N NaOH was added and cells were incubated at room temperature for 5 min, then centrifuged for 2 min at 10,000 g. After elimination of the supernatant, pellets were suspended in Laemmli buffer (60 mM TrisHCl pH 6.8; 50% glycerol; 2% SDS; 5% β-mercaptoethanol; 2% bromophenol blue). Total protein extract amount was quantified by measuring absorption at 280 nm (NanoDrop™ 2000 spectrophotometer, Thermo Fisher Scientific). The samples were boiled for 5 min or incubated at 65°C for 10 min, kept on ice for 2 min and centrifuged at 10,000 g for 1 min, then loaded on 8–10% acrylamide (Sigma-Aldrich) gel for SDS-PAGE. After electrophoresis, proteins were transferred to PVDF transfer membrane (Merck Millipore). Western blotting was performed with different primary antibodies (sc-7392 anti-HA Santa Cruz Biotechnology; sc-9996 anti-GFP Santa Cruz Biotechnology; F4042 anti-flag Sigma-Aldrich) and horseradish peroxidase-conjugated secondary antibody (sc-516102 anti-mouse Santa Cruz Biotechnology). Detection was performed with ECL Western blotting detection reagents (LiteAblot EXTEND, EuroClone or Western Bright Quantum, Advansta) and visualized by ChemiDoc™ MP Imaging System (Biorad). α-Tubulin (sc-53030 Santa Cruz Biotechnology) or Ada2 (ab215524 AbCam) detections were used as loading controls.

Catalase and Superoxide Dismutase Activity

Cells (3–4 OD_{600} units) were collected from cultures, and extracts were prepared by glass beads crushing in lysis buffer (50 mM Tris-HCl pH 6.8; 100 mM NaCl). Protein content in samples was determined at 280 nm (NanoDrop™ 2000, Thermo Fisher Scientific). To determine catalase activity, 1–1.5 μl aliquots of samples were added to 0.5 ml of 11 mM H_2O_2 (Sigma-Aldrich) in 50 mM phosphate buffer pH 7.0; 1 μM EDTA. H_2O_2 decomposition was monitored at 25°C at 240 nm (ε_{240} = 39.4 M^{-1} cm^{-1}). Superoxide dismutase activity was determined by measuring the rate of WST1-Formazan formation, using the SOD Assay kit-WST (Sigma-Aldrich), as suggested by the supplier. Calibration curve was determined using a commercial Sod enzyme (Sigma-Aldrich).

Activity measurements have been performed in two to four biological repetitions, each of them in technical triplicates. Standard deviations and statistical significances (*P*-values) have been determined.

Fluorescence Microscopy

Exponentially growing cells on YPD medium were observed with a Zeiss Axio Imager Z1 fluorescence microscope with an AxioVision 4.8 digital image processing system, and oil 63× objective lens. Culture (100 μl) was centrifugated, washed with sterile water, and then resuspended in 100 μl of 0.1 mM 2-(p-dimethylaminostryryl)-l-methylpyridinium iodine (DASPMI). Fluorescence could be detected 5–10 min after addition of the dye to the cells. The fluorescence was observed using DASPMI filter sets (550/25 nm excitation and 605/670 nm emission). DASPMI maximal absorption wavelength is 429 nm, and maximal emission wavelength (excitation at 467 nm) is 557.5 nm in water (Bereiter-Hahn, 1976; Ramadass and Bereiter-Hahn, 2008).

Respiration

Respiration was analyzed by measuring the oxygen consumption rate using a Clark oxygen electrode (Hansatech Instruments) as described in De Luca et al. (2009). Cells (1×10^6) from exponential cultures ($1 \div 4 \times 10^6$ cells ml^{-1}) were collected, washed with 1 ml sterile water, suspended in 1 ml sodium phosphate buffer (10 mM pH 7.4, containing glucose 4 g L^{-1}), and loaded in the reaction vessel of the previously calibrated oxygen electrode chamber.

Fatty Acid Extraction and HPLC-MS/MS Analysis

FAs were extracted from cells grown to OD_{600} = 1 in light or dark exposition. Lyophilized cells of *K. lactis* were extracted following the method described in Ludovici et al. (2014). Internal reference standard was the 9(S)-HODE-d4 (Cayman) at the final concentration of 1 μM. The samples were extracted with 2 ml of isopropyl alcohol:water:ethyl acetate (1:1:3 v/v) mixture with 0.0025% w/v of butylated hydroxytoluene. The extracts were dried by nitrogen flux and resuspended with 100 μl of methanol. The samples have been analyzed with LC (HPLC 1200 series rapid resolution) coupled to a triple quadrupole MS (G6420 series triple quadrupole, QQQ) equipped with an electrospray ionization source (ESI). The equipment, the chromatographic column, and the analysis software were from Agilent Technologies. The chromatographic separation has been performed with a Zorbax ECLIPSE XDB-C18 rapid resolution HT 4.6 × 50 mm 1.8 μm p.s. column. FAs were analyzed by single ion monitoring (SIM) method in negative. The elution program requires the following mobile phase: phase A water/acetonitrile 97:3 v/v containing 0.1% formic acid and 3% acetonitrile, and phase B: acetonitrile/isopropyl alcohol 90:10 v/v. The injection volume was 10 μl. Instrument setting was reported previously (Ludovici et al., 2014). The SIM parameters have been obtained by flow injection of authentic standard and agreed with the literature (Yang et al., 2009; Beccaccioli et al., 2021). FA mass and relative parameters of analysis are reported in **Table 2**. SIM data have been processed using Mass Hunter Quantitative software. Membrane fluidity, expressed as the FA unsaturation index (UI), was calculated as follows: [(%C16:1 + %C18:1) + (%C18:2 × 2) + (%C18:3 × 3)]/100.

RESULTS

Growth of *KlMGA2*, *KlCRZ1*, and *KlMSN2* Mutant Strains in Light or Dark Condition

In order to test the role of *Kl*Mga2, *Kl*Msn2, and *Kl*Crz1 in light-dependent response, we constructed deletion mutants into *K. lactis* MWL9S1 strain (Wésolowski-Louvel, 2011). The identification of *KlMGA2* has been described previously (Micolonghi et al., 2012). The homologs of *CRZ1* and *MSN2* were identified in *K. lactis* genome using BLAST: *KlMSN2* (ORF *KLLA0F26961g*) had 24% identity and 35% similarity with *MSN2*; *KlCRZ1* (ORF *KLLA0E08713g*) had 28% identity and 40% similarity with *CRZ1* (Bussereau et al., 2006; Barsoum et al., 2011). These mutant strains were named *Klmga2*Δ, *Klcrz1*Δ, and *Klmsn2*Δ, respectively. Likewise, we generated an additional *Klmga2*Δ mutant strain harboring a truncated form of *KlMGA2* (*mga2*ΔTM strain): the latter contained *Kl*Mga2 lacking C-terminal transmembrane domain (TM), that in *S. cerevisiae* represses Mga2 protein activity (Chellappa et al., 2001; Huang and Kao, 2018). We assumed that the *mga2*ΔTM strain coded for an always active truncated *Kl*Mga2 protein. Genotypes of these four mutant strains, obtained as described in the "Materials and Methods" section, are reported in **Table 1**.

We have previously shown (Ottaviano et al., 2015) that the deletion of *KlMGA2* in the wild type GDK strain caused a reduced growth rate compared to wild type. We performed the growth experiment on standard glucose medium in light or darkness condition with MWL9S1 strain and the derived *Klmga2*Δ mutant strain (**Figure 1**). According to our previous results with the mutant strain GDK/*Klmga2*Δ, we observed that the deleted strain presented a longer lag phase and a slower growth rate as compared to wild type MWL9S1. Interestingly, incubation in dark or light conditions significantly affected the growth rate of mutant strain: in fact, the duplication time of deleted strain in the exponential phase shifted from about 6 h in light to 4 h in darkness, while the wild type duplication time only changed from 2.7 h in light to 2.2 h in darkness condition, respectively.

Previous studies showed that the desaturase gene *FAD2* is a target of *Kl*Mga2 (Ottaviano et al., 2015). However, light or dark

TABLE 2 | Fatty acid SIM method.

Compound name	Ion mass $[M-H]^-$	Fragmentor (V)	Polarity
16:0	255.2	140	Negative
16:1	253.2	140	Negative
18:0	283.2	140	Negative
18:1	281.2	140	Negative
18:2	279.2	140	Negative
18:3	277.2	140	Negative

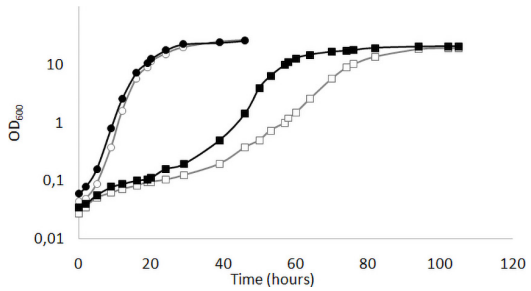

FIGURE 1 | Growth profiles of *Klmga2*Δ strain in light or dark exposure. Typical growth curves of the wild type MWL9S1 (circles) and the *Klmga2*Δ mutant strains (squares) in standard YPD medium are reported as optical density (OD_{600}) vs. time (hours). Black and white symbols refer to darkness and light cultivation, respectively. Repeated experiments gave similar results.

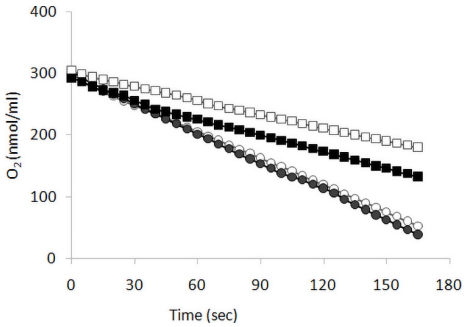

FIGURE 2 | Respiration rate. Respiration was determined as oxygen consumption rate (oxygen slope: nmol O_2 ml^{-1} s^{-1}) by wild type (circles) and of *Klmga2*Δ mutant cells (squares), grown exponentially in YPD medium. Black and white symbols refer to dark and light cultivation, respectively. Repeated experiments gave similar slopes: average values and standard deviations of the repeated experiments are reported in text.

incubation did not interfere with growth rates of *fad2*Δ strain (LDA2 strain, **Table 1**). The presence of light or darkness did not interfere significantly also with strain *Klmsn2*Δ: both results are reported in **Supplementary Figure 1**.

Effects of Light and Dark Exposure on Respiration and Mitochondrial Morphology

We previously reported (Ottaviano et al., 2015) that *KlMGA2* deletion affected FA biosynthesis, respiration rate, and mitochondrial morphology. To establish the occurrence of a light-dependent connection between growth and respiration rates of *Klmga2*Δ strain, we measured oxygen consumption rates of exponentially growing MWL9S1 wild type and *Klmga2*Δ mutant cells cultured in light or darkness using a Clark electrode, as described in the section "Materials and Methods." Results are reported in **Figure 2**. Average of three independent measurements indicated that the wild type cells consumed oxygen faster than deleted strain and consumption rate was independent on light (1.5 ± 0.05 nmol O_2 ml^{-1} s^{-1}) or dark (1.54 ± 0.04 nmol O_2 ml^{-1} s^{-1}) growth. Differently, the deleted strains showed higher oxygen consumption rate when grown in darkness (0.92 ± 0.01 nmol O_2 ml^{-1} s^{-1}) than in light condition (0.69 ± 0.03 nmol O_2 ml^{-1} s^{-1}). Similarly to growth rate, the defective respiration rate of the deleted strain was exacerbated by light exposure while no effect of light could be recorded in the presence of *Kl*Mga2. Data reported in **Supplementary Figure 2** showed that light or dark did not affect the respiration rates of *Klmsn2*Δ and *fad2*Δ strains.

In order to investigate mitochondrial morphology and activity, cells were stained with the functional dye DASPMI. This staining allows to visualize functional mitochondrial membranes with an active potential by fluorescence microscopy (Bereiter-Hahn, 1976). Results, reported in **Figure 3A** and **Supplementary Figure 3**, revealed that the mitochondrial membranes of the *Klmga2*Δ mutant strains, as well as those of the wild type strain, were visualized by DASPMI staining suggesting a correct mitochondrial functionality. Nevertheless, as previously reported (Ottaviano et al., 2015), mitochondrial network of *Klmga2*Δ strain frequently showed a non-tubular collapsed morphology under light conditions. However, when the *Klmga2*Δ cells were grown in the darkness, the percentage of cells bearing normal tubular mitochondria was significantly increased to the same level as the wild type (**Figure 3B**). We observed a normal mitochondrial morphology in *Klmsn2*Δ, *fad2*Δ, and *mga2*ΔTM strains (data not shown).

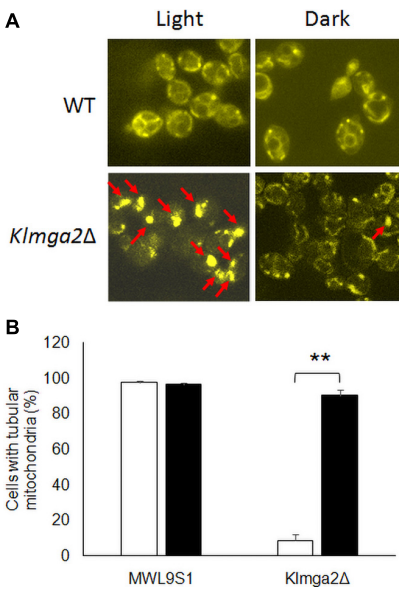

FIGURE 3 | Fluorescence microscopy analysis of wild type and mutant strains *Klmga2*Δ. **(A)** Reports DASPMI staining of the mitochondrial network of wild type MWL9S1 and *Klmga2*Δ strains. The red arrows show the non-tubular collapsed mitochondrial network. **(B)** Shows histogram reporting the percentages of tubular mitochondria-containing cells. White and black blocks refer to light and darkness cultivation, respectively. Growth medium was YPD. Two or three independent cultures were performed for each strain/condition, and 100–700 cells were analyzed. Standard deviations (SD) are reported. ** indicates $p < 0.01$.

The *Klmga2*Δ strain in the MWL9S1 background had a rag- phenotype (sensitivity to the mitochondrial drug antimycin A on high glucose concentration: GAA medium, **Figure 4**) as previously reported for another *K. lactis* strain (Micolonghi et al., 2012). The rag- phenotype is usually due to defects in the glycolytic and/or fermentative pathways or in their regulation (Wésolowski-Louvel et al., 1992) pointed out by respiration blockage; however, the deletion of *KlMGA2* did not impeded hypoxic growth or ethanol production (Ottaviano et al., 2015), indicating that the inability of the deleted strain to grow when oxidative phosphorylation is impaired was not to be ascribed to mere metabolic defect. We assayed the effect of darkness on the rag- phenotype of the deleted strain (**Figure 4**), but no difference with light stress could be recorded, suggesting that blockage of electron transport required *Kl*Mga2 for growth in both conditions. Surprisingly, the deletion of *KlMSN2* did not affect growth in the presence of antimycin A under light stress but a slight reduction of growth was observed in darkness. Deletion of *FAD2* and *KlCRZ1* did not influence growth on antimycin A in light or darkness (**Supplementary Figure 4**). Expression of the *Kl*Mga2 truncated form in strain *mga2*ΔTM allowed wild type growth in the presence of light (**Supplementary Figure 4**); however, growth in darkness was more similar to the deleted strain than the wild type and the presence of antimycin A slightly reduced grow rate in both light and darkness.

Activation of *Kl*Mga2 Protein

In *S. cerevisiae* Mga2 is present in two forms: p120, an inactive 120 kDa precursor form that is anchored to the ER membrane by the C-terminus, and p90, a soluble 90 kDa N-terminus fragment which is the nuclear active form. Mga2 activation requires appropriate stimuli, such as hypoxia or low temperature, to induce p120 ubiquitylation and the consequent proteolytic activation process by the proteasome. Activation of the precursor p120 releases the soluble and active transcriptional activator p90 from the ER to the nucleus, where it drives the gene expression mediated by stress responsive elements (STRE) (Covino et al., 2016).

In order to assess the role of light in KlMga2 activation, we transformed the *Klmga2*Δ strain with a plasmid containing a modified *KlMGA2*^{Flag} gene, encoding a N-terminus tagged protein, and we investigated *Kl*Mga2 protein maturation under light or dark growth conditions by Western blot. Results (not shown) revealed that *Kl*Mga2 proteolytic activation occurred independently on light or dark conditions with similar efficiency.

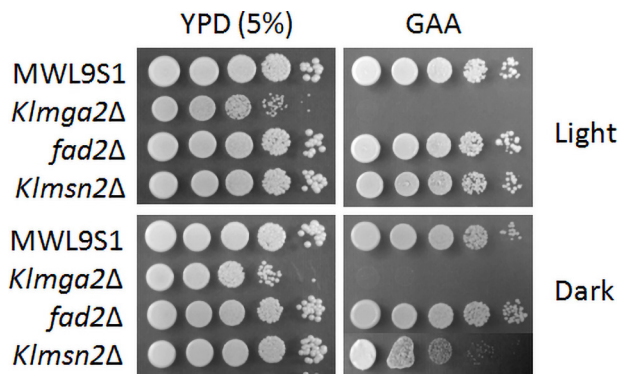

FIGURE 4 | Growth on different media of wild type strain MWL9S1 and mutant strains. Cultures were grown overnight in YPD at 28°C in light or dark conditions, serially diluted, and plated onto YPD plates (5% glucose) without or with antimycin A (GAA plates). Plates were incubated at 28°C under light or dark conditions for 3–4 days. Two or three independent cultures were performed for each strain/condition. Representative samples are shown.

Effects of Light on Catalase and Superoxide Dismutase Enzyme Production

Collapsed mitochondria are often associated to ROS accumulation and impaired response to oxidative stress: we previously observed that GDK/*Klmga2*Δ strain showed a stronger protection against ROS by over-expressing ROS detoxification enzymes catalase (Cat) and superoxide dismutase (SOD) in the exponential growth phase as compared to wild type strain (Santomartino et al., 2019a). The deletion of *KlMGA2* also caused an increased chronological life span (Santomartino et al., 2019a).

Studies on *S. cerevisiae* reported that light is converted to an oxidative stress signal inside the cell (Bodvard et al., 2017). To assess if light exposition activates an oxidative stress response in *K. lactis*, we assayed the production of SOD and *Kl*Ctt1/*Kl*Cta1 enzymes by transcription analysis of *KlSOD1*, *KlSOD2*, *KlCTA1*, and *KlCTT1* genes (**Figure 5**) and by measuring SOD and catalase enzymes activity (**Figure 6**). Wild type and *Klmga2*Δ strains were cultivated in standard YPD medium in light and dark conditions to exponential growth phase. Results of transcription analysis, performed by qRT-PCR, showed that in the wild type strain transcript levels of the four genes did not change between light and dark growth condition (**Figure 5**). On the contrary, the transcription levels of *KlSOD1* (cytosolic SOD) and *KlSOD2* (mitochondrial SOD) genes were higher in the mutant strain than the wild type when cells were grown in light (**Figures 5A,B**). We also observed a 10-fold higher transcription level of *KlCTT1* (cytosolic Cat) gene in the mutant strain with respect to the wild type cells in both light and dark condition (**Figure 5D**). Differently, the transcription levels of *KlCTA1* (peroxisomal Cat) gene were not significantly different between *Klmga2*Δ mutant and wild type cells (**Figure 5C**).

To assess if increased transcription of the selected genes corresponded to increased enzyme activities, SOD and *Kl*Ctt1/*Kl*Cta1 activities were measured in cell extracts at the exponential growth phase. Results are reported in **Figure 6**. Both SOD and *Kl*Ctt1/*Kl*Cta1 activity levels in wild type strain resulted independent on light or dark exposition. On the contrary, SOD activity in *Klmga2*Δ mutant cells (**Figure 6A**) resulted higher in light condition (10.9 ± 0.73 U mg^{-1} mg^{-1}), while in dark condition it was very similar to wild type (6.4 ± 0.04 U mg^{-1}). Differently, *Kl*Ctt1/*Kl*Cta1 activity (**Figure 6B**) in *Klmga2*Δ mutant cells was higher both in dark (12.0 ± 1.31 U mg^{-1}) and light (13.8 ± 1.18 U mg^{-1}) growth conditions compared

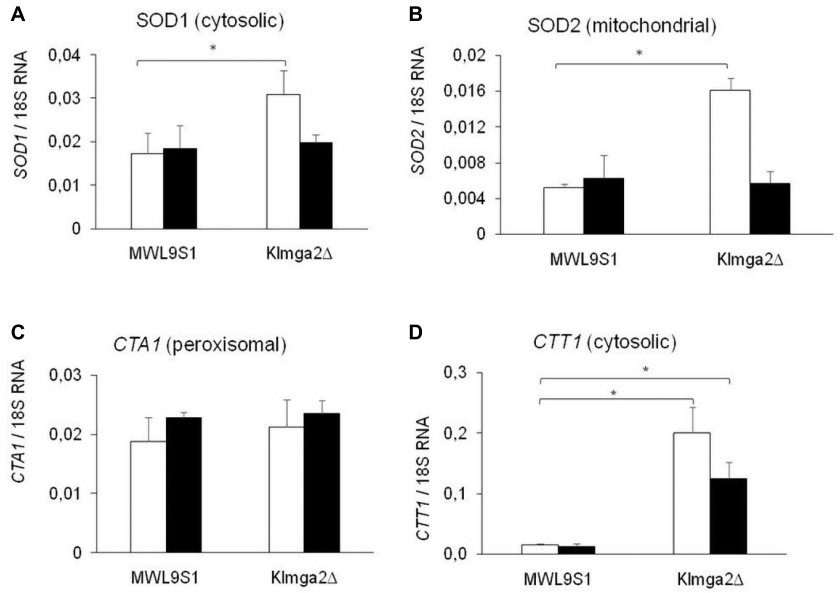

FIGURE 5 | Transcription of *KlSOD1*, *KlSOD2*, *KlCTA1*, and *KlCTT1* genes. Results of qRT-PCR analysis of Catalase (Cat) and SOD genes in wild type MWL9S1 and in *Klmga2*Δ mutant strain grown in YPD flask cultures in light (white blocks) or dark (black blocks) condition are reported. **(A–D)** report *KlSOD1*, *KlSOD2*, *KlCTA1*, and *KlCTT1* transcription analysis, respectively. Ribosomal 18S gene transcription has been used as reference. Values are averages of three independent determinations, each measured by two technical repetitions, with SD reported. * indicates $p < 0.05$.

to wild type (4.8 ± 1 and 4.7 ± 0.33 U mg^{-1} in dark and light, respectively).

We performed enzyme activities assays in the *Klmsn2*Δ strain too, since in *S. cerevisiae* Msn2 upregulates the cytosolic catalase gene *CTT1* (Hasan et al., 2002), which resulted strongly transcribed in *Klmga2*Δ mutant cells (**Figure 5D**). In the *Klmsn2*Δ strain, we found a significantly decrease of *Kl*Ctt1/*Kl*Cta1 activity (3.2 ± 0.38 U mg^{-1} and 3.5 ± 0.14 U mg^{-1} in light and dark condition, respectively; **Figure 6B**) in respect to wild type cells, suggesting that also in *K. lactis* Msn2 upregulates the activity of catalases. No significant changes of SOD activity compared to wild type were found in the *Klmsn2*Δ mutant.

Effects of Light on Fad2 Desaturase Production

Previous studies showed that FA composition of membranes is modulated by hypoxia in *S. cerevisiae* (Vasconcelles et al., 2001), by temperature and also by light exposure, especially in plant and bacterial cells (Kis et al., 1998; Hernández et al., 2011), as a stress adaptation response. We reported that *K. lactis* strain GDK/Klmga2Δ has an altered membrane composition and an inhibited hypoxic induction of the desaturase gene *FAD2*, which was the main FA desaturation target gene of *Kl*Mga2 (Ottaviano et al., 2015). We aimed studying a possible light regulation of desaturases expression in *K. lactis*, in particular, a *Kl*Mga2-dependent response to light. To this purpose, we first focused our study to the desaturase *FAD2* gene expression after light to dark and dark to light shifts. Results of qRT-PCR, reported in **Figure 7**, showed that the transcription levels of *FAD2* in wild type strain were influenced by light exposure. In detail, the shift from light to darkness caused a transient increase of transcription with a significant peak at 40 min from transition, while a progressive *FAD2* transcript reduction could be observed by shifting from darkness to light. Differently, the expression of *FAD2* in the *Klmga2*Δ mutant strain resulted substantially unchanged during light/dark shifts.

The expression profile of *FAD2* in wild type strain was confirmed assaying Fad2 protein levels by Western blot (**Figure 8**). The shift from light to darkness caused a transient increase of Fad2 expression with a significant peak at 60 min from induction; from darkness to light, our results showed a Fad2 reduction after 120 min of light exposure.

Effects of Light/Darkness Growth on FA Composition in Wild Type and *Klmga2*Δ Strains

Desaturases control the synthesis of unsaturated FAs and, consequently, composition of membranes. We performed FA analysis of wild type and *Klmga2*Δ mutant cells grown overnight in light or darkness (**Figure 9**). In the wild type strain, we observed a significant higher level of total FAs when cells were grown in light rather than in darkness, while in the mutant strain, FAs were high independently on light or darkness (values: **Figure 9A**). We calculated the Unsaturation Index (UI), a parameter of membrane fluidity: a low UI indicates a low fluidity of the membrane lipids due to a reduced percentage of unsaturated carbon–carbon bonds in FA molecules. Results in **Figure 9B** indicated a lower UI for the mutant strain with respect to the wild type, as also previously reported (Ottaviano et al.,

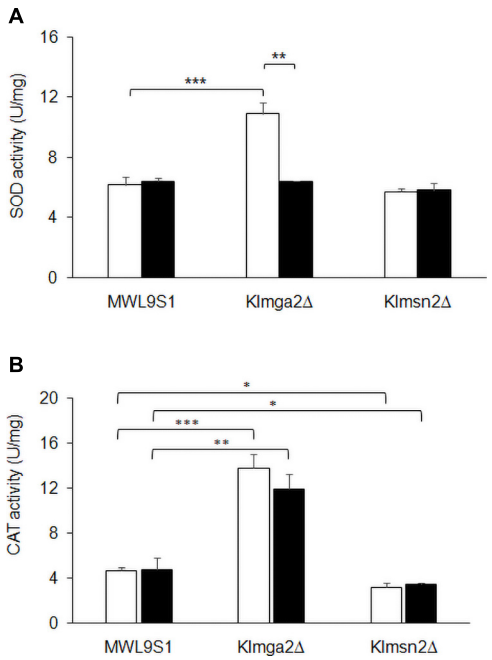

FIGURE 6 | Activity of SOD and catalase enzymes. Total extracts from wild type MWL9S1, *Klmga2*Δ and *Klmsn2*Δ strains, grown in light (white blocks) and dark (black blocks) conditions up to exponential phase, were assayed for catalase and superoxide dismutase activities. **(A)** shows SOD activities (U mg^{-1}): values are averages of three independent determinations, each measured by three technical repetitions, with standard deviations reported. **(B)** shows *Kl*Ctt1/*Kl*Cta1 activities (U mg^{-1}): values are averages of two to four independent determinations, each measured by three technical repetitions, with SD reported. Significances: *$p < 0.05$; **$p < 0.01$; and ***$p < 0.001$.

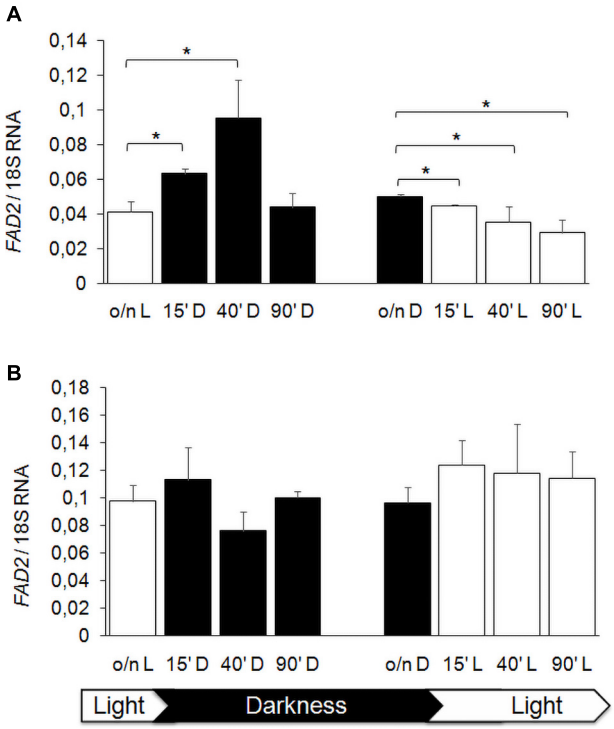

FIGURE 7 | *FAD2* transcription after light and darkness shifts. Wild type **(A)** and *Klmga2*Δ **(B)** strain cells were grown overnight in light (o/n L) or darkness (o/n D) and then shifted to darkness (D) or light (L), respectively, for 15, 40, and 90 min before nucleic acid extraction and qRT-PCR. Values are averages of three independent determinations with SD. Transcription of ribosomal 18S gene was used as reference. * indicates $p < 0.05$.

2015), regardless on light (1.71 ± 0.005 vs. 1.93 ± 0.03) or dark (1.65 ± 0.004 vs. 1.81 ± 0.03) exposure. In addition, we have observed that UI was higher in both strains when cultivated in light condition as compared to darkness.

The detailed analysis of palmitic (C16:0), palmitoleic (C16:1), stearic (C18:0), oleic (C18:1), linoleic (C18:2), and linolenic (C18:3) acids is reported in **Figure 9C**. In the wild type strain, the growth in darkness resulted in an increase of saturated palmitic and stearic acids and of the mono-unsaturated (MUFA) oleic acid: the reduction of UI in darkness depended on the compensatory decrease of poly-unsaturated (PUFA) linoleic and linolenic acids. In the mutant strain we observed slightly different profile: the significant increase of palmitoleic acid was compensated by the decrease of C18 unsaturated oleic, linoleic and linolenic acids. The most relevant differences between the wild type and the mutant strains were significant increase of palmitoleic acid in the mutant strain, both in light and darkness growth (and oleic, but only in light), and the significant reduction of linoleic acid in the mutant strain, again in both light and darkness conditions.

These changes might depend on different production of the desaturases Ole1 and Fad2 in the mutant strain. To verify this hypothesis, we determined the amount of Fad2 by Western blotting in the wild type and in the mutant strains grown in light and darkness. Results, reported in **Figure 10**, showed a significant reduction of Fad2 in the mutant strain with respect to the wild type, when grown under light stress, suggesting that, at least in light condition, the reduction of linoleic acid could be correlated to reduction of the corresponding biosynthetic enzyme.

DISCUSSION

Light is an ubiquitous and free source of energy. Light availability allowed the evolution of organisms endowed of biochemical systems able to capture and use this energy for biosynthesis. Also organisms lacking such molecules or proteins are subjected to light and are possibly set to respond to its exposure. Microorganisms like the unicellular yeasts *K. lactis* and *S. cerevisiae* do not have recognized light-responsive protein or photo-receptive molecules but are transparent to light and their metabolism and physiology might be influenced by light.

Light Stress in *K. lactis*

Very few data, related to the light response in yeast, are available. In *S. cerevisiae*, the two regulatory factors Msn2 and Crz1 are environmental-stress regulators and a similar

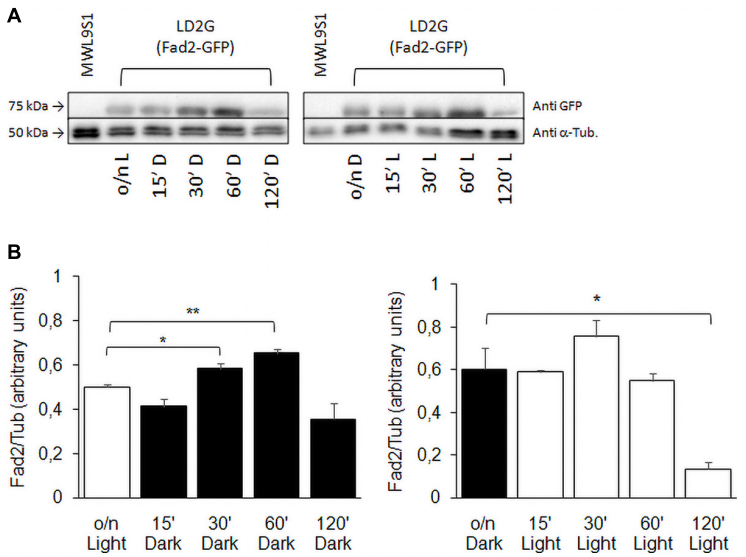

FIGURE 8 | Fad2 enzyme production in wild type strain with *FAD2* fused to *EGFP*. **(A)** Shows Western blot against GFP-fused Fad2 protein, using strain LD2G (De Angelis et al., 2016). Cells were grown overnight in light or darkness and then shifted to darkness or light for 15, 30, 60, and 120 min. α-Tubulin detection was used as loading control. **(B)** Reports Fad2-GFP signal quantification with respect to α-Tubulin: values are averages of three independent determinations with SD. Significances: $*p < 0.05$; $**p < 0.01$.

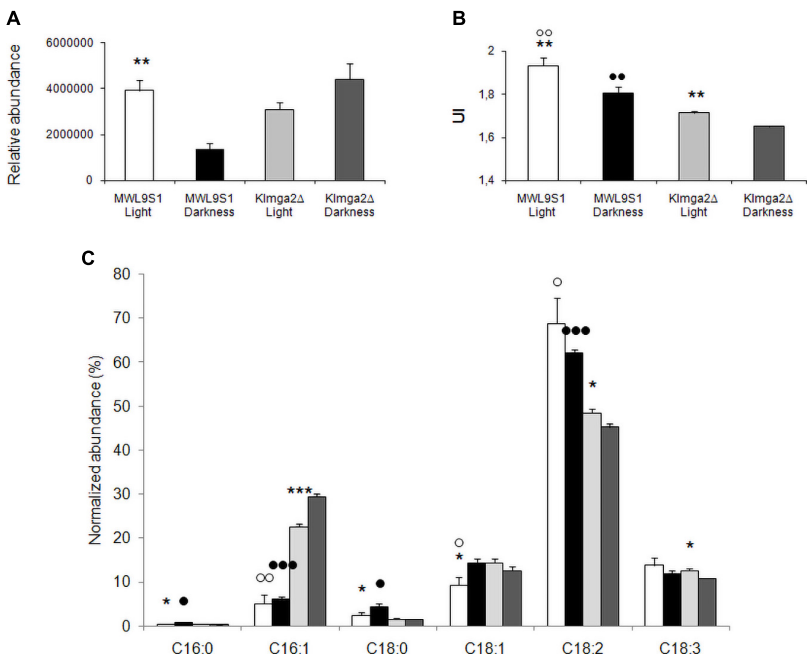

FIGURE 9 | Fatty acid composition of the wild type MWL9S1 and *Klmga2*Δ mutant strain. Cells were grown in overnight light or darkness. **(A,B)** Report total fatty acid (FA) content (relative abundance with respect to 9-hydroxy octadecadienoic d_4 acid, 9-HODE d_4) and unsaturation indexes (UI) of the wild type and deleted mutant strain, respectively, with SD reported. **(C)** Reports amounts of palmitic (C16:0), palmitoleic (C16:1), stearic (C18:0), oleic (C18:1Δ9), linoleic (C18:2Δ9,Δ12), and linolenic (C18:3Δ9,Δ12,Δ15) acids (relative abundance with respect to HODE, normalized to the total amount of FAs). Results with SD are means of three independent determinations. Statistical relevance: stars = light vs dark, white dots = wild type vs mutant (light conditions), black dots = wild type vs mutant (dark conditions); one star or white/black dot = $p < 0.05$, two stars or white/black dots = $p < 0.01$ and three stars or white/black dots = $p < 0.001$.

function has been recorded also for Msn2 in *K. lactis* (Barsoum et al., 2011). Msn2 and Crz1 are also light-dependent proteins in *S. cerevisiae*, translocated to nuclei under light exposition (Cai et al., 2008; Bodvard et al., 2011), suggesting a possible light-stress response dependent on the expression of specific target genes. Light signaling can be mediated in

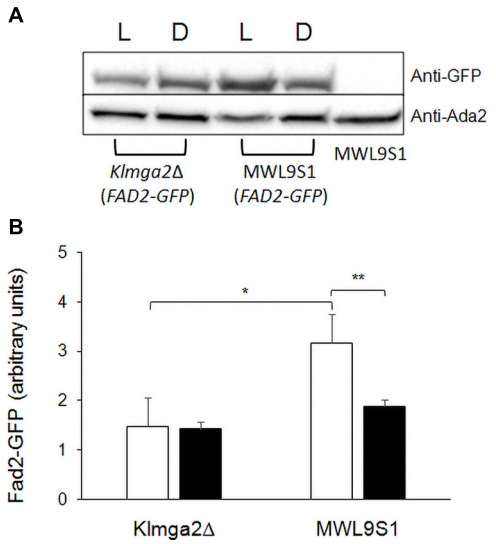

FIGURE 10 | Fad2 production in *Klmga2*Δ mutant strain and wild type. **(A)** Shows a Western blot against Fad2-GFP protein, using extracts of strains LD2G and *Klmga2*Δ/Fad2-GFP grown overnight in light (L) and dark (D) conditions. Ada2 protein was used as loading control. **(B)** Reports a Fad2-GFP signal quantification of repeated Western blot experiments. White blocks represent Fad2-GFP in light and black blocks in darkness, respectively. SD are indicated. Statistical significance: $^{*}p < 0.05$, $^{**}p < 0.01$.

S. cerevisiae by the synthesis of hydrogen peroxide and the activity of PKA through the action of Pox1/Tsa1/Trx1 enzymes (Bodvard et al., 2017). All these elements are also present in *K. lactis* (*TPK1/2*: *KLLA0B07205g*, *TPK2*: *KLLA0D03190g*, *BCY1*: *KLLA0E04181g*, *POX1*: *KLLA0F09933g*, *TSA1*: *KLLA0B01628g*, *TRX1*: *KLLA0E16347g*), suggesting that a similar mechanism might be active also in this yeast.

In wild type *K. lactis* cells, light had no effects on growth rate. Differently, in the absence of *KlMGA2* gene, growth in darkness proceeded faster than in light, suggesting that that light could act as stressing element respect to growth and that *Kl*Mga2 could counteract light effect, protecting cells from adverse events. An altered membrane composition of the *Klmga2*Δ strain is a direct consequence of the reduced expression of *FAD2*, which is a main target of *Kl*Mga2 (Ottaviano et al., 2015). However, the deletion of *FAD2* gene did not affect light growth, suggesting that the differences in growth between light and dark conditions observed in the *Kl*mga2Δ strain should not be a direct consequence of the altered FAs membrane composition that characterizes the mutant strain.

Mitochondrial Functions

We have previously reported that the deletion of *KlMGA2* causes altered mitochondrial morphology and respiration rate (Ottaviano et al., 2015). The recovery of normal mitochondrial morphology and the increase of respiration rate of the *Klmga2*Δ strain in the darkness confirm that *K. lactis* can sense light and that *Kl*Mga2 could play a role to mediate or attenuate phenotypes specifically correlated to respiration and/or mitochondrial functions in response to light. The deletion of *KlMSN2* did not caused sensitivity to the mitochondrial drug antimycin A (rag- phenotype), as in the case of *KlMGA2*. A slight sensitivity to the drug in darkness suggests an opposite regulatory effect of *Kl*Msn2, respect to *Kl*Mga2, in the mechanism of antimycin A resistance in light/dark conditions. The deletion of *KlCRZ1* did not cause evident phenotypes in the conditions explored in this work.

Activation of *Kl*Mga2

Our results indicated that light or dark exposition did not induce the *Kl*Mga2 maturation process. However, the slight sensitivity to antimycin A, especially in darkness, of the constitutively active *mga2*ΔTM strain suggests a possible role of the full-sized membrane-bound *Kl*Mga2 form in contrasting drug activity. A detailed study of *Kl*Mga2 maturation and the physiological characterization of the strain harboring the *Kl*Mga2 truncated form, such as growth, oxygen consumption, and protein localization, will require further targeted investigations.

Oxidative Stress

We have demonstrated in previous work (Santomartino et al., 2019a) that *Kl*Mga2 is involved in the response to oxidative stress and regulates chronological life span. It has been reported that light can induce ROS generation and oxidative stress in *S. cerevisiae* (Bodvard et al., 2017). In *K. lactis*, we found that the activity profiles of *Kl*Ctt1/*Kl*Cta1 and SOD enzymes and the transcriptional profiles of the corresponding genes were consistent with a general overactive ROS response in the absence of *KlMGA2* when the cells were exposed to light, especially as far as SOD expression was concerned. Our results also suggested a possible role of *Kl*Mga2 as downregulator of Msn2, because we observed high *Kl*Ctt1/*Kl*Cta1 activity in the absence of *Kl*MGA2, which was instead reduced in the absence of *KlMSN2*. In the latter case, the mechanism of action seemed to be independent on light/dark exposition.

Lipids

FA composition of membranes determines their properties and functionality and depends on the expression FA biosynthetic enzymes, especially desaturases. The expression of yeast FAs desaturases is regulated by various environmental factors, including hypoxia, temperature, and the presence of specific chemicals. In addition, different yeasts are endowed with different desaturases (Santomartino et al., 2017). Another environmental factor that might influence membrane composition is light: it has been shown that the expression of the desaturase gene *FAD2* in plant depends on light exposure (Kargiotidou et al., 2008; Dar et al., 2017). Our study on the expression of *FAD2* desaturase gene in *K. lactis* indicated that *Kl*Mga2 mediates the transient light-dependent regulation of *FAD2* observed in wild type cells, suggesting a light-stress dependent modulation of membrane composition. Our results showed opposite light regulation of transcription of *FAD2* and *SOD1/2* or *CTT1* genes in the wild type and in the *Klmga2*Δ mutant, suggesting that light stress influenced differently ROS metabolism and PUFA biosynthesis in *K. lactis* and indicating the

involvement of other specific elements in the *Kl*Mga2-dependent response mechanisms.

Major differences between *K. lactis* cells cultivated in light and in darkness were in the total amount of FAs and in the unsaturation index (UI). Light cultivation caused a consistent increase of cellular FAs and an increase of UI. Light also caused specific changes in the amount of individual FA species. As far as FA biosynthesis and accumulation were concerned, the absence of *Kl*Mga2 simulated a light stress-like status with abundant FAs content. On the other hand, light stress could be associated with increased membrane fluidity but this response was not dependent on *Kl*Mga2. It remains to be investigated the specific connection between light stress and high FAs content and high UI. For example, the high FAs content might derive from accumulation of triacylglycerol, due to metabolic imbalance, or increase of functional membranes, dependent on organelle proliferation. These hypotheses could be further investigated by assessing lipid droplets in light and dark conditions.

Interestingly, the amount of oxylipins (oxidized FA, **Supplementary Figure 5**) increased in dark conditions concomitantly to FA decrease in both strains. Especially 13-hydoxyoctadecenoic acid (13-HODE), an oxidation product of linoleic acid, increased in darkness (not shown). We can suggest that part of the loss of linoleic acid under dark conditions experiments by both strains could be partly due to the synthesis of oxylipins. This synthesis can be spontaneous, i.e., occurring from double bond oxidation by ROS, and enzymatically, i.e., catalyzed by lipoxygenases or dioxygenases.

CONCLUSION

Results reported in this work indicate that the yeast *K. lactis* is responsive to light and that the regulatory factor *Kl*Mga2 has a role in this response. It has been shown that light induces oxidative stress in *S. cerevisiae* (Bodvard et al., 2017) and a similar activity could be envisaged also in *K. lactis* with the involvement of *Kl*Mga2, because of the effect of light on the detoxifying enzymes catalase and SOD. The deletion of *KlMGA2* gene has pleiotropic effects, suggesting that *Kl*Mga2, possibly because of its biochemical characteristics (Camponeschi et al., 2020), participates in various pathways: uncovering the detail of these pathways requires further investigation.

One of the most relevant pathway regulated by *Kl*Mga2 is the biosynthesis of FAs, and we showed here that also this pathway is influenced by light stress. The connection among light stress, membrane composition or functionality, and *Kl*Mga2 is highlighted by the fact that phenotypes of the *Klmga2*Δ strains, like growth rate, respiration rate, and mitochondrial morphology, are partially or completely suppressed either by darkness or by unsaturated FAs (Micolonghi et al., 2012; Ottaviano et al., 2015; Santomartino et al., 2019a). Finally, our findings open new perspectives on the role of light in the biology of organisms (apparently) deprived of light sensing proteins and on the role of lipids and membranes in the response to light stress.

DATA AVAILABILITY STATEMENT

The original contributions presented in the study are included in the article/ **Supplementary Material**, further inquiries can be directed to the corresponding author/s.

AUTHOR CONTRIBUTIONS

IC performed and conceived the experiments and wrote the manuscript. AM, MR, and CM performed the critical reading. MB performed the experiments and critical reading. MMB conceived the experiments, wrote the manuscript, and provided the funding. All authors contributed to the article and approved the submitted version.

FUNDING

This work was supported by the Ateneo Sapienza 2019 and 2020, MAECI Progetti Grande Rilevanza PGR00208; PGR00209; PGR00748.

ACKNOWLEDGMENTS

We are indebted to the colleague Paola Ballario of the Department of Biology and Biotechnology 'C. Darwin', Sapienza University of Rome, who inspired and promoted this research of light effects on yeast.

SUPPLEMENTARY MATERIAL

The Supplementary Material for this article can be found online at: https://www.frontiersin.org/articles/10.3389/fmicb.2021.705012/full#supplementary-material

REFERENCES

Barsoum, E., Rajaei, N., and Aström, S. U. (2011). RAS/cyclic AMP and transcription factor Msn2 regulate mating and mating-type switching in the yeast *Kluyveromyces lactis*. *Eukaryot Cell* 10, 1545–1552. doi: 10.1128/EC.05158-11

Beccaccioli, M., Salustri, M., Scala, V., Ludovici, M., Cacciotti, A., D'Angeli, S., et al. (2021). The effect of *Fusarium verticillioides* fumonisins on fatty acids, sphingolipids, and oxylipins in maize germlings. *Int. J. Mol. Sci.* 22:2435. doi: 10.3390/ijms22052435

Bereiter-Hahn, J. (1976). Dimethylaminostyrylmethylpyridiniumiodine (daspmi) as a fluorescent probe for mitochondria in situ. *Biochim. Biophys. Acta* 423, 1–14. doi: 10.1016/0005-2728(76)90096-7

Bodvard, K., Jörhov, A., Blomberg, A., Molin, M., and Käll, M. (2013). The yeast transcription factor Crz1 is activated by light in a Ca2+/calcineurin-dependent and PKA-independent manner. *PLoS One* 8:e53404. doi: 10.1371/journal.pone.0053404

Bodvard, K., Peeters, K., Roger, F., Romanov, N., Igbaria, A., Welkenhuysen, N., et al. (2017). Light-sensing via hydrogen peroxide and a peroxiredoxin. *Nat. Commun.* 8:14791. doi: 10.1038/ncomms14791

Bodvard, K., Wrangborg, D., Tapani, S., Logg, K., Sliwa, P., Blomberg, A., et al. (2011). Continuous light exposure causes cumulative stress that affects the localization oscillation dynamics of the transcription factor Msn2p. *Biochim. Biophys. Acta* 1813, 358–366. doi: 10.1016/j.bbamcr.2010.12.004

Bussereau, F., Casaregola, S., Lafay, J. F., and Bolotin-Fukuhara, M. (2006). The *Kluyveromyces lactis* repertoire of transcriptional regulators. *FEMS Yeast Res.* 6, 325–335. doi: 10.1111/j.1567-1364.2006.00028.x

Byfield, G. E., and Upchurch, R. G. (2007). Effect of temperature on delta-9 stearoyl-ACP and microsomal omega-6 desaturase gene expression and fatty acid content in developing soybean seeds. *Crop Sci.* 47, 1698–1704. doi: 10.2135/cropsci2006.04.0213

Cai, L., Dalal, C. K., and Elowitz, M. B. (2008). Frequency-modulated nuclear localization bursts coordinate gene regulation. *Nature* 455, 485–490. doi: 10.1038/nature07292

Camponeschi, I., Damasco, A., Uversky, V. N., Giuliani, A., and Bianchi, M. M. (2020). Phenotypic suppression caused by resonance with light-dark cycles indicates the presence of a 24-hours oscillator in yeast and suggests a new role of intrinsically disordered protein regions as internal mediators. *J. Biomol. Struct. Dyn.* 39, 2490–2501. doi: 10.1080/07391102.2020.1749133

Chellappa, R., Kandasamy, P., Oh, C. S., Jiang, Y., Vemula, M., and Martin, C. E. (2001). The membrane proteins, Spt23p and Mga2p, play distinct roles in the activation of *Saccharomyces cerevisiae* OLE1 gene expression. fatty acid-mediated regulation of Mga2p activity is independent of its proteolytic processing into a soluble transcription activator. *J. Biol. Chem.* 276, 43548–43556. doi: 10.1074/jbc.M107845200

Covino, R., Ballweg, S., Stordeur, C., Michaelis, J. B., Puth, K., Wernig, F., et al. (2016). A eukaryotic sensor for membrane lipid saturation. *Mol. Cell* 63, 49–59. doi: 10.1016/j.molcel.2016.05.015

Cyert, M. S. (2003). Calcineurin signaling in *Saccharomyces cerevisiae*: how yeast go crazy in response to stress. *Biochem. Biophys. Res. Commun.* 311, 1143–1150. doi: 10.1016/s0006-291x(03)01552-3

Dar, A. A., Choudhury, A. R., Kancharla, P. K., and Arumugam, N. (2017). The fad2 gene in plants: occurrence, Regulation, and Role. *Front Plant Sci.* 8:1789. doi: 10.3389/fpls.2017.01789

De Angelis, L., Rinaldi, T., Cirigliano, A., Bello, C., Reverberi, M., Amaretti, A., et al. (2016). Functional roles of the fatty acid desaturases encoded by KlOLE1, FAD2 and FAD3 in the yeast *Kluyveromyces lactis*. *Microbiology* 162, 1435–1445. doi: 10.1099/mic.0.000315

De Luca, C., Zhou, Y., Montanari, A., Morea, V., Oliva, R., Besagni, C., et al. (2009). Can yeast be used to study mitochondrial diseases? Biolistic tRNA mutants for the analysis of mechanisms and suppressors. *Mitochondrion* 9, 408–417. doi: 10.1016/j.mito.2009.07.004

Estruch, F. (2000). Stress-controlled transcription factors, stress-induced genes and stress tolerance in budding yeast. *FEMS Microbiol. Rev.* 24, 469–486. doi: 10.1111/j.1574-6976.2000.tb00551.x

Görner, W., Durchschlag, E., Martinez-Pastor, M. T., Estruch, F., Ammerer, G., Hamilton, B., et al. (1998). Nuclear localization of the C_2H_2 zinc finger protein Msn2p is regulated by stress and protein kinase A activity. *Genes Dev.* 12, 586–597. doi: 10.1101/gad.12.4.586

Hao, N., and O'Shea, E. K. (2011). Signal-dependent dynamics of transcription factor translocation controls gene expression. *Nat. Struct. Mol. Biol.* 19, 31–39. doi: 10.1038/nsmb.2192

Hasan, R., Leroy, C., Isnard, A. D., Labarre, J., Boy-Marcotte, E., and Toledano, M. B. (2002). The control of the yeast H_2O_2 response by the Msn2/4 transcription factors. *Mol. Microbiol.* 45, 233–241. doi: 10.1046/j.1365-2958.2002.03011.x

Hernández, M. L., Padilla, M. N., Sicardo, M. D., Mancha, M., and Martínez-Rivas, J. M. (2011). Effect of different environmental stresses on the expression of oleate desaturase genes and fatty acid composition in olive fruit. *Phytochemistry* 72, 178–187. doi: 10.1016/j.phytochem.2010.11.026

Hnatova, M., Wésolowski-Louvel, M., Dieppois, G., Deffaud, J., and Lemaire, M. (2008). Characterization of KlGRR1 and SMS1 genes, two new elements of the glucose signaling pathway of *Kluyveromyces lactis*. *Eukaryot Cell* 7, 1299–1308. doi: 10.1128/EC.00454-07

Hockberger, P. E., Skimina, T. A., Centonze, V. E., Lavin, C., Chu, S., Dadras, S., et al. (1999). Activation of flavin-containing oxidases underlies light-induced production of H_2O_2 in mammalian cells. *Proc. Natl. Acad. Sci. U.S.A.* 96, 6255–6260. doi: 10.1073/pnas.96.11.6255

Hoppe, T., Matuschewski, K., Rape, M., Schlenker, S., Ulrich, H. D., and Jentsch, S. (2000). Activation of a membrane-bound transcription factor by regulated ubiquitin/proteasome-dependent processing. *Cell* 102, 577–586. doi: 10.1016/s0092-8674(00)00080-5

Huang, M., and Kao, K. C. (2018). Identifying novel genetic determinants for oxidative stress tolerance in Candida glabrata via adaptive laboratory evolution. *Yeast* 35, 605–618. doi: 10.1002/yea.3352

Idnurm, A., Verma, S., and Corrochano, L. M. (2010). A glimpse into the basis of vision in the kingdom Mycota. *Fungal Genet. Biol.* 47, 881–892. doi: 10.1016/j.fgb.2010.04.009

Janke, C., Magiera, M. M., Rathfelder, N., Taxis, C., Reber, S., Maekawa, H., et al. (2004). A versatile toolbox for PCR-based tagging of yeast genes: new fluorescent proteins, more markers and promoter substitution cassettes. *Yeast* 21, 947–962. doi: 10.1002/yea.1142

Jiang, Y., Vasconcelles, M. J., Wretzel, S., Light, A., Martin, C. E., and Goldberg, M. A. (2001). MGA2 is involved in the low-oxygen response element-dependent hypoxic induction of genes in *Saccharomyces cerevisiae*. *Mol. Cell Biol.* 21, 6161–6169. doi: 10.1128/mcb.21.18.6161-6169.2001

Kainou, K., Kamisaka, Y., Kimura, K., and Uemura, H. (2006). Isolation of Delta12 and omega3-fatty acid desaturase genes from the yeast *Kluyveromyces lactis* and their heterologous expression to produce linoleic and alpha-linolenic acids in *Saccharomyces cerevisiae*. *Yeast* 23, 605–612. doi: 10.1002/yea.1378

Kargiotidou, A., Deli, D., Galanopoulou, D., Tsaftaris, A., and Farmaki, T. (2008). Low temperature and light regulate delta 12 fatty acid desaturases (FAD2) at a transcriptional level in cotton (*Gossypium hirsutum*). *J. Exp. Bot.* 59, 2043–2056. doi: 10.1093/jxb/ern065

Kis, M., Zsiros, O., Farkas, T., Wada, H., Nagy, F., and Gombos, Z. (1998). Light-induced expression of fatty acid desaturase genes. *Proc. Natl. Acad. Sci. U.S.A.* 95, 4209–4214. doi: 10.1073/pnas.95.8.4209

Köhrer, K., and Domdey, H. (1991). Preparation of high molecular weight RNA. *Methods Enzymol.* 194, 398–405. doi: 10.1016/0076-6879(91)94030-g

Ludovici, M., Ialongo, C., Reverberi, M., Beccaccioli, M., Scarpari, M., and Scala, V. (2014). Quantitative profiling of oxylipins through comprehensive LC-MS/MS analysis of *Fusarium verticillioides* and maize kernels. *Food Addit. Contam. Part A Chem. Anal. Control Expo. Risk Assess.* 31, 2026–2033. doi: 10.1080/19440049.2014.968810

Medvedik, O., Lamming, D. W., Kim, K. D., and Sinclair, D. A. (2007). MSN2 and MSN4 link calorie restriction and TOR to sirtuin-mediated lifespan extension in *Saccharomyces cerevisiae*. *PLoS Biol.* 5:e261. doi: 10.1371/journal.pbio.0050261

Micolonghi, C., Ottaviano, D., Di Silvio, E., Damato, G., Heipieper, H. J., and Bianchi, M. M. (2012). A dual signalling pathway for the hypoxic expression of lipid genes, dependent on the glucose sensor Rag4, is revealed by the analysis of the KlMGA2 gene in *Kluyveromyces lactis*. *Microbiology* 158, 1734–1744. doi: 10.1099/mic.0.059402-0

Natter, K., and Kohlwein, S. D. (2013). Yeast and cancer cells - common principles in lipid metabolism. *Biochim. Biophys. Acta* 1831, 314–326. doi: 10.1016/j.bbalip.2012.09.003

Ottaviano, D., Montanari, A., De Angelis, L., Santomartino, R., Visca, A., Brambilla, L., et al. (2015). Unsaturated fatty acids-dependent linkage between respiration and fermentation revealed by deletion of hypoxic regulatory KlMGA2 gene in the facultative anaerobe-respiratory yeast *Kluyveromyces lactis*. *FEMS Yeast Res.* 15:fov028. doi: 10.1093/femsyr/fov028

Ramadass, R., and Bereiter-Hahn, J. (2008). How DASPMI reveals mitochondrial membrane potential: fluorescence decay kinetics and steady-state anisotropy in living cells. *Biophys. J.* 95, 4068–4076. doi: 10.1529/biophysj.108.135079

Rossi, M., Buzzini, P., Cordisco, L., Amaretti, A., Sala, M., Raimondi, S., et al. (2009). Growth, lipid accumulation, and fatty acid composition in obligate psychrophilic, facultative psychrophilic, and mesophilic yeasts. *FEMS Microbiol. Ecol.* 69, 363–372. doi: 10.1111/j.1574-6941.2009.00727.x

Salani, F., and Bianchi, M. M. (2006). Production of glucoamylase in pyruvate decarboxylase deletion mutants of the yeast *Kluyveromyces lactis*. *Appl. Microbiol. Biotechnol.* 69, 564–572. doi: 10.1007/s00253-005-0148-x

Santhanam, A., Hartley, A., Düvel, K., Broach, J. R., and Garrett, S. (2004). PP2A phosphatase activity is required for stress and Tor kinase regulation of yeast stress response factor Msn2p. *Eukaryot Cell* 3, 1261–1271. doi: 10.1128/EC.3.5.1261-1271.2004

Santomartino, R., Camponeschi, I., Polo, G., Immesi, A., Rinaldi, T., Mazzoni, C., et al. (2019a). The hypoxic transcription factor KlMga2 mediates the response

to oxidative stress and influences longevity in the yeast *Kluyveromyces lactis*. *FEMS Yeast Res.* 19:foz020. doi: 10.1093/femsyr/foz020

Santomartino, R., Ottaviano, D., Camponeschi, I., Landicho, T. A. A., Falato, L., Visca, A., et al. (2019b). The hypoxic expression of the glucose transporter RAG1 reveals the role of the bHLH transcription factor Sck1 as a novel hypoxic modulator in *Kluyveromyces lactis*. *FEMS Yeast Res.* 19:foz041. doi: 10.1093/femsyr/foz041

Santomartino, R., Riego-Ruiz, L., and Bianchi, M. M. (2017). Three, two, one yeast fatty acid desaturases: regulation and function. *World J. Microbiol. Biotechnol.* 33:89. doi: 10.1007/s11274-017-2257-y

Sikorski, R. S., and Hieter, P. (1989). A system of shuttle vectors and yeast host strains designed for efficient manipulation of DNA in *Saccharomyces cerevisiae*. *Genetics* 122, 19–27.

Thewes, S. (2014). Calcineurin-Crz1 signaling in lower eukaryotes. *Eukaryot Cell* 13, 694–705. doi: 10.1128/EC.00038-14

Vasconcelles, M. J., Jiang, Y., McDaid, K., Gilooly, L., Wretzel, S., Porter, D. L., et al. (2001). Identification and characterization of a low oxygen response element involved in the hypoxic induction of a family of *Saccharomyces cerevisiae* genes. implications for the conservation of oxygen sensing in eukaryotes. *J. Biol. Chem.* 276, 14374–14384. doi: 10.1074/jbc.M009546200

Wach, A., Brachat, A., Pööhlmann, R., and Philippsen, P. (1994). New heterologous modules for classical or PCR-based gene disruptions in Saccharomyces cerevisiae. *Yeast* 10, 1793–1808. doi: 10.1002/yea.320101310

Wésolowski-Louvel, M. (2011). An efficient method to optimize *Kluyveromyces lactis* gene targeting. *FEMS Yeast Res.* 11, 509–513. doi: 10.1111/j.1567-1364.2011.00741.x

Wésolowski-Louvel, M., Prior, C., Bornecque, D., and Fukuhara, H. (1992). Rag-mutations involved in glucose metabolism in yeast: isolation and genetic characterization. *Yeast.* 8, 711–719. doi: 10.1002/yea.320080904

Yang, J., Schmelzer, K., Georgi, K., and Hammock, B. D. (2009). Quantitative profiling method for oxylipin metabolome by liquid chromatography electrospray ionization tandem mass spectrometry. *Anal. Chem.* 81, 8085–8093. doi: 10.1021/ac901282n

Yuan, S.-W., Wu, X.-L., Liu, Z.-H., Luo, H.-B., and Huang, R.-Z. (2012). Abiotic stresses and phytohormones regulate expression of FAD2 gene in *Arabidopsis thaliana*. *J. Integr. Agric.* 11, 62–72. doi: 10.1016/S1671-2927(12)60783-4

Zhang, S., Skalsky, Y., and Garfinkel, D. J. (1999). MGA2 or SPT23 is required for transcription of the delta9 fatty acid desaturase gene, OLE1, and nuclear membrane integrity in *Saccharomyces cerevisiae*. *Genetics* 151, 473–483.

Conflict of Interest: The authors declare that the research was conducted in the absence of any commercial or financial relationships that could be construed as a potential conflict of interest.

frontiers in Microbiology

ORIGINAL RESEARCH
published: 23 July 2021
doi: 10.3389/fmicb.2021.706349

Effect of Osmotic Stress on the Growth, Development and Pathogenicity of *Setosphaeria turcica*

Yuwei Liu[1,2,3†], Xiaodong Gong[1,2,3†], Moxiao Li[1,2,3], Helong Si[1,2,3], Qihui Zhou[1,2,3], Xingchen Liu[1,2,3], Yu Fan[1,2,3], Xiaoyu Zhang[1,2,3], Jianmin Han[1,2,3], Shouqin Gu[1,2,3] and Jingao Dong[1,2,4]**

[1] State Key Laboratory of North China Crop Improvement and Regulation, Baoding, China, [2] College of Life Sciences, Hebei Agricultural University, Baoding, China, [3] Key Laboratory of Hebei Province for Plant Physiology and Molecular Pathology, Baoding, China, [4] College of Plant Protection, Hebei Agricultural University, Baoding, China

OPEN ACCESS

Edited by:
Joaquin Arino,
Universitat Autònoma de Barcelona, Spain

Reviewed by:
David Turra,
Università degli Studi di Napoli Federico II, Italy
István Pócsi,
University of Debrecen, Hungary

***Correspondence:**
Shouqin Gu
gshq@hebau.edu.cn
Jingao Dong
shmdjg@hebau.edu.cn

† These authors have contributed equally to this work and share first authorship

Specialty section:
This article was submitted to Microbial Physiology and Metabolism, a section of the journal Frontiers in Microbiology

Received: 07 May 2021
Accepted: 29 June 2021
Published: 23 July 2021

Citation:
Liu Y, Gong X, Li M, Si H, Zhou Q, Liu X, Fan Y, Zhang X, Han J, Gu S and Dong J (2021) Effect of Osmotic Stress on the Growth, Development and Pathogenicity of Setosphaeria turcica. Front. Microbiol. 12:706349. doi: 10.3389/fmicb.2021.706349

Osmotic stress is a severe condition frequently encountered by microorganisms; however, there is limited knowledge on the influence of hyperosmotic stress on the growth, development and pathogenicity of phytopathogenic fungi. Here, three osmotic conditions (0.4 M NaCl, 0.4 M KCl, and 0.6 M sorbitol supplemented in potato dextrose agar medium) were used to identify the effect of osmotic stress on the growth, development and pathogenicity of *Setosphaeria turcica* which is a plant pathogenic fungus and causes northern corn leaf blight disease in maize, sorghum, and related grasses. In osmotic stress, the growth rate of mycelium was decreased, and the number of vesicular structures and flocculent secretion outside the hypha cell wall were significantly increased. The qRT-PCR results showed that the osmotic stress quickly activated the HOG-MAPK pathway, up-regulated the expression of the downstream genes, and these genes were most highly expressed within 30 min of exposure to osmotic stress. Furthermore, the germination rate and the yield of conidia were significantly higher under osmotic stress than in the control. A pathogenicity analysis confirmed that pathogenicity of the conidia which were cultured under osmotic stress was significantly enhanced. By analyzing the knock-out mutants of an osmotic stress responsed gene *StFPS1*, an aquaglyceroporin downstream of the HOG-MAPK pathway, we found that *StFPS1* was involved in the formation of appressorium and penetration peg, which affected the penetration ability of *S. turcica*. In summary, our work explained the correlation between osmotic stress and growth, development, and pathogenicity in *S. turcica*.

Keywords: *Setosphaeria turcica*, osmotic, pathogenicity, HOG-MAPK, *StFPS1*

INTRODUCTION

Organisms are constantly exposed to abiotic stress factors, such as ultraviolet radiation, temperature fluctuations, osmotic imbalance and oxidative damage, during their life cycle (Gasch et al., 2000; Duran et al., 2010; Abu Bakar et al., 2020). Hyperosmotic stress is a prevalent, adverse condition that could cause osmotic dehydration and cell death (Bremer and Krämer, 2019).

Previous studies have shown that exposure of microorganisms to specific incremental stress enhances their resistance to that particular stress factor and other stresses. This is known as cross-protection or cross-resistance (Gasch, 2003). Therefore, evaluating the cellular response induced by stress could reveal the mechanisms by which the cell responds to other stress factors (Brown et al., 2014). You et al. (2012) showed that cells can "remember" previous hyperosmotic stress conditions for some time beyond the duration of signal transduction, and thus they can quickly adapt to subsequent exposure. Filamentous fungi exposed to priming stress show a better response to temperature stress than those that have not been exposed to priming stress (Andrade-Linares et al., 2016).

When exposed to stress, the fungi initiate a series of reprogramming processes to adapt to the environmental changes. For example, under hyperosmotic stress conditions, the hyphae of *Glomus intraradices* grow in a curled hyphae instead of the typical straight runner hyphae and the spore number was significantly decreased (Hammer and Rillig, 2011). In *Ashbya gossypii*, it was found that the growth rate and the total biomass were significantly decreased in the medium supplemented with NaCl (Förster et al., 1998). At the cellular level, hyperosmotic stress causes water outflow from the cell, an increase in cytoplasmic ion concentration, and the contraction of protoplasts (Saito and Posas, 2012). In addition, the molecular regulation of cellular responses to osmotic pressure has been well studied. The high osmolarity glycerol mitogen-activated protein kinase (HOG-MAPK) pathway, which is composed of Ste11/Ssk2/Ssk22 (MAPKKK) -Pbs2 (MAPKK)-Hog1 (MAPK), was reported to be able to govern adaptive responses in fungi (Hohmann, 2002). Among of these components, Hog1 is the central core of the HOG-MAPK cascade (Saito and Posas, 2012). Deletion of Hog1-encoding genes in *Bipolaris oryzae* (Moriwaki et al., 2006), *Magnaporthe oryzae* (Dixon et al., 1999), *Ustilaginoidea virens* (Zheng et al., 2016), and *Fusarium graminearum* (Zheng et al., 2012) cause a defect in adaptation to high osmolarity conditions. Furthermore, it was reported that the homologs of Hog1 were involved in species and tissue-specific pathogenesis (Jiang et al., 2018). For example, Osm1 which is the homolog of Hog1 in *M. oryzae* is dispensable for pathogenesis (Dixon et al., 1999), while, our previous research demonstrated that a MAPK gene named *StSTK1* is essential for hyphal, conidial, and appressorial development; toxin biosynthesis; pathogenicity; and osmotic stress reaction in the plant pathogenic fungus *Setosphaeria turcica* (Li et al., 2016).

Although the osmotic stress response and cellular memory phenomena have been studied in fungi (You et al., 2012), the research of the correlation between osmotic stress and pathogenicity is rarely reported in plant pathogenic fungi. In the present study, the effect of osmotic stress on the growth and development, and pathogenicity in *S. turcica* was explored. Further, the functions of the osmotic stress-related gene *StFPS1*, an aquaglyceroporin gene downstream of the HOG-MAPK pathway, was investigated to confirm the relationship between osmotic stress and pathogenicity. This research will provide an example for understanding the correlation between osmotic stress and pathogenicity in plant pathogenic fungi.

MATERIALS AND METHODS

Strains and Growth Conditions

The strain of *S. turcica* used in the present study was 01–23. The strain was cultured according to our previous study with minor modifications (Gu et al., 2014). Specifically, potato dextrose agar (PDA) medium supplemented with 0.4 M NaCl, 0.4 M KCl, or 0.6 M sorbitol was used for the osmotic stress treatments (Araújo et al., 2020). Mycelium of *S. turcica* with a diameter of 0.8 cm was inoculated with the above four media, respectively, (each medium had three replicates) in darkness at 25°C and the colony diameters were measured from the first day to the sixth day after inoculation. All tests were performed in three independent times.

Colony Growth Rate, Yield of Conidium, Hyphae and Conidia Morphology

Colony growth rate was monitored and calculated using the method reported in our previous research (Gu et al., 2014). After 20 days of culture under darkness at 25°C, the effects of osmotic stress treatment on the morphology of aerial hyphae, basal hyphae, and conidium were observed. Aerial hyphae from the four media types (each medium had three replicates) were selected from the colony edges and observed under a microscope (Nikon eclipse, E-200). After scraping off the aerial hyphae on the media surfaces, the morphology of the basal hyphae and conidium were examined at 10× and 40× magnifications. Conidium yield was evaluated using a hemocytometer according to our previous report (Zhang et al., 2003), and performed in three independent times.

Appressorium Formation and Penetration Assay

The strain was cultured on PDA medium at 25°C in the dark for 20 days. 5 mL of H_2O, 1.1 M NaCl, 1.1 M KCl, and 1.3 M Sorbitol were added on the surface of the colonies to obtain conidium suspensions and each of the above solution was performed in triplicate. These suspensions were incubated at 25°C for 30 min and 3 h and then the conidia concentration was adjusted to 10^4/mL using ddH_2O. The suspensions were then placed on water agar media covered with cellophane and incubated in the dark at 25°C. The germination of conidia and the formation of invasive structures were observed 3, 6, 9, 11, 12, 24, 36, 48, 60, and 72 h post cultivation. At least 10 sights of each sample were observed. Artificial cellophane film was used for the penetration assay, as detailed in our previous report (Gong et al., 2021).

Evaluation of the Pathogenicity on Maize Seedlings

The strain was cultured on PDA medium and PDA medium supplemented with 0.4 M KCl at 25°C in the dark for 20 days.

Then, 5 mL H_2O was added on the surface of the colony to make a conidial suspension and the conidial concentration was adjusted to 10^4/mL. Further, 200 μL of suspension was inoculated on three maize seedling whorls at the 4–6 leaf stage. Inoculated seedlings were placed in a dark growth chamber with 80% humidity for 24 h and cultivated in 12 h of light, 12 h of darkness at 25°C for 7–15 days to evaluate the pathogenicity on maize leaves.

Observation of Cell Wall Ultrastructure

After 3 days of growth in PDA medium or PDA medium supplemented with 0.4 M NaCl, the aerial and basal hyphae were sampled and quickly placed in a 1.5 mL EP tube containing the initial fixative solution [2.5% glutaraldehyde (w/v) made up in 0.1 M phosphate buffer (pH 7.2)]. The methods for scanning electron microscopy and transmission electron microscopy were those presented in our previous report (Gong et al., 2017a). At least 10 cell were observed for each sample.

Expression Analysis of Key Genes in the *S. turcica* HOG-MAPK Pathway Under Osmotic Stress

The search of HOG-MAPK pathway homologous genes in *S. turcica* was using the local Blastp program (version 2.7.1+). The protein sequences related to HOG-MAPK pathway in *S. cerevisiae* were as queries to search the GeneCatalog proteins[1] of *S. turcica*. For the blast results, the best alignment of *S. turcica* protein was regarded as the homolog of *S. cerevisiae*. For the qRT-PCR analysis, the strain was sampled during active growth. A mycelium with a diameter of 0.8 cm was inoculated in potato dextrose (PD) medium and incubated in the dark at 25°C for 5–7 days. The PD medium was poured out and completely drained off between filter papers. Then, the pathogen was cultivated in PD medium supplemented with 0.4 M NaCl for 0, 5, 10, 15, 20, and 30 min, and 1, 3, 12, 24, 36, 48, and 72 h. Subsequently, the pathogen was taken out and the excess water was removed using filter paper. RNA extraction was conducted using the UNIQ-10 column Trizol total RNA extraction kit following the manufacturer's protocol (Songon Biotech, China). Total RNA was reverse transcribed to complementary DNA (cDNA) using M-MLV reverse transcriptase (Promega) according to the manufacturer's instructions. The qRT-PCR analysis was performed using TransStart Top Green qPCR SuperMix (TransStart, China) and the primers are shown in **Supplementary Table 1**. PCR reactions were performed in triplicate for each sample.

Transformation-Mediated Gene Disruption

Gene knock-out was done based on a previously published method (Ruiz-Roldán et al., 2001). Briefly, an upstream flanking fragment of *StFPS1* (*StFPS1-A*) was amplified by StFPS1-AL/StFPS1-AR primers, while StFPS1-BL/StFPS1-BR was used to amplify a downstream flanking fragment of *StFPS1* (*StFPS1-B*). After amplicon purification using the TaKaRa DNA Fragment Purification Kit ver. 2.0 (TaKaRa, Japan), the fragments *StFPS1-A* and *StFPS1-B* were cloned into the vector pBS, which confers resistance to hygromycin B phosphotransferase. The resulting plasmid, named pBS-A-HPH-B, was used to transform wild-type (WT) of *S. turcica* protoplasts. The transformed protoplasts were incubated on PDA medium containing hygromycin B (50 μg/mL) at 25°C for 6–7 day until hygromycin B-resistant transformants were observed. All transformants were individually preserved and subjected to verification by PCR using the primers *HPH*-L/*HPH*-R and a primer which was in the upstream of *StFPS1* (*StFPS1*-UpL) and a primer in *HPH* (*HPH*-UpR).

HT-Toxin Isolation and HPLC Analysis Assay

After 21 day of culture in the dark at 25°C, the mycelia of Δ*StFPS1* and WT were filtered away with 4-layer gauze. The filtrate was centrifuged (2,000 × *g*, 10 min), and the supernatant was extracted with acetic ether ethyl acetate (AEEC) at 25°C and 200 r min^{-1} for 12 h. The water-soluble extract was further extracted with AEEC. The residue was dissolved in methanol and used in the subsequent HPLC analysis and toxicity assay, as described previously (Zhang et al., 2007).

RESULTS

Osmotic Stress Affects the Growth of *S. turcica*

To determine the effects of osmotic conditions on the growth and development of *S. turcica*, the strain was inoculated into PDA medium supplemented with 0.4 M NaCl, 0.4 M KCl, and 0.6 M sorbitol. Firstly, the colony diameter was measured every day after inoculation and the colony morphology was observed on the sixth day. The results showed poor hypha growth under osmotic stress (**Figure 1A**). Compared with the 0.6 M sorbitol treatment, the colonies were significantly limited under the 0.4 M NaCl and 0.4 M KCl treatments (**Figure 1B**), indicating that the hypha are more sensitive to ionic stress than non-ionic stress. Furthermore, obvious granular substances were observed in the hyphae of *S. turcica* in the 0.4 M NaCl treatment (**Figure 1C**). In addition, it was found that osmotic stress had a significant effect on the growth of the basal hyphae. The hypha septum of *S. turcica* in the medium supplemented with 0.4 M NaCl, 0.4 M KCl, and 0.6 M sorbitol were significantly shorter than control (**Figure 1D**). Some of the hyphae even expanded to form a spherical shape (**Figure 1E**). Overall, these results indicate that both aerial and basal hyphae exhibited short turns and swellings to various degrees when cultivated in osmotic media.

Prompted by the granular substances observed in hyphae grown on PDA medium with 0.4 M NaCl, we determined whether osmotic stress affects the formation and transport of vesicles. Therefore, following 3-day culture in PDA and PDA supplemented with 0.4 M NaCl, hyphae were observed via electron microscopy (**Figure 2A**). The hyphae cultivated

[1] https://genome.jgi.doe.gov/Settu3/Settu3.home.html

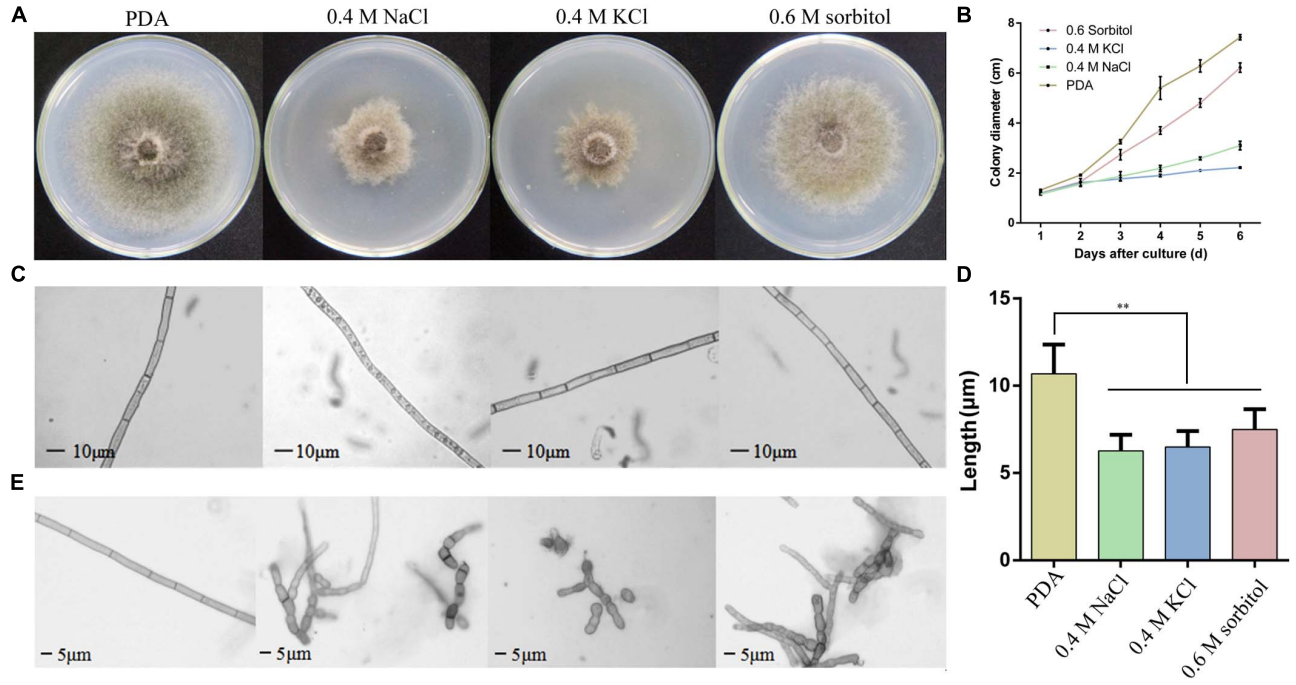

FIGURE 1 | Observation of the *Setosphaeria turcica* phenotype when cultured under osmotic conditions. **(A)** Colony morphology and **(B)** the growth rate of *S. turcica* in potato dextrose agar (PDA) and 0.4 M NaCl, 0.4 M KCl, and 0.6 M sorbitol culture media. The results are shown as mean colony diameter from three independent experiments. **(C)** Morphology and **(D)** the growth rate of aerial hyphae under the above four culture mediums; **(E)** morphology of basal hyphae under the above four culture conditions. These results are shown as mean length of hyphae from three independent experiments. Data are presented as the mean ± SD of three independent experiments. $^{**}P < 0.01$.

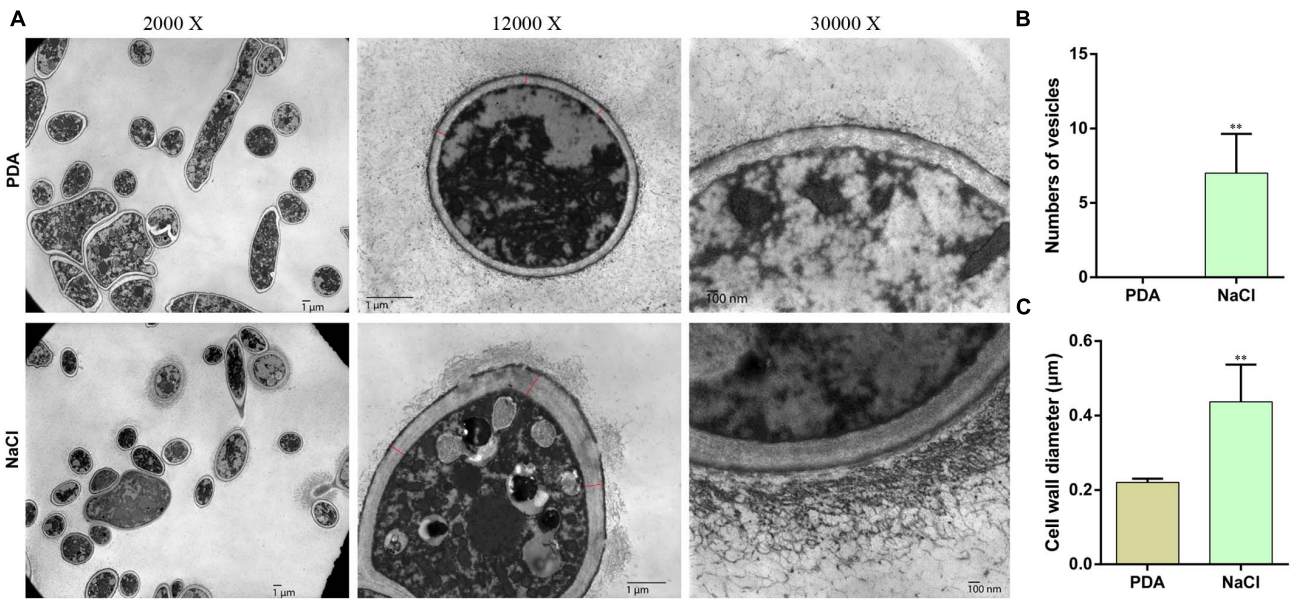

FIGURE 2 | Transmission electron microscopy (TEM) of hyphae of *S. turcica* cultured on PDA and 0.4 M NaCl. **(A)** Representative TEM images (magnification, ×2,000, ×12,000, and ×30,000, respectively) of hyphae. **(B)** The mean number of vesicles in each cell. **(C)** The mean diameter of the cell wall. Data are presented as the mean ± SD of each cell. $^{**}P < 0.01$.

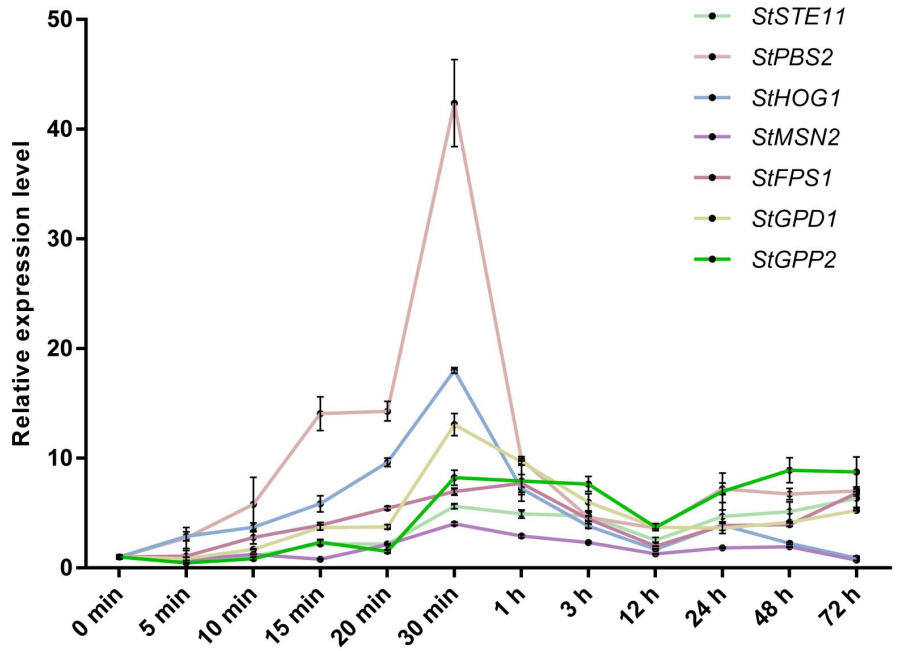

FIGURE 3 | qRT-PCR analysis of the relative expression of HOG-MAPK related genes at different treatment times in 0.4 M NaCl treatment. Data are presented as the mean ± SD of three independent experiments.

under osmotic conditions produced numerous membrane vesicles, whereas this was not found in cells cultured in PDA alone (**Figure 2B**). In addition, the hypha cell wall in the osmotic medium became significantly thicker and the flocculent secretions outside the cell wall increased compared with those in the control (**Figure 2C**). These results indicated that vesicle transport was increased under osmotic stress in *S. turcica*.

Identification of Genes Responsive to Osmotic Stress in *S. turcica*

In light of the osmotic stress has a great influence on the growth of *S. turcica*, we wanted to explore the genes that can respond to hypertonic stress. Previous studies have indicated that HOG-MAPK pathway contributes to osmotic regulation (Hohmann, 2002). To explore whether the HOG-MAPK pathway can respond to osmotic stress in *S. turcica*, the dynamic changes of gene expression related to HOG-MAPK pathways were studied. Specifically, seven genes involved in the HOG-MAPK pathways, namely *StSTE11* (Locus ID from Joint Genome Institute: 158652), *StPBS2* (138151), and *StHOG1* (47672), and the downstream genes of the HOG-MAPK cascade, namely *StMSN2* (101099), *StFPS1* (153214), *StGPD1* (166570), and *StGPP2* (1414693), were evaluated. The expression levels of *StPBS2*, *StHOG1*, *StMSN2*, *StFPS1*, and *StGPD1* increased first and then decreased with the increase in osmotic stress treatment time (0.4 M NaCl; **Figure 3**). The mRNA level of *StFPS1* was highest after 1 h of osmotic treatment, whereas the mRNA levels of the other four genes reached a peak value after 30 min of osmotic treatment. Notably, the relative expression level of *StHOG1* and *StMSN2* decreased to its lowest level after 72 h of osmotic stress treatment (**Figure 3**). This finding agrees with the previous report that to adapt to osmotic stress, yeast cells re-establish osmotic balance and decrease the relative expression level of *StHOG1* to its lowest level (Saito and Posas, 2012). In addition, the results showed that the expression of almost all the tested genes was significantly reduced at 12 h after osmotic stress treatment (**Figure 3**). These results indicate that both the HOG-MAPK pathway genes and the key downstream genes respond to osmotic stress via dynamic gene transcription in *S. turcica*.

Osmotic Stress Strengthens the Formation of Infection Structures

The HOG pathway plays a species-specific role in pathogenesis (Jiang et al., 2018). In our previous study, we found the *StHOG1* was required for pathogenicity in *S. turcica* (Li et al., 2016). Therefore, the strong transcriptional induction of *StHOG1* in osmotic stress led us to consider the possibility that osmotic stress have a certain relationship to pathogenicity. To test this, the germination of conidia and appressorium formation and the formation of infection structures which cultured on PDA medium with different osmotic stress conditions were observed. We found that the hyphae could induce conidia under different culture conditions, but the conidia yield was significantly decreased ($P < 0.05$) under hypertonic culture (**Figure 4A**). Among of them, the conidia yield was the lowest in the medium supplemented with 0.6 m sorbitol (**Figure 4A**). In addition, the conidium could germinate after 3 h of cultivation in the PDA medium and the three osmotic

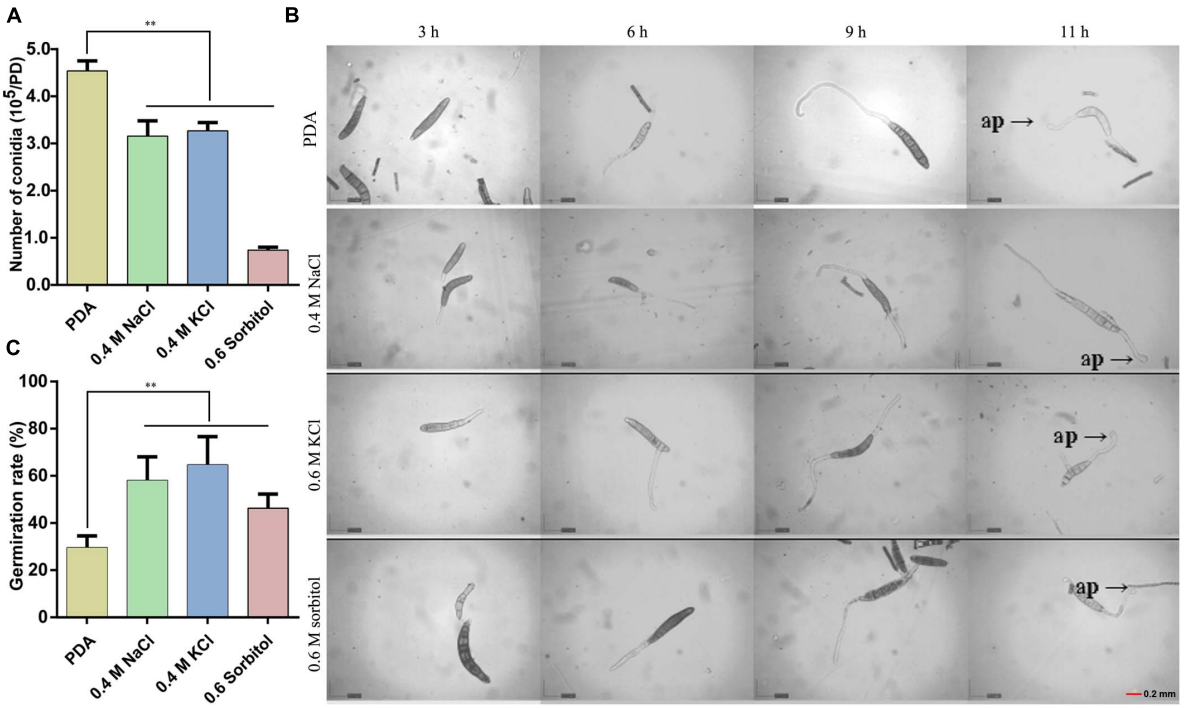

FIGURE 4 | Observation of conidia germination after 20 days of culture under the three osmotic conditions (0.4 M NaCl, 0.4 M KCl, and 0.6 M sorbitol) and control (PDA). **(A)** The number of conidia produced by the hyphae under the four media. **(B)** The conidial suspension was incubated on cellophane at 25°C in the dark and observed at 3, 6, 9, and 11 h after inoculation under a microscope and **(C)** the quantitative statistics from three independent petri dishes. ap: appressorium, Data are presented as the mean ± SD of three independent experiments.$^{**}P < 0.01$.

media (**Figure 4B**). In the control group (PDA alone), the germination rate of conidia was 29.51%, whereas the germination rate in the media supplemented with 0.4 M NaCl, 0.4 M KCl, and 0.6 M sorbitol were 58.08, 64.63, and 46.30%, respectively, which were significantly higher than the PDA control ($p < 0.01$; **Figure 4C**). However, osmotic stress did not affect the conidial morphology and similar to the control, most conidium was fusiform with six to eight compartments (**Supplementary Figure 1**). Further, whether osmotic conditions affect the formation of infective structures was also studied. The formation of penetration pegs could be found both in the control and the three osmotic treatments after 12 h of induction (**Figure 5**). However, the morphology of invading hyphae differed between the control and osmotic conditions. Under osmotic conditions, the invading hyphae generally gathered into a bunch, grew rapidly toward a specific direction, and the tip continued to bifurcate and extend forward at 60 and 72 h. Meanwhile, the invading hyphae formed in PDA grew radially around the penetration peg (**Figure 5**). In addition, the higher osmolality (1.3 M NaCl) with shorter-term (3 h) osmotic stress treatment had the same effect on the morphology of invading hyphae in the 20-day 0.4 M NaCl treatment. However, there was no obvious difference among the morphology of hyphae in the other treatments (**Supplementary Figure 2**). These results suggest that osmotic stress influences the germination of conidia and the morphology of invading hyphae.

Osmotic Stress Enhances the Pathogenicity of *S. turcica*

To confirm the effect of osmotic stress on the pathogenicity of *S. turcica*, host infection experiments were performed. Leaf whorls of maize seedlings at the 4–6 leaf stage were inoculated with conidial suspension supplemented with 0.4 KCL or not. The results indicated that plants inoculated with conidial suspension supplemented with KCl showed 1–2 days earlier disease spots. Furthermore, the disease spots on these plants were expanded than on plants inoculated with conidial suspension not supplemented with KCl 12 days post inoculation (**Figure 6**). These results suggest that osmotic stress enhanced the pathogenicity of *S. turcica* in maize.

Osmotic Stress Related Gene *StFPS1* Regulates the Invasiveness of *S. turcica*

Previous study of Luyten et al. (1995) showed that Fps1, an aquaglyceroporin of yeast, facilitates glycerol transport in response to changes in extracellular osmolarity. Our results indicated that *StFPS1*, a homologous of yeast *FPS1*, was up-regulated during osmotic stress (**Figure 3**). To investigate the effect of osmotic related gene *StFPS1* in pathogen pathogenicity, mutant strain of *S. turcica*, namely, Δ*StFPS1* was generated via protoplast transformation and confirmed by PCR analysis (**Figure 7A**). The results showed that the hyphae of Δ*StFPS1* could not form any appressorium and penetration pegs after

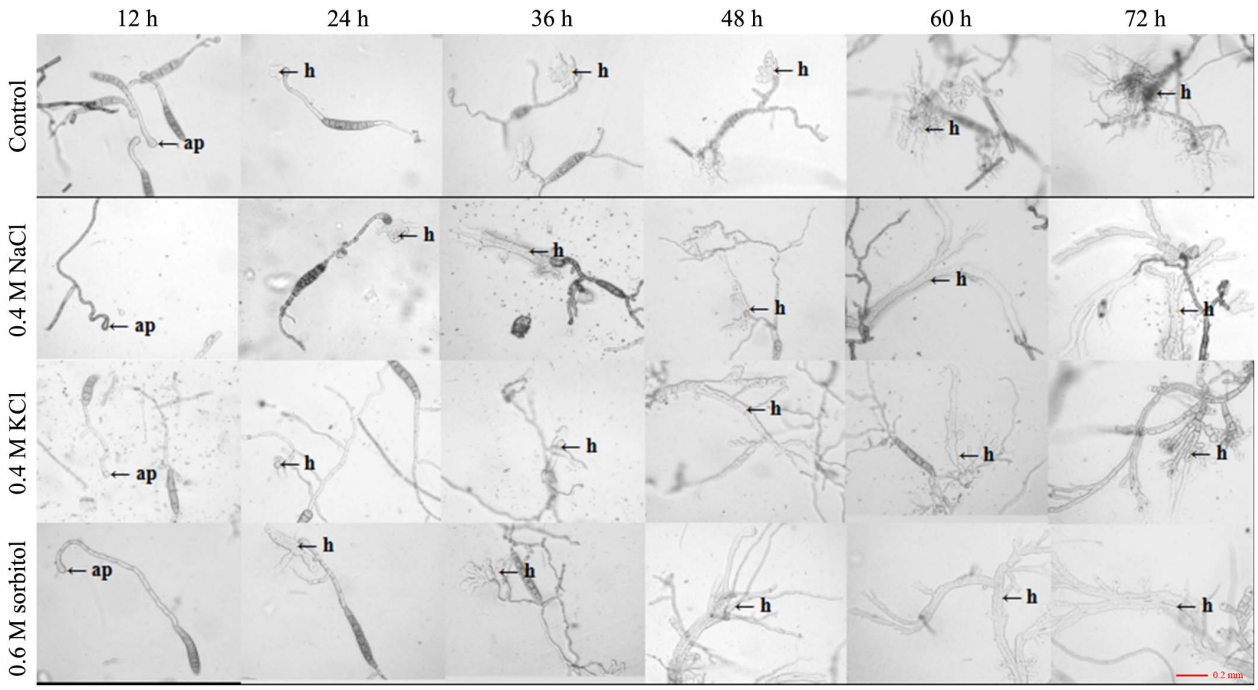

FIGURE 5 | Observation of appressorium development after 20 days of culture under the three osmotic conditions (0.4 M NaCl, 0.4 M KCl, and 0.6 M sorbitol) and control (PDA). The conidial suspension was incubated on cellophane at 25°C in the dark and observed at 12, 24, 36, 48, 60, and 72 h after inoculation under a microscope. h: invading hyphae.

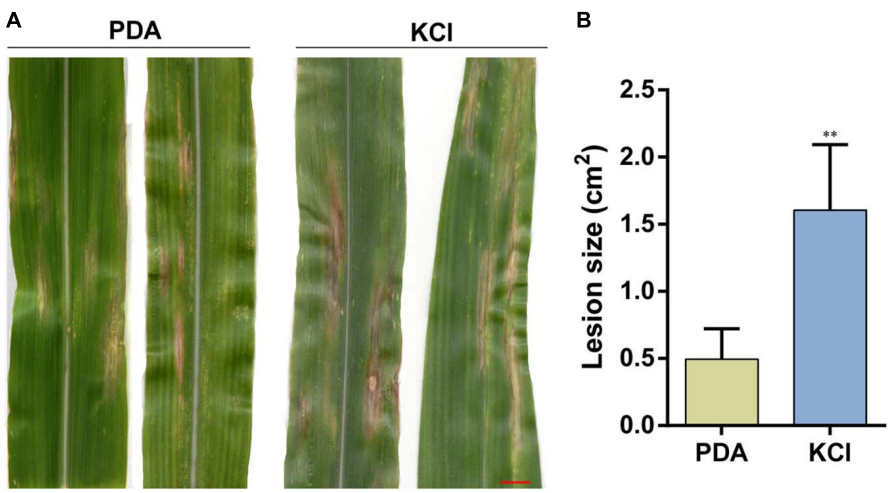

FIGURE 6 | Pathogenicity of *S. turcica* after 20 days of culture under the 0.4 M KCl and control (PDA). **(A)** Conidial suspensions were inoculated on maize B73 seedling whorl at the 4–6 leaf stage, and results were scored at 12 days post-inoculation and **(B)** the mean size of the lesion. $^{**}P < 0.01$, bar = 1 cm.

84 h of induction, while, the appressorium and penetration pegs of the WT strain were observed after 24 h and 36 h of induction (**Figure 7B**). These results suggest that *StFPS1* significantly influences the formation of infective structures. To evaluate whether *StFPS1* is essential for pathogenicity, the mycelial suspensions of WT and Δ*StFPS1* were inoculated on the maize leaves. 10 days after inoculation, the maize leaves exhibited typical fusiform lesions after inoculation with WT, while no lesions were detected after inoculation with Δ*StFPS1* (**Figure 7C**), indicating *StFPS1* is required for pathogenesis of *S. turcica*. In order to clarify the influence of *StFPS1* on pathogenicity, a penetration test was then performed to confirm the influence of *StFPS1* on penetrability. Hyphae taken from the WT strain and Δ*StFPS1* were separately inoculated on PDA media covered with artificial cellophane film which can simulate hyphal penetration into maize leaves. The results showed that

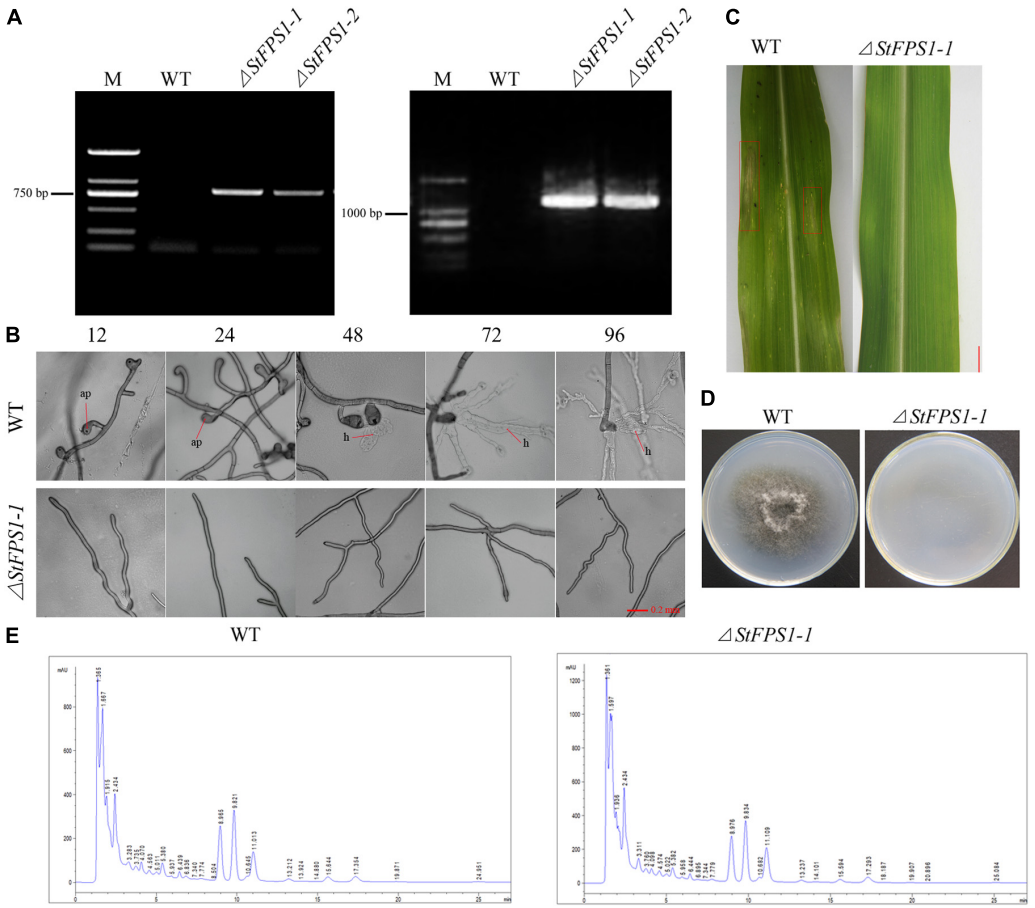

FIGURE 7 | Identification of the *StFPS1* knockout mutant (Δ*StFPS1*) and functional analysis of Δ*StFPS1*. **(A)** *S. turcica* wild-type (WT) and Δ*StFPS1*, identified by amplifying a fragment of the hygromycin B phosphotransferase gene (*HPH*) using specific primers (*HPH*-L/*HPH*-R; left) and fragment including the *StFPS1* upstream flanking fragment and *HPH* using specific primers (*StFPS1*-UpL/*HPH*-UpR; right). **(B)** Observation of the appressorium development of WT and Δ*StFPS1* at 12, 24, 48, 72, and 96 h after inoculation under a microscope. **(C)** Mycelial suspensions were inoculated on maize B73 seedling whorl at the 4–6 leaf stage, and results were scored at 10 days post-inoculation, bar = 1 cm. **(D)** Comparison of the cellophane penetrating ability of WT and Δ*StFPS1* after the strains were incubated on cellophane at 25°C in the dark for 5 days and then removed the cellophane and continued to incubate for 2 days for observation. **(E)** High performance liquid chromatography analysis of HT-toxins of WT and Δ*StFPS1*.

Δ*StFPS1* could not penetrate the cellophane to form a colony, while the WT strain showed the opposite results (**Figure 7D**). To further elucidate whether *StFPS1* influence the pathogenicity of *S. turcica*, the components of crude HT-toxin which is an important pathogenic factor in *S. turcica* were analyzed by HPLC (Gu et al., 2014). The results showed that the Δ*StFPS1* and WT strains had absorption peaks at the same time, and the peak areas were almost the same, indicating that the deletion of *StFPS1* did not change the composition and content of HT-toxin (**Figure 7E**). Based on the above results, we inferred that *StFPS1* effects the development of appressorium and the penetration ability of *S. turcica*.

DISCUSSION

To adapt to hyperosmotic stress, microorganisms have formed a set of effective osmoadaptation mechanisms over the course of evolution. One of the most common mechanisms of osmoadaptation mechanisms is the production and accumulation of osmoregulatory substances to maintain intracellular water balance (Saito and Posas, 2012). In *S. turcica*, our previous study confirmed that hyperosmotic stress significantly changed the contents of glycerol, trehalose and mannitol in mycelial cells (Gong et al., 2017b). To further explore the effect of osmotic stress on the growth, development, and pathogenicity in *S. turcica*, the pathogen was exposed to NaCl, KCl, and sorbitol. Relative to sorbitol, both NaCl and KCl severely inhibited pathogen growth (**Figure 1A**). These findings are in accordance with the study on hyperosmotic stress in *Ashbya gossypii*, which reported that the growth rate of NaCl-treated cells was significantly decreased, whereas there was a minor effect on grown in the mannitol treatment (Förster et al., 1998). Further analysis found that many granular substances were in the hyphae which were cultured on medium with 0.4 M NaCl, while it was not found in other cases. These

results further confirm that osmotic stress caused by Na^+ could have an additional influence on the content in the hyphae (**Figure 1B**). This finding is similar to a previous report revealing that sodium toxicity poses additional influence on the growth of *S. cerevisiae* (Prista et al., 2005). Furthermore, electron microscopy demonstrated a significant influence of osmotic conditions on the morphology of *S. turcica* cells. Therefore, cell resistance to external osmotic stress conditions involves multiple coordinated responses.

The osmoadaptation mechanism in yeast has been studied intensively, and the HOG-MAPK pathway is the main pathway that acts in response to hyperosmotic stress. Moreover, the role of HOG-MAPK in osmoregulation is conserved in many fungi, such as in *Verticillium dahliae* (Wang et al., 2016), *B. oryzae* (Turrà et al., 2014), *U. virens* (Zheng et al., 2016), and *S. turcica* (Li et al., 2016). In yeast, HOG-MAPK mediated osmoregulation by phosphorylating the activation site of Hog1 (peaking at 5 min), after which most Hog1 are transported to the nucleus to regulate transcription and the cell cycle, and after 30 min, glycerin accumulates in the cell to produce high osmotic pressure (Hao et al., 2007; Muzzey et al., 2009; Wosika and Pelet, 2020). In addition, in yeast, the greatest changes in the high osmolarity-regulated genes were observed within the first 40 min of treatment, with the maximal induction after 20 min of treatment (O'Rourke and Herskowitz, 2004). In the present study, genes related to the HOG-MAPK pathway participate in osmotic stress response via transcriptional regulation (**Figure 2**). The results of this study showed that most of these genes were maximally up-regulated within 30 min of osmotic treatment, suggesting that the HOG-MAPK pathway-related genes could rapidly respond to osmotic stress at the mRNA level (**Figure 2**). In addition, some reports have focused on the influence of osmotic stress on secondary metabolism and/or morphogenesis, such as in the yeast *S. cerevisiae*, *Aspergillus species* (Hohmann et al., 2007; Miskei et al., 2009). However, few reports focus on the influence of osmotic stress on the pathogenicity in plant pathogenic fungi. It's worth noting that the HOG-MAPK pathway has species-specific differences in pathogenesis of plant pathogenic fungi (Dixon et al., 1999; Wang et al., 2016; Segorbe et al., 2017; Jiang et al., 2018). In *S. turcica*, for instance, we previously found that the MAPK gene *StHOG1* is required for pathogenicity (Li et al., 2016). In the present study, we further found that the downstream gene *StFPS1* is also involved in regulating fungal invasiveness (**Figure 7**). A previous study on yeast showed that the Fps1p channel plays an important role in facilitating glycerol efflux (Beese-Sims et al., 2011). Therefore, it is possible that *StFPS1* reduces glycerol transport and the hyphae subsequently lack the pressure to form infective structure. For *M. oryzae*, the appressorium develops a high internal turgor pressure for penetration of the rice leaf and glycerol accumulation plays an important role in appressorium turgor (Foster et al., 2017). These results demonstrate the significance of the HOG-MAPK pathway in fungal development and pathogenicity.

Cross-protection is a common phenomenon in microorganisms. For instance, in *Zygosaccharomyces rouxii* and *Rhodotorula mucilaginosa*, heat preadaptation could improve resistance to salt stress (Cheng et al., 2016; Wang et al., 2021). However, the mechanisms by which cross-protection occurs remains obscure. Previous studies have shown that two homologous transcription factors Msn2p and Msn4p, which are downstream of the HOG-MAPK cascade (Verghese et al., 2012), were associated with the basis of cross-stress resistance (Święciło, 2016). These findings reveal the important role of HOG-MAPK in cross-protection. In our previous research, we found that *StHOG1* is not only involved in osmotic stress but also related to pathogenicity (Li et al., 2016), indicating that there must be some relationship between osmotic stress reaction and pathogenicity in *S. turcica*. In accordance with our hypothesis, in the present study, we found the osmotic stress strengthens the formation of infection structures and enhances the pathogenicity of *S. turcica*. In addition, in the life cycle of phytopathogenic fungi, at conidium germination and the penetration phase, fungi are in a state of starvation, which can be regarded as starvation stress (Divon and Fluhr, 2007). During these periods, nutrients are entirely obtained from internal stores, of which glycerol is a major component (Thines et al., 2000; Weber et al., 2001). As for *S. turcica*, we speculate that exposure to osmotic stress strengthens its ability to synthesis glycerol via the HOG-MAPK pathway in *S. turcica*. Via pretreatment with hypertonic stress, fungi can quickly synthesize glycerol to meet the nutrient demand when they infect maize leaves. Subsequently, the glycerol produces the high turgor pressure required for appressorium, thereby increasing pathogenicity. Therefore, our experiment confirmed from a new perspective that osmotic stress as an important abiotic stress factor effects the growth and development, and pathogenicity by activating gene expression in HOG MAPK pathway, and the cell memory of osmotic stress can enhance the pathogenicity of *S. turcica*.

CONCLUSION

In this study, qRT-PCR analysis indicated that the activation of the HOG-MAPK pathway and the expression of its downstream genes are quickly up-regulated at the transcriptional level to respond to osmotic stress. Importantly, it was demonstrated that osmotic stress affects the morphology of hypha, shortens the germination time of conidia, alters the structure of invasive hyphae, and enhances the pathogenicity of *S. turcica*. Genetic analysis revealed that *StFPS1*, a key gene downstream of HOG-MAPK pathway, influences the development of appressorium and the penetration ability to maize, but is not related to the virulence in *S. turcica*. In summary, our findings confirmed that there is a close relationship between osmotic stress response and pathogenicity in *S. turcica*.

DATA AVAILABILITY STATEMENT

The original contributions presented in the study are included in the article/**Supplementary Material**; further inquiries can be directed to the corresponding author/s.

AUTHOR CONTRIBUTIONS

SG and JD conceived and designed the experiments. YL participated in the experiments and wrote the manuscript. XG, ML, HS, QZ, XL, YF, and XZ performed the experiments. JH collect the experimental materials. All authors read and approved the final manuscript.

FUNDING

This work was supported by the National Natural Science Foundation of China (Nos. 31671983 and 31701741), the Natural Science Foundation of Hebei Province (No. C2019204211), and the China Agriculture Research System (CARS-02-25).

SUPPLEMENTARY MATERIAL

The Supplementary Material for this article can be found online at: https://www.frontiersin.org/articles/10.3389/fmicb.2021.706349/full#supplementary-material

Supplementary Figure 1 | Morphology of conidia culture under the three osmotic conditions (0.4 M NaCl, 0.4 M KCl, and 0.6 M sorbitol) and control (PDA) conditions.

Supplementary Figure 2 | Observation of appressorium development of *S. turcica* grown for 3 h in 1.1 M NaCl, 1.1 M KCl, and 1.3 M sorbitol media. ap: appressorium; h: invading hyphae.

Supplementary Figure 3 | The phenotype of *StFPS1* knockout mutants.

Supplementary Table 1 | The primers used in this study.

REFERENCES

Abu Bakar, N., Karsani, S. A., and Alias, S. A. (2020). Fungal survival under temperature stress: a proteomic perspective. *PeerJ*. 8:e10423. doi: 10.7717/peerj.10423

Andrade-Linares, D. R., Veresoglou, S. D., and Rillig, M. C. (2016). Temperature priming and memory in soil filamentous fungi. *Fungal Ecol.* 21, 10–15. doi: 10.1016/j.funeco.2016.02.002

Araújo, C. A. S., Ferreira, P. C., Pupin, B., Dias, L. P., Avalos, J., Edwards, J., et al. (2020). Osmotolerance as a determinant of microbial ecology: a study of phylogenetically diverse fungi. *Fungal Biol.* 124, 273–288. doi: 10.1016/j.funbio.2019.09.001

Beese-Sims, S. E., Lee, J., and Levin, D. E. (2011). Yeast Fps1 glycerol facilitator functions as a homotetramer. *Yeast* 28, 815–819. doi: 10.1002/yea.1908

Bremer, E., and Krämer, R. (2019). Responses of microorganisms to osmotic stress. *Annu. Rev. Microbiol.* 73, 313–334. doi: 10.1146/annurev-micro-020518-115504

Brown, A. J. P., Budge, S., Kaloriti, D., Tillmann, A., Jacobsen, M. D., Yin, Z., et al. (2014). Stress adaptation in a pathogenic fungus. *J. Exp. Biol.* 217, 144–155.

Cheng, Z., Chi, M., Li, G., Chen, H., Sui, Y., Sun, H., et al. (2016). Heat shock improves stress tolerance and biocontrol performance of *Rhodotorula mucilaginosa*. *Biol. Control* 95, 49–56. doi: 10.1016/j.biocontrol.2016.01.001

Divon, H. H., and Fluhr, R. (2007). Nutrition acquisition strategies during fungal infection of plants. *FEMS Microbiol. Lett.* 266, 65–74. doi: 10.1111/j.1574-6968.2006.00504.x

Dixon, K. P., Xu, J. R., Smirnoff, N., and Talbot, N. J. (1999). Independent signaling pathways regulate cellular turgor during hyperosmotic stress and appressorium-mediated plant infection by *Magnaporthe grisea*. *Plant Cell* 11, 2045–2058. doi: 10.2307/3871096

Duran, R., Cary, J. W., and Calvo, A. M. (2010). Role of the osmotic stress regulatory pathway in morphogenesis and secondary metabolism in filamentous fungi. *Toxins* 2, 367–381. doi: 10.3390/toxins2040367

Förster, C., Marienfeld, S., Wendisch, F., and Krämer, R. (1998). Adaptation of the filamentous fungus *Ashbya gossypii* to hyperosmotic stress: different osmoresponse to NaCl and mannitol stress. *Appl. Microbiol. Biotechnol.* 50, 219–226. doi: 10.1007/s002530051280

Foster, A. J., Ryder, L. S., Kershaw, M. J., and Talbot, N. J. (2017). The role of glycerol in the pathogenic lifestyle of the rice blast fungus *Magnaporthe oryzae*. *Environ. Microbiol.* 19, 1008–1016. doi: 10.1111/1462-2920.13688

Gasch, A. P. (2003). "The environmental stress response: a common yeast response to diverse environmental stresses" in *Yeast Stress Responses*. eds S. Hohmann and W. H. Mager (Berlin: Springer). 11–70. doi: 10.1007/3-540-45611-2_2

Gasch, A. P., Spellman, P. T., Kao, C. M., Carmel-Harel, O., Eisen, M. B., Storz, G., et al. (2000). Genomic expression programs in the response of yeast cells to environmental changes. *Mol. Biol. Cell.* 11, 4241–4257. doi: 10.1091/mbc.11.12.4241

Gong, X. D., Feng, S. Z., Zhao, J., Tang, C., Tian, L., Fan, Y. S., et al. (2017a). StPBS2, a MAPK kinase gene, is involved in determining hyphal morphology, cell wall development, hypertonic stress reaction as well as the production of secondary metabolites in Northern Corn Leaf Blight pathogen *Setosphaeria turcica*. *Microbiol. Res.* 201, 30–38. doi: 10.1016/j.micres.2017.04.009

Gong, X. D., Liu, X., Zhao, L. Q., Zheng, Y. N., Fan, Y. S., Han, J. M., et al. (2017b). Effect of hyperosmotic stress on growth and development of *Setosphaeria turcica* and determination of osmolytes in the mycelium cells of the pathogen. *Sci. Agricult. Sin.* 50, 1922–1929.

Gong, X. D., Liu, Y. W., Bi, H. H., Yang, X. R., Han, J. M., Dong, J. G., et al. (2021). StKU80, a component in the NHEJ repair pathway, is involved in mycelial morphogenesis, conidiation, appressorium development, and oxidative stress reactions in *Exserohilum turcicum*. *J. Integr. Agricult.* 20, 147–158. doi: 10.1016/s2095-3119(20)63233-6

Gu, S. Q., Li, P., Wu, M., Hao, Z. M., Gong, X. D., Zhang, X. Y., et al. (2014). *StSTE12* is required for the pathogenicity of *Setosphaeria turcica* by regulating appressorium development and penetration. *Microbiol. Res.* 169, 817–823. doi: 10.1016/j.micres.2014.04.001

Hammer, E. C., and Rillig, M. C. (2011). The influence of different stresses on glomalin levels in an arbuscular mycorrhizal fungus–salinity increases glomalin content. *PLoS One* 6:e28426. doi: 10.1371/JOURNAL.PONE.0028426

Hao, N., Behar, M., Parnell, S. C., Torres, M. P., Borchers, C. H., Elston Timothy, C., et al. (2007). A systems-biology analysis of feedback inhibition in the sho1 osmotic-stress-response pathway. *Curr. Biol.* 17, 659–667. doi: 10.1016/j.cub.2007.02.044

Hohmann, S. (2002). Osmotic stress signaling and Osmoadaptation in yeasts. *Microbiol. Mol. Biol. Rev.* 66, 300–372. doi: 10.1128/mmbr.66.2.300-372.2002

Hohmann, S., Krantz, M., and Nordlander, B. (2007). Yeast osmoregulation. *Methods Enzymol.* 428, 29–45. doi: 10.1016/s0076-6879(07)28002-4

Jiang, C., Zhang, X., Liu, H., and Xu, J. R. (2018). Mitogen-activated protein kinase signaling in plant pathogenic fungi. *PLoS Pathog.* 14:e1006875. doi: 10.1371/JOURNAL.PPAT.1006875

Li, P., Gong, X. D., Jia, H., Fan, Y. S., Zhang, Y. F., Cao, Z. Y., et al. (2016). MAP kinase gene STK1 is required for hyphal, conidial, and appressorial development, toxin biosynthesis, pathogenicity, and hypertonic stress response in the plant pathogenic fungus *Setosphaeria turcica*. *J. Integr. Agricult.* 15, 2786–2794. doi: 10.1016/s2095-3119(16)61472-7

Luyten, K., Albertyn, J., Skibbe, W. F., Prior, B. A., Ramos, J., Thevelein, J. M., et al. (1995). Fps1, a yeast member of the MIP family of channel proteins, is a facilitator for glycerol uptake and efflux and is inactive under osmotic stress. *EMBO J.* 14, 1360–1371. doi: 10.1002/j.1460-2075.1995.tb07122.x

Miskei, M., Karanyi, Z., and Pocsi, I. (2009). Annotation of stress-response proteins in the aspergilli. *Fungal Genet. Biol.* 46, S105–S120.

Moriwaki, A., Kubo, E., Arase, S., and Kihara, J. (2006). Disruption of SRM1, a mitogen-activated protein kinase gene, affects sensitivity to osmotic and ultraviolet stressors in the phytopathogenic fungus *Bipolaris oryzae*. *FEMS Microbiol. Lett.* 257, 253–261. doi: 10.1111/j.1574-6968.2006.00178.x

Muzzey, D., Gómez-Uribe, C. A., Mettetal, J. T., and Oudenaarden, A. V. (2009). A systems-level analysis of perfect adaptation in yeast osmoregulation. *Cell* 138, 160–171. doi: 10.1016/j.cell.2009.04.047

O'Rourke, S. M., and Herskowitz, I. (2004). Unique and redundant roles for HOG MAPK pathway components as revealed by whole-genome expression analysis. *Mol. Biol. Cell* 15, 532–542. doi: 10.1091/mbc.e03-07-0521

Prista, C., Loureiro-Dias, M. C., Montiel, V., García, R., and Ramos, J. (2005). Mechanisms underlying the halotolerant way of *Debaryomyces hansenii*. *FEMS Yeast Res.* 5, 693–701. doi: 10.1016/j.femsyr.2004.12.009

Saito, H., and Posas, F. (2012). Response to Hyperosmotic Stress. *Genetics* 192, 289–318. doi: 10.1534/genetics.112.140863

Segorbe, D., Di Pietro, A., Pérez-Nadales, E., and Turrà, D. (2017). Three *Fusarium oxysporum* mitogen-activated protein kinases (MAPKs) have distinct and complementary roles in stress adaptation and cross-kingdom pathogenicity. *Mol. Plant Pathol.* 18, 912–924. doi: 10.1111/mpp.12446

Święciło, A. (2016). Cross-stress resistance in *Saccharomyces cerevisiae* yeast—new insight into an old phenomenon. *Cell Stress Chaperones* 21, 187–200. doi: 10.1007/s12192-016-0667-7

Ruiz-Roldán, M. C., Maier, F. J., and Schäfer, W. (2001). PTK1, a Mitogen-activated-protein kinase gene, is required for conidiation, appressorium formation, and pathogenicity of pyrenophora teres on barley. *Mol. Plant-Microbe Interact.* 14, 116–125. doi: 10.1094/MPMI.2001.14.2.116

Thines, E., Weber, R. W., and Talbot, N. J. (2000). MAP kinase and protein kinase A-dependent mobilization of triacylglycerol and glycogen during appressorium turgor generation by *Magnaporthe grisea*. *Plant Cell* 12, 1703–1718. doi: 10.1105/tpc.12.9.1703

Turrà, D., Segorbe, D., and Di Pietro, A. (2014). Protein kinases in plant-pathogenic fungi: conserved regulators of infection. *Annu. Rev. Phytopathol.* 52, 267–288. doi: 10.1146/annurev-phyto-102313-050143

Verghese, J., Abrams, J., Wang, Y., and Morano, K. A. (2012). Biology of the heat shock response and protein chaperones: budding yeast (*Saccharomyces cerevisiae*) as a model system. *Microbiol. Mol. Biol. Rev.* 76, 115–158. doi: 10.1128/mmbr.05018-11

Wang, D., Zhang, M., Huang, J., Zhou, R., Jin, Y., Zhao, D., et al. (2021). Heat preadaptation improved the ability of *Zygosaccharomyces rouxii* to salt stress: a combined physiological and transcriptomic analysis. *Appl. Microbiol. Biotechnol.* 105, 259–270. doi: 10.1007/s00253-020-11005-z

Wang, Y., Tian, L., Xiong, D., Klosterman, S. J., Xiao, S., and Tian, C. (2016). The mitogen-activated protein kinase gene, VdHog1, regulates osmotic stress response, microsclerotia formation and virulence in *Verticillium dahliae*. *Fungal Genet. Biol.* 88, 13–23. doi: 10.1016/j.fgb.2016.01.011

Weber, R. W. S., Wakley, G. E., Thines, E., and Talbot, N. J. (2001). The vacuole as central element of the lytic system and sink for lipid droplets in maturing appressoria of *Magnaporthe grisea*. *Protoplasma* 216, 101–112. doi: 10.1007/bf02680137

Wosika, V., and Pelet, S. (2020). *Single-particle View of Stress-promoters Induction Dynamics: an Interplay Between MAPK Signaling, Chromatin and Transcription Factors*. Switzerland: University of Lausanne.

You, T., Ingram, P., Jacobsen, M. D., Cook, E., McDonagh, A., Thorne, T., et al. (2012). A systems biology analysis of long and short-term memories of osmotic stress adaptation in fungi. *BMC Res. Notes* 5:258. doi: 10.1186/1756-0500-5-258

Zhang, L. H., Dong, J. G., Wang, C. H., and Li, Z. P. (2007). Purification and structural analysis of a selective toxin fraction produced by the plant pathogen *Setosphaeria turcica*. *Agric. Sci. China* 6, 452–457. doi: 10.1016/S1671-2927(07)60069-8

Zhang, L. H., Liu, Y. H., Dong, J. G., and Li, Z. P. (2003). Isolation and purification of specific toxin fractions produced by *Exserohilum turcicum*. *Acta Phytopathol. Sin.* 33, 67–71.

Zheng, D., Wang, Y., Han, Y., Xu, J. R., and Wang, C. (2016). UvHOG1 is important for hyphal growth and stress responses in the rice false smut fungus *Ustilaginoidea virens*. *Sci. Rep.* 6:24824. doi: 10.1038/SREP24824

Zheng, D., Zhang, S., Zhou, X., Wang, C., Xiang, P., Zheng, Q., et al. (2012). The FgHOG1 pathway regulates hyphal growth, stress responses, and plant infection in *Fusarium graminearum*. *PLoS One* 7:e49495. doi: 10.1371/JOURNAL.PONE.0049495

Conflict of Interest: The authors declare that the research was conducted in the absence of any commercial or financial relationships that could be construed as a potential conflict of interest.

Publisher's Note: All claims expressed in this article are solely those of the authors and do not necessarily represent those of their affiliated organizations, or those of the publisher, the editors and the reviewers. Any product that may be evaluated in this article, or claim that may be made by its manufacturer, is not guaranteed or endorsed by the publisher.

frontiers in Microbiology

REVIEW
published: 09 August 2021
doi: 10.3389/fmicb.2021.715891

The Plasma Membrane at the Cornerstone Between Flexibility and Adaptability: Implications for *Saccharomyces cerevisiae* as a Cell Factory

*Luís Ferraz[1,2], Michael Sauer[3], Maria João Sousa[1] and Paola Branduardi[2]**

[1] Center of Molecular and Environmental Biology, University of Minho, Braga, Portugal, [2] Department of Biotechnology and Biosciences, University of Milano Bicocca, Milan, Italy, [3] Department of Biotechnology, Institute of Microbiology and Microbial Biotechnology, BOKU University of Natural Resources and Life Sciences, Vienna, Austria

In the last decade, microbial-based biotechnological processes are paving the way toward sustainability as they implemented the use of renewable feedstocks. Nonetheless, the viability and competitiveness of these processes are often limited due to harsh conditions such as: the presence of feedstock-derived inhibitors including weak acids, non-uniform nature of the substrates, osmotic pressure, high temperature, extreme pH. These factors are detrimental for microbial cell factories as a whole, but more specifically the impact on the cell's membrane is often overlooked. The plasma membrane is a complex system involved in major biological processes, including establishing and maintaining transmembrane gradients, controlling uptake and secretion, intercellular and intracellular communication, cell to cell recognition and cell's physical protection. Therefore, when designing strategies for the development of versatile, robust and efficient cell factories ready to tackle the harshness of industrial processes while delivering high values of yield, titer and productivity, the plasma membrane has to be considered. Plasma membrane composition comprises diverse macromolecules and it is not constant, as cells adapt it according to the surrounding environment. Remarkably, membrane-specific traits are emerging properties of the system and therefore it is not trivial to predict which membrane composition is advantageous under certain conditions. This review includes an overview of membrane engineering strategies applied to *Saccharomyces cerevisiae* to enhance its fitness under industrially relevant conditions as well as strategies to increase microbial production of the metabolites of interest.

Keywords: plasma membrane, yeast, membrane engineering, microbial cell factories, robustness, lipids

OPEN ACCESS

Edited by:
Cristina Mazzoni, Sapienza University of Rome, Italy

Reviewed by:
Estéfani García Ríos, Instituto de Salud Carlos III, Spain
Di Liu, Sandia National Laboratories, United States

****Correspondence:***
Paola Branduardi
paola.branduardi@unimib.it

Specialty section:
This article was submitted to Microbial Physiology and Metabolism, a section of the journal Frontiers in Microbiology

Received: *27 May 2021*
Accepted: *19 July 2021*
Published: *09 August 2021*

Citation:
Ferraz L, Sauer M, Sousa MJ and Branduardi P (2021) The Plasma Membrane at the Cornerstone Between Flexibility and Adaptability: Implications for Saccharomyces cerevisiae as a Cell Factory. Front. Microbiol. 12:715891. doi: 10.3389/fmicb.2021.715891

INTRODUCTION

The urge for the production of goods and services for a growing population, adopting the principles of linear economy, has led to massive consumption of natural resources, resulting in an unbalance between the request and the supply of these resources. Biorefineries are intended to address this urgency by utilizing and converting residual and renewable biomasses into a

spectrum of marketable products such as biofuels, materials, chemicals, feed, and food (Branduardi, 2021). Among the diverse methods of valorization of biomass, microbial fermentations offer many possibilities for obtaining the desired products. The diverse nature of the feedstocks, together with the biodiversity of microorganisms, has the potential to lead to the production of many classes of products (Hong and Nielsen, 2012). Yeasts are among the most prominent microorganisms used in industrial biotechnology because they unify the advantage of unicellular organisms with eukaryotic nature. *Saccharomyces cerevisiae*, in particular, plays a major role, mainly thanks to its ancient history of domestication by humans (Branduardi and Porro, 2012). Moreover, microbial biotechnology applications have increased in the last decades, with the constant evolution of genomics, metabolic engineering, systems, and synthetic biology. This has enabled the production of numerous valuable products of primary and secondary metabolism, enzymes and biopharmaceutical proteins, which are of high demand in various industrial sectors. Once more, *S. cerevisiae* is still scoring positive returns as a cell factory (Li and Borodina, 2015).

Nonetheless, harsh industrial conditions put microbial cell factories in very stressful environments. The development of tolerant strains, able to handle the requirements of industrial processes is therefore highly desirable. During industrial processes, microorganisms can be subjected to many and different kinds of stresses: high metabolite concentration, substrate variety, high osmotic pressure and ion toxicity, high temperature, extreme pH, high concentrations of weak acids, among others that compromise cell metabolism (Deparis et al., 2017). In this regard, the plasma membrane plays a key role since it is a physical barrier that separates the extracellular environment and intracellular components, is responsible for maintaining the correct ion homeostasis and is the sensor of the overall cellular environment, rearranging its composition in response to different stimuli (Stewart, 2017). Moreover, increased production of metabolites of interest by the microbial cell factory also puts augmented pressure on the plasma membrane. It is therefore evident that the plasma membrane is crucial for the successful development of many bioprocesses (Jezierska and Van Bogaert, 2017).

Thus, the plasma membrane has to be considered when designing strategies for the development of versatile, robust and efficient cell factories ready to tackle the harshness of industrial processes while delivering high yield, titer and productivity. In this sense, the concept of membrane engineering has emerged. The plasma membrane is a complex and dynamic system, whose behavior is challenging to predict due to the connections, competitions, dependencies, or other types of interactions between its components. Furthermore, the behavior of a system is also influenced by its surrounding environment. This is precisely what happens at the membrane level, where lipids and proteins interact and influence each other. For this reason, it is not trivial to predict which element(s) should be changed to trigger a specific rewiring of the overall system.

When employing membrane engineering strategies, researchers have mainly been focusing on alterations in single elements of the plasma membrane rather than on the membrane as a whole system. Changes in single elements might trigger an overall response of the membrane resulting in a global reshaping of the system. On the other hand, being a highly interconnected network, the plasma membrane might not be affected by single modifications as it can counteract minor alterations by different regulation mechanisms (Sandoval and Papoutsakis, 2016; Jezierska and Van Bogaert, 2017).

This review aims to describe the most recent efforts to engineer the plasma membrane of microbial cell factories, with particular emphasis on *S. cerevisiae*, to increase its fitness and performance in biotechnological processes.

YEAST PLASMA MEMBRANE

All cells are surrounded by a plasma membrane that defines the boundary between the cell itself and the environment. In *S. cerevisiae*, the cell envelope alone (plasma membrane and cell wall) occupies about 15% of the total cell volume (Stillwell, 2016).

In bacteria and eukaryotic cells, the plasma membrane is structured as a bilayer mainly composed of a mixture of (phospho)lipids and proteins which, by their interactions, govern the structure of the membrane and determine its physicochemical properties.

Lipids represent around 50% of the membrane composition. The major lipid classes present in the *S. cerevisiae* membrane are glycerophospholipids (about 70%), sphingolipids (about 15%) and sterols (about 15%) (**Table 1**; Klose et al., 2012). Glycerophospholipids have a glycerol backbone connected to two fatty acyl chains by an ester-linkage and can be further divided according to their head group, attached to glycerol through phosphate, into: phosphatidylcholine (PC), phosphatidylethanolamine (PE), phosphatidylinositol (PI), phosphatidylserine (PS), phosphatidylglycerol (PG), and phosphatidic acid (PA) (Klug and Daum, 2014). The fatty acyl chains of glycerophospholipids are usually C_{16}–C_{18}. Sphingolipids contain a sphingoid backbone connected by an amide link to a fatty acyl chain and are classified by their head group into inositol phosphoryl ceramide (IPC), mannosyl-inositol phosphoryl ceramide (MIPC) and mannosyl-di-inositol phosphoryl ceramide (MIP_2C). Sphingolipids have long-chain

TABLE 1 | Main classes and subclasses of lipids in *S. cerevisiae*.

Lipid classes	Lipid subclasses
Glycerophospholipids	Phosphatidylcholine (PC)
	Phosphatidylethanolamine (PE)
	Phosphatidylinositol (PI)
	Phosphatidylserine (PS)
	Phosphatidylglycerol (PG)
	Phosphatidic acid (PA)
Sphingolipids	Ceramide (CER)
	Inositol phosphoryl ceramide (IPC)
	Mannosyl-inositol phosphoryl ceramide (MIPC)
	Mannosyl-di-inositol phosphoryl ceramide (MIP_2C)
Sterols	Ergosterol

bases (LCB) originating from C_{16}–C_{18} fatty acids combined with very-long-chain fatty acid (VLCFA), usually C_{24}–C_{26}. Sphingolipids acyl chains are completely saturated, differently, the acyl chains of glycerophospholipids can be unsaturated (Megyeri et al., 2016). Saturated fatty acyl chains increase lipid packing and membrane thickness due to their straight conformation, in comparison to unsaturated fatty acyl chains, which have a bent conformation. Furthermore, long fatty acyl chains increase membrane rigidity by increasing the membrane thickness and lipid packaging (Slotte, 2016). Ergosterol is the main sterol in yeast: its general structure comprises a hydroxyl head group, an alkenyl side chain and a four-ring nucleus (Klug and Daum, 2014). Sterols increase membrane rigidity by ordering fatty acyl chains allowing tighter lipid packing (Caron et al., 2014). Nonetheless, portraying the impact of lipid species on the membrane physicochemical properties is an oversimplification and the reality is not as straightforward. The lipid composition of membranes is not constant. In *S. cerevisiae*, the ratios of lipids may differ not only among different strains but also depending on the carbon source and cultivation conditions (Patton and Lester, 1991). Changes in the lipid composition can have profound effects on cellular functions, including signal transduction, membrane elasticity, and membrane trafficking (Santos and Preta, 2018). Moreover, the biosynthesis pathways leading to different lipid species are tightly connected with complex cross-talks (Henry et al., 2012).

Another major component of the plasma membrane is proteins, representing around 40% of the membrane composition. A total of 1,000 different proteins are estimated to be located in the yeast plasma membrane (Stewart, 2017). Not all of these proteins are present at the same time and the amount and type of proteins changes according to different cellular stimuli, which means that the actual number of functional membrane proteins is much smaller. The majority are transport proteins while other membrane proteins are involved in cell wall synthesis, signal transduction or take part in the definition of the cytoskeleton. Remarkably, the activity and stability of membrane proteins is dependent on the lipids that surround them (Coskun and Simons, 2011). Membrane proteins require specific lipids, as cofactors for their functions or as "co-structures" for their correct folding and stability. Therefore, the composition of the lipid bilayer must be optimal for obtaining the correct activity or the desired biological function of the membrane proteins (Lee, 2004). This awareness is very important (and far from being trivial) when introducing heterologous proteins in different microorganisms (Opekarová and Tanner, 2003). Also, the physicochemical properties of the plasma membrane, such as thickness, viscosity, tension and permeability are affected by the interactions between lipids and proteins (Lee, 2004). Lipid rafts are a good example of the interaction between lipids and proteins (Klose et al., 2010). Lipid rafts are dynamic nanoscale ergosterol and sphingolipid-enriched clusters with higher order than the surrounding membrane areas. It has been suggested that the bulky sterol rings pack better next to saturated acyl chains of sphingolipids and are shielded from the aqueous environment by the large sphingolipids head groups. Membrane rafts house several membrane proteins as some concentrate in these specific areas, among which, the proton pump H + -ATPase Pma1 (Ferreira et al., 2001). This is the major proton pump present in the yeast plasma membrane and represents 15% of all plasma membrane proteins. The importance of this proton pump for yeast cells under different stress conditions has been highlighted [see for a recent example Lee et al. (2017)]. The correct positioning and activity of Pma1 into plasma membrane lipid rafts has been correlated with the presence of very long chain fatty acids and ergosterol (Eisenkolb et al., 2002; Gaigg et al., 2006). These studies highlighted the importance of membrane lipid composition for the correct integration and functioning of proteins in the plasma membrane.

EXPLORING MICROBIAL MEMBRANES

It becomes evident that either for understanding biological functions or for exploiting cellular systems in microbial-based processes, biochemical and physical understanding of plasma membranes is essential. Nevertheless, it is difficult to predict which membrane composition will lead to a specific emerging property. However, it is possible to use and integrate the data deriving from different research technologies (**Table 2**) to describe the plasma membrane not as a sum of elements, but as a whole system.

Lipids are highly complex and dynamic molecules with thousands of species dynamically changing to support variations in physiological and environmental conditions. For this reason, the identification and quantification of lipids over time is very difficult (Yang and Han, 2016). Lipidomics is the technology that aims to analyze and quantify lipid species in a cell, organism or context (Klose and Tarasov, 2016). Lipidomics methods reveal the lipid status of a cellular phenotype at a particular time point and therefore allow researchers to correlate a specific membrane lipid composition with specific conditions. However, it does not allow researchers to understand the cellular mechanism which led to a specific membrane composition.

To obtain further information related to the structure and the dynamics of the plasma membrane molecular dynamics (MD) simulations are used (Pluhackova and Böckmann, 2015). MD simulation studies can be used to investigate the physicochemical properties of the membrane, the interdependent influence of proteins and lipids and also the formation of membrane nanodomains (Lindahl et al., 2016, 2018). MD simulations may also be used as predictive, to provide strategies for membrane engineering. However, most MD simulations are performed using very simple membrane models which limits the biological relevance of these studies.

Atomic Force Microscopy (AFM) is another valuable tool used in membrane research. AFM has emerged as a powerful tool to investigate microbial cells at the nanoscale level and to measure the nanomechanical properties of cell surface topology such as stiffness, elasticity or roughness (Dague et al., 2010; Shi et al., 2018). AFM provides three-dimensional views of biological structures in real-time, on living cells and also under biologically relevant conditions (Alsteens et al., 2017). AFM can provide complementary information on how cells can cope

TABLE 2 | Overview of research techniques used to characterize different parameters of the plasma membrane.

Technique	Strengths	Limitations	Relevant works cited within this review
Lipidomics	Identification and quantification of lipids	Accuracy	Klose and Tarasov (2016)
Molecular dynamic simulations	Physiochemical characterization of the plasma membrane	Simplicity of the models available	Pluhackova and Böckmann (2015)
Atomic force microcopy	Working on living cells under physiological relevant conditions, Investigation of cell surface nanomechanical properties	Sample preparation, Scanning speed, Low scan image size	Dufrêne (2002), Francois et al. (2013), Shi et al. (2018)
In vitro membrane models	Enables the prediction of physiochemical properties of lipid bilayers	Limited to the classes of lipids commercially available	Lopes et al. (2017)
Genomic scale metabolic models (GEMs)	Helpful to predict phenotypes based on genotype manipulation.	Reproducibility of simulations "*in vivo*" is dependent on the quality of the GEM	Garcia-Albornoz and Nielsen (2013)

with a certain type of stress, which can be relevant in the design of novel strategies for the development of improved microbial cell factories. Using AFM, Niu et al. (2016) studied the effect of ethanol stress on *S. cerevisiae* plasma membrane elasticity and fluidity. Under ethanol stress, the integrity of the plasma membrane was reduced which led an increased membrane permeability and fluidity. Furthermore, an increase on the plasma membrane elasticity was also observed. For a more detailed information on the application of AFM to explore yeast cells under stress conditions the reader should look at the following manuscripts (Dufrêne, 2002; Francois et al., 2013; Schiavone et al., 2016).

In vitro membrane models represent another way to study the physicochemical properties of lipid bilayers (Lopes et al., 2017). However, these models rely on commercially available lipids. There is still a lack of internal standards for some lipids classes and therefore, these types of studies are usually done using very simple membrane models consisting of only some classes of lipids. For these reasons, the physiological relevance of these studies is often limited.

Genome-scale metabolic models (GEMs) can also be a valuable tool for the design and optimization of microbial cell factories. The reproducibility of the simulations in "*in vivo*" data is, however, dependent on the quality of the GEM (Garcia-Albornoz and Nielsen, 2013). Recently, Tsouka and Hatzimanikatis (2020) developed a metabolic model called "Reduced lipids-centric model" (redLips), which focused on the lipid metabolism of *S. cerevisiae*. "RedLips" was constructed through the integration of detailed lipid metabolic pathways into already existing genome-scale metabolic models. Overall, this model can be used as a scaffold for integrating lipidomics data to improve predictions in studies of lipid-related biological functions (Tsouka and Hatzimanikatis, 2020).

MEMBRANE ENGINEERING IN MICROBIAL WORKHORSES

Overall, the different technologies that allow researchers to study the plasma membrane are still incomplete in describing what is occurring at the membrane level at a certain time point, and even more in the fluctuating conditions of industrial processes. Notably, several approaches involving the plasma membrane have been used to ameliorate yeast cell factories. In this section, we provide an overview of membrane engineering strategies applied to *S. cerevisiae* to improve its robustness toward different stress conditions present at industrial levels, strategies focusing on improving *S. cerevisiae* productivity, yield and production will also be described (**Figure 1**).

Improving the Robustness of Microbial Cell Factories

Robustness is an important beneficial trait for any microorganism to acquire improved fitness, which in some cases correlates with an efficient biosynthesis of desirable molecules (Nicolaou et al., 2010). During biotechnological processes, yeasts encounter different kinds of stresses that are generally associated with the growth conditions (temperature, pH, oxygenation, ...), the starting substrates and the final products or byproducts (Gibson et al., 2007). Because the economic viability of bioprocesses is often limited by damage to the microbial plasma membrane, assessing changes due to stressors becomes essential to design counteractions.

Ethanol

The effects of ethanol on *S. cerevisiae* membrane permeability were firstly described by Leão and Van Uden (1984), who reported an increased permeability of the plasma membrane to protons in the presence of ethanol. Later it was shown that ethanol also increases the diffusion of acetic acid in *S. cerevisiae* (Casal et al., 1998). More recently, a similar effect was also reported by Niu et al. (2016), who showed that the exposure of yeast cells to ethanol resulted in increased membrane permeability (characterized by relative electric conductivity) together with an increase in cell swelling rate, indicating that the plasma membrane integrity was reduced in the presence of ethanol. Furthermore, using AFM, Schiavone et al. (2016) demonstrated that ethanol stress caused a reduction of the plasma membrane thickness.

The relationship between ethanol tolerance and lipid composition of the plasma membrane is strongly dependent on the experimental conditions that are used. For this reason, a clear connection between plasma membrane composition and ethanol tolerance remains to be elucidated (Henderson and Block, 2014).

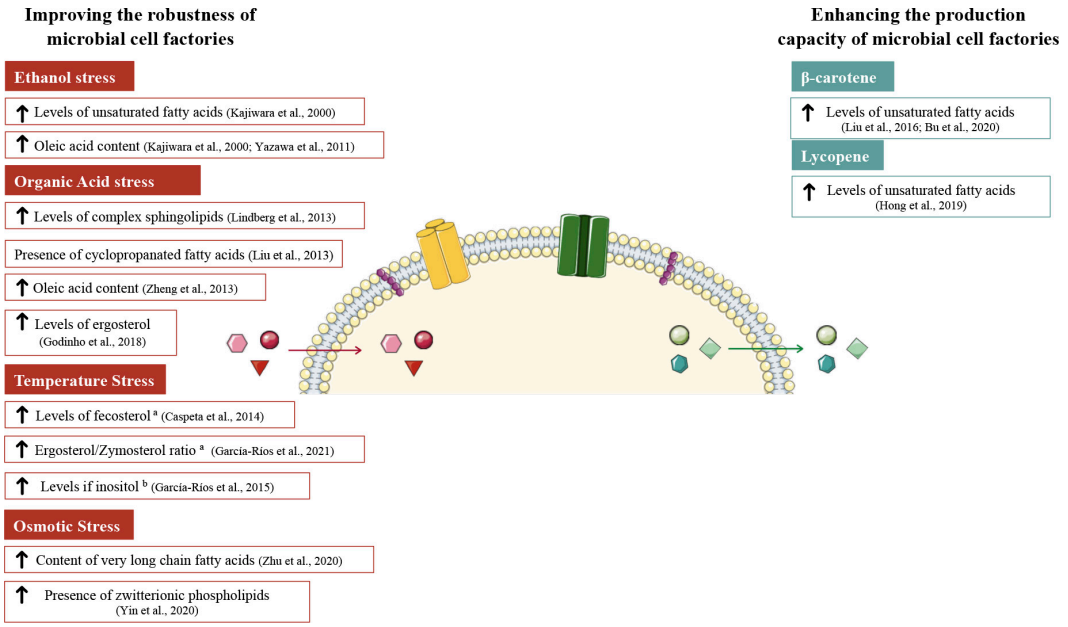

FIGURE 1 | Plasma membrane modifications in *S. cerevisiae* aiming to improve yeast fitness on industrial bio-processes. On the left side are represented modifications to increase yeast robustness toward stress conditions (ethanol, organic acids, temperature, and osmotic stress). Plasma membrane modifications on the right side were done to enhance the production capacity of microbial cell factories. Red arrows indicate the entrance of the stress agents. Green arrows indicate the exit of metabolites of interest. [a] and [b] stand for works performed at high and low temperatures, respectively. The figure was produced using the vector image bank of Servier Medical Art (http://smart.servier.com/).

A common strategy to improved *S. cerevisiae* robustness to ethanol has been the development of strains with an increased fraction of glycerophospholipids containing oleic acid ($C_{18:1}$). Oleic acid has unique properties: on one side its 18 carbon chain length contributes to increasing membrane thickness, but on the other side its degree of unsaturation contributes to an increase of membrane fluidity and decreases membrane thickness. The effect of increased amounts of oleic acid in the plasma membrane is difficult to predict and must be verified experimentally case by case, considering the overall changes in fatty acyl chain length and saturation, and the experimental conditions. Kajiwara et al. (2000) reported a 33% increase in oleic acid content at the expense of palmitic acid ($C_{16:0}$) when *OLE1*, encoding for a stearoyl-CoA 9-desaturase which catalyzes the transformation of saturated fatty acids ($C_{16:0}$ and $C_{18:0}$) to unsaturated fatty acids ($C_{16:1}$ and $C_{18:1}$), was overexpressed in *S. cerevisiae*, overall measuring a 7% increase in unsaturated fatty acids. The engineered strain showed improved growth and ethanol production at low temperatures (10°C). Since lowering of the temperature leads to a more ordered membrane structure and hence a reduction in fluidity (Shinitzky and Henkart, 1979) which is largely determined by the packing of oleic acid ($C_{18:1}$) and palmitoleic acid ($C_{16:1}$), the impact of the observed increase in oleic acid in membrane fluidity could potentially underlay the improved performance of the strain.

Differently, in other study, conducted at 30°C, the overexpression of *OLE1* did not result in changes in the content of oleic acid (Zheng et al., 2013). This discrepancy might be because cells increase their membrane unsaturation at lower temperatures (Aguilera et al., 2007).

Saccharomyces cerevisiae membrane engineering can also be based on the introduction of heterologous genes or lipid species. Yazawa et al. (2011) expressed the rat elongase 1 gene (*rELO1*) in *S. cerevisiae*, obtaining vaccenic acid instead of oleic acid, but with no effect on ethanol tolerance. The desired effect was reached by the introduction of rat elongase 2 (*rELO2*), which increased oleic acid content by 18%. Importantly, under these conditions the unsaturation index was very similar to that of the control, meaning that the increase of oleic acid was determinant for ethanol tolerance. Furthermore, *rELO2* overexpression also conferred tolerance to n-butanol, n-propanol, and 2-propanol.

Despite the positive results obtained, it is not clear if the advantage derives from the oleic acid content or other alterations affecting the membrane properties, as they were not measured. Indeed, other attempts seem to suggest that we are still exploring trial and error strategies.

Organic Acids

The effects of weak organic acids on *S. cerevisiae* have been generally ascribed to acidification of the cytosol by protons released and/or accumulation of the anionic form of the acid. These, in turn, can cause several cell alterations such as the disruption of the proton gradient across the plasma membrane, increased turgor pressure, oxidative stress, protein aggregation, lipid peroxidation, inhibition of membrane trafficking, and perturbation of plasma and vacuolar membranes spatial organization (Piper, 2011).

Guo et al. (2018) performed a comparative analysis of lipids in *S. cerevisiae* grown in the presence of four different weak acids, which are known to be detrimental for yeast growth: acetic, cinnamic, formic, and levulinic acids.

Yeast cells counteract the stress caused by organic acids by modulating the plasma membrane lipid composition and the modifications differ depending on the molecular conformations of the acids. Formic, levulinic and acetic acids did not affect the levels of PA in comparison to the control, while in cells exposed to cinnamic acid there was a decrease of 30% in PA content. Furthermore, the contents of PE, PC, and PS decreased in yeast cells under any acid condition compared to the control. Differently, the content of PI increased in yeast cells subjected to acid stress during growth on glucose, but decreased during the adaptation phase on ethanol, compared to the control. Concerning the fatty acids (profile FAs), in yeast cells under acid stress, the amount of myristic acid ($C_{14:0}$) was around 5% of the total FAs, similar to that of the control. However, a decrease in palmitic acid ($C_{16:0}$) and palmitoleic acid ($C_{16:1}$) and an increase in elaidic acid ($C_{18:1}$) and stearic acid ($C_{18:0}$) were observed for all the acid-stressed cells. While the unsaturation index in cells exposed to cinnamic acid was unaffected, exposure to acetic, formic and levulinic acid resulted in an increase in the saturation index of FAs in comparison to the control. Exposure of the cells to acids led to a continuous increase of the sterol content during the different phases of growth, while the control showed a gradual decrease in ergosterol from the exponential phase to the stationary phase. Ergosterol, the major yeast sterol, is essential for the structure of the plasma membrane, modulating its thickness, fluidity and permeability and regulating the activity of membrane-associated transporters (Abe and Hiraki, 2009; Kodedová and Sychrová, 2015). Therefore, ergosterol plays a key role in the resistance toward inhibitory compounds.

The work developed by Guo et al. (2018) has the important merit to describe how the plasma membrane lipid composition adapt to different stress factors and could be used as a guide for membrane engineering strategies, despite it did not take into account the membrane physicochemical properties as well as the rearrangement of membrane proteins.

Lindberg et al. (2013) explored a comparative approach: in an attempt to increase *S. cerevisiae* tolerance to acetic acid, the authors studied the lipid profile of *Zygosaccharomyces bailii*, a food spoilage yeast well known for its resistance to weak organic acids (Fleet, 1992). After exposure to acetic acid, *Z. bailii* revealed large lipidomic changes while smaller changes were observed in *S. cerevisiae*. A higher degree of saturation of the glycerophospholipids and increased amounts of complex sphingolipids at the expense of glycerophospholipids were the most noticeable changes in the adaption of *Z. bailii* to acetic acid. These results are consistent with the previously described role of sphingolipids in cell death induced by acetic acid in *S. cerevisiae*, where the deletion of *ISC1*, coding for the inositol phosphosphingolipid phospholipase C, responsible for the hydrolysis of complex sphingolipids, lead to increased resistance to acetic acid (Rego et al., 2012).

By combining lipidomic analysis with molecular dynamic simulations, in a multidisciplinary work, Lindahl et al. (2016) reported that membranes with high content of sphingolipids are thicker and denser than control and membrane permeability decreases. Taking this into account, Lindahl et al. (2017) tried to increase the fraction of complex sphingolipids in the plasma membrane of *S. cerevisiae* by altering the expression of genes associated with the production of long-chain base (LCB) and very-long-chain fatty acids (VLCFA) (C_{24-26}), and with the conversion of ceramides into complex sphingolipids. The authors overexpressed *ELO3*, involved in fatty acid elongation and *AUR1*, encoding an enzyme that catalyzes the formation of complex sphingolipids, and deleted *ORM1* and *ORM2*, encoding negative regulators of sphingolipids biosynthesis. However, neither the overexpression of *ELO3* or *AUR1* influenced the lipid metabolism. The deletion of *ORM1* and *ORM2* lead to a decrease in both complex sphingolipids and phosphatidylinositol, which diminished cell viability. When combined, the reduction in growth caused by the *orm1/2* deletion was alleviated by the overexpression of *ELO3* and *AUR1*, which also determined an increase in the fatty acyl chain length. Overall, the authors were not successful in the attempt to increase levels of complex sphingolipids in *S. cerevisiae*.

Increasing the length of fatty acids has been a common strategy employed to increase microorganisms' fitness toward organic acids. Zheng et al. (2013) overexpressed *ELO1*, encoding a fatty acid elongase, in *S. cerevisiae* to improve cellular tolerance to acetic acid. These authors observed an 18% increase in the cellular content of oleic acid, which resulted in a 44% increase in survival after acetic acid exposure, but the molecular system was not completely described.

Godinho et al. (2018) unveiled the relation between the yeast ABC transporter Pdr18 and ergosterol levels in yeast adaptation and tolerance to acetic acid stress. Pdr18 has been proposed to mediate the incorporation of ergosterol in the plasma membrane. The authors reported a coordinated activation of the transcription of Pdr18 and several ergosterol biosynthesis pathway genes during the period of adaptation to acetic acid. Therefore, Pdr18 has been suggested to be essential to keep maximum ergosterol content in the plasma membrane in the presence of acetic acid, thus maintaining the plasma membrane order, electrochemical potential and permeability in the presence of acetic acid. The role of Pdr18 in the maintenance of the plasma membrane physicochemical properties in the presence of acetic acid is crucial for the adequate functioning of the membrane.

The expression of heterologous genes in *S. cerevisiae* to increase its robustness to organic acids has also been attempted. Cyclopropane ring formation on fatty acyl chains occurs in both bacteria and archaea and it has been associated with an increase in the plasma membrane rigidity (Oger and Cario, 2013). Liu et al. (2013) expressed *Escherichia coli cfa* gene in *S. cerevisiae* and successfully converted 10% of fatty acids into cyclopropanated fatty acids. However, mutants failed to show octanoic acid resistance and no further stress conditions were tested.

Thermotolerance

Thermotolerance is a desirable trait in microbial cell factories: it can result in reduced cooling costs, and contamination risks and can boost enzyme activity during simultaneous saccharification

and fermentation (Abdel-Banat et al., 2010). However, heat is also a stress factor, known to disturb protein stability, cell membrane order, and cytoskeleton structures, with consequences such as protein dysfunction, metabolic imbalances and loss of metabolic activity (Verghese et al., 2012).

Caspeta et al. (2014) set up an adaptive laboratory evolution (ALE) experiment to select yeast strains with improved growth and ethanol production at temperatures higher than 40°C. Sequencing of the evolved strain, capable to grow at high temperatures, revealed, among other findings, a point mutation in the *ERG3* gene, encoding a structural enzyme in the ergosterol biosynthesis pathway. In this strain, fecosterol, a sterol precursor, became the major sterol in the plasma membrane rather than ergosterol. The authors reported that the substitution of the "flat" ergosterol by the "bended" fecosterol in the evolved *S. cerevisiae* strain seems to be responsible for the maintenance of optimal membrane fluidity at high temperatures and therefore crucial for the thermotolerant phenotype (Caspeta et al., 2014).

More recently, García-Ríos et al. (2021) aimed to generate a robust *S. cerevisiae* strain to be used in cocoa fermentation. ALE was conducted in a defined medium at 40°C for 150 generations. The evolved strain exhibited a significantly increased growth rate in comparison to the parental strain. Lipidomic analysis revealed that, at 40°C, the evolved strain exhibited a higher ergosterol/zymosterol ratio compared to the parental strain. Authors claim that this difference could be responsible for the adaptation of the evolved strain to higher temperatures. Differently from the higher levels of fecosterol reported by Caspeta et al. (2014), in the obtained evolved strain García-Ríos et al. (2021) observed the accumulation of episterol, which is the next intermediate in the sterol biosynthesis pathway. Furthermore, no significant differences were found in terms of the fatty acid profile between the two strains.

These results highlight that the adaptation of the yeast plasma membrane to heat stress is not straightforward and membrane lipid composition changes differently according to the background of the strain used and also with the conditions in which the ALE experiments are carried out.

In another work, Liu et al. (2017) compared the thermotolerance of *erg2*Δ, *erg3*Δ, *erg4*Δ, *erg5*Δ, *erg3*Δ*erg4*Δ, *erg3*Δ*erg5*Δ, and *erg4*Δ*erg5*Δ *S. cerevisiae* strains. The mutants lacking either of the four enzymes are viable, with intermediate sterols instead of ergosterol accumulated in the membrane. All mutant strains displayed a higher growth rate than wild type at 39.5°C. The *erg3*Δ*erg5*Δ strain, in particular, exhibited and 2.24-fold increase in growth rate relative to wild type at this temperature (Liu et al., 2017). Modifications of the sterol composition directly affect the fluidity and permeability of the plasma membrane, as well as the localization and activity of membrane proteins (Kodedová and Sychrová, 2015). This work highlighted the importance of the sterol composition on yeast response to high temperatures and can be used as a guide for future membrane engineering approaches.

Different from these approaches, the study of the membrane composition of thermotolerant yeasts such as *Kluyveromyces marxianus* can be valuable to provide guidelines and ideas to engineering the plasma membrane of *S. cerevisiae*.

Temperature is also one of the most important parameters affecting wine fermentation. Low fermentation temperature improves the characteristic taste and aroma of wines. However, low temperature fermentations result in increased lag phases and lower growth rates for yeasts, causing fermentation to stop (Bisson, 1999). As mentioned above, low temperatures also affect the plasma membrane, leading to a decrease in membrane fluidity (Shinitzky and Henkart, 1979). Metabolic profiling done by López-Malo et al. (2013b) revealed that the main metabolic differences between *S. cerevisiae* growing at 12°C (common fermentation temperature for wine) and 28°C were related to lipid metabolism.

Genes involved in the phospholipid, sphingolipid and ergosterol metabolism were identified as those causing the most significant effects on yeast growth at low temperatures (López-Malo et al., 2013a). *OLE1* was one of the genes identified and its overexpression lead to an improved fermentation ability at lower temperatures (12°C) in synthetic must. Furthermore, the wine produced from this strain revealed a specific aroma profile (López-Malo et al., 2014). As previously mentioned, *OLE1* encodes a stearoyl-CoA 9-desaturase which catalyzes the transformation of saturated fatty acids (C16:0 and C18:0) to unsaturated fatty acids (C16:1 and C18:1). The presence of unsaturated fatty acids contributes to increased membrane fluidity, which is advantageous for the cells at low temperatures (Aguilera et al., 2007).

In a different approach, López-Malo et al. (2015) performed an ALE in synthetic must to obtain a wine yeast strain able to ferment at low temperatures. The evolved strain exhibited improved growth and higher fermentation performance at low-temperature in comparison to the parental strain. Genome sequencing of the evolved strain revealed the presence of a single nucleotide polymorphism (SNP) in the *GAA1* gene, which encodes a subunit of the glycosylphosphatidylinositol (GPI) transamidase complex. This complex adds GPI, required for inositol synthesis, to newly synthesized proteins, including mannoproteins. Inositol is an essential phospholipid precursor in yeast cells and could be incorporated into phosphatidylinositol (PI), sphingolipids and glycosylphosphatidylinositol anchors. Using a reverse engineering strategy, a site-directed mutation (*GAA1*Thr108) was introduced in the parental strain, which resulted in improved fermentation performances. This result reveals a higher inositol requirement for *S. cerevisiae* cells grown at low temperatures.

Overall, these works highlighted the importance of the plasma membrane lipid composition in yeast response to sub-optimal temperatures.

Osmotic Stress

Osmoregulation is fundamental for living cells and is particularly relevant for industrial biotechnology. Yeast adaptation to osmotic stress is an active process based on sensing and counterbalancing osmotic changes. Morphologic changes are key toward osmotic stress as yeast cells change their volume in response to osmotic challenges, decreasing volume in response to hypertonic stress and increasing volume in the presence of hypotonic stresses. Therefore, the ability to tolerate osmotic

stress is strongly influenced by plasma membrane permeability (Gonzalez et al., 2016).

Through an adaptive laboratory evolution experiment, Zhu et al. (2020) were able to isolate a strain with improved tolerance to osmotic stress. Transcriptome sequencing (RNA-seq) suggested that mRNA levels of *ELO2* were differentially upregulated in the isolated strain. Using a reverse engineering strategy, *ELO2* was overexpressed in a wild-type strain, resulting in enhanced very long fatty acids content (the contents of $C_{20:0}$, $C_{22:0}$, and $C_{24:0}$ were increased by 52.3, 94.1, and 14.4%, respectively). Furthermore, the levels of complex sphingolipids were increased. These modifications have been reported to promote a thicker and less permeable membrane. Flow cytometry analysis of cells stained with SYTOX green revealed that the *ELO2* overexpressing strain exhibited a 24.4% higher membrane integrity than the wild-type strain, resulting in an enhanced osmotic tolerance.

Similarly, Yin et al. (2020) were able to increase the tolerance of *S. cerevisiae* to salt stress by significantly improving the yeast membrane potential and integrity. Using a nitroguanidine mutagenesis strategy, authors identified *CDS1,* encoding a phosphatidate cytidylyltransferase, and *CHO1*, encoding a phosphatidylserine (PS) synthase, as key factors to yeast tolerance toward salt stress. The combined overexpression of *CDS1* and *CHO1* resulted in a redistribution of membrane phospholipids and a decreased anionic-to-zwitterionic phospholipid ratio. In *S. cerevisiae*, anionic phospholipids are mainly PA, PI, and PS, while zwitterionic phospholipids are PE and PC. These results indicate that a higher presence of zwitterionic phospholipids may be beneficial to deal with salt stress (Yin et al., 2020).

These works highlight that different membrane compositions can be advantageous toward the same stress agent. In both works, Yin et al. (2020) and Zhu et al. (2020), the levels of PS and PE were increased, 35.5% and 15, 25.2, and 18.9%, respectively. However, when *ELO2* was overexpressed the levels of PC, PA, and PI did not change. On the other hand, the double overexpression of *CDS1* and *CHO1* led to a 28.6% increase in PC and to a decrease in the levels of PA and PI of 14.6 and 39.8%, respectively.

Enhancing the Production Capacity of Microbial Cell Factories: When Membrane Composition Can Contribute to Increasing Product Export

Microorganisms can be exploited for the production of several compounds with applications in a wide range of industrial sectors, and whenever possible the export of the product into the medium is preferable, mainly for limiting the downstream processing costs, but very often also for increasing the flux toward the product itself (Chung et al., 2015; Tsuge et al., 2016; Porro and Branduardi, 2017). Therefore, a proper export of the products of interest is often indispensable for a profitable and efficient cell factory. Researchers have been focusing on maximizing the export of the compounds of interest by overexpressing specific membrane transporters, engineering transporters for improved efficiency or even introducing heterologous transporters in the cell factory (Boyarskiy and Tullman-Ercek, 2015; Kell et al., 2015; Erian et al., 2020; Soares-Silva et al., 2020). For more detailed information on the engineering of membrane transporters for industrial biotechnology applications, the reader should look the works mentioned above.

However, many times, the simple overexpression of a transporter does not result in the intended increased export rates. This is why in this review we wanted to focus on and highlight strategies where the plasma membrane composition was changed, and in turn influencing the properties of the entire structure, considered as a system. Indeed, the plasma membrane composition is very crucial and must be considered since it determines physiochemical properties such as fluidity, permeability and elasticity, which can facilitate the export of the products of interest (Royce et al., 2015). So far there are not many examples of membrane engineering strategies focusing on increasing metabolites secretion in yeast and in particular in *S. cerevisiae*. However, there are many works performed in *E. coli* (Tan et al., 2016, 2017; Wu et al., 2017; Kanonenberg et al., 2019) which may serve as guidance for future work in yeast.

One interesting example in *S. cerevisiae* relates to the work of Liu et al. (2016) who reported a decrease in the fluidity of the plasma membrane caused by the decrease of unsaturated fatty acids in *S. cerevis*iae strain producing β-carotenes. Carotenoids accumulate in the cell membrane and therefore, high production levels of carotenoids can cause membrane stress (Gruszecki and Strzałka, 2005).

In this strain, carotenoid biosynthesis shares the precursors acetyl-CoA and farnesyl pyrophosphate (FPP) with unsaturated fatty acids and ergosterol, respectively. Therefore, heterologous carotenoid biosynthesis could decrease the content of unsaturated fatty acids and ergosterol due to competition for these precursors. Given the importance of plasma membrane fluidity in cellular metabolism and physiology (such as facilitating the absorption of essential substances), authors sought to restore it. The addition of linoleic acid ($C_{18:2}$) to the culture media restored the plasma membrane fluidity by the incorporation of unsaturated fatty acids in the membrane. This resulted in a 24.3% increase in the production of β -carotene (Liu et al., 2016).

A different approach was used by Bu et al. (2020). The authors were able to counteract the decrease of membrane fluidity caused by the accumulation of β-carotenes by overexpressing *OLE1*. Overexpression of *OLE1* could improve the fatty acid unsaturation and membrane flexibility, which conferred cells a high tolerance to various types of stress, as reported above (Fang et al., 2017; Nasution et al., 2017). Indeed, the overexpression of *OLE1* promoted cell membrane fluidity (measured by fluorescence anisotropy) and resulted in an improved β-carotene secretion (Bu et al., 2020). The same strategy was also used by Hong et al. (2019) for the production of lycopene, a red carotenoid pigment. *OLE1* overexpression led to improved lycopene production suggesting that an increase in unsaturated fatty acids content in the cell membrane might relieve the carotenoid toxicity (Hong et al., 2019).

Another example of how the membrane composition affects the export of molecules was reported by Wang et al. (2013). The addition of surfactants, such as Triton X-100, led to increased permeability and fluidity of the plasma membrane in the yeast *Monascus purpureus*, which resulted in a 56.8% higher production of pigments. The addition of Triton X-100 led to

an increased degree of unsaturation in the membrane lipids. According to the authors, these changes, facilitated the secretion of intracellular pigment to the broth thus alleviated the product feedback inhibition and enhanced pigment production (Wang et al., 2013). These results suggested that Triton X-100 could markedly affect the fatty acid composition of *M. purpureus* H1102 by significantly increasing the degree of unsaturation of the cell membrane lipids, thus improving the fluidity and permeability of the cell membrane.

CONCLUSION

Overall, despite its great potential, membrane engineering is still a highly complex approach as membrane lipids and membrane homeostasis are vital for many cellular functions. Moreover, it is difficult to predict the outcomes of altering membrane elements in the whole membrane system. The understanding of membranes and their structure has changed enormously over the last years. The availability and development of high-throughput methods have allowed researchers to deepen their knowledge on the plasma membrane conformation and dynamics. However, the analysis of the plasma membrane composition is still challenging which hampers a detailed association between specific composition and physicochemical properties of the plasma membrane. The interdependency between membrane lipids and proteins can not be neglected. In the future, a combination of efforts between researchers from different areas of study, such as lipidomics, molecular dynamics simulations and membrane biophysics will be crucial to gain a better understanding of the plasma membrane and therefore plan strategies to tailor it at a systems level.

AUTHOR CONTRIBUTIONS

LF and PB drafted the manuscript. LF wrote the manuscript. MS, MJS, and PB provided the writing guidance and revised the manuscript. All authors read and approved the final manuscript.

FUNDING

This project has received funding from the European Union's Horizon 2020 Research and Innovation Program under the Marie Skłodowska-Curie Grant Agreement No. 764927 and by the Portuguese Foundation for Science and Technology (FCT) under the scope of the strategic funding of "Contrato-Programa" UIDB/04050/2020. This work was funded through the COST Action "Understanding and exploiting the impacts of low pH on micro-organisms" (EuroMicropH) CA18113.

REFERENCES

Abdel-Banat, B. M. A., Hoshida, H., Ano, A., Nonklang, S., and Akada, R. (2010). High-temperature fermentation: how can processes for ethanol production at high temperatures become superior to the traditional process using mesophilic yeast? *Appl. Microbiol. Biotechnol.* 85, 861–867. doi: 10.1007/s00253-009-2248-5

Abe, F., and Hiraki, T. (2009). Mechanistic role of ergosterol in membrane rigidity and cycloheximide resistance in *Saccharomyces cerevisiae*. *Biochim. Biophys. Acta Biomembr.* 1788, 743–752. doi: 10.1016/j.bbamem.2008.12.002

Aguilera, J., Randez-Gil, F., and Prieto, J. A. (2007). Cold response in *Saccharomyces cerevisiae*: new functions for old mechanisms. *FEMS Microbiol. Rev.* 31, 327–341. doi: 10.1111/j.1574-6976.2007.00066.x

Alsteens, D., Müller, D. J., and Dufrêne, Y. F. (2017). Multiparametric Atomic Force Microscopy Imaging of Biomolecular and Cellular Systems. *Acc. Chem. Res.* 50, 924–931. doi: 10.1021/acs.accounts.6b00638

Bisson, L. F. (1999). Stuck and sluggish fermentations. *Am. J. Enol. Vitic.* 50, 107–119.

Boyarskiy, S., and Tullman-Ercek, D. (2015). Getting pumped: membrane efflux transporters for enhanced biomolecule production. *Curr. Opin. Chem. Biol.* 28, 15–19. doi: 10.1016/j.cbpa.2015.05.019

Branduardi, P. (2021). Closing the loop: the power of microbial biotransformations from traditional bioprocesses to biorefineries, and beyond. *Microb. Biotechnol.* 14, 68–73. doi: 10.1111/1751-7915.13713

Branduardi, P., and Porro, D. (2012). "Yeasts in Biotechnology," in *Yeast: Molecular and Cell Biology, Second Edition*, ed. H. Feldmann (Hoboken: Wiley-Blackwell), 347–370.

Bu, X., Lin, J. Y., Cheng, J., Yang, D., Duan, C. Q., Koffas, M., et al. (2020). Engineering endogenous ABC transporter with improving ATP supply and membrane flexibility enhances the secretion of β-carotene in *Saccharomyces cerevisiae*. *Biotechnol. Biofuels* 13:168. doi: 10.1186/s13068-020-01809-6

Caron, B., Mark, A. E., and Poger, D. (2014). Some like it hot: the effect of sterols and hopanoids on lipid ordering at high temperature. *J. Phys. Chem. Lett.* 5, 3953–3957. doi: 10.1021/jz5020778

Casal, M., Cardoso, H., and Leão, C. (1998). Effects of ethanol and other alkanols on transport of acetic acid in *Saccharomyces cerevisiae*. *Appl. Environ. Microbiol.* 64, 665–668. doi: 10.1128/aem.64.2.665-668

Caspeta, L., Chen, Y., Ghiaci, P., Feizi, A., Baskov, S., Hallström, B. M., et al. (2014). Altered sterol composition renders yeast thermotolerant. *Science* 346, 75–78. doi: 10.1126/science.1258137

Chung, H., Yang, J. E., Ha, J. Y., Chae, T. U., Shin, J. H., Gustavsson, M., et al. (2015). Bio-based production of monomers and polymers by metabolically engineered microorganisms. *Curr. Opin. Biotechnol.* 36, 73–84. doi: 10.1016/j.copbio.2015.07.003

Coskun, Ü, and Simons, K. (2011). Cell membranes: the lipid perspective. *Structure* 19, 1543–1548. doi: 10.1016/j.str.2011.10.010

Dague, E., Bitar, R., Ranchon, H., Durand, F., Yken, H. M., and François, J. M. (2010). An atomic force microscopy analysis of yeast mutants defective in cell wall architecture. *Yeast* 27, 673–684. doi: 10.1002/yea.1801

Deparis, Q., Claes, A., Foulquié-Moreno, M. R., and Thevelein, J. M. (2017). Engineering tolerance to industrially relevant stress factors in yeast cell factories. *FEMS Yeast Res.* 17:fox036. doi: 10.1093/femsyr/fox036

Dufrêne, Y. F. (2002). Atomic force microscopy, a powerful tool in microbiology. *J. Bacteriol.* 184, 5205–5213. doi: 10.1128/JB.184.19.5205-5213.2002

Eisenkolb, M., Zenzmaier, C., Leitner, E., and Schneiter, R. (2002). A specific structural requirement for ergosterol in long-chain fatty acid synthesis mutants important for maintaining raft domains in yeast. *Mol. Biol. Cell* 13, 4414–4428. doi: 10.1091/mbc.E02-02-0116

Erian, A. M., Egermeier, M., Rassinger, A., Marx, H., and Sauer, M. (2020). Identification of the citrate exporter Cex1 of *Yarrowia lipolytica*. *FEMS Yeast Res.* 20:foaa055. doi: 10.1093/femsyr/foaa055

Fang, Z., Chen, Z., Wang, S., Shi, P., Shen, Y., Zhang, Y., et al. (2017). Overexpression of *OLE1* enhances cytoplasmic membrane stability and confers resistance to cadmium in *Saccharomyces cerevisiae*. *Appl. Environ. Microbiol.* 83, e02319–16. doi: 10.1128/AEM.02319-16

Ferreira, T., Mason, A. B., and Slayman, C. W. (2001). The Yeast Pma1 Proton Pump: a model for understanding the biogenesis of plasma membrane proteins. *J. Biol. Chem.* 276, 29613–29616. doi: 10.1074/jbc.R100022200

Fleet, G. (1992). Spoilage yeasts. *Crit. Rev. Biotechnol.* 12, 1–44. doi: 10.3109/07388559209069186

Francois, J. M., Formosa, C., Schiavone, M., Pillet, F., Martin-Yken, H., and Dague, E. (2013). Use of atomic force microscopy (AFM) to explore cell wall properties and response to stress in the yeast *Saccharomyces cerevisiae*. *Curr. Genet.* 59, 187–196. doi: 10.1007/s00294-013-0411-0

Gaigg, B., Toulmay, A., and Schneiter, R. (2006). Very long-chain fatty acid-containing lipids rather than sphingolipids per se are required for raft association and stable surface transport of newly synthesized plasma membrane ATPase in yeast. *J. Biol. Chem.* 281, 34135–34145. doi: 10.1074/jbc.M603791200

Garcia-Albornoz, M. A., and Nielsen, J. (2013). Application of genome-scale metabolic models in metabolic engineering. *Ind. Biotechnol.* 9, 203–214. doi: 10.1089/ind.2013.0011

García-Ríos, E., Lairón-Peris, M., Muñiz-Calvo, S., Heras, J. M., Ortiz-Julien, A., Poirot, P., et al. (2021). Thermo-adaptive evolution to generate improved *Saccharomyces cerevisiae* strains for cocoa pulp fermentations. *Int. J. Food Microbiol.* 342:109077. doi: 10.1016/j.ijfoodmicro.2021.109077

Gibson, B. R., Lawrence, S. J., Leclaire, J. P. R., Powell, C. D., and Smart, K. A. (2007). Yeast responses to stresses associated with industrial brewery handling. *FEMS Microbiol. Rev.* 31, 535–569. doi: 10.1111/j.1574-6976.2007.00076.x

Godinho, C. P., Prata, C. S., Pinto, S. N., Cardoso, C., Bandarra, N. M., Fernandes, F., et al. (2018). Pdr18 is involved in yeast response to acetic acid stress counteracting the decrease of plasma membrane ergosterol content and order. *Sci. Rep.* 8:7860. doi: 10.1038/s41598-018-26128-7

Gonzalez, R., Morales, P., Tronchoni, J., Cordero-Bueso, G., Vaudano, E., Quirós, M., et al. (2016). New genes involved in osmotic stress tolerance in *Saccharomyces cerevisiae*. *Front. Microbiol.* 7:1545. doi: 10.3389/fmicb.2016.01545

Gruszecki, W. I., and Strzałka, K. (2005). Carotenoids as modulators of lipid membrane physical properties. *Biochim. Biophys. Acta* 1740, 108–115. doi: 10.1016/j.bbadis.2004.11.015

Guo, Z., Khoomrung, S., Nielsen, J., and Olsson, L. (2018). Changes in lipid metabolism convey acid tolerance in *Saccharomyces cerevisiae*. *Biotechnol. Biofuels* 11:297. doi: 10.1186/s13068-018-1295-5

Henderson, C. M., and Block, D. E. (2014). Examining the role of membrane lipid composition in determining the ethanol tolerance of *Saccharomyces cerevisiae*. *Appl. Environ. Microbiol.* 80, 2966–2972. doi: 10.1128/AEM.04151-13

Henry, S. A., Kohlwein, S. D., and Carman, G. M. (2012). Metabolism and regulation of glycerolipids in the yeast *Saccharomyces cerevisiae*. *Genetics* 190, 317–349. doi: 10.1534/genetics.111.130286

Hong, J., Park, S. H., Kim, S., Kim, S. W., and Hahn, J. S. (2019). Efficient production of lycopene in *Saccharomyces cerevisiae* by enzyme engineering and increasing membrane flexibility and NAPDH production. *Appl. Microbiol. Biotechnol.* 103, 211–223. doi: 10.1007/s00253-018-9449-8

Hong, K. K., and Nielsen, J. (2012). Metabolic engineering of *Saccharomyces cerevisiae*: a key cell factory platform for future biorefineries. *Cell. Mol. Life Sci.* 69, 2671–2690. doi: 10.1007/s00018-012-0945-1

Jezierska, S., and Van Bogaert, I. N. A. (2017). Crossing boundaries: the importance of cellular membranes in industrial biotechnology. *J. Ind. Microbiol. Biotechnol.* 44, 721–733. doi: 10.1007/s10295-016-1858-z

Kajiwara, S., Aritomi, T., Suga, K., Ohtaguchi, K., and Kobayashi, O. (2000). Overexpression of the *OLE1* gene enhances ethanol fermentation by *Saccharomyces cerevisiae*. *Appl. Microbiol. Biotechnol.* 53, 568–574. doi: 10.1007/s002530051658

Kanonenberg, K., Royes, J., Kedrov, A., Poschmann, G., Angius, F., Solgadi, A., et al. (2019). Shaping the lipid composition of bacterial membranes for membrane protein production. *Microb. Cell Fact.* 18:131. doi: 10.1186/s12934-019-1182-1

Kell, D. B., Swainston, N., Pir, P., and Oliver, S. G. (2015). Membrane transporter engineering in industrial biotechnology and whole cell biocatalysis. *Trends Biotechnol.* 33, 237–246. doi: 10.1016/j.tibtech.2015.02.001

Klose, C., and Tarasov, K. (2016). "Profiling of yeast lipids by shotgun lipidomics," in *Methods in Molecular Biology*, ed. F. Devaux (Totowa: Humana Press), 309–324. doi: 10.1007/978-1-4939-3079-1_17

Klose, C., Ejsing, C. S., García-Sáez, A. J., Kaiser, H. J., Sampaio, J. L., Surma, M. A., et al. (2010). Yeast lipids can phase-separate into micrometer-scale membrane domains. *J. Biol. Chem.* 285, 30224–30232. doi: 10.1074/jbc.M110.123554

Klose, C., Surma, M. A., Gerl, M. J., Meyenhofer, F., Shevchenko, A., and Simons, K. (2012). Flexibility of a eukaryotic lipidome - insights from yeast lipidomics. *PLoS One* 7:e35063. doi: 10.1371/journal.pone.0035063

Klug, L., and Daum, G. (2014). Yeast lipid metabolism at a glance. *FEMS Yeast Res.* 14, 369–388. doi: 10.1111/1567-1364.12141

Kodedová, M., and Sychrová, H. (2015). Changes in the sterol composition of the plasma membrane affect membrane potential, salt tolerance and the activity of multidrug resistance pumps in *Saccharomyces cerevisiae*. *PLoS One* 10:e0139306. doi: 10.1371/journal.pone.0139306

Leão, C., and Van Uden, N. (1984). Effects of ethanol and other alkanols on passive proton influx in the yeast *Saccharomyces cerevisiae*. *Biochim. Biophys. Acta Biomembr.* 774, 43–48. doi: 10.1016/0005-2736(84)90272-4

Lee, A. G. (2004). How lipids affect the activities of integral membrane proteins. *Biochim. Biophys. Acta Biomembr.* 1666, 62–87. doi: 10.1016/j.bbamem.2004.05.012

Lee, Y., Nasution, O., Lee, Y. M., Kim, E., Choi, W., and Kim, W. (2017). Overexpression of *PMA1* enhances tolerance to various types of stress and constitutively activates the SAPK pathways in *Saccharomyces cerevisiae*. *Appl. Microbiol. Biotechnol.* 101, 220–239. doi: 10.1007/s00253-016-7898-5

Li, M., and Borodina, I. (2015). Application of synthetic biology for production of chemicals in yeast *Saccharomyces cerevisiae*. *FEMS Yeast Res.* 15, 1–12. doi: 10.1111/1567-1364.12213

Lindahl, L., Genheden, S., Eriksson, L. A., Olsson, L., and Bettiga, M. (2016). Sphingolipids contribute to acetic acid resistance in *Zygosaccharomyces bailii*. *Biotechnol. Bioeng.* 113, 744–753. doi: 10.1002/bit.25845

Lindahl, L., Genheden, S., Faria-Oliveira, F., Allard, S., Eriksson, L. A., Olsson, L., et al. (2018). Alcohols enhance the rate of acetic acid diffusion in *S. cerevisiae*: biophysical mechanisms and implications for acetic acid tolerance. *Microb. Cell* 5, 42–55. doi: 10.15698/mic2018.01.609

Lindahl, L., Santos, A. X. S., Olsson, H., Olsson, L., and Bettiga, M. (2017). Membrane engineering of *S. cerevisiae* targeting sphingolipid metabolism. *Sci. Rep.* 7:41868. doi: 10.1038/srep41868

Lindberg, L., Santos, A. X. S., Riezman, H., Olsson, L., and Bettiga, M. (2013). Lipidomic Profiling of *Saccharomyces cerevisiae* and *Zygosaccharomyces bailii* Reveals Critical Changes in Lipid Composition in Response to Acetic Acid Stress. *PLoS One* 8:e73936. doi: 10.1371/journal.pone.0073936

Liu, G., Chen, Y., Færgeman, N. J., and Nielsen, J. (2017). Elimination of the last reactions in ergosterol biosynthesis alters the resistance of S*accharomyces cerevisiae* to multiple stresses. *FEMS Yeast Res.* 17:fox063. doi: 10.1093/femsyr/fox063

Liu, P., Chernyshov, A., Najdi, T., Fu, Y., Dickerson, J., Sandmeyer, S., et al. (2013). Membrane stress caused by octanoic acid in *Saccharomyces cerevisiae*. *Appl. Microbiol. Biotechnol.* 97, 3239–3251. doi: 10.1007/s00253-013-4773-5

Liu, P., Sun, L., Sun, Y., Shang, F., and Yan, G. (2016). Decreased fluidity of cell membranes causes a metal ion deficiency in recombinant *Saccharomyces cerevisiae* producing carotenoids. *J. Ind. Microbiol. Biotechnol.* 43, 525–535. doi: 10.1007/s10295-015-1728-0

Lopes, D., Jakobtorweihen, S., Nunes, C., Sarmento, B., and Reis, S. (2017). Shedding light on the puzzle of drug-membrane interactions: experimental techniques and molecular dynamics simulations. *Prog. Lipid Res.* 65, 24–44. doi: 10.1016/j.plipres.2016.12.001

López-Malo, M., Chiva, R., Rozes, N., and Guillamon, J. M. (2013a). Phenotypic analysis of mutant and overexpressing strains of lipid metabolism genes in *Saccharomyces cerevisiae*: implication in growth at low temperatures. *Int. J. Food Microbiol.* 162, 26–36. doi: 10.1016/j.ijfoodmicro.2012.12.020

López-Malo, M., García-Ríos, E., Chiva, R., and Guillamon, J. M. (2014). Functional analysis of lipid metabolism genes in wine yeasts during alcoholic fermentation at low temperature. *Microb. Cell* 1, 365–375. doi: 10.15698/mic2014.11.174

López-Malo, M., García-Rios, E., Melgar, B., Sanchez, M. R., Dunham, M. J., and Guillamón, J. M. (2015). Evolutionary engineering of a wine yeast strain revealed a key role of inositol and mannoprotein metabolism during low-temperature fermentation. *BMC Genomics* 16:537. doi: 10.1186/s12864-015-1755-2

López-Malo, M., Querol, A., and Guillamon, J. M. (2013b). Metabolomic Comparison of *Saccharomyces cerevisiae* and the Cryotolerant Species *S. bayanus* var. *uvarum* and *S. kudriavzevii* during Wine Fermentation at Low Temperature. *PLoS One* 8:e60135. doi: 10.1371/journal.pone.0060135

Megyeri, M., Riezman, H., Schuldiner, M., and Futerman, A. H. (2016). Making Sense of the Yeast Sphingolipid Pathway. *J. Mol. Biol.* 428, 4765–4775. doi: 10.1016/j.jmb.2016.09.010

Nasution, O., Lee, Y. M., Kim, E., Lee, Y., Kim, W., and Choi, W. (2017). Overexpression of *OLE1* enhances stress tolerance and constitutively activates the MAPK HOG pathway in *Saccharomyces cerevisiae*. *Biotechnol. Bioeng.* 114, 620–631. doi: 10.1002/bit.26093

Nicolaou, S. A., Gaida, S. M., and Papoutsakis, E. T. (2010). A comparative view of metabolite and substrate stress and tolerance in microbial bioprocessing: from biofuels and chemicals, to biocatalysis and bioremediation. *Metab. Eng.* 12, 307–331. doi: 10.1016/j.ymben.2010.03.004

Niu, Y. P., Lin, X. H., Dong, S. J., Yuan, Q. P., and Li, H. (2016). Indentation with atomic force microscope, *Saccharomyces cerevisiae* cell gains elasticity under ethanol stress. *Int. J. Biochem. Cell Biol.* 79, 337–344. doi: 10.1016/j.biocel.2016.09.003

Oger, P. M., and Cario, A. (2013). Adaptation of the membrane in Archaea. *Biophys. Chem.* 183, 45–56. doi: 10.1016/j.bpc.2013.06.020

Opekarová, M., and Tanner, W. (2003). Specific lipid requirements of membrane proteins - A putative bottleneck in heterologous expression. *Biochim. Biophys. Acta Biomembr.* 1610, 11–22. doi: 10.1016/S0005-2736(02)00708-3

Patton, J. L., and Lester, R. L. (1991). The phosphoinositol sphingolipids of *Saccharomyces cerevisiae* are highly localized in the plasma membrane. *J. Bacteriol.* 173, 3101–3108. doi: 10.1128/jb.173.10.3101-3108.1991

Piper, P. W. (2011). "Resistance of Yeasts to Weak Organic Acid Food Preservatives," in *Advances in Applied Microbiology*, eds A. I. Laskin, S. Sariaslani, and G. M. Gadd (Amsterdam: Elsevier), 97–113. doi: 10.1016/b978-0-12-387044-5.00004-2

Pluhackova, K., and Böckmann, R. A. (2015). Biomembranes in atomistic and coarse-grained simulations. *J. Phys. Condens. Matter.* 27:323103. doi: 10.1088/0953-8984/27/32/323103

Porro, D., and Branduardi, P. (2017). "Production of organic acids by yeasts and filamentous fungi," in *Biotechnology of Yeasts and Filamentous Fungi*, ed. A. Sibirny (Berlin: Springer), 205–223. doi: 10.1007/978-3-319-58829-2_7

Rego, A., Costa, M., Chaves, S., Matmati, N., Pereira, H., Sousa, M. J., et al. (2012). Modulation of mitochondrial outer membrane permeabilization and apoptosis by ceramide metabolism. *PLoS One* 7:e48571. doi: 10.1371/journal.pone.0048571

Royce, L. A., Yoon, J. M., Chen, Y., Rickenbach, E., Shanks, J. V., and Jarboe, L. R. (2015). Evolution for exogenous octanoic acid tolerance improves carboxylic acid production and membrane integrity. *Metab. Eng.* 29, 180–188. doi: 10.1016/j.ymben.2015.03.014

Sandoval, N. R., and Papoutsakis, E. T. (2016). Engineering membrane and cell-wall programs for tolerance to toxic chemicals: beyond solo genes. *Curr. Opin. Microbiol.* 33, 56–66. doi: 10.1016/j.mib.2016.06.005

Santos, A. L., and Preta, G. (2018). Lipids in the cell: organisation regulates function. *Cell. Mol. Life Sci.* 75, 1909–1927. doi: 10.1007/s00018-018-2765-4

Schiavone, M., Formosa-Dague, C., Elsztein, C., Teste, M.-A., Martin-Yken, H., De Morais, M., et al. (2016). An Atomic Force Microscopy study of yeast response to ethanol stress: evidence for a role of the plasma membrane in the nanomechanical properties of the cell walls. *Appl. Environ. Microbiol.* 82, 4789–4801. doi: 10.1128/AEM.01213-16

Shi, Y., Cai, M., Zhou, L., and Wang, H. (2018). The structure and function of cell membranes studied by atomic force microscopy. *Semin. Cell Dev. Biol.* 73, 31–44. doi: 10.1016/j.semcdb.2017.07.012

Shinitzky, M., and Henkart, P. (1979). Fluidity of Cell Membranes - Current Concepts and Trends. *Int. Rev. Cytol.* 60, 121–147. doi: 10.1016/S0074-7696(08)61261-9

Slotte, J. P. (2016). The importance of hydrogen bonding in sphingomyelin's membrane interactions with co-lipids. *Biochim. Biophys. Acta Biomembr.* 1858, 304–310. doi: 10.1016/j.bbamem.2015.12.008

Soares-Silva, I., Ribas, D., Sousa-Silva, M., Azevedo-Silva, J., Renduliæ, T., and Casal, M. (2020). Membrane transporters in the bioproduction of organic acids: state of the art and future perspectives for industrial applications. *FEMS Microbiol. Lett.* 367:fnaa118. doi: 10.1093/femsle/fnaa118

Stewart, G. G. (2017). "The Structure and Function of the Yeast Cell Wall, Plasma Membrane and Periplasm," in *Brewing and Distilling Yeasts*, ed. G. G. Stewart, (Berlin: Springer), 55–75.

Stillwell, W. (2016). "Introduction to Biological Membranes," in *An Introduction to Biological Membranes*, ed. W. Stillwell, (Amsterdam: Elsevier), 3–15. doi: 10.1016/b978-0-444-63772-7.00001-4

Tan, Z., Khakbaz, P., Chen, Y., Lombardo, J., Yoon, J. M., Shanks, J. V., et al. (2017). Engineering *Escherichia coli* membrane phospholipid head distribution improves tolerance and production of biorenewables. *Metab. Eng.* 44, 1–12. doi: 10.1016/j.ymben.2017.08.006

Tan, Z., Yoon, J. M., Nielsen, D. R., Shanks, J. V., and Jarboe, L. R. (2016). Membrane engineering via trans unsaturated fatty acids production improves *Escherichia coli* robustness and production of biorenewables. *Metab. Eng.* 35, 105–113. doi: 10.1016/j.ymben.2016.02.004

Tsouka, S., and Hatzimanikatis, V. (2020). redLips: a comprehensive mechanistic model of the lipid metabolic network of yeast. *FEMS Yeast Res.* 20:foaa006. doi: 10.1093/femsyr/foaa006

Tsuge, Y., Kawaguchi, H., Sasaki, K., and Kondo, A. (2016). Engineering cell factories for producing building block chemicals for bio-polymer synthesis. *Microb. Cell Fact.* 15:19. doi: 10.1186/s12934-016-0411-0

Verghese, J., Abrams, J., Wang, Y., and Morano, K. A. (2012). Biology of the Heat Shock Response and Protein Chaperones: budding Yeast (*Saccharomyces cerevisiae*) as a Model System. *Microbiol. Mol. Biol. Rev.* 76, 115–158. doi: 10.1128/mmbr.05018-11

Wang, Y., Zhang, B., Lu, L., Huang, Y., and Xu, G. (2013). Enhanced production of pigments by addition of surfactants in submerged fermentation of *Monascus purpureus* H1102. *J. Sci. Food Agric.* 93, 3339–3344. doi: 10.1002/jsfa.6182

Wu, T., Ye, L., Zhao, D., Li, S., Li, Q., Zhang, B., et al. (2017). Membrane engineering - A novel strategy to enhance the production and accumulation of β-carotene in *Escherichia coli*. *Metab. Eng.* 43, 85–91. doi: 10.1016/j.ymben.2017.07.001

Yang, K., and Han, X. (2016). Lipidomics: techniques, applications, and outcomes related to biomedical sciences. *Trends Biochem. Sci.* 41, 954–969. doi: 10.1016/j.tibs.2016.08.010

Yazawa, H., Kamisaka, Y., Kimura, K., Yamaoka, M., and Uemura, H. (2011). Efficient accumulation of oleic acid in *Saccharomyces cerevisiae* caused by expression of rat elongase 2 gene (*rELO2*) and its contribution to tolerance to alcohols. *Appl. Microbiol. Biotechnol.* 91, 1593–1600. doi: 10.1007/s00253-011-3410-4

Yin, N., Zhu, G., Luo, Q., Liu, J., Chen, X., and Liu, L. (2020). Engineering of membrane phospholipid component enhances salt stress tolerance in *Saccharomyces cerevisiae*. *Biotechnol. Bioeng.* 117, 710–720. doi: 10.1002/bit.27244

Zheng, D. Q., Liu, T. Z., Chen, J., Zhang, K., Li, O., Zhu, L., et al. (2013). Comparative functional genomics to reveal the molecular basis of phenotypic diversities and guide the genetic breeding of industrial yeast strains. *Appl. Microbiol. Biotechnol.* 97, 2067–2076. doi: 10.1007/s00253-013-4698-z

Zhu, G., Yin, N., Luo, Q., Liu, J., Chen, X., Liu, L., et al. (2020). Enhancement of sphingolipid synthesis improves osmotic tolerance of *Saccharomyces cerevisiae*. *Appl. Environ. Microbiol.* 86, e2911–19. doi: 10.1128/AEM.02911-19

Conflict of Interest: The authors declare that the research was conducted in the absence of any commercial or financial relationships that could be construed as a potential conflict of interest.

frontiers in Microbiology

ORIGINAL RESEARCH
published: 16 August 2021
doi: 10.3389/fmicb.2021.705326

Effects of NaCl Concentrations on Growth Patterns, Phenotypes Associated With Virulence, and Energy Metabolism in *Escherichia coli* BW25113

Fen Li[1†], Xue-Song Xiong[1†], Ying-Ying Yang[2], Jun-Jiao Wang[3], Meng-Meng Wang[4,5], Jia-Wei Tang[3], Qing-Hua Liu[6], Liang Wang[3,7] and Bing Gu[1,8*]*

[1] Medical Technology School of Xuzhou Medical University, Xuzhou, China, [2] School of Life Sciences, Xuzhou Medical University, Xuzhou, China, [3] Department of Bioinformatics, School of Medical Informatics and Engineering, Xuzhou Medical University, Xuzhou, China, [4] Jiangsu Key Laboratory of New Drug Research and Clinical Pharmacy, School of Pharmacy, Xuzhou Medical University, Xuzhou, China, [5] Department of Pharmaceutical Analysis, School of Pharmacy, Xuzhou Medical University, Xuzhou, China, [6] State Key Laboratory of Quality Research in Chinese Medicines, Macau University of Science and Technology, Taipa, China, [7] Institut Pasteur of Shanghai, Chinese Academy of Sciences, Shanghai, China, [8] Laboratory Medicine, Guangdong Provincial People's Hospital, Guangdong Academy of Medical Sciences, Guangzhou, China

OPEN ACCESS

Edited by:
Jose M. Mulet, Universitat Politècnica de València, Spain

Reviewed by:
Muthita Vanaporn, Mahidol University, Thailand
Natalia Gottig, CONICET Instituto de Biología Molecular y Celular de Rosario (IBR), Argentina
Xiangke Duan, Southwest University, China

***Correspondence:**
Liang Wang
healthscience@foxmail.com
Bing Gu
gb20031129@163.com

† These authors have contributed equally to this work

Specialty section:
This article was submitted to Microbial Physiology and Metabolism, a section of the journal Frontiers in Microbiology

Received: *05 May 2021*
Accepted: *21 July 2021*
Published: *16 August 2021*

Citation:
Li F, Xiong X-S, Yang Y-Y, Wang J-J, Wang M-M, Tang J-W, Liu Q-H, Wang L and Gu B (2021) Effects of NaCl Concentrations on Growth Patterns, Phenotypes Associated With Virulence, and Energy Metabolism in Escherichia coli BW25113. Front. Microbiol. 12:705326. doi: 10.3389/fmicb.2021.705326

According to the sit-and-wait hypothesis, long-term environmental survival is positively correlated with increased bacterial pathogenicity because high durability reduces the dependence of transmission on host mobility. Many indirectly transmitted bacterial pathogens, such as *Mycobacterium tuberculosis* and *Burkhoderia pseudomallei*, have high durability in the external environment and are highly virulent. It is possible that abiotic stresses may activate certain pathways or the expressions of certain genes, which might contribute to bacterial durability and virulence, synergistically. Therefore, exploring how bacterial phenotypes change in response to environmental stresses is important for understanding their potentials in host infections. In this study, we investigated the effects of different concentrations of salt (sodium chloride, NaCl), on survival ability, phenotypes associated with virulence, and energy metabolism of the lab strain *Escherichia coli* BW25113. In particular, we investigated how NaCl concentrations influenced growth patterns, biofilm formation, oxidative stress resistance, and motile ability. In terms of energy metabolism that is central to bacterial survival, glucose consumption, glycogen accumulation, and trehalose content were measured in order to understand their roles in dealing with the fluctuation of osmolarity. According to the results, trehalose is preferred than glycogen at high NaCl concentration. In order to dissect the molecular mechanisms of NaCl effects on trehalose metabolism, we further checked how the impairment of trehalose synthesis pathway (*otsBA* operon) via single-gene mutants influenced *E. coli* durability and virulence under salt stress. After that, we compared the transcriptomes of *E. coli* cultured at different NaCl concentrations, through which differentially expressed genes (DEGs) and differential pathways with statistical significance were identified, which provided molecular insights into *E. coli*

responses to NaCl concentrations. In sum, this study explored the in vitro effects of NaCl concentrations on *E. coli* from a variety of aspects and aimed to facilitate our understanding of bacterial physiological changes under salt stress, which might help clarify the linkages between bacterial durability and virulence outside hosts under environmental stresses.

Keywords: *Escherichia coli*, bacterial survival, biofilm formation, glycogen, trehalose, transcriptome

HIGHLIGHTS

- Elevated NaCl concentration generally inhibits *E. coli* growth and phenotypes associated with virulence, such as biofilm formation, oxidative resistance and motile ability.
- Elevated NaCl concentration reduces glucose consumption and glycogen accumulation while improving trehalose production.
- Disruption of trehalose synthesis pathway OtsAB completely abolishes trehalose accumulation and greatly suppresses glycogen accumulation.
- Disruption of trehalose synthesis pathway OtsAB facilitates biofilm formation at low NaCl concentrations.
- Transcriptomic study provides clues into the molecular mechanisms of *E. coli* responses to the alteration of NaCl concentrations.

INTRODUCTION

Bacterial pathogens must have certain routes to be transmitted from one host to another, either directly through physical contact or indirectly via an intermediate agent. Although bacterial transmission is central to host infection, the transmission modes are complex and diverse, which involves direct host-to-host transmission, vector-borne transmission, and environmental transmission, and are often under genetic control of the host or the pathogen (Antonovics et al., 2017). According to the conventional wisdom of virulence evolution, all pathogens should be in a relationship of commensalism or mutualism with their hosts, that is, being avirulent to their hosts, because no pathogen wants to "kill the chicken for the eggs" (Wang et al., 2017). However, this traditional idea started to be challenged in mid-20th century and it was argued that avirulence should not be so inevitable for pathogens (Alizon et al., 2009). Later, more and more studies indicated that linkages existed between bacterial transmission modes and the evolution of bacterial virulence, one of the reasonings behind which is that increasing bacterial abundance within-host promotes the potential of pathogen transmission, but also increases host mortality (Cressler et al., 2015).

Through a series of cross-species studies, it was observed that vector-borne pathogens, such as Yellow Fever virus and *Rickettsia prowazekii* etc., tended to be more virulent than directly transmitted diseases like Coronavirus and *Haemophilus influenzae* since vector-borne pathogens did not rely on the well beings of hosts for transmission (Ewald, 1983). However, further studies showed that some non-vector-borne pathogens such as *Mycobacterium tuberculosis* and *Corynebacterium diphtheriae* could also cause high mortality in hosts (Ewald, 1983; Walther and Ewald, 2004). Epidemiological studies revealed that the high virulence of non-vector-borne pathogens were positively correlated with the long-term survival time in the environment because high durability increased transmission opportunities with less reliance on host mobility, which was later termed as the sit-and-wait hypothesis (Walther and Ewald, 2004). Thus, long-term environmental survival could play important roles in bacterial pathogenicity (Wang et al., 2017). In particular, when being outside the hosts, bacterial pathogens constantly encounter abiotic stresses such as nutrient deficiency, temperature fluctuation, and osmotic imbalance, etc. (Guan et al., 2017). It is possible that abiotic stresses may activate certain pathways or the expressions of certain genes, which also contributions to bacterial virulence such as self-replication, cellular adhesion and host invasion, etc. and is worthy of further investigation since it may provide molecular insights into the changing patterns of bacterial pathogenicity (Boor, 2006).

In fact, a variety of studies have revealed that abiotic stresses could improve virulent phenotypes of bacterial pathogens. For example, Sundberg et al. explore how long-term starvation influences virulence of the environmentally transmitting fish pathogen *Flavobacterium columnare*, which found that starved rhizoid isolates evolved toward significantly higher virulence after 5 months when compared with the ancestral rhizoid (Sundberg et al., 2014). Mihaljevic et al. studied the effects of environmental stress factors on the survival and virulence of *Campylobacter jejuni*, according to which oxygen exposure increased invasion capability and intraepithelial survival of the clinical isolate (Mihaljevic et al., 2007). Thus, it concludes that aeration is associated with the pathogenic potential of *C. jejuni* (Mihaljevic et al., 2007). In addition, Pinto et al. used RNA sequencing to identify the differentially expressed genes of *Corynebacterium pseudotuberculosis* in response to abiotic stresses, which uncovered that, under thermal, osmotic or acidic stress conditions, biological processes such as cellular adhesion and/or oxidoreduction become the most evident in terms of induced genes (Pinto et al., 2014). Recently, Vanaporn and Titball (2020) systematically reviewed the functions of trehalose in bacterial virulence, according to which trehalose biosynthesis is typically induced when exposed to abiotic stress while threhalose is associated with host colonization, within-host growth, and the modulation of host defense mechanisms. For a schematic illustration of the potential interactions between abiotic stress and bacterial pathogens, please refer to **Figure 1**.

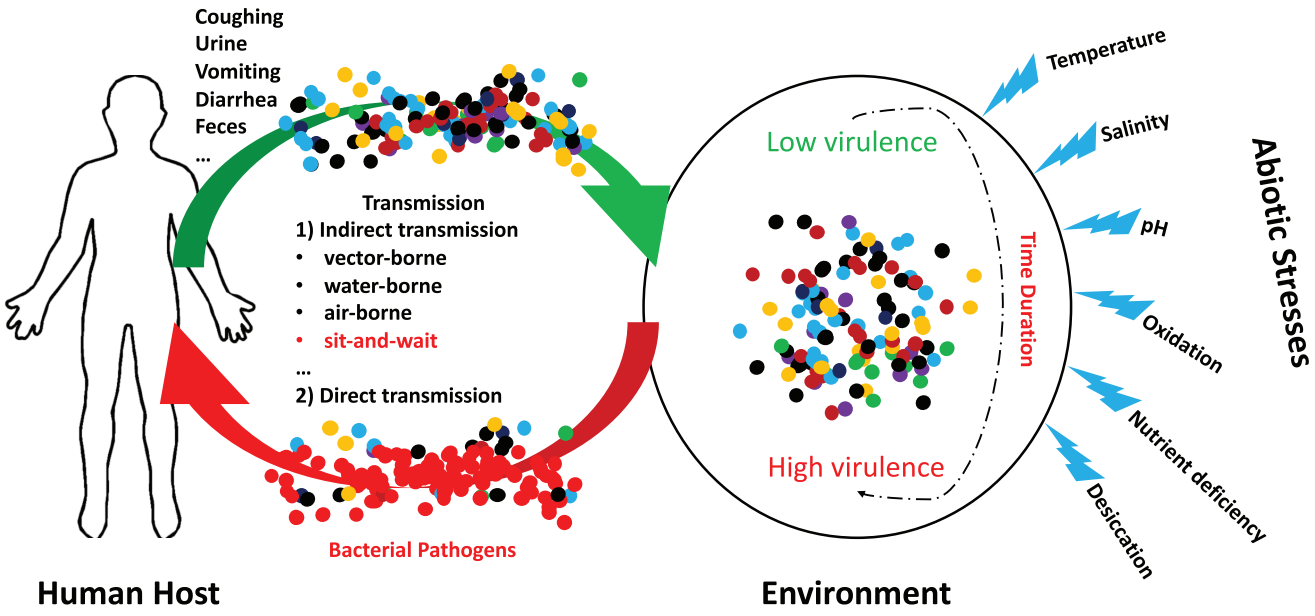

FIGURE 1 | Schematic illustration of the potential interactions between abiotic stress and bacterial pathogens. A group of indirectly transmitted bacterial pathogens shed from human hosts were spread to environment via a variety of routes, where they encounter many abiotic stresses for a certain duration. During the period, it is possible that bacterial pathogenic phenotypes could be altered from low virulence to high virulence due to the influences of abiotic stresses. These bacteria may cause severe consequences after being transmitted to new hosts.

Among these abiotic stresses, fluctuating osmotic pressure is commonly encountered by bacterial pathogens. Dinnbier et al. (1988) first revealed that *E. coli* K-12 transiently accumulated potassium glutamate for elevated NaCl concentration and then replaced it with trehalose as an osmoprotectant during adaptation. Later, a variety of studies investigated how bacteria responded to the stress and showed the corresponding effects on bacterial physiology like virulence (Strom and Kaasen, 1993; Sleator and Hill, 2002; Macintyre et al., 2020). In this study, we used *Escherichia coli* K-12 BW25113 as a model organism to comprehensively explore how NaCl concentrations influenced growth pattern, biofilm formation ability, oxidative stress resistance, and motile capacity, all of which were associated with bacterial environmental survival and within-host pathogenicity. In addition, since energy metabolism also contributed to osmotic pressure response, we investigated how glycogen and trehalose metabolisms were influenced by different NaCl concentrations and their potential interconnections, which revealed that glycogen level was significantly reduced while trehalose level was greatly increased in response to high NaCl concentrations. In order to further understand the osmoprotection roles of trehalose, we investigated the physiological changes of two single-gene knockout strains, *E. coli* BW25113 Δ*otsA* and Δ*otsB*, under salt stresses, respectively. Moreover, for elucidating the molecular mechanisms of *E. coli* response to osmotic stress, we compared transcriptomes of *E. coli* cultured under different NaCl concentrations. Differentially expressed genes (DEGs) with statistical significance, together with differential metabolic pathways, were identified, which might provide insights into the relationship between environmental durability and bacterial virulence. In sum, our study showed that salt stress could greatly and significantly alter bacterial phenotypes, which not only facilitated our understanding of physiological changes under NaCl concentrations in bacteria, but also provided clues for the evolution of bacterial virulence outside hosts from the perspective of the sit-and-wait hypothesis.

MATERIALS AND METHODS

Bacterial Strains and Growth Conditions

The commonly used lab strain *Escherichia coli* K-12 BW25113 (Horizon Discovery Ltd., United States) and two single-gene knockout mutants, *E. coli* K-12 BW25113 Δ*otsA* and K-12 BW25113 Δ*otsB*, as part of the KEIO collection (Horizon Discovery Ltd., United States) were studied in this project. Inactivation of the two genes at expression level was double-checked via quantitative reverse-transcription PCR (qRT-PCR). The strains were initially stored in ultra-low temperature freezer (Thermo Fisher, United States) at −80°C. When doing experiment, the strains were thawed on ice, streaked on Luria–Bertani (LB) agar (VICMED, China) plates, and incubated at 37°C overnight for recovery. Single colonies were picked up from the agar plate, which were then used to inoculate LB liquid medium culture and 1 × M9 minimal medium culture (Sigma-Aldrich, United States) consisting of 6.78 g/L Na_2HPO_4, 3 g/L KH_2PO_4, 1 g/ L NH_4Cl, and 0.5 g/L NaCl for subsequent experiments as designated.

Measurement of Bacterial Growth Curves

A single colony (wild-type, Δ*otsA*, Δ*otsB*) was picked up from the LB agar plate and inoculated into 10 mL of LB broth. After vortexing, the culture was incubated overnight at 37°C and 220 rpm. The overnight culture was then used to inoculate fresh LB broth at the ratio of 1:100, which was cultured for 4 h at 37°C and 220 rpm. For the effects of glucose concentrations on bacterial growth, the culture was used to inoculate 1 × M9 minimal medium supplemented with 0.2, 0.4, and 0.8% glucose at a ratio of 1:20, respectively, which was then cultured at 37°C and 220 rpm for 24 h. For the effects of NaCl, the culture was used to inoculate sterile LB broth containing 0%, 1%, 3.5%, and 5% NaCl at the ratio of 1:1000. At 0, 2, 4, 6, 8, 10, 12, 14, 16, 18, 20, 24 h, the optical density value OD_{600} was measured via microplate reader while the number of viable cells (colony forming units per milliliter, CFU/mL) was counted via Miles and Misra method for the two tests, respectively (Hedges, 2002). Three independent replicates were performed for the number of viable cells, the average of which, together with standard error means, was used to draw growth curve (**Figure 2**). As for the OD_{600}-based growth curves for the two tests, please refer to **Supplementary Figure 1**.

Quantification of Biofilm Formation

The quantification of bacterial biofilm formation of *E. coli* strains (wild-type, Δ*otsA*, Δ*otsB)* was performed by following the procedures as previously described by Wang et al. (2015) with modifications. In particular, a single *E. coli* colony was picked up from LB agar plate and inoculated into 10 mL LB broth, which was then cultured overnight at 37°C and 220 rpm. Fresh LB broth with different salt concentrations (0, 1, 3.5, 5%) were mixed with the overnight bacterial culture at the ratio of 100:1. Take 200 μL solution from each of the above-prepared LB broths as experimental group, together with 200 μL solution of sterile LB broth with corresponding salt concentration as control group to a 96-well plate. For each sample, three technical repeats and three biological repeats were performed. The 96-well plates were incubated statically at 30°C for 20 h. After that, bacterial solutions were discarded and the plates were thoroughly but gently washed with deionized water for three times. Then, 200 μL of 0.1% crystal violet solution (Dalian Meilun Biotechnology Co. Ltd., China) was added to each well for a 10-min incubation at room temperature in order to stain the biofilm. After staining, all the solutions were discarded and the plates were washed with deionized water for three times. In order to quantify biofilm formation capacity, 200 μL of the mixed solution with 20% ethanol and 80% acetone (Sinopharm Chemical Reagent Co. Ltd., China) was added to each well for 10 min for decolorization. 150 μL of the solution from each well was then transferred to a new 96-well plate. A microplate reader (Thermo Fisher, United States) was used to measure the absorbance of the solution at 590 nm, the values of which represented bacterial biofilm formation abilities.

Measurement of Oxidative Stress Resistance

A single colony (wild-type, Δ*otsA*, Δ*otsB*) was picked up from the LB agar plate and inoculated into 10 mL LB broth for overnight culture at 37°C and 220 rpm. The bacterial solution was then mixed with fresh LB broth at a ratio of 1:100, which was cultured for 4 h at 37°C and 220 rpm. After that, 20 μL bacterial solutions were well mixed with LB broths containing 0.8% agar and different concentrations of NaCl (0, 1, 3.5, 5%), which were then poured into 90 mm petri dishes and solidified. 10 μL H_2O_2 solution (6.6 mol/L) was then dropped onto 6 mm round filter paper sheet that was placed in the center of each petri dish. The plates were then incubated statically overnight at 37℃. The diameter of the inhibition zone from three different directions was recorded. The experiment for each sample was repeated for three times independently. The average value and standard error were present for each sample.

Motility Test

Single colonies (wild-type, Δ*otsA*, Δ*otsB*) picked up from LB agar plate were used to inoculate 10 mL LB broth that was further cultured at 37°C and 220 rpm overnight. 100 mL fresh LB broth was inoculated with the overnight culture at a ratio of 100:1, which was then cultured for 4 h at 37°C and 220 rpm (starting culture). Centrifuge the culture at 6,000 *g* for 10 min, discard the supernatant, resuspend bacterial pellet in LB broth to reach a final OD_{600} of 2. Transfer 2 μL of the resuspended culture to the center of LB agar plates (0.3% agar) with different NaCl concentrations (0, 1, 3.5, 5%), which were then incubated statically at 37℃ for 24 h. Diameters of the near-circle growth zones were measured from three different directions, which reflected bacterial motile abilities. The experiment was repeated independently for three times. Averaged diameter and standard errors were visualized and present.

Quantification of Glucose Consumption Rate

Starting culture was prepared as described above, which was then inoculated (ratio = 20:1) into 1 × M9 minimal medium containing 0.8% glucose and different concentrations of NaCl (0, 1, 3.5, 5%). The mixed culture was incubated at 37°C with shaking rate of 220 rpm. At 16 h, 20 h, and 24 h, 1 ml of culture was taken out for centrifugation at 6,000 *g* for 10 min, respectively. It is noteworthy that for the two *E. coli* mutants Δ*otsA* and Δ*otsB*, the experiment was only performed at 20 h. 10 μL of the supernatant was transferred into an Eppendorf (EP) tube with 990 μL GOPOD solution (Megazyme, Ireland). The tube was vortexed and incubated at 50℃ for 20 min. After reaction, the absorbance value was measured at 510 nm, which was then transformed into glucose content in the culture (mg/mL) by using glucose standard curve produced by following the manufacturer's instructions. Since the initial glucose content (0.8%) was known, the percentage of left-over glucose was easily calculated. The experiment was repeated for three times independently. Averaged values and standard errors were visualized and present.

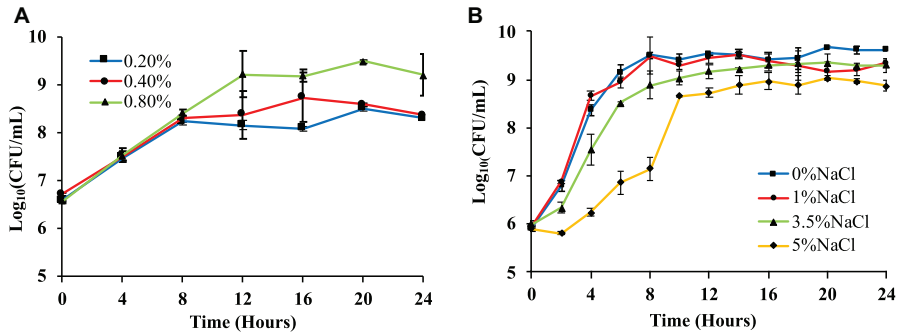

FIGURE 2 | Effects of glucose and NaCl concentrations on the growth rates of *Escherichia coli* BW25113. **(A)** *E. coli* growth curves in 1 × M9 minimal medium with three different glucose concentrations (0.2, 0.4, and 0.8%) measured via logarithmic value of CFU with base 10. **(B)** *E. coli* growth curves in LB broth supplemented with four different NaCl concentrations (0, 1, 3.5, and 5%) measured via logarithmic value of CFU with base 10. Three independent replicates were performed for the number of viable cells, the average values and standard error means were used to draw the curves.

Glycogen/Protein Ratio Assay

Wild-type *E. coli* BW25113 was incubated in 1 × M9 minimum medium containing 0.8% glucose and different concentrations of NaCl (0, 1, 3.5, 5%) for 16, 20, and 24 h. It is noteworthy that for the two *E. coli* mutants Δ*otsA* and Δ*otsB*, the experiment was only performed at 20 h. 10 mL of the culture was then centrifuged at 6,000 *g* for 10 min. The bacterial pellet was resuspended in 1 mL glycogen extraction buffer (50 mM Tris, pH 8, 150 mM NaCl, 2 mM EDTA, 50 mM NaF, 5 mM sodium pyrophosphate, and Roche protease inhibiting cocktail) and lysed by sonication (25% amplitude, 10 s on, 30 s off, 3 repeats). Two groups were set-up for further analysis, which were experimental group and blank control group. In the experimental group, 20 μL of lysed bacterial culture was mixed with 100 μL of pH 4.5 acetic acid-sodium acetate buffer solution, and then mixed with 5 μL of 3,260 U/mL amyloglucosidase (MegaZyme, Ireland), which was made up to 500 μL with deionized water. Composition of the blank control group was exactly the same as that of the experimental group except that amyloglucosidase was not added. After vortexing, samples were incubated at 50°C for 30 min. After the reaction, centrifuge the samples at 6,000 *g* for 10 min at room temperature. After centrifugation, take 300 μL of the supernatant to mix with 700 μL of GOPOD reagent, which was then incubated at 50℃ for 20 min. When the reaction complete, take 150 μL of the sample in a 96-well plate (three technical repeats for each sample), and use a microplate reader to determine the absorbance values of the experimental group and the blank control sample at 510 nm. The absorbance value of the experimental group is subtracted from the absorbance value of the blank control group, which was then brought into the standard curve to obtain the glycogen content. As for protein content determination, we used commercial Bradford method kit (Shanghai Biyuntian Biotechnology Co., Ltd., China). All the procedures were done by following the manufacturer's instructions. Briefly, bacterial homogenate was diluted 20 times with deionized water, 5 μL of which was then added to a 96-well plate. 250 μL of G250 staining solution was added to each well. Measure the absorbance with a microplate reader at of 595 nm. Protein content was obtained by using standard protein curve. Glycogen/protein ratio was calculated by simple division. All the procedures were repeated for three times, independently.

Trehalose Content Assay

Commercial trehalose assay kit (Megazyme, Ireland) was used for its content determination. Manufacturer's instructions were followed for content quantification. Briefly, 200 μL of lysed bacterial homogenate as described above in section 2.7 was mixed with 200 μL of alkaline sodium borohydride, which was stirred and reacted in a metal bath at 40°C for 30 min. 500 μL of 200 mM glacial acetic acid was added to the mixed and vortexed to remove excess sodium borohydride. After 5 min, add 200 μL of 2 M imidazole buffer, and adjust the solution to pH 7. Take 20 μL of the neutral solution to a 96-well plate, add 20 μL kit buffer, 10 μL NADPH + /ATP, 2 μL HK/G-6-PDH, and 200 μL ddH_2O to each well. Mix and react at 25°C for 5 min. After that, absorbance value (A1) was measured at 340 nm. Add 2 μL trehalase to each well. Mix and react for 5 min at 25℃. Measure the absorbance value (A2) of the sample at 340 nm. Obtain the final value by subtracting A2 with A1 (A2-A1). The trehalose content of the sample was calculated based on the standard trehalose curve. The tests were repeated independently for three times.

Comparative Transcriptome Analysis

Bacterial Culture and RNA Extraction

A single colony of wild-type *E. coli* BW25113 was picked up from LB agar plate, which was used to inoculate 10 mL of fresh LB broth. The inoculated medium was well mixed and incubated overnight at 37°C and 220 rpm, which was then added to fresh LB broth at the ratio of 1:100 for 4-h incubation at 37°C and 220 rpm. Fresh 1 × M9 minimal media (0.8% glucose) containing 0%, 1%, 3.5%, 5% NaCl were then mixed with the 4-h bacterial culture at a ratio of 20:1. The four groups of mixed culture were incubated for 20 h at 37°C and 220 rpm. After culture, transfer 1 mL of the bacterial solution into a 2 mL sterile tube, centrifuge the solution at 6,000*g*, 4°C for 10 min, discard the supernatant and retain the pellet for RNA extraction. Total RNA was extracted via Total RNA Extractor Kit (Sangon, Shanghai) by following the

manufacturer's instructions, which was then treated with RNase-free DNase I in order to get rid of genomic DNA contaminant. RNA completeness was assessed with 1.0% agarose gel. The quality and quantity of RNA were then evaluated by using Qubit Flurometer (Life Technologies, CA, United States). High quality RNA samples were sent submitted to Sangon Biotech Co., Ltd. (Shanghai, China) for library preparation. Paired-end sequencing of the library was performed at Sangon Biotech Co., Ltd. on the HiSeq XTen sequencers (Illumina, San Diego, CA, United States).

Transcriptome Analysis

Data assessment and reference genome alignment

FastQC (version 0.11.2) was used for evaluating the quality of sequenced data. Raw reads were filtered by Trimmomatic (version 0.36), which involved deletions of adaptor sequence, low quality bases ($Q < 20$), and short reads (< 35 nt). Clean reads were then used for further analysis through mapping to the reference genome *Escherichia coli* K-12 substr. MG1655 (NCBI Genome ID NC_000913.3) by HISAT2 (version 2.0) with default parameters. RSeQC (version 2.6.1) was used to statistically check the alignment results. The homogeneity distribution and the genome structure were checked by Qualimap (version 2.2.1). BEDTools (version 2.26.0) was used to analyze gene coverage ratio. Quality of the RNA sequencing data was summarized in **Table 1**.

Differentially expressed genes

Transcripts were computed by StringTie (version 1.3.3b) in terms of expression levels. Sample distance and difference were analyzed via Principal Component Analysis (PCA) and Principal co-ordinates analysis (PCoA). Transcripts Per Million (TPM) was used for eliminating the influence of gene lengths and sequencing discrepancies, which enabled direct comparison of gene expression levels between samples. Differentially expressed genes (DEGs) between two samples were determined by DESeq2 (version 1.12.4). DEGs were considered as statistically significant if *P*-value was less than 0.05 and $\log_2$(FoldChange) was greater than 1. For those genes with normalized expression difference equal to zero between two samples, the expression value was adjusted to 0.01 because 0 cannot be plotted on a log plot. If the normalized expression of a certain gene in two libraries was all lower than 1, further differential expression analysis was conducted without this gene. Gene expression differences were visualized by volcano plot and heatmap while sample clusters were generated via principal component analysis (PCA).

Network analysis

As for the identification of hub genes, up- and down-regulated genes were analyzed, separately. In specificity, up- or down-regulated genes were input into the String database https://string-db.org/ for building interaction networks (Szklarczyk et al., 2021), respectively. The results were shown in **Supplementary Figure 2**. These data were then input into CytoScape and visualized for highly-connected proteins via the number of degrees and hub proteins calculated by using the cytoHubba algorithm (Shannon, 2003; Chin et al., 2014).

Functional analysis of DEGs

Functional analyses including Gene Ontology (GO) annotation, Kyoto Encyclopedia of Genes and Genomes (KEGG) pathways, and hub genes were performed to identify which DEGs were significantly enriched in GO terms, metabolic pathways, and clusters of genes. Gene Ontology (GO) is a standard classification system for gene functions (Consortium, 2019). For GO annotation, DEGs were mapped to the GO terms (biological process, cellular component, molecular function) in the database. The number of genes in every term was then calculated, and a hypergeometric test is performed to identify significantly enriched GO terms in the gene list out of the background of the reference gene list. KEGG is a public database of pathway data (Kanehisa et al., 2017). KEGG pathway analysis identifies DEGs that are significantly enriched in metabolic pathways or signal transduction pathways compared to a reference gene background via the hypergeometric test. GO terms and KEGG pathway with false discovery rate (Q-value < 0.05) were considered as significantly altered.

Statistical Analysis

A two-tailed unequal variance Student's *t*-test was calculated for pairwise comparison wherever applicable, unless otherwise instructed. Significant difference is defined as *P*-value less than 0.05. The single-step multiple comparison procedure and statistical test, Tukey's Honestly Significant Difference (HSD) test, was performed via the R software TukeyC package wherever applicable, which compared the means of every group to the means of every other group simultaneously. Means denoted by a different letter indicated significant differences among groups (*P*-value <0.05).

RESULTS

Bacterial Growth

We first tested *E. coli* BW25113 growth pattern on different concentration of glucose and survival ability under different concentrations of NaCl. Both OD_{600} values and the number of viable cells (CFU/mL) were measured, where only the number of viable cells was present while OD_{600} values were present in **Supplementary Figure 1**. For glucose concentration, 1 × M9 minimal medium supplemented with higher level of glucose (0.8%) showed the highest number of viable cells in the culture, which was significantly different from those with 0.2% and 0.4% glucose (*P*-value <0.05) after culturing for 20 h (**Figure 2A**). This result is similar with previous studies performed on *E. coli* BL21(DE3) and *E. coli* DH5α, which confirms that high level of carbon source facilitates the replication of bacterial cells (Wang et al., 2018, 2020b). As for osmotic stress, four sodium chloride (NaCl) concentrations (0, 1, 3.5, and 5%) were explored and statistical analysis showed that the number of viable cells in LB broth supplemented with 0% NaCl at 24 h is significantly higher than other tested groups, that is, LB broth supplemented with 1%, 3.5%, and 5% NaCl (**Figure 2B**). The result is consistent with previous reports that elevated concentration of NaCl could

TABLE 1 | RNA sequencing data for the eight samples in the four *E. coli* groups cultured in different NaCl concentrations.

Sample	Repeats	Clean reads	Total bases	Mapped reads	Q10*	Q20*	Q30*	GC content
0% NaCl	R1	45850638	6349937612	71.92%	100%	98.83%	95.64%	52.76%
	R2	37508466	5101337699	99.65%	100%	98.74%	95.41%	52.31%
1% NaCl	R1	42539228	5767997978	99.7%	100%	98.81%	95.57%	52.33%
	R2	38463266	5232506247	99.7%	100%	98.78%	95.51%	52.41%
3.5% NaCl	R1	31624808	4431748030	99.53%	100%	98.79%	95.53%	52.82%
	R2	23246030	3208991183	99.31%	100%	98.74%	95.35%	52.64%
5% NaCl	R1	35416518	4824466216	99.36%	100%	98.87%	95.74%	52.75%
	R2	33649560	4647777496	99.01%	100%	98.76%	95.44%	52.82%

**Q10 means the sequencing error rate of the base was less than 10%; Q20 means the sequencing error rate of the base was less than 1%; Q30 means the sequencing error rate of the base was less than 0.1%.*

inhibit the growth patterns of bacterial species (Rath et al., 2016; Pang et al., 2020).

Biofilm Formation, Oxidative Resistance and Motility

Biofilm normally consists of bacterial cells and extracellular polymeric substances (EPS) that helps bacteria to survive in harsh environmental conditions and facilitate host infection (Sharma et al., 2016). Thus, biofilm formation is a survival strategy of bacteria. In this study, we investigated how NaCl concentrations impacted on *E. coli* biofilm formation. According to the results in **Figure 3A**, NaCl showed a positively dose-dependent inhibition of biofilm growth in *E. coli*, though statistical significance was only detected when comparing *E. coli* in culture of 0% NaCl with that in the culture of 3.5% and 5% NaCl, respectively. In fact, *E. coli* growing in culture with 3.5% and 5% NaCl had negligible amount of biofilm. However, the relationship between hyperosmotic stress and biofilm formation in bacteria is actually controversial. For example, Kawarai et al. (2009) reported that *E. coli* K-12 did not form biofilm in LB broth supplemented with 1 M NaCl, which is consistent with the result in this study, while another study revealed that biofilm formation of *Staphylococcus aureus* was significantly enhanced with the increase of NaCl concentrations (Lee et al., 2014). Thus, how NaCl concentration influences the formation of bacterial biofilm should probably be investigated and explained on a case-by-case basis.

Aerobic bacteria use oxygen to oxidize nutrients for energy or to respire, which leads to the generation of reactive oxygen species (oxidants) for the necessity of various physiological functions. However, if there is an imbalance between the production of oxidants and antioxidants, oxidative stress emerges, which has harmful effects on protein structure and functions with the possibility of causing cell death (Ezraty et al., 2017). Thus, in this study, we tested the roles that NaCl played in combating oxidative stress resistance in *E. coli*. According to the results in **Figure 3B**, hyperosmolarity induced by 5% NaCl could significantly increase the effects of oxidative damages when compared with other NaCl concentrations (0, 1, and 3.5%). Although we can see that 3.5% NaCl also increases the oxidative stress of H_2O_2 on *E. coli* colonies, there is no statistical significance detected when compared with lower NaCl concentrations.

As for motility, it is a common behavior for most bacterial species, through which bacteria are able to reach new environments, looking for niches with high nutrient and low toxins (Mitchell and Kogure, 2006). Some studies suggest that bacterial virulence and motile ability are closely associated via complex regulatory networks (Josenhans and Suerbaum, 2002), while others hold different opinions (Kao et al., 2014). In this study, we explored the effects of NaCl concentrations on the motility of *E. coli* on soft agar plates, the results of which indicated that there was dose-dependent inhibition of bacterial movement with statistical significance among the four NaCl concentrations (**Figure 3C**).

Energy Metabolism

In order to grow and replicate in a fast pace, bacteria need to get access to abundant nutrients and absorb sufficient energy from surrounding compounds (Rohmer et al., 2011). In addition, bacterial viability and virulence are also tightly correlated with energy metabolism (Passalacqua et al., 2016). Thus, it is important to understand that how abiotic stress influences bacterial energy metabolism. Glucose is an optimal carbon source for *E. coli* that supports faster growth when compared with other sugars, the dynamic change of which have been explored by a variety of studies (Fuhrer et al., 2005; Yamamotoya et al., 2012). As a widely present carbohydrate reserve in bacteria, glycogen contributes to bacterial survival in the environment under a variety of stresses, such as temperature fluctuation, nutrient deprivation, and osmolarity instability (Wang et al., 2020a). In addition, glycogen also plays important roles in physiological activities such as osmotic regulation and pH maintenance, etc. (Liu et al., 2021). As for trehalose, it is a disaccharide of two glucose molecules linked by α 1,1-glycosidic bond. It is well known that trehalose protects microbes like *Saccharomyces cerevisiae* and *E. coli* from desiccation (Welsh and Herbert, 1999; Tapia et al., 2015). Studies also show that trehalose and trehalose derivatives play important roles in bacterial virulence in terms of host colonization and within-host adaptation (Vanaporn and Titball, 2020) while the deletion of trehalose-synthesizing gene leads to the virulence abolishment of bacterial pathogens (Puttikamonkul et al., 2010; Gebhardt et al., 2015). In this study, we explored the impacts of salt concentrations on the interconnections of these three important energy compounds.

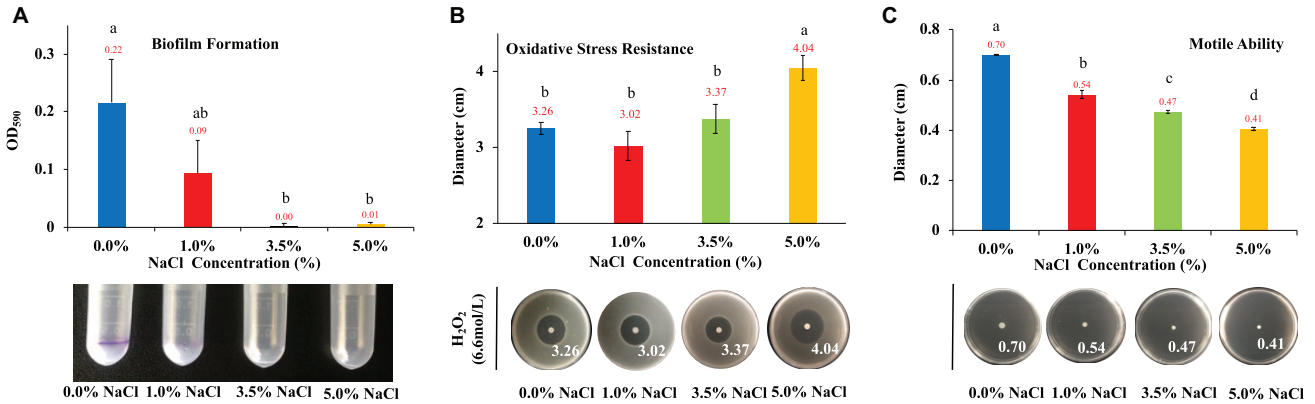

FIGURE 3 | Effects of NaCl on *E. coli* biofilm formation, oxidative stress resistance, and motile ability. **(A)** Effects of different NaCl concentrations on *E. coli* biofilm formation. **(B)** Influences of different NaCl concentrations on *E. coli* oxidative stress resistance. **(C)** Effects of different NaCl concentrations on *E. coli* motile abilities. Tukey's Honestly Significant Difference (HSD) test was performed, which compared the means of every group to the means of every other group simultaneously. Means denoted by a different letter indicated significant differences among groups (*P*-value <0.05).

E. coli was cultured in 1 × M9 minimal medium containing 0.8% glucose and different concentrations of NaCl (0, 1, 3.5, and 5%). The general changing patterns of glucose consumption rates at the three time points (16, 20, and 24 h) were the same, which indicated that the effects of NaCl concentrations on *E. coli* glucose uptake from the culture were consistent. In specificity, *E. coli* growing in 1% NaCl had the highest glucose uptake value while 3.5% and 5% NaCl inhibited the absorption of external glucose with statistical significance at both 16-h and 20-h (**Figures 4A–C**). At 24-h, 5% NaCl had the lowest level of glucose absorption than cultures containing other concentrations of NaCl (**Figure 4C**). As for glycogen metabolism, it was obvious that NaCl had a dose-dependent inhibitory effect on glycogen accumulation in *E. coli* (**Figures 4D–F**). In addition, glycogen accumulation also showed a time-dependent pattern when the culture was the same, that is, higher at 20-h and lower at 16- and 24-h, which was also consistent with previous studies (Wang et al., 2020b). Moreover, trehalose accumulation in cultures with different NaCl concentrations also showed dose-dependent changing patterns (**Figures 4G–I**). However, in contrast to glycogen accumulation, NaCl facilitated the accumulation of trehalose in *E. coli* BW25113 in response to hyperosmotic stress. According to the statistical analysis, *E. coli* cultured at 3.5% and 5% NaCl conditions accumulated significantly more trehalose than bacteria cultured at 0% and 1% NaCl, which was independent of time points. It was also obvious that *E. coli* accumulated the highest amount of trehalose at 24-h (**Figure 4I**). Thus, trehalose accumulation could play important roles in *E. coli* response to hyperosmotic stress as previously confirmed (Dinnbier et al., 1988; Purvis et al., 2005).

Effects of NaCl Concentrations on *Escherichia coli* Δ*otsA* and Δ*otsB*

Previous study showed that trehalose content was significantly enhanced in wild-type *E. coli* under high salinity concentration (**Figures 4G–I**). In bacteria, three trehalose synthesis pathways have been reported, which are OtsAB, TreYZ and TreS (Avonce et al., 2006), among which the pathway consisting of OtsA (trehalose-6-phosphate synthase) and OtsB (trehalose-6-phosphate phosphatase) uses UTP-glucose as a substrate, which is essential for trehalose synthesis in some bacteria such as *Mycobacterium tuberculosis* (Murphy et al., 2005). As for TreYZ pathway, TreY (maltooligosyl-trehalose synthase) and TreZ (maltooligosyltrehalose trehalohydrolase) work together to convert maltodextrin to maltooligosyltrehalose and then hydrolyze this product to form free trehalose (Elbein, 2003). TreS is trehalose synthase that inter-convert trehalose (α-D-1,1-glucose) to maltose (α-D-1,4-glucose) (De Smet et al., 2000). Since OtsAB pathway is directly linked with glucose for trehalose synthesis while the other two pathways used maltodextrin and maltose, we focused on single-gene inactivation of the OtsAB pathway in terms of their responses to the fluctuations of NaCl concentrations in this study.

A variety of studies have explored how the inactivation of *otsA* and/or *otsB* influenced bacterial physiology in different bacterial specie under different conditions. For example, a recent study by Hubloher et al. showed that deletion of *otsB* in *Acinetobacter baumannii* led to growth impairments at high salt conditions (Hubloher et al., 2020). Another study of *E. coli* Δ*otsA* showed that trehalose played a protective role in stabilizing outer membrane when *E. coli* was under abiotic stress (Chang et al., 2019). In addition, Algara et al. revealed that trehalose protected *E. coli* against carbon stress because *E. coli* Δ*otsA*, a trehalose-abolished strain, showed increased Nε-lysine acetylation and protein aggregation (Moruno Algara et al., 2019). Although this study showed that high salt condition facilitated trehalose accumulation and inhibited glucose uptake and glycogen accumulation in wild-type *E. coli*, whether the disruption of trehalose synthesis could lead to any different physiological changes when compared with the wide-type strain in response to hyperosmotic stress is unknown.

In this study, we compared the two single-gene inactivated *E. coli* BW25113 mutants Δ*otsA* and Δ*otsB* in terms of their

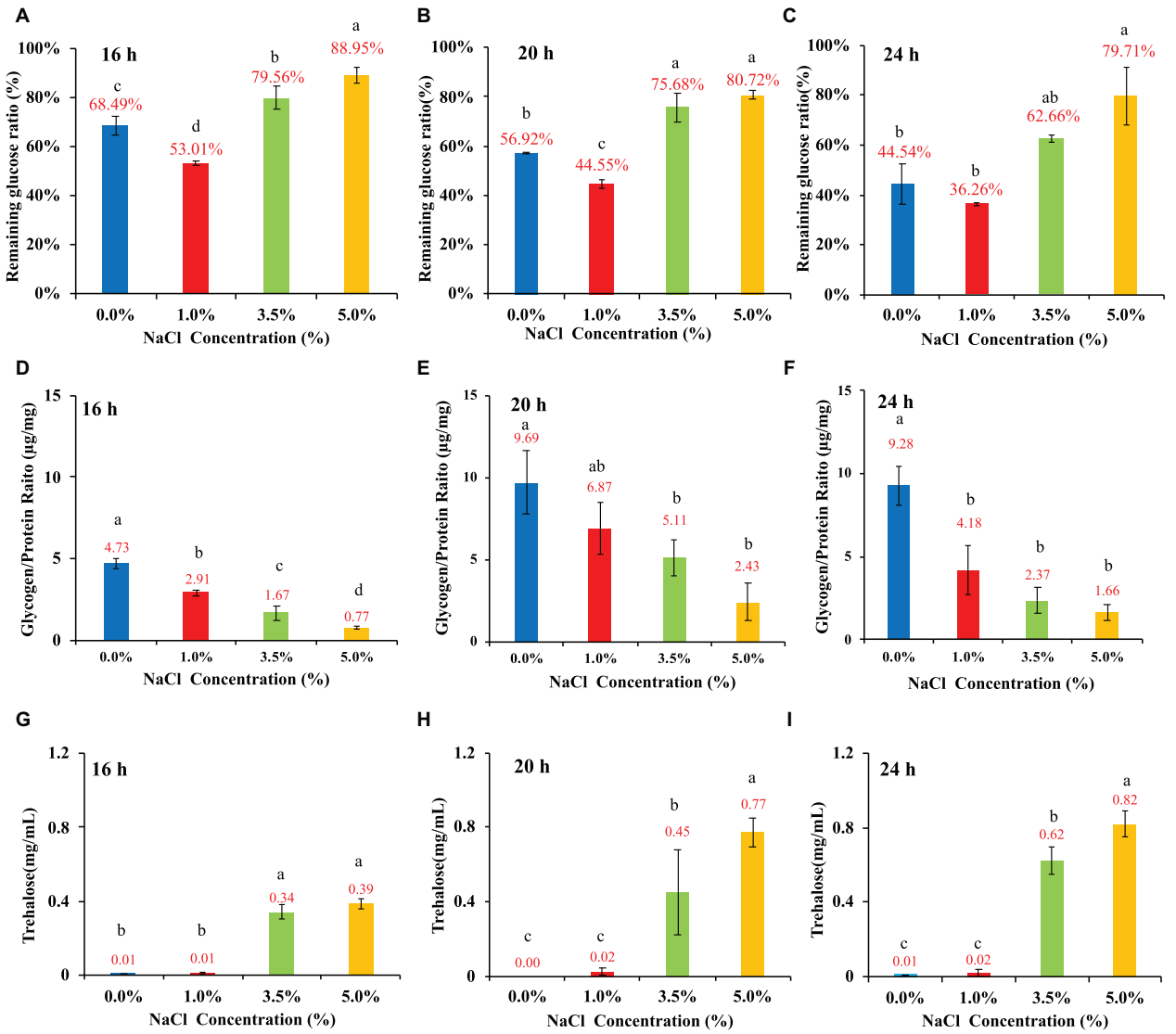

FIGURE 4 | Influences of NaCl concentrations (0, 1, 3.5, and 5%) on *E. coli* glucose consumption rate, glycogen accumulation, and trehalose content at three time points, that is, 16, 20, and 24 h. **(A–C)** Glucose consumption rate. **(D–F)** Glycogen accumulation capacity. **(G–I)** trehalose content. Tukey's Honestly Significant Difference (HSD) test was performed. Means denoted by a different letter indicated significant differences among groups (*P*-value <0.05).

growth pattern, biofilm formation, oxidative stress resistance, and motile abilities with the wild-type strain. Both *E. coli* mutants showed abolishment of trehalose accumulation at 20 h (**Supplementary Figure 3**), which indicated that inactivation of Δ*otsA* and Δ*otsB* led to the disruption of trehalose synthesis. In addition, both mutants showed analogous growth patterns as wild-type *E. coli* strain when no NaCl was supplemented in the LB broth while increased NaCl concentration inhibited the general growth trends of the two mutants in a dose-dependent manner that is similar to wild-type strain, though *E. coli* Δ*otsB* seemed to have extended lag phase (**Figures 5A,B**). As for biofilm formation, the capacity of *E. coli* Δ*otsB* was significantly higher than *E. coli* Δ*otsA* at both 0% and 1% NaCl while both mutants showed significantly increased biofilm formation than wild-type strain at 0% and 1% NaCl. When NaCl concentrations increased to 3.5 and 5%, no biofilm could be detected in both mutant and wild-type strains (**Figures 5C,D**). As for oxidative resistance and mobile ability, both mutants showed similar patterns as the wild-type strain with no statistical significance (**Figures 5E–H**). In sum, physiological analysis showed that inactivation of trehalose synthesis pathway in *E. coli* BW25113 mainly impacted on bacterial biofilm formation while other features were not significatnly influenced.

As for glucose consumption in the 20-h culture, the two mutants showed very different abilities with each other and also when compared with wild-type strain. In particular, glucose uptake of strain Δ*otsA* decreased proportionally with the increase of NaCl concentration; in contrast, strain Δ*otsB* showed the

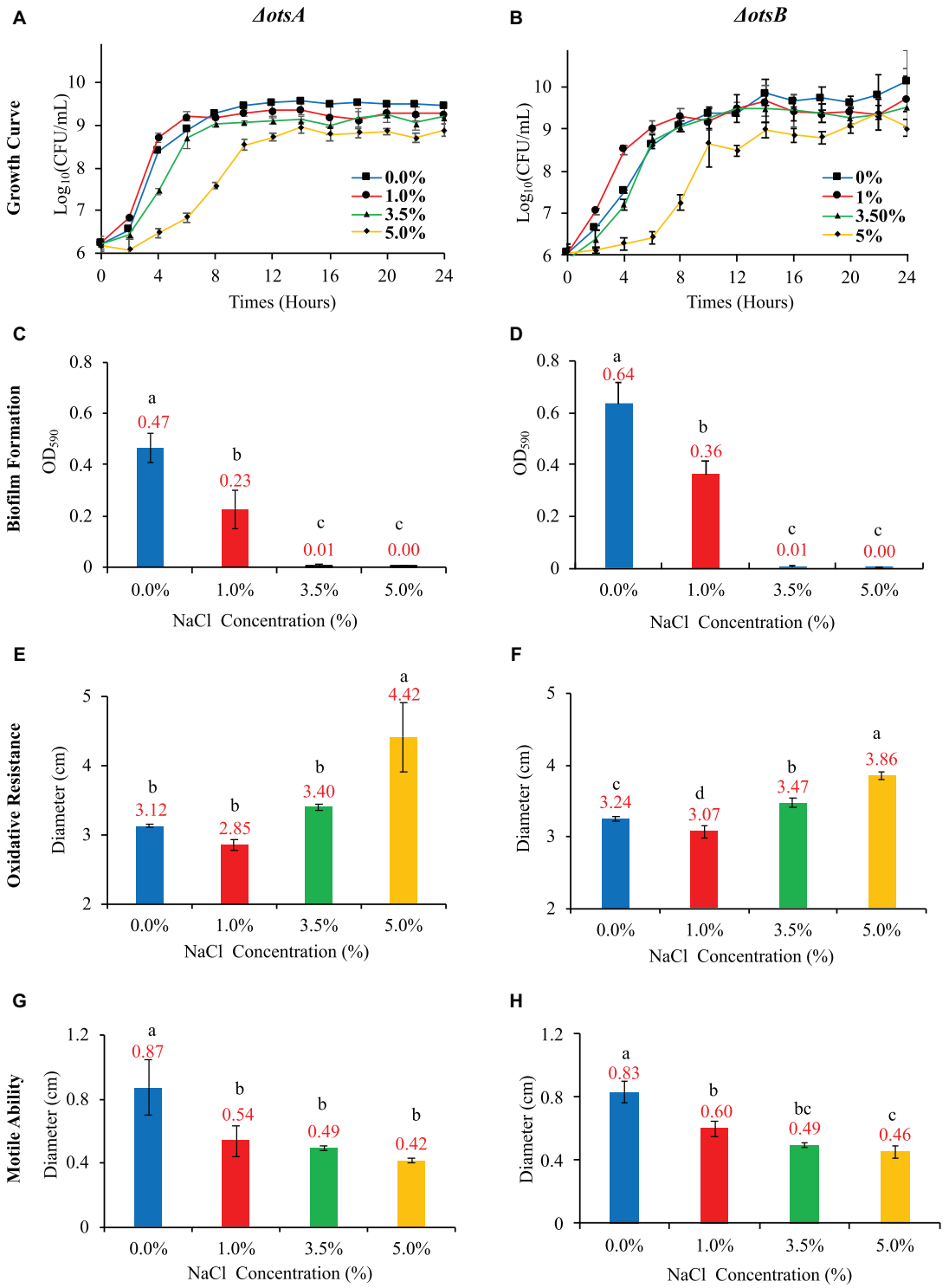

FIGURE 5 | Effects of NaCl on growth rate, biofilm formation, oxidative resistance, and motile ability in *E. coli* Δ*otsA* and Δ*otsB*. **(A,B)** Effects of different NaCl concentrations on the growth rates of *E. coli* mutants. **(C,D)** Effects of different NaCl concentrations on *E. coli* mutant biofilm formation. **(E,F)** Influences of different NaCl concentrations on the oxidative stress resistance of *E. coli* mutants. **(G,H)** Effects of different NaCl concentrations on *E. coli* mutant motile abilities. Tukey's Honestly Significant Difference (HSD) test was performed, which compared the means of every group to the means of every other group simultaneously. Means denoted by a different letter indicated significant differences among groups (*P*-value <0.05).

highest glucose uptake at 1% NaCl, which was similar as the wild-type strain. In addition, glucose consumption ability of strain Δ*otsA* was significantly higher than both wild-type and Δ*otsB* strains at the concentrations of 3.5% and 5% NaCl while wild-type and Δ*otsB* strains showed a similar changing glucose uptake pattern (**Figures 6A,B**). As for glycogen accumulation, the two trehalose-deficient mutants showed similar NaCl-concentration-dependent trends as the wild-type strain, though strain Δ*otsB* seemed to have higher amount of accumulated glycogen than strain Δ*otsA* at each NaCl concentration (**Figures 6C,D**). However, the accumulated glycogen contents in the two mutated strains were significantly reduced when compared with wild-type strain, especially at higher NaCl concentrations.

Transcriptome Analysis

Basic Info of RNA Sequencing

In order to understand bacterial physiological changes in response to salt stress at gene transcriptional level, we performed transcriptomic study on *E. coli* culture at four NaCl concentrations (0, 1, 3.5, and 5%). cDNA libraries prepared from 8 samples of *E. coli* were sequenced on the HiSeq XTen sequencers platform. A total of 297,780,562 raw reads were generated. After the sequencing adapters and low-complexity reads were removed, 288,298,514 clean reads were generated with an average of 41679552, 40501247, 27435419, and 34533039 reads in the cDNA libraries of *E. coli* cultured in 0%, 1%, 3.5%, and 5% NaCl concentrations, respectively. The clean reads which were perfectly mapped to the reference genomes without mismatch were all greater than 70% while reads with sequencing errors less than 1% in all samples are more than 98%. A detailed summary of the sequencing results is shown in **Table 1**.

Differentially Expressed Genes

In order to better elucidate the phenotype changes of the wild-type *E. coli* under salt stress, we first divided *E. coli* cultured in the four concentrations of NaCl into two groups, high salinity group (3.5% and 5% NaCl) and low salinity group (0 and 1%). We then investigated the differentially expressed genes (DEGs) of *E. coli* cultured in high and low salinity conditions by Illumina high-throughput RNA sequencing, respectively. Using genome-wide transcriptional analysis, a total of 1,117 genes (653 upregulated and 464 downregulated genes) were found to be differentially expressed by the criteria of $\log_2$(Fold_Change) > 1 and *P*-value <0.05. All the up- and down-regulated genes, together with basic information such as gene names, UniProt IDs, fold changes and P-values, could be found in **Supplementary Table 1**. The top 20 genes in terms of fold changes in the up- and down-regulated gene sets in this study were present in **Supplementary Table 2**, respectively. In particular, for the up-regulated genes, *stpA* (log2|Fold_Change| = 8.09, *P*-value = 2.23E-57) has the highest differential expression level with significant difference, which encode a DNA-binding protein. In contrast, among the down-regulated genes, *glrK* (log2|Fold_Change| = −4.50, *P*-value = 5.98E-134) shows the highest differential expression level. It encodes a sensor protein that plays important roles in sensing histidine kinase.

Network Analysis

Considering the large number of up- and down-regulated genes caused by hyper-saline pressure in the *E. coli* transcriptome, we performed two types of network analyses in order to identify the hub genes (proteins). The first analysis relies on the functional protein association network automatically constructed by STRING database, which was then imported into CytoScape for visualization. In a network, some nodes (proteins) are connected with one or more nodes while other nodes are independent; if a node is highly connected within a network., then the node is considered as a potential hub with important functions (Berlingerio et al., 2011). Based on the up- and down-regulated gene networks constructed by STRING (**Supplementary Figure 2**), we ranked the genes according to their degrees, that is, the number of connected nodes in descending order. Top 20 genes in each network were collected and annotated via UniProt database (Consortium, 2015) (**Supplementary Table 3**). According to the result, *ppsA* (log2|Fold_Change| = 1.28, *P*-value = 2.85E-8) has the highest degree ($n = 58$) among the up-regulated genes, which encodes phosphoenolpyruvate synthase (PEP synthase) in *E. coli*. Meanwhile, *metG* (log2|Fold_Change| = −1.68, *P*-value = 1.98E-29) is the most connected hub ($n = 56$) among all the down-regulated genes, which encodes methionine-tRNA ligase in *E. coli*.

However, topology of PPI network is rather complex and node degree is just one of the features. Thus, in order to make sure that our study predicts essential proteins with better performance and high precision, we used the cytoHubba plug-in in the CytoScape software by choosing the recommended algorithm Maximal Clique Centrality (MMC) (Chin et al., 2014). According to the up-regulated gene network in **Supplementary Table 4**, the top 20 hub genes are mainly responsible for cell division and cell wall formation (*ftsZ*, *ftsI*, *ftsW*, *ftsL*, *murE*, *murG*, *murF*, *mraZ*, *mraY*, *murC*, *murD*, *lpxC*), which belong to the so-called "division and cell wall (dcw) cluster" in *E. coli* (**Figure 7D**). In addition, ribosomal RNA small subunit methyltransferase H (*rsmH*), DNA translocase (*ftsK*), and molybdenum/molybdate related proteins (*moaA*, *moaE*, *moaD*, *moaC*, *modA*, *mobA*) are also recognized. As for the down-regulated gene network, the top 20 hub genes all encode ribosomal protein subunits (**Figure 7E**), which include *rpsD*, *rpsE*, *rplE*,*rplB*, *rplD*, *rplC*, *rplQ*, *rplO*, *rpsK*, *rplF*, *rpsC*, *rplW*, *rpsM*, *rpsH*, *rpmD*, *rplX*, *rplV*, *rpmA*, *rplU* and *rplR* (**Supplementary Table 4**).

GO Enrichment Analysis of DEGs

GO annotation system is an international standard for gene function classification, which includes biological process (BP), cellular component (CC), and molecular function (MF). In order to understand the biological roles of the most significantly up- or down-regulated genes, GO enrichment analysis was performed by using the Fisher's Exact Test with *P*-value <0.05 as the threshold. In specificity, the up-regulated DEGs were enriched to 24 GO terms and classified into categories of BP with 11 GO terms, CC with 3 GO terms, and MF with 10 GO terms. As shown in **Figures 7F,G**, the top three enriched terms in BP were "translation (GO:0006412)," "phosphorelay

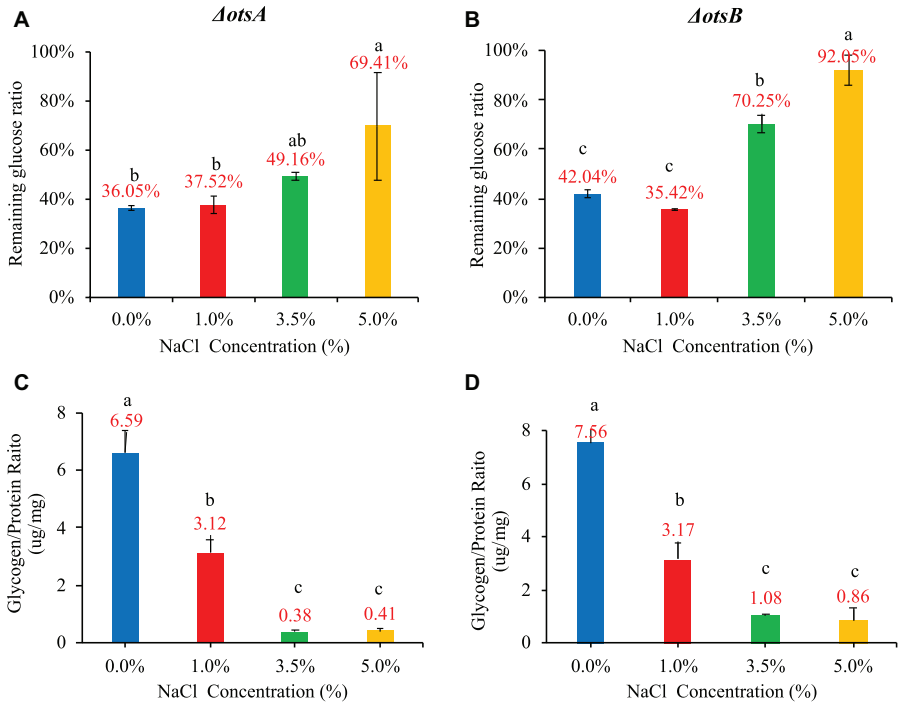

FIGURE 6 | Influences of NaCl concentrations (0, 1, 3.5, and 5%) on *E. coli* Δ*otsA* and Δ*otsB* in terms of glucose consumption rate and glycogen accumulation at 20 h. **(A,B)** Glucose consumption rates. **(C,D)** Glycogen accumulation capacity. Tukey's Honestly Significant Difference (HSD) test was performed. Means denoted by a different letter indicated significant differences among groups (*P*-value <0.05).

signal transduction system (GO:0000160)," and "proteolysis (GO:0006508)," with the number of DEGs being 29, 29, and 17, respectively. In the CC category, all three enriched terms were "cytosol (GO:0005829)," "cytosolic large ribosomal subunit (GO:0022625)," and "cell division site (GO:0032153)" with the number of DEGs being 348, 18, and 16. In the category of MF, genes were significantly enriched into the top three terms of "protein binding (GO:0005515)," "identical protein binding (GO:0042802)," and "magnesium ion binding (GO:0000287)," and the number of DEGs being 249, 109, and 69, respectively. More information about the involved genes of GO enrichment is shown in **Supplementary Table 5**.

KEGG Pathway Analysis of DEGs

KEGG pathway was used for biological pathway analysis, in which up- and down-regulated genes were mapped to the reference pathways of KEGG. For the up-regulated genes, the significantly enriched top six pathways (P-value < 0.05) were "metabolic pathways (eco01100, $n = 144$)," "biosynthesis of secondary metabolites (eco01110, $n = 76$)" and "biosynthesis of antibiotics (eco01130, $n = 46$)," "biosynthesis of amino acids (eco01230, $n = 33$)," "pyrimidine metabolism (eco00240, $n = 21$)" and "oxidative phosphorylation (eco00190, $n = 13$)" (**Figure 7H**). As for the down-regulated genes, all three significantly enriched pathways were "ribosome (eco03010, $n = 27$)," "sulfur metabolism (eco00920, $n = 10$)," and "folate biosynthesis (eco00790, $n = 7$)" (**Figure 7I**). More information about the results of KEGG enrichment is presented in **Supplementary Table 6**.

DISCUSSION

Environmentally-transmitted pathogenic bacteria frequently encounter a variety of abiotic stresses, such as temperature, oxidation, pH and osmosis, et al. (Wang et al., 2017). These stresses impose selection pressure on bacterial environmental durability and virulence with immediate effects at shorter time scale and evolutionary effects at longer time scale (Brouwer et al., 2019). So far, many studies have explored the effects of abiotic stresses on bacterial phenotypes (Boor, 2006; Mihaljevic et al., 2007; Pinto et al., 2014; Ezraty et al., 2017; Guan et al., 2017). However, few studies tried to explore stress responses by linking bacterial environmental durability and virulence. For example, it was noted that high level of salinity led to the expression of genes related with potential virulence factors, phage capsid proteins, and drug resistance proteins in *Burkholderia pseudomallei*, which indicated the potential positive linkages between bacterial stress adaptation and virulence factors (Dai et al., 2015). Dayma et al. also noticed that low salinity stress facilitated the virulence potential and biofilm formation of marine bacterium *Vibrio alginolyticus* (Dayma et al., 2016). In this study, we investigated the potential influences of salt stress on wild-type *E. coli* and two trehalose-deficient mutants in terms of growth pattern, phenotypes associated with pathogenic virulence, and energy metabolism, from which we tried to understand the short-term effects of this particular environmental stress on bacterial durability and virulence. After that, in order to understand the potential molecular mechanisms of *E. coli* adaptation to

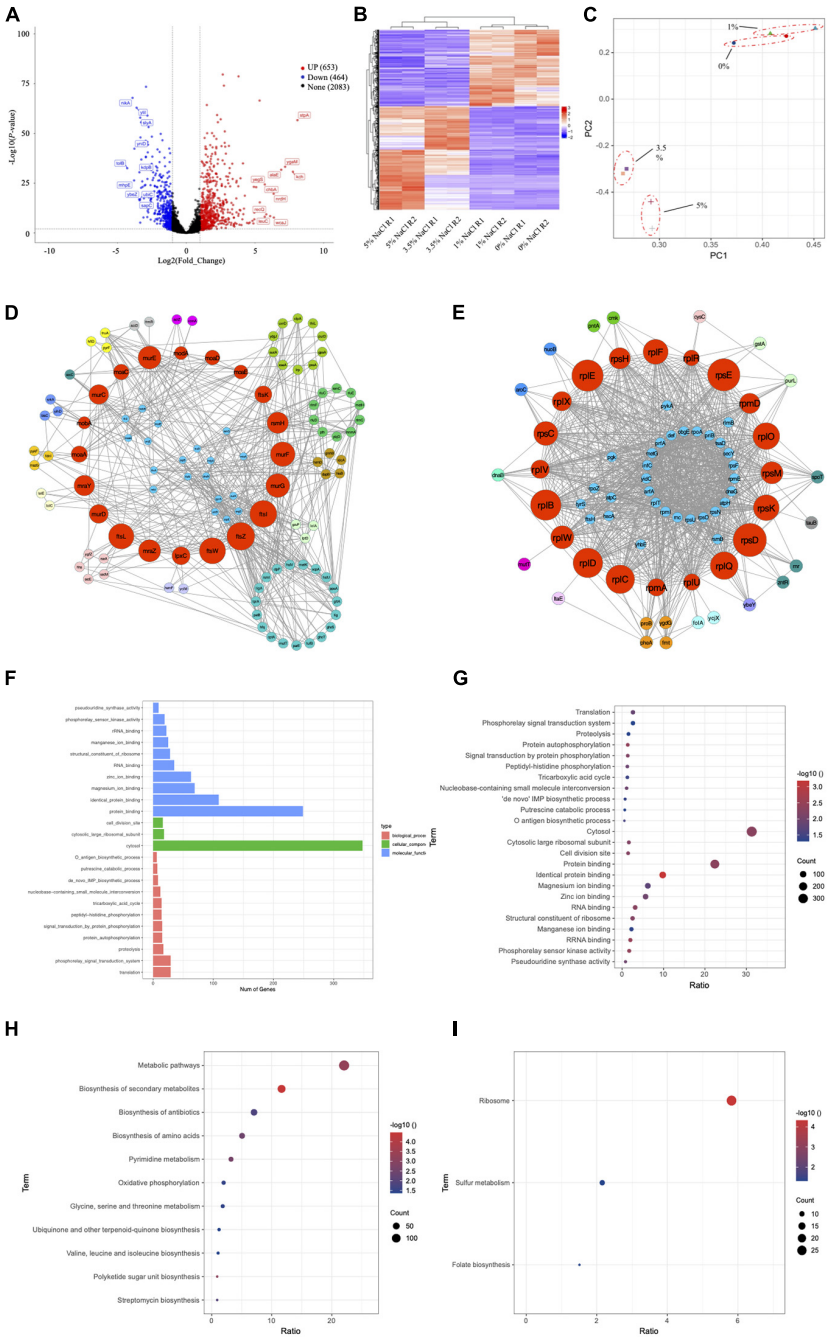

FIGURE 7 | Transcriptomic study of *E. coli* BW25113 under four NaCl concentrations of 0, 1, 3.5, and 5%. Since the phenotypes of *E. coli* under 0% and 1% NaCl are more consistent, while the phenotypes of *E. coli* under 3.5% and 5% NaCl are more similar, we combine 0% and 1% NaCl samples together as Group 1 and 3.5% and 5% NaCl samples together as Group 2 for the analysis. **(A)** Volcano plot for DEGs. **(B)** Heatmap plot for DEGs. **(C)** PCA analysis for group clusters. **(D)** Hub nodes among up-regulated genes. **(E)** Hub nodes among down-regulated genes. **(F)** Bar plot of GO term enrichment analysis. **(G)** Bubble plot of GO term enrichment analysis. **(H)** KEGG pathway enrichment for up-regulated genes. **(I)** KEGG pathway enrichment for down-regulated genes.

different concentrations of NaCl, we performed a comparative transcriptome study. DEGs and significantly enriched pathways were identified for a better understanding of the molecular mechanisms of bacterial responses to high salinity stress. Among the DEGs, potential virulence genes that were up-regulated in high salinity conditions were discussed, which could contribute to the elucidation of the potential linkages between bacterial environmental adaptation and the evolution of virulence.

Nutrient fluctuation is a commonly encountered abiotic stress for bacteria during their transmission between hosts and external

environment (Wang et al., 2020b). Its driving force will change bacteria at both physiological and genetic level. For example, Ratib et al. studied *E. coli* in long-term stationary phase (LTSP) for over 1,200 days, which revealed that two physically distinct lineages evolved from the culture (Ratib et al., 2021). Tenaillon et al. studied the evolution of *E. coli* for 2000 generations at high temperature, finding two distinct adaptive pathways (Tenaillon et al., 2012). As for short-term adaptation, Biselli et al. discovered that *E. coli* tended to decrease growth and maintenance rate in exchange of longer survival during carbon deficiency (Biselli et al., 2020). In this study, we examined the response of *E. coli* BW25113 to nutrient fluctuation, according to which, higher glucose concentration (0.8%) significantly improved the number of viable cells during 24-h culture (**Figure 1A**), which is consistent with previous studies (Wang et al., 2018, 2020b). Bacterial replication is a key factor for host colonization, resource exploitation, and between-host transmission (Rohmer et al., 2011), high rate of which could contribute to bacterial virulence. A study using the environmentally transmitted bacterial fish pathogen *Flavobacterium columnare* as a model organisms revealed that abundant nutrients in environment could act as a selective pressure for higher virulence and faster evolutionary rate (Kinnula et al., 2017). On the other hand, nutrient deficiency has been reported to diversify population structure and virulence strategies in opportunistic pathogens (Sundberg et al., 2014). Further studies showed that osmotic stress had negative influences on *E. coli* growth. Although *E. coli* requires NaCl to grow, high concentrations of NaCl significantly inhibited the growth rate of *E. coli* (**Figure 1B**). In fact, *E. coli* has the optimal concentration of NaCl at 0.5% (w/v) for growth (Abdulkarim et al., 2009) while it could gradually adapt to 11% NaCl, though it is not a halophilic bacterium (How et al., 2013).

As for biofilm, it is a bio-matrix of extracellular polymeric substances (EPSs) that consist of exopolysaccharides, fibril proteins, and DNA (Bremer and Krämer, 2019). In this study, NaCl concentrations showed a dose-dependent inhibitory effect on *E. coli* (**Figure 3A**). In particular, *E. coli* growing in the culture media supplemented with 0% and 1% NaCl had detectable amount of biofilm while 3.5% and 5% NaCl completely inhibited biofilm formation. Previously, studies had already showed that osmotic stress could induce biofilm production in a variety of microbes such as *Staphylococcus epidermidis*, *Clostridium ljungdahlii* and *Candida albicans* (Pemmaraju et al., 2016; Yang et al., 2017; Ferreira et al., 2019). Lee et al. (2014) used quantitative real-time PCR to analyze the expression levels of biofilm-related genes, which included *icaA*, *atl*, *clfA*, *fnbA*, *sarA* and *rbf*, which revealed that elevated NaCl concentration increased the formation of biofilm in *S. aureus* via the up-regulation of *icaA*. Another study by Lim et al. (2004) showed that biofilm formation in *S. aureus* was multi-phasic; although increased NaCl concentration facilitated the formation of biofilm, the process was actually controlled by different genes at different stages, while no biofilm formation could be detected when NaCl concentration was higher than 5.6%. Thus, the results are not consistent in terms of effects of NaCl concentrations on biofilm formation among bacterial species. In sum, it is worthy of further investigation into the inhibitory effects of NaCl on *E. coli* biofilm formation at molecular level via transcriptomic analysis.

In terms of oxidative stress, previous studies showed that increased NaCl concentration could enhance bacterial oxidative resistance via chloride and sodium ion channels rather than degradation of hydrogen peroxide in the bacterial pathogen *Burkhoderia pseudomallei* (Pumirat et al., 2017). In a recent study conducted by Hassan et al., it was revealed that salinity stress was able to enhance the antioxidant capacity of *Bacillus* and *Planococcus* species isolated from saline lake environment; however, the two species showed strain-specific responses in terms of oxidative resistance (Hassan et al., 2020). For *Planococcus*, high-salinity-induced resistant strains increased glutathione cycle, phenols, flavonoids, antioxidant capacity, catalase, and/or superoxide dismutase while *Bacillus* species used phenols, flavonoids, peroxidase, glutaredoxin, and/or SOD to combat oxidative stress (Hassan et al., 2020). In addition, studies also inter-linked oxidative stress with bacterial virulence, which showed that the deletion of YqhG gene encoding periplasmic protein in uropathogenic *E. coli* not only decreased bacterial virulence but also increased sensitivity to oxidative stress (Bessaiah et al., 2019). In this study, as for the effects of NaCl concentrations on *E. coli* adaptive response to oxidation, it was found that high salt condition actually reduced oxidative resistance (**Figure 3B**). In *E. coli*, some enzymes related with oxidative stress resistance were previously reported, which included but not limited to OxyR, SoxRS, and RpoS (Chiang and Schellhorn, 2012). However, how alteration of NaCl concentrations in the culture medium influenced the expression of these genes have not been clearly elucidated yet, which requires further investigation.

Our study also identified that enhanced NaCl level could significantly reduce bacterial motile abilities in a dose-dependent manner (**Figure 3C**). It was previously reported that the fish pathogen *Edwardsiella tarda* moved much faster in low salt conditions than in high salt conditions (Yu et al., 2011) while Ikeda et al. (2020) showed that the hypoosmotic stress induces flagellar biosynthesis and swimming motility in the food pathogen *Escherichia albertii*. In a genome-wide screening analysis, Inoue et al. used Keio collection, a set of single-gene knockout mutants of all the nonessential genes in *E. col*i K-12, to find all the motility-related genes in *E. coli*, according to which 78 genes were strongly related with *E. coli* motile ability (Inoue et al., 2007). However, how these genes were influenced by differential NaCl concentrations is worthy of further investigations.

Glycogen and trehalose have been widely investigated due to their roles in osmoprotection (Seibold et al., 2007; Wang et al., 2020a). In addition, the metabolic pathways of the two compounds, together with glucose and maltose, were also inter-connected (Pan et al., 2008). However, how salt stress influences the inter-conversion process of these carbohydrates is not clear. Thus, in this study, we investigated the potential correlations among glucose consumption rate, glycogen accumulation, and trehalose content under different NaCl concentrations (**Figure 4**). For glucose uptake rate, the results showed that high salinity significantly inhibited the uptake of glucose in the culture medium (**Figures 4A–C**). However, by checking the

expression levels of the five regulatory genes (EI:*pstI*, HPr:*pstH*, EIIA^{Glucose}:*crr*, EIICB^{Glucos}e:*ptsG*, and AC:*cyaA*) for glucose uptake via the phosphoenolpyruvate phosphotransferase system, no significant up- or down-regulations were identified (Steinsiek and Bettenbrock, 2012). Thus, the molecular mechanisms behind the glucose uptake inhibition should be further investigated. Meanwhile, both glycogen and trehalose contents showed dose-dependent relationship with NaCl concentrations. The difference is that increased NaCl concentration inhibits glycogen accumulation but facilitates the build-up of trehalose. It is well documented that storing around 55,000 glucose molecules as a single glycogen particle as an energy reserve has little effect on bacterial internal osmotic pressure (Wilson et al., 2010). In fact, halophilic archaea, when compared with thermophilic archaea, do not even have complete glycogen metabolism pathways based on a large number of genomic analysis (Wang et al., 2019). In contrast, many studies have reported that trehalose accumulation provides strong protection for bacteria under osmotic stress via a variety of pathways, such as glycogen degradation and trehalose synthesis, etc. (Welsh and Herbert, 1999; Pan et al., 2008; Tapia et al., 2015). However, in this study, we neither observed significantly enhanced gene levels for glycogen degradation nor noticed significantly improved levels of trehalose synthesis genes, which suggested that there might be missing links between glycogen and trehalose metabolism under high salt stress.

Previous studies have already reported the protection mechanism of trehalose in *E. coli* under low temperature stress (Kandror et al., 2002) while enhanced trehalose production improves growth of *E. coli* under osmotic stress (Purvis et al., 2005). In order to understand the roles of trehalose in *E. coli* growing in different NaCl concentrations, we explored two *E. coli* strains with trehalose synthesis deficiency, that is, *E. coli* Δ*otsA* and Δ*otsB*. Our study confirmed that growth rate of the two mutants decreased smoothly with increasing NaCl (**Figures 5A,B**). However, no significant difference was identified between mutated strains and the wild-type strain in terms of growth rate at the same NaCl concentration. Thus, there should be other metabolites facilitating the survival of *E. coli* at high salt level. The impacts of high salinity on biofilm formation (**Figures 5C,D**), oxidative resistance (**Figure 5E,F**), and motile ability (**Figures 5G,H**) of the two mutants were also similar to wild-type *E. coli* in terms of the general trend. However, trehalose deficiency seems to facilitate biofilm formation under low salinity condition (0 and 1%) for both *E. coli* Δ*otsA* and Δ*otsB* when compared with wide-type strain, which is worthy of further investigation. As for glucose consumption and glycogen accumulation, *E. coli* Δ*otsA* showed better glucose metabolism ability than *E. coli* Δ*otsB*, especially at high NaCl concentrations (3.5 and 5%) while glycogen accumulation abilities of both mutated strains were significantly inhibited with no clear explanation (**Figure 6**). Thus, how the trehalose and glycogen metabolism pathways are inter-twined under salt stress should be further explored at the levels of transcriptome, proteome, and metabolome.

Further transcriptomic analysis provided an overview of how *E. coli* BW25113 responded to the stimulation of high salinity stress (**Figure 7**). Volcano plot, heatmap, and PCA clusters confirmed that *E. coli* responded to high salinity stimulus systematically at molecular level. The up- and down-regulated gene sets provide highly valuable info for further molecular studies of *E. coli* adaptation to high salinity condition. In terms of bacterial growth rate, we first checked the expression level of *dnaA*, the gene encoding the initiator protein of chromosome replication (Sekimizu et al., 1987); however, no significant change was identified in low and high salt concentrations. As for biofilm, a group of genes were previously reported to affect biofilm formation and architecture upon over-expression (Tenorio et al., 2003), among which ten genes was found to reduce biofilm formation when over-expressed while only gene *secY* (secretion pathway component) was present in the list of DEGs in this study. However, our study showed that the expression level of *secY* was actually suppressed when biofilm formation was abolished at high NaCl concentration (**Supplementary Table 1**). Thus, the two results showed inconsistency, which requires further exploration. As for the abnormality of biofilm architecture, we noticed that 4 out of 36 genes were present in our DEGs list (Tenorio et al., 2003), among which *evgS* (FC = 5.91), *wcaJ* (FC = 6.37) and *yfcS* (FC = 1.18) were significantly over-expressed, indicating the formation of abnormal biofilm at high NaCl concentrations. Studies also revealed that three transcription factors, OxyR (hydrogen peroxide-inducible genes activator), SoxR (Redox-sensitive transcriptional activator SoxR), and SoxS (Regulatory protein SoxS), play critical roles in the regulation of oxidative stress resistance in bacteria (Seo et al., 2015). Both OxyR and SoxR were not identified as differential expressed genes in this study while SoxS was significantly up-regulated to 2.02 folds, which links SoxS with the salt-induced oxidative stress susceptibility and requires further exploration. Genome-wide screening of motility related genes via Keio collection in *E. coli* found 78 genes, the mutation of which could cause strongly repressed swarming and swimming (Inoue et al., 2007). Through searching the 78 genes in the list of DEGs in this study, we identified 23 genes that were significantly expressed due to high salt level, among which 13 genes were significantly down-regulated (**Supplementary Table 7**). It should be highlighted that the gene *tolB* encoding the Tol-Pal system protein TolB was significantly down-regulated by 4.29 folds, which ranked the second of all down-regulated genes by salt stress (**Supplementary Table 1**). In addition to its close association with *E. coli* motility (Inoue et al., 2007), it was also reported that Tol-Pal system contributed to the enteric pathogenesis of enterohemorrhagic *E. coli* (EHEC) associated with the Type III secretion system (T3SS) (Hirakawa et al., 2020). Thus, high NaCl concentration potentially had synergistic effects on inhibiting both motility and virulence in *E. coli*.

Moreover, the highest up-regulated gene *stpA* encodes a DNA-bind protein, which condenses supercoiled DNA in preference to linear DNA and protects bacterial DNA from digestion under stress conditions (Keatch, 2005). The specific molecular mechanism of the process has not been studied under osmotic stress, which could provide novel insights into bacterial survival strategies. As for other differentially expressed genes and functionally-important hub genes, similar analyses should be performed in order to understand *E. coli* responses to osmotic

stress in details. It was also worthy of mentioning that both STRING and cytoHubba analyses revealed that most of the down-regulated hub genes belonged to ribosomal proteins, which indicated that the translation initiation was generally inhibited during osmotic stress (Uesono and Toh-E, 2002). As for the GO term enrichment, it is obvious to see that most of the DEGs fall into the cellular component term cytosol (GO:0005829), which reflects that *E. coli* responds to osmotic stress mainly via physiological activities internally. As for the KEGG pathways, up-regulated genes are mainly enriched in the "Metabolic pathway" and "Biosynthesis of secondary metabolites" while down-regulated genes in "Ribosome" pathway, which indicates that *E. coli* responds to osmotic stress via metabolic change and also a variety of secondary metabolites, rather than synthesis of novel proteins. Further metabolomic and proteomic studies could provide more details in terms of the molecular mechanisms. As for potential virulence factors in *E. coli*, such as lipopolysaccharides and fimbria, the results showed inconsistent up- and down-regulation patterns in response to osmotic stress. For example, the expression levels of fimbria-relavant genes such as *ecpB*, *yfcR*, *yfcS* and *yehA* were significantly up-regulated while *ycfP*, *yadV*, *sfmH*, *yehC*, *yehD*, *yadK* and *sfmF* were significantly down-regulated. Such inconsistency might explain the diversification of virulent phenotypes of the fish pathogens during long-term starvation survival in the environment (Sundberg et al., 2014) since the evolution of virulence is a sophisticated but delicated process that requires the balance of many molecular processes.

CONCLUSION

In this study, we investigated the influences of NaCl concentrations on growth patterns, phenotypes associated with virulence, and energy metabolism in wild-type *Escherichia coli* BW25113 and its two single-gene mutants Δ*otsA* and Δ*otsB*. The results indicated that elevated NaCl concentrations in the culture medium generally inhibited bacterial growth, biofilm formation, oxidative resistance, and motile ability in both wild-type strain and trehalose-deficient mutants. As for energy metabolism, it was confirmed that trehalose was preferred under hyper-saline conditions than glycogen in *E. coli* BW25113, while glucose uptake was significantly inhibited at higher NaCl levels. As for the *E. coli* Δ*otsA* and Δ*otsB*, trehalose was completely abolished in the two mutated strains. However, when compared *E. coli* wild-type strain with its two mutants, it was shown that inactivation of trehalose synthesis pathway facilitated biofilm formation at low salinity level. Further transcriptomic analysis revealed the significantly up- and down-regulated genes that were responsible for *E. coli* responses in high salinity condition. Hub genes and enriched pathways were also identified for general understanding of *E. coli* survival strategy under osmotic pressure. Although representative phenotypes associated with pathogenic characteristics in *E. coli* were negatively impacted by hyperosmotic pressure in this study, transcriptomic analysis revealed that gene expressions related with salt response and virulence were actually inter-connected. Thus, this study does not necessarily disapprove the sit-and-wait hypothesis since evolution involves long-term interactions with and adaptations to environment. Further studies may need to examine the phenotype changes of *E. coli* after long-term adaptation to hyperosmotic conditions, investigating specific pathways and gene clusters by experimental methodologies at molecular level for a better understanding of *E. coli* adaptations to abiotic stresses.

DATA AVAILABILITY STATEMENT

The datasets presented in this study can be found in online repositories. The names of the repository/repositories and accession number(s) can be found in the article/ **Supplementary Material**.

AUTHOR CONTRIBUTIONS

BG and LW conceived and designed the experiments. LW, BG, and Q-HL contributed to project administration. FL, X-SX, Y-YY, J-JW, M-MW, and Q-HL carried out the experimental work. LW and J-WT performed the transcriptome analysis. LW, QH-L, FL, X-SX, M-MW, and J-WT wrote and revised the manuscript. LW and Q-HL provided platform and resources. All authors read and approved the final manuscript.

FUNDING

LW would like to thank the financial support of National Natural Science Foundation of China (No. 31900022), Natural Science Foundation of Jiangsu Province (No. BK20180997), Young Science and Technology Innovation Team of Xuzhou Medical University (No. TD202001), and Jiang-Su Qing-Lan Project (2020). BG thank the financial support of National Natural Science Foundation of China (Nos. 81871734 and 81471994), Key R & D Program of Jiangsu Province (No. BE2020646), Jiangsu Privincial Medical Talent (No. ZDRCA2016053), Six Talent Peaks Project of Jiangsu Province (No. WSN-135), Advanced Health Talent of Six-One Project of Jiangsu Province (No. LGY2016042), and Research Foundation for Advanced Talents of Guandong Provincial People's Hospital (No. KJ012021097).

ACKNOWLEDGMENTS

We greatly appreciate the reviewers whose comments and suggestions help improve and clarify this manuscript.

SUPPLEMENTARY MATERIAL

The Supplementary Material for this article can be found online at: https://www.frontiersin.org/articles/10.3389/fmicb.2021.705326/full#supplementary-material

REFERENCES

Abdulkarim, S., Fatimah, A. B., and Anderson, J. G. (2009). Effect of salt concentrations on the growth of heat-stressed and unstressed *escherichia coli*. *J. Food Agric. Environ.* 7:4.

Alizon, S., Hurford, A., Mideo, N., and Van Baalen, M. (2009). Virulence evolution and the trade-off hypothesis: history, current state of affairs and the future. *J. Evol. Biol.* 22, 245–259. doi: 10.1111/j.1420-9101.2008.01658.x

Antonovics, J., Wilson, A. J., Forbes, M. R., Hauffe, H. C., Kallio, E. R., Leggett, H. C., et al. (2017). The evolution of transmission mode. *Philos. Trans. R. Soc. Lond. B Biol. Sci.* 372:20160083. doi: 10.1098/rstb.2016.0083

Avonce, N., Mendoza-Vargas, A., Morett, E., and Iturriaga, G. (2006). Insights on the evolution of trehalose biosynthesis. *BMC Evol. Biol.* 6:109. doi: 10.1186/1471-2148-6-109

Berlingerio, M., Coscia, M., Giannotti, F., Monreale, A., and Pedreschi, D. (2011). The pursuit of hubbiness: Analysis of hubs in large multidimensional networks. *J. Comput. Sci.* 2, 223–237. doi: 10.1016/j.jocs.2011.05.009

Bessaiah, H., Pokharel, P., Habouria, H., Houle, S., and Dozois, C. M. (2019). yqhG Contributes to oxidative stress resistance and virulence of uropathogenic *Escherichia coli* and identification of other genes altering expression of Type 1 fimbriae. *Front. Cell. Infect. Microbiol.* 9:312. doi: 10.3389/fcimb.2019.00312

Biselli, E., Schink, S. J., and Gerland, U. (2020). Slower growth of *Escherichia coli* leads to longer survival in carbon starvation due to a decrease in the maintenance rate. *Mol. Syst. Biol.* 16:e9478. doi: 10.15252/msb.20209478

Boor, K. J. (2006). Bacterial stress responses: what doesn't kill them can make them stronger. *PLoS Biol.* 4:e23. doi: 10.1371/journal.pbio.0040023

Bremer, E., and Krämer, R. (2019). Responses of microorganisms to osmotic stress. *Ann. Rev. Microbiol.* 73, 313–334. doi: 10.1146/annurev-micro-020518-115504

Brouwer, A. F., Eisenberg, M. C., Love, N. G., and Eisenberg, J. N. S. (2019). Phenotypic variations in persistence and infectivity between and within environmentally transmitted pathogen populations impact population-level epidemic dynamics. *BMC Infect. Dis.* 19:449. doi: 10.1186/s12879-019-4054-8

Chang, A., Gu, Y., Hui, K., and Xi, C. (2019). otsA single gene knock-out in *Escherichia coli* increases cell sensitivity to outer membrane destabilization by SDS and EDTA treatment. *Undergr. J. Exper. Microbiol. Immunol.* 24:9.

Chiang, S. M., and Schellhorn, H. E. (2012). Regulators of oxidative stress response genes in *Escherichia coli* and their functional conservation in bacteria. *Arch. Biochem. Biophys.* 525, 161–169. doi: 10.1016/j.abb.2012.02.007

Chin, C.-H., Chen, S.-H., Wu, H.-H., Ho, C.-W., Ko, M.-T., and Lin, C.-Y. (2014). cytoHubba: identifying hub objects and sub-networks from complex interactome. *BMC Syst. Biol.* 8:S11. doi: 10.1186/1752-0509-8-S4-S11

Consortium, T. G. O. (2019). The gene ontology resource: 20 years and still going strong. *Nucleic Acids Res.* 47, D330–D338.

Consortium, T. U. (2015). UniProt: a hub for protein information. *Nucleic Acids Res.* 43, D204–D212.

Cressler, C. E., Mcleod, D. V., Rozins, C., Van Den Hoogen, J., and Day, T. (2015). The adaptive evolution of virulence: a review of theoretical predictions and empirical tests. *Parasitology* 143, 915–930. doi: 10.1017/s003118201500092x

Dai, S. J., Rubiano-Labrador, C., Bland, C., Miotello, G., Armengaud, J., and Baena, S. (2015). Salt stress induced changes in the exoproteome of the Halotolerant Bacterium tistlia consotensis deciphered by proteogenomics. *Plos One* 10:e0135065. doi: 10.1371/journal.pone.0135065

Dayma, P., Raval, I. H., Joshi, N., Patel, N. P., Haldar, S., and Mody, K. H. (2016). Influence of low salinity stress on virulence and biofilm formation potential inVibrio alginolyticus, isolated from the Gulf of Khambhat, Gujarat India. *Aquatic Living Resour.* 28, 99–109. doi: 10.1051/alr/2016004

De Smet, K. A. L., Weston, A., Brown, I. N., Young, D. B., and Robertson, B. D. (2000). Three pathways for trehalose biosynthesis in mycobacteria. *Microbiology* 146, 199–208. doi: 10.1099/00221287-146-1-199

Dinnbier, U., Limpinsel, E., Schmid, R., and Bakker, E. P. (1988). Transient accumulation of potassium glutamate and its replacement by trehalose during adaptation of growing cells of *Escherichia coli* K-12 to elevated sodium chloride concentrations. *Arch. Microbiol.* 150, 348–357. doi: 10.1007/bf00408306

Elbein, A. D. (2003). New insights on trehalose: a multifunctional molecule. *Glycobiology* 13, 17–27.

Ewald, P. W. (1983). Host-parasite relations, vectors, and the evolution of disease severity. *Ann. Rev. Ecol. Syst.* 14, 465–485. doi: 10.1146/annurev.es.14.110183.002341

Ezraty, B., Gennaris, A., Barras, F., and Collet, J.-F. (2017). Oxidative stress, protein damage and repair in bacteria. *Nat. Rev. Microbiol.* 15, 385–396. doi: 10.1038/nrmicro.2017.26

Ferreira, R. B. R., Ferreira, M. C. S., Glatthardt, T., Silvério, M. P., Chamon, R. C., Salgueiro, V. C., et al. (2019). Osmotic stress induces biofilm production by Staphylococcus epidermidis isolates from neonates. *Diagn. Microbiol. Infect. Dis.* 94, 337–341. doi: 10.1016/j.diagmicrobio.2019.02.009

Fuhrer, T., Fischer, E., and Sauer, U. (2005). Experimental identification and quantification of glucose metabolism in seven bacterial species. *J. Bacteriol.* 187, 1581–1590. doi: 10.1128/jb.187.5.1581-1590.2005

Gebhardt, M. J., Gallagher, L. A., Jacobson, R. K., Usacheva, E. A., Peterson, L. R., Zurawski, D. V., et al. (2015). Joint transcriptional control of virulence and resistance to antibiotic and environmental stress in *Acinetobacter baumannii*. *mBio* 6:e01660–15. doi: 10.1128/mBio.01660-15

Guan, N., Li, J., Shin, H.-D., Du, G., Chen, J., and Liu, L. (2017). Microbial response to environmental stresses: from fundamental mechanisms to practical applications. *Appl. Microbiol. Biotechnol.* 101, 3991–4008. doi: 10.1007/s00253-017-8264-y

Hassan, A. H. A., Alkhalifah, D. H. M., Al Yousef, S. A., Beemster, G. T. S., Mousa, A. S. M., Hozzein, W. N., et al. (2020). Salinity stress enhances the antioxidant capacity of *Bacillus and Planococcus* species isolated from Saline Lake environment. *Front. Microbiol.* 11:561816. doi: 10.3389/fmicb.2020.561816

Hedges, A. J. (2002). Estimating the precision of serial dilutions and viable bacterial counts. *Int. J. Food Microbiol.* 76, 207–214. doi: 10.1016/s0168-1605(02)00022-3

Hirakawa, H., Suzue, K., Takita, A., Awazu, C., Kurushima, J., and Tomita, H. (2020). Roles of the Tol-Pal system in the Type III secretion system and flagella-mediated virulence in enterohemorrhagic *Escherichia coli*. *Sci. Rep.* 10:15173. doi: 10.1038/s41598-020-72412-w

How, J. A., Lim, J. Z. R., Goh, D. J. W., Ng, W. C., Oon, J. S. H., Lee, K. C., et al. (2013). Adaptation of *Escherichia coli* ATCC 8739 to 11% NaCl. *Dataset Papers Biol.* 2013, 1–7. doi: 10.7167/2013/219095

Hubloher, J. J., Zeidler, S., Lamosa, P., Santos, H., Averhoff, B., and Müller, V. (2020). Trehalose-6-phosphate-mediated phenotypic change in *Acinetobacter baumannii*. *Environ. Microbiol.* 22, 5156–5166. doi: 10.1111/1462-2920.15148

Ikeda, T., Shinagawa, T., Ito, T., Ohno, Y., Kubo, A., Nishi, J., et al. (2020). Hypoosmotic stress induces flagellar biosynthesis and swimming motility in *Escherichia* albertii. *Commun. Biol.* 3:87. doi: 10.1038/s42003-020-0816-5

Inoue, T., Shingaki, R., Hirose, S., Waki, K., Mori, H., and Fukui, K. (2007). Genome-wide screening of genes required for swarming motility in *Escherichia coli* K-12. *J. Bacteriol.* 189, 950–957. doi: 10.1128/jb.01294-06

Josenhans, C., and Suerbaum, S. (2002). The role of motility as a virulence factor in bacteria. *Int. J. Med. Microbiol.* 291, 605–614. doi: 10.1078/1438-4221-00173

Kandror, O., Deleon, A., and Goldberg, A. L. (2002). Trehalose synthesis is induced upon exposure of *Escherichia coli* to cold and is essential for viability at low temperatures. *Proc. Natl. Acad. Sci.* 99, 9727–9732. doi: 10.1073/pnas.142314099

Kanehisa, M., Furumichi, M., Tanabe, M., Sato, Y., and Morishima, K. (2017). KEGG: new perspectives on genomes, pathways, diseases and drugs. *Nucleic Acids Res.* 45, D353–D361.

Kao, C. Y., Lin, W. H., Tseng, C. C., Wu, A. B., Wang, M. C., and Wu, J. J. (2014). The complex interplay among bacterial motility and virulence factors in different *Escherichia coli* infections. *Eur. J. Clin. Microbiol. Infect. Dis.* 33, 2157–2162. doi: 10.1007/s10096-014-2171-2

Kawarai, T., Furukawa, S., Narisawa, N., Hagiwara, C., Ogihara, H., and Yamasaki, M. (2009). Biofilm formation by *Escherichia coli* in hypertonic sucrose media. *J. Biosci. Bioengin.* 107, 630–635. doi: 10.1016/j.jbiosc.2009.01.018

Keatch, S. A. (2005). StpA protein from *Escherichia coli* condenses supercoiled DNA in preference to linear DNA and protects it from digestion by DNase I and EcoKI. *Nucleic Acids Res.* 33, 6540–6546. doi: 10.1093/nar/gki951

Kinnula, H., Mappes, J., Valkonen, J. K., Pulkkinen, K., and Sundberg, L.-R. (2017). Higher resource level promotes virulence in an environmentally transmitted bacterial fish pathogen. *Evolut. Appl.* 10, 462–470. doi: 10.1111/eva.12466

Lee, S., Choi, K.-H., and Yoon, Y. (2014). Effect of NaCl on biofilm formation of the isolate from *Staphylococcus aureus* outbreak linked to Ham. *Korean J. Food Sci. Anim. Resour.* 34, 257–261. doi: 10.5851/kosfa.2014.34.2.257

Lim, Y., Jana, M., Luong, T. T., and Lee, C. Y. (2004). Control of glucose- and NaCl-induced biofilm formation by rbf in *Staphylococcus aureus*. *J. Bacteriol.* 186, 722–729. doi: 10.1128/jb.186.3.722-729.2004

Liu, Q., Tang, J. W., Wen, P. B., Wang, M. M., Zhang, X., and Wang, L. (2021). From prokaryotes to eukaryotes: insights into the molecular structure of glycogen particles. *Front. Mol. Biosci.* 8:673315. doi: 10.3389/fmolb.2021.67331

Macintyre, A. M., Barth, J. X., Pellitteri Hahn, M. C., Scarlett, C. O., Genin, S., and Allen, C. (2020). Trehalose synthesis contributes to osmotic stress tolerance and virulence of the bacterial wilt PathogenRalstonia solanacearum. *Mol. Plant-Microbe Interac.* 33, 462–473. doi: 10.1094/mpmi-08-19-0218-r

Mihaljevic, R. R., Sikic, M., Klancnik, A., Brumini, G., Mozina, S. S., and Abram, M. (2007). Environmental stress factors affecting survival and virulence of *Campylobacter jejuni*. *Microbial. Pathog.* 43, 120–125. doi: 10.1016/j.micpath.2007.03.004

Mitchell, J. G., and Kogure, K. (2006). Bacterial motility: links to the environment and a driving force for microbial physics. *FEMS Microbiol. Ecol.* 55, 3–16. doi: 10.1111/j.1574-6941.2005.00003.x

Moruno Algara, M., Kuczyńska-Wiśnik, D., Dębski, J., Stojowska-Swędrzyńska, K., Sominka, H., Bukrejewska, M., et al. (2019). Trehalose protects *Escherichia coli* against carbon stress manifested by protein acetylation and aggregation. *Mol. Microbiol.* 112, 866–880. doi: 10.1111/mmi.14322

Murphy, H. N., Stewart, G. R., Mischenko, V. V., Apt, A. S., Harris, R., Mcalister, M. S. B., et al. (2005). The OtsAB pathway is essential for trehalose biosynthesis in *Mycobacterium tuberculosis*. *J. Biol. Chem.* 280, 14524–14529. doi: 10.1074/jbc.m414232200

Pan, Y. T., Carroll, J. D., Asano, N., Pastuszak, I., Edavana, V. K., and Elbein, A. D. (2008). Trehalose synthase converts glycogen to trehalose. *FEBS J.* 275, 3408–3420. doi: 10.1111/j.1742-4658.2008.06491.x

Pang, H., Xin, X., He, J., Cui, B., Guo, D., Liu, S., et al. (2020). Effect of NaCl concentration on microbiological properties in NaCl assistant anaerobic fermentation: hydrolase activity and microbial community distribution. *Front. Microbiol.* 11:589222. doi: 10.3389/fmicb.2020.589222

Passalacqua, K. D., Charbonneau, M.-E., and O'riordan, M. X. D. (2016). Bacterial metabolism shapes the host–pathogen interface. *Microbiol. Spectr.* 4:10.1128. doi: 10.1128/microbiolspec.VMBF-0027-2015

Pemmaraju, S. C., Padmapriya, K., Pruthi, P. A., Prasad, R., and Pruthi, V. (2016). Impact of oxidative and osmotic stresses on *Candida albicans* biofilm formation. *Biofouling* 32, 897–909. doi: 10.1080/08927014.2016.1212021

Pinto, A., De Sá, P. H. C. G., Ramos, R. T. J., Barbosa, S., Barbosa, H. P. M., Ribeiro, A., et al. (2014). Differential transcriptional profile of *Corynebacterium* pseudotuberculosis in response to abiotic stresses. *BMC Genom.* 15:14. doi: 10.1186/1471-2164-15-14

Pumirat, P., Vanaporn, M., Boonyuen, U., Indrawattana, N., Rungruengkitkun, A., and Chantratita, N. (2017). Effects of sodium chloride on heat resistance, oxidative susceptibility, motility, biofilm and plaque formation of *Burkholderia pseudomallei*. *MicrobiologyOpen* 6:e00493. doi: 10.1002/mbo3.493

Purvis, J. E., Yomano, L. P., and Ingram, L. O. (2005). Enhanced trehalose production improves growth of *Escherichia coli* under osmotic stress. *Appl. Environ. Microbiol.* 71, 3761–3769. doi: 10.1128/aem.71.7.3761-3769.2005

Puttikamonkul, S., Willger, S. D., Grahl, N., Perfect, J. R., Movahed, N., Bothner, B., et al. (2010). Trehalose 6-phosphate phosphatase is required for cell wall integrity and fungal virulence but not trehalose biosynthesis in the human fungal pathogen *Aspergillus fumigatus*. *Mol. Microbiol.* 77, 891–911. doi: 10.1111/j.1365-2958.2010.07254.x

Rath, K. M., Maheshwari, A., Bengtson, P., Rousk, J., and Cullen, D. (2016). Comparative toxicities of salts on microbial processes in soil. *Appl. Environ. Microbiol.* 82, 2012–2020. doi: 10.1128/aem.04052-15

Ratib, N. R., Seidl, F., Ehrenreich, I. M., Finkel, S. E., and Ballard, J. D. (2021). Evolution in long-term stationary-phase batch culture: emergence of divergent *Escherichia coli* lineages over 1,200 Days. *mBio* 12:e03337–20. doi: 10.1128/mBio.03337-20

Rohmer, L., Hocquet, D., and Miller, S. I. (2011). Are pathogenic bacteria just looking for food? Metabolism and microbial pathogenesis. *Trends Microbiol.* 19, 341–348. doi: 10.1016/j.tim.2011.04.003

Seibold, G., Dempf, S., Schreiner, J., and Eikmanns, B. J. (2007). Glycogen formation in *Corynebacterium* glutamicum and role of ADP-glucose pyrophosphorylase. *Microbiology* 153, 1275–1285. doi: 10.1099/mic.0.2006/003368-0

Sekimizu, K., Bramhill, D., and Kornberg, A. (1987). ATP activates dnaA protein in initiating replication of plasmids bearing the origin of the E. coli chromosome. *Cell* 50, 259–265. doi: 10.1016/0092-8674(87)90221-2

Seo, S. W., Kim, D., Szubin, R., and Palsson, B. O. (2015). Genome-wide reconstruction of OxyR and SoxRS transcriptional regulatory networks under oxidative stress in *Escherichia coli* K-12 MG1655. *Cell. Rep.* 12, 1289–1299. doi: 10.1016/j.celrep.2015.07.043

Shannon, P. (2003). Cytoscape: A software environment for integrated models of biomolecular interaction networks. *Genome Res.* 13, 2498–2504. doi: 10.1101/gr.1239303

Sharma, G., Sharma, S., Sharma, P., Chandola, D., Dang, S., Gupta, S., et al. (2016). *Escherichia coli* biofilm: development and therapeutic strategies. *J. Appl. Microbiol.* 121, 309–319. doi: 10.1111/jam.13078

Sleator, R. D., and Hill, C. (2002). Bacterial osmoadaptation: the role of osmolytes in bacterial stress and virulence. *FEMS Microbiol. Rev.* 26, 49–71. doi: 10.1111/j.1574-6976.2002.tb00598.x

Steinsiek, S., and Bettenbrock, K. (2012). Glucose transport in *Escherichia coli* mutant strains with defects in sugar Transport Systems. *J. Bacteriol.* 194, 5897–5908. doi: 10.1128/jb.01502-12

Strom, A. R., and Kaasen, I. (1993). Trehalose metabolism in *Escherichia coli*: stress protection and stress regulation of gene expression. *Mol. Microbiol.* 8, 205–210. doi: 10.1111/j.1365-2958.1993.tb01564.x

Sundberg, L.-R., Kunttu, H. M. T., and Valtonen, E. (2014). Starvation can diversify the population structure and virulence strategies of an environmentally transmitting fish pathogen. *BMC Microbiol.* 14:67. doi: 10.1186/1471-2180-14-67

Szklarczyk, D., Gable, A. L., Nastou, K. C., Lyon, D., Kirsch, R., Pyysalo, S., et al. (2021). The STRING database in 2021: customizable protein–protein networks, and functional characterization of user-uploaded gene/measurement sets. *Nucleic Acids Res.* 49, D605–D612.

Tapia, H., Young, L., Fox, D., Bertozzi, C. R., and Koshland, D. (2015). Increasing intracellular trehalose is sufficient to confer desiccation tolerance to *Saccharomyces cerevisiae*. *Proc. Natl. Acad. Sci.* 112, 6122–6127. doi: 10.1073/pnas.1506415112

Tenaillon, O., Rodriguez-Verdugo, A., Gaut, R. L., Mcdonald, P., Bennett, A. F., Long, A. D., et al. (2012). The molecular diversity of adaptive convergence. *Science* 335, 457–461. doi: 10.1126/science.1212986

Tenorio, E., Saeki, T., Fujita, K., Kitakawa, M., Baba, T., Mori, H., et al. (2003). Systematic characterization of*Escherichia coli*genes/ORFs affecting biofilm formation. *FEMS Microbiol. Lett.* 225, 107–114.

Uesono, Y., and Toh-E, A. (2002). Transient inhibition of translation initiation by osmotic stress. *J. Biol. Chem.* 277, 13848–13855. doi: 10.1074/jbc.m108848200

Vanaporn, M., and Titball, R. W. (2020). Trehalose and bacterial virulence. *Virulence* 11, 1192–1202. doi: 10.1080/21505594.2020.1809326

Walther, B. A., and Ewald, P. W. (2004). Pathogen survival in the external environment and the evolution of virulence. *Biol. Rev.* 79, 849–869. doi: 10.1017/s1464793104006475

Wang, L., Liu, Q., Du, Y., Tang, D., and Wise, M. (2018). Optimized M9 minimal salts medium for enhanced growth rate and glycogen accumulation of *Escherichia coli* DH5 □ □. *Microbiol. Biotechnol. Lett.* 46, 194–200. doi: 10.4014/mbl.1804.04010

Wang, L., Liu, Q., Wu, X., Huang, Y., Wise, M. J., Liu, Z., et al. (2019). Bioinformatics analysis of metabolism pathways of archaeal energy reserves. *Sci. Rep.* 9:1034. doi: 10.1038/s41598-018-37768-0

Wang, L., Liu, Z., Dai, S., Yan, J., and Wise, M. J. (2017). The Sit-and-Wait hypothesis in bacterial pathogens: a theoretical study of durability and virulence. *Front. Microbiol.* 8:2167. doi: 10.3389/fmicb.2017.02167

Wang, L., Regina, A., Butardo, V. M., Kosar-Hashemi, B., Larroque, O., Kahler, C. M., et al. (2015). Influence of in situ progressive N-terminal is still controversial truncation of glycogen branching enzyme in *Escherichia coli* DH5α on glycogen structure, accumulation, and bacterial viability. *BMC Microbiol.* 15:96. doi: 10.1186/s12866-015-0421-9

Wang, L., Wang, M., Wise, M. J., Liu, Q., Yang, T., Zhu, Z., et al. (2020a). Recent progress in the structure of glycogen serving as a durable energy reserve in bacteria. *World J. Microbiol. Biotechnol.* 36:14. doi: 10.1007/s11274-019-2795-6

Wang, M., Liu, Q., Kang, X., Zhu, Z., Yang, H., Xi, X., et al. (2020b). Glycogen metabolism impairment via single gene mutation in the glgBXCAP operon

alters the survival rate of *Escherichia coli* under various environmental stresses. *Front. Microbiol.* 11:588099. doi: 10.3389/fmicb.2020.588099

Welsh, D. T., and Herbert, R. A. (1999). Osmotically induced intracellular trehalose, but not glycine betaine accumulation promotes desiccation tolerance in*Escherichia coli*. *FEMS Microbiol. Lett.* 174, 57–63. doi: 10.1111/j.1574-6968.1999.tb13549.x

Wilson, W. A., Roach, P. J., Montero, M., Baroja-Fernández, E., Muñoz, F. J., Eydallin, G., et al. (2010). Regulation of glycogen metabolism in yeast and bacteria. *FEMS Microbiol. Rev.* 34, 952–985. doi: 10.1111/j.1574-6976.2010.00220.x

Yamamotoya, T., Dose, H., Tian, Z., Fauré, A., Toya, Y., Honma, M., et al. (2012). Glycogen is the primary source of glucose during the lag phase of E. coli proliferation. *Biochim. Biophys. Acta* 1824, 1442–1448. doi: 10.1016/j.bbapap.2012.06.010

Yang, S., Philips, J., Rabaey, K., Lovley, D. R., and Vargas, M. (2017). Biofilm formation by *Clostridium ljungdahlii* is induced by sodium chloride stress: experimental evaluation and transcriptome analysis. *Plos One* 12:e0170406. doi: 10.1371/journal.pone.0170406

Yu, J.-E., Park, J.-M., and Kang, H.-Y. (2011). Effects of salt concentration on motility and expression of flagellin genes in the fish pathogen *Edwardsiella tarda*. *J. Life Sci.* 21, 1487–1493. doi: 10.5352/jls.2011.21.10.1487

Conflict of Interest: The authors declare that the research was conducted in the absence of any commercial or financial relationships that could be construed as a potential conflict of interest.

Publisher's Note: All claims expressed in this article are solely those of the authors and do not necessarily represent those of their affiliated organizations, or those of the publisher, the editors and the reviewers. Any product that may be evaluated in this article, or claim that may be made by its manufacturer, is not guaranteed or endorsed by the publisher.

frontiers in Microbiology

ORIGINAL RESEARCH
published: 17 September 2021
doi: 10.3389/fmicb.2021.726935

Growth and Characteristics of Two Different *Epichloë sinensis* Strains Under Different Cultures

*Yang Luo and Pei Tian**

State Key Laboratory of Grassland Agro-ecosystems, Key Laboratory of Grassland Livestock Industry Innovation, Ministry of Agriculture and Rural Affairs, College of Pastoral Agriculture Science and Technology, Lanzhou University, Lanzhou, China

In the present study, two *Epichloë sinensis* endophyte strains isolated from different *Festuca sinensis* ecotypes were inoculated on potato dextrose agar (PDA) and potato dextrose broth (PDB) media with or without (control) exogenous additives. After 4 weeks of growth, the growth (colony diameter, hyphal diameter, and mycelial biomass) and other characteristics (pH and antioxidant capacity of culture filtrate, mycelial ion contents, and hormone contents) were measured. The results showed that the culture conditions had significant effects ($p < 0.05$) on the hyphal diameter, mycelial biomass, and hormone content of the two strains. The mycelial biomass of the two strains in PDB was significantly higher ($p < 0.05$) than that on PDA. Except for strain 1 with indole-3-acetic acid (IAA) treatment and strain 84F with control and VB_1 treatments, the hyphal diameter of the two strains in PDB under the other treatments was significantly higher ($p < 0.05$) than that on PDA. In most cases, the IAA, cytokinins (CTK), abscisic acid (ABA), and gibberlic acid (GA) contents in the mycelia on PDA of the two strains were significantly higher ($p < 0.05$) than those in PDB. The two *E. sinensis* strains exhibited significantly different performances ($p < 0.05$) under the five treatments. The indices, including colony diameter, mycelial biomass, scavenging ability of superoxide anion radicals and hydroxyl radicals, pH of culture filtrate, ion contents, hyphal diameter, and IAA, CTK, GA, and ABA contents were significantly different ($p < 0.05$) between the two strains, although the performance was inconsistent. Exogenous additives had significant effects ($p < 0.05$) on the performance of the two *E. sinensis* strains. Indole-3-acetic acid and VB_1 treatments significantly promoted ($p < 0.05$) the growth of the two strains on both PDA and PDB. Indole-3-acetic acid treatment also significantly increased the hyphal diameters of the two strains in PDB ($p < 0.05$). Indole-3-acetic acid and VB_1 treatments significantly reduced ($p < 0.05$) the antioxidant ability of these two strains in PDB. NaCl and $ZnCl_2$ treatments had significant inhibitory effects ($p < 0.05$) on fungal growth and promotion effects on the antioxidant ability of the two strains. The treatments also had significant effects ($p < 0.05$) on hyphal diameters and ion and hormone contents, although the effects varied with different indices.

Keywords: *Epichloë sinensis*, potato dextrose agar, potato dextrose broth, exogenous additives, growth, characteristics

OPEN ACCESS

Edited by:
Jose M. Mulet, Universitat Politècnica de València, Spain

Reviewed by:
Anwar Hussain, Abdul Wali Khan University Mardan, Pakistan
Dewa Ngurah Suprapta, Udayana University, Indonesia

***Correspondence:**
Pei Tian
tianp@lzu.edu.cn

Specialty section:
This article was submitted to Microbial Physiology and Metabolism, a section of the journal Frontiers in Microbiology

Received: *17 June 2021*
Accepted: *18 August 2021*
Published: *17 September 2021*

Citation:
Luo Y and Tian P (2021) Growth and Characteristics of Two Different Epichloë sinensis Strains Under Different Cultures. Front. Microbiol. 12:726935. doi: 10.3389/fmicb.2021.726935

INTRODUCTION

The grass endophytes live asymptomatically and internally within host plant tissues without causing visible damage to the plant (Siegel et al., 1987). Fungal hyphae grow in intercellular spaces in mostly leaf sheaths, culms, and seeds, while strains of *Epichloë* can be transmitted either vertically *via* seeds or horizontally *via* spores in stromata (Faeth et al., 2010). Fungal endophytes exhibit a variety of interactions with the host plant (Hume et al., 2016). The grass provides fungal endophytes with nutrients and space for growth, and in turn, fungal endophytes confer many benefits to grass hosts, including persistence/fitness, resistance/deterrence to insects, drought and salinity tolerance, and resistance to nematodes and fungal pathogens (Gundel et al., 2013; Vázquez-de-Aldana et al., 2013; Xia et al., 2018; Song et al., 2015a). This is attributed to the production of abundant and diverse secondary metabolites, as observed in a host and pure culture (Song et al., 2015b). Also, a diverse array of secondary metabolites isolated from *Epichloë* endophytes and symbionts is a rich source for developing new pesticides and drugs. However, some toxic alkaloids produced through the symbiosis also impair animal performance, which has significant economic consequences for the pastoral agricultural sectors (Schardl et al., 2012, 2013).

At present, studies on the biology and physiology of endophytes *in vitro* are mainly focused on the effects of media, conditions including temperature and pH, and carbon and nitrogen sources. For example, several studies suggested that the optimal growth conditions for *E. coenophiala* are 25°C and pH 9, whereas the optimal growth conditions of *E. gansuensis* are 25°C and pH 7 (Li et al., 2008). Latch et al. (1984) found that 25°C is the optimal temperature for the growth of *Epichloë festucae* var. *lolii*, *Epichloë coenophialum*, and *Epichloë typhina*. The optimal growth conditions for *E. festucae* are 25°C and pH 7–9 or 5 (Li et al., 2008; Ma, 2009), and the optimal growth conditions for *Epichloë bromicola* are 25°C and pH 5.09–6.10 or 9 (Zhang, 2013; Chen et al., 2016). Several studies have selected optimal nutrition resources for endophyte growth. Mannitol and tryptone are optimal carbon and nitrogen sources for *E. coenophiala* (Kulkarni and Nielsen, 1986; Pope and Hill, 1991), and maltose and tryptone are optimal carbon and nitrogen sources for *E. bromicola* (Chen et al., 2016). Lactose and casein are the optimal carbon and nitrogen sources for *E. festucae* (Li et al., 2008). Ferguson et al. found that the best nitrogen sources for the mycelial growth of *E. coenophiala* are proline and potassium nitrate (Ferguson et al., 1993). The growth of *E. festucae* is significantly improved by cellulase, tryptone, casein peptone, proline, and peptone (Ma, 2009).

Festuca sinensis is native to the cool semi-arid regions of China and is an important perennial cool-season bunchgrass involved in grassland establishment and ecological management programs in the Qinghai-Tibetan plateau in China (Tian et al., 2015; Zhou et al., 2015a; Wang et al., 2016). It is frequently symbiotic with *Epichloë* endophytes (Nan, 1996a). This endophyte has been isolated and identified through morphology with colony, texture, conidia, conidiophores, and its phylogeny studied through housekeeping genes. These evaluations confirmed that the endophyte that establishes symbiosis with *F. sinensis* is the new species, *Epichloë sinensis* (Tian et al., 2020). This species needs further and comprehensive studies to fully understand its characteristics and provides more reference for utilization. Previous studies have indicated that *E. sinensis* isolated from different host ecotypes performed morphological diversity which had different growth rates (Wang, 2019). Jin et al. (2009) showed that *E. sinensis* grows at 10–30°C and stop growing at 5°C and 35°C. The optimal growth conditions for *E. sinensis* are 25°C and pH 7–9, and the optimal carbon and nitrogen sources are mannitol and yeast extract. The ability to use carbon and nitrogen nutrients is different for different endophyte strains. Wang (2019) found that plant growth regulators [PGRs; VB_1, VB_5, VB_9, Indole-3-acetic acid (IAA), gibberellin (GA_3), and KT-30] promote *E. sinensis* strain growth, whereas ions (Na^+, Cd^{2+}, Cr^{6+}, and Zn^{2+}) inhibit their growth although the effects depend on additives and concentrations. These studies have mainly focused on the growth of *E. sinensis* under different temperatures, pH, carbon, nitrogen sources, vitamins, and heavy metals. However, little is known about the biological and physiological characteristics of *E. sinensis* in different media.

Production of fungal mycelium with high levels of secondary metabolites is critical for endophyte utilization. Compared with PDB culture for mycelium production, potato dextrose agar (PDA) culture is usually used to production (You et al., 2012), but PDA medium is not well for short-term culture to produce fungal mycelium. In addition, biomass and the biological activity of the mycelium of *Epichloë* endophytes have never been compared as between PDA and PDB culture.

In the present study, we selected two *E. sinensis* endophyte strains (strain ID 1, 84F) which were isolated from different *F. sinensis* ecotypes distributed in Gansu Province (1) and Qinghai Province (84F), China. The biological and physiological characteristics of these two strains on PDA and in PDB with different additives were measured. The objectives of this study were to: (1) compare the biological and physiological characteristics of these two *E. sinensis* strains grown in various media with exogenous additives; (2) clarify the response mechanisms of these two strains to different additives; and (3) explore the optimal enrichment conditions for *E. sinensis* mycelia.

MATERIALS AND METHODS

Biological Materials

Epichloë sinensis strain 1 isolated from wild *F. sinensis* seeds in Xiahe County, Gansu Province, and strain 84F isolated from wild *F. sinensis* seeds in Ping'an County, Qinghai Province, were provided by our research groups (Kuang, 2016) and preserved in the Mycological Herbarium of Lanzhou University, China. The hyphae were transferred onto fresh PDA plates ($D = 90$ mm) and incubated in the dark at 25 ± 1°C for 4 weeks before the experiment.

Experimental Design

Exogenous additives, including Vitamin B_1 (VB_1), IAA, sodium chloride (NaCl), and zinc chloride ($ZnCl_2$), were dissolved in

sterile water to make 30 g/L, 20 g/L, 23376 g/L, and 750 g/L concentrated solutions; 10 μl or 100 μl of each concentrated solution was added to 1 L sterilized PDA or 100 ml sterilized PDB, respectively, to reach final concentrations of 30 mg/L, 20 mg/L, 0.4 mol/L, and 750 mg/L, respectively. potato dextrose agar and PDB without additives were prepared as controls. A 6-mm-diameter inoculum plug of each fungus was inoculated on cellophane-overlaid PDA ($D = 90$ mm) containing different additives and incubated in the dark at 25 ± 1°C for 4 weeks. Each fungus had four replicates per treatment. Three 6-mm-diameter inoculum plugs of each fungus were also inoculated into PDB (100 ml in 250 ml flask). Each fungus had four replicates per treatment. All flasks were incubated at 25 ± 1°C with 145 rpm for 4 weeks.

Experimental Evaluations

Colony Diameter on PDA

The colony diameter on PDA was measured weekly during the first 4 weeks of growth.

Hypha Diameter

Pieces of adhesive tape were gently pressed over actively growing margins of colonies on PDA to collect the mycelium. The tapes were aseptically placed on sterile glass slides for observation using an Olympus optical microscope (BX51 SZX12 type; Mm et al., 2012). Pieces of mycelia in PDB were placed on sterile glass slides and then gently covered with coverslips. Each hypha was measured through microscopy with at least 50 measurements to determine the average mycelial diameter.

Mycelial Biomass

Mycelia on PDA were harvested by gentle scraping with a scalpel. Mycelia and culture filtrate in PDB were separated by centrifugation at 4°C and 8,000 rpm for 5 min. The culture filtrate was stored at −20°C until further use. The mycelia were washed thoroughly with sterile water, and sterile water was drained off with sterilized filter paper. Each harvested mycelium was transferred into an Eppendorf tube and weighed.

The pH Value of Culture Filtrate

A pH meter (PB-20 type) was used to measure the pH value of the culture filtrate.

Antioxidant Activity of Culture Filtrate

The culture filtrate was centrifuged at 10,000 rpm for 10 min, and the supernatant was collected to measure the total antioxidant capacity (T-AOC). Total antioxidant capacity was determined with an ultraviolet-visible spectrophotometer according to the procedure of the Total Antioxidant Capacity Assay Kit (Nanjing Jiancheng Company, China). The absorbance of the mixture was measured at 520 nm (Zeng et al., 2015).

The culture filtrate was evaporated under reduced pressure (8 × 103 Pa) and extracted twice with 75% ethyl alcohol. Subsequently, the extract was centrifuged at 5,000 rpm for 10 min. The supernatant was evaporated under reduced pressure to obtain the final extract, which was stored at 4°C for further testing.

The scavenging ability of superoxide anion radicals and hydroxyl radicals was determined through the pyrogallol autoxidation and salicylic acid methods, respectively (Kim et al., 1995; Škerget et al., 2005).

Ion Content of Mycelia

The mycelia were freeze-dried and ground to determine the ion content. Na^+, K^+, and Ca^{2+} ions were measured using atomic absorption spectrometry (M6AA system, Thermo, United States) after mineralization in a mixture of acids (HNO_4: $HClO_4$ = 4:1), and the Na^+/K^+ ratio was calculated (Hanway and Heidel, 1952).

Endogenous Hormone Content

After 28 days of growth, hyphae and culture filtrate were collected for GA_3, IAA, cytokinins (CTK), and abscisic acid (ABA) content determination using enzyme-linked immunosorbent assay (Danshi biology, Shanghai, China; Weiler, 1984). The percentage of hormone content in the culture filtrate in total content was calculated by dividing the hormone content in the culture filtrate by the total content secreted by *E. sinensis*.

Statistical Analyses

Statistical data analysis was performed with SPSS 25.0 (SPSS, Inc., Chicago, IL, United States). All averages and the standard error of the difference (*SE*) of the measurements were recorded in Excel2010. Univariate analysis of general linear models was employed to estimate the effects of single factor and their interaction on indices of *E. sinensis* strains in the present study (**Supplementary Tables S1, S2, S3**). Significant difference between single factor (exogenous additive, strain, and culture condition) was assessed by least significant difference tested at $p < 0.05$ and generated from one-way ANOVA based on the separated dataset. Statistical significance was defined at the 95% confidence level.

RESULTS

Colony Diameter

The colony diameters of the two *E. sinensis* strains were significantly different ($p < 0.05$), and the colony diameter of strain 1 was always significantly higher ($p < 0.05$) than that of strain 84F (**Table 1**).

Exogenous additives had significant effects ($p < 0.05$) on the growth of the two strains. Compared with control, IAA and VB_1 significantly promoted ($p < 0.05$) the growth of strains 1 and 84F, whereas NaCl and $ZnCl_2$ significantly inhibited ($p < 0.05$) the growth of the two strains (**Table 1**).

Hyphal Diameter

Culture conditions significantly affected the hyphal diameters of the two *E. sinensis* strains. The hyphal diameter of strains

TABLE 1 | Colony diameter of *Epichloë sinensis* under different treatments for 4 weeks (cm).

Treatment	Strain ID	
	1	84F
CK	2.93 ± 0.08c	1.95 ± 0.13c
Indole-3-acetic acid (IAA)	3.24 ± 0.08b	2.11 ± 0.07b
VB_1	3.52 ± 0.06a	2.41 ± 0.11a
NaCl	2.3 ± 0.12d	1.5 ± 0.08d
$ZnCl_2$	1.94 ± 0.07e	1.14 ± 0.16e
	*	

**in the table indicates significant differences between different strains ($p < 0.05$). Different lowercase letters in the table indicate significant differences between different exogenous additives ($p < 0.05$).*

in PDB was significantly higher ($p < 0.05$) than that on PDA (**Figure 1A**).

The hypha diameters of the two strains in PDB were significantly different ($p < 0.05$). The hyphal diameter of strain 1 was significantly lower ($p < 0.05$) than that of strain 84F (**Figure 1A**).

Exogenous additives had significant effects ($p < 0.05$) on hyphal diameters of the two strains. The hyphal diameters of strain 1 on PDA with control, VB_1, and NaCl treatments had no significant difference and were significantly lower ($p < 0.05$) than that with $ZnCl_2$ treatment. The hyphal diameters of strain 84F on PDA with control, IAA, and VB_1 treatments had no significant difference, which was significantly higher ($p < 0.05$) than that with NaCl and $ZnCl_2$ treatments. The hyphal diameters of strain 1 in PDB with IAA and $ZnCl_2$ were significantly higher ($p < 0.05$) than those with the other three treatments; the hyphal diameters of strain 84F in PDB were significantly different and were the highest with $ZnCl_2$ and the lowest with control and VB_1 (**Figure 1A**).

Mycelial Biomass

Culture conditions had significant effects ($p < 0.05$) on the mycelial biomass of the two *E. sinensis* strains. The mycelial biomass of the two strains in PDB was significantly higher ($p < 0.05$) than that on PDA (**Figure 1B**).

The mycelial biomass of the two strains in PDB was significantly different ($p < 0.05$). The mycelial biomass of strain 1 was significantly higher ($p < 0.05$) than that of strain 84F (**Figure 1B**).

Exogenous additives had significant effects ($p < 0.05$) on mycelial biomass of the two strains. On PDA, the mycelial biomass of strain 1 was significantly different ($p < 0.05$) under these five treatments and changed according to the following order depending on the additive: $VB_1 > IAA > CK > NaCl > ZnCl_2$. The mycelial biomass of strain 84F was also significantly different ($p < 0.05$) and changed according to the following order of additives: VB_1, $IAA > CK > NaCl > ZnCl_2$. In PDB with IAA and VB_1, the mycelial biomass of strain 1 was significantly higher ($p < 0.05$) than that with control treatment; however, in PDB with NaCl and $ZnCl_2$, biomass of strain 1 was significantly lower ($p < 0.05$) than that with control. In PDB with IAA, VB1, and control treatments, biomass of strain 84F were not significant difference ($p > 0.05$), which were significantly higher ($p < 0.05$) than those with NaCl and $ZnCl_2$ treatments (**Figure 1B**).

PH

Exogenous additives had significant effects ($p < 0.05$) on the pH of the culture filtrate of the two *E. sinensis* strains. The pH of strain 1 was the highest with NaCl treatment and was significantly higher ($p < 0.05$) than that with IAA, VB_1, and $ZnCl_2$ treatments. The pH of the filtrate of strain 84F with NaCl treatment was significantly higher ($p < 0.05$) than that with the other treatments, and the pH of strain 84F with VB_1 treatment was significantly lower ($p < 0.05$) than that with IAA, NaCl, and $ZnCl_2$ treatments (**Figure 2A**).

The Antioxidant Activity

Total Antioxidant Activity

Exogenous additives had significant effects ($p < 0.05$) on the T-AOC of the two *E. sinensis* strains. The T-AOC of strain 1 with control, NaCl, and $ZnCl_2$ treatments was significantly higher ($p < 0.05$) than that with IAA and VB_1 treatments. The T-AOC of strain 84F with NaCl and $ZnCl_2$ was significantly higher ($p < 0.05$) than that with IAA and VB_1 treatments (**Figure 2B**).

Superoxide Anion Radical and Hydroxyl Radical Scavenging Ability

The superoxide anion radical and hydroxyl radical scavenging abilities of the two *E. sinensis* strains were significantly different ($p < 0.05$). The superoxide anion radical and hydroxyl radical scavenging abilities of strain 84F were always significantly higher ($p < 0.05$) than that of strain 1 (**Figures 2C**,**D**).

Exogenous additives had significant effects ($p < 0.05$) on the superoxide anion radical and hydroxyl radical scavenging abilities of the two strains. The superoxide anion radical scavenging ability of strain 1 with $ZnCl_2$ treatment was significantly higher ($p < 0.05$) than that with control, IAA, and VB_1 treatments, and that with NaCl treatment was significantly higher ($p < 0.05$) than that with control and IAA treatments. The superoxide anion radical scavenging ability of strain 1 was the lowest with IAA treatment. The superoxide anion radical scavenging ability of strain 84F with IAA and VB_1 treatments was significantly lower ($p < 0.05$) than that with control, NaCl, and $ZnCl_2$ treatments. The hydroxyl radical scavenging ability of strains 1 and 84F with NaCl treatment was significantly higher ($p < 0.05$) than that with the other four treatments, while the scavenging ability with $ZnCl_2$ treatment was significantly higher ($p < 0.05$) than that with control, IAA, and VB_1 treatments (**Figures 2C**,**D**).

Ion Content of Mycelia

Exogenous additives had significant effects ($p < 0.05$) on the Na^+, K^+, and Ca^{2+} contents of the two *E. sinensis* strains. Na^+ and K^+ contents of strain 1 with IAA, VB_1, and $ZnCl_2$ were significantly higher ($p < 0.05$) than those with control and NaCl treatments. The Na^+ content of strain 84F with VB_1 treatment was significantly higher ($p < 0.05$) than that with control and

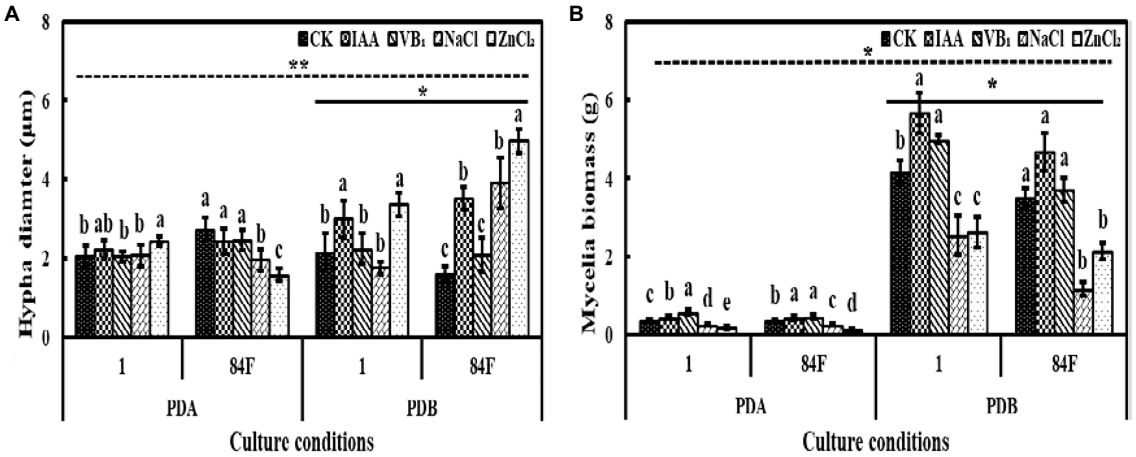

FIGURE 1 | Hyphal diameter and mycelial biomass of *Epichloë sinensis* under different treatments for 4 weeks. **(A)** is hyphal diameter, and **(B)** is mycelial biomass. Different lowercase letters in the figure indicate significant differences between different exogenous additives ($p < 0.05$); *on the real line in the figure indicates significant differences between different strains under same culture conditions ($p < 0.05$); *on the dotted line in the figure indicates significant differences between different cultures ($p < 0.05$).

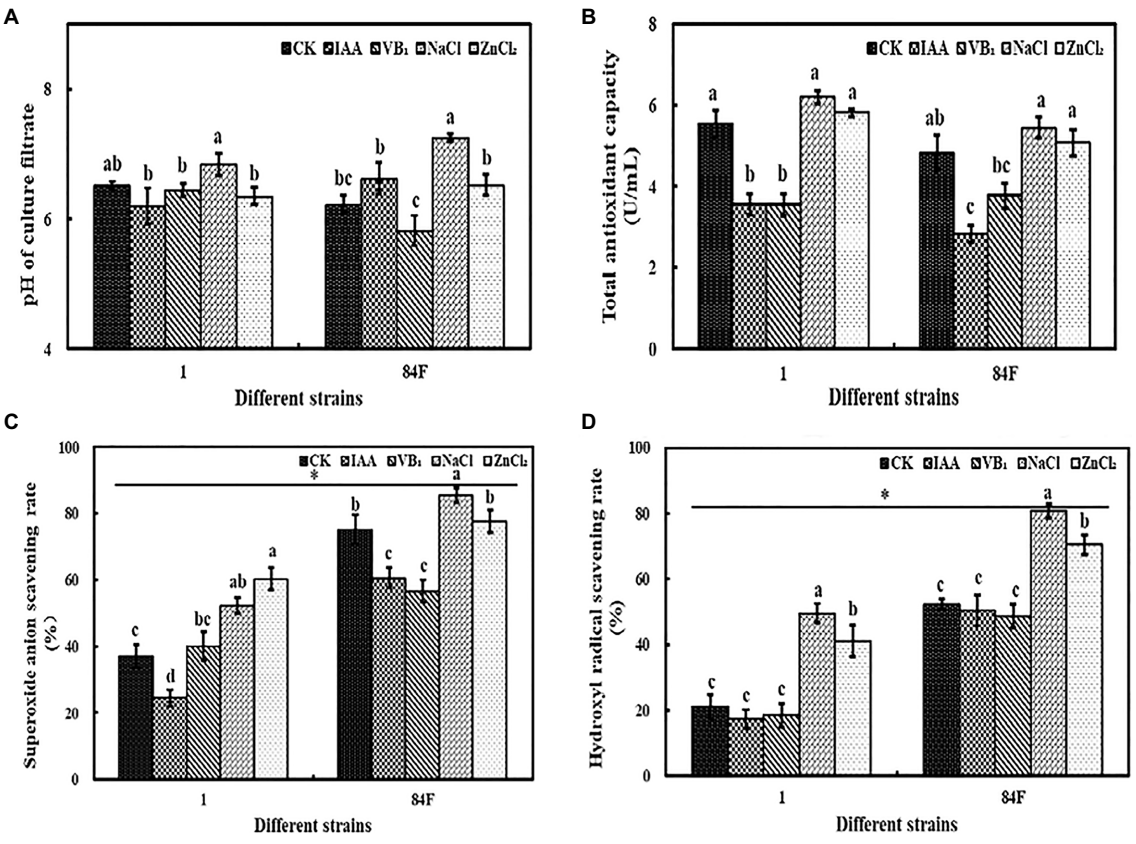

FIGURE 2 | PH and antioxidant ability of *E. sinensis* under different treatments for 4 weeks. **(A)** is PH, **(B)** is total antioxidant capacity of culture filtrate, **(C)** is superoxide anion radicals scavenging ability, and **(D)** is hydroxyl radical scavenging ability. The same as **Figure 1**.

NaCl treatments. The K^+ content of strain 84F with VB_1 treatment was significantly higher ($p < 0.05$) than that with IAA, NaCl, and $ZnCl_2$ treatments. The Ca^{2+} content of strain 1 with VB_1 treatment was significantly higher ($p < 0.05$) than that with control, NaCl, and $ZnCl_2$ treatments. The Ca^{2+} content of strain 84F with VB_1 treatment was significantly higher ($p < 0.05$) than

that with $ZnCl_2$ treatment. There was no significant difference between Na^+, K^+, and Ca^{2+} contents in mycelia of the two strains (**Figures 3A–C**).

Exogenous additives had significant effects on the Na^+/K^+ ratio of the two strains. Na^+/K^+ of strain 1 with NaCl treatment was significantly lower ($p < 0.05$) than that with control. Na^+/K^+ of strain 84F with control was significantly lower ($p < 0.05$) than that of IAA, VB_1, and $ZnCl_2$ treatments, and the ratio with IAA treatment was significantly higher ($p < 0.05$) than that with the other three treatments (**Figure 3D**).

Hormone Content

CTK Content

Culture conditions had significant effects ($p < 0.05$) on CTK content in mycelia of the two *E. sinensis* strains. The CTK content in mycelia of *E. sinensis* strains on PDA was significantly higher ($p < 0.05$) than that in PDB (**Figure 4**).

Cytokinins content in mycelia of the two strains on PDA and in PDB was not significantly different ($p < 0.05$). Cytokinins contents in the culture filtrate of strain 84F were significantly higher ($p < 0.05$) than that of strain 1 (**Figure 4**).

Exogenous additives had significant effects ($p < 0.05$) on CTK content on PDA and in PDB of the two strains. Cytokinins contents in mycelia of strain 1 on PDA and in PDB were not significantly different among the five treatments. The CTK contents of strain 84F on PDA with IAA and $ZnCl_2$ treatments were significantly higher ($p < 0.05$) than those with VB_1 treatment. In PDB with IAA, the CTK content in mycelia of strain 84F was significantly higher ($p < 0.05$) than that with NaCl treatment. Cytokinins content in the culture filtrate of strain 1 with IAA treatment was significantly higher ($p < 0.05$) than that with control and NaCl treatments; CTK content in the culture filtrate of strain 84F with control treatment was significantly higher ($p < 0.05$) than that with VB_1 treatment (**Figure 4**).

ABA Content

Culture conditions had significant effects ($p < 0.05$) on CTK content in mycelia of the two *E. sinensis* strains. Abscisic acid content in mycelia of *E. sinensis* strains on PDA was significantly higher ($p < 0.05$) than that in PDB (**Figure 5**).

The ABA content in mycelia of these two strains was significantly different ($p < 0.05$). In the culture filtrate, the ABA content of strain 84F was significantly higher ($p < 0.05$) than that of strain 1 (**Figure 5**).

Exogenous additives had significant effects ($p < 0.05$) on the ABA content of the two strains. On PDA, the ABA contents of strain 1 with control and $ZnCl_2$ treatments were significantly higher ($p < 0.05$) than those with NaCl treatment; the ABA

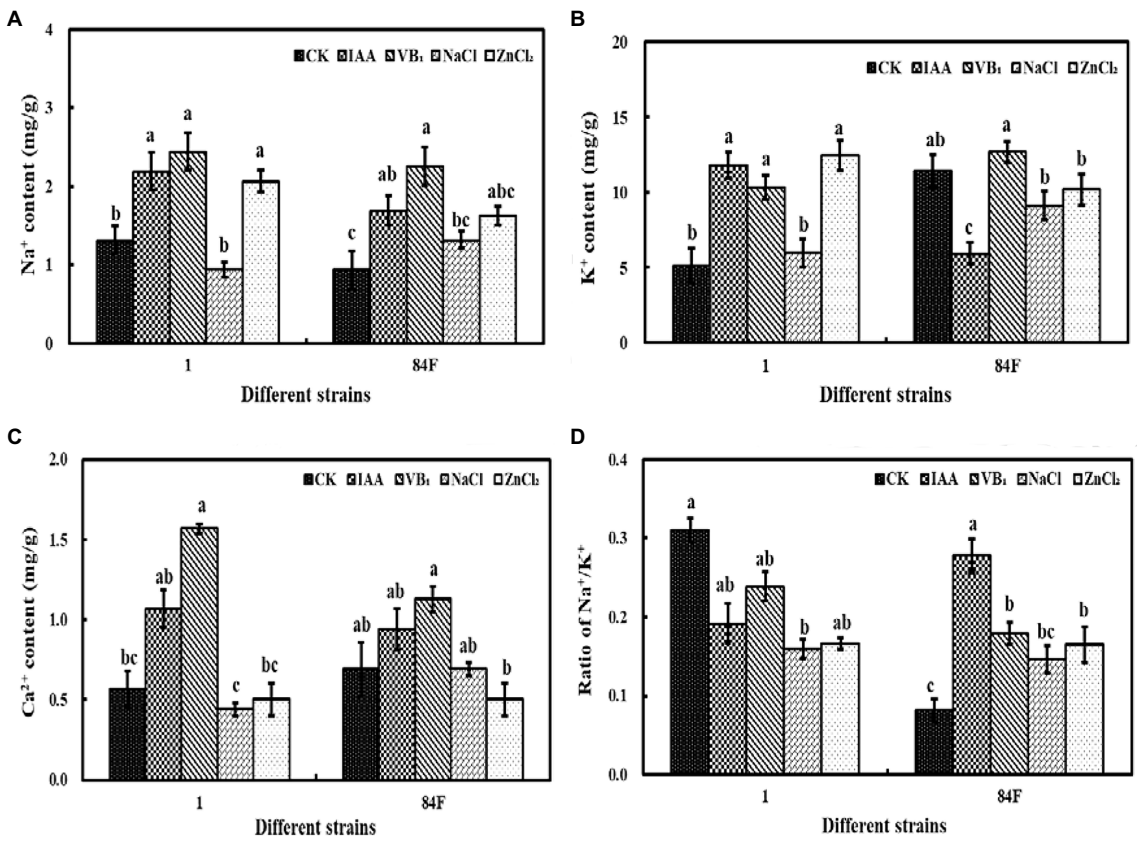

FIGURE 3 | Na^+, K^+, and Ca^{2+} contents and ratio of Na^+/K^+ of mycelium of *E. sinensis* under different treatments for 4 weeks. **(A)** is Na^+ content, **(B)** is K^+ content, **(C)** is Ca^{2+} content, and **(D)** is ratio of Na^+/K^+. The same as **Figure 1**.

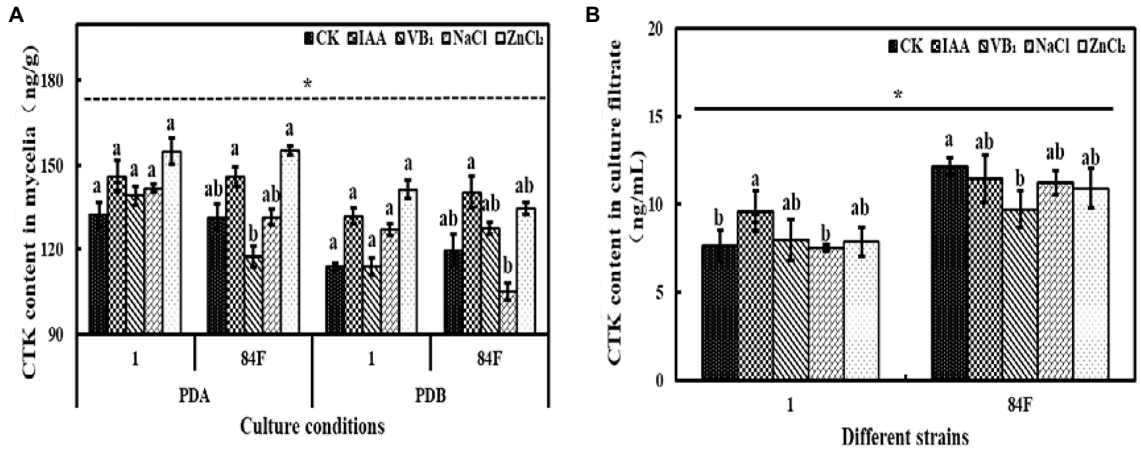

FIGURE 4 | Cytokinins content of *E. sinensis* under different treatments for 4 weeks. **(A)** is CTK content in mycelia, and **(B)** is CTK content in culture filtrate. The same as **Figure 1**.

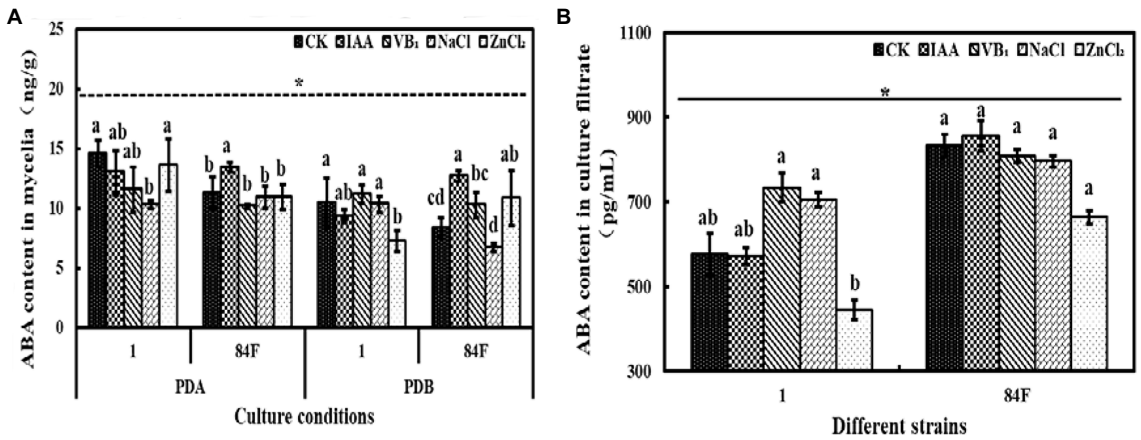

FIGURE 5 | Abscisic acid content of *E. sinensis* under different treatments for 4 weeks. **(A)** is ABA content in mycelia, and **(B)** is ABA content in culture filtrate. The same as **Figure 1**.

content for strain 84F with IAA treatment was significantly higher ($p < 0.05$) than that with the other four treatments. In PDB, ABA contents in the mycelia of strain 1 with control, VB_1, and NaCl treatments were significantly higher ($p < 0.05$) than those with $ZnCl_2$ treatment. Abscisic acid content in the mycelia of strain 84F with IAA treatment was significantly higher ($p < 0.05$) than that with control, VB_1, and NaCl treatments. In PDB with $ZnCl_2$ treatment, ABA content in mycelia of strain 84F was significantly higher ($p < 0.05$) than that with control and NaCl treatments. The ABA contents in the culture filtrate of strain 1 with VB_1 and NaCl treatments were significantly higher ($p < 0.05$) than those with $ZnCl_2$ treatment (**Figure 5**).

GA Content

Culture conditions had significant effects ($p < 0.05$) on GA content in mycelia of the two *E. sinensis* strains. GA content in mycelia of *E. sinensis* strains on PDA was significantly higher ($p < 0.05$) than that in PDB (**Figure 6**).

GA content in mycelia of the two strains was significantly different ($p < 0.05$). On PDA, the GA content of strain 1 was significantly higher ($p < 0.05$) than that of 84F. In PDB, no significant difference was observed between the two strains. In the culture filtrate, the GA content of strain 84F was significantly higher ($p < 0.05$) than that of strain 1 (**Figure 6**).

Exogenous additives had significant effects ($p < 0.05$) on the GA content of the two strains. On PDA, the GA content of strain 1 with control was significantly higher ($p < 0.05$) than that with VB_1 treatment. The GA content of strain 84F with IAA treatment was significantly higher ($p < 0.05$) than that with control, NaCl, and $ZnCl_2$ treatments. In PDB, there were no significant differences between GA contents in mycelia of strains 1 and 84F under the five treatments. GA content in the culture filtrate of strain 1 with IAA treatment was significantly lower ($p < 0.05$) than that with control, NaCl, and $ZnCl_2$ treatments; GA contents in the culture filtrate of strain 84F with IAA

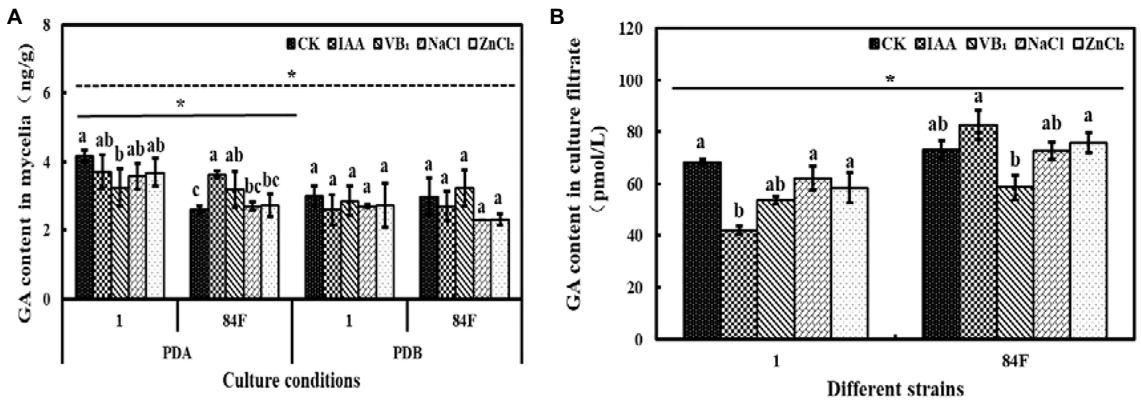

FIGURE 6 | Gibberlic acid content of *E.* sinensis under different treatments for 4 weeks. **(A)** is GA content in mycelia, and **(B)** is GA content in culture filtrate. The same as **Figure 1**.

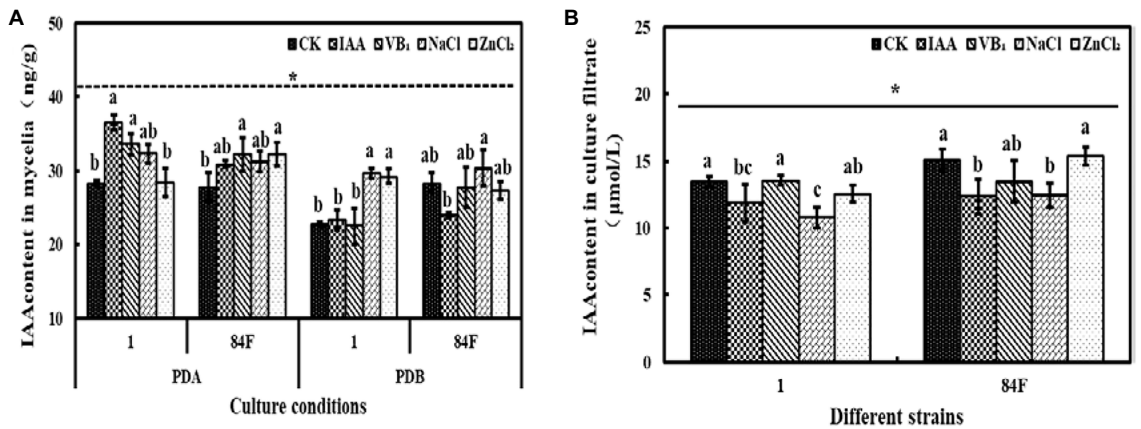

FIGURE 7 | Indole-3-acetic acid content of *E.* sinensis under different treatments for 4 weeks. **(A)** is IAA content in mycelia, and **(B)** is IAA content in culture filtrate. The same as **Figure 1**.

and $ZnCl_2$ treatments were significantly higher ($p < 0.05$) than those with VB_1 treatment (**Figure 6**).

IAA Content

Culture conditions had significant effects ($p < 0.05$) on IAA content in mycelia of the two *E. sinensis* strains. The IAA content in mycelia of *E. sinensis* strains on PDA was significantly higher ($p < 0.05$) than that in PDB (**Figure 7**).

IAA content in mycelia of the two strains on PDA and in PDB was not significantly different ($p < 0.05$). IAA contents in the culture filtrate of strain 84F were significantly higher ($p < 0.05$) than those of strain 1 (**Figure 7**).

Exogenous additives had significant effects ($p < 0.05$) on the IAA content of the two strains. On PDA with IAA and VB_1 treatments, IAA contents of strain 1 were significantly higher ($p < 0.05$) than those with control and $ZnCl_2$ treatments. In PDB, IAA content in mycelia of strain 1 with NaCl and $ZnCl_2$ treatments was significantly higher ($p < 0.05$) than those with control, IAA, and VB_1 treatments. Indole-3-acetic acid content in mycelia of strain 84F with NaCl treatment was significantly higher ($p < 0.05$) than those with IAA treatment. Indole-3-acetic acid content in the culture filtrate of strain 1 with control and VB_1 treatments was significantly higher ($p < 0.05$) than those with IAA and NaCl treatments. Indole-3-acetic acid content in the culture filtrate of strain 84F with control and $ZnCl_2$ treatments was significantly higher ($p < 0.05$) than those with IAA and NaCl treatments (**Figure 7**).

The Percentage of Hormone Content in the Culture Filtrate in Total Content Secreted

The percentages of CTK, ABA, and GA contents in the culture filtrate in total contents secreted by these two strains were significantly different ($p < 0.05$). The percentage of strain 84F was significantly higher ($p < 0.05$) than that of strain 1 (**Table 2**).

Exogenous additives had significant effects ($p < 0.05$) on the percentage of IAA content in the culture filtrate in total content secreted by strain 1. The percentage of strain 1 with control and VB_1 treatments was significantly higher ($p < 0.05$) than

TABLE 2 | Percentage of hormone content in the culture filtrate in total content (%).

Treatment	Cytokinins (CTK)		Abscisic acid (ABA)		Gibberlic acid (GA)		Indole-3-acetic acid (IAA)	
	1	84F	1	84F	1	84F	1	84F
CK	40.17a	50.41a	36.03a	49.26ab	44.23a	46.28b	50.86a	48.24a
IAA	42.31a	44.80b	37.37a	40.17ab	36.23a	51.59a	47.03b	47.38a
VB'	41.16a	43.56b	39.60a	43.89ab	38.80a	39.13a	51.41a	45.95ab
NaCl	37.38a	51.63a	40.23a	53.96a	44.21a	52.00ab	38.91d	41.77b
ZnCl'	35.75a	44.84b	37.78a	38.21b	43.14a	53.15a	42.89c	49.73a
	*		*		*			

**in the table indicates significant differences between different strains ($p < 0.05$).*
Different lowercase letters in the table indicate significant differences between different exogenous additives ($p < 0.05$).

that with the other four treatments; the percentage of strain 1 was significantly different ($p < 0.05$) and changed according to the following order of additives: CK, $VB_1 > IAA > NaCl > ZnCl_2$. Exogenous additives had significant effects ($p < 0.05$) on the percentage of CTK content in the culture filtrate in total content secreted by strain 84F ($p < 0.05$). The percentages of CTK content in the culture filtrate in total content secreted by strain 84F with control and NaCl treatments were significantly higher ($p < 0.05$) than that with IAA, VB_1, and $ZnCl_2$ treatments. The percentage of ABA content in the culture filtrate in total content secreted by strain 84F with NaCl treatment was significantly higher ($p < 0.05$) than that with $ZnCl_2$ treatment and was not significantly different with control, IAA, and VB_1 treatments. The percentage of GA content in the culture filtrate in total content secreted by strain 84F with VB_1 treatment was significantly higher ($p < 0.05$) than that with IAA, NaCl, and $ZnCl_2$ treatments. The percentage of IAA content in the culture filtrate in total content secreted by strain 84F with NaCl treatment was significantly lower ($p < 0.05$) than that with the other treatments (**Table 2**).

DISCUSSION

The endophyte strains isolated from different host ecotypes showed a rich diversity in morphological and growth characteristics (Wei et al., 2010). Ahlholm et al. (2002) showed that host genotypes, along with prevailing environmental conditions, influenced the genetic variation of endophytes. Endophyte strains isolated from a globally distributed collection of perennial ryegrass accessions presented rich gene diversity after evaluation with simple sequence repeat markers (van Zijll De Jong et al., 2008a, 2008b). The genetic polymorphism of grass endophytes is beneficial to select non-toxic strains that do not produce toxic alkaloids to livestock. These selected endophytes were artificially inoculated into grass and established a new grass-endophyte symbiosis that is both stress-resistant and non-toxic to domestic animals and, therefore, improves the quality of grasses and ensures animal safety (Johnson et al., 2013; Young et al., 2013). Yang et al. (2011) found differences in the culture characteristics and growth rates of various endophyte strains isolated from wild *F. sinensis* seeds from Sangke and Ganjia grasslands in the Gansu Province, China (Yang et al., 2011). Significant diversity was observed among the five *E. sinensis* endophyte strains isolated from different *F. sinensis* ecotypes on PDA with a variety of additives at different growth rates (Wang, 2019). The results of the present study support these findings and indicated that *E. sinensis* strains are biodiverse, and the growth and physiological characteristics of *E. sinensis* are affected by host ecotypes. The selection of appropriate markers for genetic polymorphism analysis of *E. sinensis* strains was conducted to reveal the relationship between their growth rate, physiological changes, and host genotype.

The endophyte growth is influenced not only by host genotype, environmental conditions but also by culture conditions (Ahlholm et al., 2010; Wei et al., 2010). We studied the growth of five *E. sinensis* endophyte strains on PDA with different additives and found that PGRs (VB_1, VB_5, VB_9, IAA, GA_3, and KT-30) promoted fungal growth, whereas ions (Na^+, Cd^{2+}, Cr^{6+}, and Zn^{2+}) inhibited it (Wang, 2019). The growth of four *E. sinensis* strains with 30 mg/l VB_1 and five *E. sinensis* strains with 20 mg/L IAA significantly increased ($p < 0.05$), whereas the five strains had the strongest resistance with 0.4 mol/L Na^+ and 750 mg/L Zn^{2+}. Therefore, the four different treatments which included 30 mg/L VB_1, 20 mg/L IAA, 0.4 mol/L NaCl, and 750 mg/L $ZnCl_2$ in this study were set up based on previous experiments and were initiated to determine the response mechanism of these two strains to different additives.

Numerous studies have shown that IAA and VB_1 promote mycelial growth of fungi (Ren et al., 2007; Li et al., 2016; Luo et al., 2021). High concentrations of NaCl and $ZnCl_2$ inhibited the colony diameter of *E. gansuensis* and *Penicillium chrysogenum*, respectively (Jin, 2009; Wang et al., 2020). The present results are similar to those of other studies. Numerous reports have indicated that the application of PGRs, including phytohormones, promotes cell division and enhances plant and microbe growth (Naeem et al., 2004). However, vitamins only play a regulatory role in plant metabolism to maintain normal central metabolic processes (Liao et al., 2018). In this experiment, compared with the control treatment, the promotion effect of IAA treatment on *E. sinensis* was higher than that of VB_1, which may be related to the different effects of vitamins and plant hormones in the organism. The resistance of *E. sinensis* to Na^+ was stronger than that of Zn^{2+}, indicating that *E. sinensis* has different resistance to different metal ions.

Endophytes produce numerous antioxidant compounds that may play roles in enhancing stress tolerance (Schulz et al., 2002; Malinowski and Belesky, 2006; Yuan et al., 2010). Most abiotic (desiccation and/or rehydration, nutrient limitation, and UV radiation) and biotic stresses (pathogens and insect herbivory) induce reactive oxygen species (ROS) production (Beckett et al., 2005). Cells need appropriate systems to allow rapid removal of ROS. Previous studies have found that the optimal zinc concentration in the medium may improve *Lentinus edodes* mycelium growth and the zinc content of the *L. edodes* mycelium, and increase antioxidant enzyme activities (Gang et al., 2017). The antioxidant capacity of endophytes from *Myricaria laxiflora* was extraordinarily high under mild saline-alkali stress (Gao et al., 2016). The present study found that the two *E. sinensis* culture filtrates showed high free radical scavenging ability with NaCl and $ZnCl_2$ treatments, which demonstrated that the antioxidant capacity played an important role during stress resistance of *E. sinensis*. The scavenging ability of superoxide anion radicals and hydroxyl radicals of strain 84F was higher than that of strain 1 under different treatments, which could be used to further investigate the natural antioxidants of the two *E. sinensis* strains.

Potato dextrose broth is currently widely used in the industrial production of medicinal and edible fungi because of the short fungal production cycle (Yang et al., 2000; Huang and Zhang, 2005). In the present study, the mycelial biomass and hyphae diameter in PDB were generally higher than those on PDA. These differences confirmed that PDB medium has the advantage of uniform distribution of nutrients during microbial cultivation, which is conducive to full contact and absorption of nutrients by mycelia cells, and eventually increases the production of mycelia and nutrients. Therefore, PDB can also be applied to enrich more *E. sinensis* mycelium.

Hormones are naturally occurring organic molecules that regulate plant growth and its developmental processes (Costacurta and Vanderleyden, 1995; Hoyerova et al., 2006; Berger et al., 2007) and present in a wide variety of organisms, including fungi (Battista et al., 1990; Zhang et al., 1999; Yue et al., 2000; Yuan et al., 2004; Nambara and Marionpoll, 2005; Hartung, 2010; Spichal, 2012; Ban, 2013). In the present study, IAA, CTK, IAA, and GA_3 in mycelia and fermentation of two *E. sinensis* strains under five treatments were quantified, suggesting that the *E. sinensis* strain produces growth-promoting hormones (Lee, 1990; Abd, 1997; Deotale et al., 1998; Klingler et al., 2011; Chanclud et al., 2016). Previous studies have found *Epichloë* endophyte change hormones to improve host stress tolerance (Battista et al., 1990; Saikkonen et al., 2004; Xia et al., 2018). In this study, hormones were detected in both mycelia and fermentation, indicating that the hormone concentration increased in E+ plants may be also adjusted by endophyte. In most case, the percentages of hormone contents in the culture filtrate in total contents secreted by *E. sinensis* were about 50%. These results provide a basis for the development and utilization of *E. sinensis* strains. In addition, host ecotypes, culture conditions, and exogenous additives affected the hormone content of the strains. However, these effects were not consistent.

Maintaining a constant intracellular K^+ and Na^+ balance is essential for metabolic processes in cells (Zhu, 2003). Restriction of the transport of Na^+ and increase in the K^+ concentration to ensure a high cytosolic K^+/Na^+ ratio are very important for cells to tolerate stress (Berthomieu et al., 2003; Cuin et al., 2003). Ca^{2+} is essential for selective ion transport mechanisms and for the maintenance of K^+ influx and Na^+/K^+ selectivity. This study is one of the few studies on ion response of *E. sinensis* in various media with exogenous additives. Our results showed exogenous additives had effects on Na^+, K^+, and Ca^{2+} contents and the Na^+/K^+ ratio of these two strains and the effects on two strains were inconsistent. This finding suggested *E. sinensis* may adapt to changing environment by regulating ion contents. Compared with other treatments, Na^+ content in mycelia of the two strains was not significantly different or significantly reduced with the NaCl treatment. This may be because organisms selectively absorb or transport ions to reduce their stress damage and maintain normal physiological metabolism. Therefore, exogenously added Na^+ might remain in the culture filtrate. Ion contents on PDA and in the culture filtrate should be further studied to understand the resistance mechanism of *E. sinensis* strains.

CONCLUSION

Our results demonstrate that *E. sinensis* strains isolated from different host ecotypes showed a rich diversity in physiology and biochemistry characteristics in various media with exogenous additives. *E. sinensis* strain might adapt to environmental changes by changing its antioxidant capacity or intracellular ion content. Additionally, PDB culture with IAA and VB_1 additives was the optimal enrichment conditions for *E. sinensis* mycelia and the two *E. sinensis* strains produced IAA, ABA, GA, and CTK to a certain level under different treatments. Collectively, our findings provide a theoretical basis for fully understanding *E. sinensis* and obtain more reference for utilization.

DATA AVAILABILITY STATEMENT

The raw data supporting the conclusions of this article will be made available by the authors, without undue reservation.

AUTHOR CONTRIBUTIONS

PT designed the experiments. YL did the experiment and analysis. All authors wrote the manuscript, contributed to the article, and approved the submitted version.

FUNDING

The research reported here was funded by the National Nature Science Foundation of China (31971768; 32061123004),

China Agriculture Research System (CARS-22 Green Manue), and Lanzhou University enterprise-funded project [(19)0439].

SUPPLEMENTARY MATERIAL

The Supplementary Material for this article can be found online at: https://www.frontiersin.org/articles/10.3389/fmicb.2021.726935/full#supplementary-material

Supplementary Table S1 | Univariate analysis of general linear models was employed to estimate the effects of single factor and their interaction on hypha diameter and mycelia biomass of *Epichloë sinensis* strains in the present study.

Supplementary Table 2 | Univariate analysis of general linear models was employed to estimate the effects of single factor and their interaction on cytokinins, abscisic acid, gibberlic acis, and indole-3-acetic acid contents of *E. sinensis* strains in the present study.

Supplementary Table 3 | Univariate analysis of general linear models was employed to estimate the effects of single factor and their interaction on pH, total antioxidant capacity, scavenging abilities of superoxide anion radical and hydroxyl radical, and ion contents of *E. sinensis* strains in the present study.

REFERENCES

Abd, E. I. (1997). Effect of phosphorus, boron, GA_3 and their interactions on growth, flowering, pod setting, abscission and both green pod and seed yields of broad been (*Viciafaba* L.) plant. *Alexandria J. Agrc. Res.* 42, 311–332.

Ahlholm, J. U., Helander, M., Henriksson, J., Metzler, M., and Saikkonen, K. (2002). Environmental conditions and host genotype direct genetic diversity of *Venturia ditricha*, a fungal endophyte of birth trees. *Evolution* 56, 1566–1573. doi: 10.1111/j.0014-3820.2002.tb01468.x

Ahlholm, J. U., Helander, M., Henriksson, J., Metzler, M., and Saikkonen, K. (2010). Environmental conditions and host genotype direct genetic diversity of *Venturia ditricha*, a fungal endophyte of birch trees. *Evolution* 56, 1566–1573. doi: 10.1111/j.0014-3820.2002.tb01468.x

Ban, Y. H. (2013). Mechanisms of dark septate endophyte isolated from Pb-Zn mine improving plant lead tolerance. dissertation/master's thesis. Yangling: Xianyang. Northwest Agriculture and Forestry University, China.

Battista, J. P. D., Bacon, C. W., Severson, R., Plattner, R. D., and Bouton, J. H. (1990). Indole acetic acid production by the fungal endophyte of tall fescue. *Agron. J.* 82, 878–880. doi: 10.2134/agronj1990.00021962008200050006x

Beckett, R. P., Minibayeva, F. V., and Laufer, Z. (2005). Extracellular reactive oxygen species production by lichens. *Lichenologist* 37, 397–40. doi: 10.1017/S0024282905014921

Berger, S., Sinha, A. K., and Roitsch, T. (2007). Plant physiology meets phytopathology: plant primary metabolism and plant-pathogen interactions. *J. Exp. Bot.* 58, 4019–4026. doi: 10.1093/jxb/erm298

Berthomieu, P., Conéjéro, G., Nublat, A., Brackenbury, W. J., Lambert, C., Savio, C., et al. (2003). Functional analysis of *AtHKT1* in *Arabidopsis* shows that Na^+ recirculation by the phloem is crucial for salt tolerance. *EMBO J.* 22, 2004–2014. doi: 10.1093/emboj/cdg207

Chanclud, E., Kisiala, A., Emery, N. R. J., Chalvon, V., Ducasse, A., Romiti-Michel, C., et al. (2016). Cytokinin production by the rice blast fungus is a pivotal requirement for full virulence. *PLoS Pathog.* 12:e1005457. doi: 10.1371/journal.ppat.1005457

Chen, T. X., Li, C. J., and Li, X. Z. (2016). Biological and physiological characteristics of *Epichloë bromicola* endophyte symbiotic with *Hordeum brevisubulatum*. *Pratacult Sci.* 33, 1658–1664. doi: 10.11829/j.issn.1001-0629.2015-0617

Costacurta, A., and Vanderleyden, J. (1995). Synthesis of phytohormones by plant-associated bacteria. *Crit. Rev. Microbiol.* 21, 1–18. doi: 10.3109/10408419509113531

Cuin, T. A., Miller, A. J., Laurie, S. A., and Leigh, R. A. (2003). Potassium activities in cell compartments of salt-grown barley leaves. *J. Exp. Bot.* 54, 657–661. doi: 10.1093/jxb/erg072

De Jong, E. V., Dobrowolski, M. P., Bannan, N. R., Stewart, A. V., Smith, K. F., Spangenberg, G. C., et al. (2008a). Global genetic diversity of the perennial ryegrass fungal endophyte *Neotyphodium lolii*. *Crop Sci.* 48, 1487–1501. doi: 10.2135/cropsci2007.11.0641

De Jong, E. V., Dobrowolski, M. P., Sandford, A., Smith, K. F., Willocks, M. J., Spangenberg, G. C., et al. (2008b). Detection and characterisation of novel fungal endophyte genotypic variation in cultivars of perennial ryegrass *(Lolium perenne* L.). *Aust. J. Agric. Res.* 59, 214–221. doi: 10.1071/AR07270

Deotale, R. D., Mask, V. G., Sorte, N. V., Chimurkar, B. S., and Yerne, A. Z. (1998). Effect of GA_3 and IAA on morpho-physiological parameters of soybean. *J. Soils Crops* 8, 91–94.

Faeth, S. H., Helander, M. L., and Saikkonen, K. T. (2010). Asexual Neotyphodium endophytes in a native grass reduce competitive abilities. *Ecol. Lett.* 7, 304–313. doi: 10.1111/j.1461-0248.2004.00578.x

Ferguson, N. H., Rice, J. S., and Allgood, N. G. (1993). Variation in nitrogen-utilization in *Acremonium coenophialum* isolates. *Appl. Environ. Microbiol.* 59, 3602–3604. doi: 10.1128/aem.59.11.3602-3604.1993

Gang, J., Zhang, S., Liu, Y., Xie, B., and Pang, S. L. (2017). Effects of zinc on the growth and antioxidant enzymes of *lentinus edodes* mycelium. *Food Ferment. Ind.* 43, 146–151. doi: 10.13995/j.cnki.11-1802/ts.201706024

Gao, Y., Lei, Q., Jiang, W., Kong, Y. S., Xue, Y. H., and Liu, S. P. (2016). Molecular characterization and phenolic acids analysis of an endophytic fungus with high antioxidant activity. *Microbiology* 43, 1235–1243. doi: 10.13344/j.microbiol.china.150534

Gundel, P. E., Pérez, L. I., Helander, M., and Saikkonen, K. (2013). Symbiotically modified organisms: nontoxic fungal endophytes in grasses. *Trends Plant Sci.* 18, 425–432. doi: 10.1016/j.tplants.2013.03.003

Hanway, J. J., and Heidel, H. (1952). Soil analysis methods as used in lowa state college soil testing laboratory. *Iowa Agric.* 57, 1–31.

Hartung, W. (2010). The evolution of abscisic acid (ABA) and ABA function in lower plants, fungi and lichen. *Funct. Plant Biol.* 37, 806–812. doi: 10.1071/FP10058

Hoyerova, K., Gaudinova, A., Malbeck, J., Dobrev, P. I., Kocabek, T., Solcova, B., et al. (2006). Efficiency of different methods of extraction and purification of cytokinins. *Phytochemistry* 67, 1151–1159. doi: 10.1016/j.phytochem.2006.03.010

Huang, Q., and Zhang, L. (2005). Solution properties of (1→3)-alpha-D-glucan and its sulfated derivative from *Poriacocos mycelia* via fermentation tank. *Biopolymers* 79, 28–38. doi: 10.1002/bip.20332

Hume, D. E., Ryan, G. D., Gibert, A., Helander, M., Mirlohi, A., and Sabzalian, M. R. (2016). *Epichloë* fungal endophytes for grassland ecosystems. *Sustainable Agric. Rev.* 19, 233–305.

Jin, W. J. (2009). Diversity of *Neotyphodium* endophytes symbiotic with *Achnatherum inebrians*. dissertation/master's thesis. (Lanzhou (Gansu): LanZhou University).

Jin, W. J., Li, C. J., and Nan, Z. B. (2009). Biological and physiological characteristics of *Neotyphodium* endophyte symbiotic with *Festuca sinensis*. *Mycosystema* 28, 363–369.

Johnson, L. J., Bonth, A., Briggs, L. R., Garadus, J. R., Finch, S. C., Fleetwood, D. J., et al. (2013). The exploitation of epichloae endophytes for agricultural benefit. *Fungal Divers.* 60, 171–188. doi: 10.1007/s13225-013-0239-4

Kim, S. J., Han, D., Moon, K. D., and Rhee, J. S. (1995). Measurement of superoxide dismutase-like activity of natural antioxidants. *Biosci. Biotechnol. Biochem.* 59, 822–826. doi: 10.1271/bbb.59.822

Klingler, J. P., Batelli, G., and Zhu, J. K. (2011). ABA receptors: the START of a new paradigm in phytohormone signalling. *J. Exp. Bot.* 61, 3199–3210. doi: 10.1093/jxb/erq151

Kuang, Y. (2016). Characteristics of *Epichloë* endophyte-*Festuca sinensis* symbiote. dissertation/master's thesis. Lanzhou (Gansu): LanZhou University.

Kulkarni, R. K., and Nielsen, B. D. (1986). Nutritional requirements for growth of a fungus endophyte of tall fescue grass. *Mycologia* 78, 781–786. doi: 10.2307/3807523

Latch, G., Christensen, M. J., and Samuels, G. J. (1984). Five endophytes of *Lolium* and *Festuca* in New Zealand. *Mycotaxon* 20, 338–342. doi: 10.1192/bjp.167.3.338

Lee, H. S. (1990). Effect of pre-sowing seed treatments with GA_3 and IAA on flowering and yield components in groundnuts. *Korean J. Crop Sci.* 35, 1–9.

Li, Z., Lv, P. H., Du, S. T., Ding, J., and Lv, C. L. (2016). Effects of different types of plant growth regulators on the hypha growth of *Grifola frondose*. *J. Northwest For. Univ.* 31, 188–194.

Li, C. J., Nan, Z. B., and Li, F. (2008). Biological and physiological characteristics of *Neotyphodium gansuense* symbiotic with *Achnatherum inebrians*. *Microbiol. Res.* 163, 431–440. doi: 10.1016/j.micres.2006.07.007

Liao, Z., Suo, Y., Xue, C., Fu, H., and Wang, J. (2018). Improving the fermentation performance of *Clostridium acetobutylicum* ATCC 824 by strengthening the VB_1 biosynthesis pathway. *Appl. Microbiol. Biotechnol.* 102, 8107–8119. doi: 10.1007/s00253-018-9208-x

Luo, Y., Guan, Y. Q., Qi, Z. X., Hao, J. Z., Nuerziya, Y. L. M. M. T., Wei, P., et al. (2021). Effects of exogenous nutrition factors on mycelia growth of *Agaricus balchaschensis*. *Xinjiang Agric. Sci.* 58, 133–142.

Ma, M. Z. (2009). Biology, physiology and anti-fungal activities characteristics of *Neotyphodium lolii* of ryegrass. dissertation/master's thesis. Lanzhou (Gansu): LanZhou University.

Malinowski, D. P., and Belesky, D. P. (2006). Ecological importance of *Neotyphodium* spp. grass endophytes in agroecosystems. *Grassl. Sci.* 52, 1–14. doi: 10.1111/j.1744-697X.2006.00041.x

Mm, A., Vm, A., Fp, B., and Gi, A. (2012). Fungal biodeterioration of historical library materials stored in Compactus movable shelves. *Int. Biodeter. Biodegr.* 75, 83–88. doi: 10.1016/j.ibiod.2012.03.011

Naeem, M., Bhatti, I., Ahmad, R. H., and Ashraf, M. Y. (2004). Effect of some growth hormones (GA_3, IAA and Kintin) on the morphology and early or delayed iniation of bud of lintil (Lens culinaris Medik). *Pak. J. Bot.* 36, 801–809.

Nambara, E., and Marionpoll, A. (2005). Abscisic acid biosynthesis and catabolism. *Annu. Rev. Plant Biol.* 56, 165–185. doi: 10.1146/annurev.arplant.56.032604.144046

Nan, Z. B. (1996a). Incidence and distribution of endophytic fungi in seeds of some native and introduced grasses in China. *Acta Pratacul. Sin.* 5, 1–8.

Pope, D. D., and Hill, N. S. (1991). Effects of various culture media, antibiotics, and carbon sources on growth arameters of *Acremonium coenophialum*, the fungal endophyte of *tall fescue*. *Mycologia* 183, 110–115. doi: 10.2307/3759839

Ren, G. M., Zhou, M. L., Wu, N., and Gao, Y. (2007). Influence of Vitamin B_1 on several kinds of basidiomycete mycelia growth. *J. Anhui Agric. Sci.* 35, 8075–8076.

Saikkonen, K., Wäli, P., Helander, M., and Faeth, S. H. (2004). Evolution of endophyte–plant symbioses. *Trends Plant Sci.* 9, 275–280. doi: 10.1016/j.tplants.2004.04.005

Schardl, C. L., Young, C. A., Faulkner, J. R., Florea, S., and Pan, J. (2012). Chemotypic diversity of epichloae, fungal symbionts of grasses. *Ecology* 5, 331–344. doi: 10.1016/j.funeco.2011.04.005

Schardl, C. L., Young, C. A., Hesse, U., Amyotte, S. G., Andreeva, K., Calie, P. J., et al. (2013). Plant-symbiotic fungi as chemical engineers: multi-genome analysis of the clavicipitaceae reveals dynamics of alkaloid loci. *PLoS Genet.* 9:e1003323. doi: 10.1371/journal.pgen.1003323

Schulz, B., Boyle, C., Draeger, S., Rommert, A. K., and Krohn, K. (2002). Endophytic fungi: a source of novel biologically active secondary metabolites. *Mycol. Res.* 106, 996–1004. doi: 10.1017/S0953756202006342

Siegel, M. R., Latch, G. C. M., and Johnson, M. C. (1987). Fungal endophytes of grasses. *Annu. Rev. Phytopathol.* 25, 293–315. doi: 10.1146/annurev.py.25.090187.001453

Škerget, M., Kotnik, P., Hadolin, M., Hras, H. R., Simonic, M., and Knez, Z. (2005). Phenols, proanthocyanidins, flavones and flavonols in some plant materials and their antioxidant activities. *Food Chem.* 89, 191–198. doi: 10.1016/j.foodchem.2004.02.025

Song, Q. Y., Li, F., Nan, Z. B., Coulter, J. A., and Wei, W. J. (2015a). Do *Epichloë* endophytes and their grass symbiosis only produce toxic alkaloids to insects and livestock? *J. Agric. Food Chem.* 68, 1169–1185. doi: 10.1021/acs.jafc.9b06614

Song, M. L., Chai, Q., Li, X. Z., Yao, X., Li, C. J., Christensen, M. J., et al. (2015b). An asexual Epichloë endophyte modifies the nutrient stoichiometry of wild barley (Hordeum brevisubulatum) under salt stress. *Plant Soil.* 387, 153–165. doi: 10.1007/s11104-014-2289-0

Spichal, L. (2012). Cytokinins—recent news and views of evolutionally old molecules. *Funct. Plant Biol.* 39, 267–284. doi: 10.1071/FP11276

Tian, P., Kuang, Y., and Nan, Z. B. (2015). The characteristics of *Festuca sinensis* and its breeding potential. *Pratacul. Sci.* 32, 1079–1087.

Tian, P., Xu, W. B., Li, C. J., Song, H., and Nan, Z. B. (2020). Phylogenetic relationship and taxonomy of a hybrid *Epichloë* species symbiotic with *Festuca sinensis*. *Mycol. Prog.* 19, 1069–1081. doi: 10.1007/s11557-020-01618-z

Vázquez-de-Aldana, B. R., García-Ciudad, A., García-Criado, B., Vicente-Tavera, S., and Zabalgogeazcoa, I. (2013). Fungal endophyte (*Epichloë festucae*) alters the nutrient content of *Festuca rubra* regardless of water availability. *PLoS One* 8, 201–213. doi: 10.1371/journal.pone.0084539

Wang, M.N. (2019). Culture characteristics and resistance to metal ions *Epichloë* endophyte of *Festuca sinensis*. dissertation/master's thesis. Lanzhou (Gansu): LanZhou University.

Wang, X. Y., Liu, Y., Gao, T. P., Xue, L. G., Liu, Y. B., Wan, Z. D., et al. (2020). Effect of heavy-metal stress on fungal growth and pH of fermentation broth. *Microbiology* 47, 3226–3236. doi: 10.13344/j.microbiol.china.200678

Wang, X. H., Yi, M., Liu, H., Han, Y. S., and Yi, H. L. (2016). Reactive oxygen species and Ca^{2+} are involved in cadmium-induced cell killing in yeast cells. *Can. J. Microbiol.* 63, 153–159. doi: 10.1139/cjm-2016-0258

Wei, Y. K., Gao, Y. B., Xu, H., Su, D., Zhang, X., and Wang, Y. H. (2010). Occurrence of endophytes in grasses native to northern China. *Grass Forage Sci.* 61, 422–429. doi: 10.1111/j.1365-2494.2006.00551.x

Weiler, E. W. (1984). Immunoassay of plant growth regulators. *Annu. Rev. Plant Physiol.* 35, 85–89. doi: 10.1146/annurev.pp.35.060184.000505

Xia, C., Christensen, M. J., Zhang, X. X., and Nan, Z. B. (2018). Effect of *Epichloë gansuensis* endophyte and transgenerational effects on the water use efficiency, nutrient and biomass accumulation of *Achnatherum inebrians* under soil water deficit. *Plant Soil* 424, 555–571. doi: 10.1007/s11104-018-3561-5

Yang, Y., Chen, N., and Li, C. J. (2011). The morphological diversity of endophytic fungal in *Festuca sinensis* in Gansu Province. *Pratacult. Sci.* 28, 273–278.

Yang, F. C., Ke, Y. F., and Kuo, S. S. (2000). Effect of fatty acids on the mycelial growth and polysaccharide formation by *Ganoder malucidum* in shake flask cultures. *Enzym. Microb. Technol.* 27, 295–301. doi: 10.1016/S0141-0229(00)00213-1

You, B. J., Lee, H. Z., Chung, K. R., Lee, M. H., Huang, M. J., Tien, N., et al. (2012). Enhanced production of ganoderic acids and cytotoxicity of *Ganoderma lucidum* using solid-medium culture. *Biosci. Biotechnol. Biochem.* 76, 1529–1534. doi: 10.1271/bbb.120270

Young, C. A., Hume, D. E., and Mcculley, R. L. (2013). Forages and pastures symposium: fungal endophytes of tall fescue and perennial ryegrass: pasture friend or foe? *J. Anim. Sci.* 91, 2379–2394. doi: 10.2527/jas.2012-5951

Yuan, Z. L., Dai, C. C., Shi, Y., Wang, A. Q., and Zhang, D. Z. (2004). Study on the mechanism of endophytic fungus B3 promoting rice growth. *Jiangsu Agric. Sci.* 2, 10–13.

Yuan, Z. L., Zhang, C. L., and Lin, F. C. (2010). Role of diverse non-systemic fungal endophytes in plant performance and response to stress: progress and approaches. *J. Plant Growth Regul.* 29, 116–126. doi: 10.1007/s00344-009-9112-9

Yue, Q., Miller, C. J., White, J. F., and Richardson, M. D. (2000). Isolation and characterization of fungal inhibitors from *Epichloë festucae*. *J. Agric. Food Chem.* 48, 4687–4692. doi: 10.1021/jf990685q

Zeng, W., Qin, W., Tian, W., Xue, Y., and Liu, S. (2015). Antioxidant activity in vitro of endophytic fungi from *Myricaria laxiflora*, a riparian plant with strong tolerance ability of flooding. *J. Pure Appl. Microbiol.* 9, 87–95.

Zhang, P. P. (2013). Characteristic of endophytic fungi isolated from Elymus and their effect on host resistances. Xinjiang Agricultural University, China. dissertation/master's thesis. Urumchi (Xingjiang): Xinjiang Agricultural University.

Zhang, J. H., Wang, C. L., Guo, S. X., Chen, J. M., and Xiao, P. G. (1999). Phytohormones produced by 5 endophytic fungi of orchidaceous medicinal plants. *Acta Academiae Medicinae Sinicae*, 49–54.

Zhou, L. Y., Li, C. J., Zhang, X. X., Johnson, R., Bao, G. S., Yao, X., et al. (2015a). Effects of cold shocked *Epichloë* infected *Festuca sinensis* on ergot

alkaloid accumulation. *Fungal Ecol.* 14, 99–104. doi: 10.1016/j.funeco.2014.12.006

Zhu, J. K. (2003). Regulation of ion homeostasis under salt stress. *Curr. Opin. Plant Biol.* 6, 441–445. doi: 10.1016/S1369-5266(03)00085-2

Conflict of Interest: The authors declare that the research was conducted in the absence of any commercial or financial relationships that could be construed as a potential conflict of interest.

Publisher's Note: All claims expressed in this article are solely those of the authors and do not necessarily represent those of their affiliated organizations, or those of the publisher, the editors and the reviewers. Any product that may be evaluated in this article, or claim that may be made by its manufacturer, is not guaranteed or endorsed by the publisher.

frontiers in Microbiology

ORIGINAL RESEARCH
published: 17 December 2021
doi: 10.3389/fmicb.2021.652477

Membrane Homeoviscous Adaptation in *Sinorhizobium* Submitted to a Stressful Thermal Cycle Contributes to the Maintenance of the Symbiotic Plant–Bacteria Interaction

Natalia Soledad Paulucci[1,2], Adriana Belén Cesari[1,2], María Alicia Biasutti[3,4], Marta Susana Dardanelli[1,2]* and María Angélica Perillo[5,6]**

[1] Facultad de Ciencias Exactas, Físico-Químicas y Naturales, Departamento de Biología Molecular, Universidad Nacional de Río Cuarto, Río Cuarto, Argentina, [2] Instituto de Biotecnología Ambiental y Salud (INBIAS), Consejo Nacional de Investigaciones Científicas y Técnicas (CONICET), Río Cuarto, Argentina, [3] Facultad de Ciencias Exactas, Físico-Químicas y Naturales, Departamento de Química, Universidad Nacional de Río Cuarto, Río Cuarto, Argentina, [4] Instituto para el Desarrollo Agroindustrial y de la Salud (IDAS), Consejo Nacional de Investigaciones Científicas y Técnicas (CONICET), Río Cuarto, Argentina, [5] Facultad de Ciencias Exactas, Físicas y Naturales, Instituto de Ciencia y Tecnología de Alimentos (ICTA), Departamento de Química, Cátedra de Química Biológica, Universidad Nacional de Córdoba, Córdoba, Argentina, [6] Instituto de Investigaciones Biológicas y Tecnológicas (IIBYT), Consejo Nacional de Investigaciones Científicas y Técnicas (CONICET), Córdoba, Argentina

Here, we estimate fast changes in the fluidity of *Sinorhizobium meliloti* membranes submitted to cyclic temperature changes (10°C–40°C–10°C) by monitoring the fluorescence polarization (*P*) of DPH and TMA-DPH of the whole cell (WC) as well as in its outer (OM) and inner (IM) membranes. Additionally, the long-term response to thermal changes is demonstrated through the dynamics of the phospholipid and fatty acid composition in each membrane. This allowed membrane homeoviscous adaptation by the return to optimal fluidity levels as measured by the PDPH/TMA-DPH in WC, OM, IM, and multilamellar vesicles of lipids extracted from OM and IM. Due to probe-partitioning preferences and membranes' compositional characteristics, DPH and TMA-DPH exhibit different behaviors in IM and OM. The rapid effect of cyclic temperature changes on the *P* was the opposite in both membranes with the IM being the one that exhibited the thermal behavior expected for lipid bilayers. Interestingly, only after the incubation at 40°C, cells were unable to recover the membrane preheating *P* levels when cooled up to 10°C. Solely in this condition, the formation of threads and nodular structures in *Medicago sativa* infected with *S. meliloti* were delayed, indicating that the symbiotic interaction was partially altered but not halted.

Keywords: *Sinorhizobium meliloti*, homeoviscous adaptation, temperature change, plant-bacteria interaction, outer and inner membrane

OPEN ACCESS

Edited by:
Sukesh Chander Sharma, Panjab University, India

Reviewed by:
Marta Palusinska-Szysz, Marie Curie-Skłodowska University, Poland
Carlos Muñoz-Garay, Universidad Nacional Autónoma de México, Mexico

***Correspondence:**
Natalia Soledad Paulucci
npaulucci@exa.unrc.edu.ar
Marta Susana Dardanelli
mdardanelli@exa.unrc.edu.ar
María Angélica Perillo
mperillo@unc.edu.ar

Specialty section:
This article was submitted to Microbial Physiology and Metabolism, a section of the journal Frontiers in Microbiology

Received: *12 January 2021*
Accepted: *15 November 2021*
Published: *17 December 2021*

Citation:
Paulucci NS, Cesari AB, Biasutti MA, Dardanelli MS and Perillo MA (2021) Membrane Homeoviscous Adaptation in Sinorhizobium Submitted to a Stressful Thermal Cycle Contributes to the Maintenance of the Symbiotic Plant–Bacteria Interaction. Front. Microbiol. 12:652477. doi: 10.3389/fmicb.2021.652477

INTRODUCTION

Sinorhizobium meliloti are Gram-negative bacteria usually applied in the formulation of commercial inoculants because of their ability to promote the growth and yield of legume crops (e.g., *Medicago sativa,* alfalfa) through a symbiotic atmospheric nitrogen (N)-fixing relationship.

N is fundamental for the development of plants because it is needed for the synthesis of proteins and nucleic acids. To counteract the deficit of N in certain soils, alfalfa establishes N-fixing symbiosis with the bacterium *S. meliloti* through a series of continuous signal exchanges that results in structural changes of *Medicago* roots (Jones et al., 2007). The first structural change is the formation of tightly curled root hairs entrapping *S. meliloti* cells (Gage, 2004). The presence of bacterial cells inside curled root hairs leads to the formation of tube-like infection threads (Gage and Margolin, 2000) which extend toward the bases of root hairs, branch into multiple infection threads, pass layers of root cortical cells, and reach the developing nodule primordia (Kijne, 1992; Timmers et al., 1999). Nodule primordia continue to generate new plant cells and form elongated indeterminate alfalfa nodules (van Brussel et al., 2002). *S. meliloti* cells are released from infection threads into the cytoplasm of new nodule cells surrounded by a plant cell membrane in the small nodule invasion zone (Hirsch et al., 1983). Thus, if all internal conditions are favorable, *S. meliloti* cells differentiate into bacteroids and convert atmospheric N_2 into NH_4^+.

Inoculation is the technology developed with the purpose of incorporating highly infectious and highly efficient rhizobia in legumes of agricultural interest. The inoculants must overcome two major problems inherent to living microorganisms: (1) loss of viability during short storage in the grower's warehouse, and (2) long shelf life and stability of the product over a range of −5 to 30°C within the grower's storage conditions.

During storage of the inoculants, bacteria experience fluctuations in temperature that are both regular (diurnal and seasonal) and random (as a result of physical disturbances of the environment). Most studies that address the issue of adverse environmental factors are designed so that different bacterial samples are exposed to either optimal or adverse conditions. However, there are few or no studies addressing different conditions on the same bacterial population to know the dynamics of the adaptation processes to environmental changes that bacteria can undergo in natural conditions.

Among environmental factors, temperature is the one exerting the strongest impact on the cell (WC) envelope of rhizobacterias (Paulucci et al., 2011, 2015; Cesari et al., 2016, 2018). Poikilothermic organisms, including bacteria do not control their temperature and must adapt their membrane lipid composition to maintain an optimal membrane fluidity level (Ernst et al., 2016). This adaptive response is termed "homeoviscous adaptation" (Sinensky, 1974) and in Gram-negative bacteria has been frequently studied on the WC envelope with a specific focus on the inner membrane (IM) (cytoplasmatic membrane). To our knowledge, except for a few studies on *Escherichia coli* and *Yersinia pseudotuberculosis* (Lugtenberg and Peters, 1976; Davydova et al., 2016), the role of the outer membrane (OM) in the thermal adaptation process has not received much attention, whereas in the case of rhizobacteria, this kind of data are null. In this work, we describe for the first time the biophysical behavior and mechanisms of homeoviscous adaptation due to cyclic temperature changes to maintain the OM and IM fluidity of a rhizobacteria.

The fluorescent probes 1,6-diphenyl-1,3,5-hexatriene (DPH) and its trimethylammonium derivative (TMA-DPH) are widely used to study the physical state of biological membranes (Konopasek et al., 2000; Balogh et al., 2011; do Canto et al., 2016). In typical lipid bilayers, DPH is known to penetrate in the membrane interior while its polar derivative, TMA-DPH, remains at the membrane surface within the lipid polar headgroup region (Lentz, 1989). However, when DPH is used as a probe in Gram-negative bacteria, the complex cell envelope may produce misleading results from fluorescence polarization experiments obtained in WC and OM, leading to erroneous interpretations. This is because the OM is a lipid bilayer containing phospholipids (PL), which are confined to the inner monolayer of the lipid bilayer, whereas the outer monolayer is mainly composed of lipopolysaccharides (LPS) (Bos et al., 2007). The hydrophilic polymeric moiety of LPS faces the outermost part of the cell and affects the partitioning of DPH in the core of the bilayer. DPH works well as a sensor of the behavior of the IM. In turn, the interpretation of the fluorescence polarization values of both probes in OM may be hindered by other physical phenomena such as solvent polarization and the molecular dynamics of the hydrophilic environment provided by the polysaccharide chains of LPS. There, TMA-DPH achieves a concentration higher than that of DPH and the highest with respect to other membrane regions.

Lipid components of the bacterial cell envelope largely influence the bacteria–plant symbiotic interaction process (Siebers et al., 2016). Phosphatidylcholine (PC) is a PL present in the membranes of bacteria of the rhizobiaceae family (Sohlenkamp et al., 2003; Basconcillo et al., 2009; Paulucci et al., 2011, 2013, 2014, 2015) and is essential for symbiotic interactions of rhizobia with legumes. For example, root nodule formation on soybean with efficient N fixation after infection with *Bradyrhizobium japonicum* depends on the presence of PC in the bacterium (Hacker et al., 2008). Although the process of symbiotic interaction between *S. meliloti* and alfalfa is deeply studied (Sieberer et al., 2005; Peck et al., 2006; Jones et al., 2007), to our knowledge, there are no studies that analyze the effects of environmental conditions exerted on biochemical changes in the cell envelope and the subsequent events of early colonization of alfalfa root simultaneously in the same samples.

In this work, we perform steady-state measurements of the DPH and TMA-DPH fluorescence polarization and fluorescence calculations to study the short-term effects of cyclic temperature changes (10°C–40°C–10°C) on the molecular dynamics of each membrane of *S. meliloti*, using WCs, spheroplasts, and isolated OM. Then, through lipid composition analysis, we study the homeoviscous response achieved by the bacteria in each membrane after the temperature change to establish if it could reverse the initial effects. In addition, we analyze the effects

of cyclic temperature changes on early interaction events of *S. meliloti* with roots of *M. sativa*. Although homeoviscous adaptation was successfully achieved through changes in the lipid composition of OM and IM, the plant–bacteria interaction was affected after exposure of *S. meliloti* to 40°C.

Two main issues, the study of successive thermal changes within the same bacterial population and the dissection of OM and IM, differentiate our work from others appearing in the literature in the research field of thermal adaptation in bacteria membranes. Moreover, studying the thermal-induced changes in lipid composition of the *S. meliloti* envelope not only sheds light on its biochemical mechanisms of adaptation, but might also contribute to explain the thermal-mediated *Sinorhizobium* and *Medicago* crosstalk at the molecular level.

MATERIALS AND METHODS

Materials

Thin layer chromatography (TLC) plates (silica gel GHLF, UV254, 250 micron) were purchased from Analtech, Inc. (Newark, DE, United States). Lipid standards were purchased from Sigma-Aldrich Co. (St. Louis, MO, United States). Fluorescent probes were from Invitrogen™, Thermo Fisher Scientific, Argentina. All reagents were of analytical grade and solvents of HPLC grade.

Bacteria and Growth Conditions

Sinorhizobium meliloti 1021 was cultured at 28°C in Luria-Bertani (LB) medium until the stationary phase, then an aliquot of the culture was separated and the rest placed at 10°C for 24 h. Then, an aliquot was separated and the rest subjected to 40°C for 24 h. In the same way afterward, an aliquot was separated, and the rest was exposed for 24 h at 10°C again to complete the cooling–heating–cooling cycle (10°C–40°C–10°C). The aliquots of culture separated at each point of the cycle were centrifuged and the biomasses used for the different determinations.

Isolation of Outer Membrane and Inner Membrane

Fractions of internal and external membrane were obtained according to the technique of Mizuno and Kageyama (1978). Cells were harvested by centrifugation at 8,000 rpm for 10 min at room temperature and washed with saline buffer pH 7. Cells (ca. 1.5 g wet weight) were suspended in 18 mL of ice cold 20% (w/v) sucrose. Ice cold reagents were slowly added to the suspension in an ice bath in the following order: 9 mL of 2 M sucrose, 10 mL of 0.1 M Tris–HCl (pH 7.8), 0.8 mL of 1% Na-EDTA (pH 7.0), and 1.8 mL of 0.5% lysozyme. Then, the mixture was warmed to 30°C within a few minutes and kept at that temperature for 60 min. During the incubation, the mixture became viscous due to the cell disruption. Then, the suspension was centrifuged at 13,000 rpm for 15 min at 30°C to obtain the spheroplasts in the pellet. Crude OM were recovered from the supernatant by centrifugation at 30,000 rpm for 60 min. The spheroplasts were burst in 40 mL of 5 mM $MgCl_2$ and the spheroplast membranes (IM) were recovered by centrifugation at 15,000 rpm for 20 min.

Two membrane markers, the KDO (2-ketodeoxyoctonate) content for the OM and the NADH oxidase activity for the IM (de Maagd and Lugtenberg, 1986) were used to check the purity of each membrane fraction. The KDO content was 4.2/100 μg protein and 0.6/100 μg protein for the OM and IM, respectively. NADH oxidase activity was 760 and 17.6 U/mg protein/min for the IM and OM, respectively. The content of these markers demonstrates efficient separation and purity of the isolated OM and IM fractions.

Determination of Membrane Fluidity

Membrane fluidity was determined by measuring the fluorescence polarization (*P*) of the DPH or TMA-DPH probe inserted into the membrane. *P* quantifies the degree of depolarization of light emitted by the embedded fluorescent probe and is an indirect measure of the membrane organizational state (Kuhry et al., 1985). *P* and membrane fluidity are inversely correlated. As the fluidity of the bacterial membrane decreases, *P* increases and vice versa (Lakowicz, 1999).

For all samples, fluorescence intensity (FI) measurements were performed using a FluoroMax®-Spex 4 Jovin Yvon (Horiba, NJ, United States) spectrofluorometer equipped with excitation and emission polarizers. The widths of the excitation and emission beam slits were set at 5 nm. FI were measured at excitation (λ_{ex}) and emission (λ_{em}) wavelengths for DPH and TMA-DPH set at 358 and 428 nm, respectively. The degree of polarization

P was calculated from the FI as follows (Equation 1):

$$P = \frac{I_{VV} - I_{VH}.G}{I_{VV} + I_{VH}.G}$$

where I_{VV} and I_{VH} are the FI of vertically and horizontally polarized light components emitted after excitation by vertically polarized light, respectively, and $G = I_{HV}/I_{HH}$ is the sensitivity factor of the detection system (Lakowicz, 1999).

$P_{TMA\text{-}DPH}$ and P_{DPH} data were used to determine the short-term effects of cyclic temperature changes on the fluidity of *S. meliloti* membranes in WC. In turn, the P_{DPH} was used to determine the short-term effects of cyclic temperature changes on the fluidity of different fractions of *S. meliloti* membranes such as spheroplast (IM) and isolated OM. The long-term response (homeoviscous adaptation) was confirmed by the $P_{TMA\text{-}DPH}$ and P_{DPH} measured in WC and multilamellar vesicles (MLV) prepared with lipids extracted from OM and IM membranes.

In Whole Living Cells

Following the procedures described by Trevors (2003), aliquots (25 mL) of *S. meliloti* cell suspension were collected at 28°C (control) and after each temperature change, harvested, washed in sterile 15 mmol L^{-1} Tris–HCl buffer (pH 7.0), and resuspended in the same buffer up to OD = 0.2 at 600 nm. For FI measurement, 1 μL of DPH (12 mmol L^{-1} stock solution in tetrahydrofuran) or TMA-DPH 12 mmol L^{-1} (stock solution in DMSO) were added to 3 ml of resuspended cells to obtain a final probe concentration of 4 μmol L^{-1} (a typical concentration used for microviscosity studies in model (Sanchez et al., 2007)

and natural (England et al., 2003) membranes) and incubated for 10 min in the dark with magnetic stirring at 200 rpm.

In Spheroplast (Inner Membrane) and Outer Membrane

Three milliliters of a spheroplast solution (OD = 0.2 at 600 nm) obtained as described above from control cells (28°C) and from cells submitted to each temperature treatment were used to determine the FI of DPH with parallel and perpendicular oriented polarizers as already described for living cells. In addition, spheroplast from control cells were subjected to rapid changes in temperature (10 min), and the FI was determined to understand the rapid effects of temperature changes. The same tests were performed for OM samples with the difference that, for this, 3 mL of an OM suspension containing 0.5 mg/ml of protein were used.

In Multilamellar Vesicles of Lipids Extracted From Outer Membrane and Inner Membrane

Multilamellar vesicles were prepared according to Yamazaki et al. (1989). Briefly, 1 mL of Tris/HCl buffer (pH 7) was added to dry lipids extracted (see below) from OM or IM of *S. meliloti* control cell and cells subjected to each thermal treatment. The lipid suspension (3×10^{-3} M total lipids) was heated up to ∼40°C for 20 min and vortexed several times for approximately 5 min. Then, 1 μL of DPH was added to 3 mL aliquots to obtain a final probe concentration of 4 μmol L^{-1} and incubated for 10 min in the dark under stirring at 200 rpm.

Incorporation of Labeled Acetate

A total of 0.5 μCi of sterilized 1-[^{14}C]-acetate sodium salt (43 mCi $mmol^{-1}$, New England Nuclear) was added to 25 mL bacterial cultures at the time of inoculation. Cells grown under these conditions were harvested by centrifugation at 8,000 *g* for 10 min in a Beckman Allegra 64R refrigerated centrifuge. Pellets were washed twice with 0.9 % w/v NaCl and used for subsequent studies.

Total Lipid Extraction

Lipids were extracted from bacterial mass using a mixture of chloroform/methanol/water (2:1:0.2 v/v/v). The lower phase enriched in phospholipids was dried under a stream of N_2 and dissolved in an appropriate volume of 2:1 (v/v) chloroform/methanol (Bligh and Dyer, 1959).

Separation and Quantification of 1-[^{14}C]-Labeled Phospholipids

Aliquots of OM and IM lipid extracts were analyzed by TLC using a 65:25:4 chloroform/methanol/water (v/v/v) solution as the running solvent. Lipids were detected with iodine vapors, and the separated bands were identified by comparing with authentic purified standards. Lipid bands were resolved properly (see **Supplementary Figure 3**).

The bands separated in the TLC plates were scraped, dispersed in 2 mL of scintillation cocktail (25%v/v Triton X-100, 0.3% w/v diphenyloxazole in toluene), and the radioactivity was measured using a liquid scintillation counter (Beckman LS 60001 C) at a 60% efficiency.

Analysis of Fatty Acids by GC-MS

Fatty acid methyl esters (FAMEs) were obtained from *S. meliloti* OM and IM lipid extracts treated with 10% BF3 in methanol for 90 min at 100°C (Morrison and Smith, 1964).

FAMEs were analyzed by gas chromatography (GC) using an Agilent 7890B coupled to a Mass Spectrometer Agilent 5977A (MS) equipped with a ZB-WAX (30 mm × 0.25 mm ID) Zebron column. The following GC-MS conditions were used: injector temperature, 240°C; column temperature, 180°C, maintained for 30 min; increase of 5°C/min to 240°C, maintained for 10 min. Run time: 46 min. MS: full SCAN, 40–500. Injection volume: 1 μl. Split: 1:10.

FAMEs were identified by comparing the retention times of the peaks resolved in a run of the sample under study with those exhibited by the components of a mixture of commercial standards run in the same experimental conditions (Sigma Chemical Co., St. Louis, MO, United States) (Kates, 1972). Afterward, MS was used to confirm FA structures. Relative percentages of each FA were calculated.

Assays of *S. meliloti–M. sativa* Interaction

Sinorhizobium meliloti strain L5-30/pDG71 (p*trp-Gfp*mut3) that constitutively produced green fluorescent protein (GFP) under the control of a *Salmonella enterica* serovar Typhimurium *trp* promoter (Gage, 2002) were assayed for their symbiotic phenotypes on *M. sativa*.

M. sativa cv. Monarca seeds were surface sterilized as described by Gage et al. (1996). The seeds were washed extensively with sterile water and allowed to germinate for 3 days in the dark. One seedling, 1–2 cm long, was placed in one plastic pot 5 cm in diameter and 10 cm high, filled with coarse-grain vermiculite sterilized in an autoclave twice for 2 h at 121°C. To test early interaction events between *S. meliloti* and alfalfa (radical hair curvature and infection thread formation) a culture of 200 mL of *S. meliloti* was grown to stationary phase at 28°C and then had applied the thermal treatment (10°C–40°C–10°C). After each step of the thermal cycle, an aliquot of 50 mL of culture was separated, centrifuged, and the biomass resuspended in physiological solution up to a 1×10^9 CFU mL^{-1} density. The plants were inoculated with 1 mL of the bacterial suspension and were placed in a growth chamber (24°C with illumination for 16 h/day).

The plantlets were grown on N-free medium as described by Rolfe et al. (1980). After 7 and 14 postinoculation days (dpi), plants were removed and the roots visualized, at a 10 or 40 × magnification for nodules and infection thread, respectively, with a Nikon Eclipse 50*i* equipped with an epi-fluorescence attachment (Nikon Instruments Inc.).

Statistical Analysis

All experiments were carried out in triplicate. One-way ANOVA was used to analyze the results. When ANOVA indicated a significant treatment effect, the least significant differences test (Tukey, $p < 0.05$) was applied to compare the mean values.

RESULTS

Composition of Phospholipids and Fatty Acids of Outer Membrane and Inner Membrane Grown Under Control Conditions

For both membranes under control conditions, the main PLs identified were PC, PE, phosphatidylglycerol (PG), and cardiolipin (CL) (**Figure 1A**); however, some differences could be observed between OM and IM. The highest percentage of PC (34.5%) was found in IM, whereas in OM, the main PL was PE (29.7%). The anionic PLs, PG and CL, were present at the highest percentages in OM (20.1 and 18.9%, respectively). Small amounts (<7%) of a PL ninhydrin positive, probably lysophosphatidylethanolamine (LPE), were detected in both OM and IM.

In the case of FA (**Figure 1B**), under control conditions, the content of 16:0, 16:1Δ^9, 18:0, and 18:1Δ^{11} were qualitatively the same in both membranes, but OM presented a greater proportion of 16:0. Consequently, the unsaturated/saturated (U/S) FA ratio in OM was lower ($U/S_{OM} = 3$) than that of IM ($U/S_{IM} = 4.1$).

Although the 19:0 cycle FA is reported by several authors in lipids of *S. meliloti* (Tighe et al., 2000; Basconcillo et al., 2009), in this work, it has not been detected, probably due to the technique used to obtain FAMEs.

Cyclic Temperature Changes Modify the Biophysical State of the Membranes

Temperature is one of the most studied environmental factors in terms of its effect on the fluidity of the membrane in bacteria of different genus. However, there are no documented data on the effects of successive changes in temperature within the same bacterial population. DPH and TMA-DPH are extensively used to probe the membrane organization by monitoring their fluorescence polarization (*P*). Because DPH is a hydrophobic substance and TMA-DPH a derivative that, at the assayed pH, bears a net charge in its TMA moiety, they localize and, thus, sense the molecular order and mobility within the core and the polar head group regions of bilayers, respectively.

Here, we evaluated the effect of rapid temperature changes on the P_{DPH} and $P_{TMA\text{-}DPH}$ in WC of *S. meliloti* (**Figure 2A**) as well as in two subcellular fractions (IM and OM) (**Figure 2B**). WC exhibited a $P_{DPH,28} = 0.17$ in control conditions (28°C) and, after the initial incubation at 10°C for 30 min, the fluorescence polarization increased up to $P_{DPH,10i} = 0.21$. This result can be interpreted as a greater rigidity in the membrane and lesser fluctuation of the acyl chains within the lipid bilayer. A subsequent temperature increase to 40°C led to a fast decrease in P_{DPH}, reaching $P_{DPH,40} = 0.14$ after 10 min incubation, indicating an increase in the mobility of the probe within less ordered acyl chains and, thus, a higher membrane fluidity. Then, after 20 min incubation at 10°C, the final state in the cycle was reached. As expected, there was an increase in P_{DPH} with respect to the previous state ($P_{DPH,10f} = 0.19$) but slightly below the initial value of $P_{DPH,10i}$.

The environment sensed by TMA-DPH in WC at the initial state showed a $P_{TMA-DPH,28}$ ~0.23, which was significantly higher than $P_{DPH,28}$. Sequential 10 min incubation at 10°C, 40°C, and 10°C led $P_{TMA\text{-}DPH}$ to change in the opposite direction with respect to the changes observed with DPH. Hence, $P_{TMA\text{-}DPH}$ decreased up to $P_{TMA-DPH,10i} = 0.16$, increased up to $P_{TMA-DPH,40} = 0.21$, and then decreased again to $P_{TMA-DPH,10f} = 0.12$. Moreover, TMA-DPH responded faster than DPH to the initial cooling step.

P_{DPH} followed changes in the expected direction, increasing at low *T* and decreasing at high temperatures, suggesting that cyclic *T* changes (cooling–heating–cooling) induced a stiffening–fluidization–stiffening phenomenon in *S. meliloti*. However, the changes in $P_{TMA\text{-}DPH}$ did not allow for a straightforward interpretation and required further considerations (see section "Discussion"). Additionally, because these experiments were

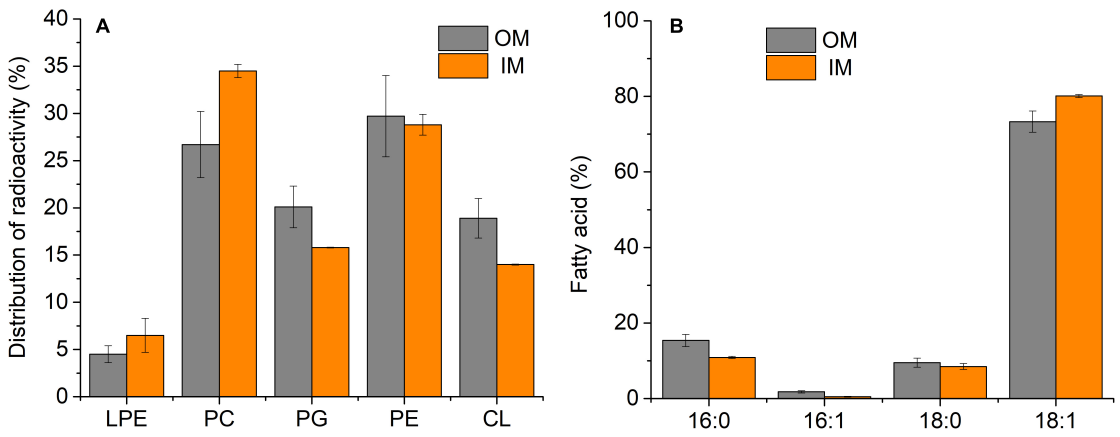

FIGURE 1 | PL **(A)** and FA **(B)** composition of *S. meliloti* OM and IM at 28°C (control). 50 mL of *S. meliloti* culture with or without [^{14}C]-acetate was grown to a stationary phase at 28°C. Afterward, OM and IM fractions were obtained. **(A)** Data from TLC of radioactively labeled PL bands scraped and quantified by liquid scintillation counting. **(B)** GC-MS analysis of FAME from total lipids. The percentage of each FA and PL is relative to the total defined as 100%. Values represent the mean ± sd of three independent experiments.

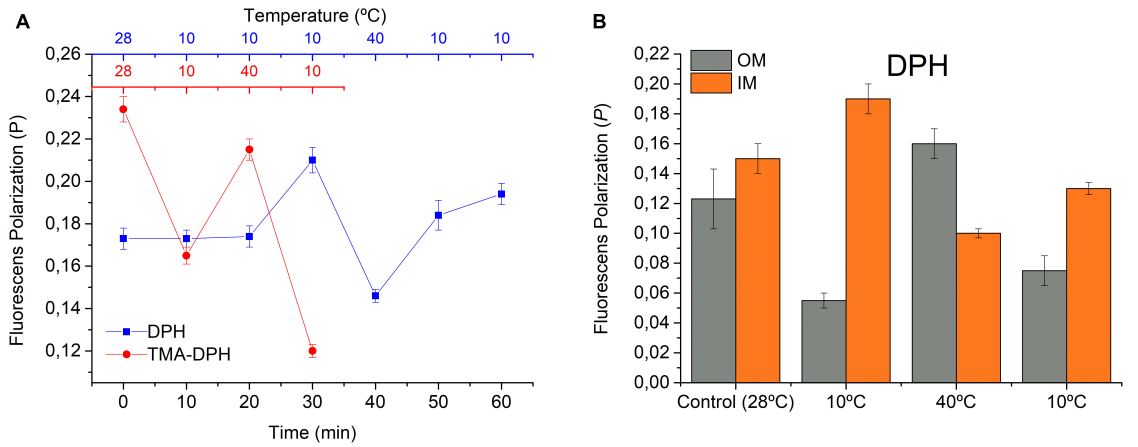

FIGURE 2 | Effect of fast cyclic temperature changes on the fluorescence polarization. **(A)** Using DPH and TMA-DPH as fluorescent probes in whole *S. meliloti* cells and **(B)** using DPH in OM and IM. *S. meliloti* culture was grown to a stationary phase at 28°C, centrifuged, and the biomass resuspended in 15 mmol L^{-1} Tris–HCl buffer (pH 7.0) up to an OD600 nm = 0.2. The fluorescent membrane probes (DPH or TMA-DPH) 4 μmol L^{-1} were added to the resuspended culture (3 mL). Fluorescence polarization was measured in one aliquot at time = 0 min at 28°C (control sample) and after each successive temperature change. OM and IM (spheroplast) fractions from control cells were incubated with DPH probe 4 μmol L^{-1} and were subjected to rapid changes in temperature (10 min), and the fluorescence polarization was determined. Values represent the mean ± sd of three independent experiments.

performed in WC, the effects of DPH might have been reflecting the behavior of membranes as well as hydrophobic cell environments, such as lipid droplets as described previously for eukaryotic K562 leukemia cells (Balogh et al., 2011). Moreover, it is important to take into account that Gram-negative cells such as *S. meliloti* have a double membrane cell envelope. The dissection of the behavior of isolated OM and IM (**Figure 2B**) seemed to help in data interpretation. In control conditions, the values of P_{DPH} in OM and IM differed between one another with $P_{DPH,OM,28} < P_{DPH,IM,28}$, and in general, they were lower than those found in WC. In control conditions, the $P_{DPH,OM,28} = 0.12$. After 30 min exposure to 10°C, $P_{DPH,OM}$ decreased, resulting in $P_{DPH,OM,10i} = 0.05$, and the opposite effect was observed in IM, where the $P_{DPH,IM,28} = 0.15$ increased up to $P_{DPH,OM,10i} = 0.19$. The difference $P_{DPH,OM,10i} << P_{DPH,IM,10i}$ widened if compared with the control at 28°C. The following step was the exposure to 40°C, which in OM, caused a considerable increase in OM ($P_{DPH,OM,40} = 0.16$) and a decrease in spheroplasts ($P_{DPH,IM,40} = 0.10$), leading to an inversion in the relationship between P_{DPH} of OM and IM, with $P_{DPH,OM,40} > P_{DPH,IM,40}$. Then, cooling up to 10°C again caused a decrease in OM ($P_{DPH,OM,10f} = 0.07$) and, on the contrary, an increase in spheroplasts ($P_{DPH,IM,10f} = 0.13$), leading to a new inversion of the relationship of P_{DPH} between both membranes. However, the difference $P_{DPH,OM,10f} < P_{DPH,IM,10f}$ was less significant than $P_{DPH,OM,10i} << P_{DPH,IM,10i}$ and the absolute value of $P_{DPH,IM,10f}$ was lower than that of $P_{DPH,IM,10i}$.

Homeoviscous Adaptation of *S. meliloti* Membranes During Cyclic Temperature Changes

To test the homeoviscous adaptation of *S. meliloti* to the effects of *T* changes on its fluidity, we measured the P_{DPH} and $P_{TMA\text{-}DPH}$ in WC after 24 h incubation at each temperature (**Figure 3**). The bacterial suspension showed the same P_{DPH} and $P_{TMA\text{-}DPH}$ as the control after the initial incubation to 10 and 40°C, clearly indicating that *S. meliloti* has the adaptive mechanisms that allow its outer and cytoplasmic membrane to return to the viscosity level of the control after the *T*-induced perturbation. However, the exposure to 10°C for the second time, after being exposed

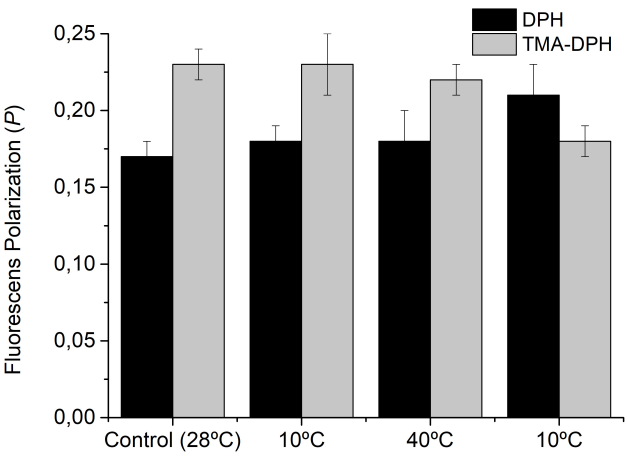

FIGURE 3 | Effect cyclic temperature changes on the fluorescence polarization of DPH and TMA-DPH in WC after 24 h of thermal change. *S. meliloti* (100 mL) culture was grown to a stationary phase at 28°C and then the thermal changes applied (10°C–40°C–10°C) for 24 h incubation periods. After exposure to each temperature, one aliquot (25 mL) was centrifuged and the biomass resuspended in 15 mmol L^{-1} Tris–HCl buffer (pH 7.0) up to an OD600 nm = 0.2. The fluorescent membrane probe (DPH or TMA-DPH) 4 μmol L^{-1} was added to the resuspended culture (3 mL). Fluorescence polarization was measured at the same temperature from which the samples come. Values are the mean ± sd of three independent experiments.

to 40°C, impaired the return to the P_{DPH} and $P_{TMA\text{-}DPH}$ values of the control. Thus, after the second exposure to 10°C, the P_{DPH} values indicate that the IM remains more rigid compared with control cells (28°C) while $P_{TMA\text{-}DPH}$ indicates that the OM remains more fluid.

Because modifications in the lipid components are usually involved in the homeoviscous adaptation phenomenon, we studied the effect of *T* on the composition of PL and FA of the cellular envelope of *S. meliloti*.

Effect of Cyclic Temperature Variations on the Composition of Phospholipid and FA From *S. meliloti* Outer Membrane and Inner Membrane

Figure 4 depicts the effect of temperature changes on the composition of PL and FA of each *S. meliloti* membrane (further details are described in **Supplementary Tables 1, 2**). Thus, 10°C caused, with respect to the control (28°C), a decrease in PC (28.8%) and an increase in CL (30.7%) and LPE (42.2%) in OM (**Figure 4A**), whereas in IM, the decrease in PC (19%) was also accompanied by an increase in the anionic PLs PG (19%) and CL (26%) (**Figure 4B**). Also, the first exposure to 10°C in OM caused a decrease in 18:1 (30.7%) and an increase in the saturated 16:0 (18%) and 18:0 (209%) (**Figure 4C**). In the IM, the response was completely the opposite to that expected for a cooling process: The content of saturated 16:0 (34.8%) and 18:0 (40%) decreased, and 18:1 increased 7.8% (**Figure 4D**).

After the incubation at 40°C, both membranes exhibited an increase in PC levels (113% and 44% for OM and IM, respectively), whereas PE decreased (36% and 15% in OM and IM, respectively)—a completely opposite response to that observed for exposure at 10°C. In addition, we observed a strong decrease in CL (31%) in IM (**Figure 4B**). Changes in the FA levels were almost opposite between both membranes, increasing 16:0 (45%) and decreasing 18:0 (40%) in OM (**Figure 4C**) and increasing 16:0 and 18:0 (95.8% and 53%, respectively) and decreasing 18:1 (10%) in IM (**Figure 4D**).

When the same cell sample was exposed again for 24 h at 10°C, we observed a decrease in PC (24.4% and 23% for OM

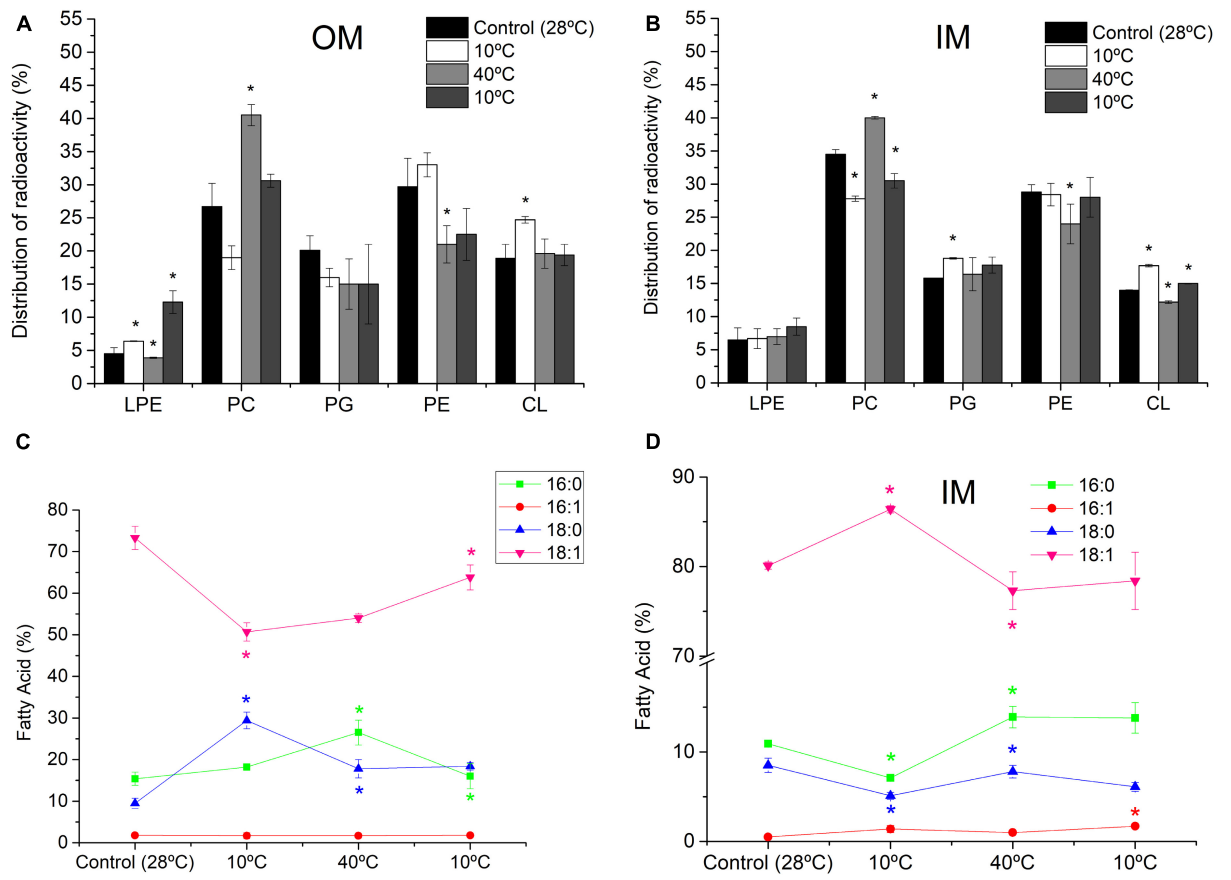

FIGURE 4 | Effect of cyclic temperature variations on the composition of PL and FA from *S. meliloti* OM **(A,C)** and IM **(B,D)**. *S. meliloti* culture (200 mL) with or without [^{14}C]-acetate was grown to a stationary phase at 28°C and then the thermal changes applied (10°C–40°C–10°C) every 24 h incubation period. After exposure to each temperature, a 50 mL aliquot of culture was separated and the biomass used to obtain OM and IM fractions. Panels **(A,B)** data from TLC of radioactively labeled PL bands scraped and quantified by liquid scintillation counting. Panels **(C,D)** GC-MS analysis FAME from total lipids. The percentage of each FA and PL is relative to the total defined as 100%. Values represent the mean ± sd of three independent experiments. Asterisks indicate statistically significant changes with respect to the previous stage.

and IM, respectively) compared with the previous condition (**Figures 4A,B**). Moreover, a strong increase in LPE (215%) was observed in OM (**Figure 4A**). The FA response of OM in this condition was different from that found in the previous exposure at 10°C, increasing 18:1 (18%) and decreasing 16:0 (40%) with respect to the control (28°C). In IM, the exposure at 10°C for the second time increased up to 40% the 16:1 content with respect to the cells subjected 24 h at 40°C.

The changes in FA composition can be synthesized in the U/S ratio. After successive 24 h incubation periods at 10°C, 40°C, and 10°C, in the OM, the U/S_{OM} ratio varied from 3.0 in the control to 1.1, 1.2, and 1.9, respectively. Interestingly, the transition to 40°C, although it did not affect the U/S_{OM}, a decrease in the mean length of the acyl chains of saturated FA was observed, by increasing 16:0 and decreasing. Underlying the process of homeoviscous adaptation is the stress-triggered catalytic activity of membrane-bound enzymes (Solís-Oviedo et al., 2012) and/or membrane sensors related to signal transduction mechanisms (Geiger et al., 2021). Thus, the membrane remodeling in composition and organization may operate as an on/off switch on the controlling mechanisms 18:0. In general, after the first 10°C incubation, the U/S_{OM} values are not in the line of compensating *T*-induced changes in membrane organization.

In turn, in IM, the U/S_{IM} of the control (4.1) changed in the following sequence, 7.2, 3.6, and 4.0 after successive 24 h incubation at 10°C, 40°C, and 10°C, respectively, along the thermal cycle. The variations in U/S_{IM} occurred in the direction expected to compensate for the *T*- induced changes in membrane microviscosity.

Fluorescence Polarization of DPH in Outer Membrane, Inner Membrane, and Multilamellar Vesicles Prepared With Lipids Extracted From Samples Submitted to the Temperature Cycle

We measured the value of P_{DPH} in isolated OM and spheroplasts (IM) as well as in MLVs prepared with the lipids extracted from OM and IM of cells previously subjected to successive 24 h incubation periods at 10, 40, and 10°C (**Figure 5**). The measurement of *P* in these systems after 24 h of exposure to each *T* allowed us to investigate if the modifications in the lipid composition were in line with restoring fluidity to optimal values after the initial disturbance. Besides this, MLVs are a more simplified system in which only the behavior of the lipid fraction (changes in *U/S* ratio) can be evaluated.

In the case of isolated OM, the P_{OM} values were 0.10, 0.13, 0.06, and 0.04, respectively, for the control, 10°C, 40°C, and 10°C, whereas MLV_{OM} exhibited the following $P_{DPH,MLV,OM}$ values for the control, 10°C, 40°C, and 10°C: 0.14, 0.24, 0.21, and 0.19, respectively. Using both systems, it can be appreciated that the OM presents a response ordering–disordering–ordering to the cooling–heating–cooling cycle, which might only be explained by the variations in U/S_{OM} during the first exposure to 10°C with respect to the previous stage.

However, in IM, the P_{IM} values were 0.15, 0.11, 0.14, and 0.09, respectively, for the control, 10°C, 40°C, and 10°C, whereas in MLV_{IM}, $P_{DPH,MLV,IM}$ values were 0.17, 0.13, 0.16, and 0.12, exhibiting a response disordering–ordering–disordering that accompanies the observed variation in U/S_{IM}.

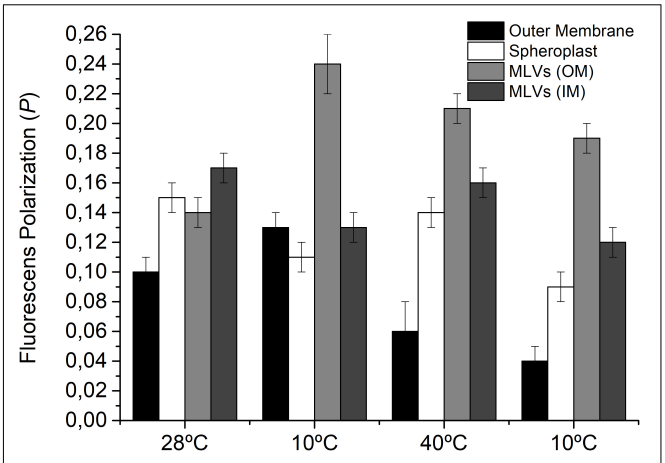

FIGURE 5 | Fluorescence polarization of DPH in IM (spheroplast) and OM as well as in MLVs of lipids extracted from *S. meliloti* OM and IM after each temperature change. *S. meliloti* culture (200 mL) was grown to a stationary phase at 28°C and then the thermal changes applied (10°C–40°C–10°C) for 24 h incubation periods. After exposure to each temperature, one aliquot (50 mL) was separated, and OM and IM fractions were obtained. MLVs were prepared from lipids obtained of OM and IM. The fluorescent membrane probe (DPH) 4 μmol L^{-1} was added to the membranes and MLVs suspension (3 mL) and incubated to facilitate incorporation of the probe. Fluorescence polarization was measured at 25°C. Values are the mean ± sd of three independent experiments.

Implications of Changes Caused by Temperature on the Ability of *S. meliloti* to Interact With *M. sativa*

We used *S. meliloti Gfp*-expressing cells in the different stages of the cycle (10°C–40°C–10°C) to perform interaction tests with *M. sativa* and evaluated the development of early symbiotic structures, such as infection threads after 7 dpi (**Figure 6A**) and their ability to evolve toward the nodule after 14 dpi (**Figure 6B**).

Medicago sativa seedlings inoculated with *S. meliloti* grown under control conditions exhibited threads of infection approximately between 5 and 7 dpi (**Figure 6A-I**) initiated from curled root hairs and extended through the epidermal cells, whereas nodular structures were detected microscopically at 14 dpi (**Figure 6B-I**).

The exposure to 10°C (**Figures 6A-II,B-II**) did not modify the bacteria's symbiotic behavior with respect to the control. However, the subsequent exposure at 40°C delayed the symbiotic events as shown by the incipient infection threads observed at 7 dpi (**Figure 6A-III**). Additionally, at 14 dpi (**Figure 6B-III**) the nodular structures were in a formation stage earlier with respect to the previous condition. When *S. meliloti* was exposed to 10°C for a second time, threads were evidenced only after 14 dpi without the formation of microscopically visible nodular structures (**Figure 6B-IV**), reflecting serious

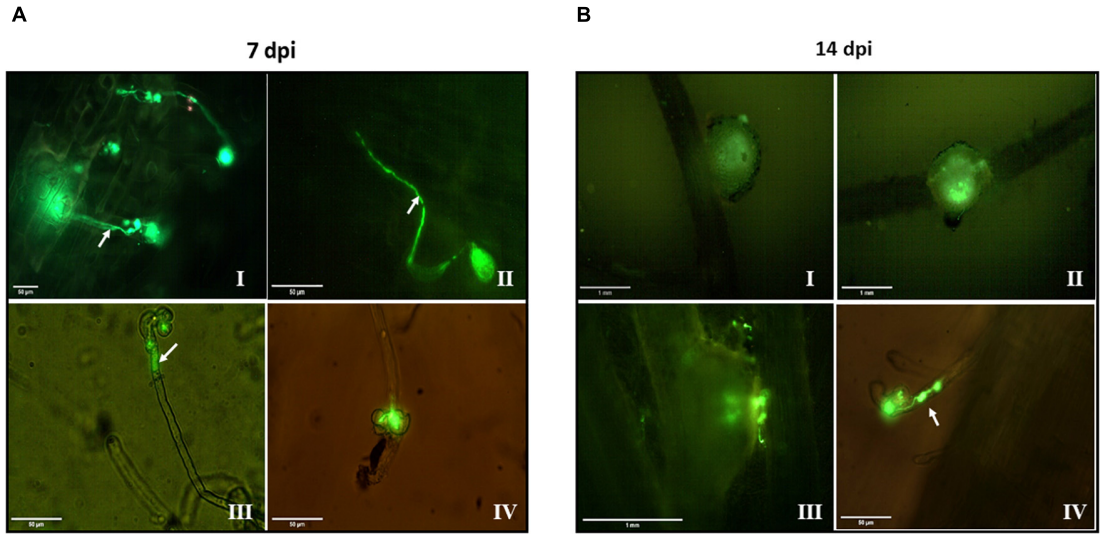

FIGURE 6 | Effect of temperature changes on the symbiotic behavior of *Gfp*-expressing *S. meliloti* with roots of *Medicago sativa*. Alfalfa roots of 7 **(A)** and 14 **(B)** dpi with *Gfp*-expressing *S. meliloti* grown under control conditions **(I)** and exposed to 10°C **(II)**, 40°C **(III)**, and 10°C **(IV)**. Arrows indicate infection threads generated by *S. meliloti* within root hairs. A culture of *Gfp*-expressing *S. meliloti* (200 mL) was grown to stationary phase at 28°C and then the thermal treatment applied (10°C–40°C–10°C). After exposure to each temperature for 24 h, an aliquot of 50 mL of culture was separated, centrifuged, and the biomass resuspended in physiological solution up to an CFU mL^{-1} of 1×10^9. Then an aliquot of that suspension (1 mL per plant) was used for inoculation tests. After 7 and 14 dpi, plants were removed, and the roots visualized in a fluorescence microscope at a 10 or 40 × magnification for nodules and infection thread respectively. Bars, 50 μm for panels **(A I–IV, B IV)**, 1 mm for panels **(B I–III)**.

problems to establish the symbiotic interaction with *M. sativa* at least until then.

DISCUSSION

In the present study, we put a dynamical insight on the capability of *S. meliloti* to respond in an adaptive manner to the fluctuations in a physical environmental variable, such as the temperature, which is crucial for controlling its development, growth, and viability.

The results obtained in the present work indicate that both *S. meliloti* membranes can sense differentially the cyclic changes in *T*. All the systems studied (WC, OM, and IM) respond dynamically to the changes in temperature, exhibiting a hysteresis along the cooling–heating–cooling cycle. The variation in P_{DPH} in WC and IM followed the expected directions, increasing upon cooling (more ordered, more anisotropic system) and decreasing upon heating (less ordered, more isotropic system). However, $P_{TMA\text{-}DPH}$ in WC and those of P_{DPH} in isolated OM implied responses to *T* changes that occurred in the direction opposite to that expected. These results can be understood if we consider that OM, present in WC as well as in the isolated OM fraction, includes LPS in its outer leaflet. The polysaccharide moiety of LPS forms a hydrophilic layer close to the OM surface, which would represent a barrier that impairs the penetration of hydrophobic substances, such as DPH to the inner cell compartments and retain and concentrate hydrophilic substances such as TMA-DPH. This would explain the relatively low FI_{DPH} and high $FI_{\text{TMA-DPH}}$ measured in O- containing samples (see **Supplementary Figure 1**). However, because the impairment would not be absolute in WC and is absent in IM, the DPH molecules that reach the IM would find an environment capable of exhibiting P_{DPH} changes that accompany the *T*-induced anisotropy dynamics (**Figures 2A,B**). Confirming this hypothesis, this behavior was not observed in OM but appeared in MLVs prepared with the lipids extracted from OM (isolated from control cells of *S. meliloti*) which lack the LPS (**Supplementary Figure 2**). The retention of TMA-DPH within the LPS layer implies that the $P_{TMA\text{-}DPH}$ would be coupled to the dynamics of the polysaccharide moiety of LPS in the outermost part of the cell envelope. This hydrophilic environment can be envisioned as a macromolecular crowded media highly hydrated in which most of the water molecules are tightly bound (structured) to the hydrophilic surfaces (Clop et al., 2014). In these conditions, the properties of water as a solvent are reduced compared with bulk water and can be modulated by the physicochemical properties of the system (*T*, ionic strength, etc.). The solubility and, thus, the partitioning of TMA-DPH within this membrane region would be reduced at low temperature. We can envision that lowering *T*, TMA-DPH could be expelled from the membrane toward the isotropic bulk water, which is reflected by a lowering of $P_{TMA\text{-}DPH}$, the opposite to what would be expected if this probe was located in a lipid bilayer. This rationale and the faster dynamics of a polymer compared with a lipid bilayer (Clop et al., 2014) also explains that the *T*-induced changes in $P_{TMA\text{-}DPH}$ were faster than those of P_{DPH} (**Figure 2A**). Other photophysical phenomena should be considered to interpret the opposite behavior of P_{DPH} in OM and IM and that of $P_{TMA\text{-}DPH}$. In this sense, the effect of decreasing the polarity and water

availability of the environment (e.g., in the polymeric LPS regions at low temperature) can increase the emission lifetimes (|) of both probes, and in the case of TM-DPH, the transition angle (⟨) between the excitation and emission dipoles may also increase. According to the Perrin equation, both phenomena contribute to the *P* decrease within the LPS region of OM when *T* becomes lower (see **Supplementary Material** for details).

It is vitally important that bacteria maintain the fluidity of their membranes at optimal values to ensure physiological homeostasis and the integrity of all the processes that occur in them. This fluidity control process, called homeoviscous adaptation, was first demonstrated in *E. coli* by observing that membrane fluidity remains relatively constant at various temperatures (Sinensky, 1974). In Gram-negative WCs, it is very difficult to test the homeoviscous adaptation of each membrane due to the lack of knowledge of the location of the fluorescent probes that are used to measure fluorescence polarization. In this work, we were able to verify that DPH is a good indicator of IM behavior. Our results also highlight that, for the correct interpretation of data obtained with DPH in OM and with TMA-DPH in both OM and IM (atypical at first sight), it is required to consider the physicochemical properties of the environment in which they are located, their partitioning properties, and the photophysical behavior of these probes (see **Supplementary Material**). Thanks to these results, we differentially monitor the behavior of each *S. meliloti* membrane during the thermal cycle in WC. After 24 h of exposure to the first cooling and subsequent heating, both membranes presented $P_{\mathrm{DPH/TMA\text{-}DPH}}$ values similar to the control (**Figure 3**), indicating that, under these conditions, there are compensatory mechanisms that allow achieving homeoviscous adaptation. At the end of the thermal cycle, the bacteria seemed to have weakened the control on its membrane fluidity.

The fluidity control was accompanied by modifications in the composition of PL; thus, the content of PC was strongly regulated at all temperatures tested in both OM and IM. Note that PC can be synthesized from PE *via* successive methylations catalyzed by pmt enzymes (Sohlenkamp and Geiger, 2016). This may explain that, in both OM and IM, mainly the exposure to 40°C led to the increase in PC accompanied by a decrease in PE. The role of PLs, mainly PC, in relation to different environmental conditions in *Bradyrhizobium* TAL1000 and SEMIA6144 (Paulucci et al., 2011, 2013; Cesari et al., 2018) and in *S. meliloti* (present work) may be related to the stabilization of the membrane because of the important function of phospholipids such as PC to form a stable lamellar structure of cell membranes, facilitated by its geometrical shape and physicochemical properties (Boumann et al., 2006). We propose that, in these types of bacteria, PC variations may be a universal response. This is not the case of the model bacterium *E. coli*, which lacks PC in the membrane (Geiger et al., 2013).

In general terms, the *T* changes applied to *S. meliloti* cause the same modifications in the composition of PL in OM and IM. An exception was the increase in the thermal-induced content of LPE in OM during the second exposure to 10°C, which was a distinctive feature between both membranes. LPE derives from the PLA-catalyzed hydrolysis of PE, and this enzyme is present in the OM of Gram-negative bacteria (Song and Rhee, 2001; Beney et al., 2007). The role of lysophospholipids in bacteria remains poorly studied; it has been proposed that the inverted cone shape of this lipid molecule could alleviate the curvature stress caused on the membrane in certain situations (Zheng et al., 2017). LPE was also found to become dominant in the OM of *Y. pseudotuberculosis* and *B.* SEMIA6144 after shifting the growth temperature from 8 to 37°C and under water deficit, respectively (Davydova et al., 2016; Cesari et al., 2018). Although both exposures to 10°C caused increased content of LPE in OM, the effect was more significant in the second exposure at 10°C (after the incubation at 40°C). Whereas in the first incubation at 10°C, the ΔT was −18°C compared with the previous state, the wider ΔT (−30°C) of the second exposure to 10°C may be responsible for the greater disturbance observed in the OM.

The control of the degree of unsaturation of FA is one of the mechanisms widely used by cells to maintain lipid packing, membrane microviscosity, and water permeability (Lande et al., 1995; de Mendoza and Pilon, 2019). In *S. meliloti,* the variations in U/S_{IM} occurred in the direction expected to compensate for the *T*-induced changes in membrane microviscosity because a decrease in *U/S* is expected to result in stabilization of membranes after heating. Surprisingly, after 24 h at 40°C, U/S_{OM} did not show variations with respect to initial 10°C, indicating the presence of other mechanisms to compensate for the perturbation induced by *T* in OM, such as the shortening of the acyl chain due to a decrease of 18:0 from 16:0. It is important to note that the change in the value of U/S_{OM} during the transition from 40 to 10°C occurs precisely in the opposite direction to that which would be expected to counteract the fluidizing effect; this could explain why, in this condition, *S. meliloti* is unable to restore the microviscosity of OM. From the few bibliographic data available on the response of OM from Gram-negative bacteria to temperature changes, the work of Davydova et al. (2016) can be cited, and they show a difference between OM and IM of *Y. pseudotuberculosis* subject to a temperature shock from 8 to 45°C. They found that IM was the membrane fraction that exhibited some features of thermal adaptation (*U/S* ratio decreased from 2.3 to 1.5), whereas in OM, although the authors claim that there were no significant changes in the composition of FA, the response observed was clearly contrary to that of IM. It is important to highlight that the biochemical changes observed are due to thermal cycling and not to bacteria aging because no significant variations were observed in FA and PL composition of *S. meliloti* under control conditions (28°C) when it was analyzed at different times (see **Supplementary Table 3**).

The *P* data obtained in MLVs prepared with the lipids extracted from OM and IM allow establishing a direct correlation between the lipid composition and the response to the *T* disturbance in the membrane. In conjunction, variations in FA and PL compositions indicate that OM and IM have their own mechanisms to respond to thermal perturbation and maintain their fluidity at optimal values, in IM the control of the degree of unsaturation being the most important. The vision of *S. meliloti* from this perspective allowed us to highlight the differences in the response to *T* of WC and the isolated OM and IM. Furthermore, considering other Gram-negative bacteria species in the response to *T* (Paulucci et al., 2011, 2013, 2015), it can be suggested that

IM is the most appropriate target to understand adaptations to thermal-induced perturbations. It is also worth noting that, although during the second exposure at 10°C, the fluidity of the *S. meliloti* membranes was not restored to control values, IM responded adequately. However, it seems that these changes did not allow reaching an optimum fluidity, probably because the long-time incubation at 40°C affected the cell viability and plasticity of their membranes to respond.

Underlying the process of homeoviscous adaptation is the stress-triggered catalytic activity of membrane bound enzymes (Solís-Oviedo et al., 2012) and/or membrane sensors related to signal transduction mechanisms (Geiger et al., 2021). Thus, the membrane remodeling in composition and organization may operate as an on/off switch on the controlling mechanisms.

The *S. meliloti* inability to control the fluidity of both membranes in the second exposure to 10°C was correlated with a delay in the formation of early symbiotic structures, such as infection threads and nodules, with respect to the other conditions, demonstrating that that maintenance of envelope integrity in *S. meliloti* is critical to achieve an effective symbiosis. The cell envelope of rhizobia is considered an important player during the establishment of symbiosis during the initial exchange of signals between the bacteria and the root (Hubac et al., 1994) as well as during their survival within the infection thread (Scheidle et al., 2005) and then in the symbiosome (Bolaños et al., 2004). Despite this and even though some components of the bacterial surface are described as essential in these processes (polysaccharides, LPS), the maintenance of integrity of the membranes after *T* disturbance had not yet been investigated in relation to the process of symbiosis.

Considering the limited available information in rhizobia on the OM and IM composition, its role in adaptation to stressful conditions, and in the symbiotic process, the data presented here could be a starting point for the design of bacteria with permanent changes in lipid composition through cell membrane engineering methods.

DATA AVAILABILITY STATEMENT

The raw data supporting the conclusions of this article will be made available by the authors, without undue reservation.

AUTHOR CONTRIBUTIONS

NP, MD, and MP designed the research and coordinated the study. NP carried out the experiments. MB and AC collaborated with fluorescence anisotropy measurements and the interpretation of the data. NP and MP wrote the manuscript. All authors contributed to the article and approved the submitted version.

FUNDING

This study was financially supported by PIP CONICET (Grant No. 11220150100232CO), SeCyT-UNRC (Grant No. 161/126), PICT (Grant No. 1065/15), PICT (Grant No. 4162/18), SeCyT-UNC (Grant No. 33620180100680CB) PICT (Grant No. 4420/2018), and PIP CONICET (Grant No. 11220200103025CO).

SUPPLEMENTARY MATERIAL

The Supplementary Material for this article can be found online at: https://www.frontiersin.org/articles/10.3389/fmicb.2021.652477/full#supplementary-material

REFERENCES

Balogh, G., Maulucci, G., Gombos, I., Horváth, I., Török, Z., Péter, M., et al. (2011). Heat stress causes spatially-distinct membrane re-modelling in k562 leukemia cells. *PLoS One* 6:e21182. doi: 10.1371/journal.pone.0021182

Basconcillo, L., Zaheer, R., Finan, T., and McCarry, B. (2009). A shotgun lipidomics approach in *Sinorhizobium meliloti* as a tool in functional genomics. *J. Lipid Res.* 50, 1120–1132. doi: 10.1194/jlr.M800443-JLR200

Beney, L., Simonin, H., and Mille, Y. (2007). Membrane physical state as key parameter for the resistance of the gram-negative *Bradyrhizobium japonicum* to hyperosmotic treatments. *Arch. Microbiol.* 187, 387–396. doi: 10.1007/s00203-006-0203-8

Bligh, E., and Dyer, W. (1959). A rapid method of total lipid extraction and purification. *Can. J. Biochem. Physiol.* 37, 911–918. doi: 10.1139/o59-099

Bolaños, L., Redondo-Nieto, M., Rivilla, R., Brewin, N., and Bonilla, I. (2004). Cell surface interactions of *Rhizobium* bacteroids and other bacterial strains with symbiosomal and peribacteroid membrane components from Pea nodules. *Mol. Plant Microbe Interact.* 17, 216–223. doi: 10.1094/MPMI.2004.17.2.216

Bos, M., Robert, V., and Tommassen, J. (2007). Biogenesis of the Gram-Negative bacterial outer membrane. *Annu. Rev. Microbiol.* 61, 191–214. doi: 10.1146/annurev.micro.61.080706.093245

Boumann, H. A., Gubbens, J., Koorengevel, M. C., Oh, C. S., Martin, C. E., Heck, A. J., et al. (2006). Depletion of phosphatidylcholine in yeast induces shortening and increased saturation of the lipid acyl chains: evidence for regulation of intrinsic membrane curvature in a eukaryote. *Mol. Biol. Cell* 17, 1006–1017. doi: 10.1091/mbc.e05-04-0344

Cesari, A. B., Paulucci, N. S., Biasutti, M. A., Morales, G., and Dardanelli, M. S. (2018). Changes in the lipid composition of *Bradyrhizobium* cell envelope reveal a rapid response to water defcit involving lysophosphatidylethanolamine synthesis from phosphatidylethanolamine in outer membrane. *Res. Microbiol.* 169, 303–312. doi: 10.1016/j.resmic.2018.05.008

Cesari, A. B., Paulucci, N. S., Biasutti, M. A., Reguera, Y. B., Gallarato, L. A., Kilmurray, C., et al. (2016). Reorganization of *Azospirillum brasilense* cell membrane is mediated by lipid composition adjustment to maintain optimal fluidity during water deficit. *J. Appl. Microbiol.* 120, 185–194. doi: 10.1111/jam.12994

Clop, E. M., Chattah, A. K., and Perillo, M. A. (2014). Water and membrane dynamics in suspensions of lipid vesicles functionalized with polyethylene glycols. *J. Phys. Chem. B* 118, 6150–6158. doi: 10.1021/jp410894x

Davydova, L., Bakholdina, S., Barkina, M., Velansky, P., Bogdanov, M., and Sanina, N. (2016). Effects of elevated growth temperature and heat shock on the lipid composition of the inner and outer membranes of *Yersinia pseudotuberculosis*. *Biochimie* 123, 103–109. doi: 10.1016/j.biochi.2016.02.004

de Maagd, R., and Lugtenberg, B. (1986). Fractionation of *Rhizobium leguminosarum* cells into outer membrane, cytoplasmic membrane, periplasmic, and cytoplasmic components. *J. Bacteriol.* 167, 1083–1085. doi: 10.1128/jb.167.3.1083-1085.1986

de Mendoza, D., and Pilon, M. (2019). Control of membrane lipid homeostasis by lipid-bilayer associated sensors: a mechanism conserved from bacteria to humans. *Prog. Lipid Res.* 76:100996. doi: 10.1016/j.plipres.2019.100996

do Canto, A., Robalo, J., Santos, P., Carvalho, A., Ramalho, J., and Loura, L. (2016). Diphenylhexatriene membrane probes DPH and TMA-DPH: A comparative molecular dynamics simulation study. *Biochim. Biophys. Acta* 11, 2647–2661. doi: 10.1016/j.bbamem.2016.07.013

England, L., Gorzelak, M., and Trevors, J. (2003). Growth and membrane polarization in *Pseudomonas aeruginosa* UG2 grown in randomized microgravity in a high aspect ratio vessel L.S. *Biochim. Biophys. Acta* 1624, 76–80. doi: 10.1016/j.bbagen.2003.09.012

Ernst, R., Ejsing, C., and Antonny, B. (2016). Homeoviscous adaptation and the regulation of membrane lipids. *J. Mol. Biol.* 428, 4776–4791. doi: 10.1016/j.jmb.2016.08.013

Gage, D. (2002). Analysis of infection thread development using Gfp- and DsRed expressing *Sinorhizobium meliloti*. *J. Bacteriol.* 184, 7042–7046. doi: 10.1128/JB.184.24.7042-7046.2002

Gage, D. (2004). Infection and invasion of roots by symbiotic, nitrogen-fixing rhizobia during nodulation of temperate legumes. *Microbiol. Mol. Biol. Rev.* 68, 280–300. doi: 10.1128/MMBR.68.2.280-300.2004

Gage, D., and Margolin, W. (2000). Hanging by a thread: invasion of legume plants by rhizobia. *Curr. Opin. Microbiol.* 3, 613–617. doi: 10.1016/s1369-5274(00)00149-1

Gage, D., Bobo, T., and Long, S. (1996). Use of green fluorescent protein to visualize the early events of symbiosis between *Rhizobium meliloti* and Alfalfa (*Medicago sativa*). *J. Bacteriol.* 178, 7159–7166. doi: 10.1128/jb.178.24.7159-7166.1996

Geiger, O., López-Lara, I. M., and Sohlenkamp, C. (2013). Phosphatidylcholine biosynthesis and function in bacteria. *Biochim. Biophys. Acta* 1831, 503–513. doi: 10.1016/j.bbalip.2012.08.009

Geiger, O., Sohlenkamp, C., Vera-Cruz, D., Medeot, D., Martínez-Aguilar, L., Sahonero-Canavesi, D. X., et al. (2021). ExoS/ChvI two-component signal-transduction system activated in the absence of bacterial phosphatidylcholine. *Front. Plant Sci.* 12:678976. doi: 10.3389/fpls.2021.678976

Hacker, S., Gödeke, J., Lindemann, A., Mesa, S., Pessi, G., and Narberhaus, F. (2008). Global consequences of phosphatidylcholine reduction in *Bradyrhizobium japonicum*. *Mol. Genet. Genomics* 280, 59–72. doi: 10.1007/s00438-008-0345-2

Hirsch, A., Bang, M., and Ausubel, F. (1983). Ultrastructural analysis of ineffective alfalfa nodules formed by nif::Tn5 mutants of *Rhizobium meliloti*. *J. Bacteriol.* 155, 367–380. doi: 10.1128/jb.155.1.367-380.1983

Hubac, C., Ferran, J., Tremolieres, A., and Kondorosi, A. (1994). Luteolin uptake by *Rhizobiurn meliloti*: evidence for several steps including an active extrusion process. *Microbiology* 140, 2769–2774. doi: 10.1099/00221287-140-10-2769

Jones, H., Kobayashi, H., Davies, B., Taga, M., and Walker, G. (2007). How rhizobial symbionts invade plants: the *Sinorhizobium–Medicago* model. *Nat. Rev. Microbiol.* 5, 619–633. doi: 10.1038/nrmicro1705

Kates, M. (1972). *Techniques of Lipidology: Isolation, Analysis and Identification of Lipids*. Amsterdam: North Holland Publishing Company.

Kijne, J. (1992). "The Rhizobium infection process," in *Biological Nitrogen Fixation*, eds G. Stacey, R. H. Burris, and H. J. Evans (New York, NY: Chapman and Hall), 349–398.

Konopasek, I., Strzalka, K., and Svobodova, J. (2000). Cold shock in *Bacillus subtilis*: deferent effects of benzyl alcohol and ethanol on the membrane organization and cell adaptation. *Biochim. Biophys. Acta* 1464, 18–26. doi: 10.1016/s0005-2736(99)00240-0

Kuhry, J. G., Duportail, G., Bronner, C., and Laustriat, G. (1985). Plasma membrane fluidity measurements on whole living cells by fluorescence anisotropy of trimethylammoniumdiphenylhexatriene. *Biochim. Biophys. Acta* 845, 60–67. doi: 10.1016/0167-4889(85)90055-2

Lakowicz, J. R. (1999). *Principles of Fluorescence Spectroscopy*, 2nd Edn. New York, NY: Kluwer Academic.

Lande, M. B., Donovan, J. M., and Zeidel, M. L. (1995). The relationship between membrane fluidity and permeabilities to water, solutes, ammonia, and protons. *J. Gen. Physiol.* 106, 67–84. doi: 10.1085/jgp.106.1.67

Lentz, B. R. (1989). Membrane fluidity as detected by diphenylhexatriene probes. *Chem. Phys. Lipids* 50, 171–190. doi: 10.1016/0009-3084(89)90049-2

Lugtenberg, E. J. J., and Peters, R. (1976). Distribution of lipids in cytoplasmic and outer membranes of *Escherichia coli* K12. *Biochim. Biophys. Acta* 441, 38–47. doi: 10.1016/0005-2760(76)90279-4

Mizuno, T., and Kageyama, M. (1978). Separation and characterization of the outer membrane of *Pseudomonas aeruginosa*. *J. Biochem.* 84, 179–191. doi: 10.1093/oxfordjournals.jbchem.a132106

Morrison, W., and Smith, L. (1964). Preparation of fatty acid methyl esters and dimethylacetals from lipids with boron fluoride. *J. Lipid Res.* 5, 600–608.

Paulucci, N. S., Dardanelli, M. S., and de Lema, M. G. (2014). Biochemical and molecular evidence of a 9 fatty acid desaturase from *Ensifer meliloti* 1021. *Microbiol. Res.* 169, 463–468. doi: 10.1016/j.micres.2013.08.003

Paulucci, N. S., Gallarato, L. A., Reguera, Y. B., Vicario, J. C., Cesari, A. B., de Lema, M. G., et al. (2015). *Arachis hypogaea* PGPR isolated from Argentine soil modifies its lipids components in response to temperature and salinity. *Microbiol. Res.* 173, 1–9. doi: 10.1016/j.micres.2014.12.012

Paulucci, N. S., Medeot, D. B., Dardanelli, M. S., and de Lema, M. G. (2011). Growth temperature and salinity impact fatty acid composition and degree of unsaturation in peanut nodulating rhizobia. *Lipids* 46, 435–444. doi: 10.1007/s11745-011-3545-1

Paulucci, N. S., Medeot, D. B., Woelke, M., Dardanelli, M. S., and de Lema, M. G. (2013). Monounsaturated fatty acid aerobic synthesis in *Bradyrhizobium* TAL1000 peanutnodulating is affected by temperature. *J. Appl. Microbiol.* 114, 1457–1467. doi: 10.1111/jam.12155

Peck, M. C., Fisher, R. F., and Long, S. R. (2006). Diverse flavonoids stimulate NodD1 binding to nod gene promoters in *Sinorhizobium meliloti*. *J. Bacteriol.* 188, 5417–5427. doi: 10.1128/JB.00376-06

Rolfe, B. G., Gresshoff, P. M., and Shine, J. (1980). Rapid screening for symbiotic mutants of *Rhizobium* and white clover. *Plant Sci. Lett.* 19, 277–284.

Sanchez, J., Turina, A., and Perillo, M. A. (2007). Spectroscopic probing of ortho-nitrophenol localization in phospholipid bilayers. *J. Photochem. Photobiol.* 89, 56–62. doi: 10.1016/j.jphotobiol.2007.08.004

Scheidle, H., Grob, A., and Niehaus, K. (2005). The Lipid A substructure of the *Sinorhizobium meliloti* lipopolysaccharides is sufficient to suppress the oxidative burst in host plants. *New Phytol.* 165, 559–566. doi: 10.1111/j.1469-8137.2004.01214.x

Sieberer, B. J., Timmers, A. C., and Emons, A. M. (2005). Nod factors alter the microtubule cytoskeleton in *Medicago truncatula* root hairs to allow root hair reorientation. *Mol. Plant Microbe Interact.* 18, 1195–1204. doi: 10.1094/MPMI-18-1195

Siebers, M., Brands, M., Wewer, V., Duan, Y., Hölzl, G., and Dörmann, P. (2016). Lipids in plant–microbe interactions. *Biochim. Biophys. Acta* 1861, 1379–1395. doi: 10.1016/j.bbalip.2016.02.021

Sinensky, M. (1974). Homeoviscous adaptation a homeostatic process that regulates the viscosity of membrane lipids in *Escherichia coli*. *Proc. Natl. Acad. Sci. U.S.A.* 71, 522–525. doi: 10.1073/pnas.71.2.522

Sohlenkamp, C., and Geiger, O. (2016). Bacterial membrane lipids: diversity in structures and pathways. *FEMS Microbiol. Rev.* 40, 133–159. doi: 10.1093/femsre/fuv008

Sohlenkamp, C., Lopez-Lara, I. M., and Geiger, O. (2003). Biosynthesis of phosphatidylcholine in bacteria. *Prog. Lipid Res.* 42, 115–162. doi: 10.1016/s0163-7827(02)00050-4

Solís-Oviedo, R., Morales, F., Geiger, O., and Sohlenkamp, C. (2012). Functional and topological analysis of phosphatidylcholine synthase from *Sinorhizobium meliloti*. *Biochim. Biophys. Acta* 1821, 573–581. doi: 10.1016/j.bbalip.2012.01.016

Song, J. K., and Rhee, J. S. (2001). Enhancement of stability and activity of phospholipase A in organic solvents by directed evolution. *Biochim. Biophys. Acta Protein Struct.* 1547, 370–378. doi: 10.1016/s0167-4838(01)00204-7

Tighe, S. W., de Lajudie, P., Dipietro, K., Lindström, K., Nick, G., and Jarvis, B. D. (2000). Analysis of cellular fatty acids and phenotypic relationships of *Agrobacterium, Bradyrhizobium, Mesorhizobium, Rhizobium* and *Sinorhizobium* species using the Sherlock microbial identification system. *Int. J. Syst. Evol. Microbiol.* 50(Pt 2), 787–801. doi: 10.1099/00207713-50-2-787

Timmers, A., Auriac, M., and Truchet, G. (1999). Refined analysis of early symbiotic steps of the *Rhizobium-Medicago* interaction in relationship with

microtubular cytoskeleton rearrangements. *Development* 126, 3617–3628. doi: 10.1242/dev.126.16.3617

Trevors, J. T. (2003). Fluorescent probes for bacterial cytoplasmic membrane research. *J. Biochem. Biophys. Methods* 57, 87–103. doi: 10.1016/s0165-022x(03)00076-9

van Brussel, A., Tak, T., Boot, K., and Kijne, J. (2002). Autoregulation of root nodule formation: signals of both symbiotic partners studied in a split-root system of *Vicia sativa* subsp. Nigra. *Mol. Plant Microbe Interact.* 15, 341–349. doi: 10.1094/MPMI.2002.15.4.341

Yamazaki, M., Ohnishi, S., and Ito, T. (1989). Osmoelastic coupling in biological structures: decrease in membrane fluidity and osmophobic association of phospholipid vesicles in response to osmotic stress. *Biochemistry* 28, 3710–3715. doi: 10.1021/bi00435a013

Zheng, L., Lina, Y., Lua, S., Zhanga, J., and Bogdanov, J. (2017). Biogenesis, transport and remodeling of lysophospholipids in Gram-negative bacteria. *Biochim. Biophys. Acta* 1862, 1404–1413. doi: 10.1016/j.bbalip.2016.11.015

Conflict of Interest: The authors declare that the research was conducted in the absence of any commercial or financial relationships that could be construed as a potential conflict of interest.

frontiers in Microbiology

ORIGINAL RESEARCH
published: 28 January 2022
doi: 10.3389/fmicb.2021.732288

The Cpx Stress Response Regulates Turnover of Respiratory Chain Proteins at the Inner Membrane of *Escherichia coli*

*Valeria Tsviklist[1], Randi L. Guest[2] and Tracy L. Raivio[1]**

[1] Department of Biological Sciences, University of Alberta, Edmonton, AB, Canada, [2] Lewis Thomas Laboratory, Department of Molecular Biology, Princeton University, Princeton, NJ, United States

The Cpx envelope stress response is a major signaling pathway monitoring bacterial envelope integrity, activated both internally by excessive synthesis of membrane proteins and externally by a variety of environmental cues. The Cpx regulon is enriched with genes coding for protein folding and degrading factors, virulence determinants, and large envelope-localized complexes. Transcriptional repression of the two electron transport chain complexes, NADH dehydrogenase I and cytochrome bo_3, by the Cpx pathway has been demonstrated, however, there is evidence that additional regulatory mechanisms exist. In this study, we examine the interaction between Cpx-regulated protein folding and degrading factors and the respiratory complexes NADH dehydrogenase I and succinate dehydrogenase in *Escherichia coli*. Here we show that the cellular need for Cpx-mediated stress adaptation increases when respiratory complexes are more prevalent or active, which is demonstrated by the growth defect of Cpx-deficient strains on media that requires a functional electron transport chain. Interestingly, deletion of several Cpx-regulated proteolytic factors and chaperones results in similar growth-deficient phenotypes. Furthermore, we find that the stability of the NADH dehydrogenase I protein complex is lower in cells with a functional Cpx response, while in its absence, protein turnover is impaired. Finally, we demonstrated that the succinate dehydrogenase complex has reduced activity in *E. coli* lacking the Cpx pathway. Our results suggest that the Cpx two-component system serves as a sentry of inner membrane protein biogenesis, ensuring the function of large envelope protein complexes and maintaining the cellular energy status of the cell.

Keywords: envelope stress response, envelope biogenesis, respiration, NADH dehydrogenase I, succinate dehydrogenase, protein folding and degradation, Cpx envelope stress response

OPEN ACCESS

Edited by:
Cristina Mazzoni, Sapienza University of Rome, Italy

Reviewed by:
Sujeet Kumar, The Ohio State University, United States
Viviana Andrea Rapisarda, Consejo Nacional de Investigaciones Científicas y Técnicas (CONICET), Argentina

****Correspondence:***
Tracy L. Raivio
traivio@ualberta.ca

Specialty section:
This article was submitted to Microbial Physiology and Metabolism, a section of the journal Frontiers in Microbiology

Received: *28 June 2021*
Accepted: *20 December 2021*
Published: *28 January 2022*

Citation:
Tsviklist V, Guest RL and Raivio TL (2022) The Cpx Stress Response Regulates Turnover of Respiratory Chain Proteins at the Inner Membrane of Escherichia coli. Front. Microbiol. 12:732288. doi: 10.3389/fmicb.2021.732288

INTRODUCTION

Gram-negative bacteria possess a unique cell envelope structure consisting of three principal layers: the outer membrane (OM), the peptidoglycan cell wall and the inner membrane (IM) (Ruiz et al., 2006; Silhavy et al., 2010). This complex multicomponent structure functions as a protective barrier, communicates changes in the external environment, and maintains the shape, stability, and rigidity of the cell (Ruiz et al., 2006; Holst et al., 2010; Silhavy et al., 2010). In addition, the bacterial envelope ensures successful host infection and colonization due to a multitude of

envelope-localized virulence factors, together with appropriate metabolism and growth of the cell (Hews et al., 2019). Bacteria have evolved a sophisticated regulatory network to maintain envelope homeostasis. Under conditions where the process of membrane biogenesis and hence envelope homeostasis is impaired, bacterial cells activate several stress response systems, including the CpxAR pathway.

CpxAR is a canonical two-component signal transduction system (TCS) that consists of the membrane-localized sensor histidine kinase CpxA and cytoplasmic response regulator CpxR (Grabowicz and Silhavy, 2017a; Delhaye et al., 2019a; Hews et al., 2019). Under non-inducing conditions, the phosphatase activity of CpxA maintains CpxR in a dephosphorylated or inactive state. When an inducing cue is present, CpxA autophosphorylates at a conserved histidine residue and transfers a phosphate group to CpxR (Raivio and Silhavy, 1997). The downstream targets of CpxR transcriptional regulation include genes whose products are involved, either directly or indirectly, in protein folding and degradation in the bacterial envelope (Pogliano et al., 1997; Raivio and Silhavy, 2001). The Cpx regulon is enriched with genes encoding virulence factors, small regulatory RNAs (sRNAs), multidrug efflux systems and peptidoglycan modifying factors (Raivio, 2014; Hews et al., 2019). Two auxiliary proteins involved in the Cpx regulatory pathway are the periplasmic protein CpxP, one of the most highly expressed members of the Cpx regulon, proposed to inhibit activation of CpxA, and the OM lipoprotein NlpE, which is thought to activate CpxA upon surface adhesion and to sense stresses related to defects in lipoprotein trafficking (Danese et al., 1995; Danese and Silhavy, 1998; Raivio et al., 1999; Otto and Silhavy, 2002; Grabowicz and Silhavy, 2017b; Delhaye et al., 2019b).

The Cpx system is triggered by a variety of signals, including alkaline pH, aminoglycoside antibiotics, NlpE overexpression, aberrant expression of Pap pilus subunits, and mutation of the IM protease FtsH (Danese et al., 1995; Nakayama and Watanabe, 1995; Jones et al., 1997; Mileykovskaya and Dowhan, 1997; Danese and Silhavy, 1998; Hung et al., 2001; Shimohata et al., 2002; Kohanski et al., 2008). These activating cues are related to potentially lethal accumulation of misfolded or mislocalized proteins at the bacterial envelope. To restore the integrity of the envelope, the Cpx response upregulates proteolytic factors and periplasmic protein folding factors, including the disulfide bond oxidoreductase DsbA, the peptidyl-prolyl isomerase PpiA, the chaperones Spy and CpxP (Danese and Silhavy, 1997, 1998; Pogliano et al., 1997; Raivio et al., 2000), and the protease/chaperone DegP (Cosma et al., 1995; Danese and Silhavy, 1997). For instance, non-productive assembly of P pili results in the activation of the Cpx pathway and subsequent upregulation of DegP, which degrades misfolded pilin subunits (Hung et al., 2001). Additionally, the Cpx pathway directly represses transcription of high molecular weight protein complexes as an adaptation to stresses that lead to protein misfolding (Raivio et al., 2013; Raivio, 2014; Hews et al., 2019). The electron transport chain (ETC) incorporates some of the largest multiprotein complexes in the *Escherichia coli* IM, making them a primary target of Cpx regulation (Guest et al., 2017).

The majority of ATP in the cell is produced via oxidative phosphorylation during aerobic growth. The ETC complexes convert the energy of reducing equivalents, such as NADH or $FADH_2$, into a proton electrochemical gradient across the membrane. This electrochemical gradient drives ATP synthesis via ATP synthase and for other energy consuming processes in the cell, including active transport and flagellar motion (Yoshida et al., 2001; Kaila et al., 2010; Price and Driessen, 2010; Borisov et al., 2011; Kaila and Wikström, 2021). The respiratory chain is composed of primary dehydrogenases and terminal oxidases coupled by the quinone pool. The first steps of electron transport are catalyzed by NADH dehydrogenase (NDH-I), the largest complex of the ETC, and the entry point for electrons carried by NADH (Brandt, 2006; Kerscher et al., 2008). In *E. coli*, the *nuo* operon contains 13 genes, *nuoA-N*, where *nuoC* encodes a fused version of NuoC and NuoD subunits (Braun et al., 1998; Price and Driessen, 2010; Friedrich et al., 2016). NDH-I is an L-shaped multisubunit structure composed of a hydrophobic membrane arm, protruding into the lipid bilayer, and a hydrophilic peripheral arm that extends into the cytoplasm (Hofhaus et al., 1991; Guénebaut et al., 1998; Baranova et al., 2007). The processes of proton translocation and quinone binding take place in the membrane arm consisting of NuoA, H, and J-N, whereas NADH oxidation is the function of the peripheral arm comprising NuoB, CD, E, F, G, and I subunits (Hofhaus et al., 1991).

Succinate dehydrogenase (SDH) is a unique membrane-bound enzyme that is a common component of the ETC and the tricarboxylic acid (TCA) cycle (Lestienne and Desnuelle, 1999). Within the TCA cycle, SDH oxidizes succinate to fumarate sequestering two electrons that are then used for the reduction of ubiquinone in the membrane (Yankovskaya et al., 2003). It is composed of four non-identical subunits encoded by the *sdhCDAB* operon, where SdhA and SdhB are the cytoplasmic catalytic subunits which contain the flavin adenine dinucleotide and iron-sulfur (Fe-S) cluster cofactors, respectively. SdhC and SdhD compose the membrane-integral part of the enzyme and contain the ubiquinone binding site and the heme b cofactor (Yankovskaya et al., 2003; Tran et al., 2006; Price and Driessen, 2010). The absence of either SdhC or SdhD structural components leads to unstable SDH activity in the cytoplasm and perturbs ubiquinone reduction at the IM (Nakamura et al., 1996).

The Cpx-mediated downregulation of *nuo* (NDH-I) and *cyo* (cytochrome *bo3*) operons, and its effect on aerobic respiration were recently demonstrated in enteropathogenic *E. coli* (EPEC), which aligns with previous RNA transcriptome findings (Raivio et al., 2013; Guest et al., 2017; Dbeibo et al., 2018). These studies proposed that, in the presence of envelope stress, *de novo* synthesis of these complexes is repressed to reduce protein traffic within the IM, and maintenance of existing complexes is performed via upregulation of the Cpx-regulated protein folding and degrading factors (Guest et al., 2017). While transcriptional repression of the genes encoding NDH-I and cytochrome bo_3 complexes of ETC has been described, additional levels of regulation remain to be investigated.

In this study, we show that the Cpx pathway regulates the expression of the SDH enzyme transcriptionally and

provide evidence that Cpx-dependent regulation extends beyond transcriptional repression of the ETC complexes. We describe the Cpx-dependent regulation of protein turnover of the NuoA subunit of the NDH-I complex and identify several Cpx-regulated protein folding and degrading factors associated with this regulation. Intriguingly, our data suggest that in the absence of the Cpx pathway the function of the SDH complex is impaired, which suggests that the Cpx response plays an essential role in maintaining the energy status of the cell, ensuring the stability, activity, and proper turnover of the ETC complexes.

MATERIALS AND METHODS

Bacterial Strains and Growth Conditions

All bacterial strains and plasmids used in this study are listed in **Supplementary Table 1**. Cultures were grown and maintained in LB broth or M9 minimal medium (Difco) at 37°C with shaking at 225 rpm, with the exception of strains bearing the *cpxA24* mutation, which were grown at 30°C in the presence of amikacin (3 μg/ml) to prevent accumulation of suppressors as previously described (Raivio et al., 1999). Isopropyl-β-D-thiogalactopyranoside (IPTG, Invitrogen) was added to a concentration of 0.1 mM to induce gene expression from pCA24N- and pMPM-K3-based vectors. Antibiotics (Sigma) were added as necessary at the following concentrations: chloramphenicol (Cam), 25 μg/mL; kanamycin (Kan), 30 or 50 μg/mL; ampicillin (Amp), 100 μg/mL; spectinomycin (Spc), 25 μg/ml.

Strain and Plasmid Construction

All BW25113 mutants were taken from the Keio collection (Baba et al., 2006). An MC4100 Δ*cpxR* knockout mutant was generated using P1 transduction to move the desired mutant allele from the Keio collection (Baba et al., 2006) into wildtype MC4100 as previously described (Silhavy et al., 1984). The inducible pCA24N-based plasmids used in this study were obtained from the ASKA collection (Kitagawa et al., 2005). Transcriptional luminescent reporters containing the promoter regions of *cpxP* and *nuoA* were constructed as previously described (Price and Raivio, 2009; Wong et al., 2013; Guest et al., 2017). The p*sdhC*::*lux* reporter was constructed similarly. Briefly, the promoter region of *sdhC* gene was amplified by PCR, using PsdhCFwdCln and PsdhCRevCln primers (**Supplementary Table 2**). Purified PCR products and the pJW15 vector (MacRitchie et al., 2008) were digested with *Eco*RI and *Bam*HI (Invitrogen), and the insert was ligated upstream of the *luxABCDE* operon in the pJW15 plasmid. Correct insertion of the promoter sequence was verified by PCR and sequencing using pNLP10F and pNLP10R primers (**Supplementary Table 2**).

For the construction of pTrc-*nlpE* vector, *nlpE* was amplified via PCR with recombinant Taq polymerase (Invitrogen) using nlpE_NcoI_F and nlpE_WT_*Hin*dIII_R primers (**Supplementary Table 2**). PCR products were purified using a QIAGEN QIAQuick PCR purification kit according to the manufacturers protocol. Amplified *nlpE* was digested along with purified pTrc99A using Fast Digest *Eco*RI and *Hin*dIII (Thermo Scientific). Digests were purified using the aforementioned PCR purification kit and were then ligated together using T4 DNA ligase. Ligations were then transformed into One Shot TOP10 chemically competent cells (Thermo Fisher). Correct insertion of the *nlpE* sequence was verified by PCR and sequencing using pTrc99A_F and pTrc99A_R primers (**Supplementary Table 2**).

The pMPM-NuoA-3 × FLAG plasmid was constructed by amplifying *nuoA* from the E2348/69 chromosome via PCR using primers nuoAFLAGFwd and nuoAFLAGrev (**Supplementary Table 2**). Primer nuoAFLAGrev contains the nucleotide sequence to insert a triple FLAG-tag directly upstream of the *nuoA* stop codon. PCR was performed using high-fidelity phusion DNA polymerase (ThermoFisher) according to the manufacturers protocol with the addition of 10% betaine. The DNA band corresponding to *nuoA*-3 × FLAG DNA was gel extracted and cleaned using the GeneJet gel purification kit (Fermentas). Both *nuoA*-3 × FLAG and pMPM-K3 DNA were digested with the *Hin*dIII and *Xba*I restriction endonucleases (Invitrogen) according to the manufacturers protocol. *nuoA*-3 × FLAG DNA was then ligated downstream of an IPTG inducible P*lac* promoter in the pMPM-K3 vector and transformed into One Shot TOP10 chemically competent *E. coli* (Invitrogen) as per the manufacturer's protocol. PCR and DNA sequencing were used to confirm the presence of *nuoA*-3 × FLAG fragment within pMPM-K3 using M13F and M13R primers (**Supplementary Table 2**). All DNA sequencing was performed by The University of Alberta Molecular Biology Services Unit (MBSU). All plasmids in this study were transformed into *E. coli* strains via chemical competency (Silhavy et al., 1984).

Luminescence Assay

Strains containing p*cpxP*::*lux*, p*sdhC*::*lux*, or p*nuoA*::*lux* reporter plasmids were grown overnight in LB broth with shaking at 37°C. Cells were pelleted by centrifugation and washed twice with phosphate-buffered saline (PBS). The cell density was standardized to OD_{600} 1.0, pelleted, and resuspended in 1 mL of 1 × PBS. Standardized cultures were serially diluted 10-fold and 10 μL of each dilution was spotted onto M9 minimal agar containing 0.4% glucose, malic acid, or succinic acid (Sigma). Glucose-succinate gradient agar plates were created by pouring M9 containing 0.4% glucose into an angled plate. The layer was allowed to solidify in the inclined position and the second portion of agar containing 0.4% succinic acid was poured into the plate, placed on a level surface and allowed to solidify (Weinberg, 1959). Agar pH was adjusted to 7.0 with sodium hydroxide. Bacteria were grown for 24–48 h at 37°C statically. Luminescence was determined by imaging the light produced by strains using the UVP Colony Doc-It Imaging Station (Biorad). Luminescence was quantified using Fiji (ImageJ).

For the assay performed in liquid medium, bacteria were grown overnight as described above, subcultured at a dilution factor of 1:100 into 5 ml of fresh LB broth and incubated for 2 h at 37°C with aeration. 200 μL of each subculture was aliquoted into a black-bottomed 96-well plate, and luminescence in counts per second (CPS) and OD_{600} were measured every 1 h for 7 h post-subculture using a PerkinElmer VICTOR^{TM} X3 multilabel reader. Luminescence and OD_{600} values measured from a blank

well containing uncultured LB were subtracted from each sample. CPS was standardized to the OD_{600} to correct for differences in cell numbers between samples. All experiments contained three technical replicates and were carried out three times.

Western Blot Analysis

Samples used for Western blot analysis were prepared by diluting overnight cultures 1:100 into 25 ml fresh LB containing appropriate concentrations of antibiotics. Bacteria were grown at 37°C with shaking to an OD_{600} of ∼ 0.35. IPTG was added to a concentration of 0.1 mM and bacteria were grown for an additional 30 mins as before. 2 × 1 mL samples were collected. Cells were pelleted by centrifugation at 21,130 × *g* for 1 min. One sample was resuspended in 50 μL 2 × Laemmli sample buffer (Sigma) and the other sample was resuspended in 50 μL 1 × PBS. Protein concentration was determined from the sample resuspended in phosphate-buffered saline using the Pierce BCA protein assay kit (ThermoFisher) according to the manufacturers' protocol. Samples resuspended in 50 μL 2 × Laemmli sample buffer were denatured by boiling for 5 mins. Sample volumes were standardized according to their determined protein concentrations and separated on a 12% SDS gel at 110 V for 1.5 h in Tris–glycine running buffer (10% SDS, 250 mM Tris, 1.2 M glycine).

Proteins were transferred onto a nitrocellulose membrane via the trans-blot semi-dry transfer system (Bio-Rad) at 15 V for 22 mins using semi-dry Towbin transfer buffer (78 mM glycine, 1.3 mM SDS, 20% methanol). Membranes were blocked in 5% MTS (2.5% skim milk powder, 154 mM NaCl, 1 mM Tris) or 2% BSA (154 mM NaCl, 1 mM Tris, 1% Tween 20, 2% bovine serum albumin) for 1 h at room temperature with shaking at 10 rpm. Primary α-FLAG (Sigma, BioLegend), α-PhoA (Abcam) and α-RNAPα (BioLegend) antibodies were diluted by a factor of 1:5,000 into 5% MTS or 2% BSA. Membranes were incubated with the primary antibody for 1 h at either room temperature with shaking at approximately 10 rpm or overnight at 4°C with rocking. Following incubation with the primary antibody, membranes were washed for 5 mins in wash solution (154 mM NaCl, 1 mM Tris, 1% Tween 20) four times. Alkaline-phosphatase (AP) anti-rabbit secondary antibodies (Sigma) were diluted at a factor of 1:10,000 in 5% MTS and were used to detect the α-PhoA (Abcam) and α-FLAG (Sigma) primary antibodies. IRDye®680RD Goat anti-Mouse 925-68070 and IRDye®800CW Goat anti-Rabbit 925-32211 secondary antibodies (LI-COR) were diluted at a factor of 1:15,000 in 5% MTS and were used to detect the α-RNAPα (BioLegend) and α-FLAG (BioLegend) primary antibodies, respectively.

Membranes were then incubated with the secondary antibody for 1 h at room temperature with shaking at approximately 10 rpm. Membranes were washed following incubation with the secondary antibody as before. Proteins from the membranes incubated with AP secondary antibodies were detected using the Immun-Star alkaline phosphatase chemiluminescence kit (Bio-Rad). All membranes were imaged with the Bio-Rad ChemiDoc MP imaging system. Quantification of each band compared to the wildtype was performed using band intensity analysis in Fiji (ImageJ). Experiments were performed in biological triplicates, and a representative blot is shown in each case.

Protein Stability Assay

Bacteria were grown overnight in 5 mL LB at 37°C with shaking. The following day, bacteria were subcultured at a 1:100 dilution into 25 mL fresh LB and grown at 37°C with shaking to an OD_{600} ∼ 0.5. IPTG was then added to a final concentration of 0.1 mM and bacteria were grown to an OD_{600} of 1.0. 1 mL samples were collected and cells were pelleted by centrifugation at 21,130 × *g* for 1 min. After the supernatant was removed, cells were resuspended in 50 μL 2 × Laemmli sample buffer (Sigma). Immediately after the sample was removed, the protein synthesis inhibitor chloramphenicol was added to the remaining culture at a concentration of 100 μg/mL. The culture was incubated at 37°C and shaken at 225 rpm. 1 mL of culture was collected right before the addition of chloramphenicol and at 1, 5, 10, 20, 30, 45, 90, and 120 min(s) after the addition of chloramphenicol. Sample collection at each timepoint was performed as described above. 10 μL of each sample was loaded onto a 12% SDS polyacrylamide gel. Incubation with primary and secondary antibodies, detection and band quantification were performed as described above. Each experiment was repeated three times, and a representative blot is shown in each case.

Succinate Dehydrogenase Activity Assay

Succinate dehydrogenase activity was measured using a kit (Abcam). Samples were prepared following the manufacturer's protocol by diluting overnight cultures 1:50 into 5 mL fresh LB and growing them to OD_{600} ∼0.5 at 37°C with shaking. 1 mL of culture was taken, pelleted by centrifugation, washed with 1 × PBS and pelleted again. Cultures were then standardized to the same optical density OD_{600} of 1.0 in the final volume of 1 mL by adding an appropriate volume of 1 × PBS, pelleting, and resuspending in 200 mL of ice-cold SDH Assay Buffer (Abcam). Cell lysis was performed by sonication. Samples were centrifuged at 10,000 × *g* for 5 mins and the supernatant was transferred into a fresh tube. 50 μL of each sample was loaded into a 96-well plate, and 50 μL of SDH reaction mix containing the SDH substrate mix, and the probe (Abcam) was added to them. Absorbance at 600 nm was measured for 30 mins at 25°C in kinetic mode using the Cytation5^{TM} Cell Imaging Multi-Mode Reader (BioTek). The succinate dehydrogenase activity of the samples was calculated according to the manufacturers' directions. Data is representative of the means and standard deviations of three biological replicates.

Minimal Media Growth Assays

Wildtype BW25113 or knockout mutants were grown overnight in 2 mL LB at 37°C with shaking. The following day, cells were pelleted by centrifugation and washed twice with 1 × PBS. The density was standardized to OD_{600} 1.0 by suspending an appropriate volume of cells in 1 ml of 1 × PBS. 20 μL of each sample was loaded into a 96-well plate, each well containing 180 μL of either 0.4% glucose (Sigma), 0.4% malic acid (Sigma) or 0.4% succinic acid (Sigma) M9 minimal medium (Difco), pH

7.0. The plate was incubated in the Cytation5^{TM} Cell Imaging Multi-Mode Reader with 330 rpm shaking at 37°C for 48 h.

RESULTS

Regulation of the Succinate Dehydrogenase Complex by the Cpx Response

Recent studies have demonstrated that the Cpx envelope stress response regulates the expression and activity of NDH-I and cytochrome bo_3 complexes in EPEC (Guest et al., 2017). In addition, Cpx-dependent downregulation of genes encoding the succinate dehydrogenase complex was observed in a large microarray dataset; however, the exact mechanism of regulation has not been revealed (Raivio et al., 2013). To investigate the impact of the Cpx pathway on the SDH, we grew strains carrying either the vector control or a reporter plasmid in which 500 bp upstream of the *sdhCDAB* operon were fused to the *luxCDABE* gene cluster in liquid LB medium aerobically for 24 h. Luminescence activity of the p*sdhC*::*lux* reporter in the presence or absence of the Cpx pathway was measured every hour until the stationary phase was reached. We chose to use the luminescence activity produced by the p*cpxP*::*lux* reporter gene as a positive control, since CpxP is one of the most upregulated members of the Cpx regulon (Price and Raivio, 2009).

In agreement with previous observations, the expression of the p*cpxP*::*lux* reporter in the wildtype BW25113 was higher than in a *cpxA* null background at every stage of growth (**Figure 1A**). Along with *cpxP*, we assayed the activity of the p*nuoA*::*lux* reporter and validated its Cpx-dependent downregulation as reported in the past (**Figure 1B**; Guest et al., 2017). Loss of Cpx response resulted in a ∼2-fold increase in the p*nuoA*::*lux* activity compared to that of the wildtype. When we assayed the luminescence activity of the p*sdhC*::*lux* reporter, we found similar increases in the absence of a functional Cpx response, while the wildtype activity of the Cpx TCS lead to transcriptional repression of the *sdhC* promoter (**Figure 1C**).

To corroborate the luminescence profile of the control and ETC reporters in liquid LB medium, we also examined expression of the reporter genes during growth on solid LB medium (**Figure 1D**). The patterns of p*nuo*::*lux*, p*sdhC*::*lux* and p*cpxP*::*lux* reporter activity observed on solid medium resembled those in the liquid medium assay. In the wildtype strain, the p*cpxP*::*lux* reporter was strongly activated, while light was not detectable in a *cpxA* null mutant background. This pattern was reversed for the p*nuo*::*lux* and p*sdhC*::*lux* reporters which demonstrated low activity in the presence of the intact Cpx pathway (**Figure 1D**).

Our results suggest that the Cpx TCS could directly inhibit the expression from the *sdhC* promoter. We thus decided to examine the region upstream of *sdhCDAB* for the presence of any putative CpxR binding sites and identified one approximately 150 bp downstream of the predicted *sdhC* transcription start site (TSS) by using Virtual Footprint[1] (Münch et al., 2005; **Supplementary Figure 1**).

[1]https://www.prodoric.de/vfp

Succinate Dehydrogenase Activity Is Affected by Excessive Activation or Absence of the Cpx Response

Our experimental results with the p*sdhC*::*lux* reporter predict that the enzymatic activity of SDH will be lower in the presence of an active Cpx TCS relative to a mutant lacking the Cpx response. To test this hypothesis, we assayed the rates of succinate oxidation in the wildtype *E. coli* strain, as well as in *cpxR*::kan and *cpxA24* mutants, reflecting a deactivated and constitutively activated Cpx pathway, respectively (Raivio and Silhavy, 1997). We also included a strain overexpressing NlpE as an alternative way to induce the Cpx response (**Figure 2**). In this assay, the oxidation of succinate is accompanied by the transfer of electrons to an artificial electron acceptor (probe), which changes color depending on the enzymatic activity of the sample. When in the oxidized state, the probe is blue with maximal absorption at 600 nm, whereas when reduced it becomes colorless. We found that the activity of the SDH complex decreased upon activation of the Cpx system in both the *cpxA24* mutant and the NlpE overexpression backgrounds. This result was predictable based on the repressive effect of the Cpx response on the *sdhC* promoter observed in **Figures 1C,D**.

Surprisingly, the loss of the Cpx response did not result in higher SDH activity, as might be anticipated with the relieved inhibition of *sdhCDAB* transcription. Instead, knocking out *cpxR* resulted in decreased succinate oxidation rates, equivalent to those observed in the presence of the strongly Cpx-activating *cpxA24* allele (**Figure 2B**). This result is reminiscent of a previously observed decrease in the oxygen consumption rate in the Δ*cpxR* mutant, despite the fact that transcription of the operons encoding NDH-I and cytochrome bo_3 are upregulated in this background (Guest et al., 2017). Together, these findings suggest that the Cpx TCS not only transcriptionally regulates the SDH protein complex, but also regulates factors responsible for its proper activity and biogenesis.

The Cellular Need for the Cpx Response Increases When Respiratory Complexes Are More Prevalent or Active

Escherichia coli is capable of growing on a number of different sugar substrates, generating the majority of its ATP via the process of oxidative phosphorylation (Ammar et al., 2018). Carbon sources that cannot be utilized through the process of substrate-level phosphorylation, or fermentation, are called non-fermentable and require a functional ETC for sufficient energy generation. Such carbon sources include succinate, malate and glutamate (Prüss et al., 1994; Chang et al., 2004; McNeil et al., 2012). Poor growth of NDH-I mutants on either malate or succinate has been proposed to reflect low energy conservation efficiency due to a low level of ATP inside the cells (Kervinen et al., 2004). Previously reported data and our observations suggest that the Cpx TCS affects transcription and function of membrane complexes required for growth on non-fermentable carbon sources, including those associated with electron transport, the TCA cycle and oxidative

phosphorylation (**Figures 1B–D**; Raivio et al., 2013; Guest et al., 2017). We thus hypothesized that the activity of the Cpx pathway would be required under conditions that create increased demand for respiration To test this, we spotted strains bearing luminescent reporter plasmids containing p*nuoA*::*lux*, p*sdhC*::*lux*, or p*cpxP*::*lux* promoter fusions along a glucose-succinate carbon source concentration gradient on minimal medium (**Figure 3**). We found that expression of the *cpxP* promoter increases as the concentration of succinate increases, whereas in the presence of glucose p*cpxP*::*lux* demonstrates background levels of luminescence comparable to the empty vector control. None of the reporters were activated to high levels in the presence of glucose, which supports our hypothesis that growth under conditions that increase demand for respiration leads to Cpx pathway activation. Due to high p*cpxP*::*lux* activity, *nuoA* and *sdhC* promoter activities were not detected by the imaging system on short exposure times, therefore we spotted the strains containing ETC reporters on a different plate and assayed them separately to image the lower luminescence activity (**Figure 3**). As expected, activity of the p*nuoA*::*lux* and p*sdhC*::*lux* reporters increased commensurate with the succinate concentration gradient. Notably, the expression of these transcriptional reporters was much higher in the absence of the Cpx response, which supports our previous findings in **Figures 1B–D** (data not shown). Based on the results of this experiment, we suggest that the cellular need for Cpx-mediated

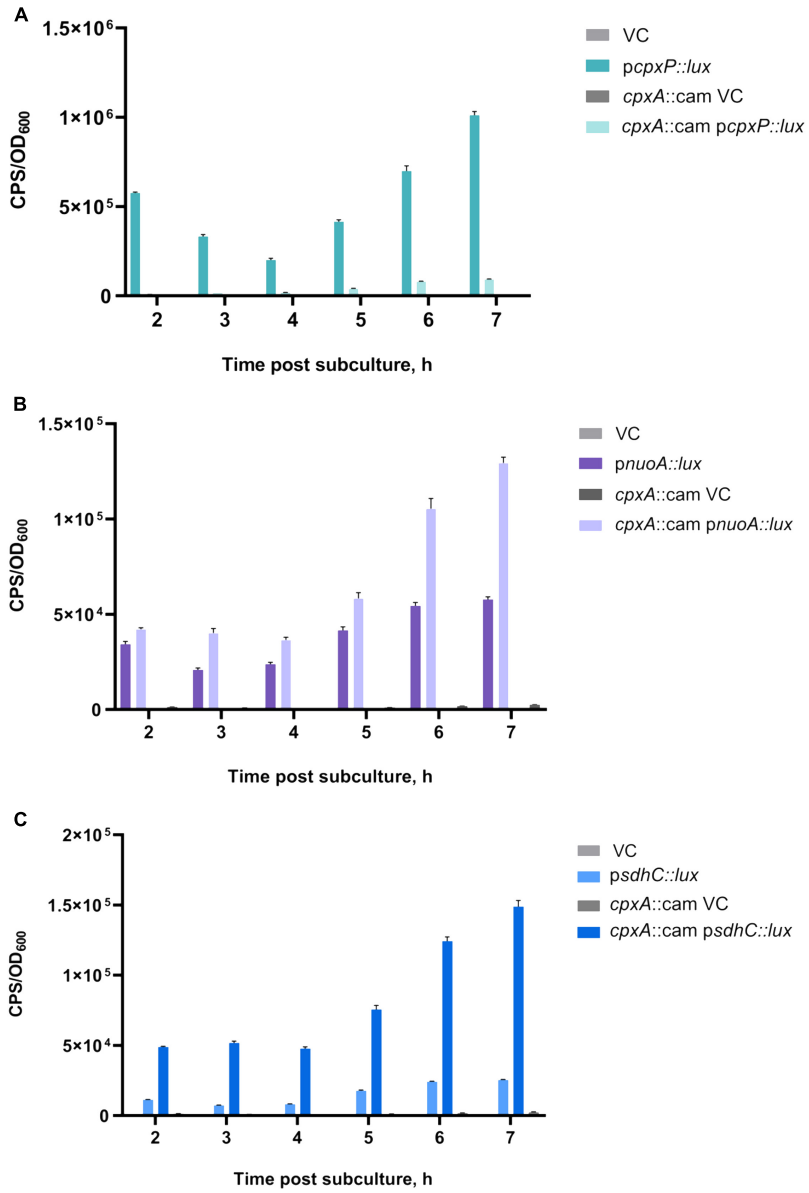

FIGURE 1 | (Continued)

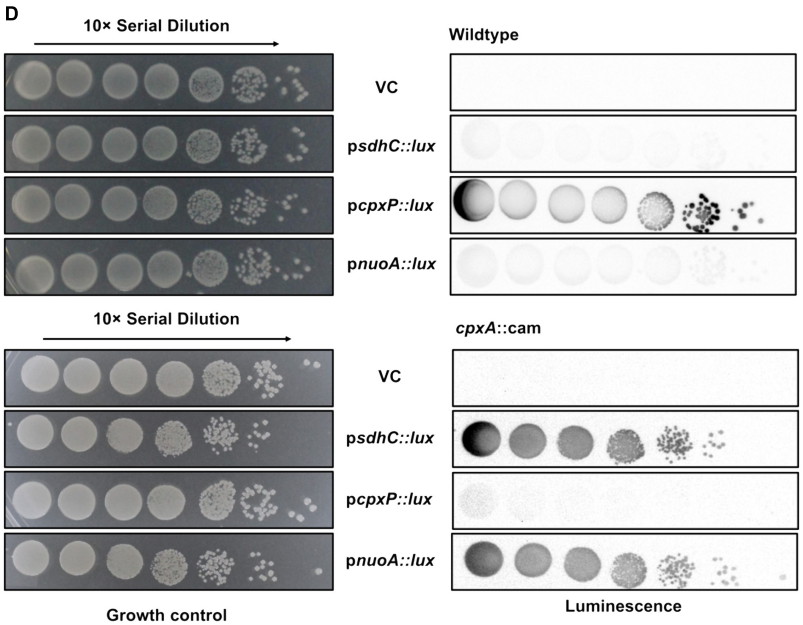

FIGURE 1 | Transcription of the *sdh* operon encoding the succinate dehydrogenase complex is downregulated by the Cpx stress response. Overnight cultures of wildtype *Escherichia coli* MC4100 or a *cpxA*::cam mutant harboring either pJW15 (vector control) or the **(A)** p*cpxP*::*lux*, **(B)** p*nuoA*::*lux*, or **(C)** p*sdhC*::*lux* reporter plasmids were subcultured 1:100 into fresh LB medium and incubated at 37°C with shaking. The luminescence and the OD_{600} were measured every hour for the duration of 7 h and a final measurement was taken at 24 h. Data correspond to the mean values from three biological replicates. Error bars depict standard deviations (SDs). **(D)** Luminescence activities are shown for wildtype *E. coli* MC4100 or a *cpxA*::cam mutant harboring either pJW15 (vector control) or the p*nuoA*::*lux*, p*sdhC*::*lux*, or p*cpxP*::*lux* reporter plasmids. Luminescence was determined by imaging the luminescence of the strains after 24 h of growth on LB plates.

stress adaptation increases when respiratory (and possibly other) protein complexes are in increased demand.

The Cpx Response Regulates NuoA Protein Levels

The Cpx response directly represses *nuo* operon transcription to ensure envelope integrity during stress and reduce excessive protein traffic within the IM (Guest et al., 2017; **Figure 1B**). The possibility of additional levels of regulation has been hypothesized because the oxygen consumption in EPEC was found to be reduced in cells with either an active or inactive Cpx pathway (Guest et al., 2017). To determine whether the Cpx response regulates respiratory proteins beyond transcription, we constructed a plasmid that expresses a triple FLAG-tagged NuoA subunit of the NDH-I complex from an exogenous, IPTG inducible promoter. We chose NuoA protein due to its scaffolding role in the assembly of the NDH-I membrane arm (Friedrich et al., 2016). Given that the NuoA-3 × FLAG construct is expressed from a CpxR-independent IPTG-inducible promoter, any effects of Cpx pathway on NuoA protein levels should be independent of transcription. To confirm that the NuoA-3 × FLAG fusion protein is functional, we complemented a chromosomal Δ*nuoA* mutant that has a growth defect on minimal medium supplemented with malate, with either the empty vector pMPM-K3 or the plasmid carrying NuoA-3 × FLAG. The exogenously expressed NuoA restored growth of the Δ*nuoA* mutant, demonstrating that the protein was expressed properly and was functional, whereas complementation with an empty vector resulted in the absence of growth (**Supplementary Figure 2**). All strains demonstrated similar growth levels on minimal medium supplemented with glucose, which is a fermentable carbon source.

We assayed the amount of NuoA-3 × FLAG protein in wildtype, Δ*cpxR* and *cpxA24* strains of *E. coli* via Western blotting and observed a decrease in NuoA-3 × FLAG levels when the Cpx response was constitutively activated. A slight accumulation of the protein was detected in the absence of Cpx response (**Figure 4A**). Expression of NuoA-3 × FLAG in the *cpxA24* mutant was 8% that of the wildtype strain 30 mins after induction, whereas NuoA-3 × FLAG levels were increased by 14% in the Δ*cpxR* mutant compared to the wildtype (**Figure 4A**).

To gain more insight into how the activity of the Cpx response affects protein turnover over time, we performed a protein stability assay by utilizing the protein synthesis inhibitor chloramphenicol and monitoring the rate of NuoA-3 × FLAG degradation over 120 mins after translation has been halted (**Figure 4B**). Relative quantification of the bands showed that in the absence of the Cpx response, approximately half of the starting amount of NuoA-3 × FLAG protein was degraded in 45 mins, which was 25 mins longer than in the wildtype strain, indicating slower protein turnover (**Figure 4C** and **Supplementary Table 3**). Unexpectedly, the rates of NuoA-3 × FLAG degradation over the course of the experiment were comparable between the *cpxA24* and the wildtype strains, although the total amount of protein degraded by the end

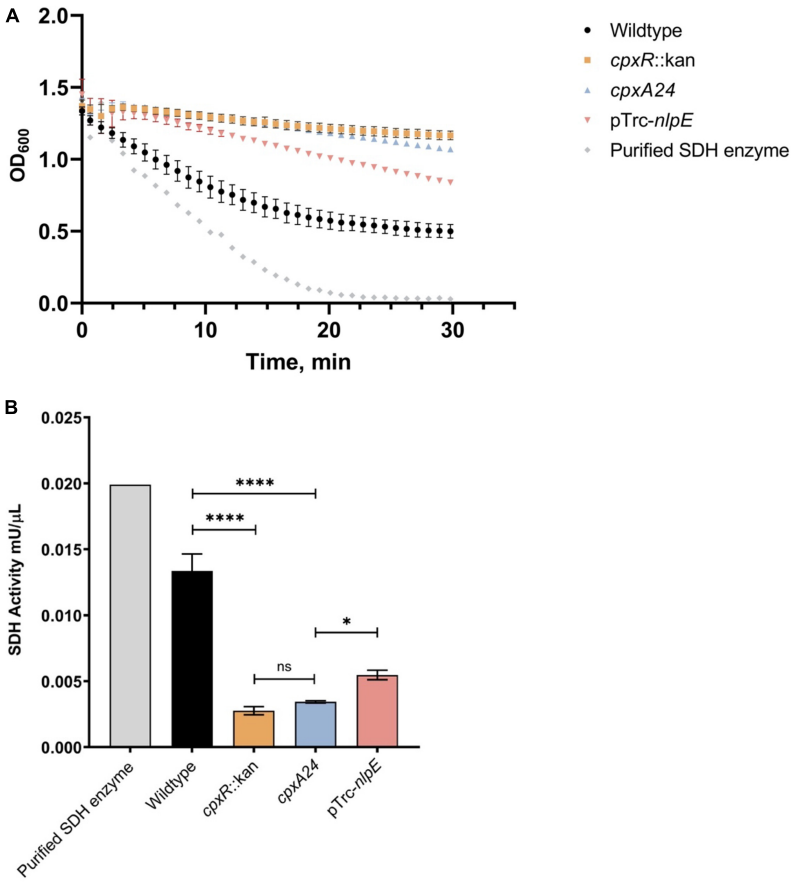

FIGURE 2 | Succinate dehydrogenase (SDH) activity is reduced by excessive activation or absence of the functional Cpx response. Wildtype MC4100, *cpxR*::kan, *cpxA24* and MC4100 harboring NlpE overexpression plasmid (pTrc-*nlpE*) were subcultured from their overnight cultures 1:50 into 5 mL fresh LB and grown to OD_{600} ~0.5 at 37°C with shaking. 1 mL samples, standardized to the same optical density OD_{600}, were pelleted, and cell pellets were resuspended in 200 µL of ice-cold SDH Assay Buffer (Abcam). Samples were prepared as per manufacturers' protocol, loaded into a 96-well plate, and mixed with 50 µL of SDH reaction mix (Abcam). **(A)** Assay data showing reduction of the DCIP artificial electron acceptor, accompanied by the color change of the dye from blue to colorless (A_{600}). Absorbance at 600 nm was measured every minute for 30 mins at 25°C with shaking using the Cytation5^{TM} Cell Imaging Multi-Mode Reader (BioTek). **(B)** Succinate dehydrogenase activity of each sample was calculated as per manufacturers' protocol and plotted. All data correspond to the means and standard deviations of three replicate cultures. Asterisks indicate a statistically significant difference from the relevant wildtype control [****$P \leq 0.0001$ (one-way ANOVA with Tukey's *post hoc* test)]. NS indicates no statistically significant difference in SDH activity.

of the experiment was larger in the *cpxA24* (**Figures 4B,C** and **Supplementary Table 3**). Together, our results suggest that Cpx-regulated protein degrading factors are responsible for faster and more efficient turnover of NuoA-3 × FLAG proteins in the wildtype strain. Counterintuitively, an increased rate of degradation does not seem to be the only reason for the diminished amount of NuoA observed in *cpxA24* strain backgrounds (**Figure 4A**).

Cpx-Regulated Protein Folding and Degrading Factors Affect Growth During High Respiratory Demand

We found that the rate of NuoA-3 × FLAG proteolysis was reduced when the Cpx response was inactivated, suggesting that the Cpx pathway assists protein turnover (**Figures 4B,C**). Given that bacteria with a compromised ETC are not able to generate sufficient amounts of ATP to support growth on non-fermentable carbon sources, we hypothesized that Cpx-regulated protein folding and degrading factors may impact the biogenesis of the ETC, together with the ability of the bacterial cells to generate proton motive force (PMF) and maintain their ATP levels. The candidate gene list for this experiment was derived from previous publications (Price and Raivio, 2009; Raivio et al., 2013) and unpublished RNASeq data. To identify genes of interest, we performed a preliminary screening of several of these envelope-associated protein folding and degrading factors (unpublished data). Cpx-regulated genes were overexpressed in a Δ*nuoA* strain containing the NuoA-3 × FLAG expression vector and NuoA-3 × FLAG protein levels were analyzed by dot blot. Overexpression of the DegP, HtpX, PpiD, and YccA proteins had the largest impact on the abundance of NuoA-3 × FLAG protein, surprisingly resulting in a greater than 2-fold increase in the amount of NuoA-3 × FLAG in comparison to

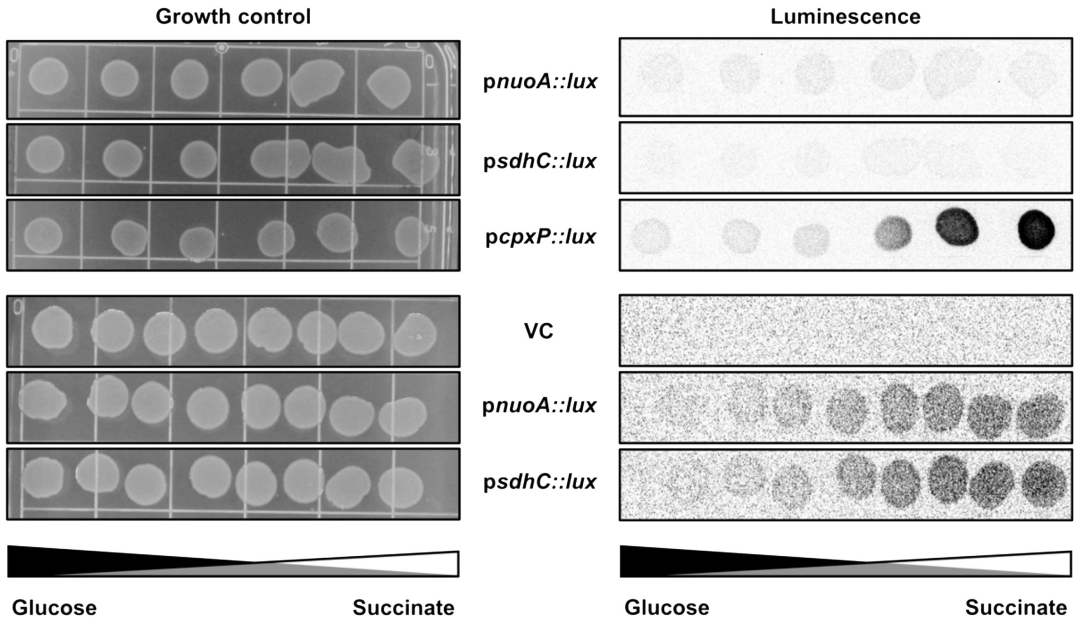

FIGURE 3 | Demand for aerobic respiration due to the presence of non-fermentable carbon sources induces the Cpx pathway. Luminescence activities are shown for wildtype *E. coli* MC4100 harboring either pJW15 (vector control) or the p*nuoA*::*lux*, p*sdhC*::*lux*, or p*cpxP*::*lux* reporter plasmids. Luminescence of the strains growing on M9 minimal media plates containing a gradient of 0.4% glucose and 0.4% succinate, pH 7.0 was determined by imaging the luminescence of the spots after 48 h of incubation at 37°C.

the vector control. Furthermore, the protease/chaperone DegP, the IM protease HtpX, proteolytic modulating factor YccA, and periplasmic chaperone PpiD, have all been implicated in maintaining the integrity of the envelope and responding to stress generated by protein misfolding (Danese et al., 1995; Shimohata et al., 2002; Yamamoto and Ishihama, 2006; Matern et al., 2010; Raivio et al., 2013).

To investigate the role these proteins may have in the quality control of the ETC complexes, we analyzed growth of their knockout mutants in minimal media supplemented with glucose, succinate or malate in BW25113 *E. coli* (**Figure 5**; Kitagawa et al., 2005). As shown in **Figure 5**, deleting *cpxR*, *ppiD*, *yccA*, *htpX*, or *degP* resulted in growth defects of differing severity in comparison to the wildtype. All strains were able to grow on media supplemented with glucose, where their growth would not solely depend on energy generated via respiration. In addition, we noticed that the growth phenotypes of some mutants differed depending on whether the media contained malate or succinate as a carbon source.

Our data demonstrate that knocking out *cpxR*, *ppiD*, or *yccA* severely attenuates growth in media supplemented with malate, whereas these defects are less pronounced in succinate. Notably, deletion of genes encoding IM protease HtpX and periplasmic protease/chaperone DegP resulted in more modest growth defects (**Figure 5**). This result was somewhat surprising, as Cpx-mediated regulation of these proteolytic factors is an important element of envelope quality control (Jones et al., 2002; Shimohata et al., 2002), although it is possible their functions overlap with other proteolytic factors. To further demonstrate that these factors are required for respiratory growth, we performed a complementation assay where the mutants were transformed with an empty vector or a plasmid expressing the gene of interest. We were partially able to complement growth defects of every mutant in media where succinate or malate were the sole carbon source (**Supplementary Figure 3**). Together, these data demonstrate that the absence of a functional Cpx system and several associated protein folding and degrading factors compromises proper biogenesis of the ETC, resulting in decreased viability in media that demand respiration.

Cpx-Regulated Protein Folding and Degrading Factors Affect NuoA Protein Levels

Our results implicate the Cpx-regulated envelope quality control factors YccA and PpiD, and to a lesser extent the proteases DegP and HtpX, in the biogenesis of the ETC (**Figures 4**, **5**). We therefore hypothesized that knocking out *ppiD*, *yccA*, *degP*, or *htpX* may impact NuoA-3 × FLAG protein abundance. Here, we demonstrate that deletion of these factors alters NuoA-3 × FLAG protein levels compared to the wildtype (**Figure 6**). Deletion of *degP*, *ppiD*, *yccA*, *or htpX* increased NuoA-3 × FLAG abundance by a factor of 5.56, 4.83, 3.95, and 1.49, respectively, in comparison to wildtype. Although the specific fold changes in NuoA-3 × FLAG levels varied between biological replicates within this experiment, we consistently detected an increased amount in the mutant strains relative to the wildtype. In agreement with our previous findings, deletion of CpxR also resulted in accumulation of NuoA-3 × FLAG (**Figures 4A**, **6**). Overall, our results suggest that several Cpx-regulated protein

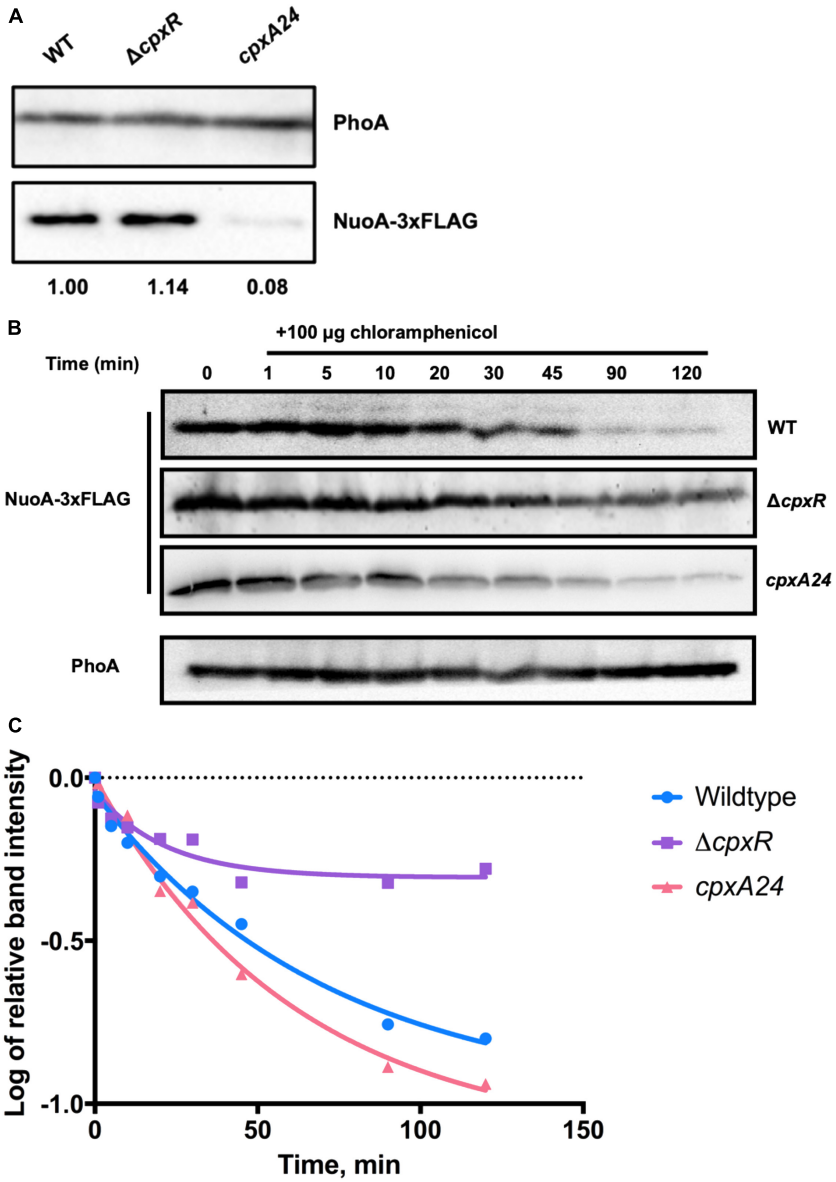

FIGURE 4 | The Cpx response affects NuoA-3 × FLAG protein levels. Western blots utilizing anti-FLAG tag antibody were performed on wildtype EPEC, *cpxA24* or Δ*cpxR* mutants **(A)** or wildtype BW25113, *cpxA24* or Δ*cpxR* mutants **(B,C)** containing the pMPM-*nuoA*-3 × FLAG expression vector **(A)** at a single time-point, where band intensity is represented by the value relative to the wildtype NuoA-3×FLAG protein level and **(B)** over time after 100 μg of chloramphenicol was added to inhibit protein synthesis. Samples were taken at 0 (before addition) 1, 5, 10, 20, 30, 45, 90, and 120 min after addition to assay NuoA-3 × FLAG protein degradation. PhoA protein levels served as a loading control. Proteins were detected using the Immun-Star alkaline phosphatase chemiluminescence kit (Bio-Rad) and the Bio-Rad ChemiDoc MP imaging system. **(C)** Relative band quantification was performed using band intensity analysis in ImageJ. The protein stability assay data were fit with a one-phase exponential decay curve to determine protein half-life using the Prism v7.0c (GraphPad) software.

folding and degrading factors affect abundance of the NuoA protein and support the hypothesis of the Cpx-dependent regulation of the NDH-I complex at the post-translational level.

DISCUSSION

The Cpx response mediates adaptation to stresses that result in envelope perturbations through a variety of mechanisms, including facilitating degradation of misfolded or mislocalized proteins. Until recently, there was only a small number of proteins whose stability was known to be affected by the Cpx stress response; the breadth of known Cpx-mediated adaptations, however, continues to expand. It was recently demonstrated that the Cpx response regulates the expression of genes encoding NDH-I and cytochrome bo_3, large envelope complexes involved in aerobic respiration (Guest et al., 2017). Transcriptional repression of the *nuo* and *cyo* promoter regions under stress is

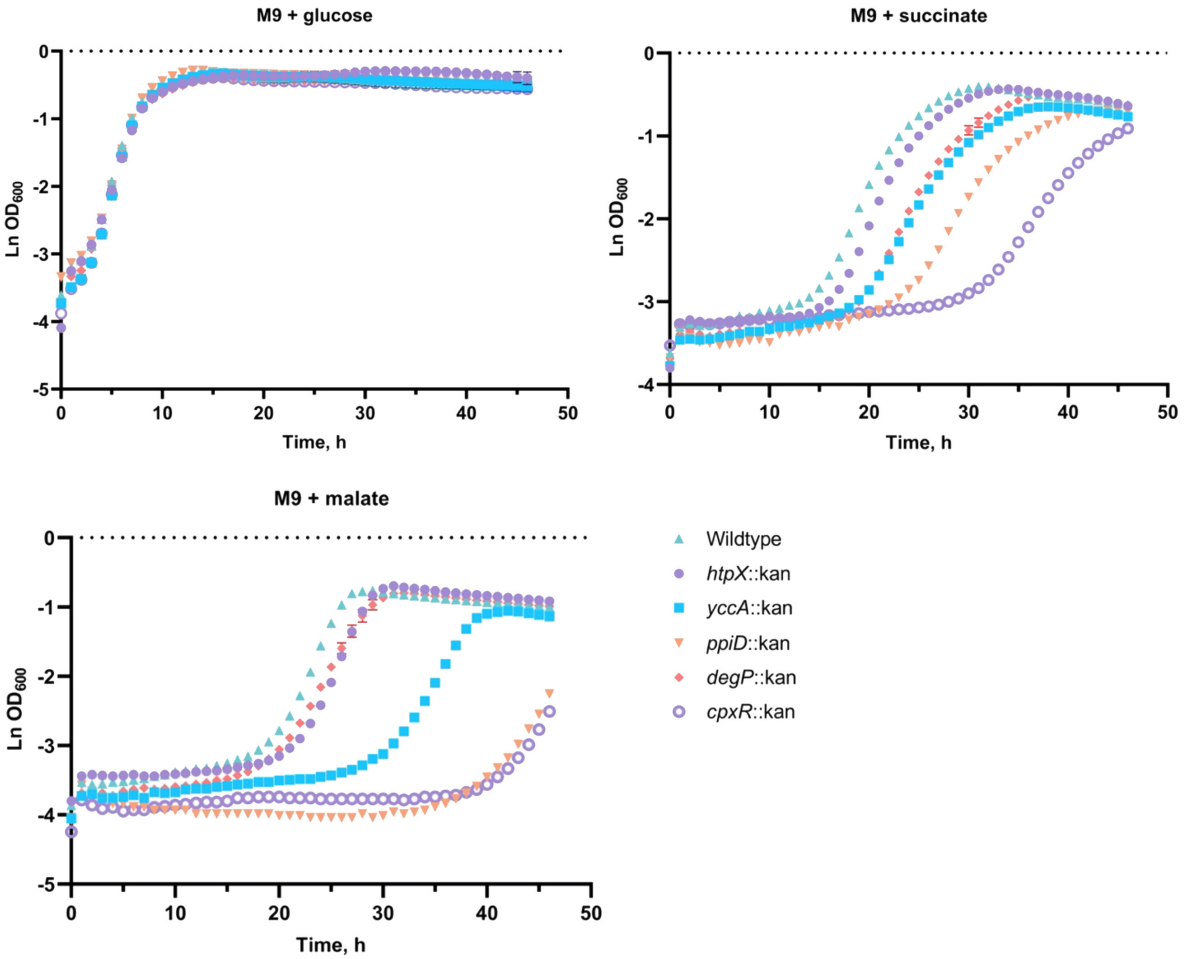

FIGURE 5 | Deletion of several Cpx-regulated protein-folding and degrading factors results in growth defects in minimal media. Wildtype BW25113 and the mutants carrying the indicated gene deletions were grown overnight in LB at 37°C, washed twice in 1x phosphate-buffered saline (PBS), and standardized to an OD_{600} of 1.0 in phosphate buffered saline. 10 μL of the culture was subcultured into M9 minimal medium containing 0.4% glucose, 0.4% malic acid, pH 7.0 (malate) or 0.4% succinic acid, pH 7.0 (succinate), and grown for 48 h at 37°C with 330 rpm linear shaking. Data correspond to the mean values from three biological replicates and are representative of three independent experiments. Error bars depict standard deviations (SDs).

thought to reduce production of new respiratory complexes and prevent excessive protein traffic within an already compromised cell envelope (Guest et al., 2017). Interestingly, when the rates of oxygen consumption were compared between Δ*cpxRA* and wildtype EPEC, it was found that despite increased transcription of the *nuo* and *cyo* operons in the Δ*cpxRA* mutant, the activity of the aerobic ETC was still impaired (Guest et al., 2017). These discoveries suggested a novel role for the Cpx TCS in monitoring protein biogenesis and regulating factors, potentially impacting the function, stability, and assembly of respiratory complexes beyond transcription.

In this study, we provide evidence that the Cpx response regulates succinate dehydrogenase, the only enzyme of the TCA cycle that interacts directly with the ETC chain, being central to cellular metabolism and energy conversion (Hederstedt and Rutberg, 1981; Cecchini et al., 2002; Yankovskaya et al., 2003; Price and Driessen, 2010; Kaila and Wikström, 2021). Raivio et al. (2013) reported that the *sdhCDAB* operon was among the genes whose transcription was downregulated upon transient NlpE overexpression, along with other genes involved in respiration, including the *nuo* and *cyo* operons. In agreement with this finding, we show that the Cpx TCS inhibits the activity of a p*sdhC*::*lux* luminescent reporter in a wildtype strain under standard laboratory conditions, whereas in the absence of a functional Cpx response, *sdhC* promoter expression is elevated (**Figures 1C,D**).

How might this operon be regulated by the Cpx response? Previous studies have shown that many Cpx-regulated genes contain a CpxR binding site within 100 bp of their transcriptional start site (Price and Raivio, 2009). Given that both the *nuo* and *cyo* promoter regions possess CpxR binding sites, and their transcription is mediated though direct binding of CpxR, it is possible *sdhCDAB* is regulated similarly. We have identified a putative CpxR binding site approximately 150 bp downstream of the *sdhCDAB* TSS by using Virtual Footprint software (Münch et al., 2005; Guest et al., 2017). However, further experimentation

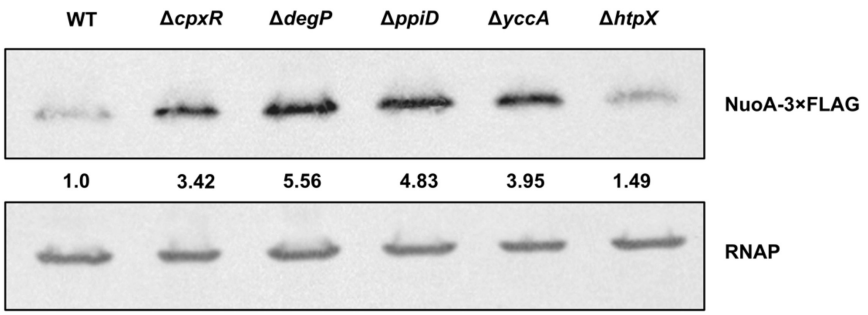

FIGURE 6 | NuoA-3 × FLAG protein levels are altered by deletion of several Cpx-regulated protein folding and degrading factors. Western blot utilizing anti-FLAG tag antibody was performed on wildtype BW25113 *E. coli* and the mutants with the indicated gene deletions containing the pMPM-*nuoA*-3 × FLAG expression vector. RNAP protein levels served as a loading control. Membranes were imaged using the Bio-Rad ChemiDoc MP imaging system. Relative band quantification was performed using band intensity analysis in ImageJ. Band intensity is represented by the value relative to the wildtype NuoA-3 × FLAG protein level.

is required to confirm this mechanism. Binding of the CpxR response regulator between the TSS and the translation start site would block transcription elongation from the *sdhC* promoter, decreasing the overall rate of *sdhCDAB* transcription. It is important to note though that this site deviates from the CpxR consensus binding sequence [5′-GTAAA(N_5)GTAAA-3′], possessing a 6 bp linker and containing a GTTAA sequence in the 5′ half of the binding site (**Supplementary Figure 1**; De Wulf et al., 2002). Interestingly, several other transcriptional regulators also have binding sites near the *sdhCDAB* TSS; there are four ArcA binding motifs (Park et al., 1995; Shen and Gunsalus, 1997) and one for the cyclic adenosine monophosphate (cAMP)-cAMP receptor protein (CRP) complex, which is located approximately 94 bp upstream of the *sdhC* TSS (Zheng et al., 2004; Surmann et al., 2020). Other known regulators of the *sdhCDAB* operon include Fur (Zhang et al., 2005; Kumar and Shimizu, 2011), Fnr (Park et al., 1995) and several sRNAs shown to inhibit *sdhCDAB* mRNA translation (Massé and Gottesman, 2002; Geissmann and Touati, 2004; Desnoyers and Massé, 2012). It is possible that some of these regulators may work in combination with CpxR or other members of the Cpx TCS to regulate the transcription and/or translation of the *sdhCDAB* operon in response to environmental changes.

Our results indicate that the wildtype activity of the Cpx pathway leads to transcriptional repression of the *sdhCDAB* gene cluster. To validate our findings, and given that oxygen consumption in EPEC was shown to be affected by excessive activation of the Cpx response (Guest et al., 2017), we examined the rates of succinate oxidation by SDH in different Cpx backgrounds (**Figure 2**). We found that both NlpE overexpression and constitutive activation of the Cpx response by the *cpxA24* allele resulted in decreased SDH activity, which is consistent with a decrease in *sdhCDAB* expression under these conditions (**Figure 2**; Raivio et al., 2013). Unexpectedly, we observed similarly low enzymatic activity in a mutant lacking the Cpx pathway, which correlated with the reduced ETC performance in Δ*cpxRA* mutant relative to the wildtype strain demonstrated previously (Guest et al., 2017).

Evidently, both excessive activation and the absence of the Cpx stress response impacts the SDH complex, directly regulating transcription of the *sdhCDAB* operon, and potentially influencing the biogenesis of the complex. Given the role of the Cpx TCS in detecting and responding to potentially lethal misfolded proteins at the IM, it has been hypothesized that its housekeeping activity contributes to proper folding, stability and regulated turnover of large envelope complexes (Hung et al., 2001; Price and Raivio, 2009; Raivio et al., 2013; Hews et al., 2019). While a significant portion of the Cpx regulon consists of proteases and chaperones that address protein misfolding at the IM, to our knowledge, there are no known proteolytic factors involved specifically in degradation or stability of the ETC. Nevertheless, general polypeptide misfolding can be recognized by other non-specific proteases, including HtpX, DegP, and FtsH, which are known responders to envelope stress and are either directly or indirectly regulated by the Cpx pathway (Kihara et al., 1995; Akiyama et al., 1996; Jones et al., 2002; Shimohata et al., 2002; Isaac et al., 2005; Sakoh et al., 2005; van Bloois et al., 2008). The absence of such quality control in a Δ*cpxRA* knockout mutant could lead to aberrant complex formation and unproductive interactions between subunits of the respiratory complexes, leading to loss of function.

We found that the increased demand for respiratory complexes resulting from utilization of non-fermentable carbon sources acts as an inducing cue for the Cpx response (**Figure 3**; Bongaerts et al., 1995). Envelope stress can be exacerbated by the elevated activity of respiratory complexes. However, in *E. coli* this stress is not likely to be due to disruption of the proton gradient; the Cpx response is not induced by the chemical protonophore carbonyl cyanide 3-chlorophenylhydrazone (CCCP) (Engl et al., 2011; Guest et al., 2017). It is possible that in order to generate sufficient energy from non-fermentable carbon sources, bacterial cells upregulate respiratory complexes, which can then be subject to misassembly, irreparable damage or insertion into an already compromised membrane, a situation that would require a functional Cpx envelope stress response. Previous studies demonstrated that bacteria carrying mutations in genes encoding components of the ETC and quinone biosynthesis exhibit growth

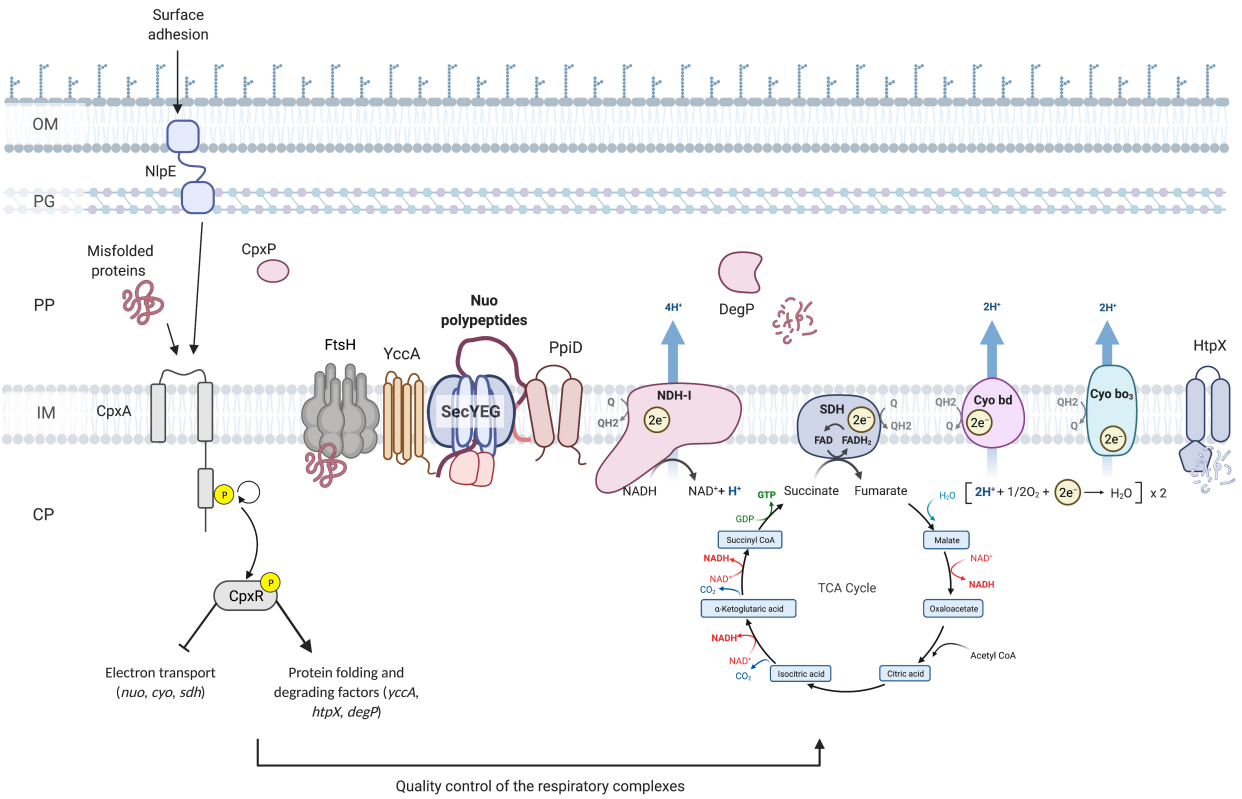

FIGURE 7 | Model of the quality control of the ETC performed by the Cpx envelope stress response at the inner membrane of *E. coli*. Upon activation of the Cpx response, CpxR represses the transcription of the operons encoding the NDH-I (*nuo*), cytochrome bo_3 (*cyo*) and succinate dehydrogenase (*sdh*) respiratory complexes. In addition, the Cpx response regulates the biogenesis of these complexes beyond transcription through increased expression of protein folding and degrading factors. Cpx-regulated protein folding factors assist with the secretion and further insertion of integral parts of the ETC complexes, whereas the proteolytic factors maintain the adequate turnover and degradation of the misfolded or mislocalized proteins. OM, outer membrane; PG, peptidoglycan; PP, periplasm; CP, cytoplasm; Q, quinone; Cyo, cytochrome.

defects on succinate, malate, lactate, and acetate (Au and Gennis, 1987; Prüss et al., 1994; Kervinen et al., 2004; McNeil et al., 2012; Aussel et al., 2014). We observe similar growth phenotypes in the absence of the Cpx response, or Cpx-regulated protein folding and degrading factors (**Figures 3**, **5**).

Upregulation of envelope quality control factors constitutes a part of Cpx-mediated adaptation under conditions in which damaged and/or misfolded proteins are predicted to accumulate (Hews et al., 2019; Mitchell and Silhavy, 2019). Regulation of proteolysis at the IM of *E. coli* is one of the least characterized parts of the Cpx response and is essential for maintaining the integrity of envelope biogenesis (Akiyama, 2009; Raivio, 2018; Delhaye et al., 2019a; Hews et al., 2019). Here, we demonstrate that the NuoA subunit of the NDH-I complex is subject to regulation by the Cpx pathway beyond transcription, and that activation of the Cpx response decreases the abundance of NuoA-3 × FLAG protein (**Figure 4A**). Furthermore, we show that the efficiency of NuoA-3 × FLAG protein turnover is reduced in the absence of the functional Cpx response (**Figures 4B,C**). These results can be interpreted in two ways. First, the Cpx system may regulate factors that inhibit translation, such as the CpxQ sRNA (Chao and Vogel, 2016), therefore decreasing the amount of successfully translated *nuoA*-3 × FLAG mRNA. Interestingly, CpxQ has been previously proposed to play a role in preserving the PMF at the IM since it downregulates the sodium-proton antiporter NhaB and counteracts the loss of membrane potential caused by CCCP treatment (Chao and Vogel, 2016). Moreover, several other sRNAs have been implicated in the post-transcriptional regulation of the ETC complexes, including RyhB that regulates both *nuo* and *sdhCDAB* transcripts under low-iron conditions (Massé and Gottesman, 2002; Massé et al., 2005; Desnoyers and Massé, 2012).

Additionally, activation of the Cpx response may result in increased proteolysis of existing NuoA-3 × FLAG proteins. This model is supported by the fact that the Cpx response regulates the expression of proteolytic factors responsible for quality control at the IM (Raivio et al., 1999, 2013; Shimohata et al., 2002; Price and Raivio, 2009; Raivio, 2014). Our data demonstrates that loss of these factors results in growth defects in media that requires a functional ETC for survival, which is in agreement with the previously suggested role of the Cpx response in the biogenesis of respiratory proteins (**Figure 5**; Guest et al., 2017). Together, these findings strengthen the link between the ETC and the Cpx TCS, where in addition to direct transcriptional

repression of respiratory complexes, the Cpx pathway regulates their biogenesis and turnover, likely through the controlled expression of protein folding and degrading factors.

Considering the impact the Cpx response has on aerobic respiration, why does the availability of relatively similar non-fermentable carbon sources in the medium yield such different growth outcomes (**Figure 5**)? Aside from the ETC biogenesis, the other key factor in the minimal media experiments is the differential energetics and interactions of the non-fermentable carbon sources with bacterial central catabolism. Despite being fed directly into the TCA cycle, malate and succinate differentially contribute to ETC bioenergetics. Malate and its oxidation product NADH are stronger reducing agents, with an E'_0 of −0.166 and −0.320 V, respectively, compared to succinate and its oxidation product $FADH_2$ with an identical E'_0 of +0.031 V (Karp, 2008). In other words, the oxidation of malate resulting in NADH production and subsequent oxidation of NADH by NDH-I provides the cell more energy for ATP production. If NDH-I is functionally deficient, NADH-derived electrons cannot be utilized directly for proton motive force generation, given that the NDH-II complex is not involved in proton translocation (Matsushita et al., 1987; Minárik et al., 2002) and ATP generation is dependent on the proton-pumping activity of the downstream cytochromes. This is supported by the fact that the inhibition of NADH oxidase subunit activity of NDH-I results in poor to no growth on malate (Kao et al., 2005). Therefore, removing factors potentially involved in the biogenesis of NDH-I may result in strong growth defects when malate is the sole carbon source. It is possible that the ability to bypass NDH-I and metabolize succinate directly through succinate dehydrogenase results in better viability of these mutants.

Here, we propose that several envelope quality control factors, some of which are Cpx-regulated, affect the biogenesis of NDH-I and, potentially, other respiratory complexes. The inability to utilize non-fermentable carbon sources (**Figure 5**) by the strains lacking envelope quality control could be caused by lethal accumulation of irreparably damaged respiratory complexes in the absence of appropriate protein turnover (**Figures 4B,C**, **6**). While we did not determine whether YccA, DegP, PpiD, or HtpX impact the ETC complexes directly, we know that most of these are associated with the non-specific protease FtsH and SecYEG-dependent translocation (Kihara and Ito, 1998; Antonoaea et al., 2008; Van Stelten et al., 2009; Leiser et al., 2012; Fürst et al., 2018). FtsH-mediated degradation of the SecY subunit of the SecYEG translocon prevents blocking of the translocase with inefficiently exported proteins (Langklotz et al., 2012).

Interestingly, not all mutations were similarly detrimental to the cell. For instance, *htpX* mutants displayed relatively mild growth defects (**Figure 5**) and reductions in NuoA-3 × FLAG protein levels (**Figure 6**), possibly because HtpX functions as a protease with cellular roles complementary or overlapping to those of FtsH (Leiser et al., 2012). In contrast, removing proteins involved in modulation of FtsH proteolytic activity, including YccA and DegP, could lead to excessive degradation of SecY, not allowing for damaged IM proteins to be replaced. PpiD, on the other hand, may assist with secretion and folding of membrane parts of the NDH-I complex. One of the proposed mechanisms of NDH-I assembly involves its co-translational translocation through the Sec translocon and further insertion of its integral protein into the membrane (Friedrich et al., 2016); however, the chaperones involved in this process are yet to be described. PpiD has been previously shown to improve translocation efficiency by clearing the Sec translocon of newly synthesized proteins (Fürst et al., 2018), while its deletion leads to delayed release of proteins from the cytoplasmic side (Antonoaea et al., 2008).

Cumulatively, our results suggest that activation of the Cpx response may stimulate FtsH proteolytic degradation and/or impact the secretion of the electron transport chain proteins. However, since *ftsH* is essential in *E. coli* (Akiyama et al., 1994), we were unable to determine if it is required for Cpx-mediated degradation of NuoA-3 × FLAG. A major future direction could involve deleting *ftsH* in a strain that carries the *sfhC21* allele, which suppresses the lethality of the *ftsH* null and assessing NuoA-3 × FLAG levels (Ogura et al., 1999).

One of the major findings of this work is that another essential component of cellular energetics, the succinate dehydrogenase complex, is a member of the Cpx regulon and that its expression is downregulated in response to stresses sensed by the Cpx TCS. Furthermore, the housekeeping activity of the Cpx response is required for proper biogenesis and performance of succinate dehydrogenase, as evidenced by the fact that SDH activity is impaired in the absence of the functional Cpx pathway. Recent studies hypothesize that during normal biogenesis of the ETC complexes, some subunits may not assemble correctly, and these subunits engage in non-productive interactions that generate the stress sensed by the Cpx response (Guest et al., 2017). This hypothesis is further supported by our findings, where increased demand for respiratory complexes induces the Cpx pathway, possibly due to a higher risk of protein misfolding. Subsequently, activation of the Cpx response results in upregulation of proteases that degrade existing complexes, possibly facilitate secretion and membrane insertion, and directly repress *nuo*, *sdhCDAB* and *cyo* transcription. Altogether, our results support a model in which the Cpx pathway maintains the function of critical cytoplasmic membrane protein complexes through modulation of an intricate balance between transcriptional repression and increased protein turnover during periods of stress, while allowing for recovery of vital cellular activities including translocation of newly synthesized proteins and their insertion into the membrane as envelope stress is alleviated (**Figure 7**).

DATA AVAILABILITY STATEMENT

All datasets generated for this study are included in the article/**Supplementary Material**.

AUTHOR CONTRIBUTIONS

VT was involved in the design of the study, the acquisition, analysis, and interpretation of the data, and wrote the manuscript. RG was involved in the design of the study,

the acquisition, analysis, and interpretation of the data. TR was involved in the conception and design of the study, the interpretation of the data, as well as wrote the manuscript. All authors contributed to the article and approved the submitted version.

FUNDING

This work was funded by operating grants (MOP 342982) from the Canadian Institutes of Health Research and discovery grant (RGPIN 238422-2013) from the Natural Sciences and Engineering Research Council awarded to TR.

ACKNOWLEDGMENTS

We are thankful to the members of the Raivio lab for their thoughtful feedback and Timothy H. S. Cho for construction of the pTrc-*nlpE* plasmid. A version of this work has been published as part of the Ph.D. thesis of Guest (2017).

SUPPLEMENTARY MATERIAL

The Supplementary Material for this article can be found online at: https://www.frontiersin.org/articles/10.3389/fmicb.2021.732288/full#supplementary-material

REFERENCES

Akiyama, Y. (2009). Quality control of cytoplasmic membrane proteins in *escherichia coli*. *J. Biochem.* 146, 449–454. doi: 10.1093/jb/mvp071

Akiyama, Y., Kihara, A., and Ito, K. (1996). Subunit a of proton ATPase F0 sector is a substrate of the FtsH protease in *Escherichia coli*. *FEBS Lett.* 399, 26–28. doi: 10.1016/s0014-5793(96)01283-5

Akiyama, Y., Ogura, T., and Ito, K. (1994). Involvement of FtsH in protein assembly into and through the membrane. I. Mutations that reduce retention efficiency of a cytoplasmic reporter. *J. Biol. Chem.* 269, 5218–5224. doi: 10.1016/S0021-9258(17)37677-9

Ammar, E. M., Wang, X., and Rao, C. V. (2018). Regulation of metabolism in *Escherichia coli* during growth on mixtures of the non-glucose sugars: arabinose, lactose, and xylose. *Sci. Rep.* 8:609. doi: 10.1038/s41598-017-18704-0

Antonoaea, R., Furst, M., Nishiyama, K. I. I., and Muller, M. (2008). The periplasmic chaperone PpiD interacts with secretory proteins exiting from the SecYEG translocon. *Biochemistry* 47, 5649–5656. doi: 10.1021/bi800233w

Au, D. C., and Gennis, R. B. (1987). Cloning of the cyo locus encoding the cytochrome o terminal oxidase complex of *Escherichia coli*. *J. Bacteriol.* 169, 3237–3242. doi: 10.1128/jb.169.7.3237-3242.1987

Aussel, L., Pierrel, F., Loiseau, L., Lombard, M., Fontecave, M., and Barras, F. (2014). Biosynthesis and physiology of coenzyme Q in bacteria. *Biochim. Biophys. Acta Bioenerg.* 1837, 1004–1011. doi: 10.1016/j.bbabio.2014.01.015

Baba, T., Ara, T., Hasegawa, M., Takai, Y., Okumura, Y., Baba, M., et al. (2006). Construction of *Escherichia coli* K-12 in-frame, single-gene knockout mutants: The Keio collection. *Mol. Syst. Biol.* 2:50. doi: 10.1038/msb4100050

Baranova, E. A., Holt, P. J., and Sazanov, L. A. (2007). Projection structure of the membrane domain of *escherichia coli* respiratory complex I at 8 Å Resolution. *J. Mol. Biol.* 366, 140–154. doi: 10.1016/j.jmb.2006.11.026

Bongaerts, J., Zoske, S., Weidner, U., and Linden, G. (1995). Transcriptional regulation of the proton translocating NADH dehydrogenase (nuoA-N) of *Escherichia coli* by electron acceptors, electron donors and gene regulators. *Mol. Microbiol.* 16, 521–534. doi: 10.1111/j.1365-2958.1995.tb02416.x

Borisov, V. B. B., Murali, R., Verkhovskaya, M. L. L., Bloch, D. A. A., Han, H., Gennis, R. B. B., et al. (2011). Aerobic respiratory chain of *Escherichia coli* is not allowed to work in fully uncoupled mode. *Proc. Natl. Acad. Sci.* 108, 17320–17324. doi: 10.1073/pnas.1108217108

Brandt, U. (2006). Energy converting NADH:quinone oxidoreductase (complex I). *Annu. Rev. Biochem.* 75, 69–92. doi: 10.1146/annurev.biochem.75.103004.142539

Braun, M., Bungert, S., and Friedrich, T. (1998). Characterization of the overproduced NADH dehydrogenase fragment of the NADH:ubiquinone oxidoreductase (complex I) from *Escherichia coli*. *Biochemistry* 37, 1861–1867. doi: 10.1021/bi971176p

Cecchini, G., Schroder, I., Gunsalus, R. P., and Maklashina, E. (2002). Succinate dehydrogenase and fumarate reductase from *Escherichia coli*. *Biochim. Biophys. Acta-Bioenerg.* 1553, 140–157. doi: 10.1016/S0005-2728(01)00238-9

Chang, D.-E., Smalley, D. J. J., Tucker, D. L. L., Leatham, M. P. P., Norris, W. E. E., Stevenson, S. J. J., et al. (2004). Carbon nutrition of *Escherichia coli* in the mouse intestine. *Proc. Natl. Acad. Sci. USA* 101, 7427–7432. doi: 10.1073/pnas.0307888101

Chao, Y., and Vogel, J. (2016). A 3' UTR-Derived Small RNA provides the regulatory noncoding arm of the inner membrane stress response. *Mol. Cell* 61, 352–363. doi: 10.1016/j.molcel.2015.12.023

Cosma, C. L., Danese, P. N., Carlson, J. H., Silhavy, T. J., and Snyder, W. B. (1995). Mutational activation of the Cpx signal transduction pathway of *Escherichia coli* suppresses the toxicity conferred by certain envelope-associated stresses. *Mol. Microbiol.* 18, 491–505. doi: 10.1111/j.1365-2958.1995.mmi_18030491.x

Danese, P. N., and Silhavy, T. J. (1997). The σ(E) and the Cpx signal transduction systems control the synthesis of periplasmic protein-folding enzymes in *Escherichia coli*. *Genes Dev.* 11, 1183–1193. doi: 10.1101/gad.11.9.1183

Danese, P. N., and Silhavy, T. J. (1998). CpxP, a stress-combative member of the Cpx regulon. *J. Bacteriol.* 180, 831–839. doi: 10.1128/JB.180.4.831-839.1998

Danese, P. N., Snyder, W. B., Cosma, C. L., Davis, L. J. B., and Silhavy, T. J. (1995). The Cpx two-component signal transduction pathway of *Escherichia coli* regulates transcription of the gene specifying the stress-inducible periplasmic protease. *DegP. Genes Dev.* 9, 387–398. doi: 10.1101/gad.9.4.387

Dbeibo, L., van Rensburg, J. J., Smith, S. N., Fortney, K. R., Gangaiah, D., Gao, H., et al. (2018). Evaluation of CpxRA as a therapeutic target for uropathogenic *escherichia coli* infections. *Infect. Immun.* 86:17. doi: 10.1128/IAI.00798-17

De Wulf, P., McGuire, A. M., Liu, X., and Lin, E. C. C. (2002). Genome-wide profiling of promoter recognition by the two-component response regulator CpxR-P in *Escherichia coli*. *J. Biol. Chem.* 277, 26652–26661. doi: 10.1074/jbc.M203487200

Delhaye, A., Collet, J.-F., and Laloux, G. (2019a). A fly on the wall: how stress response systems can sense and respond to damage to peptidoglycan. *Front. Cell. Infect. Microbiol.* 9:380. doi: 10.3389/fcimb.2019.00380

Delhaye, A., Laloux, G., and Collet, J.-F. F. (2019b). The lipoprotein NlpE is a cpx sensor that serves as a sentinel for protein sorting and folding defects in the *escherichia coli* envelope. *J. Bacteriol.* 209, 1–12. doi: 10.1128/JB.00611-18

Desnoyers, G., and Massé, E. (2012). Noncanonical repression of translation initiation through small RNA recruitment of the RNA chaperone Hfq. *Genes Dev.* 26, 726–739. doi: 10.1101/gad.182493.111

Engl, C., Beek, A., Ter Bekker, M., de Mattos, J. T., Jovanovic, G., and Buck, M. (2011). Dissipation of proton motive force is not sufficient to induce the phage shock protein response in *Escherichia coli*. *Curr. Microbiol.* 62, 1374–1385. doi: 10.1007/s00284-011-9869-5

Friedrich, T., Dekovic, D. K., and Burschel, S. (2016). Assembly of the *Escherichia coli* NADH:ubiquinone oxidoreductase (respiratory complex I). *Biochim. Biophys. Acta-Bioenerg.* 1857, 214–223. doi: 10.1016/j.bbabio.2015.12.004

Fürst, M., Zhou, Y., Merfort, J., and Müller, M. (2018). Involvement of PpiD in Sec-dependent protein translocation. *Biochim. Biophys. Acta. Mol. Cell Res.* 1865, 273–280. doi: 10.1016/j.bbamcr.2017.10.012

Geissmann, T. A., and Touati, D. (2004). Hfq, a new chaperoning role: binding to messenger RNA determines access for small RNA regulator. *EMBO J.* 23, 396–405. doi: 10.1038/sj.emboj.7600058

Grabowicz, M., and Silhavy, T. J. (2017a). Envelope Stress Responses: An Interconnected Safety Net. *Trends Biochem. Sci.* 42, 232–242. doi: 10.1016/j.tibs.2016.10.002

Grabowicz, M., and Silhavy, T. J. (2017b). Redefining the essential trafficking pathway for outer membrane lipoproteins. *Proc. Natl. Acad. Sci.* 114, 4769–4774. doi: 10.1073/pnas.1702248114

Guénebaut, V., Schlitt, A., Weiss, H., Leonard, K., and Friedrich, T. (1998). Consistent structure between bacterial and mitochondrial NADH:ubiquinone oxidoreductase (complex I). *J. Mol. Biol.* 276, 105–112. doi: 10.1006/jmbi.1997.1518

Guest, R. L., Wang, J., Wong, J. L., and Raivio, T. L. (2017). A bacterial stress response regulates respiratory protein complexes to control envelope stress adaptation. 199, 1–14. doi: 10.1128/JB .00153-17

Guest, R. L. R. L. (2017). *Regulation of respiration by the Cpx response in enteropathogenic Escherichia coli*. Edmonton: University of Alberta.

Hederstedt, L., and Rutberg, L. (1981). Succinate-dehydrogenase - a comparative review. *Microbiol. Rev.* 45, 542–555. doi: 10.1128/MMBR.45.4.542-555.1981

Hews, C. L., Cho, T., Rowley, G., and Raivio, T. L. (2019). Maintaining integrity under stress: envelope stress response regulation of pathogenesis in gram-negative bacteria. *Front. Cell. Infect. Microbiol.* 9:1–25. doi: 10.3389/fcimb.2019.00313

Hofhaus, G., Weiss, H., and Leonard, K. (1991). Electron microscopic analysis of the peripheral and membrane parts of mitochondrial NADH dehydrogenase (Complex I). *J. Mol. Biol.* 221, 1027–1043. doi: 10.1016/0022-2836(91)80190-6

Holst, O., Moran, A. P., and Brennan, P. J. (2010). "Chapter 1 - Overview of the glycosylated components of the bacterial cell envelope," in *Microbial Glycobiology*, eds J. Otto Holst Patrick and B. Mark von Itzstein (San Diego: Academic Press), 1–13. doi: 10.1016/B978-0-12-374546-0.00001-8

Hung, D. L., Raivio, T. L., Jones, C. H., Silhavy, T. J., and Hultgren, S. J. (2001). Cpx signaling pathway monitors biogenesis and affects assembly and expression of P pili. *EMBO J.* 20, 1508–1518. doi: 10.1093/emboj/20.7.1508

Isaac, D. D., Pinkner, J. S., Hultgren, S. J., and Silhavy, T. J. (2005). The extracytoplasmic adaptor protein CpxP is degraded with substrate by DegP. *Proc. Natl. Acad. Sci. USA* 102, 17775–17779. doi: 10.1073/pnas.0508936102

Jones, C. H., Danese, P. N., Pinkner, J. S., Silhavy, T. J., and Hultgren, S. J. (1997). The chaperone-assisted membrane release and folding pathway is sensed by two signal transduction systems. *EMBO J.* 16, 6394–6406. doi: 10.1093/emboj/16.21.6394

Jones, C. H., Dexter, P., Evans, A. K., Liu, C., Hultgren, S. J., and Hruby, D. E. (2002). *Escherichia coli* degp protease cleaves between paired hydrophobic residues in a natural substrate: the PapA Pilin. *J. Bacteriol.* 184, 5762–5771. doi: 10.1128/JB.184.20.5762-5771.2002

Kaila, V. R. I. I., and Wikström, M. (2021). Architecture of bacterial respiratory chains. *Nat. Rev. Microbiol.* 19, 319–330. doi: 10.1038/s41579-020-00486-4

Kaila, V. R. I. R. I., Verkhovsky, M. I. I., and Wikstrom, M. (2010). Proton-coupled electron transfer in cytochrome oxidase. *Chem. Rev.* 110, 7062–7081. doi: 10.1021/cr1002003

Kao, M.-C. C., Nakamaru-Ogiso, E., Matsuno-Yagi, A., and Yagi, T. (2005). Characterization of the membrane domain subunit NuoK (ND4L) of the NADH-quinone oxidoreductase from *Escherichia coli*. *Biochemistry* 44, 9545–9554. doi: 10.1021/bi050708w

Karp, G. (2008). *Cell and Molecular Biology: Concepts and Experiments*. 5th ed. Hoboken: John Wiley & Sons, Limited.

Kerscher, S., Dröse, S., Zickermann, V., and Brandt, U. (2008). The three families of respiratory NADH dehydrogenases. *Results Probl. Cell Differ.* 45, 185–222. doi: 10.1007/400_2007_028

Kervinen, M., Pätsi, J., Finel, M., and Hassinen, I. E. (2004). A Pair of membrane-embedded acidic residues in the nuok subunit of *Escherichia coli* NDH-1, a Counterpart of the ND4L subunit of the mitochondrial complex I, are required for high ubiquinone reductase activity. *Biochemistry* 43, 773–781. doi: 10.1021/bi0355903

Kihara, A., Akiyama, Y., and Ito, K. (1995). FtsH is required for proteolytic elimination of uncomplexed forms of SecY, an essential protein translocase subunit. *Proc. Natl. Acad. Sci. USA* 92, 4532–4536. doi: 10.1073/pnas.92.10.4532

Kihara, A., and Ito, K. (1998). Translocation, folding, and stability of the HflKC complex with signal anchor topogenic sequences. *J. Biol. Chem.* 273, 29770–29775. doi: 10.1074/jbc.273.45.29770

Kitagawa, M., Ara, T., Arifuzzaman, M., Ioka-Nakamichi, T., Inamoto, E., Toyonaga, H., et al. (2005). Complete set of ORF clones of *Escherichia coli* ASKA library (a complete set of E. coli K-12 ORF archive): unique resources for biological research. *DNA Res. Int. J. Rapid Publ. Rep. Genes Genomes* 12, 291–299. doi: 10.1093/dnares/dsi012

Kohanski, M. A., Dwyer, D. J., Wierzbowski, J., Cottarel, G., and Collins, J. J. (2008). Mistranslation of membrane proteins and two-component system activation trigger antibiotic-mediated cell death. *Cell* 135, 679–690. doi: 10.1016/j.cell.2008.09.038

Kumar, R., and Shimizu, K. (2011). Transcriptional regulation of main metabolic pathways of cyoA, cydB, fnr, and fur gene knockout *Escherichia coli* in C-limited and N-limited aerobic continuous cultures. *Microb. Cell Fact.* 10:3. doi: 10.1186/1475-2859-10-3

Langklotz, S., Baumann, U., and Narberhaus, F. (2012). Structure and function of the bacterial AAA protease FtsH. *Biochim. Biophys. Acta-Mol. Cell Res.* 1823, 40–48. doi: 10.1016/j.bbamcr.2011.08.015

Leiser, O. P., Charlson, E. S., Gerken, H., and Misra, R. (2012). Reversal of the ΔdegP Phenotypes by a Novel rpoE Allele of *Escherichia coli*. *PLoS One* 7:e33979. doi: 10.1371/journal.pone.0033979

Lestienne, P., and Desnuelle, C. (1999). *Complex II or Succinate: Quinone Oxidoreductase and Pathology BT - Mitochondrial Diseases: Models and Methods*. Berlin: Springer, 87–95. doi: 10.1007/978-3-642-59884-5_7

MacRitchie, D. M., Ward, J. D., Nevesinjac, A. Z., and Raivio, T. L. (2008). Activation of the Cpx envelope stress response down-regulates expression of several locus of enterocyte effacement-encoded genes in enteropathogenic *Escherichia coli*. *Infect. Immun.* 76, 1465–1475. doi: 10.1128/IAI.01265-07

Massé, E., and Gottesman, S. (2002). A small RNA regulates the expression of genes involved in iron metabolism in *Escherichia coli*. *Proc. Natl. Acad. Sci. USA* 99, 4620–4625. doi: 10.1073/pnas.032066599

Massé, E., Vanderpool, C. K., and Gottesman, S. (2005). Effect of RyhB small RNA on global iron use in *Escherichia coli*. *J. Bacteriol.* 187, 6962–6971. doi: 10.1128/JB.187.20.6962-6971.2005

Matern, Y., Barion, B., and Behrens-Kneip, S. (2010). PpiD is a player in the network of periplasmic chaperones in *Escherichia coli*. *BMC Microbiol.* 10:251. doi: 10.1186/1471-2180-10-251

Matsushita, K., Ohnishi, T., and Kaback, H. R. (1987). NADH-ubiquinone oxidoreductases of the *Escherichia coli* aerobic respiratory chain. *Biochemistry* 26, 7732–7737. doi: 10.1021/bi00398a029

McNeil, M. B. B., Clulow, J. S. S., Wilf, N. M. M., Salmond, G. P. C. P. C., and Fineran, P. C. C. (2012). SdhE is a conserved protein required for flavinylation of succinate dehydrogenase in bacteria. *J. Biol. Chem.* 287, 18418–18428. doi: 10.1074/jbc.M111.293803

Mileykovskaya, E., and Dowhan, W. (1997). The Cpx two-component signal transduction pathway is activated in *Escherichia coli* mutant strains lacking phosphatidylethanolamine. *J. Bacteriol.* 179, 1029–1034. doi: 10.1128/jb.179.4.1029-1034.1997

Minárik, P., Tomásková, N., Kollárová, M., and Antalík, M. (2002). Malate dehydrogenases–structure and function. *Gen. Physiol. Biophys.* 21, 257–265.

Mitchell, A. M., and Silhavy, T. J. (2019). Envelope stress responses: balancing damage repair and toxicity. *Nat. Rev. Microbiol.* 17, 417–428. doi: 10.1038/s41579-019-0199-0

Münch, R., Hiller, K., Grote, A., Scheer, M., Klein, J., Schobert, M., et al. (2005). Virtual Footprint and PRODORIC: an integrative framework for regulon prediction in prokaryotes. *Bioinformatics* 21, 4187–4189. doi: 10.1093/bioinformatics/bti635

Nakamura, K., Yamaki, M., Sarada, M., Nakayama, S., Vibat, C. R., Gennis, R. B., et al. (1996). Two hydrophobic subunits are essential for the heme b ligation and functional assembly of complex II (succinate-ubiquinone oxidoreductase) from *Escherichia coli*. *J. Biol. Chem.* 271, 521–527. doi: 10.1074/jbc.271.1.521

Nakayama, S., and Watanabe, H. (1995). Involvement of cpxA, a sensor of a two-component regulatory system, in the pH-dependent regulation of expression of *Shigella* sonnei virF gene. *J. Bacteriol.* 177, 5062–5069. doi: 10.1128/jb.177.17.5062-5069.1995

Ogura, T., Inoue, K., Tatsuta, T., Suzaki, T., Karata, K., Young, K., et al. (1999). Balanced biosynthesis of major membrane components through regulated degradation of the committed enzyme of lipid A biosynthesis by the AAA protease FtsH (HflB) in *Escherichia coli*. *Mol. Microbiol.* 31, 833–844. doi: 10.1046/j.1365-2958.1999.01221.x

Otto, K., and Silhavy, T. J. (2002). Surface sensing and adhesion of *Escherichia coli* controlled by the Cpx-signaling pathway. *Proc. Natl. Acad. Sci. USA* 99, 2287–2292. doi: 10.1073/pnas.042521699

Park, S. J., Tseng, C. P., and Gunsalus, R. P. (1995). Regulation of succinate dehydrogenase sdhCDAB operon expression in *Escherichia coli* in response to carbon supply and anaerobiosis: role of ArcA and Fnr. *Mol. Microbiol.* 15, 473–482. doi: 10.1111/j.1365-2958.1995.tb02261.x

Pogliano, J., Lynch, A. S., Belin, D., Lin, E. C. C., Beckwith, J., Genetics, M., et al. (1997). Regulation of *Escherichia coli* cell envelope proteins involved in protein folding and degradation by the Cpx two-component system. *Genes Dev.* 11, 1169–1182. doi: 10.1101/gad.11.9.1169

Price, C. E., and Driessen, A. J. M. M. (2010). Biogenesis of membrane bound respiratory complexes in *Escherichia coli*. *Biochim. Biophys. Acta-Mol. Cell Res.* 1803, 748–766. doi: 10.1016/j.bbamcr.2010.01.019

Price, N. L., and Raivio, T. L. (2009). Characterization of the Cpx regulon in *Escherichia coli* strain MC4100. *J. Bacteriol.* 191, 1798–1815. doi: 10.1128/JB.00798-08

Prüss, B. M. M., Nelms, J. M. M., Park, C., and Wolfe, A. J. J. (1994). Mutations in NADH:ubiquinone oxidoreductase of *Escherichia coli* affect growth on mixed amino acids. *J. Bacteriol.* 176, 2143–2150. doi: 10.1128/jb.176.8.2143-2150.1994

Raivio, T. L. (2014). Everything old is new again: an update on current research on the Cpx envelope stress response. *Biochim. Biophys. Acta-Mol. Cell Res.* 1843, 1529–1541. doi: 10.1016/j.bbamcr.2013.10.018

Raivio, T. L. (2018). Regulation of proteolysis in the Gram-negative bacterial envelope. *J. Bacteriol.* 200, 1–6. doi: 10.1128/JB.00639-17

Raivio, T. L., Laird, M. W., Joly, J. C., and Silhavy, T. J. (2000). Tethering of CpxP to the inner membrane prevents spheroplast induction of the Cpx envelope stress response. *Mol. Microbiol.* 37, 1186–1197. doi: 10.1046/j.1365-2958.2000.02074.x

Raivio, T. L., Leblanc, S. K. D., and Price, N. L. (2013). The *Escherichia coli* Cpx envelope stress response regulates genes of diverse function that impact antibiotic resistance and membrane integrity. *J. Bacteriol.* 195, 2755–2767. doi: 10.1128/JB.00105-13

Raivio, T. L., Popkin, D. L., and Silhavy, T. J. (1999). The cpx envelope stress response is controlled by amplification and feedback inhibition. *J. Bacteriol.* 181, 5263–5272. doi: 10.1128/JB.181.17.5263-5272.1999

Raivio, T. L., and Silhavy, T. J. (1997). Transduction of envelope stress in *Escherichia coli* by the Cpx two-component system. *J. Bacteriol.* 179, 7724–7733. doi: 10.1128/jb.179.24.7724-7733.1997

Raivio, T. L., and Silhavy, T. J. (2001). Periplasmic stress and ECF sigma factors. *Annu. Rev. Microbiol.* 55, 591–624. doi: 10.1146/annurev.micro.55.1.591

Ruiz, N., Kahne, D., and Silhavy, T. J. (2006). Advances in understanding bacterial outer-membrane biogenesis. *Nat. Rev. Microbiol.* 4, 57–66. doi: 10.1038/nrmicro1322

Sakoh, M., Ito, K., and Akiyama, Y. (2005). Proteolytic activity of HtpX, a membrane-bound and stress-controlled protease from *Escherichia coli*. *J. Biol. Chem.* 280, 33305–33310. doi: 10.1074/jbc.M506180200

Shen, J., and Gunsalus, R. P. (1997). Role of multiple ArcA recognition sites in anaerobic regulation of succinate dehydrogenase (sdhCDAB) gene expression in *Escherichia coli*. *Mol. Microbiol.* 26, 223–236. doi: 10.1046/j.1365-2958.1997.5561923.x

Shimohata, N., Chiba, S., Saikawa, N., Ito, K., and Akiyama, Y. (2002). The Cpx stress response system of *Escherichia coli* senses plasma membrane proteins and controls HtpX, a membrane protease with a cytosolic active site. *Genes Cell* 7, 653–662. doi: 10.1046/j.1365-2443.2002.00554.x

Silhavy, T., Berman, M., and Enquist, L. (1984). *Experiments with gene fusions*. New York, NY: Cold Spring Harbor Laboratory, doi: 10.1016/0168-9525(85)90025-3

Silhavy, T. J., Kahne, D., and Walker, S. (2010). The bacterial cell envelope. *Cold Spring Harb. Perspect. Biol.* 2:a000414. doi: 10.1101/cshperspect.a000414

Surmann, K., Stopp, M., Wörner, S., Dhople, V. M., Völker, U., Unden, G., et al. (2020). Fumarate dependent protein composition under aerobic and anaerobic growth conditions in *Escherichia coli*. *J. Proteomics* 212, 103583. doi: 10.1016/j.jprot.2019.103583

Tran, Q. M., Rothery, R. A., Maklashina, E., Cecchini, G., and Weiner, J. H. (2006). The quinone binding site in *Escherichia coli* succinate dehydrogenase is required for electron transfer to the heme b. *J. Biol. Chem.* 281, 32310–32317. doi: 10.1074/jbc.M607476200

van Bloois, E., Dekker, H. L., Fröderberg, L., Houben, E. N. G. G., Urbanus, M. L., de Koster, C. G., et al. (2008). Detection of cross-links between FtsH, YidC, HflK/C suggests a linked role for these proteins in quality control upon insertion of bacterial inner membrane proteins. *FEBS Lett.* 582, 1419–1424. doi: 10.1016/j.febslet.2008.02.082

Van Stelten, J., Silva, F., Belin, D., and Silhavy, T. J. (2009). Effects of antibiotics and a proto-oncogene homolog on destruction of protein translocator SecY. *Science* 325, 753–756. doi: 10.1126/science.1172221

Weinberg, E. D. (1959). Gradient Agar Plates. *Am. Biol. Teach.* 21, 347–350. doi: 10.2307/4439185

Wong, J. L., Vogt, S. L., and Raivio, T. L. (2013). Using reporter genes and the *Escherichia coli* ASKA overexpression library in screens for regulators of the gram negative envelope stress response. *Methods Mol. Biol.* 966, 337–357. doi: 10.1007/978-1-62703-245-2_21

Yamamoto, K., and Ishihama, A. (2006). Characterization of copper-inducible promoters regulated by CpxA/CpxR in *Escherichia* coli. *Biosci. Biotechnol. Biochem.* 70, 1688–1695. doi: 10.1271/bbb.60024

Yankovskaya, V., Horsefield, R., Törnroth, S., Luna-Chavez, C., Miyoshi, H., Léger, C., et al. (2003). Architecture of succinate dehydrogenase and reactive oxygen species generation. *Science* 299, 700–704. doi: 10.1126/science.1079605

Yoshida, M., Muneyuki, E., and Hisabori, T. (2001). ATP synthase - a marvellous rotary engine of the cell. *Nat. Rev. Mol. Cell Biol.* 2, 669–677. doi: 10.1038/35089509

Zhang, Z., Gosset, G., Barabote, R., Gonzalez, C. S., Cuevas, W. A., and Saier, M. H. J. (2005). Functional interactions between the carbon and iron utilization regulators. Crp and Fur, in Escherichia coli. *J. Bacteriol.* 187, 980–990. doi: 10.1128/JB.187.3.980-990.2005

Zheng, D., Constantinidou, C., Hobman, J. L., and Minchin, S. D. (2004). Identification of the CRP regulon using in vitro and in vivo transcriptional profiling. *Nucleic Acids Res.* 32, 5874–5893. doi: 10.1093/nar/gkh908

Conflict of Interest: The authors declare that the research was conducted in the absence of any commercial or financial relationships that could be construed as a potential conflict of interest.

Publisher's Note: All claims expressed in this article are solely those of the authors and do not necessarily represent those of their affiliated organizations, or those of the publisher, the editors and the reviewers. Any product that may be evaluated in this article, or claim that may be made by its manufacturer, is not guaranteed or endorsed by the publisher.

Advantages of publishing in Frontiers

OPEN ACCESS
Articles are free to read for greatest visibility and readership

FAST PUBLICATION
Around 90 days from submission to decision

HIGH QUALITY PEER-REVIEW
Rigorous, collaborative, and constructive peer-review

TRANSPARENT PEER-REVIEW
Editors and reviewers acknowledged by name on published articles

Frontiers
Avenue du Tribunal-Fédéral 34
1005 Lausanne | Switzerland

Visit us: www.frontiersin.org
Contact us: frontiersin.org/about/contact

REPRODUCIBILITY OF RESEARCH
Support open data and methods to enhance research reproducibility

DIGITAL PUBLISHING
Articles designed for optimal readership across devices

FOLLOW US
@frontiersin

IMPACT METRICS
Advanced article metrics track visibility across digital media

EXTENSIVE PROMOTION
Marketing and promotion of impactful research

LOOP RESEARCH NETWORK
Our network increases your article's readership